

Quantum Dots: Synthesis, Functionalization and Bioconjugation for Biological Applications

Ana Sofia da Cunha Miguel

Dissertation presented to obtain the Ph.D degree in Engineering Sciences
and Technology

Instituto de Tecnologia Química e Biológica | Universidade Nova de Lisboa

Oeiras, September, 2012



INSTITUTO
DE TECNOLOGIA
QUÍMICA E BIOLÓGICA
/UNL
Knowledge Creation



Quantum Dots: Synthesis, Functionalization and Bioconjugation for Biological Applications

Ana Sofia da Cunha Miguel

Dissertation presented to obtain the Ph.D degree in Engineering Sciences and Technology

Instituto de Tecnologia Química e Biológica | Universidade Nova de Lisboa

Thesis Supervisors:

Professor Dr Christopher David Maycock

(Head of the Organic Synthesis Laboratory at Instituto de Tecnologia Química e Biológica)

Dr Abel Gonzalez Oliva

(Head of the Biomolecular Diagnostic Laboratory at Instituto de Tecnologia Química e Biológica)

The research work described in this thesis was performed at Organic Synthesis and Biomolecular Diagnostic Laboratories, Instituto de Tecnologia Química e Biológica - Universidade Nova de Lisboa, Oeiras, Portugal. This work was supported by Fundação para a Ciência e Tecnologia (FCT) through a PhD grant to Ana Sofia Miguel (SFRH/BD/40303/2007) and the grant # PEst-OE/EQB/LA0004/2011. This work was also supported by the national funded project NTec/SQA/0131/2007 from FCT



Acknowledgments

I would like to express my gratitude to all the people who, in one way or another, have helped me throughout my Doctoral work:

A special thanks to **Professor Dr Christopher Maycock**, for accepting me in his lab 9 years ago, for believing in me and my work, for trusting in my capabilities when I decided to accept this project. More particularly, thank you for the guidance and advice throughout these years, for his invariable efforts to keep the laboratory in excellent condition which allowed me to proceed with my research work unhindered, for the fruitful ideas and discussions during my chemistry problems, for his great sense of humour and for the opportunity to work with him.

I would like to thank **Dr Abel Oliva**, for giving me the opportunity to work with him, for his availability and help, for all the financial efforts that he made to support my work during the past few years as well as all the research collaborations that he established giving me the opportunity to expand my work.

I thank all my colleagues (past and present members) from Organic Synthesis laboratory (ITQB-UNL), for their help, especially to Eva Lourenço, Dr Rita Ventura, Paula Rodrigues and Osvaldo Ascenso for their support, patient, enthusiasm, friendship and for all the relaxing lunches, afternoon talks and for the good moments we passed together.

I thank my colleagues (past and present members) from the Biomolecular Diagnostic laboratory (ITQB-UNL) especially Ana Raquel Santos and Joana Campos for their support and help in my work and for all the good moments that we shared together.

To **Elisa de Campos**, a deep and sincere thank you for all the support during my Doctoral work, especially for the discussions on my biological data. Thank you for sharing all your knowledge and expertise with me and for your friendship.

I would like to thank to **Dr Pedro Fevereiro** from ITQB-UNL for his sympathy, availability and for the great work resulting from our research collaboration.

A special acknowledgement to **Dr Ana Domingos** from IHMT-UNL for her help with the antibody production and helpful discussions related to biological data and for her availability and friendship.

I also thank to Analytical Services Unit (ASU) (ITQB-UNL and IBET), especially to all the members of the analytical and microbiology laboratories located in the chemistry building. I am grateful for the opportunity that was given to me to use their equipment which contributed largely to the performance and success of my work during the last four years.

I would also like to thank the Instituto de Tecnologia Química e Biológica of the Universidade Nova de Lisboa (ITQB-UNL) for the excellent conditions provided to perform my work.

I would like to express my gratitude to the Fundação para a Ciência e Tecnologia (FCT) for the PhD fellowship that was conceded to me (SFRH/BD/40303/2007).

To all my friends, a big thanks for the encouragement, support and friendship all these years! You know who you are.

I want to thank my parents for their endless affection, support, patience and for always believing in me and my capabilities. Thank you for making possible what I am today.

Finally, I especially thank Filipe Alvito for his love, support and patience. Thank you for your excellent advice, for your guidance to be always better and for being there whenever needed.

Table of Contents

Acknowledgments	v
Table of Contents	ix
Dissertation Outline	xvii
Abbreviations	xxiii
Abstract	xxix
Resumo	xxxv
Chapter 1	
General Introduction.....	1
Chapter 2	
Synthesis and Characterization of CdSe/ZnS QDs.....	27
Chapter 3	
Ligand Synthesis and Design for Water-Soluble CdSe/ZnS QDs.....	61
Chapter 4	
Conjugation of Luminescent QDs with Antibodies	141
Chapter 5	
Quantum Dot Applications	189
PART I	
Detection of RAP-1 Antigenic Protein in Infected <i>Babesia bovis</i> Erythrocytes Using QDs as Fluorescent Reagents	193
PART II	
Work Resulting From Collaboration with Other Research Groups	219
Chapter 6	
General Discussion and Future Perspectives	235
Chapter 7	
Appendix.....	251
Published papers related with this dissertation:	253
Book chapters by invitation related with this dissertation:.....	253
Submitted papers related with this dissertation:.....	253

List of Equations:

Equation 1 Expression applied to calculate the quantum yield.....	39
Equation 2 Expression of Lambert-Beer's Law given to calculate the concentration of QDs solutions.	39
Equation 3 Stokes-Einstein equation for the hydrodynamic diameter.	49
Equation 4 Expression given to estimate the number of functional amine groups available on a single QD surface.	100
Equation 5 Expression used to estimate the number of sugar molecules available on a single QD surface.....	101
Equation 6 Smoluchowski equation used to convert electrophoretic mobility of nanoparticles measured in zeta potential values.	126
Equation 7 Expression used to determine the concentration in mg/mL of the immobilized antibody in QD-antibody complexes.	155
Equation 8 Expression given to determine the QD/Ab ratios.....	155

List of Figures:

Figure 1 Electronic Energy Levels Depending on the Number of Bound Atoms.	6
Figure 2 Quantum Dots..	8
Figure 3 Surface Modification of QDs.	13
Figure 4 Bioconjugation Strategies..	15
Figure 5 Transmission Electron Microscopy Analysis.....	47
Figure 6 Size determination by dynamic light scattering.....	48
Figure 7 Correlation Data.	50
Figure 8 Determination of the extinction coefficient of QDs.	52
Figure 9 Optical Measurements:.....	53
Figure 10 ¹ H-NMR spectra of DHLA (1) and DHLA-PEG ₄₀₀ -OH (3).....	104
Figure 11 Infrared Analysis of dichloride and diazide from PEG ₄₀₀	106
Figure 12 Optical Measurements of Hydrophilic QDs.	122
Figure 13 HD Measurements of Hydrophilic QDs.	124
Figure 14 Size Determination by Dynamic Light Scattering.....	125
Figure 15 ζ -potential Measurements of Hydrophilic QDs.....	126
Figure 16 Measurement of the number of amino-PEG ₄₀₀ per QD.	128

Figure 17 Ratio of detected amine concentration vs. % of amine-terminated ligand in ligand mixture.....	129
Figure 18 Estimation of the Number of Sugar Molecules per QD.....	130
Figure 19 Structure of an IgG Molecule.	146
Figure 20 Biological Activity of the Antibody-Bioconjugated QDs.....	158
Figure 21 pH Stability of MPA and DHLA-QDs..	159
Figure 22 Electrophoretic Mobility of MPA and DHLA-QDs..	161
Figure 23 Comparison of Electrophoretic Mobility of MPA-QDs in different buffers.....	162
Figure 24 EDC Activation Step Analysed by Agarose Gel Electrophoresis.	166
Figure 25 Analysis of Bioconjugation Protocol by Agarose Gel Electrophoresis.....	169
Figure 26 Separation of the Functional Components of MPA-Bioconjugated QDs.	174
Figure 27 Separation of the Functional Components of DHLA-Bioconjugated QDs..	176
Figure 28 Testing the Functional Activity of QD-Ab complexes.....	178
Figure 29 Erythrocyte Invasion by <i>Babesia</i> Parasites.....	197
Figure 30 Apicomplexan main features for <i>Toxoplasma gondii</i> tachyzoite and <i>Plasmodium falciparum</i> merozoite.	198
Figure 31 Immunofluorescence Assays on Slide..	208
Figure 32 Immunofluorescence Assays in Solution.	209
Figure 33 Immunofluorescence Assays on Slide with Vortex Stirring.....	210
Figure 34 QDs Uptake by the Plant Cells.....	223
Figure 35 Oxidative Stress Dose Response Assay.....	224
Figure 36 DNA Damage in <i>Medicago sativa</i> cells in Suspension Cultures..	227
Figure 37 Expression of <i>Tdp1</i> β , <i>Top1</i> . β , <i>Fpg</i> , <i>SOD</i> and <i>APX</i> genes in <i>Medicago sativa</i> cells treated with MPA-QDs.	228
Figure 38 Laser Immobilization onto Solid Substrates of CdSe/ZnS core-shell QDs.....	231

List of Schemes:

Scheme 1 Reaction scheme for the synthesis of TOPO/HDA capped-CdSe QDs.	34
Scheme 2 Reaction scheme for the surface passivation of CdSe/ZnS core-shell QDs with 5 monolayers of ZnS based on SILAR method.....	37
Scheme 3 DHLA-PEG Hydrophilic Ligands.....	67
Scheme 4 DHLA and DHLA-PEG ₄₀₀ -OH Synthesis.	102
Scheme 5 Modular ligands with functional terminal groups..	105
Scheme 6 General reaction for the synthesis of ditosyl compound 20 from PEG ₄₀₀	107
Scheme 7 Amino-PEGn-DHLA and Carboxy-PEGn-DHLA Synthesis.....	107
Scheme 8 LA-NHS Synthesis.....	108
Scheme 9 Sugar-capped QDs.....	110
Scheme 10 Synthesis of 3-maleimido propionic acid NHS ester.	111
Scheme 11 Thiol linker synthesis.	112
Scheme 12 Carbohydrate Hydrophilic Ligands.	114
Scheme 13 DHLA-TEG-Mannose Synthesis.....	115
Scheme 14 Structure of collateral product TEG-N ₃ (38) formed from degradation of initial compound 31 under hydrolysis conditions.....	117
Scheme 15 DHLA-PEG ₄₀₀ -Mannose Synthesis.	118
Scheme 16 Structure of collateral product PEG ₄₀₀ -N ₃ (47) formed from degradation of initial compound 42 under hydrolysis conditions.....	119
Scheme 17 Functionalization Procedure.....	120
Scheme 18 Schematic Diagram of Covalent Conjugation.	148
Scheme 19 Bioconjugation Protocol Proposed.....	164
Scheme 20 Conjugation of Antibodies to Carboxy-QDs using EDC or EDC/NHS.	165
Scheme 21 Antibody Reduction with β -Mercaptoethanol.....	173
Scheme 22 Structure of an Individual Amino Acid Present in Proteins.....	180
Scheme 23 Schematic representation of direct and indirect immunofluorescence assay.....	207

List of Tables:

Table 1 Amount of each precursor solution added for the ZnS shell growth procedure around the CdSe cores.	36
Table 2 Glossary of terms related with quantum dots.	55
Table 3 Solvent and reagent purification.	71
Table 4 Graphical index of compounds and experiments of ligand synthesis and design.	131
Table 5 QD/Ab molar ratios obtained for the different bioconjugation reactions performed to link antibodies onto QD surface using the EDC/NHS strategy.	172
Table 6 Glossary of terms related with some molecular biology techniques applied in this work	182
Table 7 Glossary of terms related with the topic addressed in this work. .	213

Dissertation Outline

The main goal of this Doctoral work was to develop a fluorescent biomarker to identify antigenic proteins associated with specific parasites. Although it is known that fluorescent techniques making use of standard organic dyes are widely used for this purpose, the development of a new method was proposed using nanotechnology; in particular the use of nano optical reporters also called quantum dots (QDs). In order to achieve this goal, the research work was divided into four main tasks: (1) synthesis and characterization of CdSe/ZnS core-shell QDs; (2) design of dihydrolipoic acid (DHLLA) ligands appended to oligo and poly (ethylene) glycols (PEG) with different functional groups to generate biocompatible QDs; (3) bioconjugation of QDs to monoclonal antibodies based on sophisticated protocols and (4) some chemical and biological applications of the synthesized non-conjugated and conjugated nanoparticles.

Chapter 1 of this thesis is a general introduction related to nanotechnology, particularly on the subject of quantum dots. This includes a general overview of reported work related to the synthesis, functionalization, bioconjugation, toxicity and possible applications of these nanoparticles.

Chapter 2 describes protocols for the synthesis of CdSe cores and surface passivation with a ZnS multishell. Moreover, the structural and optical characterization of these nanoparticles making use of diverse techniques is also presented. Data shown in this chapter has been published in a book chapter called “Synthesis and Functionalization of CdSe/ZnS QDs using the Successive Ion Layer Adsorption Reaction and Mercaptopropionic Acid Phase Transfer Methods” within the “Nanoparticles in Biology and Medicine. Methods and Protocols.” from Springer. Ana S. Miguel is the first author of this book chapter.

Chapter 3 describes a simple and versatile scheme for the preparation of a family of heterobifunctional ligands incorporating i) dihydrolipoic acid as QD ligand, ii) a hydrophilic spacer such as polyethylene glycol with different molecular weights and iii) different functional end termini. With these ligands, different water-soluble QDs were produced by the ligand exchange method

for posterior conjugation with biomolecules. In parallel, the production of hydrophilic nanoparticles with shorter ligands such as 3-mercaptopropionic acid by the phase transfer method was also carried out and discussed. The hydrophilic nanoparticles were characterized in terms of size, surface charge and fluorescence making use of light scattering techniques and quantum yield measurements respectively. When appropriate, colorimetric assays were also used to characterize the presence of some functional groups in the QD surface. The overall data resulting from this characterization is also described and discussed in this chapter. Part of the data obtained in chapter 3 has also been published in the book chapter previously mentioned and edited by Springer.

Chapter 4 focuses on the conjugation of luminescent water-soluble QDs with monoclonal antibodies. The conjugation of MPA and DHLA-QDs with monoclonal antibodies against a recombinant antigenic protein was performed based on EDC/NHS amide bond forming chemistry. To better understand the experimental conditions necessary to carry out this reaction, the bioconjugation assay was proven by studies of the electrophoretic mobility of carboxy-QDs. Confirmation of the success of the bioconjugation process, characterization of the binding properties of the bioconjugated-QDs as well as the capacity that these bioconjugated complexes had to recognize their antigen, were analysed and discussed. The antibody/QD molar ratio was also determined.

Biological and chemical applications of the conjugated and non-conjugated QDs respectively are described in **Chapter 5**. This chapter is divided into two sections. The first part is related to the use of bioconjugated samples as fluorescent biomarkers to detect the RAP-1 antigenic protein in erythrocytes infected with *Babesia bovis*. The second part comprises the work with QDs developed in collaboration with other research groups. For example, the cytotoxic and genotoxic effects caused by the non-conjugated nanoparticles in higher plant cells was studied and is discussed. In addition, application of the native CdSe/ZnS core-shell QDs in the electronics field is described in this chapter. The work related to the study of the QD cytotoxic has been published

in *Journal of Nanobiotechnology* and in the book chapter entitled “Evaluation of Cytotoxicity of 3-Mercaptopropionic Acid-Modified Quantum Dots on *Medicago sativa* Cells and Tissues”, edited by Springer (*Nanoparticles in Biology and Medicine. Methods and Protocols*). The work related to the chemical applications of the native CdSe/ZnS QDs has been published in *Journal of Physical Chemistry C* and is also submitted in *Physica Status Solidi A*. The study of genotoxic effects of the non-conjugated nanoparticles in higher plant cells has been submitted in *Particle and Fibre Toxicology*.

Chapter 6 gathers all the results/findings obtained in this Doctoral work together to form general conclusions along with suggestions for future work.

A printed version of the published, in press or submitted papers/book chapters related to the work described in this thesis can be found in **Chapter 7** (appendix chapter).

Abbreviations

AAS atomic absorption spectroscopy
Ab antibody
ADH adipic acid dihydrazide
AFM atomic force microscopy
AMA-1 apical membrane antigen 1
A/N alkaline/neutral
a.u. arbitrary units
BCA bicinchoninic acid
BME β -mercaptoethanol
br s broad singlet
BSA bovine serum albumin
BTTS bis (trimethylsilyl) sulphide
CAT catalase
CCD charge couple device
CT C-terminal
Cys cysteine
 δ chemical shift
J coupling constant
DAB 3, 3'-diaminobenzidine
DAPI 4', 6-diamidino-2-phenylindole dihydrochloride
DCC dicyclohexylcarbodiimide
DHLA dihydrolipoic acid
DMAP 4-(dimethylamino) pyridine
DMF dimethylformamide
DLS dynamic light scattering
DSBs double strand breaks
DTNB 5, 5'-dithiobis (2-nitrobenzoic acid)
DTT dithiothreitol
EDC *N*-Ethyl-*N'*-(3-dimethylaminopropyl) carbodiimide
EDX dispersive x-ray spectroscopy
Endo III endonuclease III
ELISA enzyme-linked immunosorbent assay
ESI-MS electrospray ionization mass spectrometer
Fc fragment crystallisable

- FITC** fluorescein isothiocyanate
FPG formamidopyrimidine DNA glycosilase
FRET Förster resonance energy transfer
FTIR Fourier transform infrared spectroscopy
GPI glycosyl-phosphatidylinositol
GR glutathione reductase
HD hydrodynamic diameter
HDA 1-hexacedylamine
HOMO highest molecular orbital occupied
HRTEM high resolution transmission electronic microscopy
HRP horseradish peroxidase
H₂DCFDA 2', 7'-dichlorodihydrofluorescein diacetate
IFAT immunofluorescence antibody test
IgG immunoglobulin G
IHC immunohistochemistry
LA-NHS lipoic acid *N*-hydroxysuccinimide ester
LEDs light emitting devices
LUMO lowest molecular orbital unoccupied
MAA mercaptoacetic acid
MAPLE matrix-assisted pulsed laser evaporation
MBP maltose binding protein
MES 4-morpholineethanesulfonic acid
ML monolayer
MPA 3-mercaptopropionic acid
MW molecular weight
Na-P sodium phosphate buffer
NBT/BCIP nitro-blue tetrazolium / 5-bromo-4-chloro-3'-indolyphosphate
NC's nanocrystals
NHS *N*-Hydroxysuccinimide
Ni-NTA nickelnitriloacetic acid complex
NMR nuclear magnetic resonance
NT N-terminal
OA oleic acid
ODE 1-octadecene

PCR	polymerase chain reaction
PCS	photon correlation spectroscopy
PDI	polydispersity index
PBS	phosphate buffer saline
PEG	poly (ethylene) glycol
pI	isoelectric point
PL	photoluminescence
PMAO	maleic copolymer
PTFE	polytetrafluoroethylene
<i>p</i>-TsCl	tosyl chloride
PVDF	polyvinylidene fluoride
QD-Ab	quantum dot-antibody conjugate
QDs	quantum dots
QRT-PCR	real time quantitative polymerase chain reaction
QY	quantum yield
RAP-1	rophty associated protein
RBC	red blood cell
<i>Rf</i>	retardation factor
RLB	reverse line blotting
ROS	reactive oxygen species
r.t.	room temperature
<i>g</i>	relative centrifugal force
SBP	spherical body protein
SDS	sodium dodecyl sulphate
SILAR	successive ion layer adsorption and reaction
SMCC	4-(<i>N</i> -maleimidomethyl) cyclohexanecarboxylic acid <i>N</i> -hydroxysuccinimide ester
SOD	superoxide dismutase
SSBs	single strand breaks
Sulfo-SMCC	3-sulfo- <i>N</i> -hydroxysuccinimide ester sodium salt
TA	thioctic acid
TBE	tris borate EDTA
TBP	tributylphosphine
TBS	tris buffered saline

- Tdp** tyrosyl-DNA phosphodiesterase
TEG tri (ethylene) glycol
TEM transmission electronic microscopy
THF tetrahydrofuran
TLC thin layer chromatography
TMSOTf trifluoromethanesulfonic acid trimethyl silylester
TOP trioctylphosphine
Top topoisomerase
TOPO trioctylphosphine oxide
TRAP thrombospondin-related anonymous protein
Trp tryptophan
TTBS tris buffered saline with Tween
Tyr tyrosine
VMSA variable merozoite surface antigens
 ξ zeta potential

Abstract

During the past few decades, technology has made great improvements to enable visualisation, identification and quantitation in biological systems. In recent years, nanoparticles have become the center of attention of many researchers. The integration of inorganic synthetic methods with techniques to produce nano-sized particles of semiconducting materials has led to the creation of a class of fluorescent optical reporters, called quantum dots (QDs). These nanometer-sized crystalline particles are composed of elements of periodic groups of II-VI or III-V elements but so far the CdSe/ZnS core-shell QDs are the most used. These nanoparticles possess unique optical and electronic properties, compared to organic dyes such as size-tuneable light emission, superior signal brightness, superior resistance to photobleaching and simultaneous excitation of multiple fluorescence colours.

One of the main goals of this doctoral work was to synthesize core-shell CdSe/ZnS QDs and design ligands that permit the preparation of compact hydrophilic functionalized QDs amenable to conjugation with a variety of biomolecules via simple covalent and non-covalent binding strategies. In order to achieve this objective, detailed protocols for the preparation of CdSe nanocrystals coated with a multishell structure of ZnS were developed and described. For the controlled formation of the ZnS shells the Successive Ion Layer Adsorption and Reaction (SILAR) method was used. To analyse the size, size distribution, shape and fluorescence of the nanoparticles, a combination of optical and structural characterization techniques was used including electron transmission microscopy, dynamic light scattering and quantum yield measurements. To promote the hydrophilicity of the native QDs in aqueous environments a variety of dihydrolipoic acid (DHLLA) ligands were synthesized appended to a hydrophilic spacer, such as polyethylene glycol, of various lengths. These ligands also included a functional terminus such as an amine, a carboxylate or a sugar moiety for the posterior covalent attachment of the biomolecules. Similarly 3-mercaptopropionic acid (MPA), a short hydrophilic ligand, was attached using the phase transfer method for ligand exchange thus forming compact water soluble QDs.

Having available surface functionalized QDs, a further interesting step was their bioconjugation with antibodies and other proteins. QD/antibody bioconjugation can be carried out by several different sophisticated methods

and some of them involve the subtle modification of the antibody presumably without reduction of bioactivity. The most used procedures are covalent antibody-QD-conjugation based on cross linking reactions, between the amino groups that decorate the stem of the antibody and carboxylic acid groups which terminate the ligand chains connected to the QDs (random bioconjugation, amide bond formation catalysed by carbodiimide). Taking advantage of this methodology, the coupling of MPA and DHLA-QDs with antibodies using EDC/NHS coupling chemistry was carried out. Monoclonal antibodies against recombinant RAP-1 *Babesia bovis* protein were attached using this method. The bioconjugated nanoparticles were characterized by comparing their molecular weight and electrophoretic mobility with non-conjugated nanoparticles as well as their functional and binding properties, using SDS-PAGE, agarose gels and western blotting techniques.

Finally, the application of the developed bioconjugated nanoprobe in the biological field, namely in the detection of recombinant RAP-1 antigenic protein in infected *Babesia bovis* erythrocytes was carried out. *Babesia bovis* is an intraerythrocytic protozoan parasite transmitted by Ixodid ticks and responsible for great economic losses in cattle industry in many tropical and subtropical regions worldwide. Over the years many different methods have been applied to identify early infections in whole blood of the animals, in particular immunofluorescence antibody test (IFAT). However, one of the significant limitations presented by this method is photobleaching. Using the QDs conjugated with anti-RAP 1 antibody for detection of rhoptry associated antigenic protein (RAP-1) present in the apical complex of different *B. bovis* parasites in infected blood, these nanoparticles proved to be a good alternative to traditional IFAT and also useful tools in biosensing applications since they are much less prone to photodegradation.

Concerns about the toxic and genotoxic effects of these nanoparticles in biological systems have been raised since they contain toxic elements such as cadmium and selenium. Another interesting area of development is for possible applications in electronics for the creation of biosensors, lasers or high performance devices. This interest has led to the creation of collaborations with other research groups from different institutes/universities located in Portugal, Spain and Italy with the aim of studying the cytotoxic and

genotoxic effects in *Medicago sativa* cells (higher plant cells) when exposed to CdSe/ZnS core-shell QDs coated with 3-mercaptopropionic acid as well as the use of a recent laser-based deposition technique to immobilize the native QDs onto solid substrates for further application in electronic devices. For the cytotoxicity and genotoxicity studies, in general, the resulting work demonstrated that these effects are dependent on a number of factors including the QD's properties, dose and environmental conditions of administration. It was concluded that, QD concentrations between 1 and 5nM should not be exceeded for such biological applications. On the other hand, the native CdSe/ZnS core-shell QDs could prove to be useful tools in the electronics field since they are resistant to laser deposition techniques creating a specific network-like surface morphology of the deposited material and after the immobilization process, their functional properties (fluorescence) were not altered.

This doctoral work has demonstrated the numerous advantageous properties and some of the potentialities of the chosen QDs not only in the biological field but also in other areas.

Key-words: *Quantum dots, SILAR method, biocompatible, bioconjugation, immunofluorescence assays, Babesia bovis, cytotoxicity, genotoxicity and MAPLE technique.*

Resumo

Durante as últimas décadas, a tecnologia tem produzido notáveis avanços para permitir a identificação, a visualização e a quantificação em sistemas biológicos. Nos últimos anos, as nanopartículas tornaram-se o centro das atenções de muitos investigadores. A integração de métodos sintéticos inorgânicos com técnicas de produção de nanopartículas, constituídas por materiais semicondutores, levou à criação de uma classe de repórteres ópticos fluorescentes, denominados de *quantum dots* (QDs). Estas partículas cristalinas de tamanho nanométrico podem ser compostas por elementos dos grupos II-VI ou III-V da tabela periódica, mas até agora as que possuem um núcleo de seleneto de cádmio (CdSe) e uma cobertura de sulfureto de zinco (ZnS) têm vindo a ser as mais utilizadas. Estas nanopartículas possuem propriedades ópticas e electrónicas únicas, quando comparadas com corantes orgânicos, tais como um tamanho definido de acordo com a emissão de luz pretendida, um superior sinal de brilho, uma elevada resistência à foto-degradação e podem ser excitadas em diferentes comprimentos de onda permitindo obter múltiplas cores de fluorescência.

Um dos principais objectivos deste trabalho Doutoral foi sintetizar nanopartículas semicondutoras com a estrutura núcleo-cobertura CdSe/ZnS e criar ligandos orgânicos que permitissem a obtenção de nanopartículas compactas, funcionalizadas e hidrofílicas de forma a serem posteriormente conjugadas com diversas biomoléculas fazendo uso de ligações simples covalentes e não-covalentes. De forma a alcançar este objectivo, foram desenvolvidos e descritos protocolos detalhados para a preparação destes nano-cristais. A formação controlada das coberturas de sulfureto de zinco foi efectuada com base no método SILAR (*successive ion layer adsorption and reaction*). Para analisar o tamanho, a distribuição de tamanho, a forma e a fluorescência das nanopartículas, foi utilizada uma combinação de técnicas de caracterização estrutural e ópticas, nomeadamente microscopia de transmissão electrónica (TEM), *dynamic light scattering* (DLS) e medições do rendimento quântico. Para promover a hidrofiliabilidade das nanopartículas semicondutoras nativas em ambientes aquosos, foi sintetizada uma variedade de compostos derivados do ácido dihidrolípico (DHLLA) contendo anexada uma molécula hidrofílica, como o caso do polietileno glicol (PEG), de diferentes comprimentos. Estes ligandos contêm também na sua estrutura,

um terminal funcional que pode ser constituído por diferentes grupos funcionais, como por exemplo, uma amina, um ácido carboxílico ou um glúcido para uma posterior ligação covalente das biomoléculas. Da mesma forma, embora se trate de um ligando hidrofílico de pequeno tamanho, o ácido 3-mercaptopropiónico (MPA) foi também acoplado à superfície das nanopartículas, usando o método de transferência de fase, originando assim QDs compactos e solúveis em meios aquosos.

Após a superfície dos QDs se encontrar funcionalizada, um passo posterior interessante foi a sua conjugação com anticorpos e proteínas. A conjugação QD-anticorpo pode ser efectuada utilizando diferentes métodos sofisticados e envolvendo, alguns deles, uma modificação suave do anticorpo, sem que haja uma presumível redução da sua actividade biológica. Um dos procedimentos utilizados para a conjugação covalente QD-anticorpo é normalmente baseado em reacções cruzadas entre os grupos amino, que decoram a região Fc do anticorpo, e os ácidos carboxílicos, que terminam as cadeias dos ligandos que se encontram ligados à superfície dos QDs (bioconjugação aleatória em que a formação da ligação amida é catalizada por uma carbodiimida). Tirando partido desta metodologia, neste trabalho, a reacção de conjugação entre os QDs funcionalizados com MPA e DHLA e anticorpos monoclonais contra a proteína antigénica recombinante RAP-1 de *Babesia bovis* foi realizada usando a via química de acoplamento EDC/NHS. As nanopartículas bioconjugadas foram posteriormente caracterizadas utilizando técnicas de biologia molecular. Nesse sentido, foi efectuada uma comparação do peso molecular e da mobilidade electroforética, entre as partículas conjugadas e não conjugadas, usando géis de agarose. Adicionalmente, usando *SDS-PAGE* e *immunoblotting*, as partículas bioconjugadas foram também analisadas de forma a avaliar as propriedades de ligação dos anticorpos à superfície dos QDs assim como a sua actividade biológica.

As nanopartículas bioconjugadas desenvolvidas neste trabalho foram aplicadas no campo biológico, nomeadamente na detecção da proteína antigénica recombinante RAP-1 *B. bovis*, em eritrócitos provenientes de bovinos infectados com *Babesia bovis*. A *Babesia bovis* é um parasita protozoário intra-eritrocitário transmitido por carraças da família *Ixodidae*, e é

responsável por elevadas perdas económicas na indústria bovina em diversas áreas tropicais e sub-tropicais a nível mundial. Ao longo dos anos, diferentes métodos têm sido aplicados para identificar infecções precoces no sangue dos animais, em particular, IFAT (*immunofluorescence antibody test*). No entanto, uma das limitações significativas apresentadas por este método é a foto-degradação. De forma a ultrapassar este problema, os QDs conjugados com o anticorpo anti-RAP 1 foram testados na detecção da proteína antigénica RAP-1 presente no complexo apical de diferentes parasitas *B. bovis*, em sangue animal infectado. Os resultados obtidos demonstraram que estas nanopartículas, quando conjugadas com o anticorpo específico, podem ser uma boa alternativa ao método tradicional IFAT. Para além disso, também revelaram ser ferramentas úteis em aplicações como biosensores uma vez que são muito menos propensas ao processo da foto-degradação.

Actualmente um dos temas que tem vindo a ser desenvolvido na área da nanobiotecnologia e que tem levantado alguma preocupação são os efeitos citotóxicos e genotóxicos que estas partículas semicondutoras podem provocar em sistemas biológicos, uma vez que são constituídas por elementos tóxicos, como o cádmio e o selénio. Outro campo de aplicação, e que também tem sido alvo de estudo, é a possível utilização deste tipo de partículas na área da electrónica, nomeadamente para a criação de biosensores, lasers ou dispositivos electrónicos de elevado desempenho. Estes dois tópicos levaram à criação de colaborações com outros grupos de investigação de diferentes institutos/universidades localizados em Portugal, Espanha e Itália. Um dos principais objectivos destas colaborações foi estudar os efeitos citotóxicos e genotóxicos destas nanopartículas em células vegetais superiores de *Medicago sativa* quando expostas a QDs de CdSe/ZnS revestidos com ácido 3-mercaptopropiónico (MPA-QDs). Outro dos objectivos foi testar a imobilização das nanopartículas hidrofóbicas em substratos sólidos usando uma técnica recente de deposição com laser para posterior aplicação em dispositivos electrónicos. Relativamente aos estudos de citotoxicidade e de genotoxicidade efectuados, de uma forma geral, demonstrou-se que estes efeitos são dependentes de uma série de factores nomeadamente das propriedades das nanopartículas, da dosagem e ainda

das condições em que são administradas. Com estes estudos foi possível concluir que, para este tipo de aplicações biológicas, concentrações de QDs entre 1 e 5nM não deverão ser excedidas. No que se refere às aplicações electrónicas, os QDs nativos de CdSe/ZnS provaram ser ferramentas úteis neste tipo de área, uma vez que são resistentes a técnicas de imobilização com laser. Estas partículas demonstraram ter a capacidade de criar na superfície uma morfologia de rede específica, as quais após o processo de imobilização mantêm as suas propriedades funcionais (fluorescência) inalteradas

Com este trabalho Doutoral foi possível demonstrar, tanto no campo biológico como em outras áreas, as inúmeras propriedades vantajosas e algumas das potencialidades das nanopartículas semicondutoras escolhidas para a realização deste trabalho.

Palavras-chave: *Quantum dots, método SILAR, biocompatível, bioconjugação, ensaios de imunofluorescência, Babesia bovis, citotoxicidade, genotoxicidade e técnica MAPLE.*

Chapter 1

General Introduction

General Introduction

Introduction	5
Synthesis of QDs.....	8
Surface Modification of QDs for Stability and Biocompatibility.....	11
Conjugation of Biomolecules to QDs.....	13
Some Applications of QDs.....	16
QDs Toxicity	19
Concluding Remarks	20
References	21

Introduction

The term Nanotechnology has been employed to describe the creation and exploitation of materials with structural dimensions between those of atoms and bulk materials, with at least one dimension in the nanometer range ($1\text{nm}=10^{-9}\text{m}$)^[1]. During the last decade, engineered nanoparticles have become an important class of new materials with several properties that make them very attractive for commercial development ^[2]. Among the various classes of nanoparticles, Quantum Dots (QDs) have attracted much attention in biotechnology and biomedical fields due to the wide availability of precursors, straightforward synthesis and the unique optical and electronic properties. In particular, biosensing, drug delivery, and *in vitro* and *in vivo* imaging are the areas which have most benefitted from bioconjugated QDs ^[3]. Core/shell QDs are nanocrystals composed of a core of a semiconductor material, coated within a shell of another semiconductor material with a larger spectral band gap. They were initially prepared in colloidal solutions in 1982 ^[4], but the systematic advancement in the science and technology of these nanoparticles was fuelled only after 1984 when Louis Brus ^[5, 6] derived a relationship between size and band gap for semiconductor nanoparticles by applying a particle in a sphere model approximation to the wave function for bulk semiconductors ^[3]. QD cores are usually composed by elements from groups II and VI such as CdSe (most common) or groups III and V like InP, while the shell is typically a high band gap material such as ZnS ^[7]. The best available QD fluorophores for biological applications are made of CdSe cores coated with a layer of ZnS because their chemistry is the most refined. The ZnS passivates the core surface, protects it from oxidation, prevents leaching of the Cd/Se into the surrounding solution and also produces substantial improvement in the photoluminescence (PL) yield ^[8, 9]. These nanoparticles possess distinct properties that give them their unique capabilities when compared with standard organic dyes. Quantum dots in general are very small with a diameter in the range between 4 and 12nm and their unique optical and electronic properties originated from a combination of bulk semiconductor properties (*e.g.* band gap of the semiconductor material) and quantum confinement effect^[3]. In small nanocrystals their electronic structure is intermediate between discrete levels of an atomic system and the band

structure of a bulk solid, due to the confinement of the electron wave function within the physical dimensions of the particle. This phenomenon is called quantum confinement and this is why nanocrystals are known as QDs^[1]. In these particles, the highest occupied atomic levels of the atomic (or ionic) species interact with each other to form the valence band of the nanoparticle. Similarly, the lowest unoccupied levels combine to form the conduction band of the particle. The energy gap between the valence and conduction bands results in the band gap of the nanoparticle^[10].

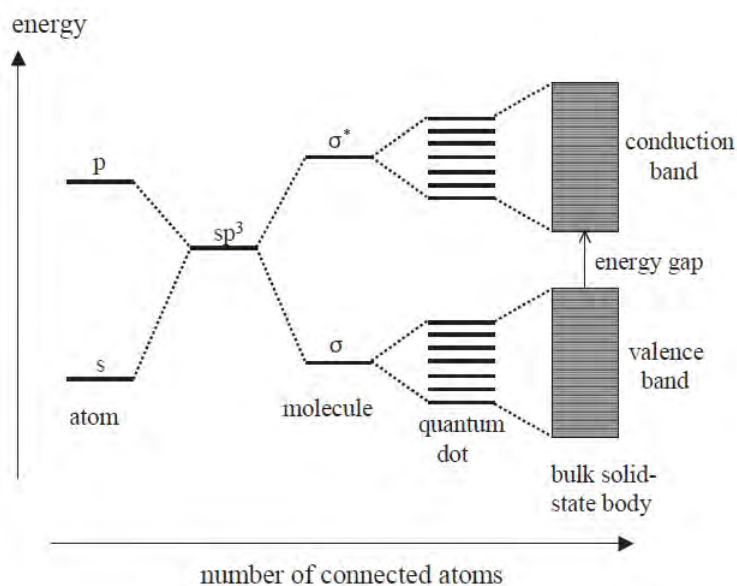


Figure 1 | Electronic Energy Levels Depending on the Number of Bound Atoms. By binding more and more atoms together, the discrete energy levels of the atomic orbitals merge into energy bands (here shown for a semiconducting material). Adapted from reference [10].

The most striking evidence of quantum confinement in semiconductor nanocrystals is their size-tuneable optical properties. In other words, the shift in the optical absorption and emission spectra of QDs is dependent on their size. When a semiconductor absorbs a photon, an electron is promoted from the valence band to the conduction band, creating an exciton (electron-hole pair) or leaving behind a region of positive charge (hole) in the valence band. During this process, both electron and hole can move around in the bulk material, but since the exciton is composed of an electron and a hole that have opposite charges, a strong Coulomb attraction causes them to remain

relatively localized within a nanometer-sized crystal. This means that due to the small size of the nanocrystals, the electron-hole separation is confined and smaller than the Bohr radius of the semiconductor^[11, 12]. Hence, when core nanocrystals are made progressively smaller, more energy is required to confine the exciton, and the energy of the emitted photons increases. Therefore, larger nanocrystals absorb and emit in the red while smaller nanocrystals absorb and emit in the blue. By controlling the core size it is possible to develop a range of nanocrystals with distinct emission spectral characteristics. The spectral characteristics of QDs offer other distinctive advantages over those of organic dyes and fluorescent proteins, particularly with regard to implementation of spectral multiplexed detection schemes (e.g. multicolour imaging). The broad absorption spectra of QDs and the fact that the absorption coefficients increase towards shorter wavelengths facilitates single wavelength excitation of multiple QD nanocrystal types. In addition to large molar absorptivity coefficients ($\sim 10^5$ - 10^6 M⁻¹cm⁻¹), the emission spectra of core-shell QDs are narrow, symmetric (Gaussian in shape) and can span a broad range of wavelengths by a careful choice of particle size and composition. QDs also possess high quantum yields due to the large capacity for photon absorption which is propagated into emission of fluorescence photons^[13].

Another property of QDs is their high photostability when not exposed to extreme conditions. This is because, generally, the core material with a narrow band gap is enclosed within a shell coating, comprised of a different semiconductor material with higher band gap. This core-shell architecture not only confines excitation and emission of the core but also enhances quantum yield and protects the core from photobleaching^[14].

These unique properties show why these nanomaterials of excellence have been applied in a variety of biological applications and have been allowing investigators to unravel biological function at the molecular level^[3, 12].

Quantum Dots, despite their many advantages, possess also some issues that must be considered, prior to their widespread adoption, including blinking, biocompatibility, larger relative size as compared to standard fluorophores and conjugation. However, all of them have been overcome to some extent and are continually being studied and improved^[14]. In this chapter, past and

ongoing efforts in synthetic methods, surface modification and bioconjugation will be addressed as well as general applications of these nanoparticles.

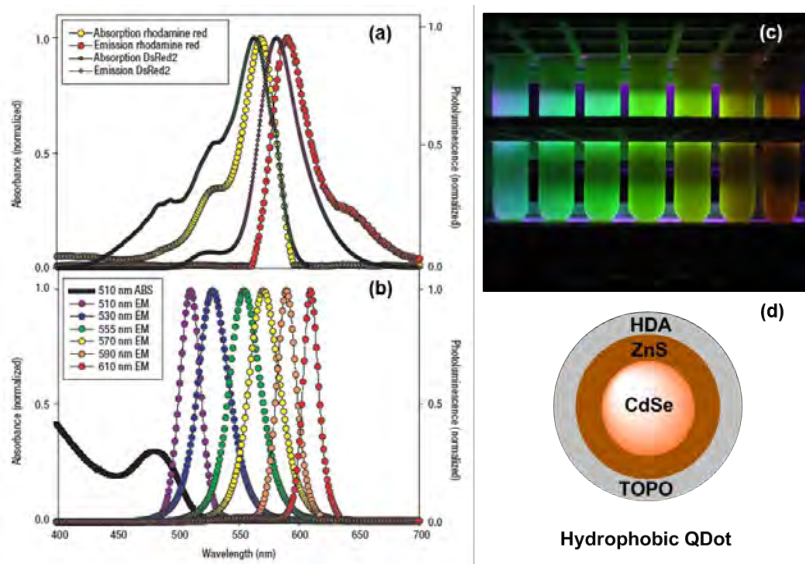


Figure 2 | Quantum Dots. (a) Absorption and Emission spectra of a standard organic dye (rhodamine red) and a genetically encoded DsRed2 protein. (b) Absorption and Emission spectra of six different QD dispersions, showing how multiple narrow and symmetric QDs emission can be used in the same spectral window when compared with an organic or genetically encoded dye. (c) Photo demonstrating the size-tunable fluorescence properties of colloidal CdSe quantum dots dispersed in hexane. (d) Structure of a lipophilic CdSe/ZnS core-shell QD with TOPO and HDA as surrounding organic ligands. Images (a) and (b) adapted by permission from Macmillan Publishers Ltd: Nature Materials[15], copyright 2005.

Synthesis of QDs

Semiconductor nanoparticle synthesis was reported for the first time in the 1980's by Alexei Ekimov^[16] and Louis Brus^[4], but it was Murray *et al*^[17] who in 1993 brought radical changes to the basic research and applications of QDs. This protocol produced QD samples that were highly monodisperse, regular in core structure, size-tunable and possessed a surface capping. Briefly, the CdSe core-QDs were synthesized using dimethyl cadmium (CdMe_2) and trioctylphosphine selenide (TOPSe) as cadmium and selenium precursors respectively in a coordinating solvent mixture composed of trioctylphosphine (TOP) and its oxide (TOPO). The synthesis was carried out in an inert atmosphere and the precursors were dissolved at 300°C followed by the growing of the nanocrystals at 230-260°C. Taking this method as the base for

the colloidal synthesis of QDs, different semiconductor nanocrystals were also obtained such as CdS or CdTe by simply replacing TOPSe by bis(trimethylsilyl) sulphide (BTSS) or TOPTe^[3]. Although this approach produced narrow size-distributed QDs with individual luminescence colours, the quality of the core-shell nanocrystals was not high in terms of size and size distribution control and the use of extremely toxic, pyrophoric, explosive and/or expensive substrates such as CdMe₂ represented a drawback. For these reasons, since that date many modifications have been made to this procedure in order to overcome these issues. The hazardous CdMe₂ was substituted by non-volatile cadmium precursors as demonstrated by Vossmeier *et al*^[18] who accomplished the synthesis of colloidal QDs by replacing the CdMe₂ with cadmium perchlorate (CdClO₄). However, it was Peng and co-workers in 2001 that more significantly contributed to the synthesis of CdX semiconductor nanocrystals eliminating the use of CdMe₂ with cadmium chloride (CdCl₂)^[19], cadmium acetate (CdAc₂)^[20] or cadmium carbonate (CdCO₃)^[21]. More recently the synthesis of QDs was simplified and optimized by the use of metal oxides such as cadmium oxide (CdO)^[22, 23].

Another important point that has also been developed in the synthesis process of colloidal QDs is the choice of coordinating solvents. This type of solution has the ability to stabilize the bulk semiconductors and prevent aggregation as the QDs grow^[17, 24]. Originally the preparation method of high quality QDs include the use of TOPO and TOP, but the synthesis of CdX nanocrystals was improved when the mixture TOPO/TOP was supplemented by alkylphosphoric acids such as dodecylphosphoric acid or more importantly by alkylamines such as 1-hexadecylamine (HDA) which proved to be very good for the production of core nanocrystals with much smaller size distribution and high PL^[24, 25]. It is important to point out that in the search for green synthetic methods for colloidal nanocrystals, non-coordinating solvents such as 1-octadecene (ODE)^[22, 26, 27] was also implemented. Among other advantages, the lower reactivity of ODE with the precursors and the excellent solvation power, made it very useful for the growth of high quality QDs in general. With the many developments made over the years, it is clear that the central synthetic methodology to provide protocols that enable core-QDs with customised properties is currently straightforward and reproducible; however

the semiconductor core material needs to be protected from degradation and oxidation to maintain optimum QD performance.

Shells on core QDs, in general, possess many functions including the protection of the core against oxidation and leaching and serve as a platform for ligand exchange and bioconjugation reactions. In addition, these shells are also made up of suitable semiconductor materials which preserve and improve the optical properties of the core^[3]. The CdSe cores coated with a ZnS shell have been the most investigated. The ZnS shell does not incorporate into the core or alter the core structure but increases the quantum yield of the CdSe core^[14]. As has happened with the core-QDs, the core-shell nanocrystals have also undergone some modifications regarding the semiconductor precursors. Dabbousi *et al*^[8] accomplished the preparation of core-shell QDs by the epitaxial growth of ZnS shells using diethyl zinc (Et₂Zn). Zinc stearate and zinc oxide (ZnO) were introduced by Reiss and co-workers^[25] to avoid the use of pyrophoric dialkyl zinc precursors. In general, semiconductor shells grown epitaxially by addition of shell precursors into the reaction mixture containing the core nanocrystals. This shell growth process was traditionally carried out by drop-wise addition^[25], but the search for homogeneous monolayer growth of the shell precursors onto all core nanocrystals in solution led to the introduction of the successive ion layer adsorption and reaction (SILAR) method. This method was introduced in 2003 by Peng *et al*^[22] and was developed for the growth of the shell where each monolayer is grown one at a time by alternating the injection of air-stable and inexpensive cationic and anionic precursors into the reaction mixture. The shell thickness may be controlled by various parameters including growth temperature, concentration and rate at which the reagents are added. The temperature is a crucial factor because if the shell growth temperature is too close to that of the core synthesis temperature, core seeds can continue to grow and negatively affect the size distribution. On the other hand, if the shell growth proceeds at lower temperatures, the crystallinity of the shell decrease leading to imperfect passivation of the core surface. The concentration and rate of addition of the shell precursors are also important to promote the heterogeneous growth^[14]. In this way a series of discrete monolayers is

produced under controlled conditions and usually does not exceed more than five.

Although semiconductor shells have been demonstrated to provide important protection, contributing to the stability of the core against degradation and photobleaching, they are poorly soluble in aqueous solutions. Thus, surface modification of QDs is needed for further stability, biocompatibility and bioconjugation.

Surface Modification of QDs for Stability and Biocompatibility

The inorganic core-shell semiconductor nanoparticles such as CdSe/ZnS QDs, once prepared, are covered and are initially only soluble in organic solvents. To be useful in biological applications, these nanoparticles must be soluble in aqueous solutions. The three main strategies used to make QDs biocompatible are: ligand exchange with bifunctional molecules, silica coating and encapsulation with amphiphilic polymers and phospholipids micelles.

The ligand exchange method is a surface exchange reaction which results in the addition of a heterobifunctional ligand and so far seems to be the methodology most applied. This ligand employs a hydrophobic and chelating end to displace the native organic ligands such as TOPO, TOP or HDA from the QD, while the hydrophilic end extends out into the aqueous phase, aiding solubility^[14]. Common heterobifunctional ligands applied for this procedure are mono and dithiols which complex with the metal ions at the surface, and having a hydrophilic group such as a carboxylic acid at the other end of a carbon chain. Since 1998, various methods for the synthesis of thiol-capped QDs have been developed. The first work was reported by Warren *et al*^[28] where CdSe/ZnS core-shell QDs were solubilized with mercaptoacetic acid (MAA). These mono-mercapto liganded QDs are obtained either commercially or by simple synthesis, but have short shell lives due to dynamic thiol-ZnS interactions^[15]. The substitution of the mono by the dithiol dihydrolipoic acid (DHLA) emerged with Mattoussi and co-workers to improve the long-term stability of the hydrophilic nanoparticles^[29]. Although DHLA allows QD dispersion in basic buffer solutions, the aggregation of DHLA-QDs under acidic conditions was registered. To overcome these limitations a coating with polymers (*e.g.* polyethyleneglycol) on the QD surface provides increased

stability and biocompatibility of the QDs. These polymers were introduced by several groups^[30-33] and offer several advantages including protection against hydrolysis and biochemical reactions, improved solubility and adapt the surface of QD for bioconjugation due to their ability to append different functional end groups (e.g. COOH, NH₂ or sugar moieties) for further coupling with biomolecules.

Silica shells and amphiphilic polymers/phospholipids micelles constitutes other alternatives to provide solubility/stability to the QDs in aqueous environments. Silane derivatives have been used to displace the coordinating ligands on the QD surface which resulted in a layer of silica around the QD. This approach is more complicated when compared for example with monothiol-capped QDs; however the difficult nature of their synthesis is countered by considerable advantages. QDs coated with silica are more stable due to the high degree of crosslinking between the silane molecules. Moreover, the experimental procedures do not change if a different type of siloxane is used. In the case of amphiphilic polymers such as octylamine-modified polyacrylic acid^[34, 35], the non-polar QD shell is used to interact with the hydrophobic region of the polymer while the hydrophilic portion of the polymer become free to increase solubility. The process of growing an amphiphilic polymer shell around quantum dots is similar to that used for silica coating but instead of forming the shell by displacing the coordinating ligands (e.g. TOPO) from QD surface, the amphiphilic polymer takes advantage of the hydrophobic nature of these ligands and creates a network with them. This methodology provides higher stability over a broader pH range however the resulting water-soluble QDs are significantly larger in terms of size which can be a limitation for certain biological applications^[14, 15].

It is clear that whatever be the surface capping methodology, the introduction of a shell is very important, not only for the improvement of the solubility but also for protection against chemical/physical/biochemical damage and ultimately for the appendage of functional groups for further bioconjugation. However, it's important to point out that the hydrodynamic size of the QDs is a parameter that has to be controlled for the optimum efficiency of the hydrophilic nanoparticles in the various biological applications.

normally used when ligands with high affinity and selectivity can carry the QD directly to the binding site of the protein of interest. A variety of small molecules have already been conjugated to QDs (e.g. PEGylated serotonin derivative, dopamine, etc.), however, this approach could represent a disadvantage because sophisticated organic chemistry is required to synthesize an optimized ligand^[12, 14].

The antibody-conjugates are often the method of choice to modify the QD surface in order to direct it to a target. For the labelling of QDs with antibodies many different strategies have been applied. The covalent attachment of biomolecules to QDs is achieved through direct linkage to the QD surface coating containing reactive groups such as an amine or carboxylic acid or using cross-linker molecules. The most used procedures for this purpose are based on cross linking reactions, (1) between carboxylic acid (-COOH) coated QDs and primary amines (-NH₂) (random bioconjugation, catalyzed by carbodiimide), (2) between amine coated QDs and sulfhydryl groups from antibody fragments obtained via disulphide reduction (coupling between Michael acceptor and sulphhydryl groups), (3) between a hydrazide (or amine) function and an aldehyde formed by oxidation of carbohydrate groups located on the antibody's Fc region (reductive amination)^[37]. Other usual conjugation chemistry is the strong biotin-streptavidin linkage. This method could be advantageous because not only a variety of antibodies but also proteins can be biotinylated for further coupling with streptavidin-coated QDs, however the increased hydrodynamic diameter could represent a limitation for certain biological applications^[12, 14]. Non-covalent biomolecular attachment has also been employed and the simple electrostatic interactions and direct adsorption are commonly used.

Electrostatic interactions' coupling was introduced by Mattoussi and co-workers. In this strategy the bifunctional recombinant protein of interest consisting of positively charged attachment domains interacts electrostatically with the negatively charged surface of the QD^[29]. The bioconjugated QDs formed in an electrostatic fashion are less stable than those formed by covalent attachment and the method is limited to nanocrystals with charged surfaces, but allows the self-assembly of a variety of individual proteins amenable to alterations of the interaction domain. Direct adsorption has also

been demonstrated, in particular, for chemically modified peptides which adsorb spontaneously on the QD surface. This conjugation strategy permits the coupling of multiple peptides to one QD leading to an increase in the binding capacity of the resulting complexes through multivalent interactions. The reagents used are usually *N*-hydroxysuccinimidyl iodoacetate (SIA) or 2-iminothiolane-HCl commonly known as Taut's reagent^[38]. Non-specific binding has also been used to couple small biomolecules to QD surface. This kind of strategy normally depends of the ionic strength, pH, temperature and surface charge of the biomolecule. However, this approach although observed in several systems, could negatively impact the results of an experiment because nonspecific attachment of unintended molecules and aggregation is possible to occur^[7, 12]. For this reason, several alternatives have been reported to address this issue, including the coating of QDs with an inert hydrophilic polymer such as polyethylene glycol (PEG)^[39].

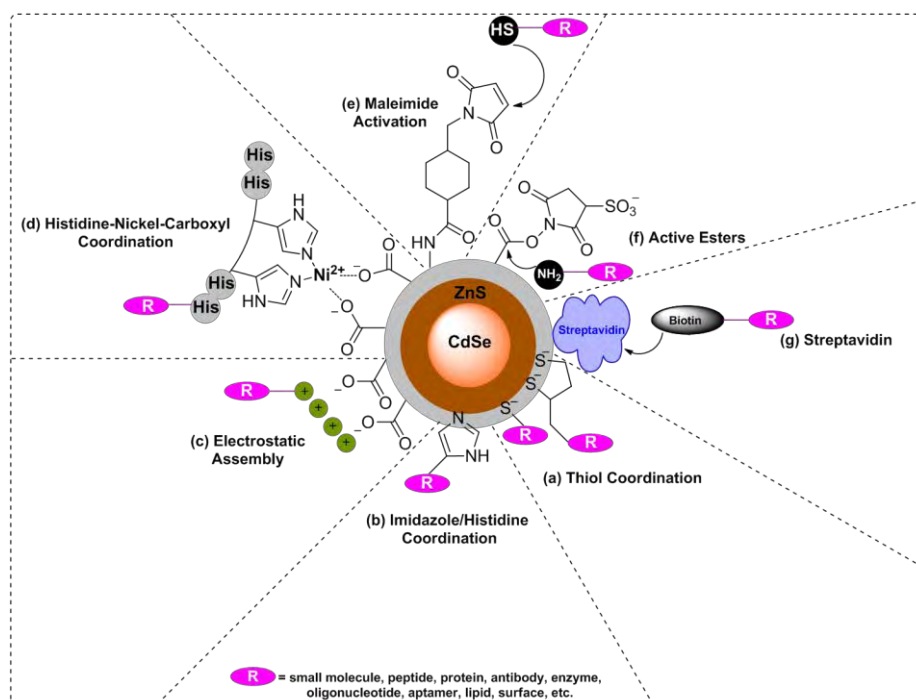


Figure 4 | Bioconjugation Strategies. An illustration of some selected biomolecule conjugation strategies applied to QDs^[40]. The grey periphery around the QD represents a general coating. Common strategies for bioconjugation include: (a) thiol modifications, (b) polyhistidine, (c) electrostatic association with coating, (d) nickel mediated assembly of polyhistidine to carboxyl coatings, (e) maleimide activation and coupling, (f) active ester and coupling and (g) biotin-labelling and streptavidin-QD conjugates.

With the variety of methods available and described above for the conjugation of biomolecules on QD surfaces it is easy to understand the amount of works that has been reported over the years to facilitate biolabeling. However, it is important to point out that bioconjugation is directly related to the development of new caps and work in this field continues in order to improve and expand the application of QDs to biological labelling.

Some Applications of QDs

Core-shell QDs possess physical and chemical properties that provide advantages for a number of different life science applications when compared with the standard fluorophores currently employed^[14]. These nanoparticles are mainly used for controlled drug delivery, bioimaging, cell labelling, biosensing, diagnosis, histochemistry and tissue engineered applications^[41].

Cellular labelling applications of QDs have been most successful and much progress has been made in the last decade. Many reports works^[42-44] has shown that QD labelling permits extended visualization of cells under continuous illumination as well as multicolour imaging, highlighting the advantages offered by these nanoparticles related to the standard fluorophores^[15]. The first labelling experiments were performed in 1998 by Alivisatos and Warren groups separately using protein interactions to specifically label 3T3 fibroblast and HeLa cells respectively to QDs^[28, 45]. These early studies demonstrated a lack of efficacy and specificity which are required requisites for QD labelling in live cell studies. However, then many developments have been made especially in surface coatings to improve aqueous solubility and the use of bioconjugation approaches such as avidin-biotin, antibody-antigen and ligand-receptor interactions to provide specificity in fixed and live cells^[46]. In general the labelling of fixed cells prepares is a harsh treatment to facilitate the entry of the QD reagent while in live cells the process must be handled carefully to maintain cellular viability. One issue of cellular labelling is the entry of the relatively large QD into the cell across lipid bilayer of the cellular membranes. Some strategies have been developed to accomplish this process including non-specific uptake by endocytosis^[47] and mechanical delivery methods such as microinjection or electroporation. In the cellular uptake, the QDs are taken up into cells by natural transport processes

(e.g. uptake of nutrients or viruses) and can be stored in granular compartments around the nucleus, without penetrating the nucleus (endocytic compartments). The micro/nano-injection of micro/nano-volumes of QDs into the cytoplasm and nucleus of individual cells was demonstrated^[48], but this strategy is a time consuming approach and the number of cells labelled limited. The electroporation process uses charge to physically deliver QDs through the membrane, but this method result in aggregation of QDs in the cytoplasm and widespread cell death^[49]. Summarizing, the labelling of cells with QDs can be carried out by methods applied by man or by methods adopted by cells and several works have been developed in this way to improve the specificity of these nanoparticles for the study of relevant biological problems.

Another important biological application of the QDs is the molecular imaging *in vitro* and *in vivo*. Due to their photostability and great resistance to photobleaching, QDs allow the acquisition of images over a longer period of time without damaging the specimen. When QDs are employed in biological imaging, some biochemical factors should be considered namely their solubility in aqueous media in order to be compatible with the biological environment. In this particular case, surface modification and conjugation of QDs plays an important role. The various surface coatings enhance solubility and provide a variety of functional groups for conjugation to antibodies, peptides and other biomolecules and/or reduce non-specific binding to the cell surface^[14, 50]. One of the most immediately successful applications of QDs *in vivo* is their use as contrast agents for the two major circulatory systems of mammals, the cardiovascular system^[51] and the lymphatic system^[52]. However, the active targeting of cancer antigens has become a unique challenge in the field of medicine because of the urgent need for sensitive and specific imaging agents for diagnostic and therapy. Since 2002 many protocols have been proposed for the conjugation of QDs with an affinity agent for various tumour cells and their vasculatures^[53, 54]. More recently, QDs labelled with a monoclonal antibody against human epidermal growth factor receptor 2 (HER2) were used to study the delivery mechanism of quantum dots in human breast cancer cells in a mouse model^[55]. Also in another study QDs conjugated with specific protein biomarkers were used for

the molecular mapping of tumour heterogeneity on human prostate cancer tissue specimens^[56]. Regarding the application of QDs in *in vitro* molecular imaging, has been described that QDs can be microinjected into the cytoplasm of fixed cells, but another interesting *in vitro* application relies on the immunostaining of fixed cells and tissue specimens. QD-based immunohistochemistry (IHC) can improve both diagnostic sensitivity and specificity. In addition, it can also provide correlated molecular and morphological information at the same time. However, this technique has had limited success, particularly in medical applications. A major drawback is the lack of robust protocols to define the key parameters and steps. For example, there is no consensus on methods for QD-antibody conjugation, tissue specimen preparation, multicolour QD staining, imaging processing and data quantification^[37, 57].

Owing to their unique spectral properties and physicochemical stability, QDs have also been used for biosensing applications. Besides immunoassays and nucleic acid detection, the Förster resonance energy transfer (FRET) is the technique that has been most extensively described in biosensing studies associated with QDs. This powerful technique allows the probing of very small changes in distance between donor and acceptor fluorophores because the efficiency of energy transfer depends in addition to this distance, also the spectral overlap and relative orientation of both donor and acceptor. This technique is commonly used to monitor biological events such as ligand-receptor binding, protein-protein interactions and conformational changes. In the large number of works already reported, QDs are predominantly used as donor molecules due their long fluorescent life time, broad absorption spectra and high extinction coefficients. In these studies^[12, 58] bioconjugated QDs have been applied to several such studies For example, Willard *et al* used QDs conjugated to bovine serum albumin (BSA) in a protein-protein assay^[59], Medintz and co-workers utilized QDs surrounded by maltose binding proteins (MBP) labelled with Cy3 for the detection of maltose sugar in solution in a dose-dependent manner^[60]. In another example, Zhang *et al* constructed a single QD-FRET biosensor for accurate and sensitive DNA detection in solution using streptavidin conjugated QDs^[61].

Despite the extended use of core-shell QDs in the biological field, QDs can also be applied in electro-optic devices. The basic advantage of this type of particles is the shell material coating the core surface, which increases the colloidal stability and prevents photodegradation of the core particle^[41]. The colloidal nanocrystals possess tunability of the emission colour from UV to near-Infrared by simply varying the nanocrystals size or narrow emission band, which has made them very useful in light-emitting devices (LEDs)^[62] development in the last decade. For this purpose, QDs have been incorporated into thin film LEDs that use a combination of semiconducting polymers, small organic molecules, III-V materials, and ceramics as charge transport layers^[63]. This class of colloidal core-shell QDs offer opportunities for inexpensive device fabrication using for example solution-based techniques such as spin or dip-coating, leading these particles to be used in thin film solar cells. The combination of CdSe QDs with polymers or the coupling of these QDs with wider gap materials such as titanium oxide (TiO₂), tin oxide (SnO₂) or zinc oxide (ZnO) maximize the efficiency of charge separation and led to the investigation of photoinduced charge transfer processes which constitute basic steps in the operation of photovoltaic devices^[64, 65].

QD Toxicity

Due to their chemical composition from toxic elements, such as cadmium and selenium, CdSe/ZnS core-shell QDs have raised many concerns about their use and application in biological systems (cells and animals)^[66]. Cadmium is the element most widely used for QD cores and for this reason various works have been reported describing methods to quantify the amount of free cadmium ions (Cd²⁺) in different biological systems^[67-69]. Studies on the exposure of cells to QDs have demonstrated the cytotoxic manifestations derived from the intracellular release of free cadmium from the QDs. The Cd²⁺ ions can be released through oxidative degradation of the QD and may then bind to sulfhydryl groups on a variety of intracellular proteins, causing decreased functionality in subcellular organelles^[70]. The cadmium was determined to be the primary cause of cytotoxicity but the tendency for nanoparticles to aggregate, precipitate on cells in culture, non-specifically

adsorb to biomolecules, and catalyse the formation of reactive oxygen species (ROS) are also possible factors that contribute to this toxicity. To reduce or eliminate this drawback, the adding of surface coatings have been the strategy most applied. For this methodology, different kinds of coating have been used including a semiconductor shell such as ZnS or small ligands such as 11-mercaptoundecanoic acid. However, the CdSe/ZnS core-shell QDs when encapsulated in amphiphilic polymers or cross-linked with silica have been found to reduce toxicity showing to be practically inert in both living cells and animals. It is clear that nanoparticle toxicity could be affected by a variety of factors. But, many different aspects have yet to be clarified and optimized such as the variety of surface coatings used by different labs, the disparity in experimental conditions tested (e.g. duration of nanoparticle exposure or media choice) or even the units of concentration used (e.g. mg/mL *versus* nM)^[66].

Cellular death or the functionality decrease of some subcellular organelles is not the only type of toxicity exhibited by QDs. Despite the lack of information and the limited published results in this area, it has been found that these nanoparticles can also damage DNA by factors such as surface coatings, in particular those bearing carboxylic acids^[14].

Concluding Remarks

Quantum dots present a highly attractive platform for a diverse array of biological applications and they are becoming a frequent tool in this field. Due to their numerous advantageous properties, in particular high fluorescence yields, stability against photobleaching and the size-dependent luminescence features, these nanoparticles are also becoming very useful in other areas. Nowadays, a selected number of QD synthetic methods, advanced surface coatings and bioconjugation techniques are available and optimized to produce nanoparticles with tailored properties. However, the challenge remain in the development of new and more efficient surface coatings to preserve bioaffinity, provide for ligand diversity and offer bioactive and stable interfaces. Issues such as biocompatibility, long-term stability and toxicity of the functionalized/bioconjugated QDs need to be more extensively studied in order to clarify and expand QD research.

References

1. Rao, C. N. R.; Müller, A.; Cheetham, A. K., *The Chemistry of Nanomaterials: Synthesis, Properties and Applications*. John Wiley & Sons: **2006**.
2. Medina, C.; Santos-Martinez, M. J.; Radomski, A.; Corrigan, O. I.; Radomski, M. W., Nanoparticles: pharmacological and toxicological significance. *Brit J Pharmacol* **2007**, 150, (5), 552-558.
3. Biju, V.; Itoh, T.; Ishikawa, M., Delivering quantum dots to cells: bioconjugated quantum dots for targeted and nonspecific extracellular and intracellular imaging. *Chem Soc Rev* **2010**, 39, (8), 3031-3056.
4. Rossetti, R.; Brus, L., Electron-Hole Recombination Emission as a Probe of Surface-Chemistry in Aqueous Cds Colloids. *J Phys Chem-Us* **1982**, 86, (23), 4470-4472.
5. Brus, L. E., Electron Electron and Electron-Hole Interactions in Small Semiconductor Crystallites - the Size Dependence of the Lowest Excited Electronic State. *J Chem Phys* **1984**, 80, (9), 4403-4409.
6. Brus, L., Electronic Wave-Functions in Semiconductor Clusters - Experiment and Theory. *J Phys Chem-Us* **1986**, 90, (12), 2555-2560.
7. Alivisatos, A. P.; Gu, W. W.; Larabell, C., Quantum dots as cellular probes. *Annu Rev Biomed Eng* **2005**, 7, 55-76.
8. Dabbousi, B. O.; RodriguezViejo, J.; Mikulec, F. V.; Heine, J. R.; Mattoussi, H.; Ober, R.; Jensen, K. F.; Bawendi, M. G., (CdSe)ZnS core-shell quantum dots: Synthesis and characterization of a size series of highly luminescent nanocrystallites. *J Phys Chem B* **1997**, 101, (46), 9463-9475.
9. Hines, M. A.; Guyot-Sionnest, P., Synthesis and characterization of strongly luminescing ZnS-Capped CdSe nanocrystals. *J Phys Chem-Us* **1996**, 100, (2), 468-471.
10. Schmid, G., *Nanoparticles: From Theory to Application*. John Wiley & Sons: **2011**.
11. Rao, C. N. R.; Müller, A.; Cheetham, A. K., *The Chemistry of Nanomaterials: Synthesis, Properties and Applications*. Wiley-VCH: **2004**.
12. Rosenthal, S. J.; Chang, J. C.; Kovtun, O.; McBride, J. R.; Tomlinson, I. D., Biocompatible Quantum Dots for Biological Applications. *Chem Biol* **2011**, 18, (1), 10-24.
13. Johnson, I. D.; Technologies, L.; Haugland, R. P.; Spence, M. T. Z., *The Molecular Probes Handbook: A Guide to Fluorescent Probes and Labeling Technologies, 11th Edition*. Life Technologies: **2010**.
14. Walling, M. A.; Novak, J. A.; Shepard, J. R. E., Quantum Dots for Live Cell and In Vivo Imaging. *Int J Mol Sci* **2009**, 10, (2), 441-491.
15. Medintz, I. L.; Uyeda, H. T.; Goldman, E. R.; Mattoussi, H., Quantum dot bioconjugates for imaging, labelling and sensing. *Nature Materials* **2005**, 4, 435-446.
16. Ekimov, A. I.; Onuschenko, A. A., Interband absorption of light in a semiconductor sphere. *Sov. Phys. Semicond.* **1982**, 16, 775-778.
17. Murray, C. B.; Norris, D. J.; Bawendi, M. G., Synthesis and Characterization of Nearly Monodisperse Cde (E = S, Se, Te) Semiconductor Nanocrystallites. *J Am Chem Soc* **1993**, 115, (19), 8706-8715.
18. Vossmeier, T.; Katsikas, L.; Giersig, M.; Popovic, I. G.; Diesner, K.; Chemseddine, A.; Eychmuller, A.; Weller, H., Cds Nanoclusters - Synthesis, Characterization, Size-Dependent Oscillator Strength, Temperature Shift of

the Excitonic-Transition Energy, and Reversible Absorbency Shift. *J Phys Chem-U*s **1994**, 98, (31), 7665-7673.

19. Peng, Z. A.; Peng, X. G., Formation of high-quality CdTe, CdSe, and CdS nanocrystals using CdO as precursor. *J Am Chem Soc* **2001**, 123, (1), 183-184.

20. Qu, L. H.; Peng, Z. A.; Peng, X. G., Alternative routes toward high quality CdSe nanocrystals. *Nano Lett* **2001**, 1, (6), 333-337.

21. Peng, Z. A.; Peng, X. G., Nearly monodisperse and shape-controlled CdSe nanocrystals via alternative routes: Nucleation and growth. *J Am Chem Soc* **2002**, 124, (13), 3343-3353.

22. Li, J. J.; Wang, Y. A.; Guo, W. Z.; Keay, J. C.; Mishima, T. D.; Johnson, M. B.; Peng, X. G., Large-scale synthesis of nearly monodisperse CdSe/CdS core/shell nanocrystals using air-stable reagents via successive ion layer adsorption and reaction. *J Am Chem Soc* **2003**, 125, (41), 12567-12575.

23. Xie, R. G.; Kolb, U.; Li, J. X.; Basche, T.; Mews, A., Synthesis and characterization of highly luminescent CdSe-Core CdS/Zn_{0.5}Cd_{0.5}/ZnS multishell nanocrystals. *J Am Chem Soc* **2005**, 127, (20), 7480-7488.

24. Talapin, D. V.; Rogach, A. L.; Kornowski, A.; Haase, M.; Weller, H., Highly luminescent monodisperse CdSe and CdSe/ZnS nanocrystals synthesized in a hexadecylamine-trioctylphosphine oxide-trioctylphosphine mixture. *Nano Lett* **2001**, 1, (4), 207-211.

25. Reiss, P.; Bleuse, J.; Pron, A., Highly luminescent CdSe/ZnSe core/shell nanocrystals of low size dispersion. *Nano Lett* **2002**, 2, (7), 781-784.

26. Yu, W. W.; Peng, X. G., Formation of high-quality CdS and other II-VI semiconductor nanocrystals in noncoordinating solvents: Tunable reactivity of monomers. *Angew Chem Int Edit* **2002**, 41, (13), 2368-2371.

27. Battaglia, D.; Peng, X. G., Formation of high quality InP and InAs nanocrystals in a noncoordinating solvent. *Nano Lett* **2002**, 2, (9), 1027-1030.

28. Warren, C. W.; Nie, S., Quantum Dot Bioconjugates for Ultrasensitive Nonisotopic Detection. *Science* **1998**, 281, 2016-2018.

29. Mattoussi, H.; Mauro, J. M.; Goldman, E. R.; Anderson, G. P.; Sundar, V. C.; Mikulec, F. V.; Bawendi, M. G., Self-assembly of CdSe-ZnS quantum dot bioconjugates using an engineered recombinant protein. *J Am Chem Soc* **2000**, 122, (49), 12142-12150.

30. Uyeda, H. T.; Medintz, I. L.; Jaiswal, J. K.; Simon, S. M.; Mattoussi, H., Synthesis of compact multidentate ligands to prepare stable hydrophilic quantum dot fluorophores. *J Am Chem Soc* **2005**, 127, (11), 3870-3878.

31. Liu, W.; Howarth, M.; Greytak, A. B.; Zheng, Y.; Nocera, D. G.; Ting, A. Y.; Bawendi, M. G., Compact biocompatible quantum dots functionalized for cellular imaging. *J Am Chem Soc* **2008**, 130, (4), 1274-1284.

32. Mei, B. C.; Susumu, K.; Medintz, I. L.; Mattoussi, H., Polyethylene glycol-based bidentate ligands to enhance quantum dot and gold nanoparticle stability in biological media. *Nat Protoc* **2009**, 4, (3), 412-423.

33. Susumu, K.; Mei, B. C.; Mattoussi, H., Multifunctional ligands based on dihydrolipoic acid and polyethylene glycol to promote biocompatibility of quantum dots. *Nat Protoc* **2009**, 4, (3), 424-436.

34. Pellegrino, T.; Manna, L.; Kudera, S.; Liedl, T.; Koktysh, D.; Rogach, A. L.; Keller, S.; Radler, J.; Natile, G.; Parak, W. J., Hydrophobic nanocrystals

coated with an amphiphilic polymer shell: A general route to water soluble nanocrystals. *Nano Lett* **2004**, 4, (4), 703-707.

35. Chen, Y.; Thakar, R.; Snee, P. T., Imparting nanoparticle function with size-controlled amphiphilic polymers. *J Am Chem Soc* **2008**, 130, (12), 3744-3745.

36. Duconge, F.; Pons, T.; Pestourie, C.; Herin, L.; Theze, B.; Gombert, K.; Mahler, B.; Hinnen, F.; Kuhnast, B.; Dolle, F.; Dubertret, B.; Tavitian, B., Fluorine-18-labeled phospholipid quantum dot micelles for in vivo multimodal imaging from whole body to cellular scales. *Bioconjugate Chem* **2008**, 19, (9), 1921-1926.

37. Xing, Y.; Chaudry, Q.; Shen, C.; Kong, K. Y.; Zhau, H. E.; WChung, L.; Petros, J. A.; O'Regan, R. M.; Yezhelyev, M. V.; Simons, J. W.; Wang, M. D.; Nie, S., Bioconjugated quantum dots for multiplexed and quantitative immunohistochemistry. *Nat Protoc* **2007**, 2, (5), 1152-1165.

38. Orndorff, R. L.; Rosenthal, S. J., Neurotoxin Quantum Dot Conjugates Detect Endogenous Targets Expressed in Live Cancer Cells. *Nano Lett* **2009**, 9, (7), 2589-2599.

39. Bentzen, E. L.; Tomlinson, I. D.; Mason, J.; Gresch, P.; Warnement, M. R.; Wright, D.; Sanders-Bush, E.; Blakely, R.; Rosenthal, S. J., Surface modification to reduce nonspecific binding of quantum dots in live cell assays. *Bioconjugate Chem* **2005**, 16, (6), 1488-1494.

40. Algar, W. R.; Tavares, A. J.; Krull, U. J., Beyond labels: A review of the application of quantum dots as integrated components of assays, bioprobes, and biosensors utilizing optical transduction. *Anal Chim Acta* **2010**, 673, (1), 1-25.

41. Chaudhuri, R. G.; Paria, S., Core/Shell Nanoparticles: Classes, Properties, Synthesis Mechanisms, Characterization, and Applications. *Chem Rev* **2012**, 112, (4), 2373-2433.

42. Wu, X. Y.; Liu, H. J.; Liu, J. Q.; Haley, K. N.; Treadway, J. A.; Larson, J. P.; Ge, N. F.; Peale, F.; Bruchez, M. P., Immunofluorescent labeling of cancer marker Her2 and other cellular targets with semiconductor quantum dots. *Nat Biotechnol* **2003**, 21, (1), 41-46.

43. Jaiswal, J. K.; Mattoussi, H.; Mauro, J. M.; Simon, S. M., Long-term multiple color imaging of live cells using quantum dot bioconjugates. *Nat Biotechnol* **2003**, 21, (1), 47-51.

44. Sukhanova, A.; Devy, M.; Venteo, L.; Kaplan, H.; Artemyev, M.; Oleinikov, V.; Klinov, D.; Pluot, M.; Cohen, J. H. M.; Nabiev, I., Biocompatible fluorescent nanocrystals for immunolabeling of membrane proteins and cells. *Anal Biochem* **2004**, 324, (1), 60-67.

45. Bruchez, M.; Moronne, M.; Gin, P.; Weiss, S.; Alivisatos, A. P., Semiconductor nanocrystals as fluorescent biological labels. *Science* **1998**, 281, (5385), 2013-2016.

46. Jaiswal, J. K.; Simon, S. M., Potentials and pitfalls of fluorescent quantum dots for biological imaging. *Trends Cell Biol* **2004**, 14, (9), 497-504.

47. Duan, H. W.; Nie, S. M., Cell-penetrating quantum dots based on multivalent and endosome-disrupting surface coatings. *J Am Chem Soc* **2007**, 129, (11), 3333-3338.

48. Yum, K.; Na, S.; Xiang, Y.; Wang, N.; Yu, M. F., Mechanochemical Delivery and Dynamic Tracking of Fluorescent Quantum Dots in the Cytoplasm and Nucleus of Living Cells. *Nano Lett* **2009**, 9, (5), 2193-2198.

49. Derfus, A. M.; Chan, W. C. W.; Bhatia, S. N., Intracellular delivery of quantum dots for live cell labeling and organelle tracking. *Adv Mater* **2004**, *16*, (12), 961-966.
50. Jin, S.; Hu, Y.; Gu, Z.; Liu, L.; Wu, H.-C., Application of Quantum Dots in Biological Imaging. *Journal of Nanomaterials* **2011**, 2011, 13.
51. Jayagopal, A.; Russ, P. K.; Haselton, F. R., Surface engineering of quantum dots for in vivo vascular imaging. *Bioconjugate Chem* **2007**, *18*, (5), 1424-1433.
52. Ballou, B.; Ernst, L. A.; Andreko, S.; Harper, T.; Fitzpatrick, J. A. J.; Waggoner, A. S.; Bruchez, M. P., Sentinel lymph node imaging using quantum dots in mouse tumor models. *Bioconjugate Chem* **2007**, *18*, (2), 389-396.
53. Akerman, M. E.; Chan, W. C. W.; Laakkonen, P.; Bhatia, S. N.; Ruoslahti, E., Nanocrystal targeting in vivo. *P Natl Acad Sci USA* **2002**, *99*, (20), 12617-12621.
54. Gao, X. H.; Cui, Y. Y.; Levenson, R. M.; Chung, L. W. K.; Nie, S. M., In vivo cancer targeting and imaging with semiconductor quantum dots. *Nat Biotechnol* **2004**, *22*, (8), 969-976.
55. Tada, H.; Higuchi, H.; Wanatabe, T. M.; Ohuchi, N., In vivo real-time tracking of single quantum dots conjugated with monoclonal anti-HER2 antibody in tumors of mice. *Cancer Res* **2007**, *67*, (3), 1138-1144.
56. Liu, J.; Lau, S. K.; Varma, V. A.; Moffitt, R. A.; Caldwell, M.; Liu, T.; Young, A. N.; Petros, J. A.; Osunkoya, A. O.; Krogstad, T.; Leyland-Jones, B.; Wang, M. D.; Nie, S. M., Molecular Mapping of Tumor Heterogeneity on Clinical Tissue Specimens with Multiplexed Quantum Dots. *ACS Nano* **2010**, *4*, (5), 2755-2765.
57. Shao, L. J.; Gao, Y. F.; Yan, F., Semiconductor Quantum Dots for Biomedical Applications. *Sensors-Basel* **2011**, *11*, (12), 11736-11751.
58. Frasco, M. F.; Chaniotakis, N., Bioconjugated quantum dots as fluorescent probes for bioanalytical applications. *Anal Bioanal Chem* **2010**, *396*, 229-240.
59. Willard, D. M.; Carillo, L. L.; Jung, J.; Van Orden, A., CdSe-ZnS quantum dots as resonance energy transfer donors in a model protein-protein binding assay. *Nano Lett* **2001**, *1*, (9), 469-474.
60. Medintz, I. L.; Clapp, A. R.; Brunel, F. M.; Tiefenbrunn, T.; Uyeda, H. T.; Chang, E. L.; Deschamps, J. R.; Dawson, P. E.; Mattoussi, H., Proteolytic activity monitored by fluorescence resonance energy transfer through quantum-dot-peptide conjugates. *Nature Materials* **2006**, *5*, (7), 581-589.
61. Zhang, C. Y.; Yeh, H. C.; Kuroki, M. T.; Wang, T. H., Single-quantum-dot-based DNA nanosensor. *Nature Materials* **2005**, *4*, (11), 826-831.
62. Talapin, D. V.; Lee, J. S.; Kovalenko, M. V.; Shevchenko, E. V., Prospects of Colloidal Nanocrystals for Electronic and Optoelectronic Applications. *Chem Rev* **2010**, *110*, (1), 389-458.
63. Wood, V.; Panzer, M. J.; Caruge, J. M.; Halpert, J. E.; Bawendi, M. G.; Bulovic, V., Air-Stable Operation of Transparent, Colloidal Quantum Dot Based LEDs with a Unipolar Device Architecture. *Nano Lett* **2010**, *10*, (1), 24-29.
64. Kamat, P. V., Quantum Dot Solar Cells. Semiconductor Nanocrystals as Light Harvesters. *J Phys Chem C* **2008**, *112*, (48), 18737-18753.

65. Guchhait, A.; Rath, A. K.; Pal, A. J., Hybrid Core-Shell Nanoparticles: Photoinduced Electron-Transfer for Charge Separation and Solar Cell Applications. *Chem Mater* **2009**, 21, (21), 5292-5299.
66. Smith, A. M.; Duan, H. W.; Mohs, A. M.; Nie, S. M., Bioconjugated quantum dots for in vivo molecular and cellular imaging. *Adv Drug Deliver Rev* **2008**, 60, (11), 1226-1240.
67. Derfus, A. M.; Chan, W. C. W.; Bhatia, S. N., Probing the cytotoxicity of semiconductor quantum dots. *Nano Lett* **2004**, 4, (1), 11-18.
68. Cho, S. J.; Maysinger, D.; Jain, M.; Roder, B.; Hackbarth, S.; Winnik, F. M., Long-term exposure to CdTe quantum dots causes functional impairments in live cells. *Langmuir* **2007**, 23, (4), 1974-1980.
69. Chang, E.; Thekkek, N.; Yu, W. W.; Colvin, V. L.; Drezek, R., Evaluation of quantum dot cytotoxicity based on intracellular uptake. *Small* **2006**, 2, (12), 1412-1417.
70. Kirchner, C.; Liedl, T.; Kudera, S.; Pellegrino, T.; Javier, A. M.; Gaub, H. E.; Stolze, S.; Fertig, N.; Parak, W. J., Cytotoxicity of colloidal CdSe and CdSe/ZnS nanoparticles. *Nano Lett* **2005**, 5, (2), 331-338.

Chapter 2

Synthesis and Characterization of CdSe/ZnS QDs

This chapter contains data published in:

Ana Sofia Miguel, Christopher Maycock and Abel Oliva. Synthesis and Functionalization of CdSe/ZnS QDs Using the Successive Ion Layer Adsorption Reaction and Mercaptopropionic Acid Phase Transfer Methods. *Nanoparticles in Biology and Medicine. Methods and Protocols*, 2012, Springer (book chapter by invitation).

The author contributed fully to this chapter, namely in the planning of the experimental work, performance of the experiments and writing of the manuscript.

Synthesis and Characterization of CdSe/ZnS QDs

Abstract	31
Introduction	31
Experimental Section	33
Materials	33
CdSe-core Nanocrystals Components	34
CdSe/ZnS core-shell Nanocrystals Components	34
Synthesis of CdSe-core Nanocrystals	34
Synthesis of CdSe/ZnS core-shell Nanocrystals based on Successive Ion Layer Adsorption Reaction (SILAR) Method	35
Characterization of the CdSe/ZnS core-shell Nanocrystals	38
Optical Measurements.....	38
Concentration Determination of QD solutions	39
Transmission Electron Microscopy (TEM).....	40
Dynamic Light Scattering Measurements.....	40
Notes	41
Results and Discussion	42
Core-QDs Synthesis and Reaction Conditions for ZnS Shell Growth. 42	
Structural Characterization	46
Concentration Determination of QDs solutions	51
Optical Characterization	52
Conclusion	54
Glossary	55
Acknowledgments	57
References	58

Abstract

This chapter describes the synthesis and surface passivation of CdSe nanocrystals for subsequent bioconjugation with a view to the development of a biomarker for antigens associated with specific parasites. Detailed protocols for the preparation of CdSe nanocrystals and their multishell coating (passivation) with ZnS based on the Successive Ion Layer Adsorption and Reaction (SILAR) method are described. Parameters such as experimental procedure, nature of the precursors materials, choice of coordinating solvent and temperature were optimized and revealed to be crucial not only in the obtention of small core-shell QDs with narrow size distribution but to allow the construction of shell layers in solution with the same thickness around each core. To analyse the size, size distribution, shape and fluorescence of the nanoparticles a combination of optical and structural techniques was used. In general, the results obtained demonstrated a CdSe/ZnS core-shell system with 5 monolayers of ZnS due to the presence of a red-shift in both absorption and emission spectra and also a narrow size distribution with a low polydispersity index; consistent with core-shell QDs.

Key-words: *quantum dots, SILAR method, photoluminescence quantum yield, dynamic light scattering.*

Introduction

Semiconductor nanocrystals, also known as Quantum Dots (QDs), are mainly composed of atoms from groups II-VI (e.g. CdSe, CdTe, CdS and ZnSe) or III-V (e.g. InP and InAs) elements in the periodic table and are defined as particles with physical dimensions smaller than the exciton Bohr radius [1,2,3,4,5]. CdSe QDs have become the most extensively developed nanocrystals in terms of the methods to prepare samples with narrow size distributions^[6,7] and also methods for surface modification in order to completely passivate the nanocrystals^[8,9].

This interest has arisen because of their potential use in many applications from electronics to biomedical tags. One of the most attractive properties associated with QDs is the size dependent emission. It is possible to synthesize differently sized CdSe nanocrystals that emit from blue to red with

very pure colour. For this reason, the control of the photoluminescence (PL) properties of these particles has been in constant development ^[10]. This property is significantly improved if the nanocrystals are passivated on their surface by a shell of a larger band gap semiconductor and the core/shell systems, CdSe/CdS and CdSe/ZnS are the most common and intensively studied ^[11,12]. The CdSe cores are covered with CdS or ZnS in order to establish a core/shell system. Basically, there are two main requirements to create “ideal” core/shell nanocrystals, one from a crystallographic and other from an electronic point of view. To produce particles with high crystallinity, the core and shell materials should have similar lattice parameters such that the shell-growth happens in an epitaxial manner ^[11], without the formation of structural defects. Second, the shell material should possess a much higher band gap than the core to suppress tunnelling of the charge carriers from the cores to the newly formed surface atoms of the shell ^[13]. Furthermore, these core/shell QDs are more robust against chemical degradation or photo-oxidation ^[11]

Since the discovery of QDs, it is clear that their synthesis has been refined tremendously by the variety of developed methods ^[14] and it is now possible to synthesize high quality, monodisperse samples of nanocrystals under relatively benign conditions or even purchase them commercially. In 2002 Quantum Dot Corporation appeared as the first commercial supplier of quantum dots and since then many different companies worldwide (e.g. Evident Technologies, Invitrogen, Nanoco, etc) have available quantum dots with a core of cadmium selenide, measuring about 2-10 nm in diameter and surrounded by a shell. Usually, this shell is composed of another semiconductor material, and an outer polymer or inorganic layer ^[15]. However, one the key barriers for purchasing these type of particles commercially is their high price. In addition, the poor reproducibility and homogeneity between samples from different batches and the lack of information about the nature of shell material is a constant. For these reasons, but particularly due to the high cost of these nanoparticles, it was decided to synthesize CdSe/ZnS core-shell QDs.

The CdSe/ZnS core-shell QD system was chosen because their shell-thickness dependent optical properties provided a convenient probe to

determine the size and size distribution of the resulting nanocrystals during growth. Moreover, these core-shell QDs, over the years, have been shown to be generally more robust against chemical degradation or photo-oxidation and more importantly exhibit tuneable emission colours covering most of the visible optical window making them a powerful tool to be applied in many scientific areas.

As precursors, metal oxides (ZnO and CdO) and elementary selenium and sulphur were used exclusively to completely avoid expensive and hazardous compounds. A mixture of TOPO/HDA was used as solvent for the preparation of the CdSe cores. Alkylamines have proven to be a very good ligand for highly luminescent plain CdSe/ZnS core-shell nanocrystals and ODE was the non-coordinating solvent used to prepare the Zn and S precursor solutions for the ZnS shell growth. The ZnS coated CdSe dots were characterized spectroscopically and structurally using a variety of techniques. The optical absorption and photoluminescence spectra of the composite dots were measured and transmission electron microscopy (TEM) and dynamic light scattering (DLS) measurements used to determine the size, shape and size distribution of the final samples.

Experimental Section

Materials

All of the reagents used for the synthesis of CdSe/ZnS QDs were stored at room temperature, unless indicated otherwise and were purchased from Sigma-Aldrich and all common solvents were p.a. ACS grade. All solutions were freshly prepared under an Argon atmosphere. We recommend using Pt 100 probe and a digital thermometer for the temperature control. Place the probe inside the reaction flask. The purification of the nanocrystals by centrifugation was performed using an Eppendorf 5804R centrifuge and the nanocrystals were dried with a high vacuum pump from Edwards. For optical and dynamic light scattering measurements, precision cells made of Quartz were used (Supracil®, type Nr 101-QS, 10mm, Helma) and the solutions were filtered using 0.2µm PTFE membrane (0.2µm pore size, filter-Ø: 15mm, Macherey-Nagel).

CdSe-core Nanocrystals Components

Cadmium oxide (CdO, 99, 99%), trioctylphosphine oxide (TOPO, technical grade), oleic acid (OA, Ph Helv), 1-hexadecylamine (HDA, tech 90%), chloroform and methanol (puriss, p.a. Reag. ACS).

Selenium/trioctylphosphine (Se/TOP) solution: In a 10mL two-neck flask under an argon flow, 0.0632g of selenium powder (99,5%, powder, 100 mesh) was placed and 2.4mL of trioctylphosphine (TOP, tech. 90%) was added and the solution was sonicated (ultrasound bath Branson 1200) until a colourless optically clear solution was obtained.

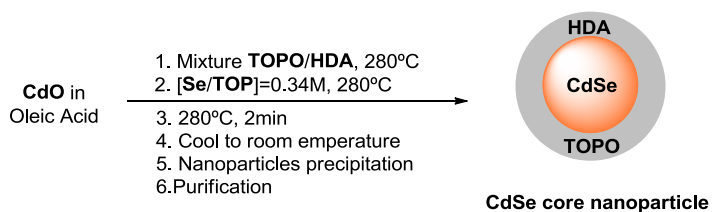
CdSe/ZnS core-shell Nanocrystals Components

Trioctylphosphine Oxide (technical grade), 1-hexadecylamine (tech. 90%), chloroform, methanol, hexane and acetone (puriss. p.a., Reag. ACS).

Zinc Oxide precursor stock solution 0.1M: In a 10mL two-neck flask, under an argon flow, 0.041g of zinc oxide (ZnO, metal basis, 99, 99%) and 1.4mL of oleic acid (Ph. Helv.) were placed. The mixture was heated at 300°C until the solution was completely clear. 3.6mL of 1-octadecene (tech. 90%) was added and the final solution was kept at 80°C until the growth shell procedure was completed.

Elemental Sulphur precursor stock solution 0.1M: In a 10mL two-neck flask, under argon, containing 0.016g of elemental sulphur (99, 98%, powder), 5mL of 1-octadecene was added. The solution was heated until a clear solution was obtained, indicating that the sulphur was completely dissolved in the solvent. The solution was kept at 80°C until the shell growth procedure was completed.

Synthesis of CdSe-core Nanocrystals



Scheme 1 | Reaction scheme for the synthesis of TOPO/HDA capped-CdSe QDs.

(TOPO/HDA)-capped CdSe nanocrystals were synthesized using standard procedures with some modifications to the reagents used^[16,17]. In a 100mL three-neck flask, under an argon atmosphere, 0.042g of cadmium oxide (CdO) and 0.6mL of oleic acid were placed. The mixture was heated using a heating mantle under stirring to 100°C until a yellow optically clear solution was obtained. Then, the flask was removed from the heat source and 2g of 1-hexadecylamine and 2g of trioctylphosphine oxide were added. The solution was heated again, but this time at to 280-300°C. When all was completely dissolved, the temperature was stabilized at 280°C and the mixture was optically clear. While keeping the mixture at 280°C, in one single injection, 2.4mL of a Se/TOP solution prepared previously was added (see **Note 1**). After 2 minutes at 280°C, the heating mantle was removed. When the temperature reached 85°C, 20mL of methanol was injected, leading to the precipitation of the nanoparticles. The reaction mixture was let cooling until to room temperature.

The nanoparticle suspension was transferred to five 50mL polypropylene centrifuge tubes (10mL in each tube) and 20mL of chloroform was added to each tube and each shaken manually to force the precipitation of nanocrystals. The tubes were left to stand for 90 minutes at room temperature and then were centrifuged at 5000g at room temperature for a period of 10 minutes. The cloudy supernatant was discarded and the concentrated pellet at the bottom of each tube was washed at least three times with 20mL of methanol and centrifuged at 5000g for a period of 10 minutes each time.

The final red-brownish pellet was dried under vacuum. These nanocrystals can then be dispersed in chloroform or hexane for further processing. Otherwise, they can be stored as a powder in the dark at 4°C for several months. This procedure typically yields CdSe nanocrystals with the first absorption peak at 568nm with a diameter of about 3.5nm.

Synthesis of CdSe/ZnS core-shell Nanocrystals based on Successive Ion Layer Adsorption Reaction (SILAR) Method

For shell growth, the SILAR method^[16] was found to be the best approach. This technique is based on alternating injections of precursor solutions containing metal oxides such as ZnO and elemental sulphur into the solution

containing the CdSe-core nanocrystals. Using this method, layers of ZnS can be grown successively around the core.

Choice of reaction system: The non-coordinating solvent, 1-octadecene was the most appropriate solvent for the growth of the shell of high-quality nanocrystals. 1-hexadecylamine was also used as ligand for the core-shell nanocrystals because alkylamines have proven to be very good ligands for highly luminescent plain CdSe/ZnS core-shell nanocrystals ^[18].

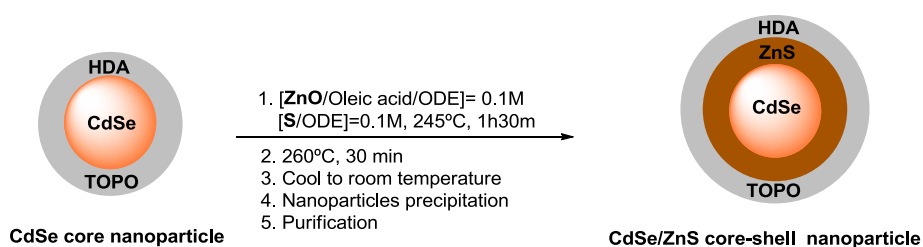
Calculations of the amount of precursor's solutions for shell growth: The growth of core-shell nanocrystals using the SILAR technique is based on alternating injections of the Zn and S precursors into the solution containing the CdSe cores. The amount of each precursor was determined by the number of the surface atoms of a given core/shell system. The theoretical calculations were based on experiments already reported in the literature ^[18], namely, the wurtzite structure of CdSe, the average thickness of one monolayer of ZnS as 0.31nm and in the concentration of the CdSe NC's as estimated by UV-visible spectra ^[19]. Hence, for a typical reaction with 1.01×10^{-4} mmols of 3.5nm CdSe cores it was injected 0.47mL of Zn and S precursors from 0.1M stock solution for the first monolayer, 0.64mL of each stock solution for the second monolayer, 0.84mL for the third monolayer, 1.064mL for the fourth monolayer and 1.32mL for the fifth monolayer with a period of 10 minutes between each addition.

Table 1 | Amount of each precursor solution added for the ZnS shell growth procedure around the CdSe cores.

Reaction time (min)	Amount of each precursor solution added (mL)	Precursor solution added	Number of ZnS monolayer (ML) being formed
0	0.47	Zn	1
10	0.47	S	
20	0.64	Zn	2
30	0.64	S	
40	0.84	Zn	3

50	0.84	S	
60	1.064	Zn	4
70	1.064	S	
80	1.32	Zn	5
90	1.32	S	

Preparation of the core/shell nanocrystals using the SILAR method: The SILAR technique allows the growth of shells around a given CdSe-core particle. Using the reaction conditions already reported by Li *et al* and Xie *et al* [18,16] with slightly modifications, a typical SILAR synthesis was performed as depicted in Scheme 2.



Scheme 2 | Reaction scheme for the surface passivation of CdSe/ZnS core-shell QDs with 5 monolayers of ZnS based on SILAR method.

3mL of 1-octadecene and 1g of 1-hexadecylamine were placed in a 100mL three-neck flask and the flask heated under vacuum at 70°C during 1h to remove any traces of water and then cooled to room temperature. About 30mg of CdSe-core nanocrystals as synthesized previously, were dispersed in 15mL of chloroform and filtered using a 0.2 μm PTFE membrane. The chloroform suspension containing the CdSe nanocrystals was placed in a flask and the chloroform and other volatiles were removed by heating under vacuum at 70°C for 30 minutes (see **Note 2**). Subsequently, the vacuum was removed and the system was heated under an argon atmosphere to 245°C where the shell growth procedure starts.

To calculate the amount of Zn- and S-precursor for the growth of the first monolayer, it was assumed that the surface of the CdSe-cores consists equally of Se and Cd atoms. For a solution containing CdSe nanocrystals with 3.5nm (1.01×10^{-4} mmols) 0.47mL of Zn and S precursor's stock solutions were added for the first layer; 0.64mL of each injection solution for the second

layer; 0.84mL of each injection solution for third layer; 1.064mL of each injection solution for the fourth layer and 1.32mL of each injection solution for the fifth layer (see **Note 3**). After the final injection, the reaction mixture was kept for 30 minutes at 260°C. Then, the reaction was cooled to room temperature and 30mL of hexane were added. For purification, the solution was transferred to a 250mL glass extraction funnel and the unreacted compounds and possible by products were removed by successive MeOH extractions (20mL, 6-8 washes) (see **Note 4**). The hexane/ODE phase containing the nanoparticles was then transferred to a 50mL centrifuge tube, washed with acetone and centrifuged at 8000g at room temperature for 10 minutes (see **Note 5**).

The final pellet was suspended in 15mL of hexane, the nanoparticles precipitated with the addition of the same volume of MeOH and centrifuged at 8000g at room temperature for 10 minutes. The colourless supernatant was discarded and the final red-brownish pellet was dried under high vacuum for 1h. The final QDs could be dispersed in chloroform or hexane for further processing. Otherwise, it was stored as a powder in the dark at 4°C and was stable for several months.

Characterization of the CdSe/ZnS core-shell Nanocrystals

Optical Measurements

UV-visible absorption spectra were measured with a Beckman DU-70 spectrophotometer and photoluminescence (PL) spectra were measured with a SPEX Fluorolog from Horiba Jobin Yvon. Fluorescence quantum yields (QY) were measured at room temperature and relative to rhodamine 6G with excitation at 530nm. A typical procedure for QY measurement was as follows: Using standard 10mm path length Quartz cuvettes, the UV/visible absorbance spectra of the CdSe/ZnS QDs in chloroform and rhodamine 6G (dye) in ethanol were recorded. The optical density for sample and dye at the excitation wavelength was below 0.1. The emission spectra with an excitation wavelength of 530nm of the solutions prepared previously were recorded in the 10 mm fluorescence cuvettes. The obtained fluorescence spectra were corrected for both samples and dye for differences in refractive index and concentration and the integrated fluorescence intensity calculated, using the

appropriate spectrometer software. Finally, to calculate the QY the following expression^[20] was used (see **Note 6**):

$$QY_{QD} = QY_{Dye} \times (A_{Dye}/A_{QD}) \times (E_{QD}/E_{Dye}) \times (\eta_{QD \text{ solvent}})^2 / (\eta_{Dye \text{ solvent}})^2$$

Equation 1 | Expression applied to calculate the quantum yield.

Concentration Determination of QD solutions

The determination of QD concentration in solution, water or a given medium is not straightforward (see **Note 7**). Measurements of optical density can in principle be used to find molar concentrations if there are established extinction coefficients for these materials. However, the published extinction coefficients for quantum dots vary by more than an order of magnitude^[19,21,22,23]. These discrepancies may arise in part from the sensitivity of absorption coefficients to both quantum dot diameter and composition. According to Peng *et al*^[19,21], the absorption spectrum method seems to be the most practical and convenient way to determine the particle concentrations. Thus, the optical density of the synthetic CdSe/ZnS QDs in chloroform solutions was measured applying this approach and using an absorption coefficient reported in the literature. To calculate the concentration of the quantum dots solutions, the Lambert-Beer's Law was applied:

$$A = \varepsilon C L$$

Equation 2 | Expression of Lambert-Beer's Law given to calculate the concentration of QDs solutions.

In Equation 2, A is the optical density or absorbance at the peak position of the first exciton absorption peak for a given sample, C is the molar concentration (mol/L) of the nanocrystals of the same sample, L is the path length (cm) of the radiation beam used for recording the absorption spectrum (in this measurements L was fixed at 1cm) and ε is the extinction coefficient per mol of nanocrystals (L/mol.cm).

To determine the concentration of a QD solution a typical procedure was performed as follow:

In a small glass vial, ~10mg of CdSe core QDs were suspended in 1.5mL of chloroform. Then, the solution was transferred for a 10mm standard path length Quartz cuvette and the UV-visible absorbance spectra were recorded. From the UV-visible spectra obtained in the previous step, the absorbance value of the highest absorption wavelength between 400 and 700nm was taken and the concentration calculated. For example, for CdSe core nanocrystals obtained previously with the first excitonic absorption peak at 568nm, according to a sizing curve from Peng *et al*^[19,21] the typical size is around 3.5nm and consequently the size-dependent extinction coefficient of nanocrystals is about $1.5 \times 10^5 \text{ M}^{-1} \text{ cm}^{-1}$. If the solution has $A=1.5$ measured in a 1cm pathlength, then according to Lambert-Beer function: $C=A/\epsilon L \Leftrightarrow C=1.5/1.5 \times 10^5 \times 1 \Leftrightarrow C=1 \times 10^{-5} \text{ M}$ (10 μM).

Transmission Electron Microscopy (TEM)

Electron transmission microscopy was the technique used to analyse the size and size distribution of CdSe/ZnS core-shell QDs. Two kinds of transmission electron microscopes were used: a JEOL 200CX transmission electron microscope operating at an acceleration voltage of 200kV was use for the low resolution images and a JEOL 2011 High Contrast Digital transmission electron microscope operating an acceleration voltage of 600kV was used for the high resolution images. The nanocrystals were deposited from diluted chloroform solutions onto cooper grids with a carbon support (Agar, 300mesh, S160-3).

Dynamic Light Scattering Measurements

Light scattering analysis was performed using a Zetasizer Nano ZS dynamic light scatterer from Malvern Instruments. With this equipment it was possible to determine the hydrodynamic diameter (HD) of synthetic lipophilic CdSe/ZnS QDs. For the HD analyses, the samples were suspended in chloroform with concentrations between 0.06 and 0.3 μM and filtered through a 0.2 μm PTFE membrane before analyses. HD was obtained from number-weighted size distribution analysis and reported as the mean of triplicate measurements. Values are reported as the average of triplicate runs consisting of 20 measurements at 25°C.

The procedure suggested by the instrument manufacturer was followed for determining the hydrodynamic diameter and was performed as follow:

10mm precision cells made of Quartz were used to ensure that the optimum signal was achieved (avoid optical interferences) in size measurements and due to their high resistance to non-aqueous solutions (e.g. chloroform). 2mL of CdSe/ZnS QDs in CHCl_3 of different concentrations between 0.06 and 0.3 μM were prepared. The sample concentration was adjusted to accommodate the scattering properties of the sample and/or the optical requirements of the specific instrument. 1mL of each sample solution using a 1mL disposable syringe was filtered with a 0.2 μm PTFE membrane before the sample was introduced into the cuvette for analysis. The cuvette was filled slowly to avoid the formation of air bubbles. Then, the cuvette was closed and placed correctly in the sample holder (quartz windows should face the incident beam and detector) and 3 measurements of 20 runs each were performed per sample at 25°C and with an equilibration time of 2 minutes. This equilibration time was used to ensure that the sample temperature was equal to the cell temperature allowing the measurement of Brownian motion of the particles and not thermal motion due to temperature gradients. The obtained data was analysed using the instrument's software (Zetasizer software, version 6.2) to evaluate parameters such as the hydrodynamic diameter, autocorrelation data, size distribution, and the polydispersity index.

Notes

1. After the addition of the Se/TOP solution, there was always a lowering of the temperature of the mixture inside the flask and normally dropped to temperatures between 255-265°C. In this case, it is necessary to wait until the temperature stabilized again to 280°C to control the crystal growth time.
2. As the system was under high vacuum, the temperature could not exceed 70°C in order to avoid possible evaporation of the mixture of solvent/ligand 1-octadecene/1-hexadecylamine from the reaction vessel.
3. With fast stirring, there was no need for dropwise injections. A period of 10 min, between each addition was sufficient for the reaction to be complete. The whole procedure for covering CdSe-cores with five monolayers 'of ZnS took about 1h30m.

4. In the extraction procedure, the undesired products were soluble in MeOH. Therefore, this phase was discarded and the hexane/ODE phase which contains the nanocrystals was kept.
5. This step is important for the elimination of excess of ODE. This non-coordinating solvent can be retained by the nanoparticles during the MeOH washes. If it is not removed completely, it may appear on the walls of the tube in the form of a pale yellow powder. Washing with acetone helped to eliminate ODE, which was discarded in the yellow cloudy supernatant. This wash was repeated four times for complete removal of ODE.
6. To calculate the QY use the expression from the literature^[20], where: QY_{Dye} is the QY of the solution containing the rhodamine 6G dye in EtOH (0.95); A is the absorbance of the solutions; E is the corrected intensity areas and η is the average of refractive index of QDs and dye solvents.
7. The published extinction coefficients for QDs can vary by more than an order of magnitude. Some authors^[24] measure the optical density of the core-shell structured QDs in a medium applying an absorption coefficient that is the average of three reported in the literature^[19,21,22,23]. In this case a large error on the extinction coefficient could exist and the optical density can at best give concentrations that are only accurate to 50%.

Results and Discussion

Core-QDs Synthesis and Reaction Conditions for ZnS Shell Growth

Due the broad variety of methods and lack of consistency in some of them, in this research work, for the synthesis of CdSe/ZnS QDs different approaches were tested based on several protocols^[6, 10, 12, 13, 25, 26] to achieve the best synthesis to produce small QDs with narrow size distribution. These different experimental conditions were carried out by varying key parameters such as nature and concentration of the core and shell precursors, the choice of coordinating solvent, the type of surfactant to permit the solubilisation of core and shell materials and temperature and/or time at core synthesis and shell growth should occurred.

The synthesis of CdSe-core QDs was achieved based on the protocol reported by Aldana *et al*^[17] and posteriorly modified by Xie *et al*^[16] with some modifications in the reagents used. As cadmium source, cadmium oxide was

the reagent used and to solubilise its inorganic nature, oleic acid was the surfactant applied forming cadmium oleate which becomes soluble in organic solvents. As anionic source, a selenium/TOP (Se/TOP) solution with a molar concentration of 0.34M was prepared and used as described in the protocol taken as base ^[16], however herein tributylphosphine (TBP) was replaced by trioctylphosphine (TOP). TOP was the coordinating solvent used to suspend the selenium while the mixture TOPO/HDA was found the best solvent system for the quantum dots growth. TOP and TOPO demonstrated, as previously shown ^[6, 27], to have the ability to stabilize the bulk semiconductors and prevent aggregation as the core-QDs growth. HDA was used because over the years have been proven to be the best primary alkylamine to allow monodispersity and permit the achievement of QDs with high PL ^[10, 25]. Regarding the temperature at which Se/TOP solution should be injected and CdSe cores should growth, it was found that higher values such as 280°C were the best temperature. This result was based upon an optimization by carrying out the synthesis of CdSe cores at different temperatures in the range between 250 and 320°C. At 280°C, it was found to be easier to control the time at which the CdSe cores should leave to increase to reach nanoparticles with the desired size. It is important to point out that temperatures in the range between 70 and 150°C were also performed. However, it was observed that such temperatures do not permit the formation of CdSe QDs and in the cases that the formation and growth was achieved the fluorescence of the obtained nanoparticles was practically absent. Even though alkylamines have the capacity to improve the photoluminescence of core-QDs, the CdSe passivated by organic ligands (TOPO alone or TOPO/HDA mixtures) does not have the quantum efficiency commonly observed for organic dyes. In order to achieve high quantum efficiency, it is known that a core nanocrystal must be coated with a layer of a wider band gap semiconductor and for this purpose many methods were already been developed ^[14]. As before for the synthesis of core-QDs, different protocols were also tested and parameters such as procedure, temperature and solvent used were again considered in order to maintain the size distribution of nanocrystals during the growth of shell materials but more importantly to permit the construction of shell layers in solution with the same

thickness around each core. After several attempts based on reported work [25, 28], the successive ion layer adsorption and reaction (SILAR) method was found the best protocol for the surface passivation of CdSe cores with a ZnS shell. This method was first applied by Park *et al* [29] to achieve accurate control of film thickness in the deposition of thin films onto solid substrates in solution. Peng *et al* [18] extended this process for the growth of core-shell semiconductor nanocrystals with precise thickness control. According to this method it is possible to build several monolayers of the shell material in an alternating fashion, depositing first the cation and then the anion. Moreover, only two subsequent additions (one addition of each precursor) are required for the growth of a complete layer of the shell semiconductor. Although, this approach was revealed to be the best way to achieve the accurate control of ZnS shell thickness, an important doubt that emerged was the number of ZnS monolayers that should be constructed around each core QD. In 1997 Dabbousi *et al* [13] carried out the synthesis of CdSe/ZnS QDs by varying the ZnS shell thickness from 0.65 to 5.3 monolayers. According to his work it was found that as the coverage of ZnS on the CdSe surface increased, a huge increase in the fluorescence quantum yield was observed followed by a steady decline after 1.3 monolayers of ZnS. Taking this into consideration and keeping in mind the constant desire to obtain CdSe/ZnS QDs with high quantum yield, initially, the synthesis of the core-shell system was performed with only 2 monolayers of ZnS. However, during later attempts (chapter 3) to functionalise these QDs with water-soluble ligands the fluorescence was lost. This led to the conclusion that with only two monolayers of ZnS the shell thickness was too thin and the CdSe core was more susceptible to possible oxidation or chemical degradation imposed by the ligand exchange procedure. Furthermore, the performance of some biological goals proposed for this doctoral work could become affected or even compromised. Thereby, the number of monolayers around the CdSe cores was adjusted and designed taking into account the future applications of such nanoparticles. In this way, CdSe/ZnS core-shell QDs were synthesized with 5 monolayers of ZnS. After ligand exchange with different aqueous ligands, although a decrease in quantum yield was observed, these water-soluble QDs were more stable for further biological application.

According to this procedure, initially the CdSe core nanocrystals were placed in the surface-passivating ligand. Normally, this ligand was an alkylamine such as octadecylamine (ODA), but for the reasons mentioned above, 1-hexadecylamine (HDA) was used in the protocol developed here. In this work, the precursor solutions (0.1M in ODE) were prepared using ZnO and elemental S. The zinc oxide was solubilised using oleic acid at high temperature (300°C). The zinc oleate solution was kept at 80°C until the shell growth procedure was complete to avoid possible cooling and consequent precipitation of the components from the solution. The sulphur precursor solution was kept at 80°C for the reasons presented before.

Another crucial parameter which was also tested and that really affects the ZnS shell growth was the temperature at such reaction should be carried out. In the protocol developed herein the choice of temperature was based on an optimization procedure in the range between 200 and 260°C developed again by Peng *et al*^[18]. In this reported work, the parameter analysed was the fluorescence quantum yield of the obtained CdSe/ZnS core-shell nanoparticles after the shell growth procedure. The experimental results reported, demonstrated that at an optimum temperature of 240°C for the CdS shell resulting in nanocrystals with a narrow size distribution and a high PL quantum yield. For ZnS shell growth, the experimental results indicated that a high QY could be achieved if the growth of the shell took place at 245°C. Moreover, it was also found that a period of 10 minutes between each precursor addition was sufficient for the reaction to be completed once UV-visible spectra and PL spectra showed no further changes after this period of time. For that reasons, the surface passivation reaction of CdSe core with five monolayer's of ZnS was carried out at 245°C during 90 minutes with alternating injections of Zn and S precursor solutions with a period of 10 minutes between each addition to the solution initially containing the CdSe-cores. After the final injection, the reaction mixture was incubated for an extra period of 30 minutes at 260°C for the complete stabilization of the ZnS shell. A crucial step that is commonly described but is poorly explained in the several methods reported is the work-up and purification of the core-shell QDs after semiconductor shell growth is complete. According to the procedure developed by Xie *et al*^[16], the nanocrystal purification is usually performed by

adding hexane to the vessel containing the reaction mixture to suspend the nanocrystals formed and the unreacted compounds and by-products were posteriorly removed by successive MeOH extraction. This type of purification was applied in the synthesis of core-shell QDs developed in this work. The hexane phase containing the nanocrystals was transferred to an extraction funnel and was extracted until the MeOH phase became clear. However, one of the problems encountered was the incomplete elimination of the ODE by the MeOH phase. According to some authors, the nanocrystals suspended in the hexane/ODE can be precipitated using acetone^[19]. Hence, to overcome the ODE issue, it was found that washing the hexane/ODE phase with the same volume of acetone followed by centrifugation, the excess of ODE became soluble in the acetone phase and was completely removed^[30]. Posteriorly, the final pellet obtained was processed by redissolving it in hexane and the nanoparticles precipitated by adding the same volume of MeOH. After centrifugation, the colourless supernatant was discarded and the final red-brownish pellet containing the CdSe/ZnS QDs dried under high vacuum and kept at 4°C in the dark. Otherwise, they were dispersed in solvents such as chloroform or hexane for further processing.

Structural Characterization

The characterization of synthetic CdSe/ZnS QDs in terms of size and size distribution was carried out using transmission electron microscopy of low (TEM) and high resolution (HRTEM) and dynamic light scattering measurements. Figure 5 shows two TEM images and one HRTEM image of the synthesized QDs with a shell of five monolayers of ZnS of different syntheses performed during this work.

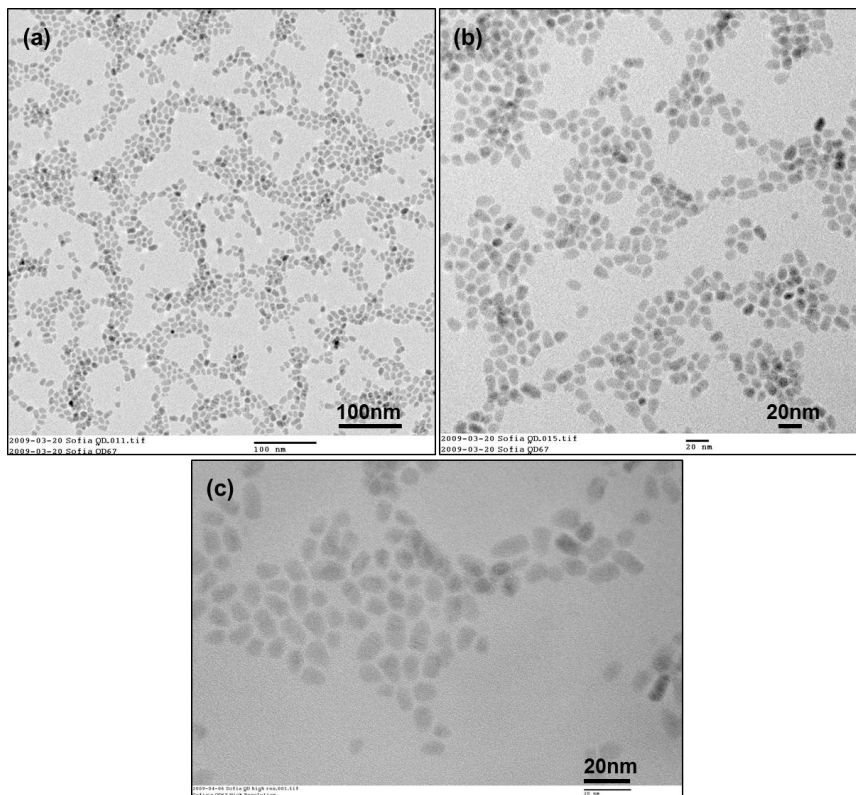
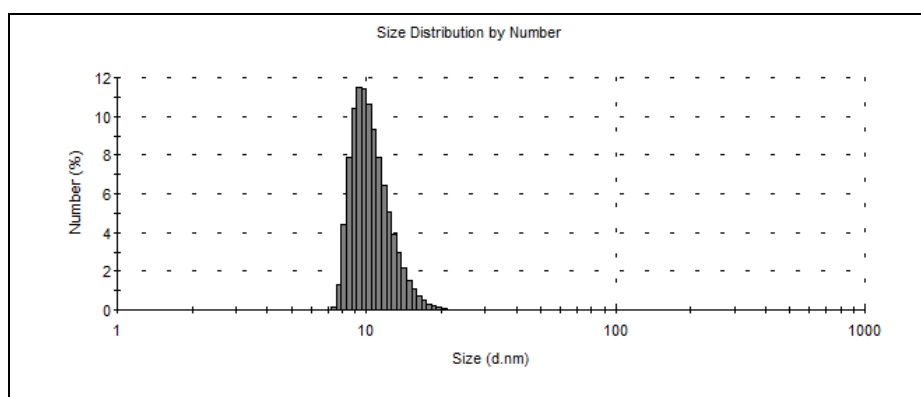


Figure 5 | Transmission Electron Microscopy Analysis. TEM (a, b) and HRTEM (c) images of CdSe/ZnS QDs synthesized and passivated with 5 monolayers of ZnS shell. Scale bar= 100nm (a) and 20nm (b, c).

The obtained nanoparticles were slightly elongated after the growth process already described in Experimental Section, were monodisperse and the size diameter is around 6 to 7nm, which is consistent with the results previously reported in the literature. In some syntheses, it was found that the CdSe/ZnS QDs showed some lattice defects or irregular shapes. This can be associated with a deficient growth of ZnS shell or with the formation of individual ZnS nanocrystals at high temperatures (245°C) that may occur when the shell thickness is more than four monolayers. These ZnS nanocrystals remained in the hexane/ODE layer as previously discussed for the reaction conditions for ZnS shell growth. In the micrographs (Figure 5) of the final CdSe/ZnS samples the results of nucleation of ZnS particles on the surface were not observed. On the other hand, the large difference in lattice parameters between CdSe and ZnS materials can also be an explanation for the presence of the elongated shape. For the growth of nanocrystals with high

crystallinity the core and shell materials should have similar lattice parameters but unfortunately this requirement is not fulfilled for CdSe and ZnS where the lattice mismatch is about 12%^[16]. Initially the growth is coherent at low coverage; however as the thickness of the shell increases, the strain due to the lattice mismatch between CdSe and ZnS is large leading to the formation of dislocations and low-angle boundaries, relaxing the structure and causing the growth to proceed incoherently^[13].

In Figure 6, a typical size distribution histogram (size/number) of the QDs analysed by dynamic light scattering is shown.



Item	HD(nm)	PDI	% Volume
CdSe/ZnS QDs	9.3	0.116	100

Figure 6 | Size determination by dynamic light scattering. Hydrodynamic diameter (histogram size/number) and polydispersity index obtained for synthetic CdSe/ZnS QDs. The results obtained were the average of triplicate runs.

DLS, also known as photon correlation spectroscopy (PCS), is probably the scattering technique most commonly used for characterizing the hydrodynamic size of nanomaterials since it is simple, non-invasive, non-destructive and relatively cheap to apply although the instrument itself can be costly^[31]. Hence, with this technique it was measured the hydrodynamic diameter of the obtained nanoparticles and the size distribution of the same particles. Briefly, due the Brownian motion of small molecules in solution, the size of a particle is calculated from the translational diffusion coefficient by using the Stokes-Einstein equation (Equation 3) where HD means the hydrodynamic diameter, D translational diffusion coefficient, k Boltzmann's

constant, T absolute temperature and η viscosity. Moreover, the translational diffusion coefficient depend not only the size of the particle core, but also on any surface structure, as well as the concentration and type of ions in the medium^[32].

$$HD = kT / 3\pi\eta D$$

Equation 3 | Stokes-Einstein equation for the hydrodynamic diameter.

This means that during the HD measurement, not only the CdSe/ZnS core-shell system was measured but also the mixture of ligands TOPO/HDA around the surface of the nanoparticles. The results displayed in Figure 6 showed an HD of about 9.3nm which is consistent with a typical behaviour for CdSe/ZnS QDs when covered with more than 4 monolayers of ZnS. Nevertheless, HD is not the only information that could be obtained from DLS size measurements. Polydispersity or polydispersity index (PDI) is also additional information that can be achieved. PDI is known as an estimative of the width of the distribution. In other words, the size distribution obtained by this technique is a plot of the relative intensity of light scattered by particles in various size classes and is therefore known as an intensity size distribution^[32]. According to histogram displayed also in Figure 6, apparently the CdSe/ZnS QDs synthesized in this work, shows a narrow size distribution and seems to form well-dispersed aggregates –free solutions as expected for this kind of system. This behaviour could be demonstrated by the obtained polydispersity index which is low (PDI=0.116) and similar with values reported in the literature^[33, 34].

Figure 7 shows typical autocorrelation data obtained when the hydrodynamic diameter of the CdSe/ZnS QDs was determined by DLS.

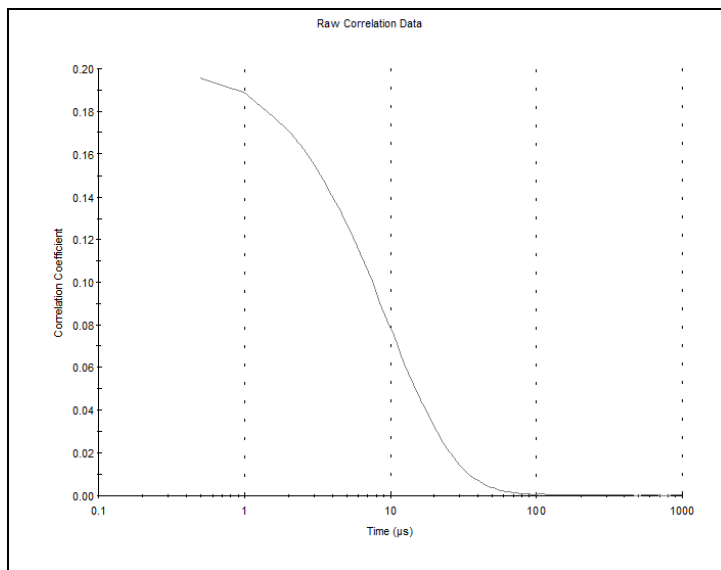


Figure 7 | Correlation Data. Measured autocorrelation function in the measurements of hydrodynamic diameter for synthetic CdSe/ZnS QDs.

An important feature of DLS is that the speed of particles that are undergoing Brownian motion is related to the size of the particles (Stokes-Einstein equation, Equation 3). Large particles move slowly, while smaller particles move quickly. As the particles move around, the constructive and destructive phase addition of the scattered light will cause the bright and dark areas to grow and diminish in intensity, or in other words, the intensity appears to fluctuate. This behaviour is translated by the correlation function and therefore the results obtained are the correlation data. If large particles are being measured, then, as they are moving slowly, the intensity of the speckle pattern will also fluctuate slowly and correlation persists for a long time. If small particles are being measured then, as they are moving quickly, the intensity of the speckle pattern will also fluctuate quickly and the correlation will reduce sooner. The data shown in Figure 7 indicates that the CdSe/ZnS QDs developed in this work are small. After 1-10 μ s the signal of correlogram starts to decay indicating the presence of small particles when comparing with large particles that in general starts to reduced only after 500-1000 μ s^[32, 35].

Concentration Determination of QDs solutions

CdSe/ZnS QDs have been applied in many different applications and for many of those applications it is crucial to determine the actual concentration of the semiconductor nanocrystals in solution or a given medium. The simple determination of concentration using spectrophotometry uses the Lambert-Beer's expression (Equation 2) and thus requires the extinction coefficient (ϵ). If the extinction coefficient is known, it is easy to obtain the concentrations of the QDs by simply taking an absorption spectrum of the sample. Over the years, many different studies have been performed for the determination of this parameter and the results obtained from the different groups differed considerably from each other. According to Schemelz *et al.*^[36] using atomic absorption spectroscopy (AAS), the extinction coefficient per particle in the size range between 1.5 and 4.5nm increases as the size of the nanocrystal increases in a cubic dependence. On the other hand, Striolo *et al.*^[22] by an osmotic method confirmed the cubic sized dependence observed by Schemelz for the extinction coefficient of nanocrystals in the size range between 2.5 and 6nm. Bawendi's group^[23] used the absorption cross section of the nanocrystals for the determination of the same parameter. Some of the methods applied by these groups were not compatible with the concentration determination of colloidal nanocrystals because of the number of ligands on their surface which are difficult to identify and may vary significantly under different conditions (*e.g.* concentration of the reactants or reaction time). So, Peng *et al.*^[19,21] suggested two approaches, atomic absorption (AA) measurements and controlled etching of the nanocrystals in a solution with a defined volume, for the accurate determination of the extinction coefficient for QDs. The results obtained show that the extinction coefficient of CdSe nanocrystals in the strong quantum confinement size regime increases as their size increases approximately as a square to a cubic function. Moreover, the integrated ϵ of the first absorption peak seemed to be independent of temperature, nature of the surface capping groups, the refractive index of the solvents, the photoluminescence and the methods employed for the synthesis of the QDs. Hence, for the advantages demonstrated, the absorption spectrum method was applied and consequently the Lambert-Beer's Law was used to determine the concentration of the synthetic QDs. The nanoparticles

were suspended in chloroform and the extinction coefficient for each sample was chosen based on the sizing curve (Figure 8, (a)) and size-dependent extinction coefficient per mole (Figure 8, (b)) at the first excitonic absorption of CdSe cores obtained by Peng's group.

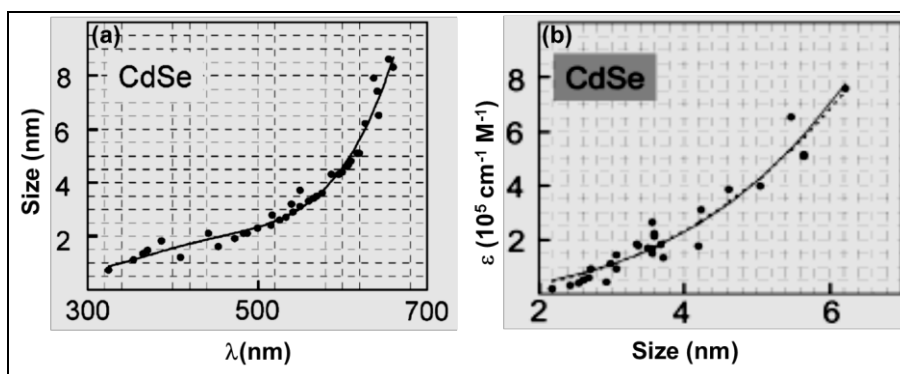


Figure 8 | Determination of the extinction coefficient of QDs. Sizing curve of CdSe cores (a) and size-dependent extinction coefficient per mole of nanocrystals at the first absorption peak of CdSe nanocrystals (b). Reprinted with permission from reference [19]. Copyright 2003, American Chemical Society.

The experimental procedure for the synthesis of CdSe cores reported previously in the Experimental section normally yields nanocrystals with the first absorption peak at 568nm. Making use of the sizing curve obtained by Peng *et al* was easy to obtain the size expected for the synthetic CdSe cores which is around 3.5nm and the corresponding extinction coefficient, $\epsilon = 1.5 \times 10^5 \text{ M}^{-1} \text{ cm}^{-1}$. Finally, the concentration was directly calculated using the Lambert-Beer's function using the measured optical density/absorption.

Optical Characterization

The synthesis presented earlier produced ZnS coated CdSe dots and Figure 9 shows the absorption spectra of CdSe dots before (black dashed line) and after (black solid line) coating with 5 monolayers of ZnS. The same figure also shows the room-temperature photoluminescence spectra (PL) (dashed green line) of the final samples (CdSe/ZnS QDs) with 12% of quantum yield (QY). In the absorption spectra of the CdSe/ZnS QDs it was observed a broader and slightly red-shift from their respective cores spectra. This data could indicate that the coating of the CdSe cores with the 5 monolayers of ZnS must have

occurred as expected. On the other hand, the position of the band maxima in photoluminescence spectra represented in green is also red-shifted and the spectra broader than the corresponding absorption spectra (black solid line) with a low QY. This could be associated with the fact that PL quantum yields are based on the structural characterization of ZnS coverage.

According to Dabbousi *et al*^[13], as the coverage of the ZnS on the CdSe surface increases, a dramatic increase in the fluorescence quantum yield followed by a steady decline after 1.3 monolayers of ZnS was observed and a value of 50% was demonstrated for this coverage.

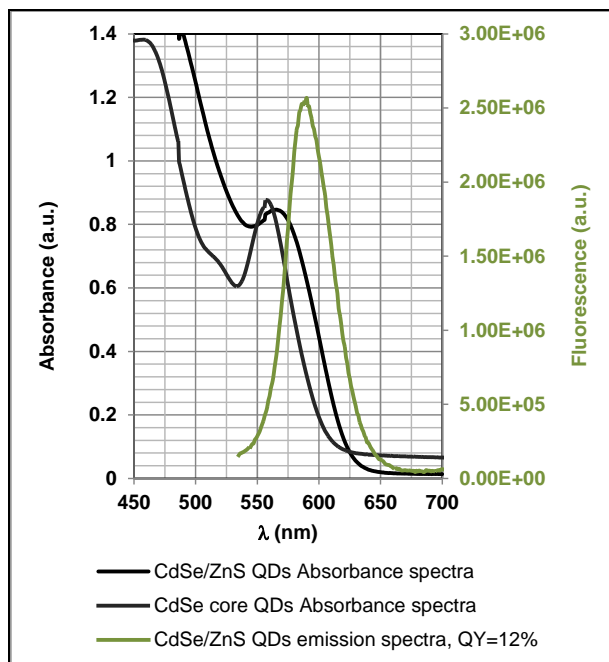


Figure 9 | Optical Measurements: Absorption spectra of CdSe cores (black dashed line) and CdSe/ZnS core-shell QDs (black solid line) and Photoluminescence spectra (dashed green line) of CdSe/ZnS QDs after the surface passivation of 5 monolayers of ZnS.

The low QY obtained for the CdSe/ZnS QDs synthesized in this work could be associated with the increase of size distribution in the samples with high coverage (~5 monolayers) and the elongated shape of some particles due to an incoherent shell growth leading to some defects in the ZnS structure. It is important to point out that this incoherent growth derives from the large lattice mismatch between CdSe and ZnS materials (~12%) causing misfit dislocations when the thickness of the ZnS layer exceeds more than 4

monolayers. Another possible explanation could be related to the use of primary alkylamines during the synthetic procedure^[16].

It was shown that the QY obtained for the core-shell system developed herein is not as high as expected, however, it is noteworthy that the CdSe/ZnS QDs with high coverage are more stable, showing a much higher photochemical stability and higher long-term fluorescence for further biological applications as desired. These enhanced properties are due to the higher band offset and lattice parameters introduced by the ZnS material when compared with other core-shell systems, namely CdSe/CdS QDs which results in a lower charge density of the photogenerated charge carriers on the particle surface and hence a lower probability of surface oxidation^[16].

Conclusion

A synthetic procedure for the production of core-shell QDs whose emission spans most of the visible spectrum that made use of the advantages of non-coordinating solvents and alkylamines as organic ligands was used. The synthesized QDs were analysed optically and structurally using different techniques. TEM and HRTEM demonstrated the elongated shape of the obtained nanoparticles and sometimes the presence of some structural defects. This derives from a deficient growth of ZnS shell that could occur at high temperatures and also the differences in lattice parameters between the ZnS and CdSe materials. The shifts present in absorption and emission spectra and the relatively low quantum yield obtained were explained as a function of the high coverage. Dynamic light scattering analysis evaluates the narrow size distribution with a very low polydispersity index which is in agreement with observations made by others for this kind of system. The high coverage sometimes bring some structural disadvantages, but in general CdSe/ZnS QDs are robust and very stable nanoparticles with optical and electronic properties that makes them very appealing for applications in many scientific areas.

Glossary

Table 2 | Glossary of terms related with quantum dots^[32,37,38].

Term	Definition
Autocorrelation data	Is a result from the correlation function measured during the HD measurement of the particles. Due to the Brownian motion of the particles the correlation function could provide information about particle size. For large particles the decay of correlation is slow because particles are moving slowly. Small particles move rapidly and the decay of correlation is also sooner.
Absorption cross section	For physics, a cross section is the effective area which governs the probability of some scattering or absorption event. For QDs, it is a crucial parameter for the design of nanocrystal quantum dot devices and to the interpretation of spectroscopic data.
Band gap	Also called energy gap, is the energy range in a solid where no electron states can exist. This means, the energy difference (normally in eV) between the valence band and a conduction band of a semiconductor.
Band-offset	Describes the relative alignment of the energy bands in the interface that occurs between two layers of a semiconductor.
Bohr radius	The natural separation distance between the positive and negative charges in the excited state of a material.
Epitaxial growth	Refers to the deposition of a crystalline overlayer on a crystalline substrate, where the overlayer is in registry with the substrate. In other words, there must be one or more preferred orientations of the overlayer with respect to the substrate for this to be termed epitaxial growth. The overlayer is called an epitaxial film or epitaxial layer.
Etching	In semiconductors, this is the process of removing unwanted material from the

surface using acids, bases or other chemicals. This process is also used to bring certain physical and chemical changes within the semiconducting materials so they become operable at desired voltages and temperatures. Semiconductor etching is carried out by three different methods: plasma, wet and orientation –dependent etching.

HOMO-LUMO gap

Is the energy difference between the highest molecular orbital occupied (HOMO) and lowest molecular orbital unoccupied (LUMO).

Hydrodynamic diameter (HD)

Effective diameter of a particle in a liquid environment. For DLS measurements the size of a sphere that moves in the same manner as the scatterer. It is useful to point out that the obtained size will include any other molecules or solvent molecules that move with the particle. (e.g. for nanoparticles with a layer of surfactant will appear larger by dynamic light scattering (which includes the surfactant layer) than by transmission electron microscopy (which does not "see" the layer due to poor contrast).

Lattice parameters

This term is related with the epitaxial growth .Lattice constant or lattice parameter is a measure of the structural compatibility between different materials. Lattice constant matching is important for the growth of thin layers of materials on other materials.

Photoluminescence

Also called fluorescence quantum yield. Is the number of emitted photons occurring per number of absorbed photons. ϕ_f is typically determined relative to a dye of known fluorescence quantum yield.

Polydispersity Index (PDI)

Is the width of the size distribution.

Quantum confinement

Is responsible for the increase of energy difference between energy states and band gap. A phenomenon tightly related with the optical and electronic properties of the materials. Thus, quantum dots of

the same material but with different sizes, can emit light of different colours (the energy levels of QDs is dependent of its size).

QD surface passivation

Modification of the surface of bare QD core to improve properties such as the fluorescence quantum yield or the resistance to chemical reaction. Achieved either by deposition of a layer of inorganic, chemically inert material and organic ligands or of a layer of organic molecules only.

Stokes shift

Difference (usually in frequency units) between the spectral position of the maxima of the lowest energy (that is, longest wavelength) absorption and the luminescence arising from the same electronic transition. In the case of QDs, this is the difference between the first excitonic absorption band and the emission maximum.

Wurtzite structure

Is a crystal structure for various binary compounds and it's an example of a hexagonal crystal system. The semiconductors such as ZnO, CdS and CdSe are wurtzite itself.

Acknowledgments

The author thank to Benjamin Hardy Wunsch from Massachusetts Institute of Technology (MIT), Cambridge, USA for the TEM and HRTEM images. The author also thank to Professor Dr António Maçanita for the opportunity to perform the photoluminescence spectra and quantum yield measurements in his laboratory at Instituto Superior Técnico (IST), Lisboa, Portugal. The help provided by Professor António Lopes from ITQB-UNL, Oeiras, Portugal in DLS measurements was also appreciated. Ana Sofia Miguel is a recipient of a PhD fellowship from the Fundação para a Ciência e Tecnologia (FCT), Portugal (SFRH/BD/40303/2007). The work was supported by the national funded project NTec/SQA/0131/2007 from FCT.

References

1. Henglein, A., Small-Particle Research - Physicochemical Properties of Extremely Small Colloidal Metal and Semiconductor Particles. *Chem Rev* **1989**, 89, (8), 1861-1873.
2. Schmid, G., Large Clusters and Colloids - Metals in the Embryonic State. *Chem Rev* **1992**, 92, (8), 1709-1727.
3. Alivisatos, A. P., Semiconductor clusters, nanocrystals, and quantum dots. *Science* **1996**, 271, (5251), 933-937.
4. Nirmal, M.; Brus, L., Luminescence photophysics in semiconductor nanocrystals. *Accounts Chem Res* **1999**, 32, (5), 407-414.
5. Chan, W. C. W.; Maxwell, D. J.; Gao, X. H.; Bailey, R. E.; Han, M. Y.; Nie, S. M., Luminescent quantum dots for multiplexed biological detection and imaging. *Curr Opin Biotech* **2002**, 13, (1), 40-46.
6. Murray, C. B.; Norris, D. J.; Bawendi, M. G., Synthesis and Characterization of Nearly Monodisperse Cde (E = S, Se, Te) Semiconductor Nanocrystallites. *J Am Chem Soc* **1993**, 115, (19), 8706-8715.
7. Peng, Z. A.; Peng, X. G., Formation of high-quality CdTe, CdSe, and CdS nanocrystals using CdO as precursor. *J Am Chem Soc* **2001**, 123, (1), 183-184.
8. Kortan, A. R.; Hull, R.; Opila, R. L.; Bawendi, M. G.; Steigerwald, M. L.; Carroll, P. J.; Brus, L. E., Nucleation and Growth of Cdse on Zns Quantum Crystallite Seeds, and Vice Versa, in Inverse Micelle Media. *J Am Chem Soc* **1990**, 112, (4), 1327-1332.
9. Mews, A.; Eychmuller, A.; Giersig, M.; Schooss, D.; Weller, H., Preparation, Characterization, and Photophysics of the Quantum-Dot Quantum-Well System Cds/Hgs/Cds. *J Phys Chem-US* **1994**, 98, (3), 934-941.
10. Qu, L. H.; Peng, X. G., Control of photoluminescence properties of CdSe nanocrystals in growth. *J Am Chem Soc* **2002**, 124, (9), 2049-2055.
11. Peng, X. G.; Schlamp, M. C.; Kadavanich, A. V.; Alivisatos, A. P., Epitaxial growth of highly luminescent CdSe/CdS core/shell nanocrystals with photostability and electronic accessibility. *J Am Chem Soc* **1997**, 119, (30), 7019-7029.
12. Hines, M. A.; Guyot-Sionnest, P., Synthesis and characterization of strongly luminescing ZnS-Capped CdSe nanocrystals. *J Phys Chem-US* **1996**, 100, (2), 468-471.
13. Dabbousi, B. O.; RodriguezViejo, J.; Mikulec, F. V.; Heine, J. R.; Mattoussi, H.; Ober, R.; Jensen, K. F.; Bawendi, M. G., (CdSe)ZnS core-shell quantum dots: Synthesis and characterization of a size series of highly luminescent nanocrystallites. *J Phys Chem B* **1997**, 101, (46), 9463-9475.
14. Dukes, A. D.; McBride, J. R.; Rosenthal, S. J., Luminescent Quantum Dots. *Ecs Transactions* **2011**, 33, (33), 3-16.
15. Sanderson, K., Quantum dots go large. *Nature* **2009**, 459, (7248), 760-761.
16. Xie, R. G.; Kolb, U.; Li, J. X.; Basche, T.; Mews, A., Synthesis and characterization of highly luminescent CdSe-Core CdS/Zn_{0.5}Cd_{0.5}S/ZnS multishell nanocrystals. *J Am Chem Soc* **2005**, 127, (20), 7480-7488.
17. Aldana, J.; Wang, Y. A.; Peng, X. G., Photochemical instability of CdSe nanocrystals coated by hydrophilic thiols. *J Am Chem Soc* **2001**, 123, (36), 8844-8850.

18. Li, J. J.; Wang, Y. A.; Guo, W. Z.; Keay, J. C.; Mishima, T. D.; Johnson, M. B.; Peng, X. G., Large-scale synthesis of nearly monodisperse CdSe/CdS core/shell nanocrystals using air-stable reagents via successive ion layer adsorption and reaction. *J Am Chem Soc* **2003**, 125, (41), 12567-12575.
19. Yu, W. W.; Qu, L. H.; Guo, W. Z.; Peng, X. G., Experimental determination of the extinction coefficient of CdTe, CdSe, and CdS nanocrystals. *Chem Mater* **2003**, 15, (14), 2854-2860.
20. Williams, A. T. R.; Winfield, S. A.; Miller, J. N., Relative Fluorescence Quantum Yields Using a Computer-Controlled Luminescence Spectrometer. *Analyst* **1983**, 108, (1290), 1067-1071.
21. Yu, W. W.; Qu, L. H.; Guo, W. Z.; Peng, X. G., Experimental determination of the extinction coefficient of CdTe, CdSe and CdS nanocrystals (vol 15, pg 2854, 2003). *Chem Mater* **2004**, 16, (3), 560-560.
22. Striolo, A.; Ward, J.; Prausnitz, J. M.; Parak, W. J.; Zanchet, D.; Gerion, D.; Milliron, D.; Alivisatos, A. P., Molecular weight, osmotic second virial coefficient, and extinction coefficient of colloidal CdSe nanocrystals. *J Phys Chem B* **2002**, 106, (21), 5500-5505.
23. Leatherdale, C. A.; Woo, W. K.; Mikulec, F. V.; Bawendi, M. G., On the absorption cross section of CdSe nanocrystal quantum dots. *J Phys Chem B* **2002**, 106, (31), 7619-7622.
24. Yu, W. W.; Chang, E.; Falkner, J. C.; Zhang, J. Y.; Al-Somali, A. M.; Sayes, C. M.; Johns, J.; Drezek, R.; Colvin, V. L., Forming biocompatible and nonaggregated nanocrystals in water using amphiphilic polymers. *J Am Chem Soc* **2007**, 129, (10), 2871-2879.
25. Reiss, P.; Bleuse, J.; Pron, A., Highly luminescent CdSe/ZnSe core/shell nanocrystals of low size dispersion. *Nano Lett* **2002**, 2, (7), 781-784.
26. Howarth, M.; Liu, W. H.; Puthenveetil, S.; Zheng, Y.; Marshall, L. F.; Schmidt, M. M.; Wittrup, K. D.; Bawendi, M. G.; Ting, A. Y., Monovalent, reduced-size quantum dots for imaging receptors on living cells. *Nat Methods* **2008**, 5, (5), 397-399.
27. Talapin, D. V.; Rogach, A. L.; Kornowski, A.; Haase, M.; Weller, H., Highly luminescent monodisperse CdSe and CdSe/ZnS nanocrystals synthesized in a hexadecylamine-trioctylphosphine oxide-trioctylphosphine mixture. *Nano Lett* **2001**, 1, (4), 207-211.
28. Wang, Q. B.; Xu, Y.; Zhao, X. H.; Chang, Y.; Liu, Y.; Jiang, L. J.; Sharma, J.; Seo, D. K.; Yan, H., A facile one-step in situ functionalization of quantum dots with preserved photoluminescence for bioconjugation. *J Am Chem Soc* **2007**, 129, (20), 6380-6381.
29. Park, S.; Clark, B. L.; Keszler, D. A.; Bender, J. P.; Wager, J. F.; Reynolds, T. A.; Herman, G. S., Low-temperature thin-film deposition and crystallization. *Science* **2002**, 297, (5578), 65-65.
30. Miguel, A. S.; Maycock, C.; Oliva, A., Synthesis and Functionalization of CdSe/ZnS QDs Using the Successive Ion Layer Adsorption Reaction and Mercaptopropionic Acid Phase Transfer Methods. In *Nanoparticles in Biology and Medicine. Methods and Protocols.*, in press ed.; Springer: 2012; Vol. 906.
31. Sapsford, K. E.; Tyner, K. M.; Dair, B. J.; Deschamps, J. R.; Medintz, I. L., Analyzing Nanomaterial Bioconjugates: A Review of Current and Emerging Purification and Characterization Techniques. *Anal Chem* **2011**, 83, (12), 4453-4488.

32. Malvern Dynamic Light Scattering: An Introduction in 30 minutes. <http://www.malvern.com/common/downloads/campaign/MRK656-01.pdf> (05/01/2012),
33. Pons, T.; Uyeda, H. T.; Medintz, I. L.; Mattoussi, H., Hydrodynamic dimensions, electrophoretic mobility, and stability of hydrophilic quantum dots. *J Phys Chem B* **2006**, 110, (41), 20308-20316.
34. Liu, W.; Howarth, M.; Greytak, A. B.; Zheng, Y.; Nocera, D. G.; Ting, A. Y.; Bawendi, M. G., Compact biocompatible quantum dots functionalized for cellular imaging. *J Am Chem Soc* **2008**, 130, (4), 1274-1284.
35. Malvern, *Zetasizer Nano Series User Manual*. Malvern Instruments Ltd: **2004**; Vol. Man0317.
36. Schmelz, O.; Mews, A.; Basche, T.; Herrmann, A.; Mullen, K., Supramolecular complexes from CdSe nanocrystals and organic fluorophors. *Langmuir* **2001**, 17, (9), 2861-2865.
37. Azzazy, H. M. E.; Mansour, M. M. H.; Kazinierczak, S. C., From diagnostics to therapy: Prospects of quantum dots. *Clin Biochem* **2007**, 40, (13-14), 917-927.
38. Resch-Genger, U.; Grabolle, M.; Cavaliere-Jaricot, S.; Nitschke, R.; Nann, T., Quantum dots versus organic dyes as fluorescent labels. *Nat Methods* **2008**, 5, (9), 763-775.

Chapter 3

Ligand Synthesis and Design for Water-Soluble CdSe/ZnS QDs

This chapter contains data published in:

Ana Sofia Miguel, Christopher Maycock and Abel Oliva; "Synthesis and Functionalization of CdSe/ZnS QDs Using the Successive Ion Layer Adsorption Reaction and Mercaptopropionic Acid Phase Transfer Methods"; *Nanoparticles in Biology and Medicine. Methods and Protocols*, Springer, 2012 (in press).

The author contributed fully to this chapter, namely in the planning of the experimental work, performance of the experiments and writing of the manuscript.

Ligand Synthesis and Design for Water-Soluble CdSe/ZnS QDs

Abstract	65
Introduction	65
Experimental Section	69
Materials and Analysis.....	69
Solvent and Reagent Purification	70
Ligand Synthesis and Design	72
Water Solubilization of CdSe/ZnS Core-Shell QDs.....	95
Preparation of 3-mercaptopropionic acid (MPA)-capped QDs.....	95
Preparation of Dihydrolipoic acid (DHLA)-capped QDs	96
Preparation of Carboxy-PEG ₄₀₀ , Mannose-TEG and Mannose-PEG ₄₀₀ - capped QDs.....	97
Preparation of Amino-PEG ₄₀₀ and Mixtures of Amino-PEG ₄₀₀ /DHLA- PEG ₄₀₀ -capped QDs	98
Characterization of Hydrophilic QDs	98
Concentration Determination in Aqueous Solutions and Optical Measurements	98
Dynamic Light Scattering Measurements.....	99
Estimation of the Number of Functional Amines Groups in Amino-QDs and Mixed-ligand Amino- QDs	100
Estimation of the Concentration of Carbohydrates Moieties in Glyco- QDs.....	101
Results and Discussion	102
Ligand Synthesis and Design.....	102
Water Solubilisation of CdSe/ZnS core-shell QDs	119
Characterization of Hydrophilic QDs	122
Determination of QDs Concentration in Aqueous Solutions and Optical Measurements	122
Tuning the Hydrodynamic Size and Surface Charge of Hydrophilic QDs	123
Probing the Number of Functional Amines Groups per QD	127
Estimation of the Number of Sugar Molecules per QD	129
Conclusion	130
Acknowledgments	131

Supplementary Information	131
Graphical Index of Compounds and Experiments of Ligand Synthesis and Design	131
References	136

Abstract

One of the common strategies to promote the transfer of QDs to an aqueous environment has relied on surface ligand exchange. Herein, is described a simple and versatile scheme for the preparation of a family of heterobifunctional ligands incorporating dihydrolipoic acid, a hydrophilic spacer such as polyethylene glycol with different molecular weights and different functional end termini for further covalent attachment to biomolecules. These ligands permit strong and stable interactions with colloidal semiconductor nanocrystals and render them soluble in aqueous media. The series of water-soluble QDs created exhibit small hydrodynamic diameter, tuneable surface charge, good quantum yield and great resistance to environmental changes, making them very amenable for use in many biological and biotechnological applications.

Key-words: *water-soluble QDs, multidentate ligands, hydrodynamic diameter, ζ -potential, absorbance and fluorescence quantitation.*

Introduction

Recent advances in water-soluble and bioconjugated QDs have made them very appealing for biosensing and bioimaging ^[1]. The best available QD fluorophores for biological applications are made of CdSe cores coated with a layer of ZnS. The ZnS layer passivates the core surface, protects it from oxidation, prevents leeching of the Cd/Se into the surrounding solution and also produces substantial improvement in the PL yield ^[2,3]. Although thin ZnS (1-2 monolayers) shells often produce the highest PL yields, thicker ZnS shells (4-6 monolayers) provide more protection against oxidation and the harsher conditions presented by biological media (e.g. acidic buffers)^[4]. These CdSe/ZnS QDs are commonly synthesized at high temperatures in coordinating solvents. As described in chapter 2, these QDs are capped with mixtures of trioctylphosphine/trioctylphosphine oxide (TOP/TOPO) and alkylamines (HDA) which are hydrophobic ligands and therefore are not suitable for use in aqueous buffers.

Since 1998, different methods have been developed to make CdSe/ZnS QDs water-soluble, so that biomolecules can be either covalently or noncovalently

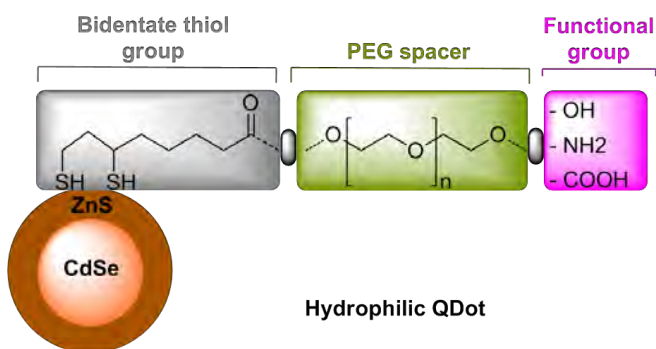
attached on the surface of the QDs. These methods include silica coating^[5,6], encapsulation of the hydrophobic (TOP/TOPO) capped QDs with amphiphilic polymer shells^[7,8] or lipid micelles^[9] and exchanging the native caps with hydrophilic ligands^[10,11]. All of these approaches have advantages and disadvantages. In the case of encapsulation with micelles or polymers, the water-soluble QDs show relatively high quantum yields because it preserves the native ligands. However, this approach tends to produce nanoparticles with larger diameter (> 15nm). This could represent a drawback in biological assays because can hamper intracellular mobility especially in mammalian cells. In comparison, the cap exchange method seems to be relatively simple and provide more compact nanocrystals (5-15nm), which may represent an advantage for size-sensitive applications such as intracellular uptake and imaging^[4,12].

In the ligand exchange method, the development of hydrophilic QDs starts with mercaptocarboxylic acids^[13,14] (e.g. 3-mercaptopropionic acid (MPA) and mercaptoacetic acid (MAA)) which seemed to be greatly advantageous due to its simplicity and also because the availability of the carboxyl group for further coupling to other biomolecules. But, for this strategy the advantages were carefully analysed against the drawbacks. MPA or MAA are mono-compact thiol ligands obtained either commercially or by simple synthesis. MPA or MAA QDs have short shelf lives (~1week) due to dynamic thiol-ZnS interactions^[4]. This issue was overcome by the strong interactions with QDs surface provided by the bidentate chelate effect introduced by dithiol Dihydrolipoic acid (DHLA) thus improving the long term stability of the water-soluble QDs. Capping QDs with DHLA permitted their dispersion in basic buffer solutions, aggregate-free dispersions that were stable for long periods of time when compared with the mono-thiol MPA. However, the aggregation of DHLA-QDs occurs under acidic conditions^[10,15].

To address these limitations and to further expand the range of techniques to prepare hydrophilic nanoparticles and also taking advantage of bidentate DHLA ligand, a poly(ethylene glycol) (PEG) has been used with success by several groups^[12, 15-18]. This polymer has great interest in the biotechnical and biomedical areas due to its suitable properties. Primarily, PEG exhibits a very low degree of nonspecific interactions with other polymers and biomolecules

in aqueous environments. In addition, it is non-toxic and does not harm active proteins or cells, although it interacts with cell membranes. It is readily amenable to chemical modification and attachment to other molecules and surfaces, and, when attached to other surfaces, it has little effect on their chemistry but controls their solubility and also increases their size thus, slowing down their diffusion and providing additional steric hindrance^[16, 19].

DHLA-PEG-OH uses the bidentate chelate interactions with the nanoparticles surface afforded by the dithiol on DHLA, combined with the hydrophilic nature of PEG chain. The presence of the PEG removes the need for charged groups to provide the solubility of the QDs^[17] as in the case of DHLA or MPA and, expanded the range of pH stability of the nanoparticles under acidic conditions. However the functional hydroxyl (OH) end group due to the absence of reactive groups (e.g. carboxyl group, COOH) represents a limitation for commonly used bioconjugation techniques such as covalent conjugation chemistry through 1-ethyl-3-(3-dimethylaminopropyl) carbodiimide (EDC) coupling. Hence, it was useful to expand the above ligand to other biocompatible functions, such as carboxyl group (COOH) or amine (NH₂) groups that can be further coupled with bifunctional molecules (e.g. dyes, peptides, proteins or antibodies).



Scheme 3 | DHLA-PEG Hydrophilic Ligands. Modular design of hydrophilic ligands with different terminal functional groups^[12].

In Scheme 3 can be observed that each ligand contains a central PEG spacer with tuneable length to promote hydrophilicity, a dithiol group for anchoring onto QD surface at one end, and, a lateral/reactive group that promotes biological linkage with target biomolecules at the other end^[12].

Much is already known about the structure, interactions and function of nucleic acids and proteins ^[20]. However, carbohydrates are also molecules that together with proteins regulate many important biological processes ^[21] (e.g. cell-cell communication) but the role of these carbohydrates in the biological systems is less clear. As is known, QDs have been used for biolabeling and imaging applications so, in 2003 Rosenzweig *et al* ^[22] used carboxymethyl dextran and polylysine to protect CdSe/ZnS QDs and demonstrated that these glyco quantum dots (glyco-QDs) are a useful tool for studying carbohydrate-protein interactions that are critical steps in many glycobiological events. Since this report many other works have been developed using carbohydrate moieties to prepare glyco-QDs. Very recently, Seeberger *et al* ^[23] used the hydrophilic nature of PEG and its ability to attach carbohydrates moieties on the surface of QDs and so the construction of glyco-QDs to be used *in vitro* and *in vivo* applications.

Once the CdSe/ZnS QDs were prepared and well characterized as described in chapter 2, one of the major goals of this work was to design ligands that permit the preparation of compact hydrophilic QDs amenable to conjugation with a variety of biomolecules via simple covalent and noncovalent binding strategies.

Herein, general procedures for the ligand synthesis and design, purification and characterization will be described. The family of ligands synthesized include a series of compounds made of polyethylene glycols (PEGs) with two different lengths, PEG₄₀₀ and PEG₂₀₀₀, where the length represents the average of molecular weight of the hydrophilic spacer. These PEG compounds were appended to dihydrolipoic acid to make use of the bidentate thiol group for further interaction with the nanoparticle surface. On the other end of the PEG, functional groups such as hydroxyl, amino or carboxyl group were created for future bioconjugation with different biomolecules as shown in Scheme 3.

The same modular design of hydrophilic ligands, DHLA-PEG-FN (where FN is the functional group), was also used to construct hydrophilic ligands with carbohydrate moieties as terminal functional group. The sugar used was mannose and the hydrophilic spacer was PEG₄₀₀ and triethyleneglycol (TEG). Although simple 3-mercaptopropionic acid and dihydrolipoic acid ligands have

demonstrated limitations in terms of pH stability and interaction with biomolecules due to the absence of a hydrophilic spacer, these two ligands were also used in this work to obtain water-soluble QDs.

For the DHLA and their corresponding PEG derivatives with different functional groups, the ligand exchange method was the approach applied. In the case of 3-mercaptopropionic acid the ligand exchange was affected by the phase transfer method^[24]. Hence the nanoparticles initially soluble in chloroform, become water soluble and the ligand exchange could be followed by this change of solubility. The general procedures for surface functionalization for both kinds of ligands will also be described here.

The water-soluble QDs were characterized by several techniques. In general all of them were analysed by optical and dynamic light scattering measurements to obtain the absorbance and photoluminescence spectra and to tune the size and the charge density of the hydrophilic QDs respectively. In addition, some of these water-soluble QDs capped with some of the DHLA-PEG-FN ligands were analysed using specific methodologies. When the functional group (FN) was an amine, the number of functional groups around the surface of nanoparticles was quantified by the fluorescamine assay^[25] and for ligands with a carbohydrate moiety as a terminal functional group the number of sugars available in the surface of QDs were quantified using the phenol-sulphuric acid assay^[26].

The results obtained, show a family of water-soluble CdSe/ZnS core-shell QDs that exhibit small hydrodynamic diameter which is substantially smaller than polymer encapsulated QDs. The QDs display a tuneable charge density and good solution stability, enhanced by the addition of a hydrophilic spacer. The presence of heterobifunctional ligands with different terminal functional groups on the surface of the QDs, make them very appealing for coupling chemistry with a variety of biomolecules.

Experimental Section

Materials and Analysis

All syntheses and manipulations of air-sensitive solutions were carried out under an argon atmosphere. Air sensitive materials were handled in a Braun MB150-GI glove box. All chemicals and solvents used in this work were

obtained from Sigma-Aldrich or Fluka and used as received unless otherwise specified. The solvents were all p.a. ACS grade. The synthesized compounds were purified by flash chromatography using silica gel 60 (0.040-0.063mm) from Merck. The analytical thin layer chromatography (TLC) plates (aluminium-backed silica gel 60 GF254, Merck) were visualised in ninhydrin solution for amine-bearing compounds, bismuth nitrate solution/aqueous barium solution (2:1) in the case of compounds containing polyethylene glycols. For all the others TLC plates an ethanolic solution of molybdotophosphoric acid was used as staining ^[27]. The melting points were determined with a capillary apparatus Büchi B-540. The NMR spectra were recorded on a Bruker Avance II⁺. The ¹H-NMR spectra were obtained at 400MHz with chemical shifts values (δ) in ppm downfield from tetramethylsilane. For spectra in D₂O the residual water peak was used as reference ¹³C-NMR spectra were obtained at 100MHz in CDCl₃ and D₂O. All coupling constant (*J*) values are reported in hertz and the number of attached protons is found in parentheses, following the chemical shift value. Peak assignments were supported by 2D data. ESI-MS was measured on a Bruker MICROTOF mass spectrometer and samples were dissolved in a solution of chloroform or water. Infrared (FTIR) spectra were recorded on a FT-IR Research series from Mattson. Samples were measured as thin films on KCl windows or as KBr discs. UV-visible absorbance spectra were taken using a Beckman DU-70 spectrophotometer. Corrected photoluminescence spectra were recorded with a SPEX Fluorolog from Horiba Jobin Yvon and a SpectraMax Gemini EM from Molecular Devices Corporation. Dynamic light scattering measurements were performed in a Zetasiser Nano ZS from Malvern Instruments. The samples of hydrophilic QDs were centrifuged in an Eppendorf 5804R centrifuge. pH measurements were performed on a Metrohm pH meter.

Solvent and Reagent Purification

Some of the solvents and reagents used needed prior purification. Table 3 describes these processes.

Table 3 | Solvent and reagent purification^[28].

Solvent/Reagent	Description
Acetic Anhydride	Was distilled under reduced pressure (20mmHg).
Anhydrous dichloromethane	Was refluxed and distilled from phosphorous pentoxide and stored over molecular sieves.
Anhydrous dimethylformamide	Was kept over calcium hydride for 24h and then distilled under vacuum (25mmHg) and stored over molecular sieves
Anhydrous pyridine	Was distilled twice from potassium hydroxide and stored over molecular sieves.
Anhydrous tetrahydrofuran	Was kept 24h over calcium hydride and distilled. It was then refluxed over sodium wire and benzophenone until it acquired a violet colour. The still was always kept at low reflux, under an inert atmosphere and only distilled immediately before use.
Anhydrous toluene	Was distilled from calcium hydride and stored over sodium wire.
Anhydrous triethylamine	Was distilled from calcium hydride and stored over molecular sieves.
Anhydrous triphenylphosphine	Was dried under vacuum (0.1mmHg) at 60°C for 4h.
Boron trifluoride diethyl etherate	Was distilled under reduced pressure (20mmHg).
Trifluoromethanesulfonic acid trimethylsilylester	Was distilled under reduced pressure (20mmHg).
Thionyl Chloride	Was freshly distilled from commercial reagent.

Ligand Synthesis and Design

Significant improvements were made to existing protocols for the synthesis of many of the ligands described below. Hence the full experimental and characterisation data is included.

Experiment 1: Synthesis of Dihydrolipoic acid (DHLA) (**1**)^[15]

Thioctic acid (0.250g, 1.21mmol) was dissolved in 5mL of 0.25M NaHCO₃ and cooled to 0°C in an ice bath. NaBH₄ (0.184g, 4.85mmol) was added slowly and the temperature kept below 4°C while stirring for an additional 2h. The reaction mixture was acidified with a solution of HCl 6M until pH=1. The aqueous phase was extracted with toluene (3x25mL). The combined organic phases were dried over Na₂SO₄ and filtered. Evaporation of the solvent yielded **1** (0.218g, 98%) as a clear colourless oil.

¹H-NMR (400MHz, CDCl₃): δ (ppm) 2.94-2.91 (m, 1H, CHSH), 2.75-2.64 (m, 2H, CH₂CH₂SH), 2.38 (t, $J=7.28$ Hz, 2H, CH₂COOH), 1.92-1.88 (m, 1H, CH₂CH₂SH), 1.77-1.71 (m, 1H, CH₂CH₂SH) 1.70-1.47 (m, 6H, 3xCH₂), 1.35 (t, $J=7.96$ Hz, 1H, SH), 1.30 (d, $J=7.64$ Hz, 1H, SH). ¹³C-NMR (100MHz, CDCl₃) δ (ppm) 22.3 (1C, CH₂), 24.3 (1C, CH₂), 26.4 (1C, CH₂), 33.8 (1C, CH₂), 38.7 (1C, CH₂), 39.3 (1C, CH), 42.7 (1C, CH₂), 179.6 (1C, C=O). I.R (KCl) ν_{\max} : 2935, 1707, 1427, 1135, 1282, 933cm⁻¹.

Experiment 2: Synthesis of TA-PEG₄₀₀-OH (**2**)^[15]

Neat PEG₄₀₀ (average MW 400g/mol) (10g, 25mmol) was heated under vacuum in a rotavapor at 60°C for 1h with stirring to remove traces of water. Thioctic acid (0.516g, 2.5mmol), 4-(dimethylamino)-pyridine (0.092g, 0.75mmol), and anhydrous dichloromethane (25mL) were added to the flask under argon. The reaction mixture was cooled to 0°C in an ice bath, and a solution of dicyclohexylcarbodiimide (DCC) (0.567g, 2.75mmol) in anhydrous dichloromethane (10mL) was added dropwise. The reaction mixture was stirred at 0°C for 1h before it was warmed to room temperature and stirred overnight. The white precipitate formed was filtered over a plug of celite and the filtrate washed with a saturated solution of sodium chloride (NaCl) (3x30mL). The combined organic extracts were dried over Na₂SO₄, filtered, and evaporated to give a yellow oil. The crude product was purified by silica

flash chromatography using a mixture of dichloromethane/methanol (9.5:0.5; R_f 0.38) and concentrated under vacuum to afford the product **2** as a yellow oil (0.77g, 77%).

$^1\text{H-NMR}$ (400MHz, CDCl_3): δ (ppm) 4.22 (t, $J=4.8$ Hz, 2H, $\text{OCH}_2\text{-PEG}$), 3.65 (m, ~32H, PEG), 3.12 (m, 2H, CH_2S), 2.67 (br s, 1H, CHS), 2.45 (m, 1H, CH_2CHS), 2.35 (t, $J=7.48$ Hz, 2H, CH_2COO), 1.91 (m, 1H, CH_2CHS), 1.68-1.47 (m, 6H, $3\times\text{CH}_2$). **$^{13}\text{C-NMR}$** (100MHz): δ (ppm) 24.5 (1C, CH_2), 28.7 (1C, CH_2), 33.9 (1C, CH_2), 34.6 (1C, CH_2), 38.5 (1C, CH_2S), 40.2 (1C, $\text{CH}_2\text{CH}_2\text{S}$), 56.3 (1C, CHS), 61.7 (1C, CH_2OH), 63.5 (1C, COOCH_2), 69.2 (1C, CH_2), 70.3-70.6 (~16C, $(\text{CH}_2\text{CH}_2\text{O})_{x-8}$, PEG), 72.5 (1C, CH_2), 173.5 (1C, C=O). **I.R** (KCl) ν_{max} : 3476, 2916, 2870, 2285, 1732, 1620, 1452, 1349, 1299, 1247, 1106, 946, 842cm^{-1} . **ESI-MS (m/z)**: $[\text{M}+\text{Na}]^+$ Calculated for $\text{C}_{26}\text{H}_{50}\text{NaO}_{11}\text{S}_2$: 625.2654; Found: 625.2687.

Experiment 3: Synthesis of DHLA-PEG₄₀₀-OH or Hydroxy-PEG₄₀₀ (**3**)^[15]

Ester **2** (0.768g, 1.92mmol) was dissolved in 7.6mL of a mixture ethanol/water (1:4 (v/v)) with stirring. NaBH_4 (0.08g, 2.12mmol) was added and stirred for 1h or until the solution became colourless. The reaction mixture was diluted with water (10mL) and extracted with chloroform (3x25mL). The combined organic phases were dried over sodium sulphate (Na_2SO_4), filtered, and concentrated under vacuum. The residue was purified by silica flash chromatography. Elution with dichloromethane/methanol (9:1; R_f 0.59) afforded **3** (0.594g, 77%) as a colourless oil.

$^1\text{H-NMR}$ (400MHz, CDCl_3): δ (ppm) 4.23 (t, $J=4.8$ Hz, 2H, $\text{OCH}_2\text{-PEG}$), 3.65 (m, ~32H, PEG), 2.92 (m, 1H, CHSH), 2.69 (m, 2H, CH_2SH), 2.35 (t, $J=7.4$ Hz, 2H, CH_2COO), 1.89 (m, 1H, CH_2CHSH), 1.79-1.70 (m, 1H, CH_2CHSH), 1.69-1.49 (m, 6H, $3\times\text{CH}_2$), 1.35 (t, $J=8$ Hz, 1H, SH), 1.31 (d, $J=7.64$ Hz, 1H, SH). **$^{13}\text{C-NMR}$** (100MHz): δ (ppm) 22.2 (1C, CH_2), 24.5 (1C, CH_2), 26.5 (1C, CH_2), 33.9 (1C, CH_2), 38.6 (1C, $\text{CH}_2\text{CH}_2\text{SH}$), 39.2 (1C, CH_2SH), 42.7 (1C, CHSH), 61.6 (1C, CH_2OH), 63.4 (1C, COOCH_2), 69.1 (1C, CH_2), 70.2-70.6 (~16C, $(\text{CH}_2\text{CH}_2\text{O})_{x-8}$, PEG), 72.5 (1C, CH_2), 173.5 (1C, C=O). **I.R** (KCl) ν_{max} : 3455, 2869, 2386, 1731, 1454, 1349, 1297, 1249, 1105, 948, 846cm^{-1} .

Experiment 4: Synthesis of Dichloride-PEG₄₀₀ (4) ^[18]

Neat PEG₄₀₀ (5.0 g, 12.5mmol) was heated under vacuum on a rotavapor at 60°C for 1h to remove traces of water. The flask was back-filled with argon and cooled on an ice bath before thionyl chloride (SOCl₂) (2.94mL, 37.5mmol) was slowly added. The solution was warmed to 25°C and stirred for 2h. The conversion was monitored by the disappearance of the broad O-H stretch at 3500 cm⁻¹ and the appearance of a C-Cl stretch at 739 cm⁻¹ in the IR spectrum. The product was diluted with anhydrous dimethylformamide (DMF) (6mL) and the solvent removed under reduced pressure. This step was repeated three (or more) times to remove all residual traces of thionyl chloride.

I.R (KCl) ν_{\max} : 2873, 1449, 1350, 1298, 1221, 994, 899, 739cm⁻¹

Experiment 5: Synthesis of Diazido-PEG₄₀₀ (5) ^[18]

Crude dichloride **4** was dissolved in a solution of sodium azide (3.25 g, 50.0mmol) in 86mL of DMF and stirred overnight at 85°C. The solvent was removed under reduced pressure, and 50mL of dichloromethane was added. The precipitate was removed by vacuum filtration and the solvent evaporated in vacuum to yield the intermediate diazide. The conversion was confirmed by the appearance of a sharp azide stretch at 2100 cm⁻¹ and the disappearance of the C-Cl stretch at 739 cm⁻¹ in the IR spectrum. The crude product obtained was purified by silica flash chromatography with a dichloromethane/methanol (9:1; *R_f*=0.55) mixture to afford **5** (6.011g) as a pale yellow oil.

¹H-NMR (400MHz, CDCl₃): δ (ppm) 3.69-3.64 (m, ~31H, PEG), 3.38 (t, *J*= 5.0 Hz, 4H, 2xCH₂-N₃). **¹³C-NMR** (100MHz): δ (ppm) 50.5 (2C, OCH₂CH₂-N₃), 69.9 (2C, OCH₂CH₂-N₃), 70.3-70.5 (~14C, (CH₂CH₂O) *x*~7, PEG). **I.R** (KCl) ν_{\max} : 2870, 2107, 1676, 1453, 1348, 1299, 1119, 945, 851cm⁻¹.

Experiment 6: Synthesis of Diamino-PEG₄₀₀ (6) ^[18]

Diazide **5** (6.011g, 15mmol) was dissolved in 94mL of anhydrous tetrahydrofuran (THF), and triphenylphosphine (8.67g, 33mmol) was added. The solution was stirred at 25°C for 4h before adding 1.24mL of water and stirring overnight. The THF was removed under vacuum, and 26mL of water

was added. The white precipitate was removed by vacuum filtration and the filtrate washed with toluene (3x50mL). The water phase was removed in vacuum to yield the pure product **6** as light-yellow oil (4.85 g, 97%).

¹H-NMR (400MHz, D₂O): δ (ppm) 3.62-3.61 (m, ~27H, PEG), 3.49 (t, $J=5.4$ Hz, 4H, OCH₂CH₂NH₂), 2.71 (t, $J=5.4$ Hz, 4H, OCH₂CH₂NH₂). **¹³C-NMR** (100MHz): δ (ppm) 39.8 (2C, OCH₂CH₂-NH₂), 69.3-69.6 (~14C, (CH₂CH₂O)_{x~7}, PEG), 72.1 (2C, OCH₂CH₂-NH₂). **I.R** (KCl) ν_{\max} : 2915, 1650, 1567, 1477, 1351, 1309, 1249, 1099, 946, 840cm⁻¹.

Experiment 7: Synthesis of TA-PEG₄₀₀-NH₂ (**7**)^[18]

To a solution of diamine **6** (4.29g, 11mmol) and sodium bicarbonate (0.924g, 11mmol) in 36mL of a dimethylformamide/water mixture (1:1) at 4°C was added dropwise a solution of lipoic acid *N*-hydroxysuccinimide ester (LA-NHS, **21**) (0.607g, 2.0mmol) (see Experiment 20) in 5mL of dimethylformamide over 1h. The solution was warmed to room temperature, stirred overnight, and extracted with chloroform (3x 20mL). The combined organic extracts were washed with water (3 x 20mL), dried over Na₂SO₄, and filtered, and the solvent was evaporated under vacuum. The crude product was purified by silica flash chromatography using a mixture of chloroform/methanol/water (7.5:2.2:0.3; $R_f=0.53$) to afford **7** as a yellow oil (0,520g, 65%).

¹H-NMR (400MHz, CDCl₃): δ (ppm) 3.83-3.80 (m, 2H, CH₂NH), 3.72-3.54 (m, ~40H, PEG), 3.47-3.39 (m, 2H, CH₂NH₂), 3.21-3.1 (m, 3H, CHS, CH₂S), 2.48-2.43 (m, 1H, CH₂CHS), 2.25-2.18 (m, 2H, CH₂COO), 1.93-1.98 (m, 1H, CH₂CHS), 1.73-1.41 (m, 6H, 3xCH₂). **¹³C-NMR** (100MHz): δ (ppm) 25.4 (1C, CH₂), 28.9 (1C, CH₂), 34.7 (1C, CH₂), 36.2 (1C, CH₂C=O), 38.5 (1C, CH₂CH₂S), 39.1 (1C, CH₂CH₂S), 40.5-40.6 (2C, CH₂NH₂, CH₂NH), 56.5 (1C, CH₂CHS), 69.7-70.6 (~14C, (CH₂CH₂O)_{x~7}, PEG), 173.2 (C=O). **I.R** (KCl) ν_{\max} : 3472, 2917, 1647, 1549, 1455, 1350, 1250, 1103, 949, 839, 753cm⁻¹. **ESI-MS (m/z)**: [M]⁺ Calculated for C₂₆H₅₃N₂O₉S₂: 601.3175; Found: 601.3187.

Experiment 8: Synthesis of DHLA-PEG₄₀₀-NH₂ or Amino-PEG₄₀₀ (**8**)^[18]

To a solution of **7** (0.457g, 1.14mmol) in 6.1mL of a mixture ethanol/water (4:1) at 4°C was slowly added 4 equivalents of sodium borohydride (NaBH₄)

(0.173g, 4.57mmol) over a 10 min period. The solution was stirred for 2h at 4°C. The mixture was then acidified to pH=2 with 3M HCl, and extracted with chloroform (3x 15mL). The combined organics were dried over Na₂SO₄ and filtered and the solvent removed under vacuum. The crude product was purified by silica flash chromatography. Elution with chloroform/methanol/water (7.5:2.2:0.3; *R_f*=0.38) afforded product **8** as a colourless oil (0,345g, 75%).

¹H-NMR (400MHz, CDCl₃): δ (ppm) 3.92-3.90 (m, 2H, CH₂NH), 3.74-3.58 (m, ~36H, PEG), 3.45 (m, 2H, CH₂NH₂), 3.20-3.0 (m, 3H, CHS, CH₂S), 2.48-2.44 (m, 1H, CH₂CHSH), 2.33-2.20 (m, 2H, CH₂COO), 1.93-1.88 (m, 1H, CH₂CHSH), 1.71-1.43 (m, 6H, 3xCH₂), 1.25-1.24 (m, 2H, 2xSH). **¹³C-NMR** (100MHz): δ (ppm) 25.3-25.6 (1C, CH₂CH₂SH), 28.9 (1C, CH₂), 34.6 (1C, CH₂), 35.8-36.2 (1C, CH₂C=O), 38.4 (1C, CH₂), 39.1 (1C, CH₂CH₂SH), 40.1-40.3 (2C, CH₂NH₂, CH₂NH), 56.4 (1C, CH₂CHSH), 60.1-70.4 (~14C, (CH₂CH₂O)_x-7, PEG), 173.4 (C=O). **I.R** (KCl) ν_{max}: 3466, 2917, 1648, 1549, 1454, 1350, 1250, 1105, 949, 842, 752cm⁻¹.

Experiment 9: Synthesis of TA-PEG₄₀₀-COOMe (**9**)^[18]

To a solution of **7** (1.23g, 3mmol) in 20mL of anhydrous dichloromethane at 0°C and under an argon atmosphere was added triethylamine (Et₃N) (0.842mL, 6mmol). Then, a solution of methylmalonylchloride (0.360mL, 3.4mmol) in 10mL of dichloromethane was slowly added at 0°C. The reaction mixture was kept at room temperature for 4h and the solvent removed under vacuum. The crude product was purified by silica flash chromatography using a dichloromethane/methanol (9:1; *R_f*=0.52) mixture to yield product **9** as a yellow oil (0.699g, 57%).

¹H-NMR (400MHz, CDCl₃): δ (ppm) 3.74 (m, 3H, OCH₃), 3.65-3.54 (m, ~34H, PEG), 3.50-3.45 (m, 4H, 2xCH₂), 3.35-3.33 (m, 1H, CHS), 3.18-3.1 (m, 2H, CH₂S), 2.48-2.43 (m, 1H, CH₂CHS), 2.23-2.19 (m, 2H, CH₂COO), 1.95-1.83 (m, 1H, CH₂CHS), 1.71-1.43 (m, 6H, 3xCH₂). **¹³C-NMR** (100MHz): δ (ppm) 25.5 (1C, CH₂), 28.8 (1C, CH₂), 34.6 (1C, CH₂), 36.6 (1C, CH₂C=O), 38.5 (1C, CH₂CH₂S), 39.5-39.7 (1C, C=OCH₂C=O), 40.2(1C, CH₂CH₂S), 41.4-41.5 (2C, (CH₂NH)_x2), 52.4(1C, CH₃), 56.4 (1C, CH₂CHS), 60.1-70.4

(~14C, (CH₂CH₂O)_x~7, PEG), 169.4 (3C, C=O). **I.R** (KCl) ν_{\max} : 3499, 3331, 2918, 2359, 2340, 1742, 1657, 1550, 1439, 1349, 1250, 1105, 949, 845cm⁻¹.

Experiment 10: Synthesis of TA-PEG₄₀₀-COOH (**10**)^[18]

Ester **9** (0.202g, 0.283mmol) was hydrolysed with 0.25M NaOH in 5mL of methanol for 5h at 60°C. After neutralizing to pH=7 with HCl 3M the solvent was removed under vacuum. The residue was dissolved in water, acidified to pH=2 and extracted with chloroform (3x10mL). The combined organic phases were dried with Na₂SO₄, filtered and the solvent evaporated under vacuum to yield the pure product **10** as a pale pink oil (0.181g, 91%).

¹H-NMR (400MHz, CDCl₃): δ (ppm) 3.66-3.63 (m, ~36H, PEG), 3.51-3.44 (m, 4H₂xCH₂), 3.38-3.36 (m, 1H, CHS), 3.19-3.1 (m, 2H, CH₂S), 2.48-2.43 (m, 1H, CH₂CHS), 2.25-2.17 (m, 2H, CH₂COO), 1.93-1.88 (m, 1H, CH₂CHS), 1.73-1.43 (m, 6H). **¹³C-NMR** (100MHz): δ (ppm) 25.4 (1C, CH₂), 28.8 (1C, CH₂), 34.6 (1C, CH₂), 36.1 (1C, CH₂C=O), 38.4 (1C, CH₂CH₂S), 38.8-39.2 (1C, C=OCH₂C=O), 39.5 (1C, CH₂CH₂S), 40.2 (2C, (CH₂NH)_x2), 56.4 (1C, CH₂CHS), 69.2-70.5 (~14C, (CH₂CH₂O)_x~7, PEG), 168.6-168.7 (1C, C=O), 168.8-168.9 (1C, C=O), 173.2-173.3 (1C, C=O). **I.R** (KCl) ν_{\max} : 3496, 3324, 2917, 1731, 1650, 1548, 1454, 1349, 1249, 1105, 948, 842, 752cm⁻¹. **ESI-MS (m/z):** [M]⁺ Calculated for C₂₉H₅₄N₂NaO₁₂S₂: 709.3021; Found: 709.3010.

Experiment 11: Synthesis of DHLA-PEG₄₀₀-COOH or Carboxy-PEG₄₀₀ (**11**)^[18]

To a solution of **10** (0.130g, 0.186mmol) in 0.25M sodium bicarbonate buffer (1.8mL) at 4°C was slowly added 4 equivalents of sodium borohydride (NaBH₄) (0.028g, 0.743mmol). The solution was stirred for 2h at 4°C, acidified to pH=2 with HCl 3M and extracted with chloroform (3x10mL). The combined organic phases were dried with Na₂SO₄, filtered and evaporated under vacuum to afford **11** as a colourless oil (0.123g, 95%).

¹H-NMR (400MHz, CDCl₃): δ (ppm) 3.66-3.55 (m, ~30H, PEG), 3.51-3.45 (m, 4H, 2xCH₂), 3.39-3.37 (m, 2H, CH₂), 2.99-2.91 (m, 1H, CHSH), 2.74-2.63 (m, 2H, CH₂SH), 2.27-2.21 (m, 2H, CH₂COO), 1.93-1.88 (m, 1H, CH₂CHSH), 1.79-1.71 (m, 1H, CH₂CHSH), 1.69-1.40 (m, 6H, 3xCH₂), 1.36 (t, J=8.0Hz,

1H, SH), 1.32 (d, $J=7.8\text{Hz}$, 1H, SH) $^{13}\text{C-NMR}$ (100MHz): δ (ppm) 22.2 (1C, $\text{CH}_2\text{CH}_2\text{SH}$), 25.2 (1C, CH_2), 26.2 (1C, CH_2), 29.7 (1C, CH_2), 36.1 (1C, $\text{CH}_2\text{C}=\text{O}$), 38.7 (1C, $\text{C}=\text{OCH}_2\text{C}=\text{O}$), 39.3 (1C, CH_2CHSH), 39.5 (2C, $(\text{CH}_2\text{NH})\times 2$), 42.7 (1C, $\text{CH}_2\text{CH}_2\text{SH}$) 69.1-70.5 (~14C, $(\text{CH}_2\text{CH}_2\text{O})\times \sim 7$, PEG), 168.72 (2C, $\text{C}=\text{O}$), 173.5 (1C, $\text{C}=\text{O}$). **I.R** (KCl) ν_{max} : 3402, 2917, 2360, 1729, 1650, 1550, 1454, 1349, 1249, 1103, 948, 836, 752cm^{-1} .

Experiment 12: Synthesis of Ditosyl-PEG₂₀₀₀ (12)

To a solution containing PEG₂₀₀₀ (8.75g, 4.38mmol) in 15mL of dry pyridine at 0°C, *p*-tosyl chloride (*p*-TsCl) (3.34g, 17.5mmol) and a catalytic amount of 4-(dimethylamino) pyridine (DMAP) was added. The reaction mixture was kept under stirring at room temperature during 48h. The pyridine was evaporated under vacuum and the white residue obtained was dissolved in dichloromethane (30mL). A saturated solution of sodium bicarbonate (NaHCO_3) was added and the aqueous phase extracted with ethyl acetate (3x30mL). The combined organic phases were dried with Na_2SO_4 , filtered and evaporated under vacuum. The crude product was purified by silica flash chromatography. Elution with dichloromethane/methanol (9:1; $R_f=0.5$) afforded product **12** as a yellow oil (4.882g, 48%).

$^1\text{H-NMR}$ (400MHz, CDCl_3): δ (ppm) 7.8 (d, $J=8.2\text{Hz}$, 4H, Ar), 7.34 (d, $J=8\text{Hz}$, 4H, Ar), 4.15 (t, $J=5\text{Hz}$, 4H, $2\times\text{CH}_2\text{OTs}$), 3.64 (m, PEG), 2.45 (s, 6H, $2\times\text{CH}_3$). $^{13}\text{C-NMR}$ (100MHz): δ (ppm) 21.5 (2C, $2\times\text{CH}_3$), 68.6 (1C, CH_2), 69.1 (1C, CH_2), 70.5-71.3 (~80C, $(\text{CH}_2\text{CH}_2\text{O})\times \sim 40$), 126.9-130.1 (8C, Ar), 132 (2C, q), 144.7 (2C, q). **I.R** (KCl) ν_{max} : 2872, 1596, 1466, 1352, 1296, 1249, 1177, 1109, 946, 842, 772cm^{-1} .

Experiment 13: Synthesis of Diazido-PEG₂₀₀₀ (13)

The reaction was carried out as in Experiment 5 using compound **12** (4.85g, 2.1mmol), sodium azide (NaN_3) (1.63g, 25mmol) and 43mL of dried dimethylformamide (DMF). The product **13** was obtained without purification as a pale yellow oil (4.02g, 96%).

$^1\text{H-NMR}$ (400MHz, CDCl_3): δ (ppm) 3.64 (m, PEG), 3.39 (t, $J=5\text{Hz}$, 4H, $2\times\text{CH}_2$). $^{13}\text{C-NMR}$ (100MHz): δ (ppm) 50.6 (2C, $\text{OCH}_2\text{CH}_2\text{-N}_3$), 69.9 (2C,

OCH₂CH₂-N₃), 70.3-70.6 (~78C, (CH₂CH₂O) x~39, PEG). **I.R** (KCl) ν_{\max} : 2882, 2360, 2103, 1467, 1359, 1279, 1147, 1114, 1060, 945, 842cm⁻¹.

Experiment 14: Synthesis of Diamino-PEG₂₀₀₀ (14)

The reaction was carried out as in Experiment 6 using diazide **13** (4.017g, 2mmol) dissolved in 25mL of dried THF, triphenylphosphine (PPh₃) (2.32g, 8.84mmol) and 0.332mL of water. The THF was removed under vacuum, and 10mL of water was added. The white precipitate was removed by vacuum filtration and the filtrate washed with toluene (3x50mL). The water phase was removed in vacuum to yield product **14** as pale yellow oil (3.722g, 93%).

¹H-NMR (400MHz, D₂O): δ (ppm) 3.62 (m, PEG), 3.51 (t, $J=5.4$ Hz, 4H, 2xCH₂), 2.75 (t, $J=5.4$ Hz, 4H, 2xCH₂). **¹³C-NMR** (100MHz): δ (ppm) 39.7 (2C, OCH₂CH₂-NH₂), 69.3-69.8 (~78C, (CH₂CH₂O)x~39, PEG), 71.5 (2C, OCH₂CH₂-NH₂). **I.R** (KCl) ν_{\max} : 2885, 1467, 1344, 1280, 1241, 1147, 1112, 1060, 962, 842cm⁻¹.

Experiment 15: Synthesis of TA-PEG₂₀₀₀-NH₂ (15)

The reaction was carried out as in Experiment 7 using compound **14** (1.38g, 0.69mmol) dissolved in 28mL of a dimethylformamide/water mixture, sodium bicarbonate (0.058g, 0.69mmol) and LA-NHS (**21**) (see Experiment 20) (0.038g, 0.125mmol) dissolved in 5mL of DMF. The crude product was purified by flash chromatography. Elution with chloroform/methanol/water (7.5:2.2:0.3; $R_f=0.63$) afforded amine **15** as a yellow oil (0.197g, 79%).

¹H-NMR (400MHz, CDCl₃): 3.91 (t, $J=4.8$ Hz, 1H, CH₂NH), 3.81 (t, $J=5$ Hz, 1H, CH₂NH), 3.76-3.52 (m, PEG), 3.49-3.42 (m, 2H, CH₂NH₂), 3.19-3.1 (m, 3H, CH₂S, CH₂S), 2.48-2.42 (m, 1H, CH₂CHS), 2.19 (t, $J=7.5$ Hz, 2H, CH₂COO), 1.95-1.88 (m, 1H, CH₂CHS), 1.73-1.43 (m, 6H, 3xCH₂). **¹³C-NMR** (100MHz): δ (ppm) 25.3 (1C, CH₂), 28.9 (1C, CH₂), 34.6 (1C, CH₂), 36.3 (1C, CH₂C=O), 38.4 (1C, CH₂CH₂S), 39.1 (1C, CH₂CH₂S), 40.1-40.4 (2C, CH₂NH₂, CH₂NH), 56.4 (1C, CH₂CHS), 69.7-70.6 (~80C, (CH₂CH₂O) x~40, PEG), 173 (C=O). **I.R** (KCl) ν_{\max} : 3465, 2885, 1648, 1554, 1467, 1344, 1282, 1243, 1112, 950, 842cm⁻¹.

Experiment 16: Synthesis of DHLA-PEG₂₀₀₀-NH₂ or Amino-PEG₂₀₀₀ (16)

The reaction was carried out as in Experiment 8, using compound **15** (0.117g, 0.060mmol) dissolved in 1.56mL of a mixture ethanol/water (4:1) at 4°C and 4 equivalents of NaBH₄ (0.009g, 0.23mmol). The crude product was purified by silica flash chromatography using a chloroform/methanol/water (7.5:2.2:0.3; *R_f*=0.51) mixture to yield the product **16** as a colourless oil (0.099g, 85%).

¹H-NMR (400MHz, CDCl₃): δ (ppm) 3.92 (t, *J*=4.8Hz, 1H, CH₂NH), 3.81 (t, *J*=5Hz, 1H, CH₂NH), 3.76-3.54 (m, PEG), 3.47-3.43 (m, 2H, CH₂NH₂), 2.92-2.91 (m, 1H, CHSH), 2.74-2.65 (m, 2H, CH₂SH), 2.19 (t, *J*=7.4Hz, 2H), 1.93-1.88 (m, 1H, CH₂CHSH), 1.78-1.71(m, 1H, CH₂CHSH), 1.69-1.41 (m, 6H, 3xCH₂), 1.35 (t, *J*=7.96Hz, 1H, SH), 1.31 (d, *J*=7.4Hz, 1H, SH). **I.R** (KCl) ν_{max}: 3527, 2873, 2360, 1650, 1548, 1465, 1348, 1282, 1247, 1112, 948, 844cm⁻¹.

Experiment 17: Synthesis of TA-PEG₂₀₀₀-COOMe (17)

The reaction was carried out as in Experiment 9 using compound **15** (0.200g, 0.1mmol) and triethylamine (28μL, 0.2mmol) dissolved in 4mL of dried dichloromethane and methylmalonylchloride (12μL, 0.11mmol) dissolved in 1mL of CH₂Cl₂. The crude product was purified by flash chromatography. Elution with dichloromethane/methanol (9:1; *R_f*=0.44) afforded methylester **17** as yellow viscous residue (0.197g, 98%).

¹H-NMR (400MHz, CDCl₃): δ (ppm) 3.81 (t, *J*=4.9Hz, 2H, CH₂NH), 3.74 (s, 3H, OCH₃), 3.66-3.54 (m, PEG), 3.50-3.45 (m, 5H, CH₂NH₂, CHS), 3.33 (s, 2H, CH₂), 3.18-3.1 (m, 2H, CH₂S), 2.48-2.43 (m, 1H, CH₂CHS), 2.21 (t, *J*=7.5Hz, 2H, CH₂COO), 1.93-1.88 (m, 1H, CH₂CHS), 1.71-1.43 (m, 6H, 3xCH₂). **¹³C-NMR** (100MHz): δ (ppm) 25.4 (1C, CH₂), 28.9 (1C, CH₂), 34.6 (1C, CH₂), 36.2 (1C, CH₂C=O), 38.4 (1C, CH₂CH₂S), 39.2-39.4 (1C, C=OCH₂C=O), 40.2(1C, CH₂CH₂S), 41.5 (2C, (CH₂NH)x2), 52.3 (1C, CH₃), 56.4 (1C, CH₂CHS), 69.6-70.5 (~80C,(CH₂CH₂O)x~40, PEG), 165.1 (2C, C=O), 173 (1C, C=O). **I.R** (KBr) ν_{max}: 3450, 2888, 1741, 1658, 1550, 1467, 1344, 1280, 1241, 1147, 1112, 1060, 962, 842cm⁻¹.

Experiment 18: Synthesis of TA -PEG₂₀₀₀-COOH (18)

Ester hydrolysis was carried out as in Experiment 10, using compound **17** (0.172g, 0.086mmol) dissolved in 5mL of a NaOH 0.25M solution prepared in methanol. The product **18** was obtained as a yellow viscous residue (0.134g, 78%).

¹H-NMR (400MHz, CDCl₃): δ (ppm) 3.81 (t, $J=4.9$ Hz, 1H, CH₂NH), 3.69-3.54 (m, PEG), 3.51-3.44 (m, 5H, CH₂NH₂, CHS), 3.36 (s, 2H, CH₂), 3.18-3.1 (m, 2H, CH₂S), 2.50-2.42 (m, 1H, CH₂CHS), 2.24 (t, $J=7.5$ Hz, 2H, CH₂COO), 1.93-1.88 (m, 1H, CH₂CHS), 1.73-1.45 (m, 6H, 3xCH₂). **¹³C-NMR** (100MHz): δ (ppm) 25.4 (1C, CH₂), 28.9 (1C, CH₂), 34.6 (1C, CH₂), 36.1 (1C, CH₂C=O), 38.4 (1C, CH₂CH₂S), 39.3 (1C, C=OCH₂C=O), 40.1 (1C, CH₂CH₂S), 40.2 (2C, (CH₂NH)x2), 56.4 (1C, CH₂CHS), 69.1-70.6 (~80C, (CH₂CH₂O)x~40, PEG), 168.6-168.7 (1C, C=O), 168.8-168.9 (1C, C=O), 173.2-173.3 (1C, C=O). **I.R** (KBr) ν_{\max} : 3448, 2886, 1735, 1656, 1548, 1467, 1344, 1280, 1241, 1114, 962, 842cm⁻¹.

Experiment 19: Synthesis of DHLA-PEG₂₀₀₀-COOH or Carboxy-PEG₂₀₀₀ (19)

The reaction was carried out as in Experiment 11 using compound **18** (0.106g, 0.053mmol), 1.5mL of 0.25M bicarbonate buffer and 4 equivalents of sodium borohydride (0.008g, 0.21mmol). The pure product **19** was obtained as colourless oil (0.105g, 99%).

¹H-NMR (400MHz, CDCl₃): δ (ppm) 3.81 (t, $J=4.8$ Hz, 2H, CH₂NH), 3.70-3.55 (m, PEG), 3.51-3.45 (m, 3H, CH₂NH₂), 3.36 (s, 2H, CH₂), 2.93-2.88 (m, 1H, CHSH), 2.74-2.63 (m, 2H, CH₂SH), 2.20 (t, $J=7.4$ Hz, 2H, CH₂COO), 1.95-1.85 (m, 1H, CH₂CHSH), 1.79-1.71 (m, 1H, CH₂CHSH), 1.69-1.41 (m, 6H, 3xCH₂), 1.35 (t, $J=7.98$ Hz, 1H, SH), 1.31 (d, $J=7.68$ Hz, 1H, SH). **I.R** (KCl) ν_{\max} : 3397, 2883, 1733, 1656, 1548, 1467, 1359, 1344, 1280, 1241, 1147, 1112, 1062, 946, 842cm⁻¹.

Experiment 20: Synthesis of *N*-hydroxysuccinimidyl (NHS) ester of lipoic acid (LA-NHS) (21)^[18]

To a solution of thioctic acid (1.0g, 4.85mmol) and *N*-hydroxysuccinimide (0.669 g, 5.82mmol) in 30mL of dried THF at 4°C was added slowly a solution of dicyclohexylcarbodiimide (DCC) (1.2g, 5.82mmol) in 10mL of THF. The mixture was warmed to room temperature and stirred for 5h. The precipitate was removed by vacuum filtration and the solvent evaporated in vacuum. The crude product was redissolved in 100mL of ethyl acetate and filtered once more by vacuum filtration. The product was recrystallized from a solution of ethyl acetate/hexane (1:1; $R_f=0.45$) to yield the pure product **21** as a pale-yellow solid (1.03g, 70%).

m.p.: 90-92°C (Lit.^[29] 90-91°C). **¹H-NMR** (400MHz, CDCl₃): δ (ppm) 3.60-3.55 (m, 1H, CHS), 3.22-3.1 (m, 2H, CH₂S), 2.84 (s, 4H, 2xCH₂, NHS), 2.63 (t, $J=7.4$ Hz, 2H, CH₂COO), 2.51-2.43 (m, 1H, CH₂CHS), 1.97-1.88 (m, 1H, CH₂CHS), 1.83-1.53 (m, 6H, 3xCH₂). **¹³C-NMR** (100MHz): δ (ppm) 24.4 (1C, CH₂), 25.6 (2C, (CH₂)x2), 28.3 (1C, CH₂), 30.5 (CH₂CH₂O), 34.6 (1C, CH₂), 38.5 (CH₂CH₂S), 40.1 (1C, CH₂CH₂S), 56.1 (1C, CH₂CHCH₂S), 168.4 (1C, C=O), 169.1 (2C, C=O). **I.R** (KBr) ν_{\max} : 2939, 2860, 1811, 1781, 1731, 1455, 1424, 1374, 1206, 1142, 1074, 990, 936, 896, 879, 810, 792, 647cm⁻¹.

Experiment 21: Synthesis of *N*-maleoyl- β -alanine (22)^[30]

β -alanine (4.0g, 45mmol) was added to a stirred solution of maleic anhydride (4.41g, 45mmol) in glacial acetic acid (45mL). After stirring for 3h the reaction product was filtered off, dried and recrystallized with hexane. The pure product **22** was obtained as a white solid (7,534g, 90%).

m.p.: 169.2-171.8°C. **¹H-NMR** (400MHz, (CD₃)₂SO): δ (ppm) 9.1 (m, 1H, NH), 6.4 (d, $J=12.4$ Hz, 1H, CH), 6.25 (d, $J=12.4$ Hz, 1H, CH), 3.4-3.35 (dd, $J=6.6$ Hz, $J=5.76$ Hz, 2H, CH₂), 2.47 (s, 2H, CH₂COOH). **¹³C-NMR** (100MHz): δ (ppm) 32.9 (1C, CH₂COOH), 3.5 (1C, CH₂), 131.3 (1C, CH), 132.7 (1C, CH), 165.3 (1C, C=O), 165.6 (1C, C=O), 172.6 (1C, C=O).

Experiment 22: Synthesis of 3-maleimido propionic acid (23)^[31]

A mixture of compound **22** (5.052g, 27.3mmol), sodium acetate (4.476g, 54.6mmol) and 26mL of acetic anhydride were stirred for 3h at 55-60°C. The mixture was allowed to cool to room temperature. After acidifying until pH 1 with HCl 1M, the mixture was extracted with ethyl acetate (3x20mL). The combined organic phases were dried with Na₂SO₄, filtered and evaporated under vacuum. The crude product was purified by silica flash chromatography. Elution with dichloromethane/methanol (9:1; *R_f*=0.58) give a pale yellow solid which was then recrystallized using a ethyl acetate/hexane (1:1) mixture to afford acid **23** as a white solid (1.110g, 24%).

m.p.: 108.1-109.5°C (Lit.^[32] 105-105.5°C). **¹H-NMR** (400MHz, CDCl₃): δ (ppm) 9.5 (br s, 1H, OH), 6.73 (s, 2H, 2xCH), 3.83 (t, *J*=7.2Hz, CH₂), 2.70 (t, *J*=7.2Hz, CH₂COOH). **¹³C-NMR** (100MHz): δ (ppm) 32.4 (1C, CH₂COOH), 33.2 (1C, CH₂), 134.2 (2C, 2xCH), 170.3 (2C, 2xC=O), 176.4 (1C, C=O).

Experiment 23: Synthesis of 3-maleimido propionic acid N-hydroxysuccinimide ester (24) – via compound 23^[33]

To a solution of acid **23** (0.113g, 0.67mmol) and *N*-hydroxysuccinimide (0.093g, 0.80mmol) in 3mL of dried THF at 0°C was added slowly to a solution of dicyclohexylcarbodiimide (DCC) (0.166g, 0.80mmol) in 2mL of THF. After 5 minutes at 0°C the solution was stirred overnight at room temperature. The resulting suspension was filtered. The obtained filtrate was evaporated under vacuum. The crude product was purified by silica flash chromatography. Elution with a dichloromethane/methanol (9:1, *R_f*=0.95) mixture give a pale yellow oil which was then recrystallized with ethyl acetate/hexane (1:1) to afford NHS ester **24** as a white solid (0.103g, 58%).

m.p.: 167-171°C (Lit.^[33] 164-166°C). **¹H-NMR** (400MHz, CDCl₃): δ (ppm) 6.73 (s, 2H, 2xCH), 3.93 (t, *J*=6.96Hz, 2H, CH₂), 3.0 (t, *J*=7Hz, 2H, CH₂), 2.82 (s, 4H, 2XCH₂). **¹³C-NMR** (100MHz): δ (ppm) 25.5 (2C, 2xCH₂), 29.7 (1C, CH₂), 32.9 (1C, CH₂), 134.3 (2C, 2xCH), 165.7 (1C, C=O), 168.7 (1C, C=O), 170.0 (1C, C=O).

Experiment 24: Synthesis of 3-maleimido propionic acid *N*-hydroxysuccinimide ester (24**) – via compound **22** ^[33]**

To a solution of **22** (0.580g, 3.13mmol) dissolved in 7mL of anhydrous dimethylformamide (DMF), NHS (0.450g, 3.91mmol) and DCC (1.292g, 6.26mmol) were added at 0°C. After 5 minutes at 0°C, the solution was stirred for 4h at room temperature. The resulting suspension was filtered. 20mL of water was then added to the filtrate. The aqueous phase was extracted with CH₂Cl₂ (3x20mL). The combined organic phases were dried with Na₂SO₄, filtered and evaporated under vacuum. The crude product was purified by silica flash chromatography. Elution with dichloromethane/methanol (9:1; *R_f*=0.95) afforded NHS ester **24** as a white solid (0.362g, 46%).

The spectroscopic characterization of NHS ester **24** was described in the previous experiment.

Experiment 25: Synthesis of Mannose Pentaacetate (25**)**

The synthesis of sugar **25** was carried out according to procedure described in the literature ^[34, 35] and was obtained in quantitative yield.

Experiment 26: Synthesis of Monotosyl-TEG (26**)**

TEG (1.0 g, 6.7mmol) was heated under vacuum in a rotavapor at 60 °C for 1h with stirring to remove traces of water and then dissolved in 15mL of dry pyridine. The flask was back-filled with argon and cooled on an ice bath before *p*-tosyl chloride (1.41g, 7.4mmol) was slowly added and a catalytic amount of DMAP. The solution was warmed to room temperature and stirred for 30 minutes. The solvent was removed under reduced pressure and the residue obtained diluted in dichloromethane and stirred with sodium bicarbonate saturated solution during 30 minutes. The mixture was extracted with ethyl acetate (3x20mL). The combined organic extracts were dried over Na₂SO₄ and filtered and the solvent evaporated under vacuum. The crude product was purified by silica flash chromatography using a dichloromethane/methanol (9.5:0.5, *R_f*=0.29) mixture to yield **26** as yellow oil (0.922g, 45%).

¹H-NMR (400MHz, CDCl₃): δ (ppm) 7.8 (d, *J*=8.2Hz, 2H, Ar), 7.3 (d, *J*=8.1Hz, 2H, Ar), 4.16 (t, *J*=4.8Hz, 2H, CH₂OTs), 3.69 (t, *J*=4.7Hz, 4H, 2xCH₂, TEG),

3.60 (s, 4H, 2xCH₂, TEG), 3.57 (t, *J*=4.6Hz, 2H, CH₂OH), 2.44 (s, 3H, CH₃). ¹³C-NMR (100MHz): δ (ppm) 21.5 (1C, CH₃), 61.6 (1C, CH₂OH), 68.5 (1C, CH₂OS), 69.1 (1C, CH₂), 70.1 (1C, CH₂), 70.6 (1C, CH₂), 72.4 (1C, CH₂), 127.9 (2C, CH), 129.8 (2C, CH), 132.8 (1C, q), 144.8 (1C, q). I.R (KCl) ν_{max}: 2877, 1598, 1452, 1353, 1297, 1245, 1176, 1122, 1012, 919, 815, 773, 663cm⁻¹.

Experiment 27: Synthesis of AcMannose-TEG-Tosyl (27)

Mannose pentaacetate (**25**) (0.331g, 0.85mmol) and monotosylated TEG (**26**) (0.775g, 2.55mmol) were dissolved in 5mL of CH₂Cl₂ and cooled to 0°C. Boron trifluoride diethyl etherate (BF₃.Et₂O) (0.428mL, 3.4mmol) was added and stirred at room temperature for 48h. The reaction was quenched with triethylamine and water and extracted with CH₂Cl₂. The combined organic extracts were dried over Na₂SO₄, filtered and the solvent evaporated under vacuum. The crude product was purified by silica flash chromatography using a hexane/ethyl acetate (1:9, *R_f*=0.26) to yield **27** as yellow oil (0.130g, 57%). ¹H-NMR (400MHz, CDCl₃): δ (ppm) 7.8 (d, *J*=8.3Hz, 2H, Ar), 7.3 (d, *J*=8.1Hz, 2H, Ar), 5.35-5.25 (m, 2H, CH₂-O-sugar), 4.86 (s, 1H, sugar), 4.29-4.08 (m, 6H, sugar), 3.71-3.59 (m, 10H, TEG), 2.45 (s, 3H, CH₃, OTs), 2.18-1.99 (m, 12H, 4xOAc). ¹³C-NMR (100MHz): δ (ppm) 20.9-21.5 (5C, 5xCH₃), 62.4 (1C, CH₂) 66.1 (1C, CH), 67.3 (1C, CH₂), 68.2-68.3 (1C, CH), 68.7 (1C, CH₂), 69 (1C, CH), 69.1-69.2 (1C, CH₂), 69.5 (1C, CH), 69.9 (1C, CH₂), 70.4 (1C, CH₂), 70.5-70.6 (1C, CH₂), 97.6 (1C, CH), 127.9 (2C, CH-Ar), 129.8 (2C, CH-Ar), 133 (1C, q), 144.8 (1C, q), 169.6-170.6 (4C, C=O). I.R (KCl) ν_{max}: 2942, 1752, 1598, 1452, 1369, 1243, 1178, 1139, 1083, 1049, 1018, 977, 921, 817, 757, 665cm⁻¹.

Experiment 28: Synthesis of AcMannose-TEG-Cl (28)

The compound **28** was prepared according to a reported procedure^[23] and was obtained in 96% of yield.

Experiment 29: Synthesis of AcMannose-TEG-SAc (29) ^[23]

AcMannose-TEG-OTs (**27**) (0.124g, 0.195mmol) and potassium thioacetate (0.067g, 0.59mmol) were dissolved in 3mL of dry DMF and stirred at room temperature for 12h. Ethyl acetate (10mL) was added to the mixture and the organic phase was washed with water (5x10mL), dried with Na₂SO₄, filtered and the solvent evaporated under vacuum. The crude product was purified by silica flash chromatography. Elution with hexane/ethyl acetate (4:6, R_f=0.47) afforded **29** as colourless oil (0,071g, 67%).

¹H-NMR (400MHz, CDCl₃): δ (ppm) 5.29-5.26 (m, 2H, CH₂-O-sugar), 4.87 (s, 1H, sugar), 4.32-4.27 (m, 1H, sugar), 4.11-4.06 (m, 2H, sugar), 3.81-3.80 (m, 1H, sugar), 3.69-3.59 (m, ~10H, TEG), 3.10 (t, J=6.44Hz, 2H, CH₂SAc), 2.33 (s, 3H, SAc), 2.15 (s, 3H, OAc), 2.10 (s, 3H, OAc), 2.05 (s, 3H, OAc), 1.99 (s, 3H, OAc). **¹³C-NMR** (100MHz): δ (ppm) 20.6-20.8 (4C, CH₃, 4xOAc), 28.7 (1C, CH₂, CH₂-SAc), 30.5 (1C, CH₃, SAc), 62.4 (1C, CH₂), 66.1 (1C, CH), 67.3 (1C, CH₂), 68.3-69.05 (3C, CH), 69.8-70.6 (4C, CH₂, TEG), 97.7 (1C, CH), 166.7-170.6 (4C, C=O, OAc), 195.5 (1C, C=O, SAc). **I.R** (KCl) ν_{max} : 2933, 1749, 1691, 1434, 1369, 1226, 1137, 1085, 1047, 977, 703, 626cm⁻¹.

Experiment 30: Synthesis of thiol linker, Mannose-TEG-SH (30) ^[23]

AcMannose-TEG-SAc (**29**) (0.064g, 0.12mmol) and a catalytic amount (0.1 equivalents) of sodium methoxide were dissolved in MeOH at room temperature for 30 minutes. The reaction mixture was neutralized until pH 7 with Dowex resin (50WX8-100) and water. The resin was filtered off and washed with MeOH and the solvent evaporated under vacuum. The crude product was dissolved in CHCl₃ and washed with water. The combined aqueous phase was evaporated under vacuum to yield **30** as colourless oil (0,023g, 59%).

¹H-NMR (400MHz, D₂O): δ (ppm) 4.81 (s, 1H, CH-sugar), 3.89-3.73 (m, 4H, 4xCH-sugar), 3.69-3.56 (m, 12H, TEG and CH₂-sugar), 2.65 (t, J=6.2Hz, 2H, CH₂-SH). **¹³C-NMR** (100MHz): δ (ppm) 23.1 (1C, CH₂-SH), 60.9 (1C, CH₂-OH), 66.4 (1C, CH₂, TEG), 66.7 (1C, CH), 69.2-69.6 (3C, 3xCH₂, TEG), 69.9 (1C, CH), 70.4 (1C, CH), 72.2 (1C, CH₂, TEG), 72.7 (1C, CH), 99.9 (1C, CH). **I.R** (KCl) ν_{max} : 3390, 2925, 1737, 1643, 1461, 1353, 1245, 1133, 1093, 1060,

975, 885, 809 cm^{-1} . **ESI-MS (m/z):** $[\text{M}+\text{M}+\text{Na}]^+$ Calculated for $\text{C}_{24}\text{H}_{46}\text{NaO}_{16}\text{S}_2$: 677.2098; Found: 677.2100.

Experiment 31: Synthesis of AcMannose-TEG-N₃ (31)

Compound **28** (0.652g, 1.3mmol) was dissolved in a solution of sodium azide (0.254 g, 3.9mmol) in 11mL of DMF and stirred overnight at 85°C. The solvent was removed under reduced pressure, and 20mL of dichloromethane was added. The precipitate was removed by vacuum filtration and the solvent evaporated in vacuum to yield the pure azide **31** as a yellow oil (0.625g, 95%). The conversion was confirmed by the appearance of a sharp azide stretch at 2109 cm^{-1} in the IR spectrum.

¹H-NMR (400MHz, CDCl_3): δ (ppm) 5.31-5.29 (m, 2H, CH_2 -O-sugar), 4.87 (s, 1H, sugar), 4.30-4.21 (m, 2H, sugar), 4.12-4.08 (m, 2H, sugar), 3.82-3.81 (m, 1H, sugar), 3.72-3.65 (m, ~6H, TEG), 3.41-3.38 (m, 4H, $\text{OCH}_2\text{CH}_2\text{N}_3$), 2.15 (s, 3H, OAc), 2.10 (s, 3H, OAc), 2.04 (s, 3H, OAc), 1.99 (s, 3H, OAc). **¹³C-NMR** (100MHz): δ (ppm) 20.8 (4C, CH_3 , 4xOAc), 50.6 (1C, CH_2 , CH_2 -N₃), 62.3 (1C, CH_2 -sugar), 66.1 (1C, CH), 63.5 (1C, CH_2 -O-sugar), 66.1 (1C, CH-sugar), 67.3 (1C, $\text{CH}_2\text{CH}_2\text{N}_3$), 68.3 (1C, CH-sugar), 69.0 (1C, CH-sugar), 69.1 (1C, CH_2 , TEG), 69.5 (1C, CH-sugar), 70.0 (1C, CH_2 , TEG), 70.6 (1C, CH_2 , TEG), 97.6 (1C, CH-O-sugar), 169.6 (4C, C=O, OAc). **I.R** (KCl) ν_{max} : 2875, 2109, 1747, 1442, 1371, 1230, 1137, 1085, 1049, 979 cm^{-1} .

Experiment 32: Synthesis of AcMannose-TEG-NH₂ (32)

Azide **31** (0.591g, 1.17mmol) was dissolved in 5mL of anhydrous tetrahydrofuran (THF), and triphenylphosphine (0.337g, 1.29mmol) was added. The solution was stirred at room temperature for 4h before adding 50 μL of water and stirring overnight. The THF was removed in vacuum, and water (2mL) was added. The resulting white precipitate was removed by vacuum filtration and the filtrate washed with toluene (3x10mL). The water phase was removed in vacuum to yield **32** as a light-yellow oil (0.432g, 77%). Compound **32** was used in the following step without any purification. Due to the limited solubility in water it was difficult to carry out the purification. For this reason no spectroscopic characterization is presented.

Experiment 33: Synthesis of AcMannose-TEG-TA (33)

To a solution of compound **32** (0.430g, 0.9mmol) and sodium bicarbonate (0.075g, 0.9mmol) in 5mL of a dimethylformamide/water mixture (1:1) at 4°C, a solution of LA-NHS (**21**) (0.272g, 0.9mmol) in 1mL of dimethylformamide was added. This solution was allowed to warm to room temperature, stirred overnight, and extracted with chloroform (3x 10mL). The combined organic extracts were washed with water (3 x 10mL), dried over Na₂SO₄, filtered, and the solvent was evaporated under vacuum. The crude product was purified by silica flash chromatography using a dichloromethane/methanol (9:1) mixture to give **33** as yellow oil.

Compound **33** (0.428g, 0.64mmol) was dissolved in 5mL of dry pyridine. The flask was back-filled with argon and cooled on an ice bath before acetic anhydride (0.364mL, 3.85mmol) and a catalytic amount of DMAP were added and the mixture was stirred for 12h at room temperature. The mixture was slowly added with stirring at 0°C to an Erlenmeyer containing a saturated solution of NaHCO₃ (20mL). The solution was extracted with CH₂Cl₂ (3x20mL). The combined organic extracts were dried over Na₂SO₄, filtered and the solvent evaporated under vacuum. The crude product was purified by silica flash chromatography. Elution with dichloromethane/methanol (9:1, *R_f*=0.55) afforded **33** as a yellow oil (0.329g, 77%).

¹H-NMR (400MHz, CDCl₃): δ (ppm) 5.37-5.26 (m, 2H, CH₂-O-sugar), 4.89 (s, 1H, CH-sugar), 4.30-4.26 (m, 1H, CH-sugar), 4.13-4.05 (m, 2H, 2xCH-sugar), 3.85-3.81 (m, 1H, CH-sugar), 3.72-3.54 (m, ~10H, TEG and CH₂-sugar), 3.47-3.43 (m, 1H, CHS), 3.19-3.09 (m, 2H, CH₂S), 2.48-2.43 (m, 1H, CH₂CHS), 2.20 (t, *J*=7.6Hz, 2H, CH₂COO), 2.16 (s, 3H, CH₃, OAc), 2.10 (s, 3H, CH₃, OAc), 2.04 (s, 3H, CH₃, OAc), 1.99 (s, 3H, CH₃, OAc), 1.93-1.88 (m, 1H, CH₂CHS), 1.73-1.43 (m, ~6H, TA). **¹³C-NMR** (100MHz): δ (ppm) 20.7 (4C, CH₃, 4xOAc), 25.3 (1C, CH₂, TA), 28.8 (1C, CH₂, TA), 34.6 (1C, CH₂, TA), 36.3 (1C, CH₂CO, TA) 38.4 (1C, CH₂S, TA), 39.1 (CH₂CH₂S, TA), 40.1 (1C, CH₂, CH₂-NH), 56.4 (1C, CHS, TA), 62.4 (1C, CH₂-sugar), 66.0 (1C, CH-sugar), 67.4 (1C, CH₂-O-sugar), 68.4 (1C, CH-sugar), 69.0 (1C, CH-sugar), 69.5 (1C, CH-sugar), 69.9-70.6 (4C, CH₂, TEG), 97.6 (1C, CH-O-sugar), 169.6-169.9 (4C, C=O, OAc), 170.0 (1C, C=O, TA).

Experiment 34: Synthesis of Mannose-TEG-TA (34)

AcMannose-TEG-TA (**33**) (0.278g, 0.42mmol) and 1 equivalent of sodium methoxide (0.022g, 0.42mmol) were dissolved in 2mL of MeOH and reacted at room temperature for 1h. The reaction mixture was neutralized to pH 7 with Dowex (50WX8-100) resin and water. The reaction was then filtered, the resin washed with MeOH and the solvent evaporated under vacuum to yield **34** as a pale yellow oil (0.205g, 98%).

¹H-NMR (400MHz, D₂O): δ (ppm) 4.80 (s, 1H, CH-sugar), 3.88-3.87 (m, 1H, CH-sugar), 3.82-3.53 (m, ~16H, TEG/sugar), 3.31 (t, $J=5.3$ Hz, 2H, CHS), 3.19-3.07 (m, 2H, CH₂S), 2.45-2.37 (m, 1H, CH₂CHS), 2.18 (t, $J=7.2$ Hz, 2H, CH₂, CH₂CO), 1.95-1.86 (m, 1H, CH₂CHS), 1.69-1.31 (m, 6H, 3xCH₂). **¹³C-NMR** (100MHz): δ (ppm) 25.0 (1C, CH₂, TA), 27.8 (1C, CH₂, TA), 33.7 (1C, CH₂, TA), 35.4 (1C, CH₂CO, TA) 38.1 (1C, CH₂S, TA), 38.9 (CH₂CH₂S, TA), 40.3 (1C, CH₂, CH₂-NH), 56.5 (1C, CHS, TA), 60.9 (1C, CH₂-sugar), 66.3 (1C, CH₂-O-sugar), 66.7 (1C, CH-sugar), 68.9 (1C, CH₂, TEG), 69.4-69.6 (3C, CH₂, TEG), 69.9 (1C, CH-sugar), 70.5 (1C, CH-sugar), 72.7 (1C, CH-sugar), 99.9 (1C, CH-O-sugar), 176.9 (1C, C=O, TA). **I.R** (KCl) ν_{\max} : 3388, 2929, 1643, 1550, 1450, 1351, 1247, 1137, 1060, 1029, 973, 881, 809cm⁻¹. **ESI-MS (m/z)**: [M+Na]⁺ Calculated for C₂₀H₃₇NaNO₉S₂: 522.1824; Found: 522.1859.

Experiment 35: Synthesis of Mannose-TEG-DHLA (35)

To a solution of compound **34** (0.235g, 0.47mmol) in 3.1mL of a mixture ethanol/water (1:4) at 4°C was slowly added 4 equivalents of sodium borohydride (NaBH₄) (0.071g, 1.88mmol). The solution was stirred for 2h at 4°C. The mixture was then acidified to pH 2 with 3M HCl, and extracted with chloroform (3x 15mL). The combined organics were dried over Na₂SO₄, filtered and the solvent removed under vacuum. The crude product was purified by silica flash chromatography using a chloroform/methanol/water (7.5:2.2:0.3, R_f=0.53) mixture to yield **35** as a colourless oil (0.172g, 73%).

¹H-NMR (400MHz, D₂O): δ (ppm) 4.82 (s, 1H, CH-sugar), 3.90-3.89 (m, 1H, CH-sugar), 3.83-3.55 (m, ~16H, TEG/sugar), 3.33 (t, $J=5.36$ Hz, 2H, CH₂-NH), 2.96-2.91 (m, 1H, CHSH), 2.67-2.65 (m, 2H, CH₂SH), 2.21 (t, $J=7.2$ Hz, 2H, OCH₂), 1.93-1.82 (m, 1H, CH₂CHSH), 1.75-1.32 (m, 9H, TA). **¹³C-NMR**

(100MHz): δ (ppm) 21.4 (1C, $\underline{\text{C}}\text{H}_2\text{SH}$), 25.0 (1C, CH_2 , TA), 25.4 (1C, CH_2 , TA), 35.5 (1C, $\underline{\text{C}}\text{H}_2\text{CHSH}$), 37.3 ($\underline{\text{C}}\text{H}_2\text{CH}_2\text{SH}$), 38.7 (1C, $\underline{\text{C}}\text{HSH}$), 41.7 (1C, $\underline{\text{C}}\text{H}_2\text{-NH}$, TEG), 60.9 (1C, $\underline{\text{C}}\text{H}_2$, sugar), 66.36 (1C, $\underline{\text{C}}\text{H}_2\text{-O-sugar}$), 66.71 (1C, CH, sugar), 68.9 (1C, CH_2 , TEG), 69.4-69.5 (3C, CH_2 , TEG), 69.9 (1C, CH, sugar), 70.5 (1C, CH, sugar), 72.7 (1C, CH, sugar), 99.9 (1C, CH-O-sugar), 176.9 (1C, C=O, TA).

Experiment 36: Synthesis of Mannose-TEG-NH₂ (36)

Via Scheme 13, strategy 2, step f): Mannose-TEG-NH₂ (**36**) was achieved as in Experiment 34, using compound **32** (0.360g, 0.75mmol) and NaOMe (0.041g, 0.75mmol) in 2mL of MeOH. The reaction was stirred for 2h at room temperature. The title compound was obtained as yellow pale oil (0.080g, 34%).

¹H-NMR (400MHz, D₂O): δ (ppm) 4.80 (s, 1H, sugar), 3.88-3.87 (m, 2H, sugar), 3.81-3.72 (m, 6H, sugar), 3.69-3.55 (m, TEG), 3.52 (t, $J=5.4\text{Hz}$, 2H, $\text{OCH}_2\text{CH}_2\text{NH}_2$), 2.78 (t, $J=5.3\text{Hz}$, 2H, $\text{OCH}_2\text{CH}_2\text{NH}_2$). ¹³C-NMR (100MHz): δ (ppm) 39.7 (1C, $\underline{\text{C}}\text{H}_2\text{NH}_2$), 60.9 (1C, $\underline{\text{C}}\text{H}_2\text{OH}$, sugar), 66.3 (1C, CH_2 , TEG), 66.7 (1C, CH, sugar), 69.3-69.6 (3C, CH_2 , TEG), 69.9 (1C, CH, sugar), 70.4 (1C, CH, sugar), 71.5-71.7 (1C, $\text{OCH}_2\text{CH}_2\text{NH}_2$), 72.7 (1C, CH, sugar), 99.9 (1C, CH, sugar). I.R (KCl) ν_{max} : 3386, 2891, 1635, 1571, 1483, 1351, 1313, 1247, 1134, 1062, 966, 887, 813 cm^{-1} .

Via Scheme 13, strategy 3, step j): To a solution of Pd/C (0.016g, 0.015mmol) previously suspended in 3mL of ethyl acetate and purged three times with H₂, was added a solution of compound **37** (0.235g, 0.7mmol) also dissolved in 3mL of ethyl acetate. The reaction was stirred at 50 Psi during 3h at room temperature. The mixture was filtered by celite and washed thoroughly with MeOH. The solvent was evaporated under vacuum. The crude obtained was dissolved in 10mL of water and washed with ethyl ether (3x10mL). The recovered aqueous phase was evaporated under vacuum to yield pure product **36** as pale yellow oil (0.208g, 95%).

The compound **36** was analysed spectroscopically as described in the procedure above.

Experiment 37: Synthesis of Mannose-TEG-N₃ (37)

The reaction was carried out as in Experiment 34 using compound **31** (0.496g, 0.98mmol) and 1 equivalent of NaOMe (0.053g, 0.98mmol) in 5mL of MeOH. Purification was accomplished by flash chromatography, eluting with a dichloromethane/methanol (9:1, $R_f=0.19$) mixture to yield **37** as a pale yellow oil (0.240g, 72%).

¹H-NMR (400MHz, CDCl₃): δ (ppm) 4.81 (s, 1H, sugar), 4.50 (s, 4H, OH, sugar), 3.96-3.75 (m, 6H, sugar), 3.69-3.54 (m, 10H, TEG), 3.40 (t, $J=5$ Hz, 2H, CH₂N₃). **¹³C-NMR** (100MHz): δ (ppm) 50.6 (1C, CH₂N₃), 60.9 (1C, CH₂OH, sugar), 66.3 (1C, CH₂, TEG), 66.2 (1C, CH, sugar), 66.7 (1C, CH₂, TEG), 70.0-70.6 (4C, CH₂, TEG), 70.8 (1C, CH, sugar), 71.5 (1C, CH, sugar), 72.2 (1C, CH, sugar), 100.1 (1C, CH, sugar). **I.R** (KCl) ν_{\max} : 3401, 2925, 2110, 1642, 1452, 1348, 1299, 1250, 1133, 1062, 975, 916, 882, 810cm⁻¹.

ESI-MS (m/z): [M+Na]⁺ Calculated for C₁₂H₂₃N₃NaO₈: 360.1362; Found: 360.1377.

Experiment 38: Synthesis of Monotosyl-PEG₄₀₀-OTs or PEG₄₀₀-OTs (39)

Neat PEG₄₀₀ (2.0g, 5mmol) was evaporated under vacuum in a rotavapor at 60°C for 1h with stirring to remove traces of water. The flask was back-filled with argon and 20mL of dried dichloromethane was added. Then, *p*-tosyl chloride (1.90g, 10mmol) and dried triethylamine (1.39mL, 10mmol) were added and the reaction was stirring at room temperature. After 40 minutes the reaction was stopped with the slowly addition of a saturated solution of sodium bicarbonate (20mL). The reaction was stirring for 30 minutes. The aqueous phase was extracted with ethyl acetate (3x30mL) and dichloromethane (3x30mL). The combined organic phases were dried with Na₂SO₄, filtered and evaporated under vacuum. The crude product was purified by silica flash chromatography. Elution with dichloromethane/methanol (9.7:0.3, $R_f=0.34$) afforded **39** as a colourless oil (0.986g, 35%).

¹H-NMR (400MHz, CDCl₃): δ (ppm) 7.79 (d, $J=8.1$ Hz, 2H, Ar), 7.34 (d, $J=8.1$ Hz, 2H, Ar), 4.16 (t, $J=4.8$ Hz, 2H, CH₂OTs), 3.72-3.58 (m, ~35H, PEG), 2.45 (s, 3H, CH₃, OTs). **¹³C-NMR** (100MHz): δ (ppm) 21.6 (1C, CH₃, OTs),

61.6 (1C, $\underline{\text{C}}\text{H}_2\text{OH}$, PEG), 68.6 (1C, $\underline{\text{C}}\text{H}_2\text{-OTs}$), 69.2 (1C, CH_2 , PEG), 70.1-70.6 (~16C, $(\text{CH}_2\text{CH}_2\text{O})_{x-8}$, PEG), 72.5 (1C, CH_2 , PEG), 127.9 (2C, CH, Ar), 129.8 (2C, CH, Ar), 132.9 (1C, q), 144.8 (1C, q). **I.R** (KCl) ν_{max} : 3471, 2875, 1729, 1648, 1598, 1454, 1353, 1294, 1249, 1176, 1099, 1012, 923, 819, 777, 665 cm^{-1} .

Experiment 39: Synthesis of AcMannose-trichloroacetimidate (40)

The compound **40** was synthesized according to the procedure described in the literature^[34, 35] and was obtained in 90% of yield.

Experiment 40: Synthesis of AcMannose-PEG₄₀₀-OTs (41)

AcMannose-trichloroacetimidate (**40**) (0.847g, 1.72mmol) and monotosylated PEG₄₀₀ **39** (0.980g, 1.72mmol) were dissolved in 20mL of CH_2Cl_2 and cooled to 0°C. TMS triflate (0.311mL, 1.72mmol) and molecular sieves were added and stirred at 0°C for 1h. The reaction was quenched with a saturated solution of NaHCO_3 (20mL) and extracted with CH_2Cl_2 (3x20mL). The combined organic extracts were dried over Na_2SO_4 , filtered and the solvent evaporated under vacuum. The crude product was purified by silica flash chromatography. Elution with dichloromethane/methanol (9.5:0.5, $R_f=0.36$) afforded **41** as a pale yellow oil (1.663g, 98%).

¹H-NMR (400MHz, CDCl_3): δ (ppm) 7.8 (d, $J=8.2\text{Hz}$, 2H), 7.3 (d, $J=8.1\text{Hz}$, 2H), 5.37-5.26 (m, 2H, sugar), 4.87 (s, 1H, sugar), 4.30-4.05 (m, 6H), 3.71-3.58 (m, ~35H, PEG), 2.45 (s, 3H, OTs), 2.16-1.99 (m, 12H, OAc). **¹³C-NMR** (100MHz): δ (ppm) 20.9-21.5 (5C, 5x CH_3), 62.3 (1C, $\text{CH}_2\text{-OH}$, sugar) 63.5 (1C, $\text{CH}_2\text{-OTs}$), 66.1 (1C, CH, sugar), 67.3 (1C, $\text{CH}_2\text{-O-sugar}$), 68.3 (1C, CH, sugar), 68.6 (1C, CH_2 , PEG), 69.1 (1C, CH, sugar), 69.2 (1C, CH_2 , PEG), 69.5 (1C, CH, sugar), 69.9 (1C, CH_2 , PEG), 70.4-70.7 (~13C, CH_2 , PEG), 97.6 (1C, CH, sugar), 127.9 (2C, CH-Ar), 129.8 (2C, CH-Ar), 144.8 (1C, q), 163.4 (1C, q), 169.4-170.6 (4C, C=O). **I.R** (KCl) ν_{max} : 2879, 1737, 1598, 1454, 1367, 1241, 1176, 1097, 1049, 921, 829, 682, 665 cm^{-1} .

Experiment 41: Synthesis of AcMannose-PEG₄₀₀-N₃ (42)

The reaction was carried out as described in Experiment 31, using compound **41** (0.356g, 0.39mmol), NaN₃ (0.076g, 1.17mmol) in 6mL of dried DMF during 3h at 85°C. The azide **42** was afforded as pale yellow oil in 98% of yield.

¹H-NMR (400MHz, CDCl₃): δ (ppm) 5.33-5.26 (m, 2H, sugar), 4.87 (s, 1H, sugar), 4.30-4.20 (m, 2H, sugar), 4.11-4.05 (m, 2H, sugar), 3.83-3.80 (m, 2H, PEG), 3.71-3.65 (m, PEG), 3.39 (t, $J=5\text{Hz}$, $\text{CH}_2\text{-N}_3$), 2.15-1.99 (m, 12H, OAc).

¹³C-NMR (100MHz): δ (ppm) 20.8 (4C, CH₃, OAc), 50.6 (1C, CH₂-N₃), 62.3 (1C, CH₂-OH, sugar), 63.5 (1C, CH₂, PEG), 66.1 (1C, CH, sugar), 67.2 (1C, $\text{CH}_2\text{CH}_2\text{N}_3$), 68.3 (1C, CH, sugar), 69.0 (1C, CH₂, PEG), 69.4 (1C, CH, sugar), 69.8 (1C, CH, sugar), 69.9-70.6 (~13C, CH₂, TEG), 97.6 (1C, CH-O-sugar), 169.6-169.8 (4C, C=O, OAc). **I.R** (KCl) ν_{max} : 2873, 2107, 1747, 1452, 1371, 1228, 1135, 1105, 1049, 979, 946 848cm⁻¹.

Experiment 42: Synthesis of Mannose-PEG₄₀₀-N₃ (43)

The reaction was carried out as in Experiment 34 using compound **42** (1.029g, 1.31mmol) and 1 equivalent of NaOMe (0.071g, 1.31mmol) in 5mL of MeOH. Purification was accomplished by silica flash chromatography, eluting with a dichloromethane/methanol (9:1, $R_f=0.43$) mixture to yield product **43** as a colourless oil (0.390g, 48%).

¹H-NMR (400MHz, CDCl₃): δ (ppm) 4.86 (s, 1H, sugar), 4.69 (br s, 3H, OH, sugar), 4.1 (br s, 1H, OH, sugar), 3.93-3.76 (m, 6H, sugar), 3.69-3.56 (m, ~37H, PEG), 3.39 (t, $J=5\text{Hz}$, 2H, CH_2N_3).

¹³C-NMR (100MHz): δ (ppm) 50.6 (1C, CH_2N_3), 61.2 (1C, CH_2OH , sugar), 66.5 (1C, CH₂, PEG), 66.6 (1C, CH, sugar), 69.9-70.6 (~16C, CH₂, PEG), 70.7 (1C, CH, sugar), 71.5 (1C, CH, sugar), 72.2 (1C, CH, sugar), 100.1 (1C, CH, sugar). **I.R** (KCl) ν_{max} : 3415, 2875, 2107, 1725, 1644, 1461, 1349, 1290, 1251, 1103, 948, 844, 680cm⁻¹.

ESI-MS (m/z): [M+Na]⁺ Calculated for C₂₄H₄₇N₃NaO₁₄: 624.2929; Found: 624.2950.

Experiment 43: Synthesis of Mannose-PEG₄₀₀-NH₂ (44)

The reaction was carried out according to the procedure described in Experiment 36, using compound **43** (0.390g, 0.63mmol) dissolved in 3mL of

AcOEt and Pd/C (0.015g, 0.014mmol) previously suspended in 3mL of AcOEt and purged with H₂. The product **44** was afforded as a pale yellow oil in 97% of yield (0.362g).

¹H-NMR (400MHz, D₂O): δ (ppm) 4.80 (s, 1H), 3.88-3.87 (m, 2H, sugar), 3.81-3.72 (m, 6H, sugar), 3.69-3.53 (m, ~40H, PEG), 2.83 (t, $J=5.3$ Hz, 2H, CH₂NH₂). **¹³C-NMR** (100MHz): δ (ppm) 39.6 (1C, CH₂NH₂), 60.9 (1C, CH₂OH, sugar), 66.3 (1C, CH₂, PEG), 66.7 (1C, CH, sugar), 69.3-69.6 (~16C, CH₂, PEG), 69.9 (1C, CH, sugar), 70.47 (1C, CH, sugar), 70.42 (1C, CH₂, PEG), 72.7 (1C, CH, sugar), 99.9 (1C, CH, sugar). **I.R** (KCl) ν_{\max} : 3396, 2915, 2875, 1641, 1461, 1351, 1301, 1249, 1093, 952, 883, 835, 809cm⁻¹.

Experiment 44: Synthesis of Mannose-PEG₄₀₀-TA (**45**):

The reaction was carried out as described in Experiment 33 using compound **44** (0.360g, 0.61mmol), LA-NHS (**21**) (0.184g, 0.61mmol) and NaHCO₃ (0.050g, 0.61mmol) in 4mL of dried DMF. The purification was accomplished by silica flash chromatography. Elution with dichloromethane/methanol (9:1, $R_f=0.3$) afforded product **45** as a yellow oil (0.296g, 61%).

¹H-NMR (400MHz, CDCl₃): δ (ppm) 4.88 (s, 1H, CH, sugar), 4.26 (br s, 2H, CH₂, sugar), 3.94-3.78 (m, 5H, sugar), 3.66-3.54 (m, ~35H, PEG), 3.44 (t, $J=5.2$ Hz, 2H, PEG), 3.21-3.08 (m, 2H, CH₂S), 2.50-2.42 (m, 1H, CH₂CHS), 2.20 (t, $J=7.5$ Hz, 2H, CH₂C=O), 1.95-1.87 (m, 1H, CH₂CHS), 1.73-1.43 (m, 6H, 3xCH₂). **¹³C-NMR** (100MHz): δ (ppm) 25.4 (1C, CH₂, TA), 28.9 (1C, CH₂, TA), 34.6 (1C, CH₂, TA), 36.3 (1C, CH₂CO, TA) 38.4 (1C, CH₂S, TA), 39.1 (CH₂CH₂S, TA), 40.2 (1C, CH₂, CH₂-NH), 56.4 (1C, CHS, TA), 61.9 (1C, CH₂-OH, sugar), 66.7 (1C, CH₂-O-sugar), 67.4 (1C, CH, sugar), 69.9-70.7 (~16C, PEG), 70.7 (1C, CH, sugar), 71.6 (1C, CH, sugar), 72.0 (1C, CH, sugar), 100.1 (1C, CH, sugar). **I.R** (KCl) ν_{\max} : 3403, 2919, 2869, 1648, 1550, 1461, 1349, 1297, 1249, 1103, 948, 883, 808cm⁻¹. **ESI-MS (m/z)**: [M+Na]⁺ Calculated for C₃₂H₆₁NNaO₁₅S₂: 786.3360; Found: 786.3375.

Experiment 45: Synthesis of Mannose-PEG₄₀₀-DHLA (**46**)

The reaction was carried out as described in Experiment 35, but using compound **45** (0.159g, 0.2mmol), NaBH₄ (0.030g, 0.8mmol) in 2mL of

ethanol/water mixture (1:4). The product **46** was afforded as colourless oil (0.122g, 77%).

¹H-NMR (400MHz, CDCl₃): δ (ppm) 4.88 (s, 1H, CH, sugar), 3.94-3.76 (m, 6H, sugar), 3.65-3.53 (m, ~38H, PEG), 3.46-3.42 (m, 2H, CH₂-NH), 2.95-2.89 (m, 1H, CH₂SH), 2.77-2.62 (m, 2H, CH₂SH), 2.20 (t, $J=7.4$ Hz, 2H, OCH₂), 1.95-1.86 (m, 1H, CH₂CHSH), 1.78-1.40 (m, 9H, TA). **¹³C-NMR** (100MHz): δ (ppm) 22.3 (1C, CH₂SH), 25.3 (1C, CH₂, TA), 28.9 (1C, CH₂, TA), 34.6 (1C, CH₂, TA), 36.2 (1C, CH₂CO, TA), 39.3 (1C, CHSH), 40.2 (1C, CH₂NH), 42.7 (1C, CH₂CH₂SH, TA), 61.7 (1C, CH₂OH, sugar), 67.3 (1C, CH₂-O-sugar), 70.0 (1C, CH, sugar), 70.1-70.6 (~16C, PEG), 70.7 (1C, CH, sugar), 71.6 (1C, CH, sugar), 72.2 (1C, CH, sugar), 100.2 (1C, CH, sugar), 173.1 (1C, C=O, TA). **I.R** (KCl) ν_{max} : 3396, 2915, 2877, 1648, 1550, 1461, 1349, 1295, 1249, 1101, 950, 879, 840, 809cm⁻¹.

Water Solubilization of CdSe/ZnS Core-Shell QDs

The surface of native trioctylphosphine oxide /1-hexadecylamine (TOPO/HDA) capped CdSe/ZnS core-shell QDs synthesized during this work (chapter 2), was exchanged with a series of designed ligands described in this chapter and also with commercial 3-mercaptopropionic acid (MPA, 99%). The exchange method was carried out according to previously reported procedures [13, 15, 18, 24, 36] with some modifications to the quantities of reagents/solvents and incubation times. The resulting hydrophilic samples of QDs were purified using centrifugal filter devices with PES membrane from Sartorius (Vivaspin) and with different MWCOs depending on the sample. The polypropylene centrifuge tubes (15 and 50mL) and polypropylene micro tubes (1.5 and 2mL) were purchased from Sarstedt.

Preparation of 3-mercaptopropionic acid (MPA)-capped QDs

A stock solution of MPA was prepared in a 10mL volumetric flask by placing 400 μ l of MPA (4.59mmol) followed by the addition of 500mg of KOH (14.3mmol) and making up to the volume of the flask with MeOH.

The MPA-capped QDs were obtained by the phase transfer method [13, 24, 36] in the following manner: 10mg of a dried pellet of CdSe/ZnS (TOPO/HDA) QDs were placed into a 5mL glass vial and dispersed in 1.5mL of chloroform to

give a highly concentrated solution (optical density , OD=1.5). 200 μ L of the MPA stock solution were then added. The vial was closed with a snap cap and manually shaken. After shaking for two minutes the chloroform solution flocculated and became turbid (the solution was not optically clear at pH 5-7, possible due to inter-particle hydrogen bonding between the carboxyl functions of the ligands). 1.5mL of NaOH solution 10mM (pH 12) was posteriorly added to the flocculate solution and the mixture of phases were manually shaken again. Immediately, the transfer of QDs from the organic to aqueous phase occurred and the aqueous phase became coloured. The two-phase solution was transferred to a 15mL polypropylene tube, centrifuged at 5500g at room temperature for 5 minutes and the aqueous phase (coloured phase) was recovered. To ensure the total collection of functionalized water-soluble QDs, the centrifugation step was repeated two more times with the addition of fresh 1.5mL of NaOH solution 10mM (pH 12) each time. The combined aqueous phases containing the MPA-capped CdSe/ZnS QDs were purified and concentrated using a centrifugal filter device (10kDa MW cutoff) at 7500g, at room temperature for 15 minutes and washed (3 times) with NaOH solution 10mM (pH 12). The final concentrated sample was dispersed in 1mL of NaOH solution 10mM (pH 12) affording an orange optically clear solution. The sample was stored in the dark at 4°C and was optically characterized for further use. With time, the stored functionalized MPA-QDs formed aggregates. To remove them, the sample was centrifuged in 2mL polypropylene tube at 2000g at room temperature for 2 minutes. The supernatant was stored again in the dark at 4°C for further use. In these cases, the new concentration had to be determined.

Preparation of Dihydrolipoic acid (DHLA)-capped QDs

The use of DHLA (1) in the ligand exchange process with the native TOPO/HDA nanoparticles was carried out as described previously ^[15]. In a 5mL glass vial, 10mg of a dried pellet of CdSe/ZnS QDs were dispersed in 50mg of pure DHLA (1) and heated to 70°C under argon for 2-3h until the solution became homogeneous. Dimethylformamide (1.5mL) was added to the solution, and the nanocrystals were precipitated with 30mg of potassium *tert*-butoxide (deprotonation of -COOH terminal group of lipoic acid) The

precipitated solution was transferred to a 15mL polypropylene centrifuge tube and centrifuged at 5500g during 5 minutes at room temperature to produce a pellet of QDs and excess of potassium *tert*-butoxide. The supernatant, free of QDs, was discarded, and the precipitate was dispersed in a NaOH solution 10mM (pH 12). The purification/concentration was carried out using a centrifugal filter device (50kDa MW cut-off) with 5mL of NaOH solution 10mM (pH 12) through four cycles (3000g, 8 minutes, r.t.). The final sample was dispersed in 1mL of NaOH solution 10mM (pH12). The sample was stored in the dark at 4°C and was optically characterized before further use.

Preparation of Carboxy-PEG₄₀₀, Mannose-TEG and Mannose-PEG₄₀₀-capped QDs

QDs ligand-exchange with carboxy-PEG₄₀₀ (**11**), mannose-TEG (**35**) and mannose-PEG₄₀₀ (**46**)-capped QDs were prepared based on the same experimental procedure described previously^[18]. As an example, carboxy-QDs were prepared in the following manner: In a 5mL glass vial, 5mg of dried pellet of CdSe/ZnS QDs were dispersed in 25mg of neat carboxy-PEG₄₀₀ (**11**) and 100µL of MeOH were added creating an homogeneous mixture. The mixture was heated under argon at 60°C, overnight. The QDs were then precipitated by adding 0.3mL of EtOH, 0.5mL of chloroform, and 0.5mL of hexane in succession (the volumes of solvent added could be increased if needed). The suspension was transferred to a polypropylene centrifuge tube (15mL) and centrifuged at 3000g for 4 minutes at room temperature. The clear supernatant was discarded and the red pellet was dispersed in 10mM NaOH solution (pH 12) and concentrated using a Sartorius Vivaspin-6 (10-50kDa MW cut-off). The final product was dispersed in 1.5mL of NaOH solution 10mM (pH 12) and stored in the fridge at 4°C. Optical characterization was performed before use.

For the hydrophilic QDs containing carbohydrate moieties the functionalization procedure was carried out as described above but final samples were washed and dispersed in sodium phosphate (Na-P) buffer 10mM (pH 7).

Preparation of Amino-PEG₄₀₀ and Mixtures of Amino-PEG₄₀₀/DHHLA-PEG₄₀₀-capped QDs

The amino-PEG₄₀₀ (**8**) ligand was used in the ligand exchange process to produce amino-QDs but also QDs with mixtures with different mole fractions of compound **8** with the non-charged DHHLA-PEG₄₀₀ (**3**) on their surface. For convenience, the nomenclature used was amino-QDs when 100% of compound **8** was coating the total surface of the nanoparticles and amino/DHHLA-PEG (*x*:*y*) when mixtures of amino-PEG₄₀₀ (**8**) and DHHLA-PEG₄₀₀ (**3**) were applied on the surface of the QDs. *x* and *y* represent the percentage of each ligand respectively. Amino/DHHLA-PEG QDs were produced using the experimental procedure applied for carboxy-QDs^[18] in different mixtures (20:80), (50:50) and (80:20). As an example for the amino/DHHLA-PEG (20:80) QDs, a mixture of ligands constituted by 5mg of amino-PEG₄₀₀ (**8**) and 20mg of DHHLA-PEG₄₀₀ (**3**) was added to a glass vial containing 5mg of dried native CdSe/ZnS QDs. The final samples were washed and dispersed in saline phosphate (PBS) buffer 10mM (pH 6).

Characterization of Hydrophilic QDs

Concentration Determination in Aqueous Solutions and Optical Measurements

The experimental procedure for the determination of the concentration of QDs in aqueous solutions were carried out as described in chapter 2 for the hydrophobic QDs using the absorption spectrum method. The MPA, DHHLA and carboxy-QD samples were dispersed in NaOH solution 10mM pH 12. For amino-QDs and mixtures with hydroxy-PEG₄₀₀ the optical density was measured in PBS buffer 10mM pH 6 and the glyco-QDs were measured in Na-P buffer 10mM pH 7. The extinction coefficient applied ($\epsilon = 1.5 \times 10^5 \text{ M}^{-1} \text{ cm}^{-1}$) was previously calculated on the first absorption peak of the CdSe cores ($\lambda = 568 \text{ nm}$) and the concentration of each sample was determined by the Lambert-Beer's Law (Equation 2). The QD concentrations in aqueous solutions obtained were in the range from 1 to 10 μM . The QY measurements and photoluminescence spectra of the same samples were performed using the experimental conditions also described in chapter 2.

Dynamic Light Scattering Measurements

Light scattering analysis was performed using a Zetasizer Nano ZS dynamic light scatterer from Malvern Instruments to characterize the hydrodynamic diameter (HD) and zeta potential (ξ -potential) of hydrophilic QDs. The samples were suspended in the aqueous solutions used for the concentration determination and optical measurements with concentrations between 0.02 and 0.1 μM and 0.1 and 0.58 μM for HD and ξ -potential measurements respectively. All the samples were filtered through a 0.2 μm PTFE membrane before analyses. HD was obtained from number-weighted size distribution analysis. For both HD and ξ -potential measurements values are reported as the average of triplicate runs consisting of 20 measurements at 25°C.

The experimental procedure for HD measurements was carried out as described in chapter 2 for hydrophobic QDs. For zeta potential analysis a typical measurement in aqueous solutions was carried out as the following procedure:

10mm precision cells made of Quartz (Type Nr. 101-QS, 10mm, Hellma) were used to avoid optical interferences and to ensure that the optimum signal was achieved during measurements. Therefore, an additional Universal “dip” cell (ZEN 1002, Malvern Instruments) was required (according to instrument manufacturer's specifications) to measure zeta potential of the aqueous samples. For example, 2mL of MPA- QDs in NaOH solution 10mM pH 12 at concentration of 0.1 μM was prepared. The sample concentration was adjusted previously to accommodate the scattering properties of the sample and/or the optical requirements of specific instrument. 1mL of the sample solution using a 1mL disposable syringe was filtered with a 0.2 μm PTFE membrane before the sample was introduced into the cuvette for analysis. The cuvette was filled slowly to avoid the formation of air bubbles and was closed by the universal “dip” cell which was inserted inside the cuvette according to manufacturer's instructions. The cuvette was placed correctly in the sample holder (quartz windows should be facing the incident beam and detector) and 3 measurements of 20 runs each were performed per sample at 25°C and with an equilibration time of 2 minutes. The obtained data was analysed using the instrument's software (Zetasizer software, version 6.2) to

evaluate surface charge (zeta potential values) and electrophoretic mobility of hydrophilic QDs.

Estimation of the Number of Functional Amines Groups in Amino-QDs and Mixed-ligand Amino- QDs

Where appropriate, the number of functional amino groups available on the QD surface was measured using the fluorescamine assay according to Udenfriend *et al* ^[25] and modified for microplates as described by Lorenzen and Kennedy ^[37].

After the water-solubilisation of native TOPO/HDA-capped QDs with pure amino-PEG₄₀₀ (**8**) and mixtures of compound **8** with hydroxy-PEG₄₀₀ (**3**), the water-soluble QDs were purified by ultrafiltration using centrifugal filter devices Vivaspin 6 (10-50kDa MW cut-off) from Sartorius to remove the presence of possible free ligand in solution. Series of 4 dilutions of free amino-PEG₄₀₀ (**8**) ligand ranging from 0 to 25µM were prepared in dried DMF to plot the calibration curve of fluorescence intensity vs. concentration of free compound **8**. The QDs solutions were suspended in PBS buffer pH 6 with a concentration of 0.25µM. After the dilutions, 150µL of each sample/standard were pipetted into a black polypropylene 96-well microplate in replicates of two to improve accuracy. The microplate was then placed in a shaker and 75µL of 10.8mM (3mg/mL) of fluorescamine freshly dissolved in dried DMF, was added to each well. The control was performed with 150µL of PBS buffer pH 6 and 75µL of fluorescamine solution. Following the addition of the fluorescamine, the plate was shaken for one minute. The fluorescence was then measured using a SpectraMax Gemini EM fluorescence plate reader from Molecular Devices with a 380-390nm excitation filter. The concentration of amino-PEG₄₀₀ (**8**) in the QDs solutions was obtained according to the calibration curve based on the integrated fluorescence intensity of standard with fluorescamine from 460-480nm, along with a linear fit. Finally, the calculated number of amines on a single QD was according the following equation:

$$N_A = C_{\text{amino-PEG400}} / C_{\text{QDs}}$$

Equation 4 | Expression given to estimate the number of functional amine groups available on a single QD surface.

Where N_A is the number of amine groups available on the surface of a single QD, $C_{\text{amino-PEG400}}$ is the concentration of amino-PEG₄₀₀ (**8**) present in the QDs solutions and C_{QDs} is the initial concentration of CdSe/ZnS QD particles.

Estimation of the Concentration of Carbohydrates Moieties in Glyco-QDs

The number of mannose molecules attached to the surface of glyco-QDs was determined by the phenol-sulfuric acid method in a microplate format described by Masuko *et al* [26]. The water-soluble sugar-capped QDs samples were first purified by ultrafiltration using centrifugal filter devices Vivaspin 6 (10-50kDa MW cut-off) to remove any kind of aggregates formed with time and eliminate the possible presence of free ligand in solution. The new concentration was determined by the absorption spectra method. A series of 10 dilutions of free mannose ranging from 0 to 200nmol were prepared in Milli-Q water to plot the calibration curve at 490nm after treatment with concentrated H₂SO₄/phenol vs. concentration of free mannose. The sugar-capped QDs were suspended in Na-P buffer 10mM pH 7.3 with a concentration ranging between 0.25-0.34μM. 50μL of each standard/sample were pipetted into a 96-well microplate in triplicate to improve accuracy. Then, 150μL of concentrated H₂SO₄ and 30μL of a fresh solution of 5% phenol in water were added to each well. 50μL of sugar-capped QD solution and 150μL of concentrated H₂SO₄ was used as control. After the addition of phenol-sulfuric acid, the microplate was heated in a water bath at 80°C during 15 minutes followed by 5 minutes at room temperature. The mannose concentration was estimated using the calibration curve of the absorbance at 490nm of free mannose after treatment with phenol-sulfuric acid, along with a linear fit and the number of sugar molecules on a single QD surface was calculated according to the following equation:

$$N_S = C_{\text{mannose}} / C_{\text{QDs}}$$

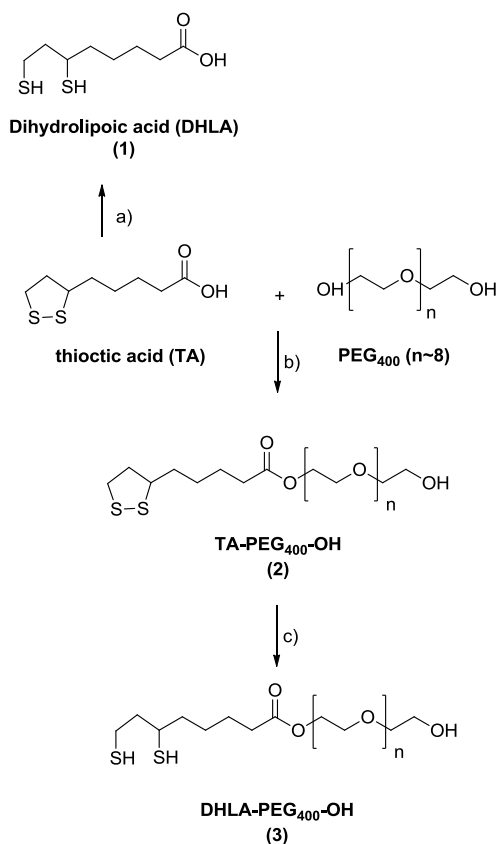
Equation 5 | Expression used to estimate the number of sugar molecules available on a single QD surface.

Where N_S is the number of sugar molecules available on the surface of a single QD, $C_{mannose}$ is the concentration of mannose present in the QDs solutions and C_{QDs} is the initial concentration of CdSe/ZnS QD particles.

Results and Discussion

Ligand Synthesis and Design

In earlier reports the use of DHLA and PEG-appended DHLA (DHLA-PEG-OH) as surface ligands was demonstrated to promote the aqueous dispersion of the luminescent CdSe/ZnS QDs^[10, 15]. Scheme 4, illustrates the synthetic route for the preparation of DHLA and PEG₄₀₀-appended to DHLA.



a) NaBH₄, NaHCO₃ 0.25M, H₂O, 0°C, 2h, 98%

b) DCC, DMAP, CH₂Cl₂, 0°C-1h, r.t - overnight, 77%; c) NaBH₄, EtOH/H₂O, r.t., 1h, 77%

Scheme 4 | DHLA and DHLA-PEG₄₀₀-OH Synthesis. Synthetic route for the production of compounds DHLA (1) and PEG₄₀₀- appended to DHLA (3) based on the Uyeda *et al* description^[15].

Dihydrolipoic acid was freshly prepared by reduction with sodium borohydride (NaBH_4) in the presence of an aqueous solvent; sodium bicarbonate (NaHCO_3) and was obtained in a quantitative yield. The synthetic scheme to make DHLA-PEG₄₀₀-OH (**3**) was relatively simple. PEG₄₀₀-appended to dihydrolipoic acid was obtained by a simple esterification reaction between PEG with molecular weight (MW) =400 (PEG₄₀₀) and thioctic acid mediated by dicyclohexylcarbodiimide (DCC) and the presence of a catalytic amount of 4-(dimethylamino)-pyridine (DMAP). The esterification reaction was followed by the reduction of the 1, 2-dithiolane with NaBH_4 in a mixture of ethanol and water to afford the desired product with an overall yield of 60% starting from thioctic acid (TA). In the synthesis and purification of DHLA-PEG₄₀₀-OH (**3**), the esterification reaction to appended PEG₄₀₀ to thioctic acid was performed using an excess of PEG. This substantially minimized the formation of bi-substituted species and thus simplified the column chromatographic purification. The unreacted PEG was eliminated by the extraction with a saturated sodium chloride (NaCl) solution where most of the glycol stayed in the aqueous phase. The ring opening of the dithiolane group of thioctic acid-terminated PEG₄₀₀ ligand (**2**) and thioctic acid (TA) was carried out, in both cases, using NaBH_4 as described above. However, the conversion of thioctic acid to dihydrolipoic acid (**1**) took place in strictly aqueous solvent whereas the reduction of compound **2** proceeded more cleanly when carried out in a mixture of ethanol/water ^[15, 38, 39]. The ring opening process was visually monitored by the gradual disappearance of the yellow colour of the precursor (oxidized form) to a final colourless solution of the final product (reduced form). The coupling of the PEG₄₀₀ to thioctic acid was demonstrated by NMR spectroscopic techniques (Figure 10). The esterification product was successfully obtained in ¹H-NMR (spectra (c)). The ¹H-NMR of the ester **2** (spectrum (c)) is essentially a composite of the two starting materials. The contribution of the PEG moiety appeared as a large broad multiplet at 3.5-3.6 ppm with an additional two-proton triplet at 4.2 ppm. Using the same technique it was also possible to analyse the completion of the reductive ring opening process. The ¹H-NMR analyses demonstrated the differences in the chemical shifts (in ppm) of the oxidized (spectrum (a) and (c)) and reduced form (spectrum (b) and (d)) of these two compounds. For compounds **1** and **3**

(spectrum (b) and (d)), the thiol protons were clearly displayed by the well-resolved triplet and doublet at 1.30 and 1.25 ppm respectively with integrated intensities of one proton each. In addition, new chemical shifts were observed again for these compounds, at 2.6 and 2.8 ppm which are completely missing in spectra (a) and (c). On the other hand, the peaks at 3.0 and 2.5 ppm are unique for the closed form of TA and compound **2** and totally absent in the reduced forms.

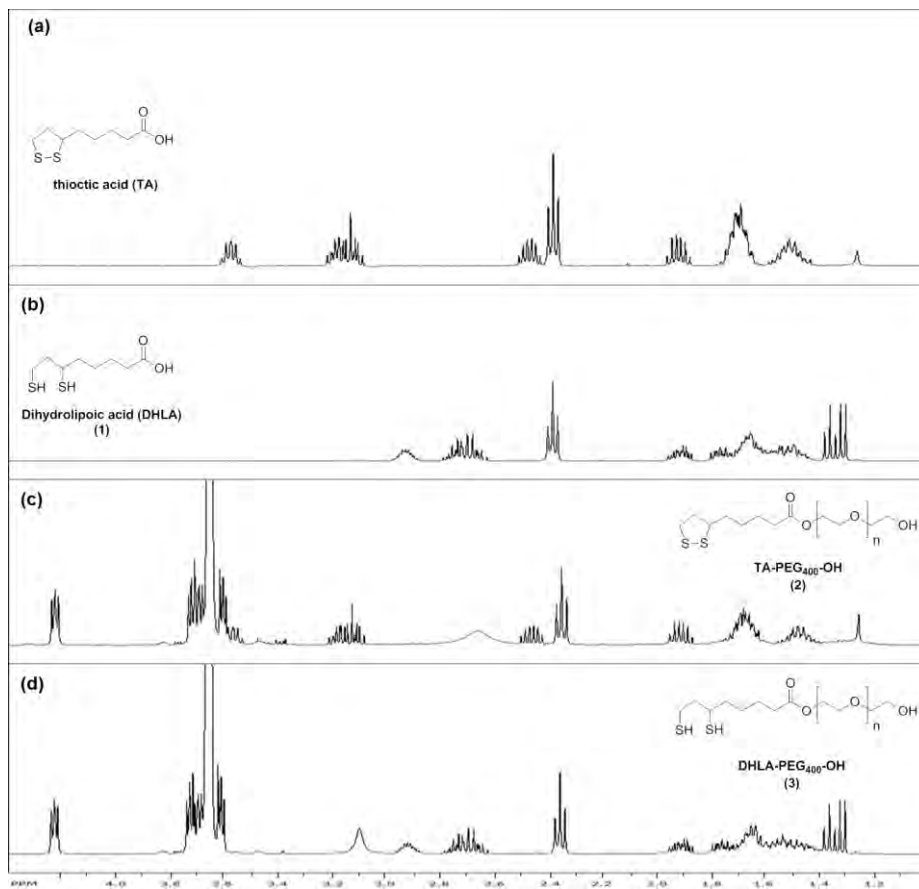
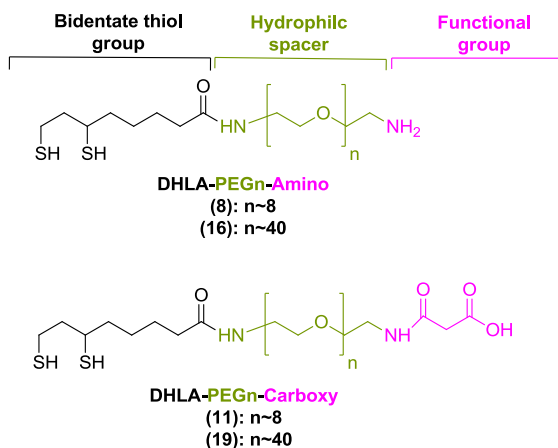


Figure 10 | $^1\text{H-NMR}$ spectra of DHLA (1) and DHLA-PEG₄₀₀-OH (3). $^1\text{H-NMR}$ spectra highlighting the coupling of PEG₄₀₀ to thioctic acid (compound **2**) and displaying the characteristics shifts resulting from the reduction of the dithiolane moiety; compounds **1** and **3**.

The synthetic route to polyethylene glycol appended dihydroliipoic acid described above provided a general and simple way to synthesize heterobifunctional ligands. At one of the ends of PEG molecule it was possible to modify with TA/DHLA maintaining the bidentate surface functionality and at

the other end it was possible to modify with other functional moieties (e.g. –OH).

Using the same type of chemistry, the synthesis and characterization was expanded to a series of modular ligands with terminal functional groups. The Scheme 5 shows a modular design of the synthesized ligands. The hydrophilic spacer used was PEG₄₀₀ and PEG₂₀₀₀ and the chosen functional groups were amine and carboxyl group



Scheme 5 | Modular ligands with functional terminal groups. General scheme of the hydrophilic ligands synthesized with different terminal functional groups and hydrophilic spacers.

Scheme 7 describes the synthetic route for DHLA-PEG_n-FN, where FN is an amine or carboxyl group and n~8 or 40. The steps were almost the same applied for both PEG₄₀₀ and PEG₂₀₀₀. The diamine functionalized polyethylene glycol **6** (n~8) or **14** (n~40) were synthesized from commercially available PEG₄₀₀ and PEG₂₀₀₀ respectively. For diamine **6** the route applied was a simple three step process affording the final ligand in high yield (97% on a 5g scale) with minimal purification steps. Reaction of neat PEG₄₀₀ with thionyl chloride as solvent was monitored by the disappearance of the broad OH stretch at 3500cm⁻¹ and the appearance of a C-Cl stretch at 739cm⁻¹ in the infrared (IR) spectra (Figure 11, spectrum (a)). After the elimination of SOCl₂ with the help of DMF under reduced pressure the chloride **4** was treated with sodium azide in order to obtain the diazide **5**. In this case, the reaction was also followed by infrared analysis where the conversion was confirmed by the presence of a sharp azide stretch at 2107cm⁻¹ and the disappearance of the

C-Cl bond at 739cm^{-1} (Figure 11, spectrum (b)). The diazide **5** in the presence of triphenylphosphine/water afforded the desired diamine **6** in large quantities.

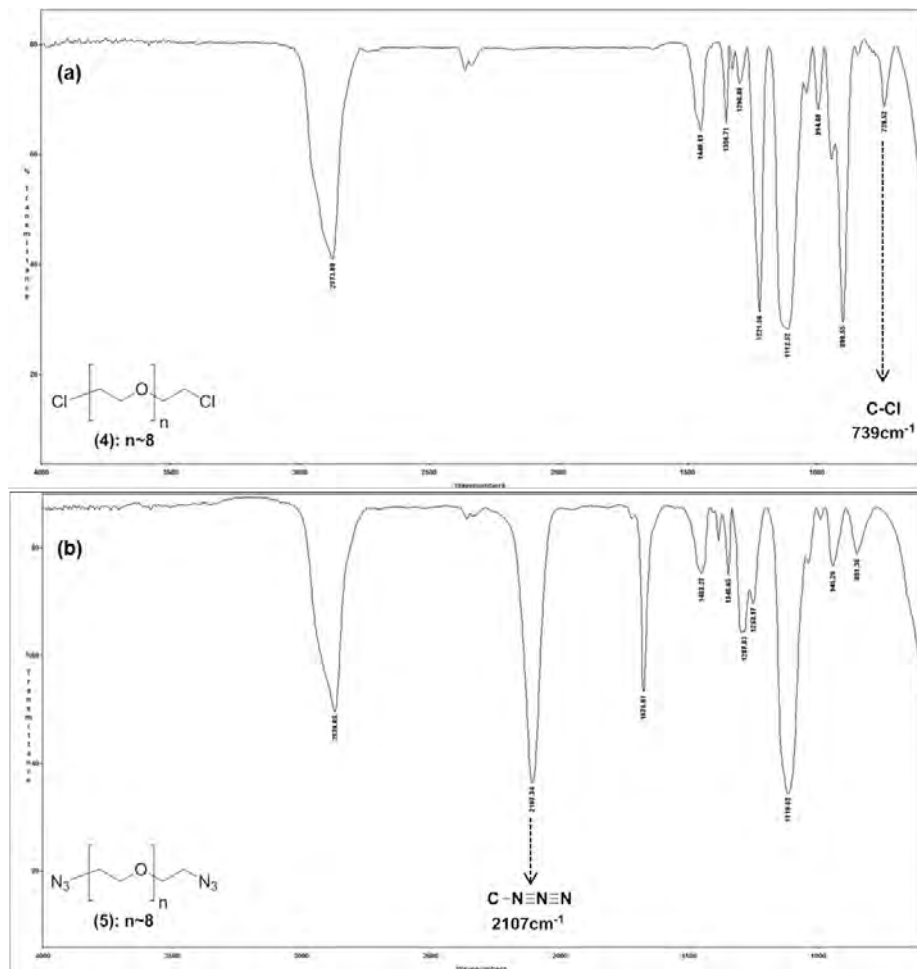
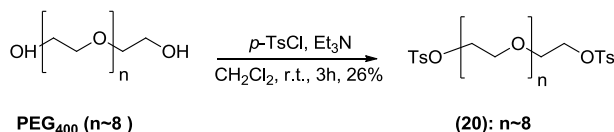


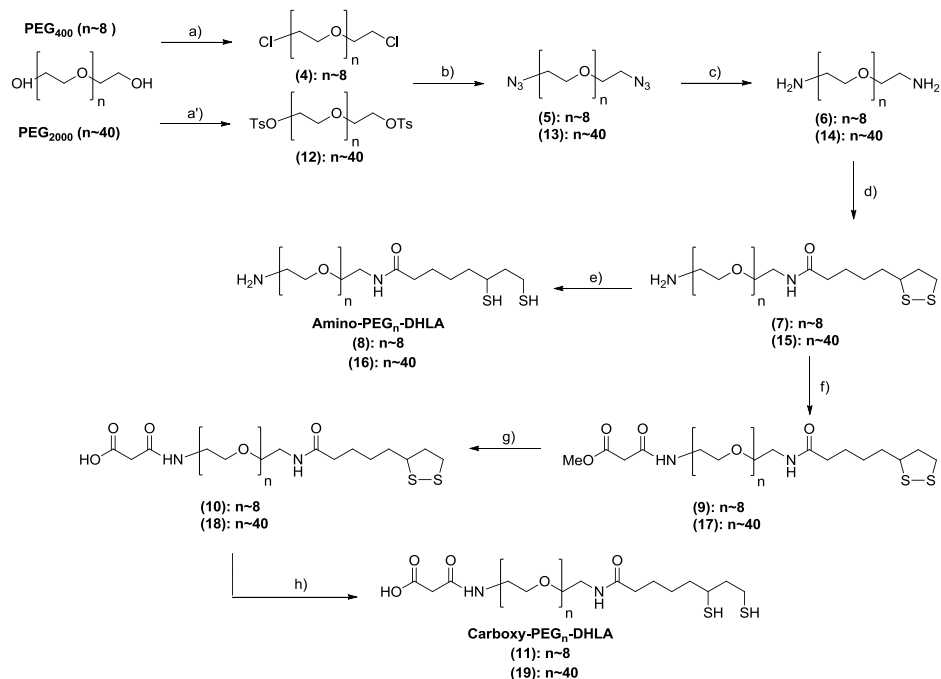
Figure 11 | Infrared Analysis of dichloride and diazide from PEG₄₀₀. Infrared spectra for the synthesis of compounds **4** and **5** where in spectra (a) is possible to visualize the presence of a C-Cl band at 739cm^{-1} and in spectra (b) the band 2107cm^{-1} indicating the formation of an azide.

Replacement of SOCl_2 by *p*-TsCl to form ditosylate **20** was also carried out (Scheme 6) but afforded the required compound in only in 26% yield and required an additional purification step. For this reason the route using dichloride **4**, although more hazardous, was more efficient.



Scheme 6 | General reaction for the synthesis of ditosyl compound **20** from PEG₄₀₀.

The heterobifunctional ligands were then obtained in a straightforward fashion from diamine **6**.



For PEG₄₀₀ (n=8):

a) SOCl₂, 0-25°C, 2h; b) NaN₃, DMF, 85°C, overnight; c) PPh₃, THF, H₂O, r.t, overnight, 97%; d) LA-NHS, NaHCO₃, DMF/H₂O (1:1), 0-25°C, overnight, 65%; e) NaBH₄, EtOH/H₂O (4:1), 2h, 75%; f) Methylmalonylchloride, Et₃N, CH₂Cl₂, 0-25°C, 4h, 57%; g) 0.25M NaHCO₃, NaBH₄, 0°C, 2h, 95% .

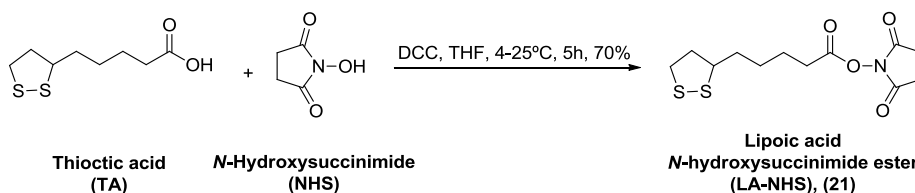
For PEG₂₀₀₀ (n=40):

a) *p*-TsCl, DMAP, py, 0-25°C, overnight, 48%; b) NaN₃, DMF, 85°C, overnight; 96% c) PPh₃, THF, H₂O, r.t, overnight, 93%; d) LA-NHS, NaHCO₃, DMF/H₂O (1:1), 0-25°C, overnight, 79%; e) NaBH₄, EtOH/H₂O (4:1), 2h, 85%; f) Methylmalonylchloride, Et₃N, CH₂Cl₂, 0-25°C, 4h, 98%; g) 0.25M NaOH, MeOH, 60°C, 5h, 78%; h) 0.25M NaHCO₃, NaBH₄, 0°C, 2h, 99% .

Scheme 7 | **Amino-PEG_n-DHLA and Carboxy-PEG_n-DHLA Synthesis.** General route for the achievement of hydrophilic ligands with an amine and carboxyl functional groups with PEG₄₀₀ and PEG₂₀₀₀ as spacer.

TA-PEG₄₀₀-NH₂ (**7**), which served as the precursor to both DHLA-PEG₄₀₀-NH₂ (**8**) and DHLA-PEG₄₀₀-COOH (**11**), resulted from the reaction of diamine **6** with the NHS ester of lipoic acid (LA-NHS) (**21**). Compound **7** was furnished smoothly by ring opening of thioctic ester into the dihydrolipoic form. The pure DHLA-PEG₄₀₀-NH₂ (**8**) was obtained in a total of five steps with 47% of overall yield. On the other hand, compound **7** was reacted with methylmalonyl chloride, followed by methylester hydrolysis to form an amide with a terminal carboxyl group (compound **10**). The reduction of the 1, 2-dithiolane ring with sodium borohydride yielded the DHLA-PEG₄₀₀-COOH (**11**) in a total of seven steps with 31% of overall yield.

Lipoic acid *N*-hydroxysuccinimide ester^[18] (LA-NHS) (**21**) was prepared in this work based on a simple esterification reaction between thioctic acid (TA) and *N*-hydroxysuccinimide (NHS) in a presence of 1.2 equivalents of DCC. The pure product was obtained as yellow powder in 70% yield (Scheme 8).



Scheme 8 | LA-NHS Synthesis. Reaction for the synthesis of lipoic acid *N*-hydroxysuccinimide ester (**21**) based on the literature^[18].

The preparation of Amino/Carboxy-PEG_{*n*}-DHLA using PEG₂₀₀₀ (*n*~40) corresponding to compounds **16** and **19** respectively was quite similar to the approach described for PEG₄₀₀ (Scheme 7). The synthesis started with conversion of PEG₄₀₀ in its corresponding dichloride **4** using an excess of thionyl chloride (SOCl₂). This reagent is toxic but the desired compound was obtained in large amounts without the need for purification. However, during the synthesis of the same intermediate using PEG₂₀₀₀, it was found that the dichloride was not formed by reaction with SOCl₂, because of the long aliphatic chain of PEG₂₀₀₀. Thus, the production of diamine **14** continues to enjoy a three steps route however, dichloride **4** was replaced by compound **12**

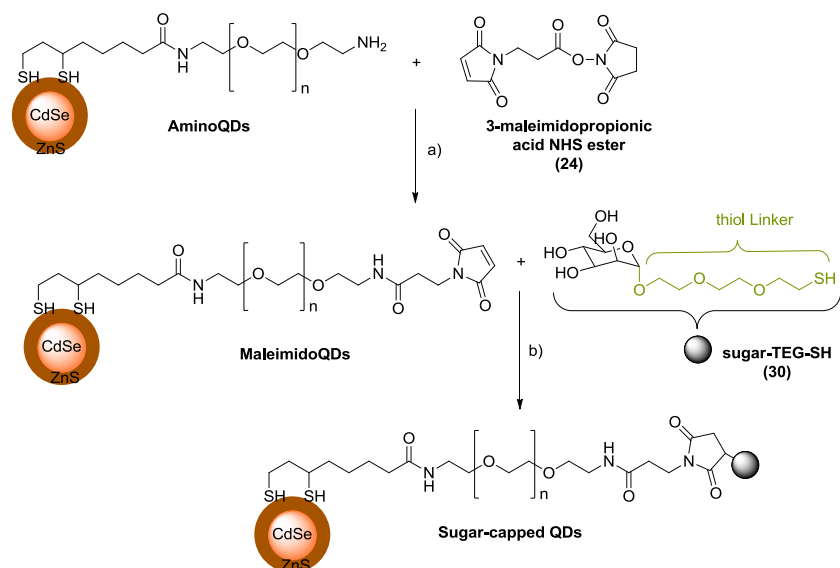
produced from reaction of PEG₂₀₀₀ with *p*-tosyl chloride affording the ditosyl-PEG₂₀₀₀ **12** in 48% yield

The heterobifunctional ligands for PEG₂₀₀₀ were synthesized in the same fashion as described for PEG₄₀₀. The intermediate **15** was obtained from the reaction between diamine **14** and LA-NHS ester (**21**) and after reduction with NaBH₄ yielded the final NH₂- terminal ligand, DHLA-PEG₂₀₀₀-NH₂ (**16**), in high yield. Compound **16** was also obtained after 5 steps but with an overall yield of 29%, lower than the corresponding intermediate for PEG₄₀₀ (47%). Alternatively, compound **15** was also used as precursor for the synthesis of DHLA-PEG₂₀₀₀-COOH (**19**). After the treatment of compound **15** with methylmalonyl chloride, followed by methyl ester hydrolysis, the final pure product was obtained by reduction with NaBH₄. The desired compound **19** was obtained after seven steps with an overall yield of 26%.

For both PEG₄₀₀ and PEG₂₀₀₀, the reductive ring opening process of 1,2-dithiolanes in the presence of NaBH₄ could be monitored by a change of colour from yellow to colourless. All of the intermediates involved in the heterobifunctional ligands synthesis were characterized by NMR as described in the Experimental section.

In general, the synthetic route illustrated in Scheme 4 and Scheme 7 demonstrated a simple means to construct heterobifunctional linkers based on polyethylene glycols of different segments appended to thioctic acid/dihydrolipoic acid with the possibility to modify one of the ends of PEG with other functional moieties (e.g. OH, NH₂, COOH). The approach used for the achievement of these ligands incorporates several advantages. The procedure outlined provided higher reaction yields coupled with the ease of product separation as the case of diamine **6** (PEG₄₀₀, n=8) that was obtained in large amounts without the need of extensive purification. The precursor **7** and **15** was obtained from diamine **6** and **14** respectively in a straightforward fashion and was used for production of both final ligands amino/carboxy-PEG_n-DHLA. Moreover these ligands incorporate amide bonds which are more robust toward hydrolysis than ester bonds^[18] and did not alter the integrity of the ligand in certain conditions (e.g. reduction with NaBH₄)^[17].

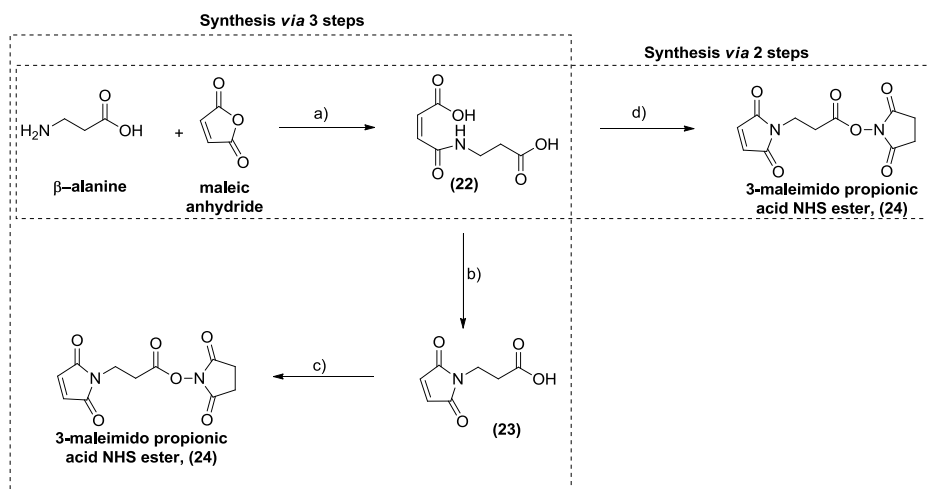
Carbohydrate moieties play a very important role in certain biological systems when coupled with proteins or lipids and it is as glyco-conjugates that they express their biological function ^[20]. One of the goals in this chapter was the preparation of water-soluble QDs using heterobifunctional ligands but also sugar-capped QDs that could be further used in biological applications. According to Seeberger *et al* ^[23] was possible to cap QDs with D-mannose and D-galactosamine using water-soluble QDs having a surface covered with amino groups (Scheme 9). The terminal NH₂ groups were reacted with 3-maleimidopropionic acid NHS ester (**24**) under borate buffer at pH 8.5. The so afforded maleimido-QDs were used directly for the next step without further purification and the final reaction with sugar-TEG-SH linker (**30**) under borate buffer at pH 7.3 produced the sugar-capped QDs



Scheme 9 | Sugar-capped QDs. General route for the production of sugar-capped QDs according to literature ^[23]. Reagents and conditions: (a) borate buffer pH 8.5, 2h, r.t.; (b) borate buffer pH 7.3, 3h, r.t.

To reproduce this strategy the 3-maleimido NHS ester (**24**) and the mannose linked thiol (**30**) were synthesized in this work. Maleimido linked active esters, such as compound **24** are widely used in biochemistry and biotechnology to crosslink high and/or low molecular weight compounds via amino groups (the active ester) and mercapto groups (the maleimido group) in many biological

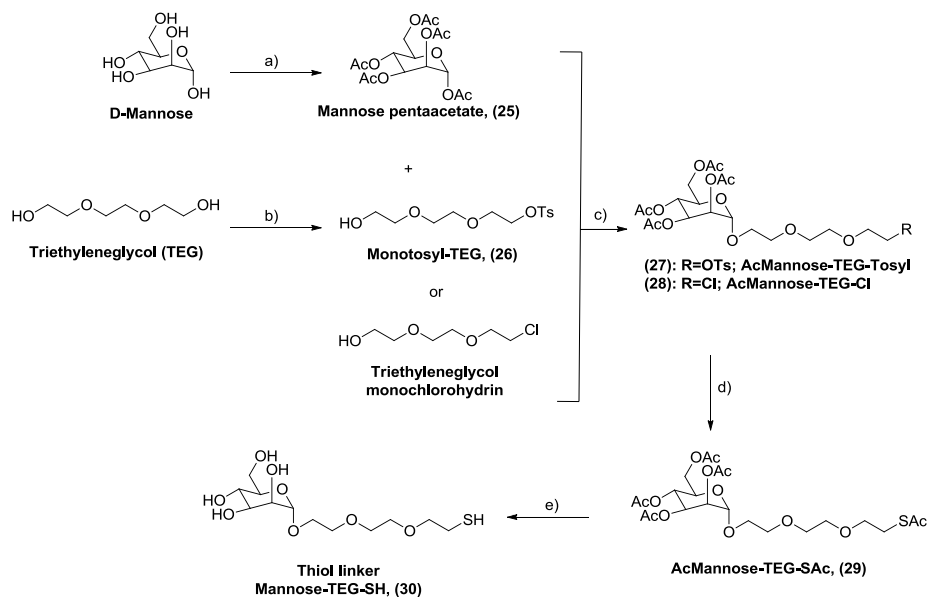
strategies (e.g. enzyme coupled immunoassays)^[33]. According to literature^[30, 31, 33], compound **24** was synthesized using two alternative ways (Scheme 10).



Scheme 10 | Synthesis of 3-maleimido propionic acid NHS ester. The scheme illustrates the two possible routes for the production of compound **24**. The synthesis *via 3 steps* is represented by the steps (a) to (c) and the synthesis *via 2 steps* is constituted by the steps (a) and (d).

The first approach was based on a three-step strategy with a very low overall yield (13%). The synthesis was carried out reacting β -alanine with maleic anhydride in the presence of glacial acetic acid to yield maleoyl- β -alanine (**22**) in a large quantity without the need of extensive purification. Consequently, compound **22** under heat reacted with acetic anhydride in the presence of sodium acetate to afford the 3-maleimidopropionic acid (**23**) which after simple esterification reaction with NHS and DCC and an additional chromatographic purification gives the final ester **24**. Alternatively, 3-maleimido propionic acid NHS ester (**24**) was obtained by a two steps route reacting maleoyl- β -alanine (**22**) directly with NHS in a simple esterification reaction in the presence of DCC. The final-product after chromatographic purification was obtained in a better yield (41%) than the first strategy.

The mannose linked thiol (**30**) was synthesized according to Kikkeri *et al*^[23] description with some modifications (Scheme 11).



- a) Ac_2O , DMAP, py, 0°C -r.t., overnight, quantitative; b) *p*-TsCl, DMAP, py, 0°C -r.t., 30min, 45%,
 c) $\text{BF}_3\cdot\text{Et}_2\text{O}$, CH_2Cl_2 , 0°C -r.t., 48h, quantitative; d) KSac, DMF, r.t, overnight, 67%;
 e) NaOMe, MeOH, r.t., 30min, 59%

Scheme 11 | Thiol linker synthesis. Synthetic route for thiol linker **30** based on the literature^[23] with some modifications.

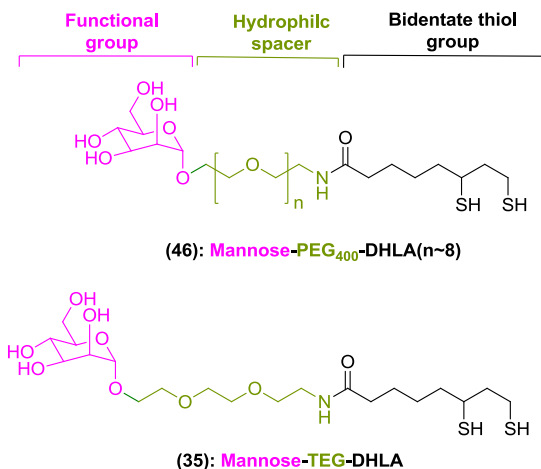
Based on the synthetic route demonstrated by Seeberger's group, it was possible to synthesize the thiol linker (**30**) in a straightforward five steps synthesis with an overall yield of 17% starting from D-mannose. The authors suggested the beginning of the synthesis using a glycosidation reaction between acetylated mannose (**25**) and the commercial triethyleneglycol monochlorohydrin in the presence of an acid Lewis ($\text{BF}_3\cdot\text{Et}_2\text{O}$) in order to obtain the compound **28**. Mannose pentaacetate (**25**) was synthesized starting from D-mannose according to literature^[34, 35] with high efficiency. The glycosidation reaction suggested was reproduced using an excess of commercial reagent and after 48h the AcMannose-TEG-Cl (**28**) was obtained in very quantitative yield. Despite the fairly efficiency of this possibility, alternatively, it was proposed in this work the use of monotosyl-TEG (**26**) instead of commercial reagent. In general this type of compounds are easy to obtain using a variety of initial reagents and show higher stability when comparing with chlorides. Hence, compound **26** was synthesized using a similar strategy applied before for PEG₄₀₀ and PEG₂₀₀₀ using *p*-TsCl, however

in this case just one side of the TEG was tosylated using 1 equivalent of *p*-TsCl and the time reduced for only 30 minutes in order to minimize the formation of bi-substituted species. After a chromatographic step the monotosyl-TEG (**26**) was afforded in 45% of yield. Subsequently, the glycosidation reaction again in the presence of BF₃.Et₂O had occurred between mannose pentaacetate (**25**) and an excess of compound **26**, and after 48h de pure AcMannose-TEG-tosyl (**27**) was also afforded in a quantitative yield.

It was not possible to obtained monotosyl-TEG (**26**) in high yield. This was a consequence of the formation of the corresponding bi-substituted type, which despite the short time used in the reaction, was hard to avoid. However, the glycosidation reaction for the production of compound **27**, demonstrated to be a very good alternative, proved by the high efficiency obtained.

The following two steps were performed using the monotosyl-TEG (**27**) instead of compound **28** that reacted with 3 equivalents of potassium thioacetate to afford the sugar-TEG-SAc (**29**) in 67%. This step was followed by an acetate deprotection reaction using sodium methoxide and MeOH to yield the desired final mannose linked thiol (**30**) in 59%.

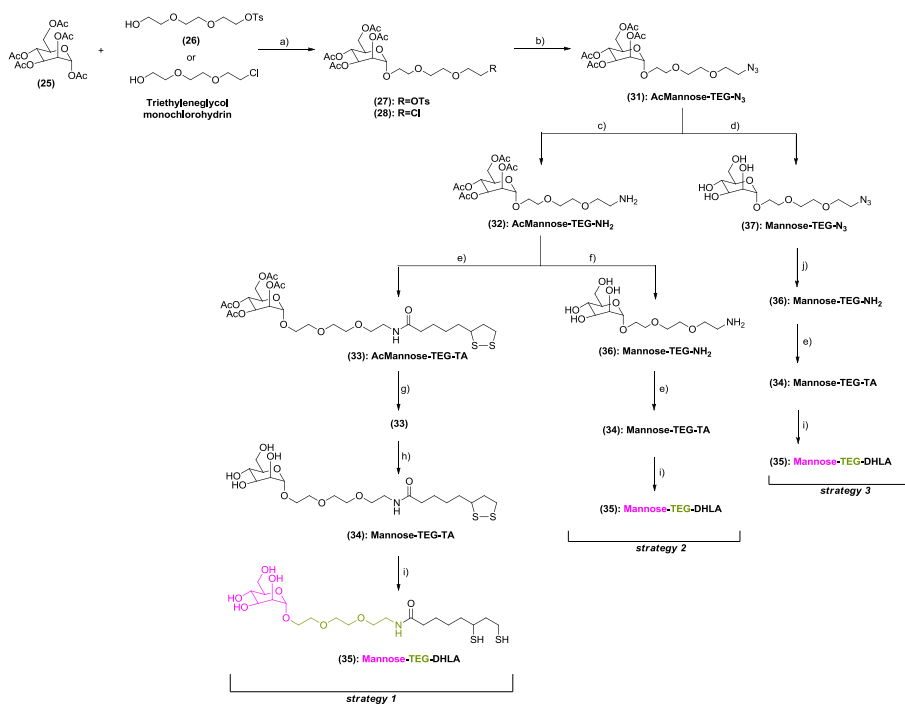
Once available the 3-maleimidopropionic acid NHS ester (**24**) and the mannose linked thiol (**30**), some attempts to obtain the sugar-capped QDs using the strategy described by Seeberger's (Scheme 9) were performed. However, many different problems and limitations were found as discussed later. To address some of these problems/limitations and further expand the range of techniques to prepare hydrophilic nanoparticles, an alternative method was devised to synthesize ligands that could incorporate carbohydrates moieties to be attached to the surface of QDs. The strategy applied was based on the approach carried out for the production of amino/carboxy-PEG_n-DHLA discussed previously and where was taken the advantage of the bidentate nature of the anchoring DHLA group and the hydrophilic nature of PEG_n chain. The structure of the final ligands with a mannose as functional group using the same modular design presented previously is shown in the follow scheme.



Scheme 12 | Carbohydrate Hydrophilic Ligands. Structure of the final ligands incorporating mannose as terminal functional group using TEG or PEG₄₀₀ as hydrophilic spacer.

The intermediates AcMannose-TEG-OTs (**27**) and AcMannose-TEG-Cl (**28**) can be used in the preparation of azide **31** (Scheme 13). In both cases, the experimental conditions were the same. The intermediates were dissolved in dried DMF and reacted with 3 equivalents of sodium azide at 85°C during 12 hours. The desired compound **31** was obtained in 95% of yield, independently of the intermediate used. This was followed by the reduction of azide group with triphenylphosphine/water followed by an aqueous work up to afford AcMannose-TEG-NH₂ (**32**) in 77% yield. After synthesis of amine **32**, the *strategy 1* displayed in Scheme 13 was followed. Compound **32** was attached to thioctic acid after reaction with its NHS ester (**21**). After 12 hours, in a DMF/water mixture and using sodium bicarbonate as base, compound **33** was obtained. Unfortunately, this step afforded the AcMannose-TEG-TA (**33**) but contaminated with a structurally similar compound lacking some acetate protecting groups in the carbohydrate moiety. This could be related to a possible migration of some acetate group to the free primary amine present in **32** leading to the formation of an acetamide as secondary product and bringing down the yield of the reaction (~57%). Hence, the mixture of compounds obtained was again subjected to an acetylation reaction with acetic anhydride/pyridine affording a single product demonstrating that the unknown number of deprotected hydroxyl groups in the sugar moiety were

reacetylated, thus producing pure **33** in 77% yield. This step was followed by a simple hydrolysis reaction with sodium methoxide to give the mannose-TEG-TA (**34**). The final pure product **35** was furnished smoothly from ring opening thioctic acid to the dihydrolipoate form by reduction with sodium borohydride in a mixture of ethanol/water. The desired mannose-TEG-DHLA (**35**) was obtained in 73% yield. Typically the reduction with sodium borohydride leads to products in quantitative yields as has been observed in the case of reduction of 1, 2-dithiolane ring for the obtention of compounds amino/carboxy-PEG_n-DHLA. In this synthesis the yield dropped slightly to 73% because the final product is soluble in water as well as the excess of NaBH₄ used in the reaction, hindering the purification step to eliminate possible impurities delivered from borohydrides. Thus, this process led to some losses of the final product.



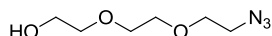
a) BF₃·Et₂O, CH₂Cl₂, 0°C-r.t., 48h, quantitative; b) NaN₃, DMF, 85°C, 12h, quantitative; c) 1. PPh₃, THF, 4h, r.t.; 2. H₂O, r.t., 12h, 77%; d) NaOMe, MeOH, r.t., 1h, 72%; e) LA-NHS (20), NaHCO₃, DMF/H₂O (1:1), 4°C-r.t., 12h, 57%; f) NaOMe, MeOH, r.t., 2h, 34%; g) Ac₂O, py, DMAP, 0°C-r.t., 12h, 77%; h) NaOMe, MeOH, r.t., 1h, 98%; i) NaBH₄, EtOH/H₂O (4:1), r.t., 2h, 73%; j) H₂, Pd/C, AcOEt, 50Psi, r.t., 3h, 95%

Scheme 13 | DHLA-TEG-Mannose Synthesis. Synthetic route developed for the achievement of compound **35**.

It was clear that the limitation presented in *strategy 1* was well overcome by the additional acetylation step to protect against the hydroxyl groups. However, once obtained the amine **32**, before the reaction with LA-NHS (**21**) was possible to follow another route (Scheme 13, *strategy 2*) where a hydrolysis reaction again using sodium methoxide in MeOH could take place first. This step removed the acetates protecting groups in the sugar, thus leading to the obtention of mannose-TEG-NH₂ (**36**) however in a low yield (34%). The deprotection of acetylated sugar moiety of compound **32** led to the formation of compound **36** with free hydroxyl groups, which is more polar and only soluble in water or polar solvents. Moreover, the work up of the reaction included the use of an ion-exchange resin (Dowex 50wx8-100) to eliminate the excess of NaOMe used in the reaction and neutralize the pH. This resin needed to be activated with HCl in order to become protonated with H⁺ protons. So, the amino group present in mannose-TEG-NH₂ (**36**) during the purification step with Dowex became protonated (NH₃⁺) and strongly interacted with the resin making it very difficult to remove even after several washes with water or MeOH. Hence, only part of the compound was recovered which led to a sharp decrease in the efficiency of the reaction. The last two steps were repeated in the same fashion as did before in *strategy 1*. The low amount obtained of mannose-TEG-NH₂ (**36**) reacted with LA-NHS (**21**) in the presence of NaHCO₃ and a DMF/water mixture to afford the mannose-TEG-TA (**34**) which after a mild reduction with sodium borohydride give the final product mannose-TEG-DHLA (**35**) in 43%. Here, a much lower yield was obtained when comparing with the result obtained for *strategy 1* (43<73%), due to the limited solubility of the final product **35** in aqueous solvents hindering the purification step as discussed above.

To turn around some of the problems discussed for *strategy 1* and *2*, a third alternative (Scheme 13, *strategy 3*) was tested. This route was enhanced by the direct deprotection of the sugar hydroxyl groups by hydrolysis of azide **31**. This step is advantageous because with the azide group it was possible to carry out the work-up with an ion-exchange resin (Dowex 50wx8-100) without the problem of mannose-TEG-N₃ (**37**) being kept in the resin. Besides, the N₃ group allowed increasing the reaction yield from 34 to 73% when compared to the same reaction with an NH₂ group presented in *strategy 2* to afford **36**. For

the obtention of **37**, it was expected a complete reaction with a quantitative yield but it was found the formation of the collateral product TEG-N₃ (**38**) from slightly degradation of initial compound **31** (Scheme 14). This was due to the use of 1 equivalent of NaOMe instead of a catalytic amount in order to ensure the total deprotection of the carbohydrate moiety.



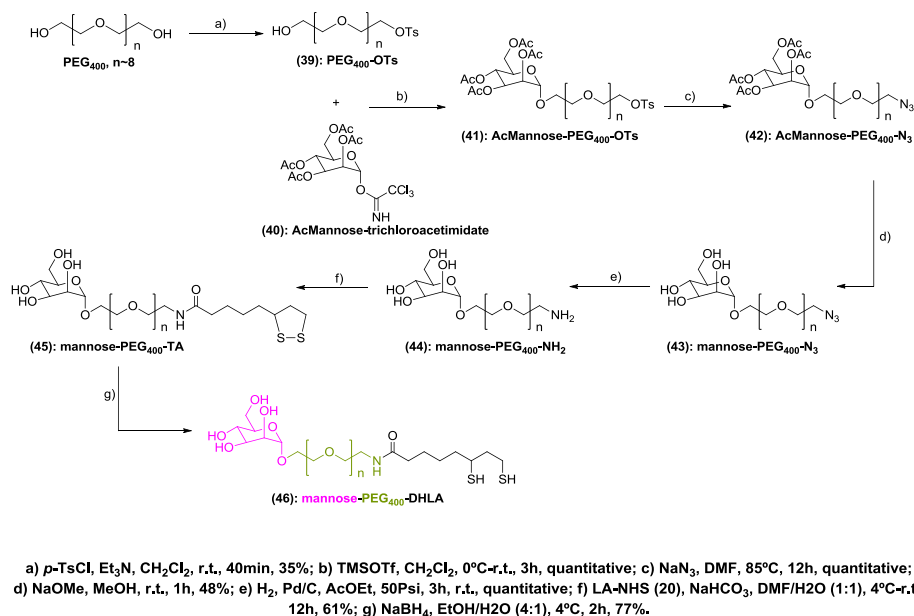
(**38**): TEG-N₃

Scheme 14 | Structure of collateral product TEG-N₃ (**38**) formed from degradation of initial compound **31** under hydrolysis conditions.

Azides may be converted to amines using the mild Staudinger reaction^[40] in the presence of PPh₃ and an aqueous work up, however this reaction is laborious since large quantities of triphenylphosphine oxide are also produced. Alternatively, mannose-TEG-NH₂ (**36**) was afforded by a catalytic hydrogenation reaction, which after 3 hours was complete (95% of yield) and the final product pure enough to be used without the need of a chromatographic purification step. Following this approach, the final product mannose-TEG-DHLA (**35**) was formed using the same conditions already described leading to an overall yield of 45%.

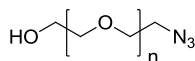
The synthesis developed for the obtention of mannose-PEG₄₀₀-DHLA (**46**) is displayed in Scheme 15.

With mannose pentaacetate (**25**) already available it was simple to think in a possibility to synthesise the monotosyl compound from PEG₄₀₀ (**39**) for a further glycosidation reaction. According to literature^[41] was possible to treat PEG₄₀₀ with a twofold excess of tosyl chloride in the presence of triethylamine. Different attempts were tested changing the reaction time from 15 minutes to 12 hours. The best result was reached for ~45 minutes with a 35% of yield, where a moderate amount of PEG₄₀₀-OTs (**39**) was formed and the production of bi-substituted species was controlled. The unreacted PEG₄₀₀ and *p*-TsCl were well eliminated by an aqueous work up and by column chromatography respectively.



Scheme 15 | DHLA-PEG₄₀₀-Mannose Synthesis. Synthetic route developed for the achievement of compound **46**.

The experiment to afford AcMannose-PEG₄₀₀-OTs (**41**) was carried out treating the mannose pentaacetate (**25**) and the PEG₄₀₀-OTs (**39**) with BF₃·Et₂O, but unfortunately the achievement of desired product was doubtful. It is well known in carbohydrate chemistry that the activation of anomeric trichloroacetimidates is usually achieved by treatment with an acid Lewis such as BF₃·Et₂O or TMS triflate (TMSOTf). Making use of these conditions the AcMannose-trichloroacetimidate (**40**) easily obtained^[35] in high yield, reacted with monotosyl compound from PEG₄₀₀ (**39**) by a simple glycosidation reaction with 1 equivalent of TMSOTf yielding compound **41** in quantitative yield. The synthesis was followed by the formation of azide **42** which was carried out under experimental conditions previously described for the obtention of **31**. The deprotection by hydrolysis of compound **42** led to the obtention of mannose-PEG₄₀₀-N₃ (**43**) in only 48% yield. This is related to the same problem found with mannose-TEG-N₃ (**37**) in *strategy 3* (Scheme 13), where a small degradation of initial compound occurred forming the secondary product PEG₄₀₀-N₃ (**47**).

(47): PEG₄₀₀-N₃, n=8

Scheme 16 | Structure of collateral product PEG₄₀₀-N₃ (**47**) formed from degradation of initial compound **42** under hydrolysis conditions.

The experimental conditions applied to the further steps were the same as those used for the formation of mannose-TEG-DHLA (**35**) in Scheme 13 (*strategy 3*). Mannose-PEG₄₀₀-NH₂ (**44**) was obtained after conversion of azide **43** to a primary amine by a hydrogenation reaction. The product **44** was obtained in quantitative yield without the need for additional purification. This step was followed by the attachment to thioctic acid using LA-NHS (**21**) to afford mannose-PEG₄₀₀-TA (**45**). The reduction of the 1,2-dithiolane ring of compound **45** was carried out with NaBH₄ in an ethanol/water mixture affording the desired final product, mannose-PEG₄₀₀-DHLA (**46**), in 77% of yield.

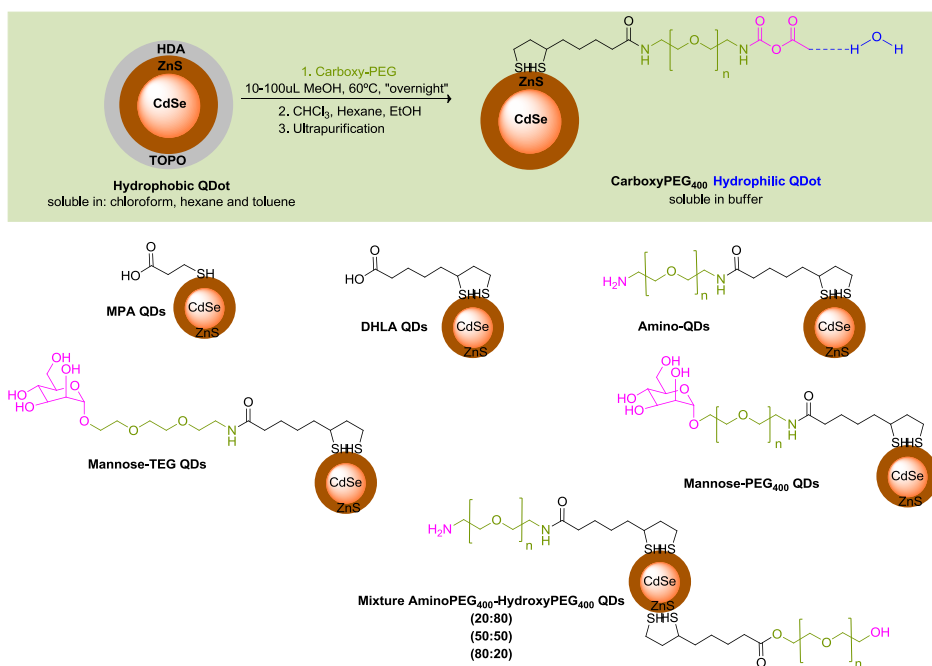
In general, the development outlined to incorporate carbohydrates moieties using the heterobifunctional strategy were successful and allowed the formation of stable glyco ligands. With the synthesis of mannose-TEG-DHLA (**35**) it was possible to address the limitations found, thus making easier the way to obtain the mannose-PEG₄₀₀-DHLA (**46**) ligand.

Water Solubilisation of CdSe/ZnS core-shell QDs

It was clear from the Introduction, that the dispersion of inorganic nanoparticles in solution environments is promoted by modification of their surface with ligands. With the cap-exchange strategy this can be realized by simply performing cap-exchange in the presence of a ligand or ligand mixtures that incorporate functional end groups for subsequent conjugation. In this particular work, the ligand exchange of CdSe/ZnS core-shell QDs was performed by displacing the native TOPO/HDA hydrophobic ligands with the monothiol group present in the commercial MPA and the dithiol group anchored in the series of ligands synthesized in this work and which can participate in binding interactions with the Zn and S atoms in the QD surface. This strategy led to a change of solubility of the surface polarity from hydrophobic to hydrophilic. Hence, the nanoparticles that were initially soluble

in chloroform become water-soluble and the ligand exchange could be followed by the change of solubility (Scheme 17).

The ligand exchange conditions for the obtention of hydrophilic QDs were relatively mild. In the case of commercial MPA the phase transfer method was applied. The hydrophobic CdSe/ZnS QDs previously suspended in a chloroform solution were shaken with a stock solution of MPA yielding a flocculate solution. After the addition of a basic aqueous solution the transfer of QDs from the organic to aqueous phase immediately occurred affording the desired hydrophilic MPA-QDs in a simple and faster way. For DHLA (**1**) ligands and their corresponding derivatives with a hydrophilic spacer and a functional end group namely amino-PEG₄₀₀ (**8**), carboxy-PEG₄₀₀ (**11**), mannose-TEG (**35**) and mannose-PEG₄₀₀ (**46**) the ligand exchange was performed under heating and inert conditions.



Scheme 17 | Functionalization Procedure. Ligand exchange strategy applied to produce hydrophilic QDs with different coatings.

Upon reduction of the 1, 2-dithiolane group of the thioic acid moiety to dithiol with NaBH₄ the resulting ligands were mixed with a dried pellet of hydrophobic QDs forming a viscous and homogeneous mixture. Under heating during from

3h to overnight, the reaction was followed by precipitation with chloroform, ethanol and hexane. The QDs were dispersed in aqueous solution or buffers and ultra-purified yielding the amino-QDs, carboxy-QDs and glyco-QDs. The same approach was used to produce hydrophilic QDs coated with mixtures of ligands. The functional amino-PEG₄₀₀ (**8**) ligand was mixed in different molar ratios with the inert hydroxy-PEG₄₀₀ (**3**) in order to control the number of reactive groups on the QDs surface. Here, three types of amino-PEG₄₀₀/hydroxy-PEG₄₀₀ (x: y) QDs were tested: (20:80), (50:50) and (80:20) where x and y represents the percentage of each ligand on the QD surface respectively. In addition, all the hydrophilic samples of QDs were purified using cycles of concentration/dilution with centrifugal filter devices with a certain MW cut-off from 10 to 50kDa depending on the sample. This procedure permitted the elimination of soluble organics (e.g. excess of ligand) and other materials from the solution and provided homogeneous and clear QD solutions.

However, careful attention was given to glyco-QDs. It was discussed previously in the ligand synthesis and design section that according to Seeberger's group ^[23] was possible to attach carbohydrates moieties to the surface of QDs. The NH₂ group available at the surface of amino water-soluble QDs reacted with maleimide **24** to afford maleimido QDs which then reacted with the mannose thiol linker **30** to yield the desired sugar-capped QDs (Scheme 9). This route was also tested during the preparation of hydrophilic QDs, but unfortunately many problems were found. The approach starts with QDs already soluble in aqueous environment, which requires that all the steps need to be performed in aqueous solution. This represents a limitation because maleimido **24** has a low solubility in borate buffer leading to a low concentration of maleimido QDs. Additionally, since the entire route needs to be performed in solution (borate buffer) was difficult to verify if the final reaction between the NHS ester present in the afforded maleimido QDs with the mannose thiol linker (**30**) occurred and no change of solubility from hydrophobic to hydrophilic could be followed.

Hence, the ligand exchange strategy proposed initially for the preparation of water-soluble QDs seems to be the easier and most appropriate since is possible to follow the change of solubility. On the other hand, the use of

PEG/TEG-modified ligands have the ability to prepare aqueous solutions of QDs that are aggregate-free and chemically stable over long periods of time

Characterization of Hydrophilic QDs

Determination of QDs Concentration in Aqueous Solutions and Optical Measurements

The concentration of QDs in aqueous solutions was estimated from measurements based on the absorption spectra method and the size-dependent extinction coefficient used was estimated by the approach developed by Peng *et al* [42, 43]. The concentrations obtained in the range 1 to 10 μ M using this method was within what was expected.

Figure 12 shows the absorption and emission spectra of a representative QD sample with emission centred at 585nm (QD585) before and after ligand exchange with commercial MPA.

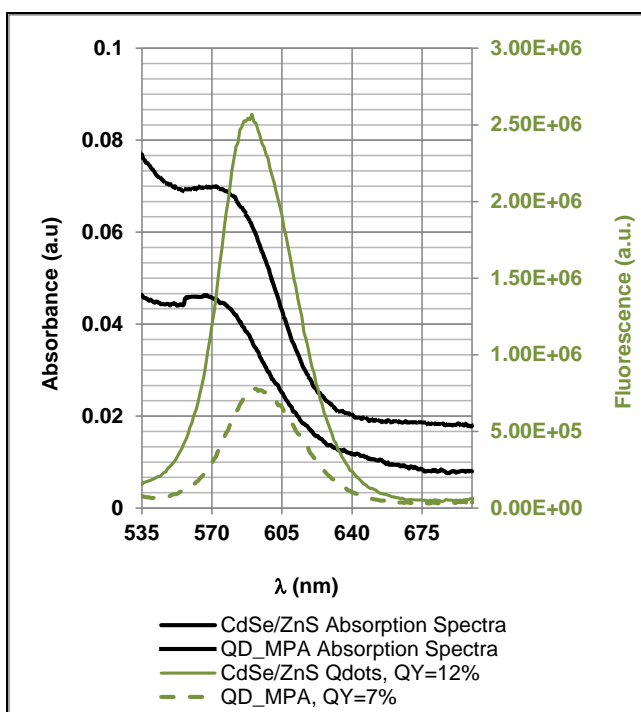


Figure 12 | Optical Measurements of Hydrophilic QDs. Representative absorption spectra of CdSe/ZnS QDs in chloroform (black solid line) and after ligand exchange with MPA (black dashed line). Fluorescence spectra of the same hydrophobic (green solid line) and hydrophilic QDs (green dashed line) with QY of 12 and 7% respectively.

The differences in the absorption and emission spectral profiles of the QDs measured in chloroform and QDs that were transferred into water using MPA are negligible with peaks shifts less than 3nm. Similar spectral properties were obtained for QDs exchanged with DHLA (**1**), amino-PEG₄₀₀ (**8**), carboxy-PEG₄₀₀ (**11**), mannose-TEG (**35**), mannose-PEG₄₀₀ (**46**) and mixtures of compound **8** with hydroxy-PEG₄₀₀ (**3**) (e.g. DHLA-QDs, QY=5%; carboxy-QDs, QY=8%). This indicates that the surface ligands have little or no effect on the electronic properties of the inorganic QD core^[15]. However, despite the absorption and emission spectra of the organic and aqueous soluble QDs were nearly identical, a considerable decrease of the photoluminescence quantum yield for the QDs dispersed in aqueous solutions was observed. The QY of QD585 in chloroform was 12% and after ligand exchange, for example, with MPA was 7%. This is consistent with previous reported work where normally the quantum yields for water-soluble QDs are smaller than those measured in organic solutions. For MPA coated CdSe cores a nearly complete quenching of the PL may be observed^[44], but the PL when MPA coated core-shell nanocrystals was only partially quenched. This phenomenon is related to the fact that the PL QY depends on the particular core-shell nanocrystals. For a CdSe/CdS core-shell system it was demonstrated a stronger decrease degree (~10 to 30%) of QY due to the smaller band offset for the CdSe and CdS materials combination, leading to a higher probability for the charge carriers to be found in the QD surface. For CdSe/ZnS QDs a similar behaviour may be observed^[36]. However, after water solubilisation the QY decrease for CdSe cores coated with a ZnS shell is smaller than those coated with a CdS shell because the lattice mismatch between CdSe core and ZnS shell materials is bigger providing a better passivation of interfacial trap states^[18]. This fact was also observed for CdSe/ZnS core-shell QDS coating with the different ligands produced in this work (amino, carboxy, glyco and mixture of ligands QDs).

Tuning the Hydrodynamic Size and Surface Charge of Hydrophilic QDs

The ligand exchange strategy was used to create the water-soluble QDs. The hydrophilicity was obtained by charged groups (e.g. carboxylic acids, amines, etc.) and polyethylene glycol (PEG) polymers. These ligands create a

solubilisation layer and strongly influence the hydrodynamic size of QDs along with their surface charge. As was discussed previously in chapter 2, DLS permits the hydrodynamic diameter (HD) measurement in an easy and cheap way. The measurement of HD is of great importance for biological applications since particles with large diameter could interfere for example in intracellular mobility assays. For that reason, in this work, the HD of the different water-soluble QDs produced and dispersed in aqueous buffers were characterized and compared with the native TOPO/HDA-capped QDs dispersed in chloroform as shown in Figure 13.

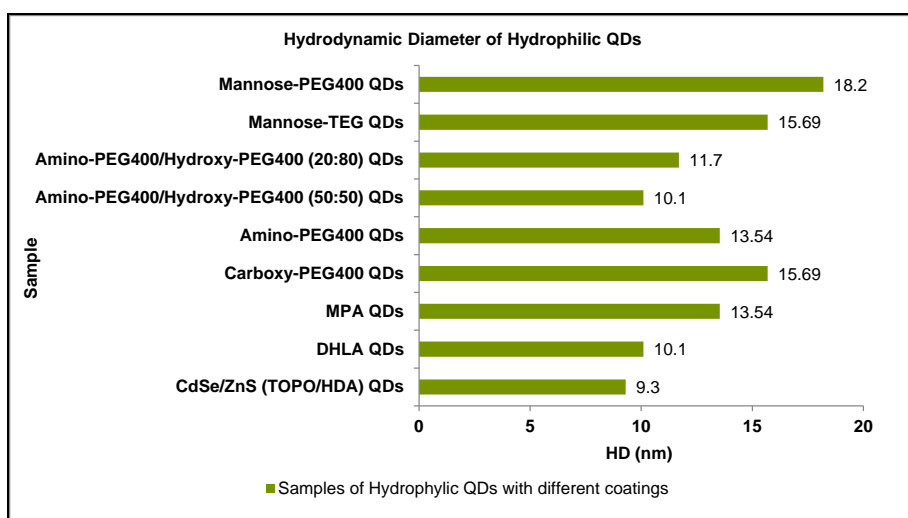
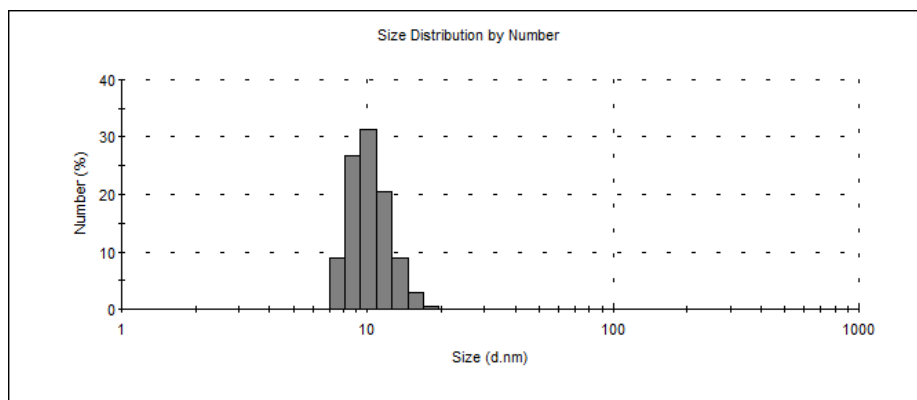


Figure 13 | HD Measurements of Hydrophilic QDs. Representative diagram of the HD results obtained for the hydrophilic QDs samples after ligand exchange with different coatings. The HD of the native TOPO/HDA QDs it's only for comparison.

The HD obtained for water-soluble QDs was in the range between 10.1 and 18.2nm. The hydrodynamic diameter of the DHLA QDs were 10% larger than their inorganic TOPO/HDA-capped counterparts which may be attributed to a larger solvation layer around the QDs in aqueous solution due to the presence of carboxylic acid groups. Similar behaviour was also observed when HD was measured for all the other samples and an increase even bigger when MPA or DHLA (1) were substituted by longer ligands such in case of carboxy-PEG₄₀₀ (11) or glyco-QDs. These larger values are consistent with what is expected for solid objects as was evaluated for Landau for hard spheres^[45]. However, QDs are nanoparticles much more complex than spheres or macromolecules.

These QDs are made of solid materials such as CdSe and ZnS and are capped with ligands that act more like polymers and can be penetrated by solvent. The main goal of these ligands (cap molecules or larger polymeric chains) was to promote the dispersion and stability of these QDs in aqueous solutions and the larger measured HD obtained for hydrophilic QDs when comparing with the hydrophobic ones, reflected this complexity. These ligands are not rigid and their contributions cannot be treated as simple geometric increase of the size. Hence, the hydrodynamic aspects of hydrophilic QDs should be viewed as a combination of solid impenetrable spherical cores and more like flexible polymer-like layer that strongly interacts with the surrounding solvent/ aqueous environment allowing aggregate-free solutions [46]. The HD histograms obtained are very similar to those obtained for the hydrophobic QDs in chapter 2 demonstrating monodisperse samples with a very low polydispersity index (PDI ~0.177). Figure 14 shows an example of these histograms for DHLA-QDs.



Item	HD(nm)	PDI	% Volume
DHLA-QDs	10.1	0.177	100

Figure 14 | Size Determination by Dynamic Light Scattering. Hydrodynamic diameter (histogram size/number) and polydispersity index obtained for DHLA-QDs. The results obtained were the average of triplicate run.

A charged particle in a buffer solution is normally surrounded by a concentration of counter ions (ions of opposite charge to that of the particle) which can be separated into distinct regions: a thin layer tightly packed around the surface called Stern layer that migrates with the particle in the

presence of an external electrical field and a more diffuse layer that migrates in the opposite direction. The surface between these two regions is defined as the surface of shear and its electrical potential is referred to as the zeta potential (ξ). Simplifying, this parameter is closely related with the charge density at the particle surface and may control colloidal properties such as stability and interparticle interactions^[46].

Among HD characterization, another feature provided by this technique is the possibility to measure the zeta potential of particles. In other words, this technique permits to measure and provide information about the surface charge or net charge of such particles. Using a dynamic light scatterer Zetasiser Nano ZS, the electrophoretic mobility of the hydrophilic QDs was determined over 20 electrode cycles and automatically converted to the zeta potential based on the Smoluchowski equation (Equation 1), where η and ϵ are the viscosity and dielectrical constant of the dispersion medium and μ_e is the electrophoretic mobility measured of the nanoparticles^[47].

$$\xi = (\eta/\epsilon)\mu_e$$

Equation 6 | Smoluchowski equation used to convert electrophoretic mobility of nanoparticles measured in zeta potential values^[47].

The zeta potential values obtained for the water-soluble QDs with different hydrophilic coatings is displayed in Figure 15.

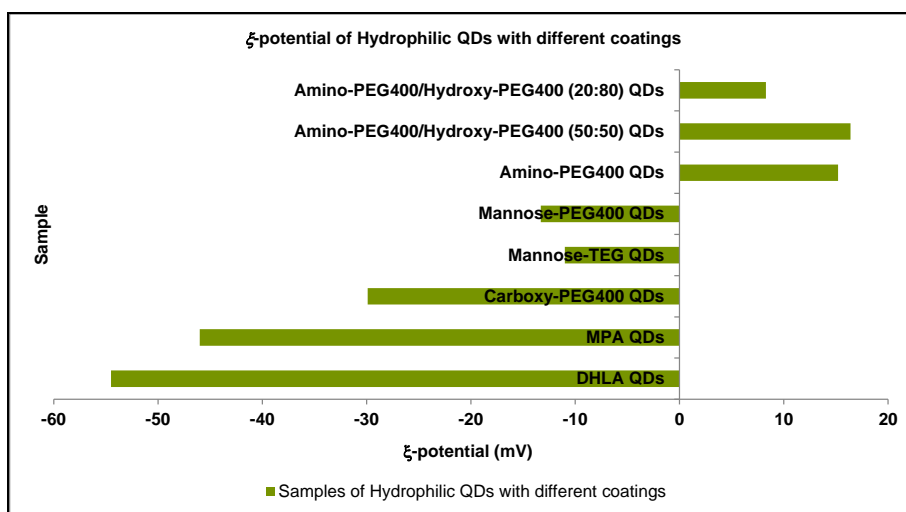


Figure 15 | ξ -potential Measurements of Hydrophilic QDs. Representative diagram of the zeta potential values obtained for the hydrophilic QDs samples after ligand exchange with different coatings.

Depending on the pH molecules bearing carboxylic acid groups (-COOH) are able to maintain a negative charge, while molecules carrying amines (-NH₂) are able to maintain a positive charge. As expected, the above graph shows that the surface charge of amino-QDs and the mixed-ligand amino-hydroxyl QDs is positive while for MPA, DHLA and carboxyPEG-QDs this surface charge is negative. Regarding the nanoparticles bearing carboxylic acid groups on their surface it is possible to observe that the zeta potential obtained for DHLA and MPA-QDs are more negative than the carboxyPEG-QDs. This could be associated with the size of the ligands. As DHLA (**1**) and MPA are smaller molecules than carboxy-PEG₄₀₀ (**11**), this means that a higher number of molecules may be attached on QD surface leading to a large density of available carboxylic acid groups and consequently a more negative zeta potential. For the amino-QDs and the corresponding mixture-ligand QDs, the zeta potential have followed a similar trend and as the percentage of ligand containing amino group's increases, the charge surface of the particles tends towards more positive values. However, for amino-PEG₄₀₀/hydroxy-PEG₄₀₀ (50:50) QD samples this behaviour was not observed. According to the same diagram, the surface of glyco-QDs seems to be poorly negatively charged. These results may be associated with a negative polarization shown by the hydroxyl groups in the carbohydrate moiety. On the other hand, the presence of a positively charge from the amide present in the Mannose-TEG (**35**) and Mannose-PEG₄₀₀ (**46**) ligands to anchor the DHLA moiety could also decrease the zeta potential of the sugar-capped QDs leading to a zero surface charge.

Probing the Number of Functional Amines Groups per QD

A fluorescamine assay was carried out in order to determine the number of reactive amine groups coupled to the amino-QDs and their mixtures with hydroxy-PEG₄₀₀ (**3**). This fluorescence-based assay is based on the rapid reaction of fluorescamine with proteins. Fluorescamine reacts with all substances containing primary amine groups to yield intensely fluorescent products (excitation at 380nm, emission at 480nm) with a fluorescence emission peak at 480nm. The emission spectra of free amino-PEG₄₀₀ (**8**) at concentrations ranging between 0-25µM after treatment with fluorescamine

was obtained as demonstrated in Figure 16. Subsequently, the integrated fluorescence of these samples were plotted from 460 to 480nm against amino-PEG₄₀₀ (8) concentration (linear fit: $y=165.83x+356.46$, $r^2=0.9997$) (Figure 16, inset).

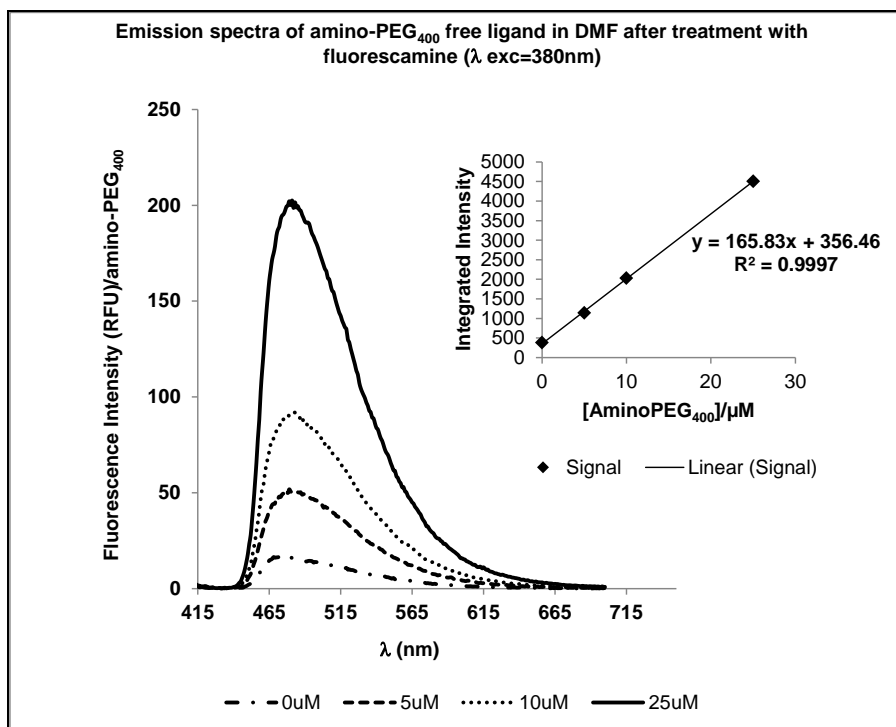


Figure 16 | Measurement of the number of amino-PEG₄₀₀ per QD. Calibration: emission spectra of amino-PEG₄₀₀ (8) free ligand in DMF after treatment with fluorescamine (380nm excitation). Inset: integrated fluorescence intensity of these samples from 460-485nm, along with a linear fit.

With this calibration curve, the concentration of compound 8 in the QD samples was determined and according to Equation 4 the number of amines available in a single QD for each sample was calculated. The results obtained are in agreement with a previously reported system^[18], where for example, an estimate of ~140 amines per QD was obtained for 100 % amino-QDs. Moreover, these results demonstrate a linear correlation for the amount of amine detected per QD with the percentage of amine-terminated ligands used in the ligand-exchange combination (Figure 17). It is important to notice that the assay was performed in duplicate to improve accuracy and in some cases values overlap as was expected.

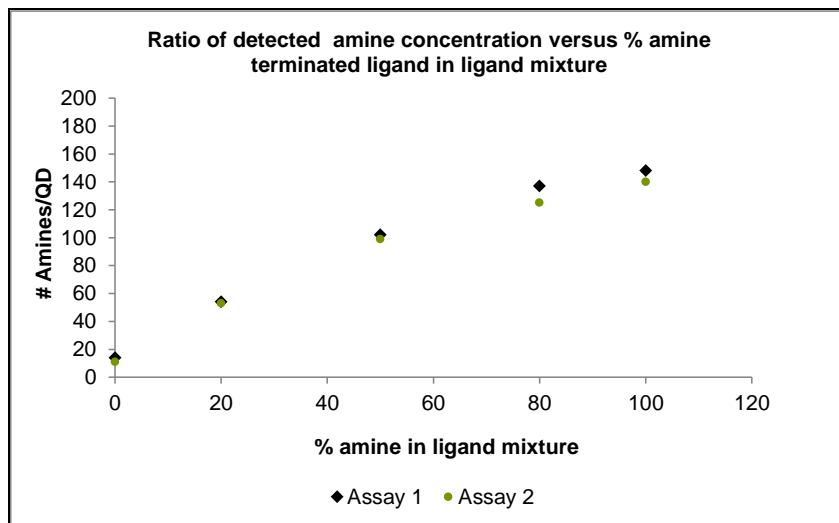


Figure 17 | Ratio of detected amine concentration vs. % of amine-terminated ligand in ligand mixture.

Estimation of the Number of Sugar Molecules per QD

Many colorimetric methods for carbohydrate determination have been reported^[48-50] but the phenol-sulphuric acid method is simple, most reliable and sensitive for measuring neutral sugars in carbohydrate chemistry. The procedure used was based in the microassay described by Masuko *et al*^[26], for high throughput, to gain greater sensitivity and to economize reagents. In terms of data treatment, this method is very similar to the fluorescamine assay previously discussed. First, the absorbance measurements at 490nm of free mannose after treatment with phenol-sulphuric acid were made in order to obtain a linear calibration curve represented by the equation: $y=0.0007x$, $r^2=0.9513$ in the range of 0-200nmol/well of mannose. Using this equation it was possible to estimate the total concentration of mannose present in the QDs samples and further the number of sugar molecules on a single QD surface using the Equation 5. The results obtained showed a range of 54 to 150 sugar molecules per QD for QDs samples with a concentration ranging from 0.25 to 0.34 μ M (Figure 18) which is consistent with a similar system reported in the literature^[23].

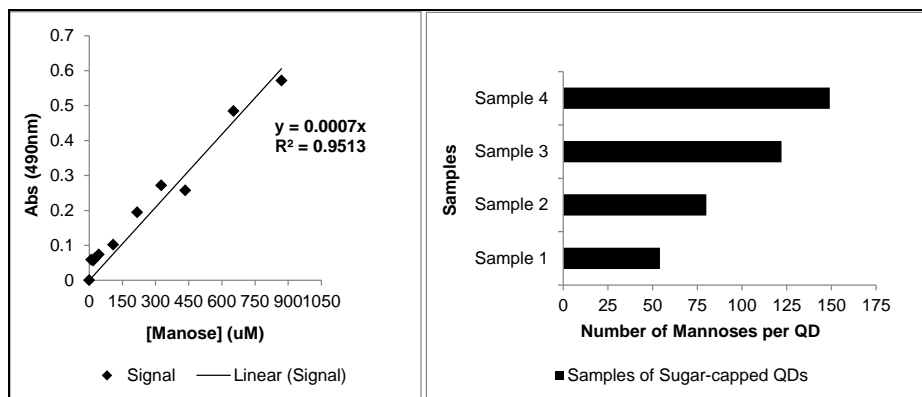


Figure 18 | Estimation of the Number of Sugar Molecules per QD. Calibration: linear curve of the absorbance measured at 490nm of free mannose after treatment with phenol-sulphuric acid (left image). Representative diagram of the number of sugar molecules per QD in four different samples of sugar-capped QDs (right image).

Conclusion

A series of polyethylene glycol/triethylene glycol-based bidentate ligands were designed and synthesized to permit the conversion of hydrophobic nanocrystals into water-soluble QDs. Moreover, these ligands were synthesized incorporating the thioctic acid moiety which after reduction of the 1, 2-dithiolane ring created a bidentate anchoring group and thus enhanced the affinity for CdSe/ZnS core-shell QDs. The ligand exchange method demonstrated to be very good strategy to create water-soluble QDs with mixed-ligands compositions including different reactive end groups and allowed access to QDs with a different charge on the surface. The hydrodynamic size and the surface charge parameters were characterized by dynamic light scattering which is a powerful tool for the characterization of hydrophilic QDs. The hydrodynamic size values showed to be strongly dependent on the size and type of capping ligand, where for example MPA or DHLA-QDs proved to be smaller than polymer-coated QDs. The results obtained for zeta potential measurements, also demonstrated a dependence of the surface composition. Where appropriate, the surface composition on a single QD was probed by known fluorimetric and colorimetric assays which reveal to be complementary methods to characterize the hydrophilic QDs. In general, a family of water-soluble QDs with small hydrodynamic diameter, good quantum yields and strong stability across a wide pH range were

produced, encouraging their use in covalent conjugation with several biomolecules to be applied in labelling and imaging applications.

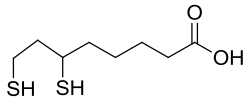
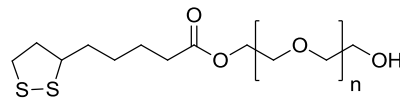
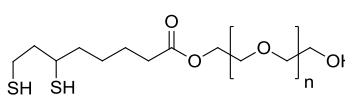
Acknowledgments

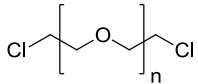
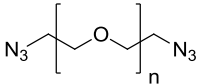
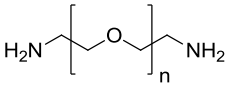
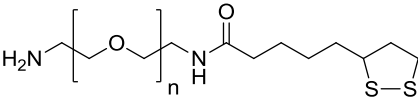
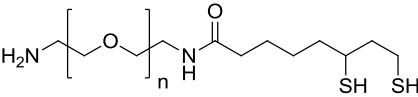
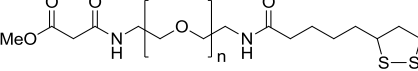
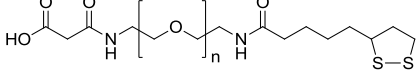
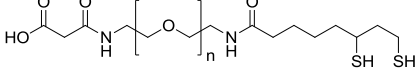
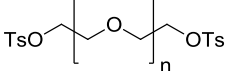
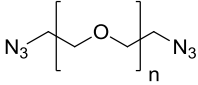
The author thank to Professor Dr António Maçanita for the opportunity to perform the photoluminescence spectra and quantum yield measurements in his laboratory at the Instituto Superior Técnico (IST), Lisboa, Portugal. The help provided by Professor António Lopes from ITQB-UNL, Oeiras, Portugal in DLS measurements was also appreciated. Ana Sofia Miguel is a recipient of a PhD fellowship from the Fundação para a Ciência e Tecnologia (FCT), Portugal (SFRH/BD/40303/2007). The work was supported by the national funded project NTec/SQA/0131/2007 from FCT.

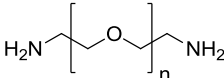
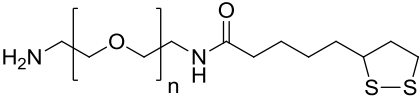
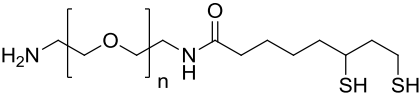
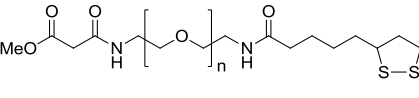
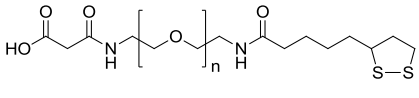
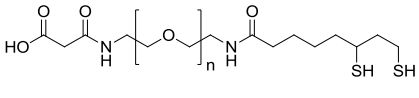
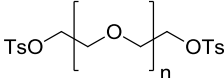
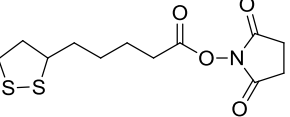
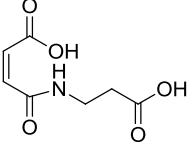
Supplementary Information

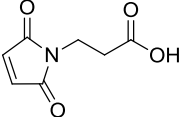
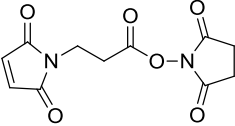
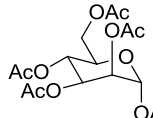
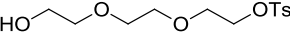
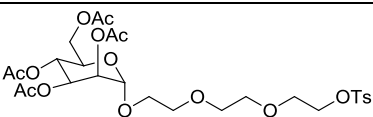
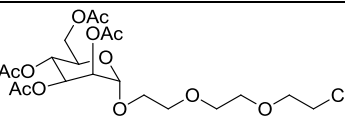
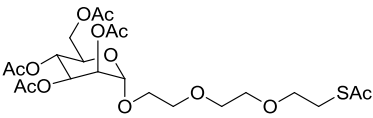
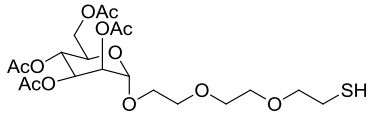
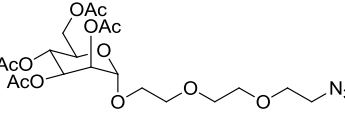
Graphical Index of Compounds and Experiments of Ligand Synthesis and Design

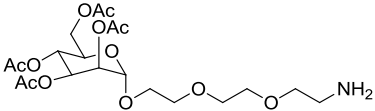
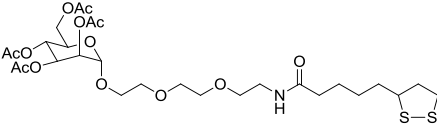
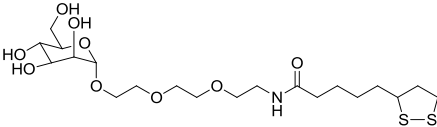
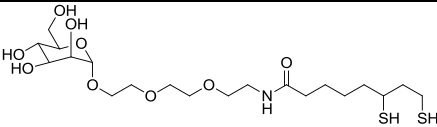
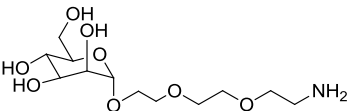
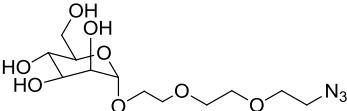
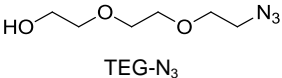
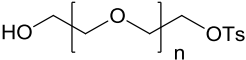
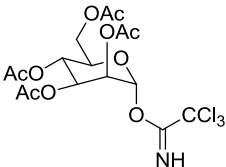
Table 4 | Graphical index of compounds and experiments of ligand synthesis and design.

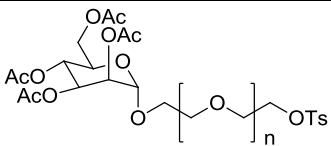
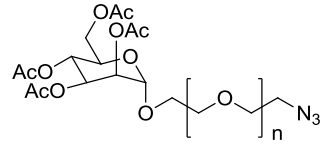
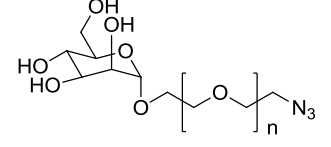
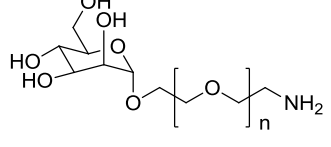
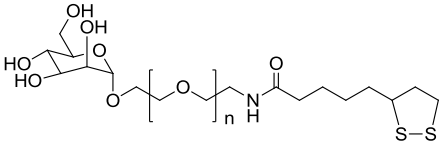
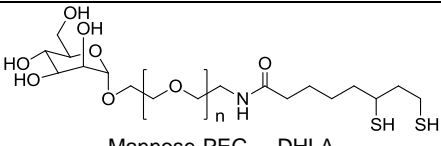
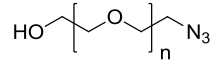
Compound N°	Synthesis of	Experiment	page
1	 Dihydrolipoic acid (DHLA)	1	72
2	 TA-PEG ₄₀₀ (n~8)	2	72
3	 DHLA-PEG ₄₀₀ -OH or Hydroxy-PEG ₄₀₀ (n~8)	3	73

4		4	74
	Dichloride-PEG ₄₀₀ (n~8)		
5		5	74
	Diazido-PEG ₄₀₀ (n~8)		
6		6	74
	Diamino-PEG ₄₀₀ (n~8)		
7		7	75
	TA-PEG ₄₀₀ -NH ₂ (n~8)		
8		8	75
	DHLA-PEG ₄₀₀ -NH ₂ or Amino-PEG ₄₀₀ (n~8)		
9		9	76
	TA-PEG ₄₀₀ -COOMe (n~8)		
10		10	77
	TA-PEG ₄₀₀ -COOH (n~8)		
11		11	77
	DHLA-PEG ₄₀₀ -COOH or Carboxy-PEG ₄₀₀ (n~8)		
12		12	78
	Ditosyl-PEG ₂₀₀₀ (n~40)		
13		13	78
	Diazido-PEG ₂₀₀₀ (n~40)		

14	 $\text{H}_2\text{N}-\left[\text{CH}_2-\text{CH}_2-\text{O}\right]_n-\text{CH}_2-\text{CH}_2-\text{NH}_2$	14	79
	Diamino-PEG ₂₀₀₀ (n~40)		
15		15	79
	TA-PEG ₂₀₀₀ -NH ₂ (n~40)		
16		16	80
	DHLA-PEG ₂₀₀₀ -NH ₂ Amino-PEG ₂₀₀₀ (n~40)		
17		17	80
	TA-PEG ₂₀₀₀ -COOMe (n~40)		
18		18	81
	TA-PEG ₂₀₀₀ -COOH (n~40)		
19		19	81
	DHLA-PEG ₂₀₀₀ -COOH or Carboxy-PEG ₂₀₀₀ (n~40)		
20		–	–
	Ditosyl-PEG ₄₀₀ (n~8)		
21		20	82
	Lipoic acid <i>N</i> -Hydroxysuccinimide ester (LA-NHS)		
22		21	82
	<i>N</i> -maleoyl- β -alanine		

23		22	83
3-maleimido propionic acid			
24		23 24	83 84
3-maleimido propionic acid <i>N</i> -hydroxysuccinimide ester			
25		25	84
Mannose Pentaacetate			
26		26	84
Monotosyl-TEG			
27		27	85
AcMannose-TEG-Tosyl			
28		28	85
AcMannose-TEG-Cl			
29		29	86
AcMannose-TEG-SAc			
30		30	86
Thiol Linker or Mannose-TEG-SH			
31		31	87
AcMannose-TEG-N ₃			

32		32	87
AcMannose-TEG-NH ₂			
33		33	88
AcMannose-TEG-TA			
34		34	89
Mannose-TEG-TA			
35		35	89
Mannose-TEG-DHLA			
36		36	90
Mannose-TEG-NH ₂			
37		37	91
Mannose-TEG-N ₃			
38		secondary product	-
TEG-N ₃			
39		38	91
Monotosyl-PEG ₄₀₀ or PEG ₄₀₀ -OTs			
40		39	92
AcMannose-trichloroacetimidate			

41		40	92
	AcMannose-PEG ₄₀₀ -OTs		
42		41	93
	AcMannose-PEG ₄₀₀ -N ₃		
43		42	93
	Mannose-PEG ₄₀₀ -N ₃		
44		43	93
	Mannose-PEG ₄₀₀ -NH ₂		
45		44	94
	Mannose-PEG ₄₀₀ -TA		
46		45	94
	Mannose-PEG ₄₀₀ -DHLA		
47		secondary product	–
	PEG ₄₀₀ -N ₃		

References

1. Wang, Q. B.; Xu, Y.; Zhao, X. H.; Chang, Y.; Liu, Y.; Jiang, L. J.; Sharma, J.; Seo, D. K.; Yan, H., A facile one-step in situ functionalization of

- quantum dots with preserved photoluminescence for bioconjugation. *J Am Chem Soc* **2007**, 129, (20), 6380-6381.
2. Dabbousi, B. O.; RodriguezViejo, J.; Mikulec, F. V.; Heine, J. R.; Mattoussi, H.; Ober, R.; Jensen, K. F.; Bawendi, M. G., (CdSe)ZnS core-shell quantum dots: Synthesis and characterization of a size series of highly luminescent nanocrystallites. *J Phys Chem B* **1997**, 101, (46), 9463-9475.
 3. Hines, M. A.; Guyot-Sionnest, P., Synthesis and characterization of strongly luminescing ZnS-Capped CdSe nanocrystals. *J Phys Chem-Us* **1996**, 100, (2), 468-471.
 4. Medintz, I. L.; Uyeda, H. T.; Goldman, E. R.; Mattoussi, H., Quantum dot bioconjugates for imaging, labelling and sensing. *Nature Materials* **2005**, 4, 435-446.
 5. Bruchez, M.; Moronne, M.; Gin, P.; Weiss, S.; Alivisatos, A. P., Semiconductor nanocrystals as fluorescent biological labels. *Science* **1998**, 281, (5385), 2013-2016.
 6. Gerion, D.; Pinaud, F.; Williams, S. C.; Parak, W. J.; Zanchet, D.; Weiss, S.; Alivisatos, A. P., Synthesis and properties of biocompatible water-soluble silica-coated CdSe/ZnS semiconductor quantum dots. *J Phys Chem B* **2001**, 105, (37), 8861-8871.
 7. Wu, X. Y.; Liu, H. J.; Liu, J. Q.; Haley, K. N.; Treadway, J. A.; Larson, J. P.; Ge, N. F.; Peale, F.; Bruchez, M. P., Immunofluorescent labeling of cancer marker Her2 and other cellular targets with semiconductor quantum dots. *Nat Biotechnol* **2003**, 21, (1), 41-46.
 8. Yu, W. W.; Chang, E.; Falkner, J. C.; Zhang, J. Y.; Al-Somali, A. M.; Sayes, C. M.; Johns, J.; Drezek, R.; Colvin, V. L., Forming biocompatible and nonaggregated nanocrystals in water using amphiphilic polymers. *J Am Chem Soc* **2007**, 129, (10), 2871-2879.
 9. Dubertret, B.; Skourides, P.; Norris, D. J.; Noireaux, V.; Brivanlou, A. H.; Libchaber, A., In vivo imaging of quantum dots encapsulated in phospholipid micelles. *Science* **2002**, 298, (5599), 1759-1762.
 10. Mattoussi, H.; Mauro, J. M.; Goldman, E. R.; Anderson, G. P.; Sundar, V. C.; Mikulec, F. V.; Bawendi, M. G., Self-assembly of CdSe-ZnS quantum dot bioconjugates using an engineered recombinant protein. *J Am Chem Soc* **2000**, 122, (49), 12142-12150.
 11. Wang, Y. A.; Li, J. J.; Chen, H. Y.; Peng, X. G., Stabilization of inorganic nanocrystals by organic dendrons. *J Am Chem Soc* **2002**, 124, (10), 2293-2298.
 12. Susumu, K.; Mei, B. C.; Mattoussi, H., Multifunctional ligands based on dihydrolipoic acid and polyethylene glycol to promote biocompatibility of quantum dots. *Nat Protoc* **2009**, 4, (3), 424-436.
 13. Warren, C. W.; Nie, S., Quantum Dot Bioconjugates for Ultrasensitive Nonisotopic Detection. *Science* **1998**, 281, 2016-2018.
 14. Willard, D. M.; Carillo, L. L.; Jung, J.; Van Orden, A., CdSe-ZnS quantum dots as resonance energy transfer donors in a model protein-protein binding assay. *Nano Lett* **2001**, 1, (9), 469-474.
 15. Uyeda, H. T.; Medintz, I. L.; Jaiswal, J. K.; Simon, S. M.; Mattoussi, H., Synthesis of compact multidentate ligands to prepare stable hydrophilic quantum dot fluorophores. *J Am Chem Soc* **2005**, 127, (11), 3870-3878.
 16. Carion, O.; Mahler, B.; Pons, T.; Dubertret, B., Synthesis, encapsulation, purification and coupling of single quantum dots in

phospholipid micelles for their use in cellular and in vivo imaging. *Nat Protoc* **2007**, 2, (10), 2383-2390.

17. Mei, B. C.; Susumu, K.; Medintz, I. L.; Mattoussi, H., Polyethylene glycol-based bidentate ligands to enhance quantum dot and gold nanoparticle stability in biological media. *Nat Protoc* **2009**, 4, (3), 412-423.

18. Liu, W.; Howarth, M.; Greytak, A. B.; Zheng, Y.; Nocera, D. G.; Ting, A. Y.; Bawendi, M. G., Compact biocompatible quantum dots functionalized for cellular imaging. *J Am Chem Soc* **2008**, 130, (4), 1274-1284.

19. Harris, J. M., *Poly(ethylene glycol) chemistry: biotechnical and biomedical applications*. Plenum Press: **1992**.

20. De la Fuente, J. M.; Penades, S., Glyconanoparticles: Types, synthesis and applications in glycoscience, biomedicine and material science. *Bba-Gen Subjects* **2006**, 1760, (4), 636-651.

21. Earhart, C.; Jana, N. R.; Erathodiyil, N.; Ying, J. Y., Synthesis of carbohydrate-conjugated nanoparticles and quantum dots. *Langmuir* **2008**, 24, (12), 6215-6219.

22. Chen, Y. F.; Ji, T. H.; Rosenzweig, Z., Synthesis of glyconanospheres containing luminescent CdSe-ZnS quantum dots. *Nano Lett* **2003**, 3, (5), 581-584.

23. Kikkeri, R.; Lepenies, B.; Adibekian, A.; Laurino, P.; Seeberger, P. H., In Vitro Imaging and in Vivo Liver Targeting with Carbohydrate Capped Quantum Dots. *J Am Chem Soc* **2009**, 131, (6), 2110-2112.

24. Gill, R.; Freeman, R.; Xu, J. P.; Willner, I.; Winograd, S.; Shweky, I.; Banin, U., Probing biocatalytic transformations with CdSe-ZnS QDs. *J Am Chem Soc* **2006**, 128, (48), 15376-15377.

25. Udenfriend, S.; Stein, S.; Bohlen, P.; Dairman, W., Fluorescamine - A Reagent for Assay of Amino-Acids, Peptides, Proteins, and Primary Amines in Picomole Range. *Science* **1972**, 178, (4063), 871-872.

26. Masuko, T.; Minami, A.; Iwasaki, N.; Majima, T.; Nishimura, S. I.; Lee, Y. C., Carbohydrate analysis by a phenol-sulfuric acid method in microplate format. *Anal Biochem* **2005**, 339, (1), 69-72.

27. Merck, E., *Dyeing Reagents for Thin Layer and Paper Chromatography*. Merck: **1978**.

28. Armarego, W. L. F.; Chai, C. L. L., *Purification of laboratory chemicals*. Butterworth-Heinemann: **2009**.

29. Graham, L. D.; Packman, L. C.; Perham, R. N., Kinetics and Specificity of Reductive Acylation of Lipoyl Domains from 2-Oxo Acid Dehydrogenase Multienzyme Complexes. *Biochemistry-Us* **1989**, 28, (4), 1574-1581.

30. Friesen, H.-J. H., Peter Compounds from biopolymers and effector substances which are linked via optically active amino acid derivatives, processes for the preparation thereof and the use thereof 14 June 1994, 1994.

31. Chadhary, B. L. H. J.; Paliwal, S. N.; Meena, S.; Chaudhary, P. R., Synthesis and Characterization of Some New Thermal Stable Polymers - Polymerization of N-[4-N'-(Benzylamino-carbonyl)phenyl]maleimide. *E-Journal of Chemistry* **2007**, 4, (2), 222-231.

32. Rich, D. H.; Gesellchen, P. D.; Tong, A.; Cheung, A.; Buckner, C. K., Alkylating Derivatives of Amino-Acids and Peptides - Synthesis of N-Maleoylamino Acids, [1-(N-Maleoylglycyl)Cysteiny]Oxytocin, and [1-(N-

- Maleoyl-11-Aminoundecanoyl)Cysteiny]Oxytocin - Effects on Vasopressin-Stimulated Water-Loss from Isolated Toad Bladder. *J Med Chem* **1975**, 18, (10), 1004-1010.
33. Nielsen, O.; Buchardt, O., Facile Synthesis of Reagents Containing a Terminal Maleimido Ligand Linked to an Active Ester. *Synthesis-Stuttgart* **1991**, (10), 819-821.
34. Schmidt, R. R.; Michel, J., Facile Synthesis of alpha- and beta-O-Glycosyl Imidates; Preparation of Glycosides and Disaccharides. *Angew Chem Int Edit* **1980**, 19, (9), 731-732.
35. Davis, B. G.; Fairbanks, A. J., *Carbohydrate chemistry*. Oxford University Press: **2002**.
36. Xie, R. G.; Kolb, U.; Li, J. X.; Basche, T.; Mews, A., Synthesis and characterization of highly luminescent CdSe-Core CdS/Zn_{0.5}Cd_{0.5}/ZnS multishell nanocrystals. *J Am Chem Soc* **2005**, 127, (20), 7480-7488.
37. Lorenzen, A.; Kennedy, S. W., A Fluorescence-Based Protein Assay for Use with a Microplate Reader. *Anal Biochem* **1993**, 214, (1), 346-348.
38. Gunsalus, I. C.; Barton, L. S.; Gruber, W., Biosynthesis and Structure of Lipoic Acid Derivatives. *J Am Chem Soc* **1956**, 78, (8), 1763-1766.
39. Wagner, A. F.; Walton, E.; Boxer, G. E.; Pruss, M. P.; Holly, F. W.; Folkers, K., Properties and Derivatives of Alpha-Lipoic Acid. *J Am Chem Soc* **1956**, 78, (19), 5079-5081.
40. Staudinger, H.; Meyer, J., On new organic phosphorus bonding III Phosphine methylene derivatives and phosphinimine. *Helv Chim Acta* **1919**, 2, 635-646.
41. van Ameijde, J.; Liskamp, R. M. J., Synthesis of novel trivalent amino acid glycoconjugates based on the cyclotrimeratrylene ('CTV') scaffold. *Org Biomol Chem* **2003**, 1, (15), 2661-2669.
42. Yu, W. W.; Qu, L. H.; Guo, W. Z.; Peng, X. G., Experimental determination of the extinction coefficient of CdTe, CdSe, and CdS nanocrystals. *Chem Mater* **2003**, 15, (14), 2854-2860.
43. Yu, W. W.; Qu, L. H.; Guo, W. Z.; Peng, X. G., Experimental determination of the extinction coefficient of CdTe, CdSe and CdS nanocrystals (vol 15, pg 2854, 2003). *Chem Mater* **2004**, 16, (3), 560-560.
44. Li, J. J.; Wang, Y. A.; Guo, W. Z.; Keay, J. C.; Mishima, T. D.; Johnson, M. B.; Peng, X. G., Large-scale synthesis of nearly monodisperse CdSe/CdS core/shell nanocrystals using air-stable reagents via successive ion layer adsorption and reaction. *J Am Chem Soc* **2003**, 125, (41), 12567-12575.
45. Landau, L. D.; Lifshits, E. M., *Fluid mechanics*. Butterworth-Heinemann: **1987**.
46. Pons, T.; Uyeda, H. T.; Medintz, I. L.; Mattoussi, H., Hydrodynamic dimensions, electrophoretic mobility, and stability of hydrophilic quantum dots. *J Phys Chem B* **2006**, 110, (41), 20308-20316.
47. Ditsch, A.; Laibinis, P. E.; Wang, D. I. C.; Hatton, T. A., Controlled clustering and enhanced stability of polymer-coated magnetic nanoparticles. *Langmuir* **2005**, 21, (13), 6006-6018.
48. Laurentin, A.; Edwards, C. A., A microtiter modification of the anthrone-sulfuric acid colorimetric assay for glucose-based carbohydrates. *Anal Biochem* **2003**, 315, (1), 143-145.

49. Irwin, M.; Leaver, A. G., Use of the Orcinol-Sulphuric Acid Reaction in the Positive Identification of Certain Monosaccharides from a Salivary Mucoid. *Nature* **1956**, 177, (4520), 1126-1126.
50. Monsigny, M.; Petit, C.; Roche, A. C., Colorimetric Determination of Neutral Sugars by a Resorcinol Sulfuric-Acid Micromethod. *Anal Biochem* **1988**, 175, (2), 525-530.

Chapter 4

Conjugation of Luminescent QDs with Antibodies

The author had full contribution in this chapter, namely in the planning of the experimental work and performance of the experiments.

Conjugation of Luminescent QDs with Antibodies

Abstract	145
Introduction	145
Experimental Section	150
Materials	150
Unconjugated QDs: Electrophoretic Mobility and pH Stability Analysis	151
EDC Activation Step	152
QD Conjugation with Antibodies via EDC/NHS Coupling	153
Estimation of QD/Antibody molar ratios	154
Characterization of Antibody-Bioconjugated QDs	155
SDS-PAGE Electrophoresis	156
Western Blotting	156
Biological Activity of the Antibody-Bioconjugated QDs	157
Results and Discussion	158
Evaluation of the Electrophoretic Mobility and pH Stability of MPA and DHLA Water-Soluble QDs	158
Coupling of Antibodies to Water-Soluble QDs through EDC/NHS Chemistry.....	162
Determination of the Antibody/QD Molar Ratio	170
Characterization of the Binding Properties of Antibody-Bioconjugated QDs.....	172
Evaluation of Antibody-Bioconjugated QDs Capacity to Recognize their Antigen.....	177
Conclusion	181
Glossary	182
Acknowledgments	185
References	185

Abstract

Several types of nanoparticles have been employed in different biological applications. The preparation of quantum dots for these applications involves many steps but the most critical is the bioconjugation with biological agents making use of specific or non-specific conjugation reactions. The subject of the work reported here was the bioconjugation of MPA-QDs and DHLA-QDs with monoclonal antibodies. In order to determine the experimental conditions for this target, preliminary studies were carried out. The pH stability and electrophoretic mobility of the carboxy-QDs was determined and it was found that these parameters were dependent upon the QD surface charge and also on the pH and the nature of the buffer. The bioconjugated nanoparticles were characterized by comparing their molecular weight and electrophoretic mobility with non-conjugated nanoparticles as well as their functional and binding properties, using agarose gel and SDS-PAGE electrophoresis and western blotting techniques. The EDC chemistry assisted by NHS for QDs activation was also analysed by agarose gel electrophoresis and the number of antibodies conjugated to a single quantum dot was determined. It was observed that this can vary from 1 to 3 depending on the working conditions. The biological nanoprobe here developed appear to be good candidates to be tested in immunofluorescence assays.

Key-words: *Quantum dots, Bioconjugation, Antibodies.*

Introduction

The ability to bioconjugate QDs makes them suitable for applications involving biological label ^[1], immunolabeling, cell motility assays *in situ* hybridization and as live cell markers ^[2, 3]. They can also be used just as a non-specific fluorescent stain ^[2, 4]. To make QDs more useful for probing live cells and other biological applications, they need to be conjugated to biomolecules without disturbing the biological function of these molecules ^[2].

Among other biomolecules, polyclonal and monoclonal antibodies have become the most important and widely used class of biological agents because their broad application in life science research, diagnostics and therapeutics. As a general rule, antibodies (*e.g.* IgG) are symmetrical

molecules made up of two identical glycosylated heavy chains and two identical non-glycosylated light chains, held together by non-covalent interactions as well as a number of disulphide bonds^[5]. The heavy chains are joined by disulphide bonds to each other in the hinge region and each light chain is disulphide-bounded to one light chain in the C_L and C_H¹ regions respectively as illustrated in a current antibody structure shown in Figure 19.

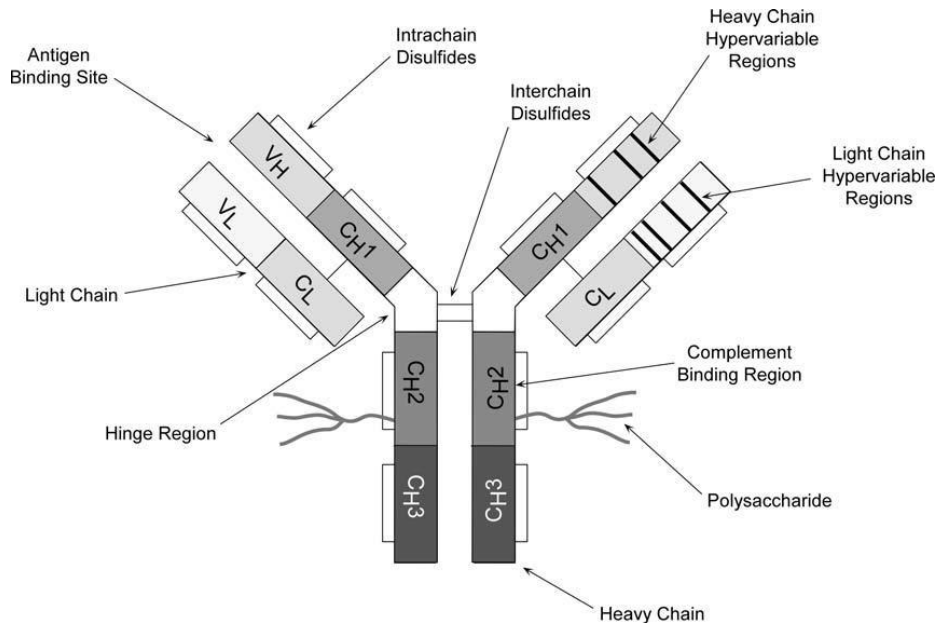


Figure 19 | Structure of an IgG Molecule. Detailed structure of an IgG antibody molecule. Adapted from reference [6]. Copyright 2008. Elsevier Inc.

Depending on the class of immunoglobulin, the molecular weight in general of the constituent subunits ranges from 50 to 75kDa for heavy chains and 25kDa for the two identical light chains. The intact molecular weight represented for all subunits achieve 150-160kDa. The light chains can be classified as either kappa (κ) or lambda (λ) type because the existing small polypeptide structural differences and these chains play an important role in determining the specificity of antibodies. However is the heavy chain variety that determines each individual class of immunoglobulin and all the master function of antibodies. The immunoglobulins may be grouped into five main classes: IgM, IgD, IgG, IgE and IgA which have distinct sizes, structural composition and different biological properties. Moreover, the heavy chains of immunoglobulin

molecules are also glycosylated in CH₂ domain inside the “fragment crystallisable” (Fc), but also contain carbohydrate moieties near the antigen binding sites ^[5-7]. Two identical heavy chains and two identical light chains comprise the Y-shaped unit. The top of this unit contains the variable region which is designed by antigen binding site. In e.g. IgG antibodies two binding sites exist and they have the conformation necessary to interact with a complementary region of the antigen molecule ^[6, 7]. In addition, the binding site is not only constituted by a linear sequence of amino acids on each chain, but also multiple weak non-covalent interactions, including electrostatic, hydrogen bonding, van der Waals and hydrophobic effects ^[5].

Looking at the global structure of antibodies it's easy to understand why these biomolecules are widely used in many different applications. In addition to possessing a number of functional groups suitable for modification and conjugation purposes, their relatively inexpensive production and design making them available for specific binding. For this purpose, several successful approaches have been used to link biological molecules to QDs, including electrostatic binding, non-covalent biotin-avidin binding, direct covalent crosslinking and nickel based histidine-tagging.

The electrostatic binding strategy was first used by Mattousi and co-workers and is based on adsorption or non-covalent self-assembly using engineered proteins ^[8-10]. This approach has proved useful for attaching a variety of engineered proteins to QDs including maltose binding protein (MBP), for purification over amylose resin and Protein G, which will bind the IgG portion of an antibody thus acting as a linker ^[10]. However, proteins can also be non-specifically adsorbed to QDs ^[11].

By using metal-affinity coordination, histidine expressing proteins (His-tag proteins) ^[12] or peptides can be directly attached on the QD surface linked to Zn atoms, where the nickel nitriloacetic acid complex (Ni-NTA) can be used a bifunctional adaptor for QD conjugation. The nitriloacetic acid group is covalently linked to the QD encapsulation polymer and the histidine tagged antibodies bind to nickel atoms (Ni²⁺) by chelation. This strategy, in comparison with other binding strategies (e.g. biotin-avidin) has several advantages such as controlled orientation of the binding ligand, because a histidine tag can be conveniently fused to proteins and peptides at a particular

site (compact overall probe size and low cost production). However, the stability of the histidine-nickel complexation could be a problem under harsh conditions [13, 14]. The covalent QD conjugation is the method most used for the labelling of biological molecules and there are essentially three different approaches for this purpose (Scheme 18).

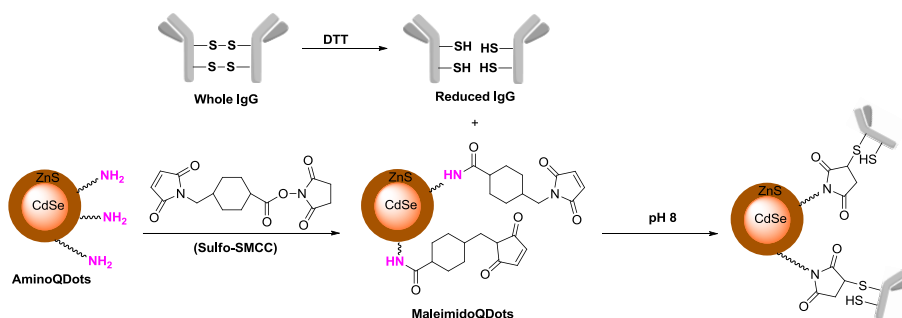
(a) Orientated Binding of Amino Groups of Antibody to CarboxyQDs



(b) Binding Carbohydrates Moieties of Antibody to AminoQDs (via NaIO₄ oxidised Antibody)



(c) Binding Sulphydryl Groups of Antibody Fragments to AminoQDs (via reduced IgG and sulfo-SMCC activated QDs)



Scheme 18 | Schematic Diagram of Covalent Conjugation. General scheme showing the three covalent approaches most used for conjugation of QDs to biomolecules: (a) covalent coupling between carboxylic acid coated QDs and primary amines on intact antibodies via EDC/NHS, (b) site-direct conjugation via oxidized carbohydrate groups on the antibody Fc portion and covalent reaction with amino-QDs, (c) QD conjugation to antibody fragments via disulphide reduction and sulphydryl-amine coupling.

The most popular covalent conjugation involves the use of 1-ethyl-3-(3-dimethylaminopropyl) carbodiimide (EDC) in the presence of *N*-

hydroxysuccinimide (NHS) to react carboxyl groups on the QD surface with biomolecules decorated with primary amino groups ^[15] (Scheme 18 (a)). An advantage of this amine-carboxylic acid crosslinking is that most proteins contain primary amines and do not need chemical modification ^[13]. However, the conjugation with EDC condensation sometimes produce intermediates aggregates due to poor QD stability in neutral/acidic buffers which also produce large conjugates with less control over the number of biomolecules attached to a single nanoparticle. Moreover, this chemistry is prone to a non-oriented conjugation. The surface functional sites available on a single QD can bind with the amine terminal groups located in the antigen binding sites of the target protein leading to loss of activity of the protein itself ^[14].

The second covalent approach commonly used involves oxidation of carbohydrates groups on the antibody's Fc portion to form reactive aldehyde groups which are then covalently linked to amino QDs by a reductive amination process (Scheme 18 (b)). This conjugation can be carried out using a suitable candidate amino-QD or carboxy-QDs (COOH-QDs) derivatized with adipic acid dihydrazide (ADH). This approach allows site specific QD conjugation at relatively low QD-antibody ratios because the known position of carbohydrates on the antibody ^[13].

The third covalent strategy that makes effective use of selective bioconjugation, targeting specific sites on the protein, is the QD conjugation to antibody fragments via disulphide reduction and sulfhydryl-amine coupling through 1, 4-addition to a maleimide functionalised QD (Scheme 18 (c)). This strategy uses of heterobifunctional cross linkers such as 4-(*N*-maleimidomethyl) cyclohexane-1-carboxylic acid 3-sulfo-*N*-hydroxysuccinimide ester sodium salt (sulfo-SMCC) or 4-(*N*-maleimidomethyl) cyclohexanecarboxylic acid *N*-hydroxysuccinimide ester (SMCC) ^[13, 15]. These reagents can form stable amide bonds with amino-QDs (NH₂-QDs). The resultant maleimido-QDs can form stable thioether bonds with a sulfhydryl-exposed antibody. The antibodies can be reduced by mild reducing agents namely cysteine HCl or dithiothreitol (DTT) where the disulphide bonds (hinge region) connecting the IgG heavy chains are selectively cleaved, leaving the other disulphide bonds, that make up the antigen binding site (hypervariable region) unaffected, and thus produce the partially reduced IgG ^[15].

The simplest and most used antibody conjugation method is the formation of amide bonds using the carbodiimide reagents as summarized above and this approach was studied for the conjugation of MPA and DHLA water-soluble QDs with anti-RAP 1 *Babesia bovis* monoclonal antibodies. Different conditions were tested and in each case the antibody conjugation efficiency was determined by calculating the number of functional antibodies conjugated to the QDs using UV-visible spectroscopy at 280nm. The QD-antibody complexes were characterized by comparing their molecular weight and electrophoretic mobility with non-conjugated nanoparticles as well as their binding properties, using agarose and SDS-PAGE electrophoresis. To evaluate the antigen recognition capacity of the antibodies linked to QDs the western blotting technique was used.

Experimental Section

Materials

CarboxyQDs, namely MPA and DHLA water-soluble QDs, used in this work were obtained as described in chapters 2 and 3. All the chemical reagents/solvents were purchased from Sigma-Aldrich unless indicated otherwise. Monoclonal antibodies anti-rRAP1 *Babesia bovis* were kindly provided by Dr. Ana Domingo's group from IHMT-UNL, Lisbon and were purified by fast liquid protein chromatography using a ÄKTAprime™ plus purifier and a Hitrap Protein G HP 1mL column, both from GE Healthcare Life Sciences. Recombinant (r) RAP-1 protein was available in the Biomolecular Diagnostic laboratory (ITQB-UNL), but was kindly produced and purified by Marta Silva^[16]. Anti-Horseradish peroxidase (anti-HRP) developed in rabbit (fractionated antiserum) was purchased from Sigma-Aldrich. Stock solutions of monoclonal antibodies, recombinant RAP-1 protein and anti-HRP were quantified using a NanoDrop 2000 UV spectrophotometer and Coomassie Plus (Bradford) assay kit from Thermo Scientific. Bioconjugated QD samples were purified using Vivaspin 500 (100-300kDa cut-off) from Sartorius. Purification by dialysis was performed using Mini-dialysis kit (2mL, 8kDa cut-off) from GE Healthcare Life Sciences. Agarose gel electrophoresis was performed using a Mini-Sub Cell GT system purchased from Bio-Rad® and agarose with low EEO from Fisher. The agarose gels were stained with

SYBR® safe DNA gel stain from Invitrogen and were loaded with GeneRuler™ 1kb and 100bp DNA ladder from Fermentas. The samples for agarose gel electrophoresis before loading on to the gel were mixed with 6xDNA loading dye purchased from Fermentas. SDS-PAGE analysis was performed using a mini vertical electrophoretic unit from Sigma-Aldrich and PAGEr™ precast gels (4-20% Tris-Gly) 10x10mm, 10 well, from LONZA. The gels were loaded with PageRuler™ Prestained Protein Ladder (MW 10-170kDa) from Fermentas. The membrane transfer in Western Blotting analysis was carried out using a semi-dry blotter from Sigma-Aldrich. The filter paper was purchased from Whatman and the 0.45µm PVDF membranes used were Immobilon™-P and Immobilon™-FL from Millipore™ depending on the assay. The membranes were incubated with secondary anti-mouse IgG-alkaline phosphatase or anti-mouse IgG-HRP purchased from Sigma-Aldrich and Santa Cruz Biotechnology respectively. One-step NBT/BCIP substrate purchased from Pierce was used for detection of alkaline phosphatase and Immobilon® western HRP substrate from Millipore™ for HRP detection. All the incubations and washing steps were carried out on an orbital shaker platform from Heidolph. Agarose and polyacrylamide gels were visualized under UV and chemiluminescence modes using a charge-couple device (CCD) ChemiDoc™ XRS+ from Bio-Rad® as well as the immuno-detection for western blotting analysis. The data treatment was accomplished by the Quantity One software also from Bio-Rad®. The natural fluorescence of water-soluble QDs was visualized with a standard UV trans-illuminator.

Unconjugated QDs: Electrophoretic Mobility and pH Stability Analysis

The electrophoretic mobility of MPA and DHLA QDs was carried out in the following manner: 100nM solutions of MPA and DHLA water-soluble QDs were diluted from their corresponding stock solutions (4.8 and 4.1µM respectively) in sodium phosphate (Na-P 10mM) buffer in the pH range between 4 and 12. The electrophoretic mobility analysis were performed by agarose gel electrophoresis in TBE 1x buffer (Tris-Borate-EDTA buffer, pH 8.4) diluted with distilled water from the 5x stock solution prepared in the laboratory. The 1% agarose gel was prepared by dissolving under heating 0.5g of agarose in 50mL of TBE 1x and 2.5µL of SYBR® safe DNA gel stain.

10 μ L of each QD solution previously prepared, were mixed with 2 μ L of 6xDNA loading dye, before loading onto the gel. 1.8 μ L of each 1kb and 100bp DNA ladder were diluted with 8.2 μ L of Na-P buffer 10mM pH 7 and loaded onto the gel for possible estimation of the molecular weight of MPA and DHLA-QDs. The gels ran at 90V during 75 minutes and were visualized under UV and chemiluminescence modes using the molecular imager ChemiDoc system and Quantity One software. The natural fluorescence of water-soluble QDs was visualized with a UV trans-illuminator.

For the pH stability analysis, 150 μ L of each 100nM solution of MPA and DHLA-QDs prepared in Na-P buffer in the pH range 4 to 12 were placed in a micro-tube support at room temperature in the dark. The stability/solubility of the different QDs solutions were excited at 365nm and monitored using a standard UV trans-illuminator at different periods of time (10 minutes to 21 days).

EDC Activation Step

Before coupling of carboxy-QDs with antibodies, the QD activation step with EDC was checked using as amino groups source two primary amines namely ethanolamine and glycine. A 0.01M EDC stock solution was prepared by placing 0.002g of EDC in a microtube and dissolving in 1mL of Na-P buffer 10mM pH 6. In separate microtubes, 6 μ L of ethanolamine was dissolved in 994 μ L of Na-P buffer 10mM pH 6 and 0.0075g of glycine were dissolved in 1mL of the same buffer in order to obtain 0.1M ethanolamine and glycine stock solutions respectively. One μ L of 0.1M ethanolamine and glycine stock solutions were then placed in separate microtubes, and each amine was incubated with 21 μ L of carboxy-QDs, 2 μ L of 0.01M EDC stock solution and 976 μ L of Na-P buffer 10mM pH 6 for 3 hours at room temperature with gentle agitation. The samples were purified by dialysis (8kDa cut-off) overnight at room temperature against 1L of Na-P buffer 10mM pH 6 to remove the excess of EDC and primary amines added. The characterization of the final samples was followed by agarose gel electrophoresis according to the following experimental procedure. 10 μ L of each sample as well as 10 μ L of 100 and 500nM free carboxy-QD solutions were mixed with 2 μ L of 6xDNA loading dye and loaded onto the gel (1% agarose gel previously prepared by heating 0.5g

of agarose in 50mL of TBE 1x buffer and 2.5 μ L of SYBR safe DNA gel stain). DNA ladder (1kb and 100bp) was also separately applied as molecular weight standard for the derivatized and non-derivatized QDs. The electrophoresis was conducted in TBE 1x running buffer at constant voltage of 90V for 50 minutes. The activated and non-activated QDs were visualized in the gel in a molecular imager ChemiDoc and the natural fluorescence of QDs observed in a standard UV trans-illuminator.

QD Conjugation with Antibodies via EDC/NHS Coupling

The QD conjugation was carried out by direct conjugation of antibodies to carboxy-QDs through amine-carboxylic acid coupling using EDC/NHS chemistry. A general procedure:

EDC and NHS stock solutions: In a 1mL microtube 0.002g of EDC was dissolved in 1mL of buffer in order to obtain a 10mM stock solution. A 2.2mM solution was then prepared taking 220 μ L of stock solution and adding 780 μ L of buffer yielding a final volume of 1mL. The NHS 10mM stock solution was prepared in a similar way dissolving 0.0012g of NHS in 1mL of buffer. A 4mM solution was then prepared taking 400 μ L from the stock solution and adding 600 μ L of buffer yielding a final volume of 1mL.

QD activation: 0.1nmol of carboxy-QDs (e.g. 24.4 μ L from a 4.1 μ M stock solution of DHLA-QDs) were placed in a 1mL microtube. 10 μ L of a 2.2mM EDC solution and 10 μ L of a 4mM NHS solution were added, followed by the addition of 55.6 μ L of buffer, yielding a final volume of 100 μ L (QD concentration \sim 1 μ M). The solution was slowly shaken during 30 minutes at room temperature. Subsequently, the activated QDs were diluted for a final concentration of 100nM with the addition of 900 μ L of buffer and purified by dialysis (8kDa cut-off) for 2 hours at room temperature against 1L of buffer to remove the excess of EDC and NHS reagents.

Bioconjugation with antibodies: The coupling between the activated QDs and antibodies was carried out by mixing the activated QD solution with 318 μ L (0.4nmol; QD/Ab molar ratio \sim 1:4) of antibody (stock solution \sim 1mg/mL) previously dialysed overnight at 4 $^{\circ}$ C against 1L of bioconjugation buffer, followed by the addition of 618 μ L of buffer in order to keep the final concentration of QDs in the reaction \sim 50nM. The reaction was incubated at

room temperature during 4 hours. Any remaining activated carboxy groups were eliminated by adding 1 μ L of a 100mM stock solution of ethanolamine (QD/ethanolamine molar ratio \sim 1:940) (previously prepared in the bioconjugation buffer) to 2mL of QD-antibody solution. After incubation overnight at room temperature the solution was purified again by dialysis (8kDa cut-off) during 2 hours at room temperature against 1L of buffer to remove the excess of ethanolamine added.

Final purification and concentration: The final purification was performed using centrifugal filtering devices (Vivaspin 500, cut-off 300kDa). The final QD-Ab samples were washed by centrifuging at 1000g, 2 minutes at room temperature. The wash procedure was repeated 4 times to ensure the total elimination of possible free antibody in solution. The final QD-antibody samples were suspended in 250-500 μ L of buffer.

Estimation of QD/Antibody molar ratios

To quantify the number of IgG molecules bound per QD, the Protein A280 assay available in the NanoDrop 2000 UV spectrophotometer from Thermo Scientific was used and the experimental measurements were carried out according to manufacturer's instructions. All of the final samples were purified using Vivaspin 500 centrifugal filter devices (300 kDa cut-off) to ensure the total elimination of free antibody in solution and the supernatants were kept for further quantitation. A reference solution having exactly the same initial antibody concentration was prepared under the same experimental conditions (pH, ionic strength) to ensure the initial mass of antibody added. As a control, the concentration of unconjugated antibody present in the supernatants resulting from the washes, were also measured. The concentration (mg/mL) of immobilized antibody was defined as the difference between the absorbance at 280nm of the QD-antibody complexes and the absorbance at 280nm of the unconjugated QDs (Equation 7) where a general reference setting based on a 0.1% (1mg/mL) protein solution producing an absorbance of 1.0 was used (pathlength 10mm). It's important to point out, that in these measurements the absorption at 280nm of the unconjugated QD was not negligible since these unconjugated nanoparticles have the ability to absorb at 280nm. For this reason the absorbance of the unconjugated QDs at this

wavelength need to be subtracted from the absorbance value obtained for the conjugated complexes at 280nm.

$$[\text{immobilized antibody}] = \text{Abs}_{280\text{nm}}(\text{QD-antibody sample}) - \text{Abs}_{280\text{nm}}(\text{QD})$$

Equation 7 | Expression used to determine the concentration in mg/mL of the immobilized antibody in QD-antibody complexes.

As the concentration of immobilized antibody was obtained in mg/mL, this means that the mass (in mg) of the immobilized antibody was obtained for 1mL. To estimate the real mass of immobilized antibody, the obtained value was then adjusted for the volume where QD-antibody complexes were suspended. Then, knowing the molecular weight of the antibody used it was possible to determine the number of moles of immobilized antibody and thus the molar ratio QD/Ab which is given by the following equation:

$$\text{QD/Ab} = n(\text{Ab})_{\text{immobilized}} / n(\text{QD})_{\text{initial}}$$

Equation 8 | Expression given to determine the QD/Ab ratios.

For this assay, it was assumed that no loss of QDs occurred and all the measurements were made in triplicate to improve accuracy.

Characterization of Antibody-Bioconjugated QDs

Agarose Gel Electrophoresis

The analysis of the QD-antibody conjugates resulted from three different experimental conditions and free carboxy-QDs as a control were characterized by agarose gel electrophoresis using the same experimental procedure described above for the characterization of the EDC activation step. However, in this case the electrophoresis was conducted at voltage ranging 45 to 90V during 3 hours because the high molecular weight of the bioconjugated samples. The derivatised and non-derivatised QDs were also visualized in the gel in a molecular imager ChemiDoc and the natural fluorescence observed in a standard UV trans-illuminator.

SDS-PAGE Electrophoresis

Samples of antibody-QD conjugates as well as free IgG were analysed by SDS-PAGE electrophoresis using the method of Laemmli ^[17], in reduced and non-reduced conditions. In the non-reduced conditions three different volumes (5, 10 and 15 μ L) of each sample were diluted in buffer yielding a final volume of 20 μ L and mixed with 5 μ L of 5x sample buffer containing 5% w/v sodium dodecyl sulphate (SDS), 10% v/v glycerol and 0.01% w/v of bromophenol blue in 0.0625M Tris-HCl, pH 6.8 ^[18]. For the reduced conditions, equal number of samples were prepared in the same way but mixed with 5 μ L of 5x sample buffer containing also 5% v/v of β -mercaptoethanol (BME). All the samples were heated at 90°C during 15 minutes and loaded into the 4-20% gradient gel. The gel was also loaded with 5 μ L of protein ladder (MW 10-170kDa) to accurately estimate the protein molecular weight. The gel was run for 1h30 minutes at constant voltage of 140V in Tris-Gly 1x running buffer (pH 8.3) diluted from a 10x stock solution (1.92mM glycine, 250mM Tris-base, 1% w/v SDS) previously prepared. The bioconjugated QDs samples were visualized in gels using a molecular imager ChemiDoc under UV light. When necessary, the gels were stained by rocking overnight at room temperature in a solution containing 0.025% Coomassie Blue R-250, 40% v/v methanol and 7% v/v acetic acid. The destaining was carried out by constant agitation in 50% v/v methanol and 7% v/v acetic acid until maximum contrast was achieved between the stained bands and the background.

Western Blotting

The western blotting analysis was performed based on standard western protocols ^[19, 20] for a semi-dry system. Six pieces of filter paper and a piece of PVDF (polyvinylidene difluoride) blotting membrane (ImmobilonTM-P) with the exact dimensions of the gel to be blotted was cut (e.g. 10x10cm). The membrane was then wetted in a plastic box with 5mL of 100% MeOH and equilibrated briefly for 5 minutes. Subsequently, the six pieces of filter paper, gel and membrane were soaked in transfer buffer pH 8.3 ^[21] (Tris base 25mM, Glycine 192mM, 10% v/v MeOH and 0.1% w/v SDS) previously prepared and stored at 4°C. All the pieces were placed in the semi-dry system for membrane transfer according to manufacturer's instructions and with careful

attention not to introduce air bubbles. The electro-transference ran under a current of 80mA during 2 hours at room temperature. After the transfer, the membrane was gently washed with 25mL of TBS pH 7.6 (Tris-buffered saline, 10mM Tris-HCl, NaCl 150mM) with constant agitation at room temperature. The blot was blocked with 50mL of freshly prepared blocking buffer (TBS, 5% non-fat milk (w/v)), for 1 hour at room temperature and followed by two washes with TBS (25mL, r.t.). Secondary antibody previously diluted in blocking buffer (1:2000-1:3000) was added and incubated for 2 hours at room temperature. The membrane was washed twice for 5 minutes each time in 25mL of TTBS (TBS containing 0.05% Tween® 20), followed by an additional wash with 25mL of TBS (5minutes, r.t.). Immunoreactive/targeted proteins were visualized with the detection reagent according to supplier instructions and the images were acquired in a molecular imager device in chemiluminescence mode.

Biological Activity of the Antibody-Bioconjugated QDs

Samples of (r) RAP-1 *B. bovis* antigenic protein were denatured at 90°C for 15 minutes with reducing sample buffer (5x) containing 5% w/v SDS and 5% v/v β -mercaptoethanol. The protein (10 μ g/well) was separated by 4-20% Tris-Gly gradient gel according to SDS-PAGE protocol previously described. The electrophoresis was conducted at a constant voltage of 140V during 90 minutes. High range SDS-PAGE protein standard (10-170kDa) was also loaded onto the gel. Proteins from the gel were blotted onto a 0.45 μ m PVDF membrane with low auto-fluorescence (Immobilon™-FL) based on the experimental procedure reported above. The blot was blocked for 30 minutes at room temperature with 50mL of freshly prepared blocking buffer (TBS, 5% non-fat milk (w/v)) followed by two washes of 5 minutes each with 25mL of TTBS. Subsequently, the blot was cut into 10 strips (Figure 20). As negative controls, 1mL of blocking buffer was used as well as 1mL of blocking buffer containing 50nM of carboxy-QDs blocked with ethanolamine and glycine and carboxy-QDs alone (Figure 20, strips 2 to 5 respectively). All the other strips were immersed in separate tubes with 1mL of blocking buffer containing different volumes of primary antibody-QD samples, in the range between 10 and 100 μ L (Figure 20, strips 6 to 10 respectively). All the samples and

respective controls were gently shaken overnight at 4°C on an orbital platform shaker. After washing with TTBS (2X, 25mL, 5min, r.t.), bioconjugated QDs were visualized on the strips with a molecular imager under UV light. Secondary antibody anti-mouse IgG with HRP conjugate freshly diluted in blocking buffer (1:3000) was added and all the strips were incubated again at room temperature for 2 hours. The immuno-detection was carried out with HRP chemiluminescence substrate. The images were acquired in a molecular imager ChemiDoc using the Quantity One software.

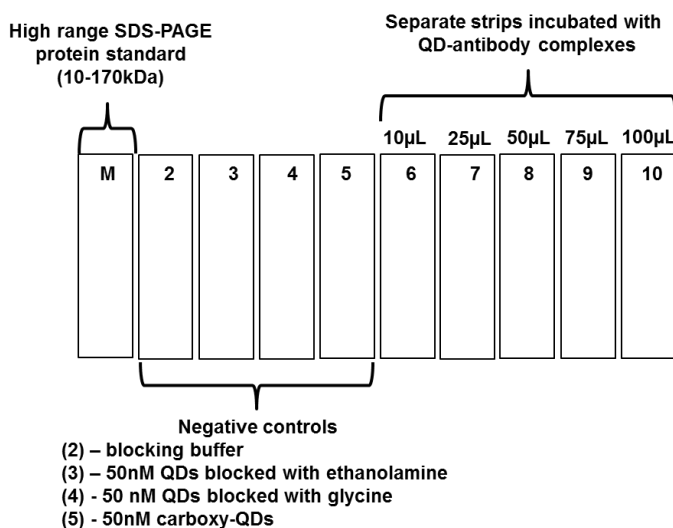


Figure 20 | Biological Activity of the Antibody-Bioconjugated QDs. Blot cut in 10 separate strips for the performance of the assay to evaluate the biological activity of the antibody-bioconjugated QDs.

Results and Discussion

Evaluation of the Electrophoretic Mobility and pH Stability of MPA and DHLA Water-Soluble QDs

Water-solubilisation of CdSe/ZnS core-shell QDs was provided by the ligand exchange strategy. With this method, monothiol and dithiol ligands were bounded on the QD surface to construct MPA and DHLA water-soluble QDs. Among others also developed, these ligands created a solubilisation (solvation) layer that strongly influenced the surface charge and mobility of hydrophilic QDs. Little is known about the charge of water-soluble QDs or bioconjugated QDs, even though this parameter is crucial, since they

influence many properties such as assay design, delivery and migration of both QDs in live cells and tissues. Therefore, during synthesis and functionalization, systematic characterization of the QD surface is needed to control and optimize QD ligand chemistry, bioconjugation and thus performance in biological assays or imaging^[22]. Hence, before the attachment of biomolecules onto the QD surface, the pH stability of aqueous dispersions of QDs coated with MPA and DHLA ligands was investigated over a period of time. The electrophoretic mobility of the same freshly prepared QD solutions using agarose gel electrophoresis was also evaluated. Figure 21 shows solutions of QDs capped with MPA and DHLA ligands in various Na-P solutions whose pH ranges from 4 to 12. It is important to notice, that pH's higher than 12 were not explored because they are not suitable for biomotivated applications.

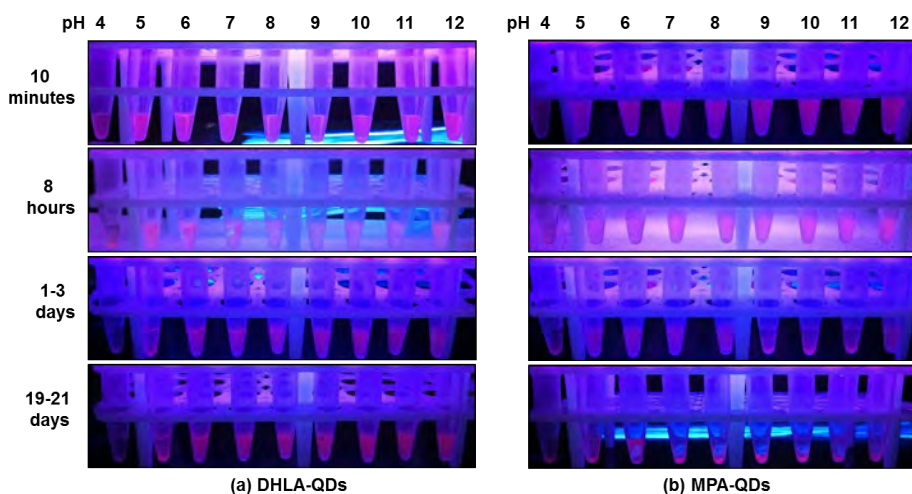


Figure 21 | pH Stability of MPA and DHLA-QDs. Luminescence image of CdSe/ZnS core-shell QDs coated with DHLA (a) and MPA (b) ligands in phosphate (Na-P) buffer in pH range between 4 and 12 after different periods of time at room temperature. The samples were excited with a UV trans-illuminator at 365nm.

It's known that DHLA capped QDs are easily dispersed in basic buffer solutions and are stable over extended periods of time in comparison with monothiol ligands, also stable in basic buffer solution but only for limited time (less than a week)^[23]. The results obtained in the pH stability assay for MPA and DHLA water-soluble QDs here developed are in agreement with this

statement. The DHLA-QDs are stable and well-dispersed in a wide pH range from 6 to 12 after 21 days at room temperature. On the other hand, after 1-3 days the MPA coated QDs were only soluble (dispersed) within a limited pH range (5 to 8) which suffered a further restriction when the solutions achieved 21 days. The formation of aggregates was a indication of degradation and ultimately the MPA-QDs became only stable at pH 6. The enhanced stability of DHLA-QDs over the monothiol capped QDs may be related to the bidentate chelate effect afforded by dithiol groups at the end of DHLA ligand. In other words, the bidentate dihydrolipoic acid can make simultaneous capping attachment to two surface sites on the ZnS coating shell, theoretically resulting in more stable cap/shell interactions ^[8]. Moreover, although the DHLA-QDs were stable in basic buffer solutions, under acidic conditions (pH 4 and 5) they tend to aggregate rapidly. This behaviour can be attributed to the fact that the stabilization of these nanoparticles relies on the deprotonation of the terminal carboxyl groups of DHLA and appears to be a crucial parameter in the solubilisation of these QDs in aqueous environments ^[23].

The pH stability results were accompanied by the electrophoretic mobility in agarose gel of the MPA and DHLA-QDs (Figure 22). The gel shifts obtained, demonstrated by the amount of QDs remained in the wells of each gel, that QDs coated with DHLA ligand resulted in aqueous dispersions that were aggregate-free in the pH regime 7-12, whereas MPA-QDs resulted in solutions well dispersed in a very small range (pH 6 and 7). The electrophoretic mobility analysis also confirmed the previous results obtained for the surface charge of this kind of particles. Outwardly, DHLA-QDs are more negatively charged than MPA-QDs. Although it has been reported that surface passivation achieved with MPA ligands result in a higher density of capping groups per QD ^[8], in our results the bidentate nature of DHLA appear to have allowed a greater ligand density and consequently a larger amount of negatively charged carboxylic acid groups onto the QD surface. This could be related to the monothiol nature of MPA which is a ligand only able to make a weak single attachment with the ZnS shell. As a consequence, these ligands could be easily removed from QD surface leading to a smaller amount of carboxylic acid groups and thus a less negative charge around QD surface.

In summary, the differences in surface properties for lipoic acid capped QDs compared with monothiol capped dots give an idea of the type of experimental conditions that should be applied for further conjugation with proteins or antibodies.

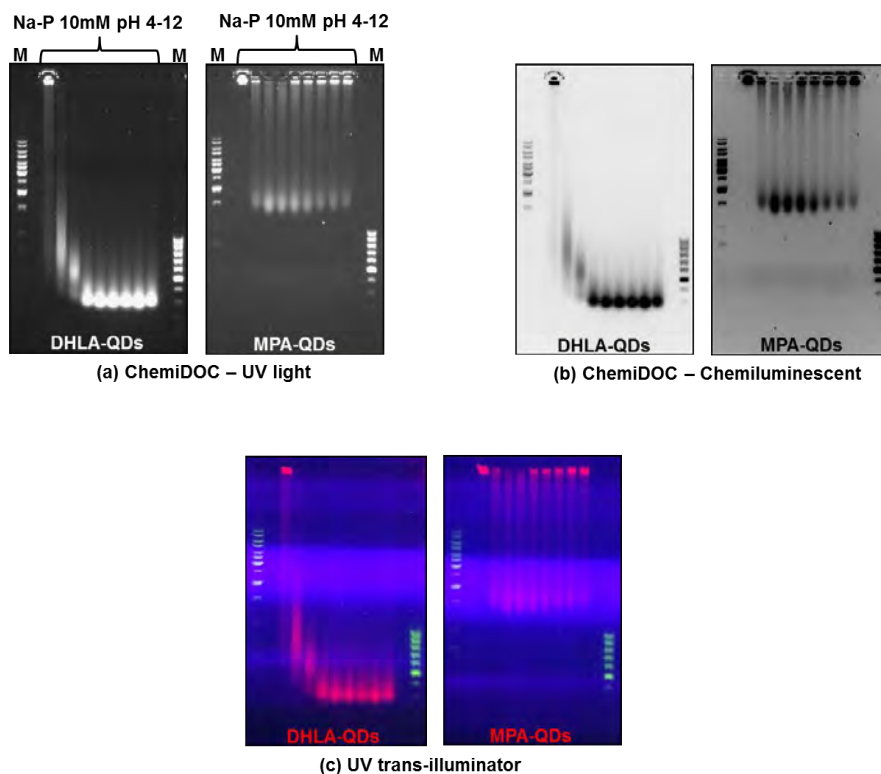


Figure 22 | Electrophoretic Mobility of MPA and DHLA-QDs. Gel shift of QDs ligand exchange with MPA and DHLA ligands using 1% agarose gel electrophoresis in TBE 1x buffer (pH 8.4) after running 1h15min at 90V. The gels were visualized under different conditions: (a) ChemiDOC molecular imager under standard UV light, (b) ChemiDOC molecular imager under chemiluminescence illumination mode and (c) UV trans-illuminator excited at 365nm to observe the natural fluorescence of water-soluble QDs.

It is noteworthy that other buffers namely 4-morpholineethanesulfonic acid (MES) or water adjusted at different pH's by acid/base addition were first tested to evaluate the electrophoretic mobility and pH stability of carboxy-QDs. However, although MES buffer demonstrated to be a suitable bioconjugation buffer for similar systems^[24, 25], for MPA-QDs this buffer proved to promote aggregation when comparing with sodium phosphate buffer, as

illustrated in Figure 23 by the strong localisation of QDs inside the wells at the top of the gel. When QDs were dispersed in Na-P, aggregation also occurred which was shown by the aggregation of QDs inside the gel, but the amount of MPA-QDs that moved through the gel was greater when compared with QDs dispersed in MES buffer or even water. This led to the conclusion that for posterior antibody/protein bioconjugation the type of buffer chosen may also exert a strong influence on a successful bioconjugation protocol in particular to maintain the dispersion of water-soluble QDs.

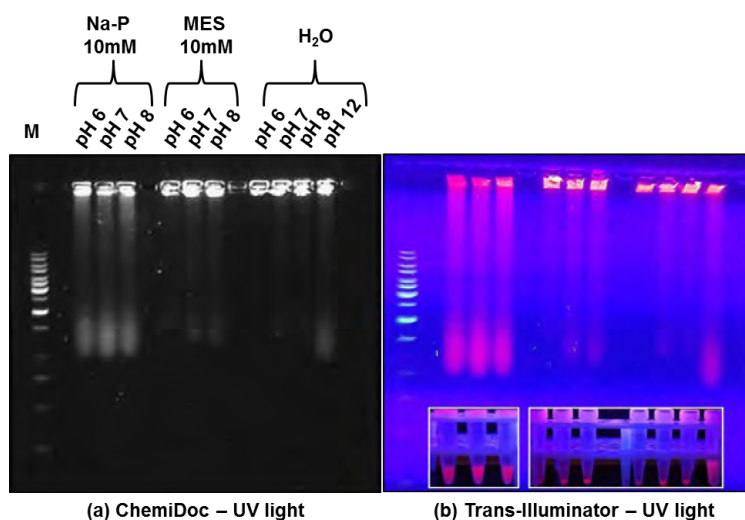


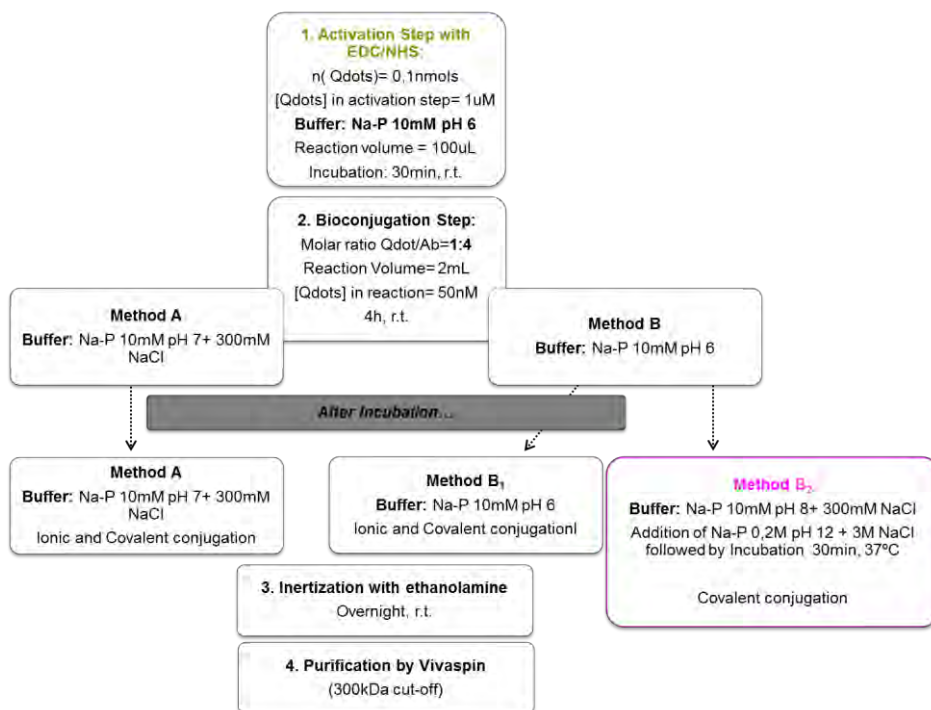
Figure 23 | Comparison of Electrophoretic Mobility of MPA-QDs in different buffers. Mobility of MPA-QDs using 1% agarose gel electrophoresis in TBE 1x buffer (pH 8.4) after running 55min at 90V. The gel was visualized using: (a) ChemiDOC molecular imager under standard UV light, (b) UV trans-illuminator excited at 365nm to observe the natural fluorescence of the QDs.

Coupling of Antibodies to Water-Soluble QDs through EDC/NHS Chemistry

One of the most popular strategies for coupling QDs to antibodies is the covalent attachment of the most reactive amine groups present on the antibodies to carboxylic acid coated QDs using EDC/NHS as a non-selective reagent. This is a simple methodology with certain advantages because it does not involve chemical modification of the antibody (Ab) since amine groups are present in most proteins and are very reactive moieties [13, 25]. However, the production of intermediate aggregates is a constant problem

due to poor QD stability in neutral/acidic buffers as well as poor control over the number of biomolecules attached to a single QD^[14]. Moreover, this strategy implies working at pH values below 8.0 which can result in a randomization of crosslinking sites of the antibody on the nanoparticle surface. This is because, at these pH values the most reactive amines reside in the antigen binding site of the antibody molecule, the Fab domain^[25, 26]. To avoid the unwanted QD-aggregates and formation of undesired secondary intermediates the use of NHS was introduced as well as other immobilization strategies to prevent the so-called antibody random orientation. Unfortunately, most of these techniques are complex and imply Ab modification through several steps of purification or the use of expensive immobilized proteins^[25]. In general, a universal methodology for the bioconjugation of non-modified antibodies onto nanoparticles making use of their Fab regions during the immobilization process is still missing. This is why EDC/NHS chemistry still continues to be the most used bioconjugation technique and the search for new and optimal experimental conditions is a constant. According to recent reports^[25], making use of the EDC/NHS chemistry, it is possible to bioconjugate nanoparticles *via* a two-step strategy which involves an initial rapid ionic adsorption of the Ab on the nanoparticle surface followed by a much slower Ab covalent attachment, taking advantage of the reversible character of ionic interactions. Covalent bond formation is evaluated after the ionic adsorption step, where the biomolecules ionically adsorbed could be eliminated by increasing the ionic strength and/or changing the global net charge of the Ab by shifting the pH of the bioconjugation buffer/media. Moreover, the covalent bond could remain at any pH or salt condition. Based on this recent reported work, it was proposed that the coupling of monoclonal antibodies onto carboxy-coated QDs through EDC and NHS chemistry using sodium-phosphate buffer 10mM as working media shifting the pH from 6 to 8 and in some cases with the addition of salt, could provide orientated coupling at the amino groups of the stem of the Ab (*i.e.* those not involved in binding to the antigen). To initially test the different experimental conditions for bioconjugation, anti-horseradish peroxidase, a robust readily available Ab was used as the working model since it differs from the general monoclonal IgG antibodies in the region at the end of the hypervariable region. The molar ratio

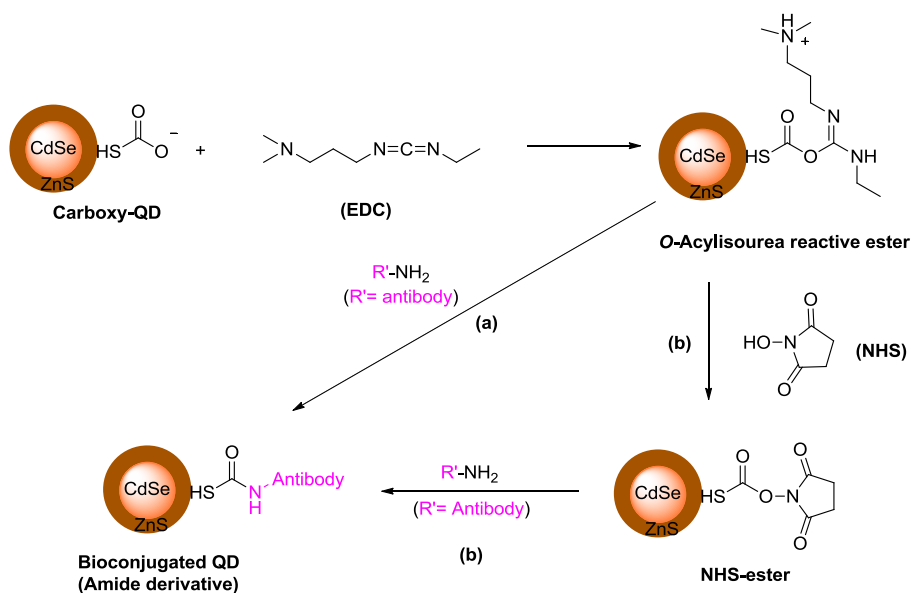
QD/antibody used was 1:4 as illustrated in the bioconjugation protocol (Scheme 19).



Scheme 19 | Bioconjugation Protocol Proposed. Schematic Illustration of the experimental conditions proposed for the conjugation of antibodies onto carboxy coated QDs.

The bioconjugation methodology herein tested required nanoparticles containing two functional groups: ionisable groups that allow ionic adsorption to the antibody and reactive groups that permit its further covalent attachment using EDC and NHS. One of the double bonds of EDC moiety reacted with the OH groups of the carboxylic acid present on the surface of QDs forming an active ester (*O*-acylisourea) leaving group. In general this active intermediate can directly react with a primary amine of the Ab, but the reaction rate is low and the intermediate can hydrolyse in aqueous solution (Scheme 20, (a)). In order to create a more stable intermediate able to react with primary amines as nucleophiles, NHS was used to assist the EDC active complex in this conjugation chemistry. In this case a NHS ester intermediate was formed resulting from the reaction of the hydroxyl group of NHS with the EDC active ester complex and thus increasing the rate of amide bond

formation (Scheme 20, (b)). This is due to the higher reactivity of NHS ester intermediate with amine containing molecules. This two-step process led to higher bioconjugation yields when compared with a single-step EDC reaction [6, 27].



Scheme 20 | Conjugation of Antibodies to Carboxy-QDs using EDC or EDC/NHS. Coupling of QDs containing carboxylate groups with amine-containing biomolecules using (a) EDC single-step reaction or the more efficient (b) EDC/NHS two-step reaction to form bioconjugated QDs (amide derivative) [6].

Formation of an NHS-ester on the surface of the particles for amide bond formation with the biomolecule of interest (amide derivative, Scheme 20 (b)) was performed using EDC. This activation step was quickly tested for carboxy-QDs. In this case the amide bond formation was carried out using ethanolamine and glycine as models and using only the single-step EDC reaction (Scheme 20 (a)). Two samples of carboxy-QDs in separate microtubes containing an excess of EDC each, were incubated with an excess of ethanolamine and with an excess of glycine respectively. Both incubations were conducted at room temperature for 3 hours, followed by 12 hours of dialysis purification. To evaluate the amide bond formation on the QDs surface (successful activation of carboxy-QDs) the molecular weight of the final QD-amide derivatives were analysed by agarose gel electrophoresis.

For comparison, natural carboxy-QDs were also loaded on the same gel (Figure 24).

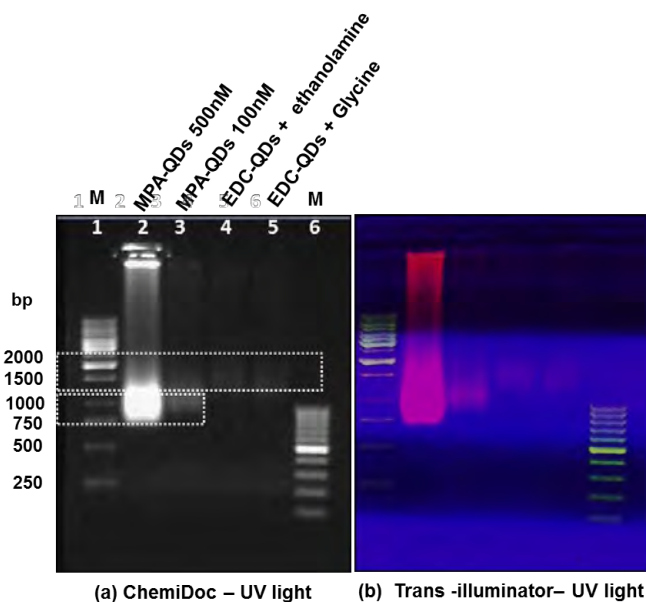


Figure 24 | EDC Activation Step Analysed by Agarose Gel Electrophoresis. Comparison of gel shift of MPA-QDs after EDC activation and amide formation and the same QDs without activation. Agarose gel electrophoresis was conducted in 1% agarose gel with TBE 1x running buffer (pH 8.4) for 55min at 90V. The gel was visualized under different conditions: (a) ChemiDOC molecular imager under standard UV light, (b) UV trans-illuminator excited at 365nm to observe the natural fluorescence of water-soluble QDs.

Gel electrophoresis monitors the electrophoretic mobility of the charged species in a gel matrix, usually agarose and polyacrylamide, when an electrical field is applied across it. On the small scale, these techniques have been used to separate and purify nanoparticles-bioconjugates and has also been used as a rapid and powerful tool for confirming molecular/biomolecular attachment to the nanoparticle through discrete changes in mobility^[28]. In this technique the migration of the nanoparticles in the electric field depends on the particle total charge but also the particle size^[29]. Figure 24 displayed the gel shift of the MPA-QDs after EDC activation and amide formation and the same QDs without activation. The results obtained appear to demonstrate that the QD-amide derivatives were successfully obtained with ethanolamine and glycine. In other words, the MPA-QDs were successfully activated with EDC

which then reacted with the corresponding amine-containing molecules to form the desired QD-amide derivatives. This result was visualized by the differences in molecular weight between the activated acid (wells 4 and 5) and the non-activated QDs (wells 2 and 3). Moreover, this result was also confirmed by differences in electrophoretic mobility where the amide-QDs moved slowly along the gel whereas the non-activated lighter QDs (natural carboxy-QDs) moved faster. These observations confirm that the activation step of carboxy-QDs can be successfully achieved using EDC chemistry.

The activation of MPA and DHLA-QDs for posterior coupling with biomolecules was carried out using the two-step EDC/NHS reaction as described. In this case the QDs were partially activated using different amounts of EDC and NHS (1:2 respectively) in order to maximise the amount of NHS ester produced and prevent the formation of unwanted surface secondary products. The activated MPA and DHLA-QDs were purified by dialysis to eliminate the excess of EDC and NHS added and immediately used for the bioconjugation step with antibodies. Over the years, many buffers such as PBS^[13], MES^[15, 24, 25], borate^[8, 30] or even Tris-glycine^[29], at different pH's, have been used for the bioconjugation of carboxy coated QDs with amine-containing biomolecules using the EDC/NHS strategy. Taking advantage of this literature and based on the pH stability of MPA and DHLA-QDs in sodium phosphate buffer previously discussed, it was decided to test the bioconjugation step proposed in Scheme 19. It is important to point out that the bioconjugated protocol displayed in this scheme was also tested with carboxyPEG₄₀₀-QDs. However, due to the long chain of PEG₄₀₀, the ligands around the QD surface fold up on themselves making impossible the posterior activation of the functional COOH groups with EDC/NHS and consequently their bioconjugation with antibodies.

Supposedly, the Ab ionic adsorption should take place at pH below its isoelectric point (pI). After the reaction of the activated QDs with antibodies at working pH, the bioconjugation media would be shifted to a higher pH and/or containing NaCl in order to dissociate the Ab ionically adsorbed and promote the Ab covalent attachment. Preliminary attempts at the bioconjugation reaction were performed under 3 different experimental conditions containing

the same concentration of activated QDs, EDC/NHS reagents and 4 equivalents of antibody (QD/Ab~1:4). Hence, keeping in mind the pI of the antibodies (around 7-7.4) ^[25], two reactions were initially suspended in Na-P 10mM pH 6 (Scheme 19, method A) and a third reaction was dispersed in Na-P 10mM pH 7 with 300mM of NaCl (Scheme 19, method B) for comparison. It is important to point out, that this last reaction was only performed because the use of pH 7 with 300mM of salt has been reported ^[25] as the best conditions to desorb the Ab attached by ionic interactions. Thus, it was thought that this could be a shortcut to directly promote the covalent binding of antibody to quantum dots. After 4h of incubation of all samples at room temperature, one of the two reactions initially prepared at pH 6 was maintained in the same buffer but the other was incubated for an additional 30 minutes at 37°C in Na-P 10mM pH 8 with 300mM of NaCl after the initial pH conditions were shifted by the addition of 20µL of a solution of Na-P 0.2M pH 12 with 3M of NaCl (Scheme 19, method B₁ and B₂ respectively). The third reaction at pH 7 with salt was also kept under the same conditions (Scheme 19, method A).

The obtained bioconjugated nanoparticle surface should be inert in order to prevent possible unspecific interactions with other components of the sample or even for a further characterization. Although BSA or PEG₅₀₀₀ has been reported to give very good results ^[24], in this work the inertization of bioconjugated QDs was carried out with an excess of ethanolamine. This step blocks the remaining activated carboxyl groups on the QDs surface and was conducted by incubating the three QD-Ab samples overnight with the amine at room temperature, followed by a purification dialysis to eliminate the unreacted ethanolamine. The bioconjugation protocol was then finished with a final purification using centrifugal filtration with a 300kDa cut-off to eliminate possible free antibody in the different QD-antibody samples. In all cases the supernatants were kept to further estimate the amount of unbound antibody. To quickly evaluate the resulting dots the final QD-Ab samples were analysed by agarose gel electrophoresis (Figure 25).

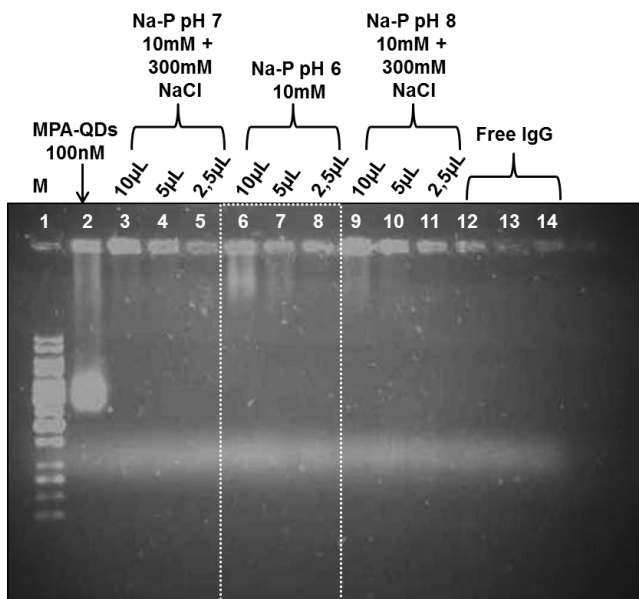


Figure 25 | Analysis of Bioconjugation Protocol by Agarose Gel Electrophoresis. Comparison of the gel shift of activated MPA-QDs after conjugation with antibodies under the different working conditions tested; (wells 3-5) Na-P 10mM pH7 with 300mM NaCl, (wells 6-8) Na-P 10mM pH 6 and (wells 9-11) Na-P 10mM pH 8 with 300mM NaCl. As a control 100nM of non-activated MPA-QDs were used (well 2). Agarose gel electrophoresis was run in 1% agarose gel with TBE 1x running buffer (pH 8.4) for 1h at 45V, 45 minutes at 60V and 1h15 minutes at 90V. The gel was visualized under UV light using a ChemiDOC molecular imager.

The migration of the nanoparticles immersed in the electric field of the electrophoresis gel depends on both the particle total charge and the particle size. Hence, it's easy to predict that CdSe/ZnS QDs bearing carboxylic ligands or biomolecules on their surface will display different electrophoretic behaviours. In Figure 25, electrophoresis results are displayed and in general they seemed to indicate that conjugation between QDs and antibodies had occurred and were also in agreement with theoretical predictions. From the differences in electrophoretic mobility, it is possible to observe that the antibody-conjugated QDs (wells 6 and 9) were always slower than natural MPA-QDs (well 2) because of the greater diameter and the reduced total charge resulting from positively charged amino groups present in the antibodies. Therefore, the reaction conducted in sodium phosphate buffer 10mM at pH 6 appeared to be the most successful since a higher fluorescence intensity of possible bioconjugated QDs was observed inside the

gel (well 6). However, well 9, although less intense, also showed the fluorescence of possible antibody-bioconjugated QDs within the gel. The reaction carried out at pH 6 apparently formed a larger quantity of antibody-conjugated QDs which could result from a possible ionic and/or covalent Ab attachment. On the other hand, the sample loaded into well 9 is the product of a reaction during which the initial working pH was increased (from 6 to 8) and the media changed by the presence of salt. This may have led to the obtention of a smaller amount of covalently conjugated QD-Ab sample and Ab's ionically adsorbed had been eliminated. The reaction conducted at pH 7 with salt, did not promote the conjugation of antibodies to QDs. It is important to point out that a lot of aggregated sample was visualized inside the wells and consequently did not migrate across the gel. This could be related to a higher QD-Ab concentration loaded on the gel or to non-optimised reaction conditions. In general, these preliminary results prove the conjugation of antibodies to QDs. However, to better confirm this data a detailed characterization of QD-Ab samples was subsequently performed as discussed below.

Determination of the Antibody/QD Molar Ratio

Before evaluating the conjugated samples for bioassay purposes, attempts to quantitate the number of IgG molecules bound per QD were made. It is known that protein concentration determination is a basic biochemical method and often necessary when protein samples are processed. Currently, there are several colorimetric assays for proteins including Lowry, Biuret, Bradford and bicinchoninic acid (BCA) assays. The Bradford assay has been extensively used due its advantages of rapidness, convenience and relative sensitivity^[31, 32]. Although not designed for nanoparticles, this method can be applied to their analysis (e.g. nanoparticle interaction and bioconjugation)^[28]. Initially, the fast and colorimetric Bradford protein assay^[33] was used. In this case a calibration curve was made using BSA as protein standard with a range of linearity from 1 to 25µg/mL. Unfortunately, the results obtained were inconclusive because the presence of the QDs in QD-Ab samples interfered with the Bradford assay as already found for similar systems^[25]. Thus, this experiment was replaced by the Protein A280 assay available in a NanoDrop

2000 UV spectrophotometer from Thermo Scientific. This assay is applicable to purified proteins that contain Trp, Tyr residues or Cys-Cys disulphide bonds and exhibit absorbance at 280 nm as was the case for the monoclonal antibodies herein used. After the inertization of antibody-bioconjugated QDs, the samples were ultra-purified by centrifuging at 1000g for 2 minutes to remove any remaining free antibodies in solution and the supernatants were all kept for posterior quantitation because the decrease in protein concentration in supernatants can be directly correlated with the amount of antibody linked to the QDs. Using this method, the concentration determination of immobilized antibody was proposed as: $Abs_{280nm}(\text{QD-Ab sample}) - Abs_{280nm}(\text{QD})$ (Equation 7). After purification the absorbance at 280nm (Abs_{280nm}) for all QD-Ab samples and their corresponding supernatants were measured as well as the UV-visible spectra of the QD-Ab samples to give the QD interference at 280nm herein designed by the $Abs_{280nm}(\text{QD})$. These measurements were based in a reference setting of 1mg/mL protein solution producing an absorbance of 1.0 (10mm pathlength). Thereby, the $Abs_{280nm}(\text{QD-Ab sample})$ as well as Abs_{280nm} of the supernatants directly represented the concentration per mL of Ab present in the samples. The real concentration of Ab present in the bioconjugated samples was then given by subtracting the undesired contribution of QD at 280nm to the initial concentration of QD-Ab samples measured at 280nm. Later, knowing the mass (in mg) of antibody attached to the QD surface and molecular weight of the antibody (~150kDa) used it was possible to calculate the number of moles of immobilized Ab. As a control, a reference solution having exactly the same initial antibody concentration was also prepared and measured to be sure about the initial mass of antibody added and all measurements were carried out in triplicate to improve accuracy. The molar ratio QD/Ab was defined as: $n(\text{Ab})_{\text{immobilized}} / n(\text{QDs})_{\text{initial}}$ (Equation 8) and it was assumed that no losses of QDs had occurred.

The meaningful results obtained are displayed in the Table 5 and are consistent with what was previously shown in the analysis of the bioconjugation protocol by agarose gel electrophoresis.

Table 5 | QD/Ab molar ratios obtained for the different bioconjugation reactions performed to link antibodies onto QD surface using the EDC/NHS strategy.

Working conditions (buffer ionic strength pH salt)	QD/Ab Molar Ratio
Na-P 10mM pH 7 with 300mM NaCl	1:0.2 ^(*) – 1:0.5
Na-P 10mM pH 6	1:2 – 1:3
Na-P 10mM pH 8 with 300mM NaCl	1:1

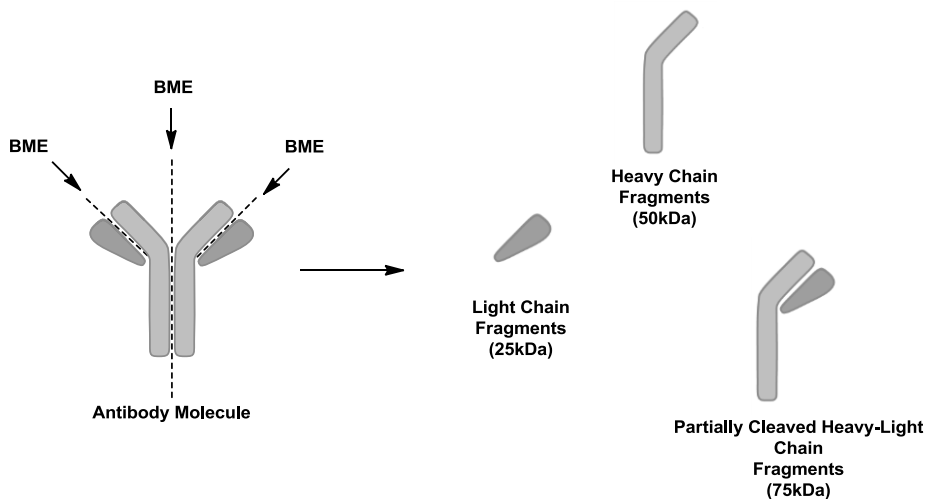
(*) Non-significant value

These results demonstrated that at pH 8 with salt and pH 6 it is possible to achieve 1 and 3 antibodies per QD respectively. This only reinforces and confirms the idea that when the working pH is lower than pI of the Ab, the ionic and covalent attachment are induced, but shifting these conditions applying a higher pH and/or salt condition apparently the antibodies ionically adsorbed could be eliminated from the QD surface and only the Ab covalently linked remained. In contrast, when the bioconjugation reaction was carried out in pH 7 with salt, the maximum QD/Ab molar ratio obtained was 1:0.5 which leads to the conclusion that the QD-antibody bond probably was not achieved. The optimised conjugation protocol applied during this work is able to produce antibody-bioconjugated QDs at least with two biomolecules per nanoparticle.

Characterization of the Binding Properties of Antibody-Bioconjugated QDs

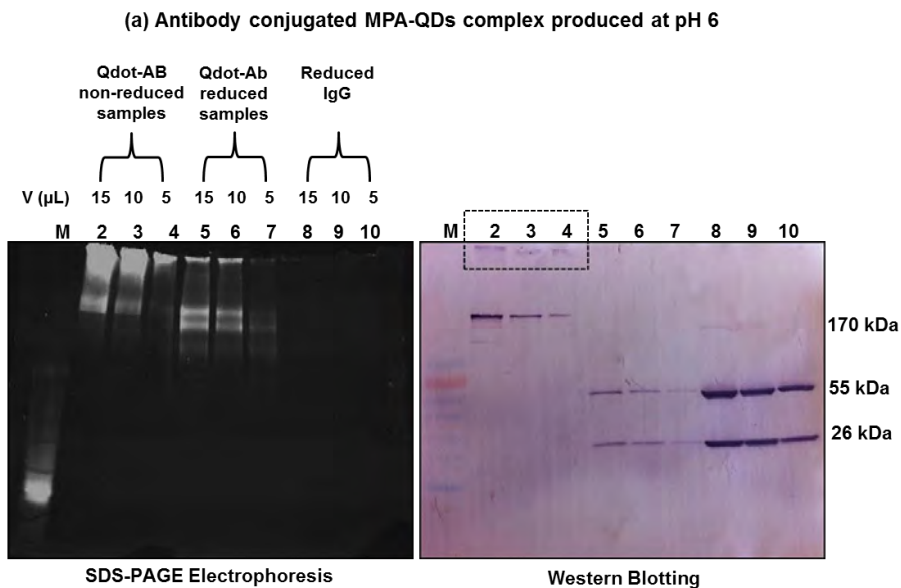
To characterize the bioconjugation of antibodies with MPA and DHLA-QDs, the antibody-QD complexes were run in a SDS-PAGE electrophoresis with and without β -mercaptoethanol (BME), where the reduction conditions were used to separate the functional components of bioconjugated QDs. The antibody fragments were then blotted onto a membrane to qualitatively analyse the attachment of antibodies to QDs. BME is one of the most commonly used agents for disulphide reduction. The reduction of disulphide proteins with this reagent proceeds rapidly via a two-step process involving an intermediate mixed disulphide ^[6]. When antibodies are reduced using BME, three distinct fragments could be generated identifiable by their molecular weights: a 25kDa light chain (includes half of the specific antigen binding site),

a 50kDa heavy chain (includes the other half of the binding site), and a 75kDa partially cleaved chain consisting of a heavy chain and a light chain held together by an unreduced disulphide bond (Scheme 21)^[34].



Scheme 21 | Antibody Reduction with β -Mercaptoethanol. Schematic antibody cleavage sites by BME at disulphide linkages.

The reaction carried out at pH 6 to link the antibodies to MPA-QDs was analysed under reducing and non-reducing conditions (Figure 26, (a)).



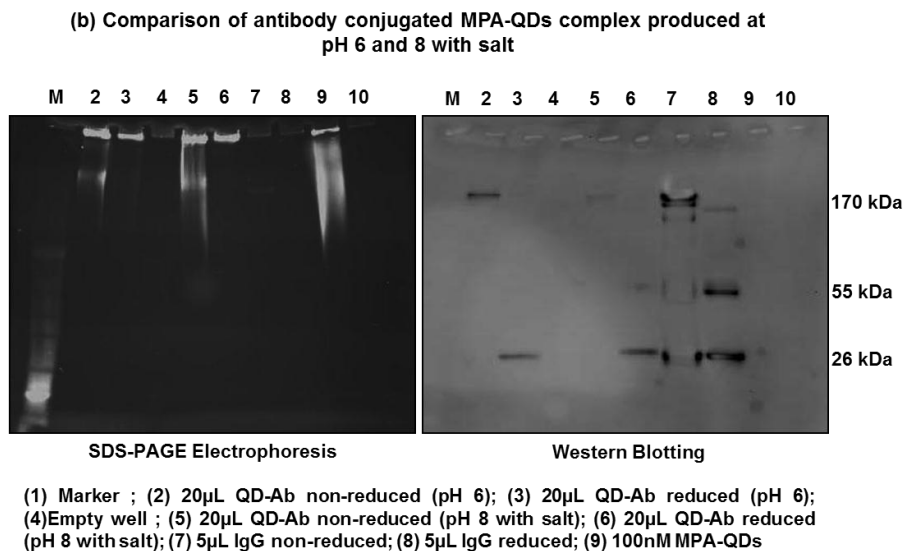


Figure 26 | Separation of the Functional Components of MPA-Bioconjugated QDs. Separation of antibody-MPA QDs complexes into fragments using SDS-PAGE electrophoresis (left images) and membrane transfer (right images) obtained under different experimental conditions. (a) Antibody conjugated MPA-QDs complex produced at pH 6. (b) Comparison of antibody conjugated MPA-QDs complexes produced at pH 6 and pH 8 with salt. For both, the SDS-PAGE was analysed under UV light before membrane transfer using a molecular imager. The SDS-PAGE electrophoresis was run at 90V for 90 minutes and electro-transfer at 80V for 2h.

For the BME reducing conditions it is possible to observe the presence of heavy (55kDa) and light (26kDa) chains cleaved from possible covalently bound Ab (Figure 26 (a), lanes 5-7). In contrast, this separation is not observed in lanes without BME (Figure 26 (a), lanes 2-4) as expected and only a band of 170kDa appears in the membrane. This type of assay was also repeated for the antibody conjugated QDs resulting from the reaction performed at pH 8 with salt and where the sample at pH 6 was loaded onto the same gel for comparison (Figure 26 (b)). Interestingly, for both pH's under reducing conditions, no heavy chains were detected in the membrane. However, the band with molecular weight around 170kDa remained under non-reducing conditions and in the same position for SDS-PAGE gel under UV light and transfer membrane. Briefly, these results suggest that bioconjugation had occurred and that the antibody was linked to the carboxy-QDs since bioconjugated QDs, which migrated in SDS-page gel, have exactly the same band position of protein as in the blotting membrane (Figure 26 (a),

lanes 2-4). For the bioconjugated QDs that remained in the wells it is also possible to visualize in the corresponding membrane position the presence of protein (dashed black box). It is noteworthy that some bioconjugated QDs remained in the wells probably due to aggregation, high concentrations of sample loaded onto the gel or high molecular weight of the sample limiting the mobility of QD-antibody complexes in the pores of the gel.

It is well known that after treatment with BME, in general each antibody molecule is split into heavy and light chain fragments which are traduced in a 50 and 25kDa bands respectively in SDS-PAGE electrophoresis. This information could be applied to evaluate the orientation of antibodies coupled to quantum dots. According to Puertas *et al*^[24], when the immobilization is done with a site-selective orientation using for example the Fc portion of antibody only the heavy chains fragments should be attached to the nanoparticles and after treatment with a reducing agent only the light chains of the Ab could be released. On the other hand, if the antibody is randomly immobilized, after reducing conditions, both light and heavy chains could be liberated. Taking advantage of this information, the presence of a most evident light chain in reducing conditions (Figure 26 (b), lanes 3 and 6) for both working pH's inspires the hypothesis that antibodies could be linked by their Fc portion and well oriented leaving their antigen binding sites available. The particular result obtained in the first SDS-PAGE assay for the sample produced at pH 6, and where after treatment with BME both light and heavy chains appeared (Figure 26 (a), lanes 5-7), could be related to the possible presence of antibodies ionically and randomly oriented onto the quantum dot surface. Repetition of the SDS-PAGE experiments was performed 24h later and perhaps during this period the bioconjugated sample may have lost antibodies ionically adsorbed on the QD surface and only the covalent linked Ab remained. It is important to remember that at pH 6 both ionic and covalent bioconjugation are favoured and with changes of pH or salt addition, predominantly covalent binding is possible. Another possible explanation could be related to the fact that these antibodies are linked to MPA water-soluble quantum dots. MPA is a monothiol ligand that is bound to the CdSe/ZnS core-shell QDs surface by a single and weak sulphur bridge. If BME could cleave the sulfhydryl bonds in proteins/antibodies it is also

possible to break these bonds in other molecules. This led to the idea that some of the antibodies linked to MPA were totally split into light and heavy chains because the sulphur bridge between ligand and the ZnS shell from native QDs was first reduced by BME. This idea was enhanced when posteriorly the coupling of antibodies to quantum dots was carried out with DHLA-QDs also at pH 6. The resulting sample was characterized by the same techniques as before running a SDS-PAGE gel and then blotted on a membrane (Figure 27). Under non-reducing conditions the presence of a 170kDa band is maintained in the same position (lanes 2-4) as well as the light chain band after treatment with BME (lanes. 5-7). Apparently, at pH 6 covalent coupling also occurred as previously discussed. On the other hand, the substitution of mono-mercapto ligands by dithiol dihydrolipoic acid ligands improves the bond stability between ligand and ZnS shell of CdSe/ZnS core-shell QDs and preventing it's destruction by the reducing agent.

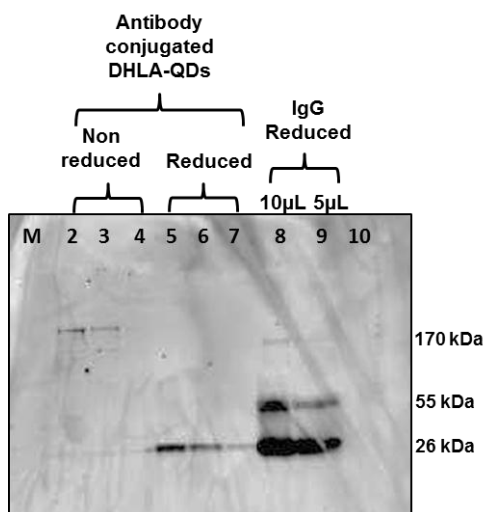


Figure 27 | Separation of the Functional Components of DHLA-Bioconjugated QDs. Separation of antibody-DHLA QDs complexes resultant from a bioconjugation reaction performed at pH 6. The SDS-PAGE electrophoresis and the electro-transfer on a PVDF membrane was conducted under the same conditions previously applied for MPA QDs-Ab samples.

Generally, the attempts to attach antibodies to CdSe/ZnS core-shell QDs capped with 3-mercaptopropionic acid and dihydrolipoic acid using EDC strategy assisted by NHS was fairly successful. However, it is evident that the

number of coupled and functional antibodies is much less than the amount of IgG added initially. The overall data, suggest that antibodies are probably more covalently than electrostatically attached due to the fact that partial Ab-QDs complexes in non-reduced lanes travel through the gel and their fluorescence is coincident with the protein band on western membrane in the same position. Additionally, some of these unreduced complexes remained in the wells because of their large size.

Evaluation of Antibody-Bioconjugated QDs Capacity to Recognize their Antigen

The term “blotting” refers to the transfer of biological samples from a gel to a membrane and their subsequent detection on the surface of the same membrane. Western blotting, also called immunoblotting was introduced by Towbin *et al*^[21] in 1979 where an antibody was used to detect its antigen. Using this technique, it was decided to perform an experiment to test the functionality of the developed antibody-conjugated QDs complexes and check if these nanoprobe were able to recognize and label their antigen. Firstly, 10µL per well of antigen (r) RAP-1 *B. bovis* was run on a SDS-PAGE gel. Later, the proteins were blotted onto a PVDF membrane with low auto-fluorescence and the gel was stained with a 0.025% coomassie blue solution to observe the electro-transfer efficiency and to estimate the molecular weight of the antigenic protein (Figure 28 (a)).

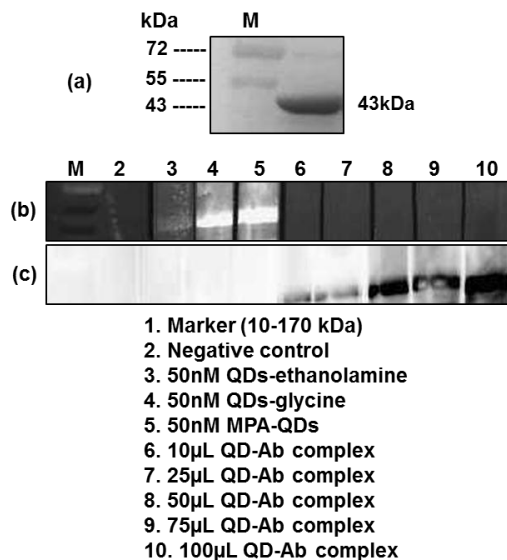


Figure 28 | Testing the Functional Activity of QD-Ab complexes. Images resulting from the assay to test the capacity of antibody-conjugated QD complexes to recognize their antigen. (a) SDS-PAGE gel loaded with 10 μ g/well of antigenic protein and stained with 0.025% coomassie blue solution. (b) Visualisation under UV-light of the natural fluorescence of QDs of the different strips containing antigen protein after incubation with 50nM of QDs inertized with ethanolamine and glycine (controls, lanes 3 and 4); 50nM of MPA-QDs (control, lane 5) and with different volumes of QD-Ab complexes (lanes 6-10). All these samples were prepared in blocking buffer containing 5% (w/v) of non-fat milk. (c) Visualisation of the same strips but after incubation with secondary antibody anti-mouse IgG-HRP. The detection method used was the chemiluminescence HRP substrate. All the images were acquired with a CCD imager ChemiDoc equipment.

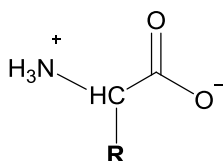
The antigenic protein, after immobilized in a PVDF membrane, was incubated overnight at 4 $^{\circ}$ C with different volumes of specific monoclonal antibodies-bioconjugated QDs. In this assay different controls were performed. As a negative control the antigenic protein was incubated with 1mL of blocking buffer only (Figure 28 (b and c), lane 2) and to ensure the absence of unspecific interactions between carboxy-QDs with the test line, the lanes 3 to 5 were incubated with 50nM of MPA-QDs blocked with ethanolamine and glycine and 50nM of natural MPA-QDs respectively. All the strips after this step were visualized under UV light to observe the natural fluorescence of QDs (Figure 28 (b)) and if an immunofluorescence reaction occurred. The subsequent immuno-detection in the membrane strips was carried out by incubating all the lanes with an anti-mouse peroxidase secondary antibody and using the chemiluminescence HRP substrate to reveal the interaction

between anti-IgG and IgG (Figure 28 (c)). Firstly, it is possible to observe in image (a) that (r)RAP-1 *B. bovis* antigen shows the presence of one band of 43kDa as expected for the purified form of this recombinant expressed antigenic protein [35]. This recombinant protein was previously produced and expressed in the Biomolecular Diagnostic laboratory (ITQB-UNL) and only the carboxyl-terminal (C-terminal) of the protein was used [16]. As already reported, when only the C-terminal is used to produce recombinant antigens spanning RAP-1 only 248 amino acids of a total of 565 were used and the molecular weight for this reduced length is about 44kDa which is consistent with the results herein obtained.

After treatment with primary antibody-conjugated QDs, the natural fluorescence of the QDs was detected with intensity in the control lanes (Figure 28 (b), lanes 3-5) for the 43kDa band. Immunofluorescence is completely absent in the lanes 6 to 10 where volumes from 10 to 100 μ L of Ab-QD sample were incubated. However, after incubation with secondary antibody the results were reversed and the reaction which reflects the antigen recognition by the antibodies attached to QDs (immunoreaction) was only visualized in the lanes incubating first with primary antibody (Figure 28 (c), lanes 6-10). These results, clearly demonstrated that the antibodies present in Ab-QD samples are functional and specifically recognized the antigen once the immunoreaction was strongly detected by the HRP substrate (Figure 28 (c), lanes 6-10). However, some doubts are raised about whether these antibodies are really attached to quantum dots or are free in solution because the immunofluorescence was not detected for these lanes before the incubation with secondary antibody. To overcome this issue the immunofluorescence reaction in controls lanes 3 to 5 was analysed (Figure 28 (b)). Interestingly, it is possible observe that the MPA-QDs in their natural form or blocked with glycine strongly interact with the antigen immobilized in the membrane. In addition, the QDs blocked with ethanolamine also interact with the antigenic protein but with less intensity.

Proteins are composed of amino acids linked together through the formation of amide bonds and the sequence and properties of these amino acids constituents determine protein structure, reactivity and function. Each amino acid is composed of an amino group and a carboxyl group bound to a central

carbon, designated the α -carbon. Also bound to the α -carbon are a hydrogen atom and a side chain unique to each amino acid which normally does not participate in polypeptide formation but is free to interact and react with the environment/other molecules ^[6]. This amine group is basic and can be protonated and thus bears a positive charge, while the carboxylate groups are negatively charged (Scheme 22).



Scheme 22 | Structure of an Individual Amino Acid Present in Proteins. Individual amino acids consist of a (α) primary amine, a carboxylic acid group, and a unique side chain structure (R). The amine is protonated and bears a positive charge, while carboxylate group is normally negatively charged at physiological pH^[6].

During the performance of this assay, were used TBS to prepare the known blocking buffer (containing also non-fat milk) and TTBS for the washes between the different steps along the experiment. As described in the Experimental Section, both buffers are prepared to have a pH around 7.6 which is very close to the physiological pH (7.4). At physiological pH each protein is composed of amino acids linked by amide bonds and bearing amino and carboxyl groups which are positively and negatively charged respectively. This suggests that in the control lanes an interaction between antigen and non-conjugated QDs could exist. More specifically, a polar interaction between the protonated NH_2 groups present in the antigen and the carboxylate groups of the MPA ligand on the QDs surface (lane 5) is possible. Similarly the terminal carboxylic acid group available in glycine (lane 4) could interact with amino groups and was indicated by the intense fluorescent band at 43kDa. In the case of lane 3 (incubated with QDs blocked with ethanolamine), the same band is less intense because the probability of interaction between the NH_2 groups present in the antigenic protein and the hydroxyl group available in QDs blocked with ethanolamine is much lower and unlikely to occur. If this explanation raises the possibility of MPA-QDs in their natural form or blocked with amine containing molecules to interact directly

with the antigen, this could lead to conclude that the antibody in Ab-QD samples must be attached to the quantum dots, because if the quantum dots were free in solution independently blocked or non-blocked at least one weak fluorescent band should have appeared in the lanes 6-10. Probably, the immunofluorescence reaction was not detected in these lanes due to the low concentration of quantum dots attached to antibodies and which was not detected by the charge-coupled device.

Conclusion

The set of data related with pH stability and electrophoretic mobility clearly demonstrated that CdSe/ZnS core-shell QDs capped with dithiol-terminated ligands are more stable and less prone to aggregation than those functionalized with monothiol ligands. Moreover, it was found that the stability of the nanoparticles strongly depend the nature of ligand but also the pH and media for their dispersion. Taking advantage of this useful information the EDC/NHS chemistry was used to bioconjugate MPA and DHLA-QDs with antibodies. The experimental conditions proposed showed that at a certain pH the antibodies are ionically and covalent attached however increasing the pH and adding some salt it's possible to promote only the covalent binding. These data were confirmed by the number of IgG molecules attached on a single quantum dot. At pH 6 was possible to achieve three antibodies per particle, assuming that some of them are only ionically bound and could be eluted form QD surface, while at pH 8 with salt no more than one antibody was obtained. Moreover, the number of attached antibodies was always lower than the amount of protein added initially indicating that with this strategy the bioconjugation reaction was not complete. The QD-antibody complexes were characterized using molecular biology techniques. By agarose gel electrophoresis it was demonstrated that the bioconjugated QDs were obtained and move slower than the non-conjugated ones. This is a result of the higher molecular weight and the reduced negative surface charge. The SDS-PAGE using BME as reducing agent was useful to clarify the binding properties of the conjugates. Additionally, the biological activity was evaluated by immunoblotting, which showed that the antibodies present in QD-Ab complexes were functional and recognized their specific antigen. However,

the use of these techniques should be optimized in order to promote less aggregation and well dispersion of the conjugated samples in the wells and thus promote a better mobility through the gels. Alternative strategies using specific sites of the antibody should also be tested to achieve higher antibody conjugation efficiency and better stability of the QD-Ab complexes.

Glossary

Table 6 | Glossary of terms related with some molecular biology techniques applied in this work ^[22, 36, 37].

Term	Definition
Agarose gel electrophoresis	Commonly electrophoresis technique using agarose gels to separate proteins, oligonucleotides or more recently nanoparticles based on their overall electrophoretic mobility, due to differences in molecular weight and/or overall charge. Is an alternative approach to using polyacrylamide gels and provides several benefits. Gels can also be run using a vertical system or a horizontal system.
Alkaline Phosphatase	An enzyme used as a detection reagent, usually conjugated to a secondary antibody probe.
Antibody	An immunoglobulin; a protein produced in response to an antigen, which specifically binds the portion of the antigen that initiated its production.
Antigen	Any molecule that specifically binds with an antibody.
Blot	Immobilization of proteins or other molecules onto a membrane; or, the membrane that has the molecules adsorbed onto its surface.
ChemiDoc™ system	Charge-coupled device camera-based imaging system for visualization and documentation of fluorescent, chemifluorescent, and colorimetric samples.

Chemiluminescence	The emission of light due to a chemical reaction; used in the specific detection of blotted molecules
Coomassie Blue	An anionic dye used in the total protein staining of gels and blots.
Electrophoretic blotting	The use of the driving force of an electric field to move proteins from gels to membranes.
Electrophoretic mobility	Is the observed rate of migration of a component divided by electric field strength in a given medium. The electrophoretic shift assay is the separation of proteins and DNA/RNA by charge and/or size and length respectively. This assay could be run in polyacrylamide or agarose gels.
Horseradish peroxidase (HRP)	An enzyme used in the specific detection of molecules on blots, usually conjugated to a secondary antibody probe.
Immunoassay	A test for a substance by its reactivity with an antibody.
Immunoblotting	Blot detection by antibody binding.
Immunodetection	Detection of a molecule by its binding to an antibody.
Ionic strength	Is a measure of the concentration of all ions in a solution.
Isoelectric point (pI)	Is sometimes abbreviated to IEF and is the pH at which a particular molecule (<i>e.g.</i> protein) or surface carries no net electrical charge. Below the pI proteins carry a net positive charge, above it a negative charge.
Nonspecific binding	The interaction between bound proteins and probes that is not a result of a specific reaction; results in spurious signals on the membrane.
PAGE	Polyacrylamide gel electrophoresis, a common method of separating proteins.

PVDF membrane	Polyvinylidene difluoride membrane is a membrane used in protein blotting, which has high chemical resistance, tensile strength, binding, and retentive capacity, making it ideal for use in protein sequencing.
Primary antibody	An antibody that binds a molecule of interest.
Prestained standard	A mixture of molecular weight marker proteins that have covalently attached dye molecules, which render the bands visible during electrophoresis and transfer; used to assess the transfer efficiency of proteins onto the membrane.
Protein G	A protein derived from <i>Streptococcus</i> that binds a wide range of immunoglobulins from various species, and has a wider range of binding capabilities than protein A.
SDS-PAGE	The separation of molecules by molecular weight in a polyacrylamide gel matrix in the presence of a denaturing detergent, sodium dodecyl sulphate (SDS).
Secondary antibody	An antibody that binds a primary antibody; used to facilitate detection.
Semi-dry blotting	The use of a semi-dry blotting apparatus, which consists of two horizontally, oriented plate electrodes. The gel and membrane sandwich is positioned between them with buffer-soaked filter paper on either side of the sandwich serving as buffer reservoirs.
Substrate	A substance that is reacted upon by an enzyme; for example, a colour development reagent.
Tween 20	A non-ionic detergent; used in blot detection procedures as a blocking reagent or added to wash buffers to minimize nonspecific binding and background.

Towbin buffer	A common protein blotting transfer buffer.
Western blotting	The immobilization of proteins onto a membrane, and the subsequent detection by protein-specific binding and detection reagents.

Acknowledgments

The author thanks to Dr Jesús M. de La Fuente and co-workers for the opportunity to work and learn molecular biology and conjugation techniques in his laboratory at Instituto de Nanociencia de Aragón (INA), Zaragoza, Spain. The author also thanks to Dr Ana Domingos from IHMT-UNL, Lisboa, Portugal for the production of mouse monoclonal antibodies against recombinant RAP-1 protein. The helpful discussions provided by Dr. Mariana Dominguez in the evaluation of the antigen recognition capacity of the antibody-bioconjugated QDs were also appreciated. Ana Sofia Miguel is a recipient of a PhD fellowship from the Fundação para a Ciência e Tecnologia (FCT), Portugal (SFRH/BD/40303/2007). The work was supported by the national funded project NTec/SQA/0131/2007 from FCT.

References

1. Azzazy, H. M. E.; Mansour, M. M. H.; Kazinierczak, S. C., From diagnostics to therapy: Prospects of quantum dots. *Clin Biochem* **2007**, 40, (13-14), 917-927.
2. Alivisatos, A. P.; Gu, W. W.; Larabell, C., Quantum dots as cellular probes. *Annu Rev Biomed Eng* **2005**, 7, 55-76.
3. Bruchez, M. P., Turning all the lights on: quantum dots in cellular assays. *Curr Opin Chem Biol* **2005**, 9, (5), 533-537.
4. Michalet, X.; Pinaud, F. F.; Bentolila, L. A.; Tsay, J. M.; Doose, S.; Li, J. J.; Sundaresan, G.; Wu, A. M.; Gambhir, S. S.; Weiss, S., Quantum dots for live cells, in vivo imaging, and diagnostics. *Science* **2005**, 307, (5709), 538-544.
5. Goding, J. W., *Monoclonal antibodies: principles and practice : production and application of monoclonal antibodies in cell biology, biochemistry and immunology*. Academic Press: **1996**.
6. Hermanson, G. T., *Bioconjugate techniques*. Academic Press: **2008**.
7. abcam, Antibody Structure and isotypes. In 2012.
8. Mattoussi, H.; Mauro, J. M.; Goldman, E. R.; Anderson, G. P.; Sundar, V. C.; Mikulec, F. V.; Bawendi, M. G., Self-assembly of CdSe-ZnS

quantum dot bioconjugates using an engineered recombinant protein. *J Am Chem Soc* **2000**, 122, (49), 12142-12150.

9. Clapp, A. R.; Goldman, E. R.; Mattoussi, H., Capping of CdSe-ZnS quantum dots with DHLA and subsequent conjugation with proteins. *Nat Protoc* **2006**, 1, (3), 1258-1266.

10. Goldman, E. R.; Anderson, G. P.; Tran, P. T.; Mattoussi, H.; Charles, P. T.; Mauro, J. M., Conjugation of luminescent quantum dots with antibodies using an engineered adaptor protein to provide new reagents for fluoroimmunoassays. *Anal Chem* **2002**, 74, (4), 841-847.

11. Hanaki, K.; Momo, A.; Oku, T.; Komoto, A.; Maenosono, S.; Yamaguchi, Y.; Yamamoto, K., Semiconductor quantum dot/albumin complex is a long-life and highly photostable endosome marker. *Biochem Bioph Res Co* **2003**, 302, (3), 496-501.

12. Susumu, K.; Medintz, I. L.; Delehanty, J. B.; Boeneman, K.; Mattoussi, H., Modification of Poly(ethylene glycol)-Capped Quantum Dots with Nickel Nitrilotriacetic Acid and Self-Assembly with Histidine-Tagged Proteins. *J Phys Chem C* **2010**, 114, (32), 13526-13531.

13. Xing, Y.; Chaudry, Q.; Shen, C.; Kong, K. Y.; Zhau, H. E.; WChung, L.; Petros, J. A.; O'Regan, R. M.; Yezhelyev, M. V.; Simons, J. W.; Wang, M. D.; Nie, S., Bioconjugated quantum dots for multiplexed and quantitative immunohistochemistry. *Nat Protoc* **2007**, 2, (5), 1152-1165.

14. Medintz, I. L.; Uyeda, H. T.; Goldman, E. R.; Mattoussi, H., Quantum dot bioconjugates for imaging, labelling and sensing. *Nature Materials* **2005**, 4, 435-446.

15. Pereira, M.; Lai, E. P., Capillary electrophoresis for the characterization of quantum dots after non-selective or selective bioconjugation with antibodies for immunoassay. *Journal of Nanobiotechnology* **2008**, 6, 10.

16. Silva, M. G.; Helali, S.; Esseghaier, C.; Suarez, C. E.; Oliva, A.; Abdelghani, A., An impedance spectroscopy method for the detection and evaluation of Babesia bovis antibodies in cattle. *Sensor Actuat B-Chem* **2008**, 135, (1), 206-213.

17. Laemmli, U. K., Cleavage of Structural Proteins during Assembly of Head of Bacteriophage-T4. *Nature* **1970**, 227, (5259), 680-&.

18. Barker, R. N., Electrophoretic analysis of erythrocyte membrane proteins and glycoproteins from different species. *Comparative Haematology International* **1991**, 1, 155-160.

19. Bolt, M. W.; Mahoney, P. A., High-Efficiency Blotting of Proteins of Diverse Sizes Following Sodium Dodecyl Sulfate-Polyacrylamide Gel Electrophoresis. *Anal Biochem* **1997**, 247, 185-192.

20. Abcam Western Blotting - A Beginner's Guide. <http://www.abcam.com/ps/pdf/protocols/WB-beginner.pdf> (03/03/2012),

21. Towbin, H.; Staehelin, T.; Gordon, J., Electrophoretic Transfer of Proteins from Polyacrylamide Gels to Nitrocellulose Sheets - Procedure and Some Applications. *P Natl Acad Sci USA* **1979**, 76, (9), 4350-4354.

22. Pons, T.; Uyeda, H. T.; Medintz, I. L.; Mattoussi, H., Hydrodynamic dimensions, electrophoretic mobility, and stability of hydrophilic quantum dots. *J Phys Chem B* **2006**, 110, (41), 20308-20316.

23. Susumu, K.; Uyeda, H. T.; Medintz, I. L.; Pons, T.; Delehanty, J. B.; Mattoussi, H., Enhancing the stability and biological functionalities of quantum

- dots via compact multifunctional ligands. *J Am Chem Soc* **2007**, 129, (45), 13987-13996.
24. Puertas, S.; Moros, M.; Fernandez-Pacheco, R.; Ibarra, M. R.; Grazu, V.; de la Fuente, J. M., Designing novel nano-immunoassays: antibody orientation versus sensitivity. *J Phys D Appl Phys* **2010**, 43, (47).
25. Puertas, S.; Batalla, P.; Moros, M.; Polo, E.; del Pino, P.; Guisan, J. M.; Grazu, V.; de la Fuente, J. M., Taking Advantage of Unspecific Interactions to Produce Highly Active Magnetic Nanoparticle - Antibody Conjugates. *Acs Nano* **2011**, 5, (6), 4521-4528.
26. Fuentes, M.; Mateo, C.; Guisan, J. M.; Fernandez-Lafuente, R., Preparation of inert magnetic nano-particles for the directed immobilization of antibodies. *Biosens Bioelectron* **2005**, 20, (7), 1380-1387.
27. Sam, S.; Touahir, L.; Andresa, J. S.; Allongue, P.; Chazalviel, J. N.; Gouget-Laemmel, A. C.; de Villeneuve, C. H.; Moraillon, A.; Ozanam, F.; Gabouze, N.; Djebbar, S., Semiquantitative Study of the EDC/NHS Activation of Acid Terminal Groups at Modified Porous Silicon Surfaces. *Langmuir* **2010**, 26, (2), 809-814.
28. Sapsford, K. E.; Tyner, K. M.; Dair, B. J.; Deschamps, J. R.; Medintz, I. L., Analyzing Nanomaterial Bioconjugates: A Review of Current and Emerging Purification and Characterization Techniques. *Anal Chem* **2011**, 83, (12), 4453-4488.
29. Bucking, W.; Massadeh, S.; Merkulov, A.; Xu, S.; Nann, T., Electrophoretic properties of BSA-coated quantum dots. *Anal Bioanal Chem* **2010**, 396, (3), 1087-1094.
30. So, M. K.; Xu, C. J.; Loening, A. M.; Gambhir, S. S.; Rao, J. H., Self-illuminating quantum dot conjugates for in vivo imaging. *Nat Biotechnol* **2006**, 24, (3), 339-343.
31. Olson, B. J. S. C.; Markwell, J., Assays for Determination of Protein Concentration. In *Current Protocols in Protein Science*, Sons, J. W., Ed. 2007; pp 3.4.1-3.4.29.
32. Han, X. X.; Xie, Y. F.; Zhao, B.; Ozaki, Y., Highly Sensitive Protein Concentration Assay over a Wide Range via Surface-Enhanced Raman Scattering of Coomassie Brilliant Blue. *Anal Chem* **2010**, 82, (11), 4325-4328.
33. Bradford, M. M., A Rapid and Sensitive Method for the Quantitation of Microgram Quantities of Protein Utilizing the Principle of Protein-dye Binding. *Anal Biochem* **1976**, 72, 248-254.
34. Pathak, S.; Davidson, M. C.; Silva, G. A., Characterization of the functional binding properties of antibody conjugated quantum dots. *Nano Lett* **2007**, 7, (7), 1839-1845.
35. Goff, W. L.; McElwain, T. F.; Suarez, C. E.; Johnson, W. C.; Brown, W. C.; Norimine, J.; Knowles, D. P., Competitive enzyme-linked immunosorbent assay based on a rhoptry-associated protein 1 epitope specifically identifies Babesia bovis-infected cattle. *Clin Diagn Lab Immunol* **2003**, 10, (1), 38-43.
36. BIO-RAD, Protein Blotting Guide - A guide to transfer and detection In Bio-Rad Laboratories, Inc.: 2003.
37. LONZA, Source Book for Electrophoresis. In Lonza Rockland, Inc.: 2009.

Chapter 5

Quantum Dot Applications

Quantum Dot Applications

PART I

Detection of RAP-1 Antigenic Protein in Infected <i>Babesia bovis</i> Erythrocytes Using QDs as Fluorescent Reagents	193
Abstract	195
Introduction	195
Experimental Section	201
Materials	201
<i>Babesia bovis</i> infected cultures	201
Immunofluorescence Assays for RAP-1 Antigenic Protein Detection in <i>B. bovis</i> Infected RBCs	202
Standard Immunofluorescence Assays	202
Direct Immunofluorescence Assays Using QD-Ab Conjugates	204
Results and Discussion	206
Conclusion	213
Glossary	213
Acknowledgments	215
References	216

PART II

Work Resulting From Collaboration with Other Research Groups	219
Introduction	221
Overview of the Work Undertaken	222
The Impact of CdSe/ZnS Quantum Dots in Cells of <i>Medicago sativa</i> in Suspension Culture	222
CdSe/ZnS Quantum Dots Trigger DNA Repair and Antioxidant Enzyme Systems in <i>Medicago sativa</i> Cells in Suspension Culture	225
Laser Immobilization onto Solid Substrates of CdSe/ZnS Core-Shell Quantum Dots	229
Acknowledgments	231
References	232

PART I

Detection of RAP-1 Antigenic Protein in
Infected *Babesia bovis* Erythrocytes Using QDs
as Fluorescent Reagents

The author had contributed fully in this section, namely in the planning of the experimental work and performance of the experiments.

Abstract

Babesia bovis is an intraerythrocytic protozoan parasite transmitted by Ixodid ticks and responsible for great economic losses in cattle industry in many tropical and subtropical regions worldwide. Over the years many different methods have been applied to identify early infections in whole blood of the animals, in particular immunofluorescence antibody test (IFAT). However, one of the significant limitations presented by this method is photobleaching and the loss of antibody activity caused by this phenomenon. In order to overcome this issue, the use of quantum dots conjugated with anti-RAP 1 antibody was proposed for the detection of its rhoptry associated antigenic protein (RAP-1) present in the apical complex of *B. bovis* parasites in infected blood. Different strains of *B. bovis* were incubated with the bioconjugated samples under three distinct experimental conditions: slide, solution and slide with vortex stirring. All the attempts demonstrated good conditions for the recognition of the antigenic protein in the infected RBCs, however the best results obtained were in the assay performed on a slide with vortex stirring. Only 16ng/ μ L of primary antibody linked to QDs were needed and the aggregation of the QD-Ab conjugates is much better controlled. Comparing this alternative immunofluorescence assay based on direct immunofluorescence principles with the traditional IFAT using FITC conjugated with secondary antibodies, the QD-Ab complexes developed in this work appear to be more resistant to large periods of excitation at different wavelengths in imaging assays. Moreover, these complexes were also demonstrated to be potential tools in the development of an immunosensor to detect early infections caused by *B. bovis* in whole blood of the animals.

Key-words: *Quantum dots, Bioconjugation, Antibodies, Immunofluorescence Assay, Babesia bovis.*

Introduction

Malaria, caused by various plasmodial species, is a disease that affects 350-500 million of people each year and is a leading killer globally^[1]. This disease is caused by the intraerythrocytic apicomplexan parasite of the genus *Plasmodia* which infects its host via the bite of a female *Anopheles*

mosquito^[2]. Similarly, Babesiosis is a parasitic infection caused by haemotropic protozoa of the genus *Babesia*, family Babesiidae, order Piroplasmida, within the phylum Apicomplexa and is transmitted by the bite of an infected tick. This malaria-like protozoan has infected the erythrocytes of a wide variety of wild and domestic animals. It is a well-recognized disease of veterinary importance in cattle, horses and dogs. Over the years, this disease has gained increasing attention as an emerging zoonotic problem due to the great economic losses in cattle industry in many tropical and subtropical regions worldwide^[3, 4].

There are over 100 species within the genus *Babesia* and this species vary in relative size from large to small members^[3]. The distribution of all the different *Babesia* species is dependent on the geographical distribution of the competent tick vectors. Moreover, several tick species have been described as *Babesia* competent vectors: *Boophilus* and *Haemaphysalis* species ticks transmit the disease mainly in the tropics, and *Rhipicephalus*, *Ixodid* and *Hyalomma* species ticks transmit the disease mainly in temperate countries^[5, 6]. In addition, the ubiquitous parasites generally have two classes of hosts, an invertebrate and vertebrate host and the maintenance of *Babesia* spp. is dependent on both hosts. *Babesia* infections have long been recognized as an important disease from the economically point of view for cattle. Among others isolated, six species appear to be responsible for bovine babesiosis particularly *Babesia bovis* and *Babesia bigemina*. Generally, babesiosis is characterized by different symptoms namely fever, extensive erythrocytic lysis leading to anemia, icterus, hemoglobinuria and death^[3].

The life cycle of *Babesia* parasites is highly complex and can be separated into three principal stages: gamogony, sporogony and merogony. After a bite from an infected tick, unlike *Plasmodium* parasites, which require hepatocyte invasion and multiplication prior to the erythrocyte stage, the sporozoites of *Babesia*, can directly invade the host erythrocytes, also called red blood cells (RBC) and undergo an asexual growth cycle in the erythrocyte stage as demonstrated in Figure 29^[3, 7]. *Babesia* sporozoites are injected into the host together with the saliva of the vector tick and directly infect the RBCs. The sporozoites, once established inside the erythrocyte of the host divide into two (sometimes four) merozoites. These in turn, follow an asexual reproduction

also called merogony. Rapid intracellular multiplication leads to a destruction of the host RBC with release of new parasites and subsequent infection and lysis of other erythrocytes ^[3]. However, the molecular interactions between *Babesia* merozoites and host RBC and their biological roles are not thoroughly understood ^[7].

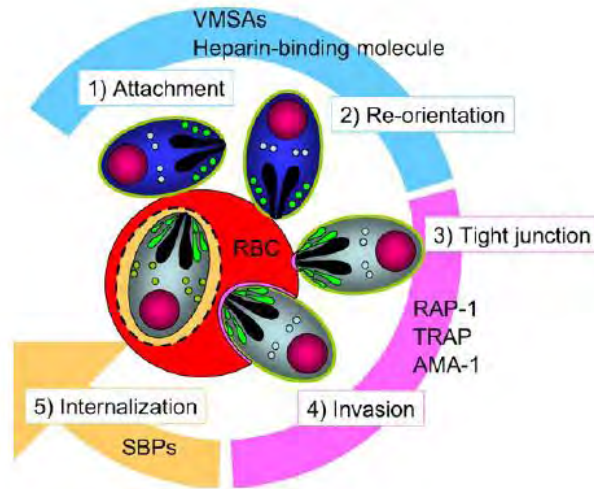


Figure 29 | Erythrocyte Invasion by *Babesia* Parasites. Schematic representation of erythrocyte invasion process of *Babesia* parasites. The erythrocyte invasion is mainly composed by five steps: (1) attachment of the parasite onto the host RBC; (2) re-orientation of the parasite; (3) formation of tight-junction between the apical part of parasite and erythrocyte surface; (4) invasion and (5) internalization of the parasite within the infected RBC. Reprinted from reference [7]. Copyright 2006, with permission from Elsevier.

Apicomplexans utilize several molecules (ligands) in their invasion process. The process of erythrocyte invasion by *Babesia* parasites is not well understood in detail, but is considered similar to other apicomplexan parasites namely *Plasmodium* or *Toxoplasma*, that have numerous proteins on the parasite surface and within the apical secretory organelles which mediate the complex multi-step invasion process ^[8]. As for malaria parasites, in the first step of erythrocyte invasion, the *Babesia* parasites use their surface molecules, coating the extracellular merozoites, to promote the attachment to RBC. For *B. bovis* a number of proteins involved in this process have been identified and grouped as surface-coating molecules, rhoptry and microneme proteins and components of the spherical body, as illustrated in Figure 30.

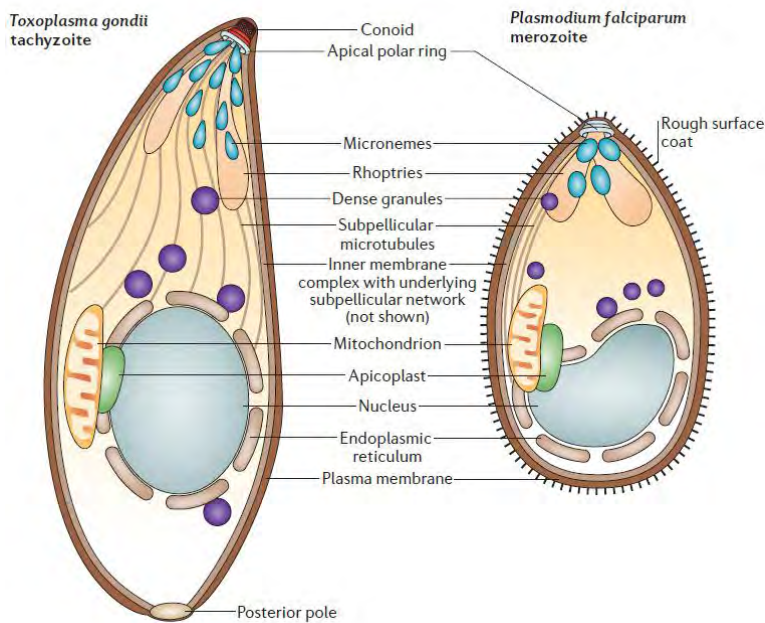


Figure 30 | Apicomplexan main features for *Toxoplasma gondii* tachyzoite and *Plasmodium falciparum* merozoite. Schematic representation of the different proteins and apical organelles involved in the multi-step erythrocyte invasion by *Plasmodium* (right side) and *Toxoplasma* (left side) parasites. Reprinted by permission from Macmillan Publishers Ltd: Nature Reviews Microbiology [9], copyright 2006.

The parasites of *B. bovis* species are known to possess at least five glycoproteins on their surface and these surface molecules belong to a family of variable merozoite surface antigens (VMSA) which is mainly composed of the antigen 1 (MSA-1; 42kDa) and antigen 2 (MSA-2; 44kDa). The antigen 2 could be organized in four genes (MSA2a₁, MSA2a₂, MSA-2b and MSA-2c) which are defined by an amino-terminal hydrophobic signal sequence, a hydrophobic central region and a conserved carboxy-terminal region containing a glycosyl-phosphatidylinositol (GPI) anchor signal sequence^[7]. Essentially, the known function of these antigens is mediate the initial attachment of the merozoite to host RBCs and facilitate the invasion in the same erythrocytes respectively^[8].

As already mentioned, from their first attachment to their complete internalization during the invasion process, apicomplexan parasites secrete proteins from their apical organelles onto the merozoite membrane or into the environment outside the parasites. For *Babesia* parasites in general, these

proteins are located in the anterior end of the parasites also called apical complex and comprises the rhoptries and micronemes proteins and spherical body ^[7].

The rhoptries proteins are long, club-shaped organelles connected by thin necks to the extreme apical pole of the parasite, and their number varies according to species. These proteins are synthesized in the endoplasmatic reticulum and passed through the Golgi complex ^[10]. In *B. bovis*, the rhoptry-associated protein-1 (RAP-1) is a 60kDa protein (full-length) that was first identified by Suarez *et al* ^[11] and is localized on the apical surface and within the rhoptries merozoites. This protein is encoded by two near identical, *rap-1a* genes; it consists of a unique N-terminal (NT) region of 316 aminoacids and a C-terminal (CT) region that contains seven tandem repeats of a degenerate 23-aminoacid sequence ^[12, 13]. Moreover, is highly conserved among diverse isolates and like MSA-1 this protein is postulated to be involved in the merozoite attachment but also in the invasion of host RBCs ^[8, 14].

Micronemes are small, cigar-shaped organelles that cluster at the apical end of the protozoan body and their number varies according to the species but also with developmental stages. They are synthesized with an N-terminal signal sequence that mediates their entrance into the secretory pathway by translocation across the endoplasmatic reticulum membrane ^[10]. Two invasion molecules are considered micronemes products in *B. bovis* merozoites. One is an apical membrane antigen 1 (AMA-1) and the other is a thrombospondin-related anonymous protein (TRAP) which are designated as BbAMA-1 and BbTRAP in *B. bovis* specie with 82 and 75kDa respectively. The BbAMA-1 is predicted to be involved in RBC invasion, while BbTRAP is involved in recognition and possible attachment and invasion of host erythrocytes ^[7, 8].

After the intracellular internalization of protozoan parasites in the host cell environment, some proteins are released into the cytoplasm of the infected RBCs in order to promote an optimal environment for the parasites. In general these proteins are called dense granules, however in the genus *Babesia*, instead of a dense granule there is a unique organelle designed spherical body. In *B. bovis*, three spherical body proteins were identified: SBP-1 (80kDa), SBP-2 (225kDa) and SBP-3 (135kDa). Their main function is

associated with the RBC membrane during the course of erythrocyte infection [7, 8].

Babesia bovis specie was first identified in Argentina in 1934 by Rees *et al* [15]. It is a widespread specie in cattle and occurs wherever tick vector *Rhipicephalus (Boophilus) microplus* is encountered which includes North and South America, Southern Europe, Africa, Asia, Australia and also in some parts of Europe where *Boophilus* does not occur, suggesting the existence of other vectors [3]. The RBC invasion is very similar to that for *B. bigemina* in which the parasite invades, grows and replicates asexually in erythrocytes of their vertebrate host causing fever, anaemia and haemoglobinuria as mutual symptoms. However, *B. bovis* infection can be distinguished from *bigemina* specie because of the additional accumulation of parasitized RBCs in the microvasculature and the consequent development of severe clinical complications, such as cerebral Babesiosis, respiratory distress and multi-organ failure [8]. For this reason, *B. bovis* is generally considered the more virulent of the two organisms [3].

Over the years, many efforts have been made in the study and control of these diseases and several diagnostic methods have been developed to identify early infections of *B. bovis* in whole blood. So far, the microscopic examination of giemsa stained blood smears is still considered the universal method of choice since it is rapid and inexpensive [4, 16]. But gradually this diagnostic method has been enhanced and replaced by molecular biological methods like immunofluorescence antibody test (IFAT)^[17], enzyme-linked immunosorbent assay (ELISA)^[16], polymerase chain reaction (PCR)^[18] and reverse line blotting (RLB)^[19] in order to increase sensitivity and specificity. Flow cytometry has also been used for this purpose^[20].

Using the luminescent quantum dots conjugated with monoclonal antibody anti-RAP 1 described previously in chapter 4, attempts to use these bionanoprobes for the detection of the rhoptry-associated protein 1 (RAP-1) based on immunofluorescence assays principles in *B. bovis* infected RBCs were made. In this study different attempts to achieve the best experimental conditions for the visualisation of the infected erythrocytes were made.

Experimental Section

Materials

Carboxy-QDs conjugated with monoclonal antibody against recombinant (r) RAP-1 protein of *Babesia bovis* (anti-rRAP-1 *B. bovis* antibody) were obtained as described in chapter 4 using the EDC/NHS chemistry. All the chemical and biochemical reagents were analytical grade and the best grade available respectively and purchased from Sigma-Aldrich unless indicated otherwise. Fluorescein isothiocyanate-conjugated (FITC) anti-mouse IgG produced in sheep was also obtained from Sigma-Aldrich and used as secondary antibody. ImmunoPen™ was purchased from Calbiochem and the glass slides from Roth. All the biological samples were handled in a laminar flow chamber NU-425-400E from NuAIRE and when centrifugation was needed a Biofuge 28RS Heraeus centrifuge from SEPATECH was used.

All the slide preparations were visualised under fluorescence microscopy using an inverted epifluorescence microscope (Nikon TE2000-S) coupled to an Evolution™ MP 5.1 colour video camera. Captured digital images were processed through the image analysis software Image-Pro Plus 7.0 (Media Cybernetics).

Babesia bovis infected cultures

The bovine erythrocyte culture infected with the parasite *B. bovis* Mexican strain (Mo7) was available as well as bovine blood smears infected with S2P strain from Argentina. The Mo7 biological clone of *Babesia bovis*, derived by limiting dilution of the Mexico strain as described elsewhere^[21, 22], was kindly provided by Dr. Erik de Vries from the Department of Infectious Diseases and Immunology, Utrecht University, The Netherlands. Stocks of *B. bovis* Mo7 cultures were cryopreserved and kept in liquid nitrogen containing 1-7% of parasitized erythrocytes. The bovine blood smears infected with *B. bovis* argentine strain S2P, were supplied by Dr Ignacio Etchaide from Estación Experimental Agropecuaria Rafaela, Instituto Nacional de Tecnología Agropecuaria, Santa Fe, Argentina. The infected smears were kept in the dark in a -80°C chamber.

Immunofluorescence Assays for RAP-1 Antigenic Protein Detection in *B. bovis* Infected RBCs

For immunofluorescence assays with QD-Ab conjugates, three different experimental conditions were attempted: on slide and on slide with vortex stirring using the infected bovine blood smears from Argentina and finally in solution. For the latter the cryopreserved infected Mo7 cultures were used. These assays were accomplished with the standard immunofluorescence assay also on slide and in solution using the same infected cultures. The experimental procedures for the different assays tested were carried out as described below.

Standard Immunofluorescence Assays

Assay on Slide: Two thin films of erythrocytes infected with *B. bovis* S2P argentine strain previously kept at -80°C were brought to room temperature, by incubating them in a 37°C chamber for 40 minutes. One of the slides was stained for 15 minutes by dipping the smear in a Coplin jar containing fresh working Giemsa stain ^[23] (2.5% v/v). The slide was then rinsed carefully and thoroughly with running tap water and left in upright position to dry. About 10 minutes later, the stained slide was visualized under a microscope to observe the presence of the parasite in the infected erythrocytes. The second thin film was divided into 10 wells using the water repelling pen (immunopen). Different dilutions of anti-rRAP-1 *B. bovis* antibody (1:25, 1:50, 1:100 and 1:200) were prepared in blocking buffer (1% BSA in PBS 1x, pH 7.2). 30µL of each dilution were dispensed in the wells and incubated for 30 minutes at 37°C in a humidified chamber. The drops of primary antibody in each well were aspirated with a pipette and the erythrocytes were then washed *in situ* twice with 30µL of PBS-T rinse buffer (PBS 1x containing 0.05% Tween® 20) for 5 minutes. Subsequently, the smear was incubated for 30 minutes at 37°C with FITC-anti-mouse IgG sheep secondary antibody diluted 1:100 and 1:200 in blocking buffer, in a humidified chamber. The erythrocytes were again washed twice *in situ* with 30µL of PBS-T and dried with filter paper for 10 minutes. As a negative control 30µL of PBS 1x and 30µL of secondary antibody in a 1:200 dilution was used. The slides were mounted with 20µL of mounting media containing glycerol/rinse buffer (1:1, v/v) and 1µL of a 1mg/mL DAPI solution

and covered with a cover glass. The preparations were left to dry during 10 minutes and the borders of the cover glass were sealed with nail polish. The result was documented by microscopic images acquired on an inverted epifluorescence microscope (Nikon T2000) coupled to a colour video camera Evolution MP with a 100x objective and the appropriate filters (UV and blue).

Assay in Solution: Liquid nitrogen cryopreserved Mo7 infected erythrocytes cultures were brought to room temperature by placing them in a water-bath at 37°C for 5 minutes. To wash the erythrocytes, the cultures were fractionated in a laminar flow chamber and transferred to separate 15mL polypropylene centrifuge tubes containing 10mL of PBS 1x. The tubes were centrifuged at 2000g for 10 minutes at 4°C. This wash procedure was repeated twice and the supernatant discarded each time. Subsequently, the lysis of the infected erythrocyte pellet was performed by adding 600µL of 0.4% (w/v) NaCl solution to each tube and incubating them for 20 minutes at room temperature. During the incubation time, the tubes were inverted 4 to 5 times. The tubes were then centrifuged at 3000g during 30 minutes at 4°C. The supernatant was removed, while the small pellets with a gel consistency remained in the tubes. Each final pellet was diluted in 100µL of blocking buffer. Two separate thin films containing 5µL of each erythrocytes culture were air-dried and fixed at room temperature for 10 minutes. Each erythrocyte smear was stained with fresh working Giemsa (2.5% v/v) stain to check aggregation and the number of parasites. Simultaneously, the immunofluorescence assay in solution was performed. 20µL of each culture pellet were placed in separate microtubes. 0.2µL of anti-rRAP-1 *B. bovis* antibody (1:100 dilution) was then added to each microtube and incubated with slow vortex stirring for 30 minutes at 37°C. Subsequently, without any wash, 0.2µL of FITC-anti-mouse IgG sheep secondary antibody (1:100 dilution) was added to each tube followed by an incubation with slow vortex stirring for 30 minutes at 37°C. Later, 2µL of each final sample were used to smear two thin films. The drop on each slide was air-dried and fixed at room temperature for 10 minutes. The slides were mounted with 5µL of mounting media containing glycerol/rinse buffer (1:1, v/v) and 1µL of a 1mg/mL DAPI solution and covered with a cover glass. The preparations were left to dry during 10 minutes with the borders sealed with

nail polish. All the images were acquired on an inverted epifluorescence microscope Nikon T200 coupled to a colour video camera Evolution MP with a 100x objective and the appropriate filters (UV and blue).

Direct Immunofluorescence Assays Using QD-Ab Conjugates

Assay on Slide: Two thin films of erythrocytes infected with *B. bovis* Argentine strain S2P previously kept at -80°C were brought to room temperature, by incubating them in a 37°C chamber for 40 minutes. One of the slides was stained for 15 minutes by dipping the smear in a Coplin jar containing fresh working Giemsa stain (2.5% v/v). The slide was then rinsed carefully under a running tap water and left in an upright position to dry. About 10 minutes later the stained slide was visualized under microscopy to observe the presence of the parasite in the infected erythrocytes. Simultaneously, the second thin film was divided into 8 wells using the water repelling pen (immunopen). Different concentrations of anti-rRAP-1 *B. bovis* antibody conjugated with DHLA-QDs (33ng/μL, 66ng/μL and 133ng/μL) were prepared in blocking buffer. 30μL of each QD-Ab concentration was dispensed in the wells and incubated overnight at 4°C in a humidified chamber. As a negative controls PBS 1x, 100nM and 200nM of natural DHLA-QDs were used. The drops of QD-Ab conjugates in each well and the corresponding controls were aspirated with a pipette and the erythrocytes also present in each well were then washed *in situ* twice with 30μL of PBS-T rinse buffer for 5 minutes and dried with filter paper for 10 minutes. The slide was mounted with 20μL of mounting media containing glycerol/rinse buffer (1:1, v/v) and 1μL of a 1mg/mL DAPI solution and covered with a cover glass. The preparation was left to dry during 10 minutes with the borders of the cover glass sealed with nail polish. The images were acquired on an inverted epifluorescence microscope Nikon T2000 coupled to a colour video camera Evolution MP with a 100x objective and the appropriate filters (UV and blue filter).

Assay in Solution: Using the same erythrocyte lysate from Mo7 culture prepared previously for the standard immunofluorescence assay in solution, three separate microtubes were prepared containing 10μL of such pellet. Then, different concentrations of anti-rRAP-1 *B. bovis* antibody conjugated

with DHLA-QDs, as described in chapter 4 (33ng/ μ L, 66ng/ μ L and 100ng/ μ L), were separately added to each microtube and incubated with slow vortex stirring for 1h at room temperature. In parallel, negative controls were also performed using the same pellet but incubating them under stirring with 100nM of DHLA-QDs, 50nM and 100nM of DHLA-QDs blocked with ethanolamine. Later, 2 μ L of each final sample as well as the respective controls were used to smear thin films. The smear on each slide was air-dried and fixed at room temperature for 10 minutes. The slides were mounted with 5 μ L of mounting media containing glycerol/rinse buffer (1:1, v/v) and 1 μ L of a 1mg/mL DAPI solution and covered with a cover glass. The preparations were left to dry during 10 minutes and the edges of the cover glass were sealed with nail polish. All the images were acquired on an inverted epifluorescence microscope NikonT2000 coupled to a colour video camera Evolution MP with a 100x objective and the appropriate filters (UV and blue).

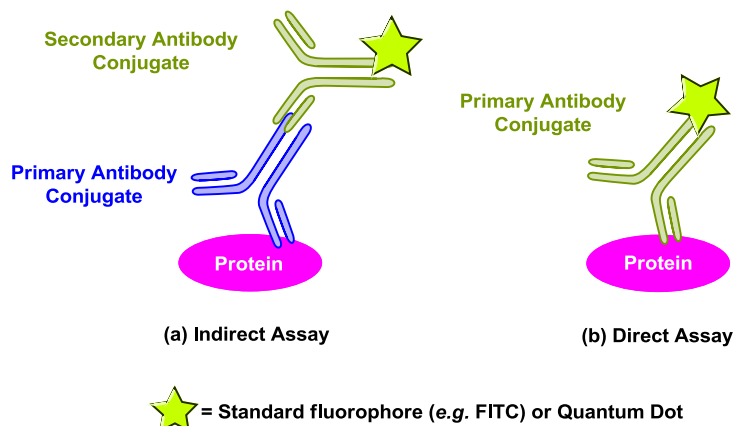
Assay on Slide with Vortex Stirring: One of the smears containing erythrocytes infected with *B. bovis* S2P argentine strain previously kept at -80°C were heated in a 37°C chamber for 40 minutes. The thin film was divided into 6 wells using the water repelling pen (immunopen). Two concentrations of anti-rRAP-1 *B. bovis* antibody conjugated with DHLA-QDs (16ng/ μ L and 100ng/ μ L) were prepared in blocking buffer. 30 μ L of each QD-Ab concentration was dispensed in the wells and incubated for 1 hour at room temperature maintaining the slide under vortex stirring in order to obtain a good homogenization and dispersion of the sample into each well. As a negative control, was used 30 μ L of PBS 1x and 50nM of DHLA-QDs blocked with ethanolamine. The drops of QD-Ab conjugates as well as the controls in each well, were aspirated with a pipette. The erythrocytes present in each well were then washed *in situ* twice with 30 μ L of PBS-T rinse buffer for 5 minutes also under vortex stirring and dried with filter paper for 10 minutes. The slide was mounted with 20 μ L of mounting media containing glycerol/rinse buffer (1:1, v/v) and 1 μ L of a 1mg/mL DAPI solution and covered with a cover glass. The preparation was left to dry during 10 minutes and the edges were sealed with nail polish. The images were acquired on an inverted epifluorescence

microscope NikonT2000 coupled to a colour video camera Evolution MP with a 100x objective having the appropriate filters (UV and blue).

Results and Discussion

As described previously, Babesiosis is an arthropod-borne disease of animals that is transmitted by *Ixodid* ticks. The most severe cases of Babesiosis are caused by *Babesia bovis*, an intraerythrocytic, apicomplexan protozoan. Apicomplexans use several molecules/ligands in their RBCs invasion process and among others *B. bovis* antigens characterized, the rhoptry associated protein (RAP-1) has been the most studied and is considered a strong candidate for vaccine development ^[7, 13]. To identify early infections a variety of methods are known and used for the detection of *B. bovis* invasion in whole blood (detecting the presence of antibodies against the parasite), however the indirect immunofluorescence antibody test (IFAT) is one of the most commonly used for this purpose and have been used for decades in diagnostic laboratories around the world. Moreover, it is considered to be a reference for the detection of antibodies against this *Babesia* specie ^[24].

Secondary or indirect immunofluorescence uses two antibodies. The unlabelled primary antibody specifically binds the target molecule while the secondary antibody (usually an anti-IgG), which carries a fluorophore, recognises the primary antibody and binds to it (Scheme 23, (a)). This technique allows more flexibility when comparing with the primary or direct immunofluorescence, because a variety of different secondary antibodies and detection techniques can be used for a given primary antibody. However, the number of steps and time consuming protocol represent a drawback. Direct immunofluorescence testing is where a single antibody chemically linked to a fluorophore binds to the target molecule and the fluorophore it bears can be detected by fluorescence microscopy (Scheme 23, (b)).



Scheme 23 | Schematic representation of direct and indirect immunofluorescence assay.

DHLA-QDs conjugated with anti-RAP1 antibody were tested as an alternative to antibodies carrying normal dyes to detect the presence of RAP-1 antigenic protein in *Babesia bovis* Argentine S2P and Mexico Mo7 strain infected erythrocytes. These cultures samples were incubated with the anti-RAP 1-QD conjugates under three different experimental conditions; slide, solution and on slide with vortex stirring as described in detail in the Experimental Section. Alongside, these experiments were accomplished with the common IFAT using anti-RAP1 and FITC anti-mouse IgG produced in sheep as primary and secondary antibodies respectively and which worked as a positive control. It is important to point out that all the preparations were mounted with mounting media containing 1 μ L of a 4', 6-diamidino-2-phenylindole dihydrochloride (DAPI) solution to easily identify the parasites. This reagent has the ability to bind to the A-T regions of parasites DNA forming a compound that is fluorescent under UV light. All preparations were microscopically observed and the results obtained for each assay are summarized in Figure 31, Figure 32 and Figure 33.

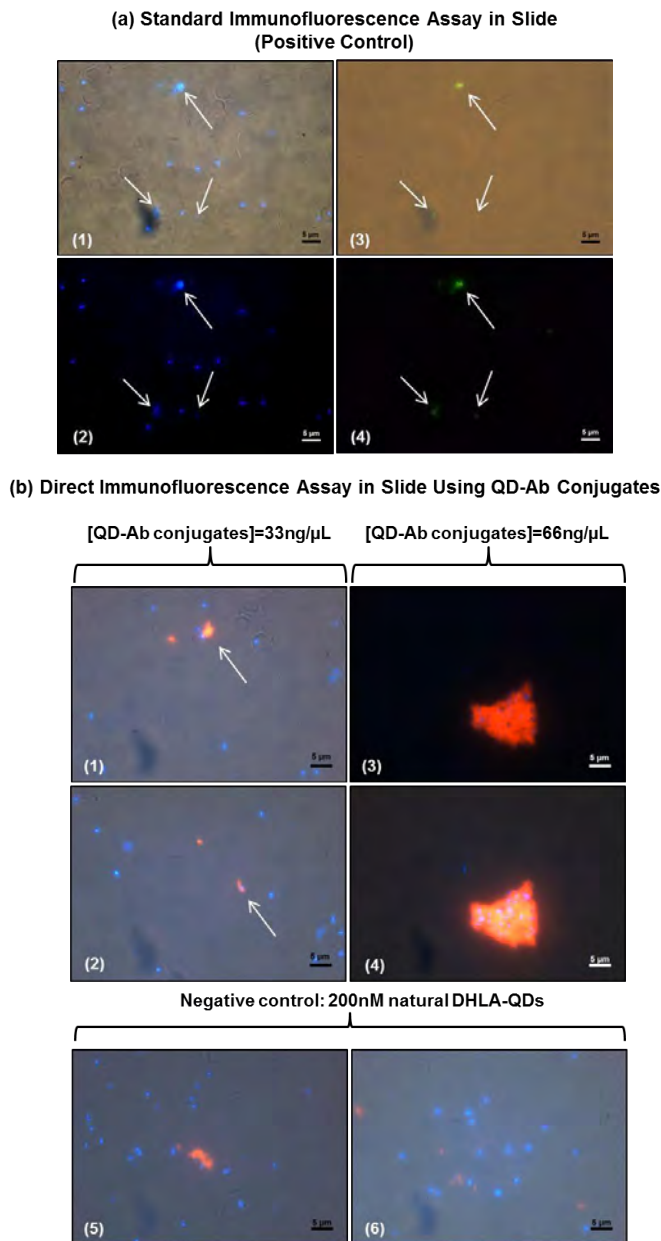


Figure 31 | Immunofluorescence Assays on Slide. (a) Visualisation of native RAP-1 protein by IFAT using primary and secondary antibodies in a 1:200 and 1:100 dilutions respectively using blood smears infected with Argentine S2P *B. bovis* strain. (b) Visualisation of the same protein in the same blood smears using 33 (images 1 and 2) and 66 (images 3 and 4) ng/μL of primary antibody anti-RAP1 conjugated with DHLA-QDs. In the assay using QD-Ab conjugates as negative controls 200nM of natural DHLA-QDs was used to incubate with the infected smears. The images were observed with 100x amplification under UV (UV-2A; λ_{exc} =330-380nm) and blue (B-2A; λ_{exc} =450-490nm) filters and bright field. Scale bar=5μm.

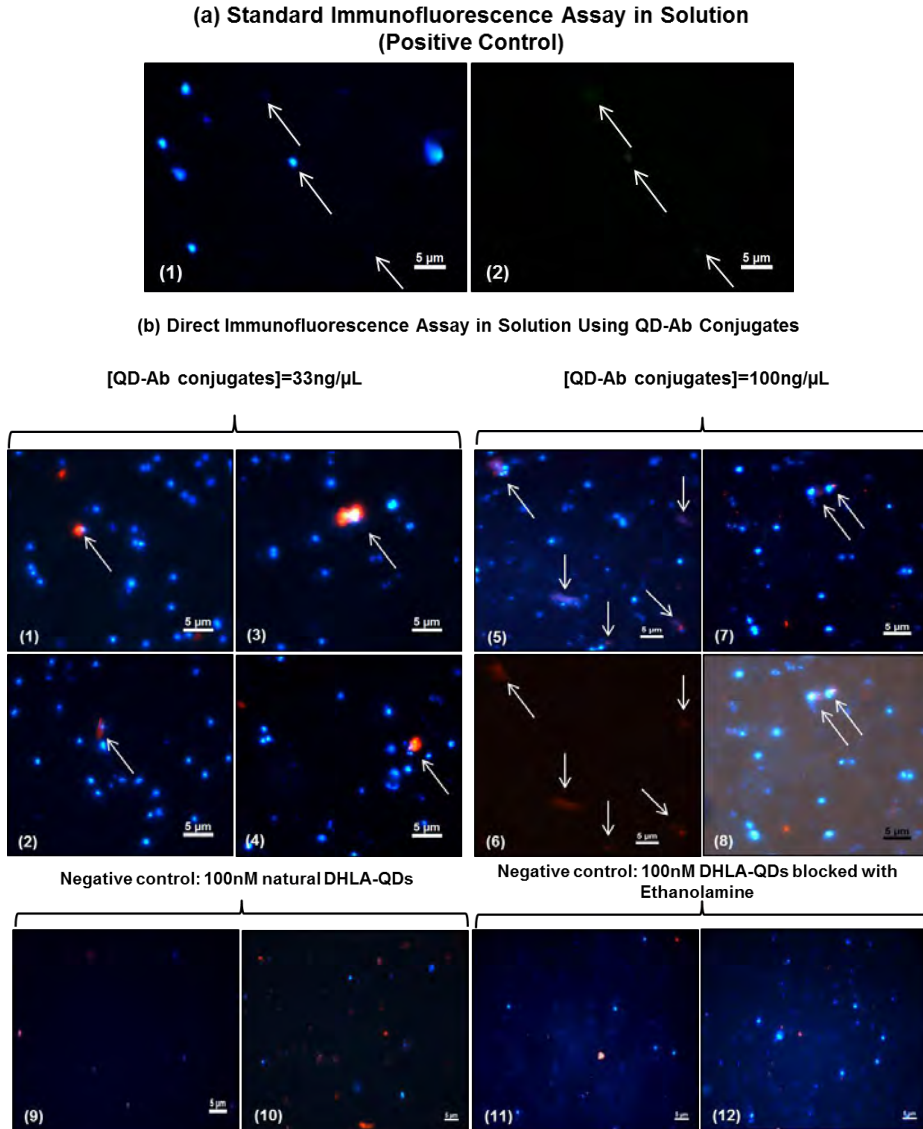


Figure 32 | Immunofluorescence Assays in Solution. (a) Visualisation of native RAP-1 protein by IFAT using primary and secondary antibodies in a 1:100 dilution in erythrocytes infected with Mo7 *B. bovis* strain. (b) Visualisation of the same protein in the same infected erythrocytes using 33 (images 1-4) and 100 (images 5-8) ng/μL of primary antibody anti-RAP1 conjugated with DHLA-QDs. In the assay using QD-Ab conjugates as negative controls 100nM of natural DHLA-QDs (images 9 and 10) and 100nM of DHLA-QDs blocked with ethanolamine (images 11 and 12) were used. The images were observed with 100x amplification under UV (UV-2A; $\lambda_{exc}=330-380\text{nm}$) and blue (B-2A; $\lambda_{exc}=450-490\text{nm}$) filters and bright field. Scale bar=5μm.

**Direct Immunofluorescence Assay in Slide with Vortex Stirring Using
QD-Ab Conjugates**

[QD-Ab conjugates]=16ng/ μ L

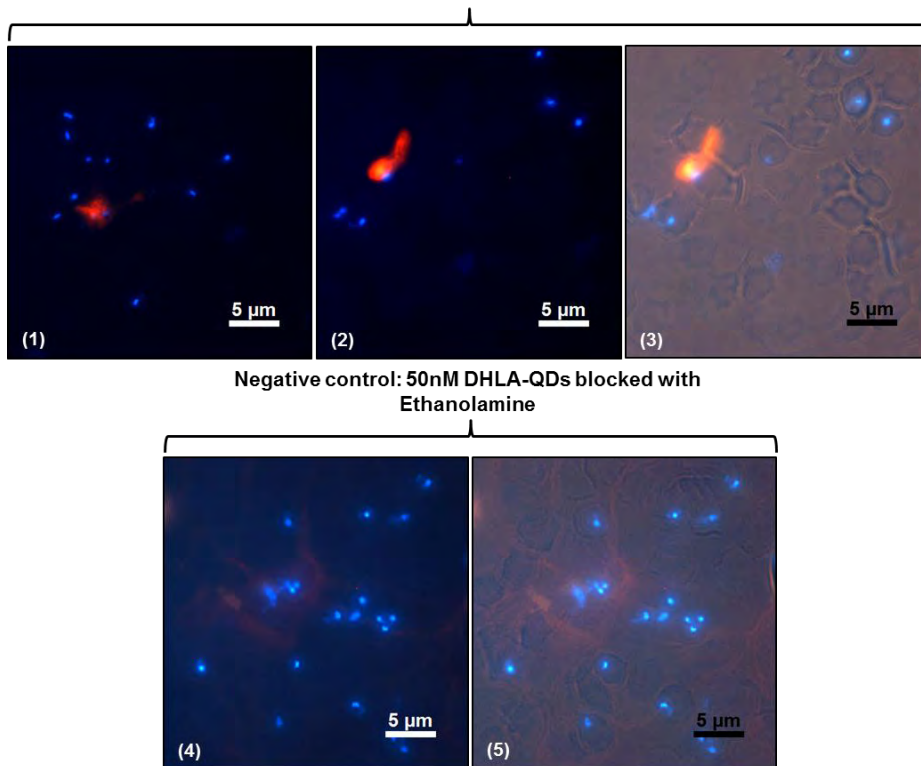


Figure 33 | Immunofluorescence Assays on Slide with Vortex Stirring. Visualisation of native RAP-1 in blood smears infected with Argentine S2P *B. bovis* strain using 16ng/ μ L (images 1-3) of primary antibody anti-RAP1 conjugated with DHLA-QDs. In this assay using QD-Ab conjugates, as negative controls 50nM of DHLA-QDs blocked with ethanolamine was used (images 4 and 5). The images were observed with 100x amplification under UV (UV-2A; λ_{exc} =330-380nm) and blue (B-2A; λ_{exc} =450-490nm) filters and bright field. Scale bar=5 μ m.

Figure 31 shows the immunofluorescence assays performed on slide using the blood smears infected with Argentine S2P *B. bovis* strain. Firstly it is possible to identify the presence of parasites seen as fluorescent blue spots and clearly in both standard (method a, images 1-4) and direct (method b, images 1-4) methods the anti-RAP 1 antibody recognizes the antigen RAP-1 in *Babesia bovis* infected erythrocytes. However, in direct immunofluorescence assay using 66ng/ μ L of anti-RAP 1 antibody conjugated with QDs (images 3 and 4), an excessive aggregation of quantum dots is also displayed. Moreover, in the negative controls using 200nM of carboxy-QDs

(DHLA-QDs) (images 5 and 6) it is possible to visualise some specificity by these nanoparticles towards the antigenic protein. Regarding these preliminary results, the aggregation may be due to the fact that the assay was performed on slide in a static way i.e. without any homogenization of the bioconjugated sample during the incubation time, thus leading to the formation of large aggregates. On the other hand, the binding demonstrated by carboxy-QDs relatively to antigenic protein may be related to what was discussed previously in chapter 4 in the western blotting analysis performed to evaluate the QD-Ab conjugates capacity to recognize their antigen. It is known that proteins in general are composed of polymerized amino acids through the formation of amide bonds and each amino acid have an amino group, a carboxylic acid group and a unique side chain structure which normally does not participate in polypeptide formation but is free to interact and react with the environment/other molecules^[25]. Moreover, at physiological pH the amines are protonated and bear a positive charge while carboxylic acid groups are negatively charged. Knowing that this assay was performed using buffers with pH close to physiological pH, it is easy to predict that the amine groups present in RAP-1 antigenic protein immobilized on the slide can interact with the carboxylate groups present in natural DHLA-QDs (COOH-QDs) carrying a negative charge.

In order to address these issues, immunofluorescence assays in solution using the erythrocytes infected with Mo7 *B. bovis* strain were carried out. The same concentrations of primary antibody linked to quantum dots tested in the slide assay were also incubated with erythrocyte lysates containing *B. bovis* parasites. To avoid the prior specificity demonstrated by the carboxylic acid groups on the surface of natural DHLA-QDs relatively to RAP-1 protein, an additional negative control was added using 100nM of DHLA-QDs inertized/blocked with ethanolamine. This control appeared to be the most appropriate, since as earlier described in chapter 4 for the bioconjugation protocol (Scheme 19, step 3), the remaining activated carboxylic acid groups present on the surface of the nanoparticles were blocked with ethanolamine to avoid the possibility of such COOH groups posteriorly interacting with NH₂ groups present in other biomolecules.

Figure 32 displays the results obtained for this assay. Once again it was easy to visualise that for *Babesia bovis* infected cultures, the anti-RAP 1 antibody linked to DHLA-QDs recognizes the antigen present in parasites (method b, images 1-8). Moreover, in this assay it was also possible to observe a reduction in the aggregates formation even for a concentration of 100ng/ μ L of primary antibody linked to QDs (method b, images 5-8). At the same time, a decrease in the recognition by the non-conjugated nanoparticles of antigenic protein when DHLA-QDs blocked with ethanolamine were used in a negative control (images 11 and 12) was also observed. Contrary, this recognition still remains when non-blocked DHLA-QDs are used (images 9 and 10). Based on these results, it was observed that the replacement of a static assay (slide assay) by the assay in solution with stirring led to a better distribution of the bioconjugated sample during the incubation with the infected erythrocytes and consequently a reduction in the aggregates formation.

Taking advantage of these results, a third assay was carried out turning to use the blood smears infected with *B. bovis* S2P strain but adding vortex stirring. Looking to Figure 33, it is noticeable that the primary antibody linked to QDs still recognizes their antigenic protein and a concentration of only 16ng/ μ L of this reagent is enough to perform this type of assay (images 1-3). In addition, it is possible to observe that DHLA QDs blocked with ethanolamine used as a negative control don't show any affinity for the parasites (images 4 and 5), since in the images they are very well distributed in the slide and never in direct contact with the blue spots.

In conclusion, it is important to point out that the indirect immunofluorescence assays which accomplished the direct immunofluorescence assay provided by the use of bioconjugated quantum dots, also showed a positive response for the detection of RAP-1 protein in infected erythrocytes, as expected. However, it is notorious that the green fluorescence emitted by the FITC fluorophore conjugated to the secondary antibody is much less intense than the orange fluorescence emitted by the bioconjugated QDs. This may be related to the poor photo-resistance demonstrated by the standard organic dyes when excited for long periods of time ^[25]. Hence, this led to the conclusion that the QDs are an useful tool for biosensing applications

because their unique photoluminescent properties and their high resistance to photo bleaching^[26].

Conclusion

After studying three different protocols, it was shown that the assay carried out on slide with vortex stirring produced the best results showing clearly that the anti-RAP 1 antibody linked to quantum dots recognizes their specific antigen (RAP-1) highly conserved in the parasites of different *Babesia bovis* strains. Only 16ng/μL of primary antibody linked to QDs were need to perform this type of assay. The optical properties of these nanoprobe, such as resistance to photobleaching, their ability to be excited for long periods of time at different wavelengths and the increased fluorescence when compared with the standard organic dyes conjugated with secondary antibodies was also demonstrated. This particular behaviour as well as these preliminary results led us to believe that CdSe/ZnS core-shell QDs, could be very useful for the development of an immunosensor for diagnosis of *B. bovis* infections in whole blood, however further studies should be performed in order to find the concentration required of primary antibody that should be linked to the quantum dots. In addition, the stability of the bioconjugated QDs should also be better controlled to avoid the aggregation phenomena of these conjugates during the performance of the immunofluorescence assay.

Glossary

Table 7 | Glossary of terms related with the topic addressed in this work^[8, 27].

Term	Definition
Apicomplexa	The Apicomplexa are a large group of protists, most of which possess a unique organelle called apicoplast and an apical complex structure involved in penetrating a host's cell. They are unicellular, spore-forming, and exclusively parasites of animals. Diseases caused by apicomplexan organisms include Babesiosis, Malaria, etc.
Dense granules	Specialised secretory organelles found

in apicomplexa parasites that contain a variety of proteins predominantly involved in modifying the host cell immediately following invasion.

Endoplasmatic reticulum (ER)

The endoplasmic reticulum (ER) is an organelle of cells in eukaryotic organisms that forms an interconnected network of tubules, vesicles, and cisternae. Rough endoplasmic reticula are involved in the synthesis of proteins and is also a membrane factory for the cell, while smooth endoplasmic reticula is involved in the synthesis of lipids, including oils, phospholipids and steroids, metabolism of carbohydrates, regulation of calcium concentration and detoxification of drugs and poisons. Sarcoplasmic reticula solely regulate calcium levels.

Haemoglobinuria

Is a condition in which the oxygen transport protein hemoglobin is found in abnormally high concentrations in the urine. The condition is often associated with hemolytic anemia, in which red blood cells (RBCs) are destroyed, thereby increasing levels of free plasma hemoglobin. The excess hemoglobin is filtered by the kidneys, which release it into the urine, giving urine a red color.

Merozoite

Is one of the organisms formed by multiple fission (schizogony) of a sporozoite within the body of the host.

Micronemes

Secretory organelles found in apicomplexa parasites that contain proteins involved with invasion of the parasite into the host cell.

Protozoa

Are a diverse group of unicellular eukaryotic organisms (whose cells contain complex structures enclosed with membranes). Many of them have the ability to move spontaneously and actively, consuming energy in the process.

Rhoptries

The largest of the apical organelles in

apicomplexa parasites. The contents of these club-shaped organelles are discharged during invasion and are believed to play a role in the formation of the parasitophorous vacuole in several parasites such as *Plasmodium* and *Toxoplasma*.

Spherical bodies

A distinct organelle found in *Babesia* and *Theileria*, considered analogous to dense granules found in other apicomplexa parasites. Up to four spherical bodies are found per *Babesia* merozoite. Proteins localised to these organelles are released after parasite invasion into the host cell but no function has yet been ascribed to any of these.

Sporozoites

Any of the minute undeveloped sporozoans produced by multiple fission of a zygote or spore, especially at the stage just before it infects a new host cell.

Vector

An organism, often an invertebrate arthropod that transmits a pathogen from reservoir to host.

Acknowledgments

The author gratefully acknowledge Dr. Erik de Vries, from the Department of Infectious Diseases and Immunology, Utrecht University, The Netherlands, who kindly provided *B. bovis* Mo7 clonal line and Dr. Ignacio Etchaide from Estación Experimental Agropecuaria Rafaela, Instituto Nacional de Tecnología Agropecuaria, Santa Fe, Argentine who provided the blood smears infected with *B. bovis* S2P strain. The fluorescence microscope handling carried out by Ana Raquel Santos is also appreciated as well as the help in the experimental protocols provided by Joana Campos. Ana Sofia Miguel is a recipient of a PhD fellowship from the Fundação para a Ciência e Tecnologia (FCT), Portugal (SFRH/BD/40303/2007). The work was supported by the national funded project NTec/SQA/0131/2007 from FCT.

References

1. Alkhalil, A.; Hill, D. A.; Desai, S. A., Babesia and plasmodia increase host erythrocyte permeability through distinct mechanisms. *Cell Microbiol* **2007**, 9, (4), 851-860.
2. Bernhardt, I.; Ellory, J. C., *Red cell membrane transport in health and disease*. Springer: **2003**.
3. Vial, H. J.; Gorenflot, A., Chemotherapy against babesiosis. *Vet Parasitol* **2006**, 138, (1-2), 147-160.
4. Kuttel, C.; Nascimento, E.; Demierre, N.; Silva, T.; Braschler, T.; Renaud, P.; Oliva, A. G., Label-free detection of Babesia bovis infected red blood cells using impedance spectroscopy on a microfabricated flow cytometer. *Acta Trop* **2007**, 102, (1), 63-68.
5. Uilenberg, G., Babesia - A historical overview. *Vet Parasitol* **2006**, 138, (1-2), 3-10.
6. Wagner, G. G.; Holman, P.; Waghela, S., Babesiosis and heartwater: threats without boundaries. *Vet Clin N Am-Food A* **2002**, 18, (3), 417-430.
7. Yokoyama, N.; Okamura, M.; Igarashi, I., Erythrocyte invasion by Babesia parasites: Current advances in the elucidation of the molecular interactions between the protozoan ligands and host receptors in the invasion stage. *Vet Parasitol* **2006**, 138, (1-2), 22-32.
8. Gohil, S.; Kats, L. M.; Sturm, A.; Cooke, B. M., Recent insights into alteration of red blood cells by Babesia bovis: moovin' forward. *Trends Parasitol* **2010**, 26, (12), 591-599.
9. Baum, J.; Papenfuss, A. T.; Baum, B.; Speed, T. P.; Cowman, A. F., Regulation of apicomplexan actin-based motility. *Nat Rev Microbiol* **2006**, 4, (8), 621-628.
10. De Souza, W., Secretory organelles of pathogenic protozoa. *An Acad Bras Cienc* **2006**, 78, (2), 271-291.
11. Suarez, C. E.; Palmer, G. H.; Jasmer, D. P.; Hines, S. A.; Perryman, L. E.; McElwain, T. F., Characterization of the Gene Encoding a 60-Kilodalton Babesia-Bovis Merozoite Protein with Conserved and Surface Exposed Epitopes. *Mol Biochem Parasit* **1991**, 46, (1), 45-52.
12. Suarez, C. E.; Palmer, G. H.; Hotzel, I.; McElwain, T. F., Structure, sequence, and transcriptional analysis of the Babesia bovis rap-1 multigene locus. *Mol Biochem Parasit* **1998**, 93, (2), 215-224.
13. Santangelo, M. P.; McIntosh, D.; Bigi, F.; Armoa, G. R. G.; Campos, A. S. D.; Ruybal, P.; Dellagostin, O. A.; McFadden, J.; Mendum, T.; Gicquel, B.; Winter, N.; Farber, M.; Cataldi, A., Mycobacterium bovis BCG as a delivery system for the RAP-1 antigen from Babesia bovis. *Vaccine* **2007**, 25, (6), 1104-1113.
14. Mosqueda, J.; McElwain, T. F.; Stiller, D.; Palmer, G. H., Babesia bovis merozoite surface antigen 1 and rhoptry-associated protein 1 are expressed in sporozoites, and specific antibodies inhibit sporozoite attachment to erythrocytes. *Infect Immun* **2002**, 70, (3), 1599-1603.
15. Rees, C. W., Characteristics of the Piroplasms Babesia argentina and B. bigemina in the United States. *J Agric Res* **1934**, 48, 0427-0438.
16. Bose, R.; Jorgensen, W. K.; Dalgliesh, R. J.; Friedhoff, K. T.; Devos, A. J., Current State and Future-Trends in the Diagnosis of Babesiosis. *Vet Parasitol* **1995**, 57, (1-3), 61-74.

17. Homer, M. J.; Aguilar-Delfin, I.; Telford, S. R.; Krause, P. J.; Persing, D. H., Babesiosis. *Clin Microbiol Rev* **2000**, 13, (3), 451-469.
18. Costa-Junior, L. M.; Rabelo, E. M. L.; Martins-Filho, O. A.; Ribeiro, M. F. B., Comparison of different direct diagnostic methods to identify *Babesia bovis* and *Babesia bigemina* in animals vaccinated with live attenuated parasites. *Vet Parasitol* **2006**, 139, (1-3), 231-236.
19. Schnittger, L.; Yin, H.; Qi, B.; Gubbels, M. J.; Beyer, D.; Niemann, S.; Jongejan, F.; Ahmed, J. S., Simultaneous detection and differentiation of *Theileria* and *Babesia* parasites infecting small ruminants by reverse line blotting. *Parasitol Res* **2004**, 92, (3), 189-196.
20. Wyatt, C. R.; Goff, W.; Davis, W. C., A Flow Cytometric Method for Assessing Viability of Intraerythrocytic Hemoparasites. *J Immunol Methods* **1991**, 140, (1), 23-30.
21. Rodriguez, S. D.; Buening, G. M.; Green, T. J.; Carson, C. A., Cloning of *Babesia-Bovis* by Invitro Cultivation. *Infect Immun* **1983**, 42, (1), 15-18.
22. Hines, S. A.; Mcelwain, T. F.; Buening, G. M.; Palmer, G. H., Molecular Characterization of *Babesia-Bovis* Merozoite Surface-Proteins Bearing Epitopes Immunodominant in Protected Cattle. *Mol Biochem Parasit* **1989**, 37, (1), 1-10.
23. Concern, L. I. o. P. o. P. H. Diagnostic Procedures, Blood Specimens Staining. <http://www.dpd.cdc.gov/dpdx/html/DiagnosticProcedures.htm> (26/03/2012),
24. Araujo, F. R.; Madruga, C. R.; Leal, C. R. B.; Schenk, M. A. M.; Kessler, R. H.; Marques, A. P. C.; Lemaire, D. C., Comparison between enzyme-linked immunosorbent assay, indirect fluorescent antibody and rapid agglutination tests in detecting antibodies against *Babesia bovis*. *Vet Parasitol* **1998**, 74, (2-4), 101-108.
25. Hermanson, G. T., *Bioconjugate techniques*. Academic Press: **2008**.
26. Dabbousi, B. O.; RodriguezViejo, J.; Mikulec, F. V.; Heine, J. R.; Mattoussi, H.; Ober, R.; Jensen, K. F.; Bawendi, M. G., (CdSe)ZnS core-shell quantum dots: Synthesis and characterization of a size series of highly luminescent nanocrystallites. *J Phys Chem B* **1997**, 101, (46), 9463-9475.
27. *The American Heritage medical dictionary*. Houghton Mifflin Co.: Boston, **2007**.

PART II

Work Resulting From Collaboration with Other Research Groups

This section was based on the manuscripts below:

Ana R. Santos, **Ana S. Miguel**, Leonor Tomaz, Rui Malhó, Christopher Maycock, Maria C. Vaz Patto, Pedro Fevereiro and Abel Oliva. The impact of CdSe/ZnS Quantum Dots in cells of *Medicago sativa* in suspension culture. *Journal of Nanobiotechnology* 2010, 8:24.

Ana Raquel Santos*, **Ana Sofia Miguel***, Anca Macovei*, Christopher Maycock, Alma Balestrazzi, Abel Oliva and Pedro Fevereiro. CdSe/ZnS Quantum Dots trigger DNA repair and antioxidant enzyme systems in *Medicago sativa* cells in suspension culture. *Particle and Fibre Toxicology* 2012 (submitted).

*Authors contributed equally

Ana Raquel Santos, **Ana Sofia Miguel**, Pedro Fevereiro and Abel Oliva. Evaluation of Cytotoxicity of 3-Mercaptopropionic Acid-Modified Quantum Dots on *Medicago sativa* Cells and Tissues. *Nanoparticles in Biology and Medicine. Methods and Protocols*, 2012, Springer (book chapter by invitation).

E. György, A. Perez del Pino, J. Roqueta, B. Ballesteros, **A. S. Miguel**, C. D. Maycock, and A. G. Oliva. Synthesis and Laser Immobilization onto Solid Substrates of CdSe/ZnS Core-Shell Quantum Dots. *The Journal of Physical Chemistry C*, 2011, 115, 15210-15216.

The cytotoxicity studies resulted from collaboration between Organic Synthesis, Biomolecular Diagnostic and Plant Cell Biotechnology Laboratories at Instituto de Tecnologia Química e Biológica (ITQB-UNL), Oeiras, Portugal. The author of this thesis had partial contribution in this work namely synthesis, functionalization and characterization of quantum dots as well as the writing of this part of the manuscript.

The genotoxicity studies are resulting from collaboration between Organic Synthesis, Biomolecular Diagnostic and Plant Cell Biotechnology Laboratories at Instituto de Tecnologia Química e Biológica (ITQB-UNL), Oeiras, Portugal and Department of Genetics and Microbiology of Università di Pavia, Pavia, Italy. The author of this thesis participated equally in the performance of the experiments and in the writing of the first draft of the manuscript.

The studies of laser immobilization onto solid substrates of CdSe/ZnS core-shell quantum dots is a work resulting from collaboration between Organic Synthesis and Biomolecular Diagnostic Laboratories at Instituto de Tecnologia Química e Biológica (ITQB-UNL), Oeiras, Portugal and PLD & Nanoionics Laboratory at Centre d'Investigacion en Nanociencia i Nanotecnologia, Institut Catala de Nanotecnologia, Bellaterra, Spain. The author of this thesis had partial contribution in this work namely synthesis and characterization of quantum dots as well as the writing of this part of the manuscript

Introduction

Multiple scientific disciplines are combining to create new materials with enhanced properties. Technology has made immeasurable improvements to enable visualization, identification, and quantitation in biological systems. The integration of inorganic synthetic methods with a size reduction in Nanotechnology has led to the creation of the class of optical reporters, called quantum dots ^[1]. These nanometer-sized crystalline particles are composed of periodic groups of II-VI or III-V materials but until now the CdSe/ZnS core-shell QDs are the most used. These nanoparticles possess unique properties that have been made them very appealing for applications in a variety of biological applications. However, concerns about their toxicity and genotoxicity effects have been raised in the recent years especially when they are used to study live cells and animals because they contain toxic elements such as cadmium and selenium ^[2]. In relation to these toxic effects some studies have already been reported ^[3-5] but so far no evidence about the toxicity and genotoxicity of CdSe/ZnS QDs coated with 3-mercaptopropionic acid have been published in plant cells. To evaluate such nanoparticle effects, the cytotoxic studies were normally conducted on cell-based assays and reactive oxygen species (ROS) production, cell viability, cell stress, cell morphology and cell-particle assays ^[6]. When the genotoxic potential of the nanoparticles needs to be evaluated, such as the examination of DNA damage, although flow cytometry have been used, the simple, inexpensive and sensitive comet assay, also called single-cell gel electrophoresis assay, is the technique most used ^[7, 8].

Apart from biological applications, the native semiconducting QDs have also been used in electronic and photonic fields in order to create biosensors, lasers or other high performance electronic devices. Normally, for this kind of applications, CdSe/ZnS core-shell QDs are deposited onto solid substrates using conventional methods including drop casting or spin coating but among other disadvantages, these methods do not permit control over the quantity of the immobilized material and its surface uniformity. To overcome some of these issues laser technologies have been shown to be a good alternative, in the form of matrix-assisted pulsed laser evaporation (MAPLE) ^[9].

These topics invite interdisciplinary collaboration with research groups from different institutes/universities with the aim of exploring other potentialities and overcome some limitations of these nanoparticles. A summary of the work developed to study the impact of CdSe/ZnS core-shell QDs in cytotoxicity and genotoxicity areas as well as their application in the electronic field follows. The complete work developed on this subject can be followed by reference to the manuscripts included in the appendix chapter (chapter 7).

Overview of the Work Undertaken

The Impact of CdSe/ZnS Quantum Dots in Cells of *Medicago sativa* in Suspension Culture

This work had as main goal to study the impact of quantum dots in cells of *Medicago sativa* in suspension culture using in particular, the CdSe/ZnS core-shell QDs coated with 3-mercaptopropionic acid (MPA-QDs) fabricated in the course of this research work and described in chapters 2 and 3. To evaluate the cytotoxicity of these nanoparticles in higher plant cells different assays to test the cellular response were carried out, namely the production and accumulation of reactive oxygen species (ROS), the cell viability, the cell stress, the cell morphology and the cell/plant particle uptake. Moreover, the MPA-QD stability in the biological system was also analysed. For the performance of the different assays, a plant cell suspension culture of *Medicago sativa* was established as a model for the evaluation of QD effects. To evaluate the cell growth and cell viability parameters, cell suspensions were grown during 8 days with and without the presence of 100nM of MPA-QDs. The studies related to quantum dot uptake by the plant cells were carried out on a four day's old *M. sativa* suspension culture using 10nM of MPA-QDs. After 48h of incubation with QDs, the samples were visualised using confocal and inverted microscopy. The ROS formation in cultures exposed to the MPA-QDs was analysed using two different probes. For the detection of H₂O₂, 3, 3'-diaminobenzidine (DAB) staining technique developed by Thordal-Christensen *et al*^[10] was used. DAB reacts rapidly with H₂O₂ in the presence of peroxidase forming a brown polymerized product. The detection of O₂⁻ was carried out using nitroblue tetrazolium (NBT) assay described by Fryer *et al*^[11]. To determine cellular oxidative stress the probe 2', 7'-

dichlorodihydrofluorescein diacetate (H₂DCFDA) was applied as reported by Ortega-Villasante *et al*^[12].

The results obtained for the different assays performed indicate that the cell growth is affected when 100nM of MPA-QDs were added during the exponential growth phase. Moreover, less than 50% of viable cells remain after 72h of MPA-QDs addition. The quantum dots were taken up by *Medicago sativa* cells and showed preferential accumulation in the cytoplasm and nucleus (Figure 34).

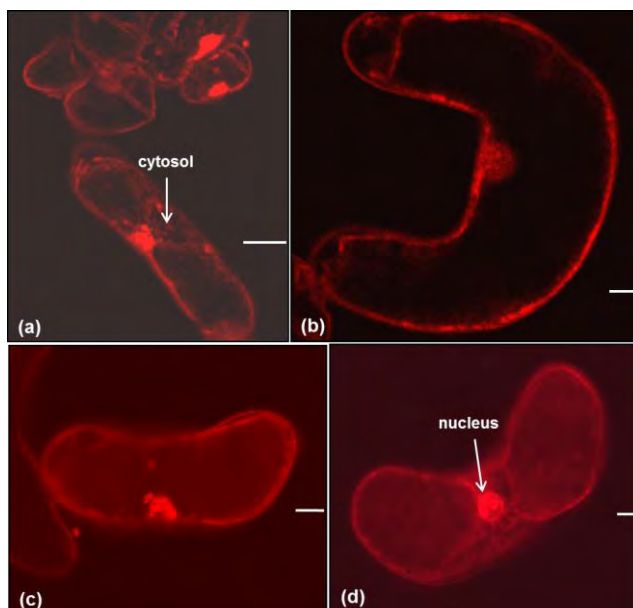


Figure 34 | QDs Uptake by the Plant Cells. Fluorescence images of *M. sativa* cells after 48h of incubation with 10nM of MPA-QDs showing QD internalization. (a, b) confocal fluorescence. (c, d) wide field fluorescence. Arrows point to nucleus and cytosol. Scale bar=20 μ m.

As part of the cellular response to internalization, *M. sativa* cells were found to increase the production of (ROS) in a dose and time dependent manner and using the fluorescent dye H₂DCFDA it was observable that MPA-QD concentrations in the range between 5 and 180nM led to a progressive and linear increase of ROS accumulation (Figure 35).

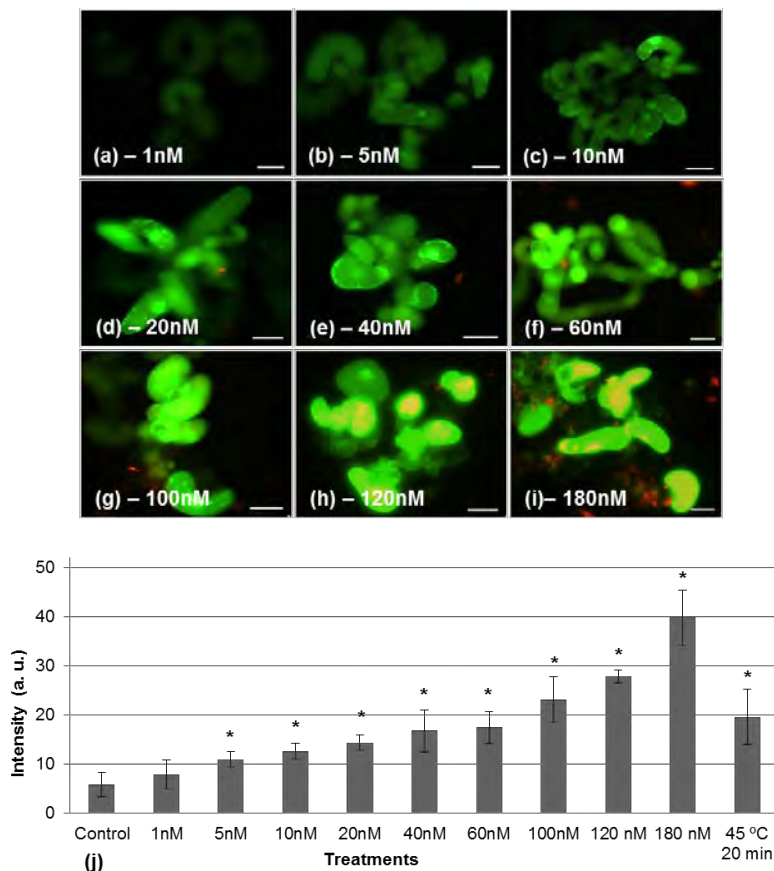


Figure 35 | Oxidative Stress Dose Response Assay. (a – i) Cell suspension cultures treated with QDs and H₂DCFDA. This nonspecific probe for reactive oxygen species accumulation is converted by ROS into a green fluorescent compound. The fluorescence increased with the increasing concentrations of MPA-QDs showing a safe range between 1 and 10nM. Scale bar=50µm. (j) Graphic representation of mean fluorescence intensity of pictures from cultures subjected to the different treatments. Columns with * indicate a significant difference from the control value with $p < 0.001$ (ANOVA). The H₂DCFDA assay was performed 48 hours after the QD addition.

The outcome of these experiments led to conclude that the extent of 3-mercaptopropionic acid coated CdSe/ZnS core-shell QD cytotoxicity in plant cells is dependent upon a number of factors including QD surface properties, dose and the environmental conditions of administration. In addition, for *Medicago sativa* cells, a safe range for biological applications of quantum dot concentrations between 1 and 5nM had been demonstrated and should not be exceeded

A complete version of this work can be found in appendix chapter in the following published publications:

Ana R. Santos, **Ana S. Miguel**, Leonor Tomaz, Rui Malhó, Christopher Maycock, Maria C. Vaz Patto, Pedro Fevereiro and Abel Oliva. The impact of CdSe/ZnS Quantum Dots in cells of *Medicago sativa* in suspension culture. *Journal of Nanobiotechnology* 2010, 8:24.

Ana Raquel Santos, **Ana Sofia Miguel**, Pedro Fevereiro and Abel Oliva. Evaluation of Cytotoxicity of 3-Mercaptopropionic Acid-Modified Quantum Dots on *Medicago sativa* Cells and Tissues. *Nanoparticles in Biology and Medicine. Methods and Protocols*, 2012, Springer (in press).

CdSe/ZnS Quantum Dots Trigger DNA Repair and Antioxidant Enzyme Systems in *Medicago sativa* Cells in Suspension Culture

As demonstrated in the previous cytotoxicity studies, plant cells increased the production of undifferentiated ROS in a dose dependent manner when exposed to MPA-QDs and that a maximum concentration of 5nM is cyto-compatible for this type of nanoparticles. Moreover, the cells accumulated these nanoparticles in the cytoplasm and nucleus. When a cell suspension culture is exposed to 100nM of MPA-QDs during 48h no noticeable production of superoxide radicals was detected and the production of H₂O₂ is far less than 10nM, if any.

There is evidence obtained from various plant systems showing that the amounts and activities of enzymes involved in scavenging ROS are altered by different stresses^[13-15]. Among others, ROS can also cause oxidative damage to DNA, lipids and proteins and occurs frequently in all cells^[16]. Therefore, genotoxic effects have been reported when nanoparticles interact with living systems^[4, 5]. However, so far, there are no reports about genotoxicity of MPA-QDs on plant cells. Based on the previous positive oxidative stress results induced by the MPA-QDs in *Medicago sativa* cell suspension cultures, work was developed to analyse the cyto- and genotoxic effects of these nanoparticles in the same plant cells. For the assessment of these effects, three different categories of experiments were carried out, including (1) antioxidant enzyme activity, (2) comet assay and (3) real time quantitative polymerase chain reaction (QRT-PCR) assay. Briefly, the antioxidant enzyme activity assay was conducted based on the evaluation of the activity of three antioxidant enzymes: superoxide dismutase (SOD), catalase (CAT) and glutathione reductase (GR). The assay was designed in order to quantify the

effect of different concentrations of MPA-QDs (10, 50 and 100nM) on the activity of these enzymes in the plant cells. The quantification of SOD activity was carried out according to Rubio *et al*^[17], the CAT activity was quantified as described elsewhere^[18] and the GR activity was quantified based on the increase in absorbance at 412 nm when 5,5'-dithiobis(2-nitrobenzoic acid) (DTNB) is reduced by glutathione (GSH)^[19, 20]. Concerning the comet assay first described by Singh *et al*^[21], four different versions were used to estimate the range and type of genotoxicity imposed by the same concentrations of MPA-QDs in *M. sativa* cells in a suspension culture: the neutral version, useful to assess DNA double strand breaks (DSBs); the alkaline/neutral version (A/N) that detects mainly DNA single strand breaks (SSBs); the A/N version followed by an enzymatic treatment with formamidopyrimidine DNA glycosylase (FPG) to evaluate the extent of purine base oxidation; and the A/N version followed by the enzymatic treatment with endonuclease III (EndoIII) to evaluate the amount of oxidized pyrimidine bases. The two enzymes (FPG and EndoIII) remove the oxidized bases and generate a DNA strand break at the position of the excised base that can be detected via the comet assay^[22]. Lastly, an experiment was carried out based on the QRT-PCR technique to evaluate the expression of genes of DNA repair enzymes when nanoparticles are placed in contact with plant cells.

The results obtained demonstrate that when *M. sativa* cells are exposed to 10, 50 and 100nM of MPA-QDs a correspondent increase in the activity of these three antioxidant enzymes is registered. The ROS scavenging mechanism seems to be activated to protect cells from reactive oxygen forms. Moreover, this activation appears to be dose dependent and effectively prevent the accumulation of H₂O₂ and radical O₂⁻. Based on the four versions explored of the comet assay, an increase of the number of DNA single and double strand breaks with the increase of the QDs concentration (Figure 36) was found. At the highest concentrations tested, purine bases were more oxidized than pyrimidine ones. Additionally, by the QRT-PCR analysis the transcription of the DNA repair enzymes was demonstrated to be up-regulated in the presence of increasing concentrations of MPA-QDs (Figure 37).

This resulting work describes for the first time the genotoxic effect of MPA-QDs in plant cells. Concentrations of MPA-QDs around 10 nM although not

lethal are cytotoxic and genotoxic to plant cells. This sets a limit for the concentrations to be used when experiments on plants using nanoparticles of this type are being considered. Furthermore, it was also possible to conclude that both DNA repair genes and the ROS scavenging mechanisms were activated when *M. sativa* cells were treated with MPA-QDs.

A full description of this work can be found in appendix chapter in the following submitted manuscript:

Ana Raquel Santos*, **Ana Sofia Miguel***, Anca Macovei*, Christopher Maycock, Alma Balestrazzi, Abel Oliva and Pedro Fevereiro. CdSe/ZnS Quantum Dots trigger DNA repair and antioxidant enzyme systems in *Medicago sativa* cells in suspension culture. *Particle and Fibre Toxicology*, 2012 (submitted). *Authors contributed equally.

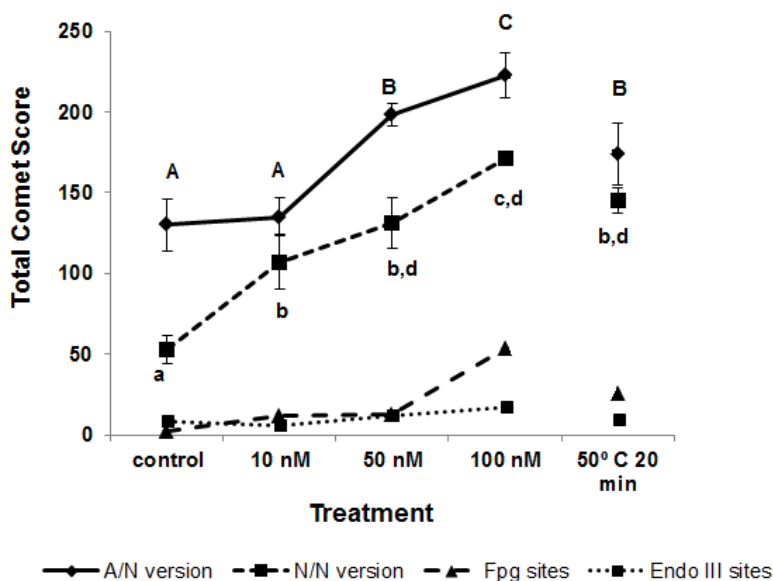


Figure 36 | DNA Damage in *Medicago sativa* cells in Suspension Cultures. DNA damage in cell suspension cultures treated with 0, 10, 50 and 100 nM of MPA-QDs for 48 hours or at 50 °C for 20 minutes, in alkaline unwinding and neutral electrophoresis (A/N), in neutral incubation and neutral electrophoresis (N/N), and also by incubation with lesion-specific FPG or EndoIII enzymes. Results are expressed as mean values with standard deviation. One –way ANOVA $P < 0.0001$. Values with different letters are significantly different at $p \leq 0.01$ with Tukey test.

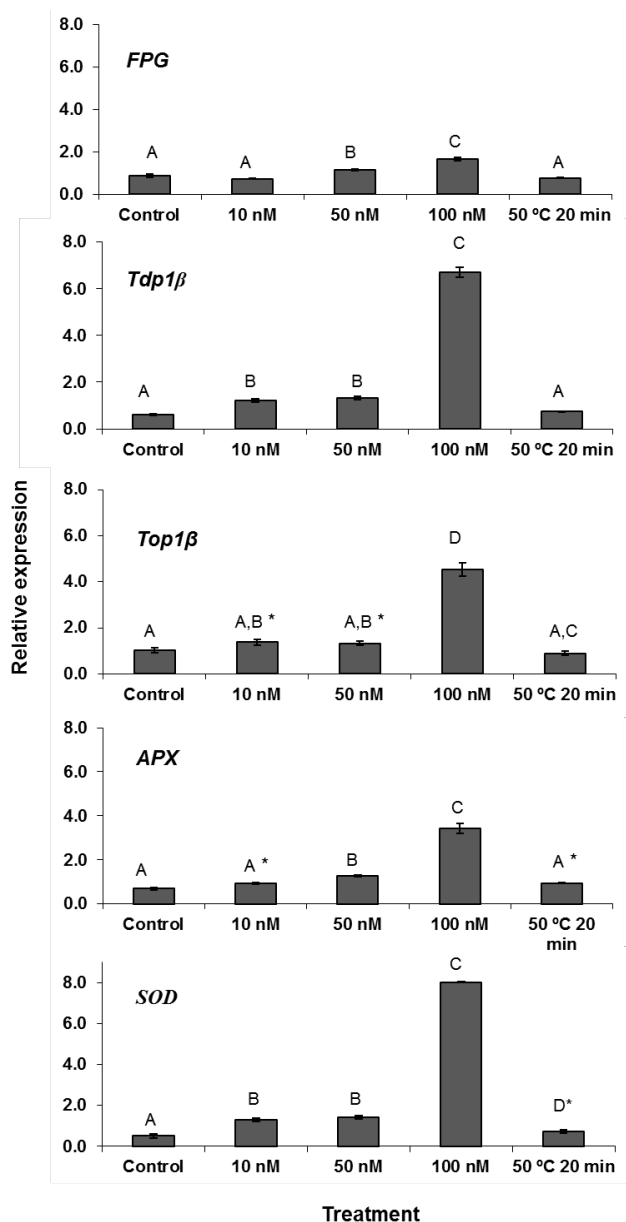


Figure 37 | Expression of *Tdp1β*, *Top1β*, *Fpg*, *SOD* and *APX* genes in *Medicago sativa* cells treated with MPA-QDs. Expression of *Tdp1β*, *Top1β*, *Fpg*, *SOD* and *APX* genes on cell suspension cultures of *M.sativa* treated for 48 hours with 0, 10, 50 and 100nM of MPA-QDs and at 50 °C for 20 minutes. For each treatment, data represent the mean values of three independent replications. One –way ANOVA $P < 0.0001$ for *Tdp1b*, *Fpg*, *APX* and *SOD* and $P < 0.01$ for *Topo1b*. Tukey test $P < 0.01$ except for * $P < 0.05$.

Laser Immobilization onto Solid Substrates of CdSe/ZnS Core-Shell Quantum Dots

Matrix-assisted pulsed laser evaporation (MAPLE) is a laser-based deposition technique developed recently, mostly for organic and bio-organic materials processing^[9]. The material to be immobilized on a solid substrate surface is diluted in a laser-absorbing solvent. After the solution is frozen in liquid nitrogen, it is submitted to laser radiation. The laser energy is mainly absorbed by the solvent which is vaporized and transports the material of interest toward the substrate placed in front of the target ensuring a gentle transfer mechanism. It's known that the physical properties of the QDs are size dependent^[23, 24] and when coated with a shell of a second semiconductor with higher band gap, their photoluminescence quantum yields could be improved when compared with shells constituted by organic materials. These features make them suitable for different applications including biological labelling^[25, 26], design of devices such as thin films LEDs^[27-29] or nanocrystals quantum dot lasers^[30-32], since both electronic and photonic characteristics can be tuned by simply controlling their shape and size. CdSe/ZnS core-shell QDs are usually deposited on solid substrates from colloidal solutions by conventional methods such as drop casting or spin coating. These deposition techniques, although simple and profitable, in addition to other drawbacks, they do not guarantee an accurate control over the amount of the immobilized material and its surface uniformity as well as unsuitability for multilayer structure growth since this implies repeated use of solvents. To overcome these disadvantages, laser technologies such as MAPLE represent a suitable alternative since these characteristics are much better controlled. Thus, using the UV-MAPLE technique, deposition of the nanocrystals was achieved creating self-organized 2D arrays constituted by the previously synthesized native CdSe/ZnS core-shell QDs immobilized on solid substrates. Here in, the synthesis of the network-like structures can be controlled by the incident laser fluence value. The formation of a photonic band gap due to the periodically changing refractive index can be used for future photonic applications implying guided light propagation or enhanced spontaneous emission.

Shortly, the native CdSe/ZnS core-shell QDs were immobilized by the UV-MAPLE technique onto SiO₂ glass substrates. The glass supports were

previously covered by silica thin films which were deposited by the dip-coating sol-gel method describe elsewhere^[33, 34]. An ultra-violet krypton fluoride (UV KrF*) excimer laser source was used for the evaporation experiments and toluene was the solvent chosen for the preparation of the composite MAPLE targets due to its highly absorption at the wavelength ($\lambda=248\text{nm}$) of the incident laser radiation. During the assays, different characteristics of the immobilized QDs were analysed. The surface morphology and growth mode of the deposited structures were investigated by optical and atomic force microscopy (AFM) in acoustic (dynamic) configuration. The crystalline structure and chemical composition of the base material used for the preparation of the MAPLE targets as well as the laser transferred QDs were studied by transmission electron microscopy (TEM) and energy dispersive X-ray spectroscopy (EDX). The functional properties of the immobilized QDs were studied by fluorescence microscopy.

Evaluating the structure of the synthesized CdSe/ZnS core-shell QDs the TEM analysis reveals that these nanoparticles possess two different crystalline structures: ZnS hexagonal wurtzite and ZnS cubic zinc-blend phases probably derived from the high number of ZnS monolayers (~5) around the CdSe cores which can lead to an epitaxial but incoherent growth. This was already observed by Dabbousi and co-workers^[35] when the shell coverage process exceed 2 monolayers of ZnS. By the analysis of AFM results it was possible to observe that using a lower fluence laser ($0.1\text{J}/\text{cm}^2$) a higher amount of material can be transferred and the surface morphology of the obtained deposited films is uniform. Contrary, when a higher ($0.2\text{J}/\text{cm}^2$) laser fluence value is used some of the material can be damaged, leading to a non-continuous deposition over the substrate. These results are in line with what was observed for fluorescence microscopy analysis. For a lower fluence laser value the fluorescence patterns are more intense.

It has been demonstrated previously that MAPLE is a useful technique for deposition of nanostructured materials such as carbon^[36] or CdSe^[37] nanoparticles and the research work carried out enhanced this data. When using lower incident laser fluence this technique reproduced a specific network-like surface morphology of the deposited material but more importantly the functional properties translated by the intense fluorescence of

the immobilized material were preserved. These led to conclude that this technique is suitable for the immobilization of CdSe/ZnS core-shell QDs making them potential tools to be applied as biosensors, lasers or high performance electronic devices.

A complete version of this work can be found in appendix chapter in the following published article:

E. György, A. Perez del Pino, J. Roqueta, B. Ballesteros, **A. S. Miguel**, C. D. Maycock, and A. G. Oliva. Synthesis and Laser Immobilization onto Solid Substrates of CdSe/ZnS Core-Shell Quantum Dots. *Journal of Physical Chemistry C*, 2011, 115, 15210-15216.

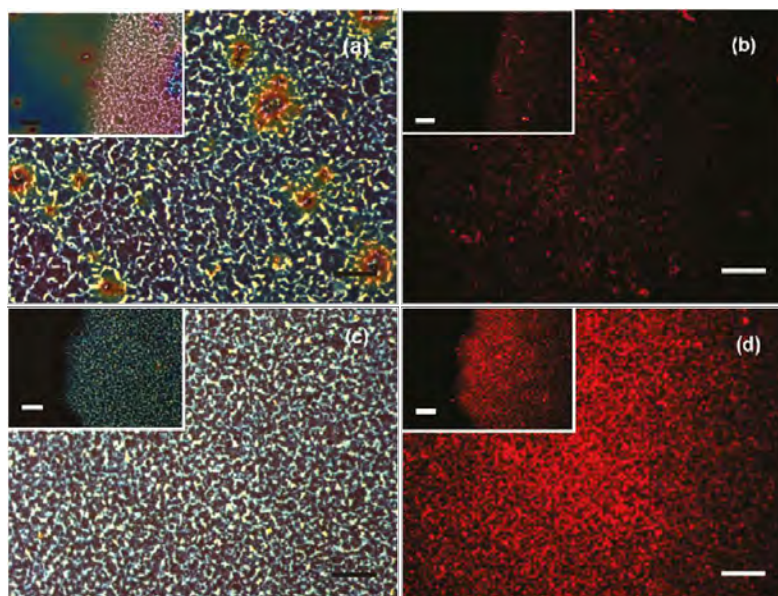


Figure 38 | Laser Immobilization onto Solid Substrates of CdSe/ZnS core-shell QDs. Optical microscopy (a, c) and fluorescence (b, d) images corresponding to the same surface area of CdSe/ZnS core-shell nanostructures obtained on SiO₂ glass substrates covered by silica solgel deposited film at 0.2 (a, b) and 0.1 J/cm² (c, d) laser fluence. The insets belong to the border between the substrate and CdSe/ZnS QDs thin films. Scale bar=20μM.

Acknowledgments

Regarding the toxicity and genotoxicity studies, the author thanks Ana Raquel Santos by her help in the performance of the majority of the experiments and the writing of the first draft of the manuscripts. The author is also thankful to Mattia Donà for his kind help and for the introduction in the Comet technique.

The author is grateful for the collaboration established with Dr. Pedro Fevereiro and Dr. Alma Balestrazzi who participated in the design and coordination of the cytotoxicity and genotoxicity studies respectively. This work was supported by the project “Development of ultra-sensitive detection methods and plant nano-vaccines for the fungi *Fusarium spp* using nanotechnological devices”, Iberian Capacitation Program in Nanotechnologies: Call 2006/2007. The author thank to Dr. Eniko György and co-workers for the kind collaboration, performance of the experiments and writing of the first draft of the manuscript in the immobilization studies using the MAPLE technique. This work was supported from the Spanish National Research Council under the Contract Nos.200860I211 and 200960I015, the Spanish Ministry of Science and Innovation for the PTA2008-1108-I contract, the Portugal-Spanish Bilateral Agreement No. 2007PT0007, and the Romanian National University Research Council under the Contract IDEAS No. 652. Ana Sofia Miguel is a recipient of a PhD fellowship from the Fundação para a Ciência e Tecnologia (FCT), Portugal (SFRH/BD/40303/2007).

References

1. Walling, M. A.; Novak, J. A.; Shepard, J. R. E., Quantum Dots for Live Cell and In Vivo Imaging. *Int J Mol Sci* **2009**, 10, (2), 441-491.
2. Alivisatos, A. P.; Gu, W. W.; Larabell, C., Quantum dots as cellular probes. *Annu Rev Biomed Eng* **2005**, 7, 55-76.
3. Wang, J. X.; Zhang, X. Z.; Chen, Y. S.; Sommerfeld, M.; Hu, Q., Toxicity assessment of manufactured nanomaterials using the unicellular green alga *Chlamydomonas reinhardtii*. *Chemosphere* **2008**, 73, (7), 1121-1128.
4. Green, M.; Howman, E., Semiconductor quantum dots and free radical induced DNA nicking. *Chem Commun* **2005**, (1), 121-123.
5. Anas, A.; Akita, H.; Harashima, H.; Itoh, T.; Ishikawa, M.; Biju, V., Photosensitized breakage and damage of DNA by CdSe-ZnS quantum dots. *J Phys Chem B* **2008**, 112, (32), 10005-10011.
6. Jones, C. F.; Grainger, D. W., In vitro assessments of nanomaterial toxicity. *Adv Drug Deliver Rev* **2009**, 61, (6), 438-456.
7. Lewinski, N.; Colvin, V.; Drezek, R., Cytotoxicity of nanoparticles. *Small* **2008**, 4, (1), 26-49.
8. Cheng-Teng Ng; Jasmine J. Li; Boon-Huat Bay; Yung, L.-Y. L., Current Studies into the Genotoxic Effects of Nanomaterials. *Journal of Nucleic Acids* **2010**.
9. Wu, P. K.; Ringeisen, B. R.; Krizman, D. B.; Frondoza, C. G.; Brooks, M.; Bubb, D. M.; Auyeung, R. C. Y.; Pique, A.; Spargo, B.; McGill, R. A.;

Chrisey, D. B., Laser transfer of biomaterials: Matrix-assisted pulsed laser evaporation (MAPLE) and MAPLE Direct Write. *Rev Sci Instrum* **2003**, 74, (4), 2546-2557.

10. Thordal-Christensen, H.; Zhang, Z.; Wei, Y.; Collinge, D. B., Subcellular localization of H₂O₂ in plants. H₂O₂ accumulation in papillae and hypersensitive response during the barley—powdery mildew interaction. *The Plant Journal* **1997**, 11, (6), 1187-1194.

11. Fryer, M. J.; Oxborough, K.; Mullineaux, P. M.; Baker, N. R., Imaging of photo-oxidative stress responses in leaves. *J Exp Bot* **2002**, 53, (372), 1249-1254.

12. Ortega-Villasante, C.; Rellan-Alvarez, R.; Del Campo, F. F.; Carpena-Ruiz, R. O.; Hernandez, L. E., Cellular damage induced by cadmium and mercury in *Medicago sativa*. *J Exp Bot* **2005**, 56, (418), 2239-2251.

13. Smeets, K.; Cuypers, A.; Lambrechts, A.; Semane, B.; Hoet, P.; Van Laere, A.; Vangronsveld, J., Induction of oxidative stress and antioxidative mechanisms in *Phaseolus vulgaris* after Cd application. *Plant Physiol Bioch* **2005**, 43, (5), 437-444.

14. Santos, A. R.; Miguel, A. S.; Tomaz, L.; Malhó, R.; Maycock, C.; Patto, M. C. V.; Fevereiro, P.; Oliva, A., The impact of CdSe/ZnS Quantum Dots in cells of *Medicago sativa* in suspension culture. *Journal of Nanobiotechnology* **2010**, 8, 24.

15. Apel, K.; Hirt, H., Reactive oxygen species: Metabolism, oxidative stress, and signal transduction. *Annu Rev Plant Biol* **2004**, 55, 373-399.

16. Valentine, J. S.; Wertz, D. L.; Lyons, T. J.; Liou, L. L.; Goto, J. J.; Gralla, E. B., The dark side of dioxygen biochemistry. *Curr Opin Chem Biol* **1998**, 2, (2), 253-262.

17. Rubio, M. C.; Gonzalez, E. M.; Minchin, F. R.; Webb, K. J.; Arrese-Igor, C.; Ramos, J.; Becana, M., Effects of water stress on antioxidant enzymes of leaves and nodules of transgenic alfalfa overexpressing superoxide dismutases. *Physiol Plantarum* **2002**, 115, (4), 531-540.

18. Bergmeyer, H. U., *Methods of enzymatic analysis: Samples, reagents, assessment of results*. Verl. Chemie: **1983**; p 539.

19. Smith, I. K.; Vierheller, T. L.; Thorne, C. A., Assay of Glutathione-Reductase in Crude Tissue-Homogenates Using 5,5'-Dithiobis(2-Nitrobenzoic Acid). *Anal Biochem* **1988**, 175, (2), 408-413.

20. Shanker, A. K.; Djanaguiraman, M.; Sudhagar, R.; Chandrashekar, C. N.; Pathmanabhan, G., Differential antioxidative response of ascorbate glutathione pathway enzymes and metabolites to chromium speciation stress in green gram (*Vigna radiata* (L.) R.Wilczek. cv CO 4) roots. *Plant Sci* **2004**, 166, (4), 1035-1043.

21. Singh, N. P.; Mccoy, M. T.; Tice, R. R.; Schneider, E. L., A Simple Technique for Quantitation of Low-Levels of DNA Damage in Individual Cells. *Exp Cell Res* **1988**, 175, (1), 184-191.

22. Petersen, E. J.; Nelson, B. C., Mechanisms and measurements of nanomaterial-induced oxidative damage to DNA. *Anal Bioanal Chem* **2010**, 398, (2), 613-650.

23. Sun, C. Q.; Chen, T. P.; Tay, B. K.; Li, S.; Huang, H.; Zhang, Y. B.; Pan, L. K.; Lau, S. P.; Sun, X. W., An extended 'quantum confinement' theory: surface-coordination imperfection modifies the entire band structure of a nanosolid. *J Phys D Appl Phys* **2001**, 34, (24), 3470-3479.

24. Jasieniak, J.; Smith, L.; van Embden, J.; Mulvaney, P.; Califano, M., Re-examination of the Size-Dependent Absorption Properties of CdSe Quantum Dots. *J Phys Chem C* **2009**, 113, (45), 19468-19474.
25. Alivisatos, P., The use of nanocrystals in biological detection. *Nat Biotechnol* **2004**, 22, (1), 47-52.
26. Riegler, J.; Ditengou, F.; Palme, K.; Nann, T., Blue shift of CdSe/ZnS nanocrystal-labels upon DNA-hybridization. *Journal of Nanobiotechnology* **2008**, 6, (7).
27. Nizamoglu, S.; Demir, H. V., Excitation resolved color conversion of CdSe/ZnS core/shell quantum dot solids for hybrid white light emitting diodes. *J Appl Phys* **2009**, 105, (8).
28. Gopal, A.; Hoshino, K.; Kim, S.; Zhang, X. J., Multi-color colloidal quantum dot based light emitting diodes micropatterned on silicon hole transporting layers. *Nanotechnology* **2009**, 20, (23).
29. Kazes, M.; Saraidarov, T.; Reifeld, R.; Banin, U., Organic-Inorganic Sol-Gel Composites Incorporating Semiconductor Nanocrystals for Optical Gain Applications. *Adv Mater* **2009**, 21, (17), 1716-1720.
30. Klimov, V. I.; Mikhailovsky, A. A.; McBranch, D. W.; Leatherdale, C. A.; Bawendi, M. G., Quantization of multiparticle Auger rates in semiconductor quantum dots. *Science* **2000**, 287, (5455), 1011-1013.
31. Klimov, V. I.; Mikhailovsky, A. A.; Xu, S.; Malko, A.; Hollingsworth, J. A.; Leatherdale, C. A.; Eisler, H. J.; Bawendi, M. G., Optical gain and stimulated emission in nanocrystal quantum dots. *Science* **2000**, 290, (5490), 314-317.
32. Smirnova, T. N.; Sakhno, O. V.; Yezhov, P. V.; Kokhtych, L. M.; Goldenberg, L. M.; Stumpe, J., Amplified spontaneous emission in polymer-CdSe/ZnS-nanocrystal DFB structures produced by the holographic method. *Nanotechnology* **2009**, 20, (24).
33. McDonagh, C.; Bowe, P.; Mongey, K.; MacCraith, B. D., Characterisation of porosity and sensor response times of sol-gel-derived thin films for oxygen sensor applications. *J Non-Cryst Solids* **2002**, 306, (2), 138-148.
34. Yu, S. Z.; Wong, T. K. S.; Hu, X.; Pita, K., The effect of TEOS/MTES ratio on the structural and dielectric properties of porous silica films. *J Electrochem Soc* **2003**, 150, (5), F116-F121.
35. Dabbousi, B. O.; RodriguezViejo, J.; Mikulec, F. V.; Heine, J. R.; Mattoussi, H.; Ober, R.; Jensen, K. F.; Bawendi, M. G., (CdSe)ZnS core-shell quantum dots: Synthesis and characterization of a size series of highly luminescent nanocrystallites. *J Phys Chem B* **1997**, 101, (46), 9463-9475.
36. Hunter, C. N.; Check, M. H.; Bultman, J. E.; Voevodin, A. A., Development of matrix-assisted pulsed laser evaporation (MAPLE) for deposition of disperse films of carbon nanoparticles and gold/nanoparticle composite films. *Surf Coat Tech* **2008**, 203, (3-4), 300-306.
37. Pate, R.; Lantz, K. R.; Stiff-Roberts, A. D., Resonant infrared matrix-assisted pulsed laser evaporation of CdSe colloidal quantum dot/poly[2-methoxy-5-(2'-ethylhexyloxy)-1,4-(1-cyano vinylene)phenylene] hybrid nanocomposite thin films. *Thin Solid Films* **2009**, 517, (24), 6798-6802.

Chapter 6

General Discussion and Future Perspectives

General Discussion and Future Perspectives

General Discussion and Future Perspectives 239
References 247

General Discussion and Future Perspectives

The research work described in this thesis was constructed with the aim of developing a fluorescent biomarker for application in biological assays, namely microscopy imaging and immunotests. Generally, for this kind of application, fluorescent techniques making use of standard organic dyes (e.g. encoded fluorescent proteins or chemically synthesized dyes) are widely used. However, due to the optical limitations presented by these fluorophores (e.g. narrow specific excitation wavelengths, photobleaching), semiconductor nanoparticles, also called Quantum dots (QDs), have been introduced to replace the dyes and their use has been evolving over the years. So far, the most studied are the CdSe/ZnS QDs due to their unique optical and electronic properties and their relatively high availability. Quantum dots emerged in science and technology in the eighties, but it was almost one decade later that the interest and constant development in nanoparticle research started. Since that date many modifications have been made to these synthetic procedures in order to produce QDs with enhanced properties for specific applications ^[1], ^[2]. The first commercial application of QDs took place in 2002, when nanotech start-up Quantum Dot Corporation launched its first QD bioimaging agent. Since that date, other companies worldwide have emerged. However, a key problem related to commercial QDs developed by these enterprises is the price that these particles can cost restricting their use to highly specialized applications ^[3]. Among the price, other disadvantages are also associated with these products. Issues such as poor reproducibility and homogeneity between samples from different batches and the lack of information about the nature of shell material is a constant. For these reasons, but particularly due to the high cost of these nanoparticles, one of the main goals of this Doctoral work was to synthesize CdSe/ZnS core-shell QDs for application in bioassays. The synthesis of a core-shell system involves two steps: the core synthesis and the shell growth. When the synthesis of core-shell QDs is considered, the main idea that should be kept in mind is to find a protocol which permits the obtention of small particles with narrow size distribution. Moreover, it is important to find a protocol which maintains the size distribution of nanocrystals during the growth of shell materials but more importantly allows the construction of shell layers in solution with the same

thickness around each core. Much work has been reported for this purpose, but many of these protocols are not reproducible, present lack of information about the experimental conditions or use dangerous/toxic reagents. In addition, parameters such as inorganic nature and concentration of core and shell precursors, coordinating solvent used and temperature applied for core synthesis and shell growth have suffered several modifications and sometimes are not coherent between protocols. Taking this into consideration and knowing that these parameters can affect the structural and optical properties of QDs, for both core synthesis and shell growth, many protocols were tested until the best conditions were found to produce QDs with enhanced properties. For the synthesis of the CdSe cores, the best procedure encountered to produce small cores with a narrow size distribution was the protocol developed by Aldana *et al* ^[4] and posteriorly modified by Xie *et al* ^[5] with some modifications in the reagents used. For the growth of a ZnS multishell around each core with precise thickness control, the successive ion layer adsorption and reaction (SILAR) method previously adapted by Peng *et al* ^[6] to the synthesis of QDs was found to be the best protocol ^[7]. Initially, the synthesis of the core-shell system was carried out with only 2 monolayers of ZnS.

At this primary phase, these nanoparticles possess on their surface only hydrophobic ligands which are not suitable for use in aqueous buffers. To have utility in biological applications, these nanoparticles should be soluble in aqueous solutions and for this purpose surface modification is required to achieve biocompatibility. To reach this goal a family of ligands consisting of dihydrolipoic acid appended to polyethylene glycols, of different molecular weights, bearing functional groups such as hydroxyl, amine, carboxyl or carbohydrate moieties were designed and synthesized. Furthermore, shorter ligands such as 3-mercaptopropionic acid (MPA) and dihydrolipoic acid (DHHLA) were also used to promote the hydrophilicity of the native QDs. Making use of the ligand exchange method, water-soluble QDs were created with these ligands. However, it was observed that the CdSe cores passivated with only two monolayers of ZnS, after solubilisation in aqueous environments, presented a very low fluorescence and in the majority of the cases their fluorescence was completely destroyed. For this reason the

synthesis of CdSe QDs was again carried out but increasing the number of ZnS monolayers around each core. Dabbousi *et al*^[8] reported previously that after more than 1.3 monolayers of ZnS around the cores a steady decline in the fluorescence quantum yield is observed. Even though a decrease in the quantum yield could occur, after passivating the CdSe cores with 5 monolayers of zinc sulphide it was found that the nanoparticles were still fluorescent, were small and monodisperse and had a slightly elongated shape. More importantly, they became more resistant to possible oxidation or chemical degradation imposed by the ligand exchange procedure making possible the biological applications initially proposed.

These data were confirmed by the structural and optical characterization performed on the lipophilic QDs using transmission electron microscopy, dynamic light scattering and UV/visible spectroscopy. Microscopic characterization indicated some irregular shapes or structural defects in some particles. These defects were derived from the large number of ZnS monolayers and the high temperature at which the procedure occurs (245°C)^[8]. A photoluminescence study indicated that the quantum yield obtained for these nanoparticles did not exceed 12%. This was also due to the high number of monolayers around the cores leading to an incoherent shell growth causing some defects in ZnS shell. Moreover, the presence of a primary amine (HDA) in the coordinating solvent mixture (TOPO/HDA) could also explain the obtention of a low QY^[9, 10]. They have also the capability to be more strongly bound when the outer surface is a ZnS shell, especially, more strongly bound to Zn-sites on the surface of QDs leading to the obtention of particles with a low QY (10-15%)^[5].

As previously mentioned, to achieve hydrophilicity and biocompatibility of the native CdSe/ZnS core-shell QDs, a ligand exchange with a variety of water-soluble ligands had occurred on their surface. Except for MPA, all the compounds used for this target were synthesized during this work. The synthesis of the DHLA ligand as well as the compounds with the structural format DHLA-PEG_n-FN (n=8 and 40; FN=OH, COOH and NH₂) were based on previously reported literature^[11, 12]. The compounds made of DHLA appended to TEG or PEG₄₀₀, but bearing a carbohydrate moiety as functional

terminal were developed during this work. The family of compounds consisting of DHLA appended to a hydrophilic spacer and support a functional end group brought some advantages when compared with shorter ligands as in the case of MPA. The incorporation of the thioctic acid moiety which after reduction of the 1,2-dithiolane ring led to the obtention of a bidentate and strong anchoring group with high affinity to the surface of native QDs. With the presence of a hydrophilic spacer such as PEG or TEG the solubility of these ligands in aqueous environments was increased. The presence of diverse reactive end groups onto the QD surface permitted the obtention of water-soluble QDs with different hydrodynamic sizes and degrees of charge. More interesting, the obtention of ligands with a carboxyl or amino reactive group allowed the obtention of water-soluble QDs with groups suitable for further conjugation with biomolecules using different chemical strategies.

In order to be applied in biological systems, QDs must be linked to biomolecules without altering the biological activity of the conjugated form. For this reason, a number of successful conjugation methods have been developed over the years including covalent and non-covalent attachment ^[1]. Taking advantage of the EDC/NHS chemistry commonly used for the conjugation of QDs with biomolecules ^[13-15], the coupling of water-soluble carboxy-QDs with monoclonal antibodies was carried out. Due to the higher solubility presented by the ligands which support a hydrophilic spacer (PEG) and the bidentate nature and strong affinity demonstrated by the DHLA group, for the surface of CdSe/ZnS QDs, such coupling to biomolecules was first attempted with carboxyPEG₄₀₀-QDs (QD-DHLA-PEG₄₀₀-COOH). However, one of the main problems encountered in the bioconjugation protocol using these QDs was the activation of the terminal COOH groups with EDC and NHS. Apparently, the length of these ligands caused by the long PEG₄₀₀ chain makes such ligands roll up on themselves, thus making the carboxy group inaccessible and turning the posterior activation of the functional COOH groups with EDC/NHS and consequently their bioconjugation with antibodies impossible. To overcome this issue, carboxyPEG₄₀₀-QDs in the bioconjugation with antibodies, were replaced by carboxy-QDs bearing shorter ligands such as MPA or DHLA.

Among other parameters, the bioconjugation of QDs to biomolecules could be affected by pH or by the buffers in which the QDs were dispersed, because depending of these conditions the nanoparticles could form large aggregates thus preventing a possible posterior bioconjugation. MPA and DHLA-QDs before the conjugation with antibodies were evaluated in terms of pH stability and electrophoretic mobility. Based on these studies it was possible to demonstrate that CdSe/ZnS core-shell QDs capped with dithiol-terminated ligands (DHLA-QDs) were more stable and well-dispersed in a wide pH range from 6 to 12 when compared with those functionalized with monothiol ligands (MPA-QDs) where the aggregates built up and were stable only at pH 6. The same studies also showed that the stability of the water-soluble QDs not only depended on the nature of the ligand and pH, but also the media (buffer) for their dispersion. Although 4-morpholineethanesulfonic acid (MES) buffer was a suitable bioconjugation buffer for similar systems ^[16, 17], for MPA-QDs this buffer promoted aggregation whereas sodium phosphate (Na-P) buffer did not.

Taking this into account, the coupling between carboxy-QDs and the monoclonal antibodies were conducted at pH 6 and 8 in Na-P buffer. Through these results it was demonstrated that using the EDC/NHS strategy, the number of antibodies attached to a single QD as well as the type of binding, strongly depends upon the pH and salt conditions of the aqueous media. By the Protein A280 assay the QD/Ab molar ratio in QD-Ab complexes was estimated. It was demonstrated that at pH 6 the ionic and covalent binding of the antibodies was promoted achieving on average three biomolecules per QD, while increasing the pH to 8 and adding some salts only the covalent attachment was achieved and no more than one biomolecule per particle was obtained. Regardless of the number of antibodies per particle, it was confirmed that after the bioconjugation reaction the antibodies linked to QDs kept their functional properties and recognized their specific antigen.

Conjugation of carboxy-QDs bearing shorter ligands with the monoclonal antibodies was successfully achieved, although one of the principal problems found after bioconjugation was the stability of the QD-Ab complexes because frequent and persistent aggregation was observed in the final conjugates. This suggested that maybe the type of ligand used to coat the hydrophobic

surface of the nanoparticles as well as the type of conjugation strategy applied was not the most efficient for this purpose.

In order to avoid the undesirable nanoparticle aggregation problem and improve the colloidal stability of conjugated and non-conjugated nanoparticles, some improvements are required. The synthesis of more complex ligands or polymers with multiple functional groups able to form direct multiple binding to the nanoparticle surface and enhance colloidal stability should be considered. Moreover, such ligands need to present high hydrophilicity to increase the solubility of the particles in aqueous environments. As a possible example, recently cysteine-functionalized polyaspartate ^[18] was synthesized by Ying's group. This polymer was designed in a way that the ligand exchange method could be applied for the coating of QDs without producing particle aggregates. The multiple thiol groups on the polymer backbone provided strong chemisorption to the nanoparticle surface, and the carboxyl group convey water solubility and provide further bioconjugation^[19].

Amphiphilic polymers such as maleic copolymer (PMAO) should also be regarded. These polymers bear a hydrophobic part which can interact hydrophobically with the organic ligands present in QD surface and a hydrophilic part constituted by maleic anhydride moieties. These reactive groups can confer stability to the nanoparticles and are able to suffer chemical modifications (e.g. hydrolysis) for further bioconjugation with biomolecules ^[20]. With this type of polymer, it may be possible to avoid the carboxyPEG₄₀₀-QDs issue related with bioconjugation. As this polymer has the ability to interact with the hydrophobic ligands on the QD surface, the functional end groups available for posterior bioconjugation are at the end of these hydrophobic chains as a network-like pointing outwards. This may avoid the possibility of such ligands rolling up and making the activation of these groups difficult or impossible.

The conjugation strategies using specific sites on the antibody should also be tested and evaluated. Even though these strategies involve the subtle modification of the biomolecules, higher or complete antibody conjugation efficiency may be achieved. In this case, covalent QD-antibody conjugation based on cross linking reactions between amino-QDs and an aldehyde

formed by oxidation of carbohydrate groups located on the antibody's Fc region (reductive amination)^[21] should be considered and performed. For this target, the amino-QDs and the QDs with ligand mixtures of aminoPEG₄₀₀/hydroxyPEG₄₀₀ on their surface developed in this thesis can be used. Using the same QDs it is also possible to conjugate them with antibodies by reacting the NH₂ groups on QD surface with sulfo-SMCC (Michael acceptor) forming maleimido-QDs, which in turn can react with the sulphhydryl groups present in antibodies fragments previously derived from IgG reduction with dithiothreitol (DTT)^[21]. With this strategy heterocyclic moieties are introduced into the system and these could have their own biological activity and hence interfere in posterior biological applications.

QDs conjugated with monoclonal anti-RAP 1 antibody were applied for the immunodetection of the rhoptry associated protein (RAP-1) present in the apical complex of *Babesia bovis* parasites of infected bovine blood samples. The results obtained were visualized by fluorescence microscopy. To control the efficiency of this assay, simultaneously, samples of the same infected red blood cells with *B. bovis* parasites were incubated with the monoclonal antibody against RAP-1 protein and the immunofluorescence reaction was monitored by the use secondary antibodies conjugated with FITC commonly used in the standard indirect immunofluorescence assay. The study developed in such application demonstrated that direct immunofluorescence assay using QD-antibody conjugates represent a good alternative method for this type of test. Furthermore, the fluorescence emitted by the QDs is more intense than the fluorescence emitted by the standard dye conjugate to secondary antibody. This evidenced the higher capability that QDs have to be more resistant to large periods of excitation at different wavelengths. In conclusion, the CdSe/ZnS core-shell QDs when coupled with specific biomolecules could be useful in the development of an immunosensor for disease diagnosis. In this particular application the identification of antibodies against the *Babesia bovis* parasite in bovine blood smears was demonstrated. It's noteworthy that during these studies the colloidal instability of the QD-Ab conjugates was persistent during the assays. This problem was partly eliminated by agitating the assay to permit a better homogeneity of the

conjugated sample. This assay could be improved by the development of more stable QDs and better conjugation processes, as mentioned above. Due to their chemical composition which includes toxic elements, such as cadmium and selenium, the use of CdSe/ZnS core-shell QDs for biological applications has raised many concerns. Although a few studies have already been conducted and reported, no data was available about the cytotoxic and genotoxic effects of this class of nanoparticles in higher plant cells. To overcome the lack of information in this area, studies on QD cytotoxicity^[22, 23] and genotoxicity were conducted. This part of the work was mainly focused on the study of the impact of CdSe/ZnS core-shell QDs coated with MPA (MPA-QDs) on *Medicago sativa* cells in suspension culture. This study demonstrated that the observed effects were dependent on a number of factors including QD properties, dose and environmental conditions of administration. This led to the conclusion that this work sets a limit for the concentrations that should be used when experiments on plants using nanoparticles are being considered. QD concentrations between 1 and 5nM are enough for imaging immunoassays and should not be exceeded for such cellular biological system.

These cytotoxic and genotoxic studies were only carried out with CdSe/ZnS core-shell QDs coated with 3-mercaptopropionic acid. It has been reported that the coatings used to increase the quantum yield of the core, or for solubility and conjugation, reduce the cytotoxicity of QDs^[1]. Moreover, such coatings bearing a hydrophilic spacer such as PEG on the nanoparticle surface could decrease the level of cytotoxicity caused by QDs in different mammalian cell lines^[24]. Taking this into consideration, it is intended to expand this kind of study to other ligands developed in the course of this work. For example, ligands containing dihydrolipoic acid bearing an oligo or polyethylene glycol as hydrophilic spacer and functional terminals (OH, COOH, NH₂ or mannose) should be applied to the same cell line of higher plants in suspension culture in order to evaluate the level of toxicity caused by the PEG and/or even by the functional terminus present in such ligands.

Apart from their extensive use in biological applications, QDs, which are semiconductors, have also been applied in electro-optic devices such as

LEDs or solar cells ^[25, 26]. For such purposes QDs are usually deposited on solid substrates from colloidal solutions by conventional methods such as drop casting or spin coating. These deposition techniques, although simple and profitable, do not guarantee an accurate control over the amount of the immobilized material deposited or its surface uniformity and is not suitable for multilayer structure growth since this implies a repeated use of solvents. Making use of the recently developed matrix assisted pulsed laser evaporation (MAPLE) technique ^[27], studies to immobilize the native CdSe/ZnS core-shell QDs onto SiO₂ substrates were conducted ^[28]. Characteristics such as surface morphology and growth mode, crystalline structure and chemical composition as well as the functional properties of the immobilized QDs were analysed using techniques including AFM, TEM, EDX and fluorescence microscopy. After the laser immobilisation using the MAPLE technique, it was demonstrated that the immobilized CdSe/ZnS core-shell QDs evidence the formation of a long-range self-organized network-like morphology but more importantly the intense fluorescence observed in the deposited QDs indicated that their functional properties were preserved after the immobilization process. This led to conclude that MAPLE is a suitable technique for the immobilization of CdSe/ZnS core-shell QDs onto solid substrates making them good candidates in electronic applications, biosensors, or lasers or devices.

Altogether, this Doctoral work contributed to enhance the knowledge of the unique optical and electronic properties of the CdSe/ZnS core-shell QDs. It was possible to show how these nanoparticles are multifunctional and can be used in biological but also in electronic applications. New ideas and improvements were addressed and new directions are still open in order to better understand and further expand QD research.

References

1. Walling, M. A.; Novak, J. A.; Shepard, J. R. E., Quantum Dots for Live Cell and In Vivo Imaging. *Int J Mol Sci* **2009**, 10, (2), 441-491.
2. Jaiswal, J. K.; Simon, S. M., Potentials and pitfalls of fluorescent quantum dots for biological imaging. *Trends Cell Biol* **2004**, 14, (9), 497-504.

3. Sanderson, K., Quantum dots go large. *Nature* **2009**, 459, (7248), 760-761.
4. Aldana, J.; Wang, Y. A.; Peng, X. G., Photochemical instability of CdSe nanocrystals coated by hydrophilic thiols. *J Am Chem Soc* **2001**, 123, (36), 8844-8850.
5. Xie, R. G.; Kolb, U.; Li, J. X.; Basche, T.; Mews, A., Synthesis and characterization of highly luminescent CdSe-Core CdS/Zn_{0.5}Cd_{0.5}S/ZnS multishell nanocrystals. *J Am Chem Soc* **2005**, 127, (20), 7480-7488.
6. Li, J. J.; Wang, Y. A.; Guo, W. Z.; Keay, J. C.; Mishima, T. D.; Johnson, M. B.; Peng, X. G., Large-scale synthesis of nearly monodisperse CdSe/CdS core/shell nanocrystals using air-stable reagents via successive ion layer adsorption and reaction. *J Am Chem Soc* **2003**, 125, (41), 12567-12575.
7. Miguel, A. S.; Maycock, C.; Oliva, A., Synthesis and Functionalization of CdSe/ZnS QDs Using the Successive Ion Layer Adsorption Reaction and Mercaptopropionic Acid Phase Transfer Methods. In *Nanoparticles in Biology and Medicine. Methods and Protocols.*, in press ed.; Springer: 2012; Vol. 906.
8. Dabbousi, B. O.; RodriguezViejo, J.; Mikulec, F. V.; Heine, J. R.; Mattoussi, H.; Ober, R.; Jensen, K. F.; Bawendi, M. G., (CdSe)ZnS core-shell quantum dots: Synthesis and characterization of a size series of highly luminescent nanocrystallites. *J Phys Chem B* **1997**, 101, (46), 9463-9475.
9. Qu, L. H.; Peng, X. G., Control of photoluminescence properties of CdSe nanocrystals in growth. *J Am Chem Soc* **2002**, 124, (9), 2049-2055.
10. Talapin, D. V.; Rogach, A. L.; Kornowski, A.; Haase, M.; Weller, H., Highly luminescent monodisperse CdSe and CdSe/ZnS nanocrystals synthesized in a hexadecylamine-trioctylphosphine oxide-trioctylphosphine mixture. *Nano Lett* **2001**, 1, (4), 207-211.
11. Uyeda, H. T.; Medintz, I. L.; Jaiswal, J. K.; Simon, S. M.; Mattoussi, H., Synthesis of compact multidentate ligands to prepare stable hydrophilic quantum dot fluorophores. *J Am Chem Soc* **2005**, 127, (11), 3870-3878.
12. Liu, W.; Howarth, M.; Greytak, A. B.; Zheng, Y.; Nocera, D. G.; Ting, A. Y.; Bawendi, M. G., Compact biocompatible quantum dots functionalized for cellular imaging. *J Am Chem Soc* **2008**, 130, (4), 1274-1284.
13. Medintz, I. L.; Uyeda, H. T.; Goldman, E. R.; Mattoussi, H., Quantum dot bioconjugates for imaging, labelling and sensing. *Nature Materials* **2005**, 4, 435-446.
14. Xing, Y.; Chaudry, Q.; Shen, C.; Kong, K. Y.; Zhou, H. E.; WChung, L.; Petros, J. A.; O'Regan, R. M.; Yezhelyev, M. V.; Simons, J. W.; Wang, M. D.; Nie, S., Bioconjugated quantum dots for multiplexed and quantitative immunohistochemistry. *Nat Protoc* **2007**, 2, (5), 1152-1165.
15. Pereira, M.; Lai, E. P., Capillary electrophoresis for the characterization of quantum dots after non-selective or selective bioconjugation with antibodies for immunoassay. *Journal of Nanobiotechnology* **2008**, 6, 10.
16. Puertas, S.; Moros, M.; Fernandez-Pacheco, R.; Ibarra, M. R.; Grazu, V.; de la Fuente, J. M., Designing novel nano-immunoassays: antibody orientation versus sensitivity. *J Phys D Appl Phys* **2010**, 43, (47).
17. Puertas, S.; Batalla, P.; Moros, M.; Polo, E.; del Pino, P.; Guisan, J. M.; Grazu, V.; de la Fuente, J. M., Taking Advantage of Unspecific Interactions to Produce Highly Active Magnetic Nanoparticle - Antibody Conjugates. *Acs Nano* **2011**, 5, (6), 4521-4528.

18. Jana, N. R.; Erathodiyil, N.; Jiang, J.; Ying, J. Y., Cysteine-Functionalized Polyaspartic Acid: A Polymer for Coating and Bioconjugation of Nanoparticles and Quantum Dots. *Langmuir* **2010**, *26*, (9), 6503-6507.
19. Erathodiyil, N.; Ying, J. Y., Functionalization of Inorganic Nanoparticles for Bioimaging Applications. *Accounts Chem Res* **2011**, *44*, (10), 925-935.
20. Moros, M.; Pelaz, B.; Lopez-Larrubia, P.; Garcia-Martin, M. L.; Grazu, V.; de la Fuente, J. M., Engineering bifunctional magnetic nanoparticles for biotechnological applications. *Nanoscale* **2010**, *2*, (9), 1746-1755.
21. Hermanson, G. T., *Bioconjugate techniques*. Academic Press: **2008**.
22. Santos, A. R.; Miguel, A. S.; Tomaz, L.; Malhó, R.; Maycock, C.; Patto, M. C. V.; Fevereiro, P.; Oliva, A., The impact of CdSe/ZnS Quantum Dots in cells of *Medicago sativa* in suspension culture. *Journal of Nanobiotechnology* **2010**, *8*, 24.
23. Santos, A. R.; Miguel, A. S.; Fevereiro, P.; Oliva, A., Evaluation of Cytotoxicity of 3-Mercaptopropionic Acid-Modified Quantum Dots on *Medicago sativa* Cells and Tissues. In *Nanoparticles in Biology and Medicine. Methods and Protocols.*, in press ed.; Springer: 2012; Vol. 906.
24. Kirchner, C.; Liedl, T.; Kudera, S.; Pellegrino, T.; Javier, A. M.; Gaub, H. E.; Stolze, S.; Fertig, N.; Parak, W. J., Cytotoxicity of colloidal CdSe and CdSe/ZnS nanoparticles. *Nano Lett* **2005**, *5*, (2), 331-338.
25. Chaudhuri, R. G.; Paria, S., Core/Shell Nanoparticles: Classes, Properties, Synthesis Mechanisms, Characterization, and Applications. *Chem Rev* **2012**, *112*, (4), 2373-2433.
26. Talapin, D. V.; Lee, J. S.; Kovalenko, M. V.; Shevchenko, E. V., Prospects of Colloidal Nanocrystals for Electronic and Optoelectronic Applications. *Chem Rev* **2010**, *110*, (1), 389-458.
27. Wu, P. K.; Ringeisen, B. R.; Krizman, D. B.; Frondoza, C. G.; Brooks, M.; Bubb, D. M.; Auyeung, R. C. Y.; Pique, A.; Spargo, B.; McGill, R. A.; Chrisey, D. B., Laser transfer of biomaterials: Matrix-assisted pulsed laser evaporation (MAPLE) and MAPLE Direct Write. *Rev Sci Instrum* **2003**, *74*, (4), 2546-2557.
28. Gyorgy, E.; del Pino, A. P.; Roqueta, J.; Ballesteros, B.; Miguel, A. S.; Maycock, C. D.; Oliva, A. G., Synthesis and Laser Immobilization onto Solid Substrates of CdSe/ZnS Core Shell Quantum Dots. *J Phys Chem C* **2011**, *115*, (31), 15210-15216.

Chapter 7

Appendix

Published papers related with this dissertation:

- I. Ana R. Santos, **Ana S. Miguel**, Leonor Tomaz, Rui Malhó, Christopher Maycock, Maria C. Vaz Patto, Pedro Fevereiro and Abel Oliva. The impact of CdSe/ZnS Quantum Dots in cells of *Medicago sativa* in suspension culture. *Journal of Nanobiotechnology* 2010, 8:24.
- II. E. György, A. Perez del Pino, J. Roqueta, B. Ballesteros, **A. S. Miguel**, C. D. Maycock, and A. G. Oliva. Synthesis and Laser Immobilization onto Solid Substrates of CdSe/ZnS Core-Shell Quantum Dots. *Journal of Physical Chemistry C*, 2011, 115, 15210-15216.
- III. E. György, J. Roqueta, B. Ballesteros, A. Perez del Pino, **A.S. Miguel**, C. Maycock and A.G. Oliva. Synthesis and characterization of CdSe/ZnS quantum dots immobilised on solid substrates through laser irradiation. *Physica Status Solidi A*, 2012, 1-7.

Book chapters by invitation related with this dissertation:

- IV. **Ana Sofia Miguel**, Christopher Maycock and Abel Oliva. Synthesis and Functionalization of CdSe/ZnS QDs Using the Successive Ion Layer Adsorption Reaction and Mercaptopropionic Acid Phase Transfer Methods. *Nanoparticles in Biology and Medicine: Methods and Protocols, Methods in Molecular Biology, 906, Part 2, 143-155*, 2012, Springer.
- V. Ana Raquel Santos, **Ana Sofia Miguel**, Pedro Fevereiro and Abel Oliva. Evaluation of Cytotoxicity of 3-Mercaptopropionic Acid-Modified Quantum Dots on *Medicago sativa* Cells and Tissues. *Nanoparticles in Biology and Medicine: Methods and Protocols, Methods in Molecular Biology, 906, Part 5, 435-449*, 2012, Springer.

Submitted papers related with this dissertation:

- VI. Ana Raquel Santos*, **Ana Sofia Miguel***, Anca Macovei*, Christopher Maycock, Alma Balestrazzi, Abel Oliva and Pedro Fevereiro. CdSe/ZnS Quantum Dots trigger DNA repair and antioxidant enzyme

systems in *Medicago sativa* cells in suspension culture. *Particle and Fibre Toxicology*, 2012 (submitted). *Authors contributed equally.

RESEARCH

Open Access

The impact of CdSe/ZnS Quantum Dots in cells of *Medicago sativa* in suspension culture

Ana R Santos^{1,2*}, Ana S Miguel^{1,3}, Leonor Tomaz², Rui Malhó⁴, Christopher Maycock^{3,4}, Maria C Vaz Patto², Pedro Fevereiro^{2,4}, Abel Oliva¹

Abstract

Background: Nanotechnology has the potential to provide agriculture with new tools that may be used in the rapid detection and molecular treatment of diseases and enhancement of plant ability to absorb nutrients, among others. Data on nanoparticle toxicity in plants is largely heterogeneous with a diversity of physicochemical parameters reported, which difficult generalizations. Here a cell biology approach was used to evaluate the impact of Quantum Dots (QDs) nanocrystals on plant cells, including their effect on cell growth, cell viability, oxidative stress and ROS accumulation, besides their cytotoxicity.

Results: A plant cell suspension culture of *Medicago sativa* was settled for the assessment of the impact of the addition of mercaptopropionic acid coated CdSe/ZnS QDs. Cell growth was significantly reduced when 100 mM of mercaptopropionic acid -QDs was added during the exponential growth phase, with less than 50% of the cells viable 72 hours after mercaptopropionic acid -QDs addition. They were up taken by *Medicago sativa* cells and accumulated in the cytoplasm and nucleus as revealed by optical thin confocal imaging. As part of the cellular response to internalization, *Medicago sativa* cells were found to increase the production of Reactive Oxygen Species (ROS) in a dose and time dependent manner. Using the fluorescent dye H₂DCFDA it was observable that mercaptopropionic acid-QDs concentrations between 5-180 nM led to a progressive and linear increase of ROS accumulation.

Conclusions: Our results showed that the extent of mercaptopropionic acid coated CdSe/ZnS QDs cytotoxicity in plant cells is dependent upon a number of factors including QDs properties, dose and the environmental conditions of administration and that, for *Medicago sativa* cells, a safe range of 1-5 nM should not be exceeded for biological applications.

Background

Nanotechnology is a fast-developing industry, having substantial impact on the economy, society and the environment [1] and predictions so far exceed the Industrial Revolution, with a \$1 trillion market by 2015 [2]. Nanotechnology has the potential to revolutionize the agricultural and food industry with new tools for the molecular treatment of diseases, rapid disease detection and enhancing plant ability to absorb nutrients. Smart sensors and smart delivery systems will help the

agricultural industry to fight viruses and other crop pathogens [3].

However, the novel size-dependent properties of nanomaterials, that make them desirable in technical and commercial uses, also create concerns in terms of environmental and toxicological impact [4].

Nanotoxicology is emerging as an important subdiscipline of nanotechnology and involves the study of the interactions of nanostructures with biological systems. Nanotoxicology aims on elucidating the relationship between the physical and chemical properties of nanostructures with the induction of toxic biological responses [5]. This information is important to characterize nanomaterial in biotechnology, ecosystems, agriculture and biomedical applications [6].

* Correspondence: raquelsantos@itqb.unl.pt

¹Biomolecular Diagnostics Laboratory, Instituto de Tecnologia Química e Biológica, Universidade Nova de Lisboa, Apartado 127, 2781-901 Oeiras, Portugal

Full list of author information is available at the end of the article

The few studies conducted to date on the effects of nanoparticles on plants have focused mainly on phytotoxicity and how certain plant metabolic functions are affected. The reported effects vary depending on the type of nanoparticle, as well as plant species, and are inconsistent among studies [2]. So far, there is only one report of nanoparticle toxicity in cells of a photosynthetic organism, the green microalgae *Chlamydomonas reinhardtii*, in which the toxicity of two types of widely used nanomaterials (TiO₂ and CdTe) was evaluated [7]. No data is available concerning toxicology of Quantum Dots (QDs) in higher plant cells [8].

QDs are inorganic semiconductor nanocrystals, typically composed of a cadmium selenide (CdSe) core and a zinc sulphide (ZnS) shell and whose excitons (excited electron-hole pairs) are confined in all three dimensions, giving rise to characteristic fluorescent properties. QDs are extremely photostable, bright and are characterized by broad absorption profiles, high extinction coefficients and narrow and spectrally tunable emission profiles [9].

Cell-based in vitro studies play an essential role on meaningful toxicity testing. They allow the setting up of high-throughput systems for rapid and cost-effective screening of hazards, while targeting the biological responses under highly controlled conditions [4]. The evaluation of five categories of cellular response, including reactive oxygen species (ROS) production and accumulation, cell viability, cell stress, cell morphology, and cell-particle uptake, are central themes in such testing [10].

Aiming to develop a nano-strategy using coated QDs conjugated with specific biomolecules to precociously identify the presence of fungal infections in *Medicago sativa* (a perennial pulse with economic relevance) we established a fine plant cell suspension culture that was subsequently used to investigate the potential cytotoxicity of CdSe/ZnS Mercaptopropionic acid coated QDs and its uptake at cellular level.

Methods

Cell suspension culture establishment

Cell suspension cultures were established from a *Medicago sativa* line M699, seeds being kindly provided by Diego Rubiales (IAS-CSIC, Spain). Well-developed petioles from 25 day old in vitro germinated M699 seedlings were used as explants for callus induction. Petioles were placed in solid Murashige & Skoog (M&S) medium supplemented with 0.5 mg/L of 2,4-D and kinetin and 5 mg/L of dithiothreitol, maintained in growth chamber under a 16 hours photoperiod and a day/night temperature of 24°/22°C (Phytotron Edpa 700, Aralab, Portugal).

Two friable portions of 8 weeks old dark grown callus from petioles were placed in a 250 mL Erlenmeyer flask with 50 mL of liquid M&S medium, supplemented with the same growth hormone composition used for callus

phase. The flasks were maintained in an orbital shaker at 110 rpm (Innova 4900, New Brunswick Scientific, Germany) in the dark, at 24°C. After 10 days, 100 mL of fresh medium was added. 10 days later, 100 mL of fresh medium was added to 20 mL of decanted cell suspension culture. Until an adequate cell density was obtained, the cells were pelleted and medium replaced every 8/9 days. When stabilized, suspensions were sub cultured every 8 days transferring 20 mL to 100 mL of fresh medium (in 250 mL Erlenmeyer flasks). Growth regulators were always filter sterilized through 0.2 µm Orange Scientific filters and added to cooled autoclaved medium (20 minutes at 121°C). These cell suspension cultures will be referred to as stock.

Synthesis, solubilisation and characterization of CdSe/ZnS core shell QDs

All chemicals unless indicated were obtained from Sigma-Aldrich and used as received. UV-vis absorbance spectra were taken using a Beckman DU-70. Photoluminescence spectra were recorded with a SPEX Fluorolog spectrofluorimeter.

TOPO/HDA - capped CdSe nanocrystals were synthesized using standard procedures [11]. This typically generates CdSe nanocrystals with the first absorption peak around 580-590 nm and a diameter of 3.6-4.5 nm. For the synthesis of core-shell CdSe/ZnS QDs, the cores obtained were monodisperse after passivation with at least 5 monolayers of ZnS. Passivation was obtained using the SILAR method [12] that consists of alternating injections of Zn and S precursors to the solution containing CdSe-core nanocrystals suspended in octadecene/hexadecylamine. After extraction with methanol, centrifugation and decantation, the particles were dispersed in chloroform for further processing.

The Mercaptopropionic acid coated nanocrystals were synthesized by the phase transfer method as described previously [12]. The obtained Mercaptopropionic acid coated CdSe/ZnS QDs were then concentrated using a Sartorius Vivaspin 6 tube (cutoff 10 kDa) at 7.500 g.

For the characterization of the synthesized CdSe/ZnS QD nanoparticles Transmission Electron Microscopy (TEM) was used. Low resolution images were obtained using a JEOL 200CX traditional TEM operating at an acceleration voltage of 200 kV.

Quantum yields were measured relative to Rhodamine 6G with excitation at 530 nm. Solutions of QDs in chloroform or water and dye in ethanol were optically matched at the excitation wavelength ($\lambda = 530$ nm).

Dynamic Light Scattering (DLS) analysis was performed using a Nano series dynamic light scatterer from Malvern. With this equipment the hydrodynamic diameter (HD) and zeta potential (ξ) of synthetic CdSe/ZnS and their corresponding Mercaptopropionic acid coated

particles were measured. For the HD analyses all the samples were between 0.06 and 0.3 μM and filtered through a 0.2 μm filter before analyses. HD were obtained from number-weighted size distribution analysis and reported as the mean of triplicate measurements. ξ -Potential for Mercaptopropionic acid coated QDs with concentration between 0.06 and 0.3 μM were measured in H_2O Milli-Q basified to $\text{pH} = 12$. Values are reported as the average of triplicate runs consisting of 20 runs at 25°C . Similarly, the ξ -potential of the mercaptopropionic acid-QDs in M&S medium was measured using the DLS equipment. Value reported is the average of triplicate runs consisting of 14 runs at 25°C .

Imaging and Microscopy settings

Unless stated otherwise, images were acquired in a Nikon Eclipse TE2000-S (Japan) inverted microscope equipped with a HMX-4 100 W Mercury lamp and appropriate filter settings. Images were acquired with an Evolution MP 5.1 megapixel digital CCD Color Camera (Media Cybernetics) controlled by Image Pro Plus 5.0 software (Media Cybernetics).

Thin time-course confocal optical sections ($\sim 2 \mu\text{m}$ thick) were acquired with a Leica SP-E Confocal Laser Scanning Microscope using $<20\%$ laser intensity and operating in the mode 1024×1024 , 400 Hz ($\sim 1/2$ sec per frame). A $\times 20$ Plan Apo dry objective ($\text{NA} = 0.75$) (Leica) was used. For quantification purposes, gain and offset settings were kept constant so that the average background pixel intensity was between 0 and 10 and the fluorescent signal coming from the cells was between 60 and 220 (0-255 scale for 8 bit images).

Effect of Mercaptopropionic acid-QDs supplement on the plant cell growth

A 250 mL Erlenmeyer flask with 120 mL of 8 days old *M. sativa* cell suspension culture was randomly taken from the stock and 4 mL aliquots were inoculated in five 100 mL Erlenmeyer flasks containing 20 mL of fresh medium. Three days after sub-culture a suspension of mercaptopropionic acid -QDs was added to two of the five Erlenmeyer flasks in order to obtain the final concentration of 100 nM in the culture medium. At day 8 of culture they were sub-cultured by gentle setting and addition of 20 mL of fresh medium. Then, every day, and during 8 days, small aliquots (about 0.5 mL) of the five Erlenmeyers were taken and cells were counted (three counts per aliquot) in a Neubauer Chamber. This allowed to establish a growth curve for the *M. sativa* cells culture.

Effect of Mercaptopropionic acid-QDs supplement on the plant cell viability

Cell viability was assessed through the activity of cytoplasmic esterases that hydrolyze FDA to yield the

fluorescent product fluorescein, which accumulates intracellularly if the cell membrane remains functional [13].

A 250 mL Erlenmeyer flask with 120 mL of a 8 days old *M. sativa* cell suspension culture was randomly taken from the stock and 2 mL aliquots were inoculated in five 50 mL Erlenmeyer flasks containing 10 mL of fresh medium. After 3 days of subculture a suspension of mercaptopropionic acid -QDs was added to two Erlenmeyer flasks in order to obtain the final concentration of 100 nM in the culture medium. Before adding the mercaptopropionic Acid-QDs and every day after, viability of the cultures was checked using the Fluorescein Diacetate (FDA) method [14].

A stock solution of FDA was prepared by adding 10 mg of FDA and 2 mL of acetone and kept at -20°C . A diluted solution of FDA was then freshly prepared at the time of the assay, adding 20 μL of the stock solution to 1 mL of MS medium. Finally, a drop of both suspension culture and diluted FDA was placed on a microscope slide. The counts were performed using an inverted microscope, with excitation at 488 nm. Two preparations were made from each Erlenmeyer and the number of viable cells was counted in five random spots per microscope slide.

QDs uptake by the plant cells

A 250 mL Erlenmeyer flask with 120 mL of 4 days old *M. sativa* suspension culture was randomly taken from the stock. From this flask, 2 mL aliquots were placed in 50 mL Erlenmeyer flasks (in triplicate), and a volume of mercaptopropionic acid -QDs to obtain the final concentration of 10 nM was added. After 48 hours samples were visualized using a confocal and an inverted microscope.

Effect of mercaptopropionic acid-QDs supplement on ROS accumulation and oxidative stress

ROS formation in cultures exposed to the mercaptopropionic acid-QDs was evaluated using three different probes: 3,3'-diaminobenzidine (DAB) and nitroblue tetrazolium (NBT) that are specific to hydrogen peroxide (H_2O_2) and superoxide anion ($\text{O}_2^- \cdot$) respectively, and 2',7'- Dichlorodihydrofluorescein diacetate (H_2DCFDA) that is a nonspecific probe for ROS accumulation.

All assays were carried out in 6 well plates (Orange Scientific) to reduce the experimental volume and subsequently the amount of mercaptopropionic acid-QDs required. This also allowed performing the assays in a standard and randomized approach.

For each experiment two controls were prepared. A negative control was used consisting of cells placed in the same conditions as the assay but without the addition of mercaptopropionic acid-QDs. As a positive control, cells were heated at 45°C during 20 minutes.

1) H₂O₂ detection

Production of H₂O₂ at the cellular level was examined by applying the (DAB) staining technique described by Thordal-Christensen *et al.* [15], with few modifications. DAB reacts rapidly with H₂O₂ in the presence of peroxidase, forming a brown polymerized product.

A 250 ml flask with 120 mL of 7 days old cell suspension culture of *M. sativa* was randomly taken from the stock to establish the following experimental setup: 2 mL of suspension culture plus 0.1 mg/mL of DAB (negative control), 2 mL of suspension culture treated 45°C for 20 minutes plus 0.1 mg/mL of DAB (positive control), 2 mL of suspension culture plus 10 mM of H₂O₂ plus 0.1 mg/mL of DAB and 2 mL of suspension culture plus 32.6 µL of mercaptopropionic acid-QDs to a final concentration 100 nM plus 0.1 mg/mL of DAB. All samples were placed in sterilized 6 well plates (in triplicate), in an orbital shaker at 110 rpm, in the dark, at 24°C. After 1 hour and half, samples were taken from each assay and observed using an inverted microscope.

2) O₂⁻ • detection

The detection of O₂⁻ • was carried out as described by Fryer *et al.* [16] with slight modifications, and similarly to the DAB assay.

Nitro-substituted aromatics such as nitroblue tetrazolium can be reduced by O₂⁻ • to the monoformazan (NBT⁺) [17,18], with the accumulation of dark spots of blue formazan [19].

A 250 ml flask with 120 mL of 7 days old cell suspension culture of *M. sativa* was randomly taken from the stock to establish the following experimental setup: 2 mL of suspension culture with a final concentration of NBT of 60 nM (negative control), 2 mL of suspension culture treated 45°C for 20 minutes with a final concentration of NBT of 60 nM (positive control), 2 mL of suspension culture plus 32.6 µL of mercaptopropionic acid-QDs to a final concentration of 100 nM plus a final concentration of NBT of 60 nM. All samples were placed in sterilized 6 well plates (in triplicate), in the orbital shaker at 110 rpm, in the dark, at 24°C. After 4 hours samples were visualized using an inverted microscope in bright field.

3) Cellular oxidative stress assay

2',7'- Dichlorodihydrofluorescein diacetate (H₂DCFDA) was used to determine cellular oxidative stress as described by Ortega-Villasante *et al.* [20], using the same procedure as for the previous assay, but adding 5 µM of H₂DCFDA instead of NBT. After 1 hour and half samples were visualized using an inverted microscope ($\lambda_{\text{ex}} = 488$ and $\lambda_{\text{em}} = 525$ nm).

H₂DCFDA diffuses passively through the cellular membrane and then is enzymatically hydrolysed by intracellular esterases to 2',7'-dichlorodihydrofluorescein (DCFH). This nonfluorescent product is converted by

ROS into DCF (2',7'-dichlorofluorescein), which can easily be visualized by a strong fluorescence around 525 nm when excited at 488 nm.

The NBT and H₂DCFDA assays were repeated for longer periods of exposure of cell suspension cultures to the mercaptopropionic acid-QDs. A 250 mL flask with 120 mL of 8 days old cell suspension culture was randomly taken from the stock, 4 mL and 20 mL aliquots were inoculated in a 100 mL and 250 mL Erlenmeyer flask containing 20 mL and 100 mL of fresh medium, respectively. Three days after subculture a suspension of mercaptopropionic acid -QDs to obtain the final concentration of 100 nM in the culture medium was added to the Erlenmeyer flask containing 24 mL of cell suspension culture. Finally, on 5th and 6th day the same experimental protocol described above for the two probes was applied.

4) Oxidative stress dose response assay

A 250 mL flask with 120 mL of 3 days old cell suspension culture was randomly taken from the stock. 2 mL (in triplicate) were placed in sterilized 6 well plates. Aliquots of mercaptopropionic acid -QDs were added to each well to obtain the following final concentrations: 1 nM, 5 nM, 10 nM, 20 nM, 40 nM, 60 nM, 100 nM, 120 nM and 180 nM. All plates were placed on an orbital shaker at 110 rpm in the dark at 24°C. After 48 hours of incubation, an aliquot of H₂DCFDA, to obtain a final concentration of 5 µM, was added to all treatments including to the negative and positive (cells heat treated 45°C for 20 minutes) controls. After 1 hour, samples from each treatment were visualized using an inverted microscope and the fluorescence was quantified in terms of average pixel intensity, using the commercial program ImageJ. Images were acquired 1 hour after the H₂DCFDA addition, always with the same settings and exposure time.

Statistical analysis

All results are presented as the mean ± standard deviation (SD). One-way ANOVA was used to test for significant differences among average fluorescence intensity (Microsoft Office Excel 2007). The result was considered significant if $p < 0.001$, when compared to the control.

Results and Discussion

mercaptopropionic acid-QD stability

The mercaptopropionic acid -QDs used in this work had a size distribution between 4 and 6 nm (Fig. 1a) and a quantum yield of 7% (relative to Rhodamine 6G) (Fig. 1b).

The properties of nanomaterials can change, sometimes dramatically, when placed in contact with biological systems [21]. Nanoparticle aggregation influences their uptake by cells, and variables such as the surface

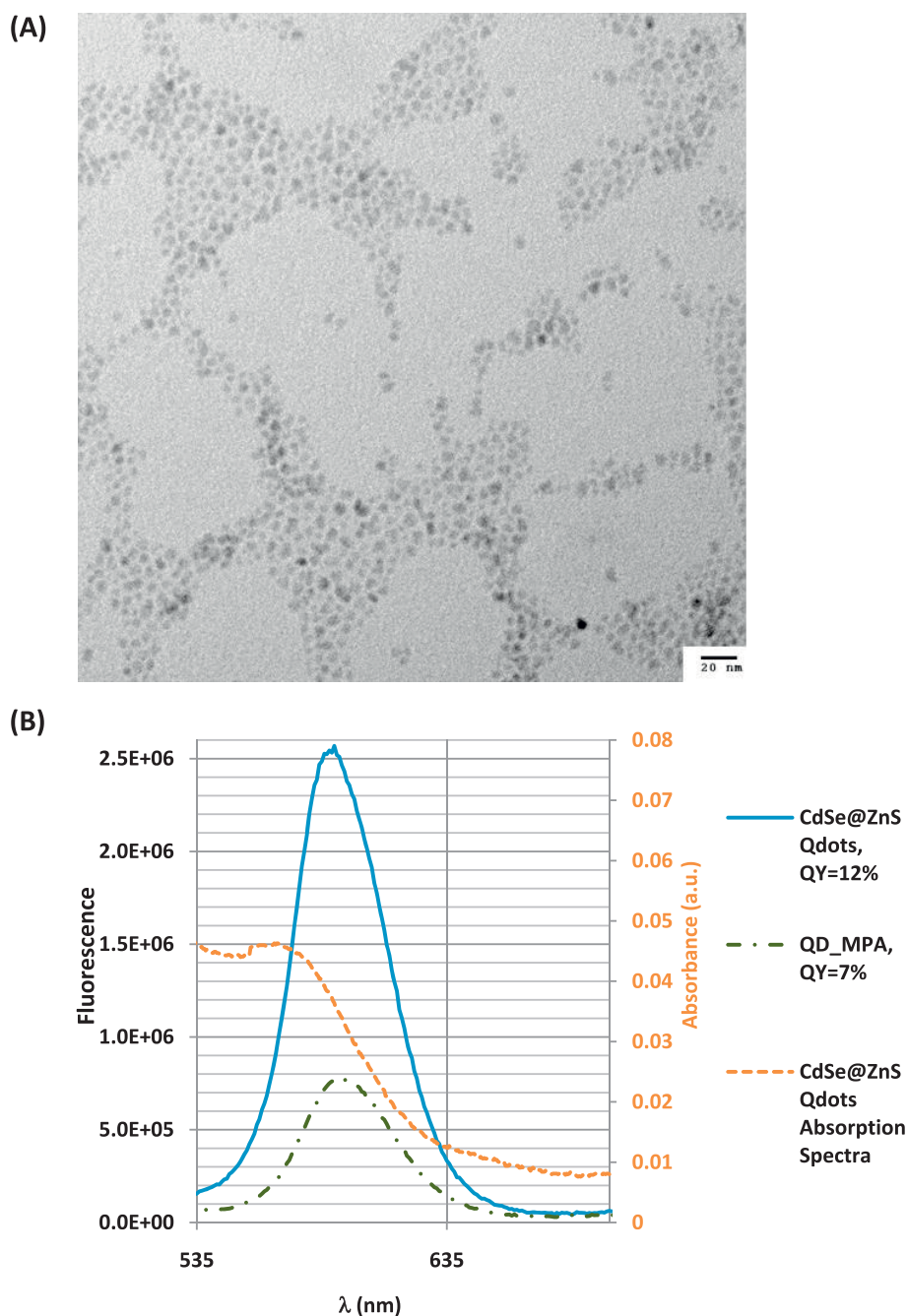


Figure 1 Characterization of the synthesized CdSe/ZnS QD nanoparticles. (A) TEM image (acceleration voltage of 200 kV) of CdSe cores after 5 monolayers of ZnS. (B) Emission spectra and quantum yields for synthetic CdSe/ZnS and their corresponding hydrophilic QDs. The orange spectra is an example of UV-Vis spectra with $abs = 0,05$ at the excitation wavelength (530 nm).

ligands and the solution composition influence nanoparticle suspension stability [22]. Assessment of mercaptopropionic acid-QD stability and aggregation under the assay conditions was then necessary to correctly interpret their biological effects.

Mercaptopropionic acid-QDs were supplied in water with a zeta (ζ) potential of -45,6 mV (Table 1), but

introduction into the M&S culture medium decreased the ζ and the mercaptopropionic acid-QDs tended to aggregate, particularly when applied to the culture at relatively high concentrations. The ζ potential of the culture medium was -12.5 mV, well under the absolute value of [25 mV], above which the system is considered to be in a disperse state.

Table 1 Results of size and zeta potential measurements for synthetic CdSe/ZnS and their corresponding hydrophilic QDs in water.

Sample	Hydrodynamic diameter (nm)	ζ -Potential (mV)
CdSe/ZnS (CHCl ₃)	9,3	-
MPA- QD (H ₂ O)	13,5	-45,6

The QD surface coating is also considered a critical factor for the extent and time scale of their potential cytotoxicity. Mercaptopropionic acid is known to be one of the smallest ligands among deprotonated thiols (thiolates) most often used to stabilize QDs in solution [23].

Effect of mercaptopropionic acid-QDs on cell growth

The mercaptopropionic acid-QD concentration used in this study (100 nM) was one order of magnitude higher than those often referred to in the literature [24,25]. It was adopted to ensure that an impact on cell viability could be detected since experiments with lower concentrations did not reveal any consistent effects (data not shown).

At the end of the cell cycle (8 days), cell suspensions grown in the presence of mercaptopropionic acid-QDs showed a reduced biomass production compared to the control and all isolated cells were plasmolyzed (data not shown). However, when cells grown with or without the

mercaptopropionic acid-QDs, were sub-cultured, all the suspensions (test and control) showed similar growth parameters (Fig. 2b). Both cultures had comparable growth profiles (Fig. 2a) but those previously treated with mercaptopropionic acid-QDs started the exponential growth phase one day sooner and reached the stationary phase earlier.

These results suggest that cultures recovered from QD damage in the second cell growth cycle which could be explained by the observed cell aggregation after the addition of the mercaptopropionic acid-QDs. Cell aggregation can be interpreted as a response by plant cells to the presence of mercaptopropionic acid-QDs, which may induce cell wall lignification and crosslinking of cell wall components. Cell aggregation was also reported in *Chlamydomonas reinhardtii* cultures in the presence of CdTe and TiO₂ nanoparticles [7]. Cellular aggregation will provide greater protection against toxic agents, particularly for cells in the middle of the aggregates. These cells will be able to act as a viable *inoculum* when subcultured in fresh culture medium.

Effect of mercaptopropionic acid-QDs on cell viability

Twenty four hours after the exposure to 100 nM of mercaptopropionic acid -QDs, cell viability had already been reduced by 6% (Fig. 3).

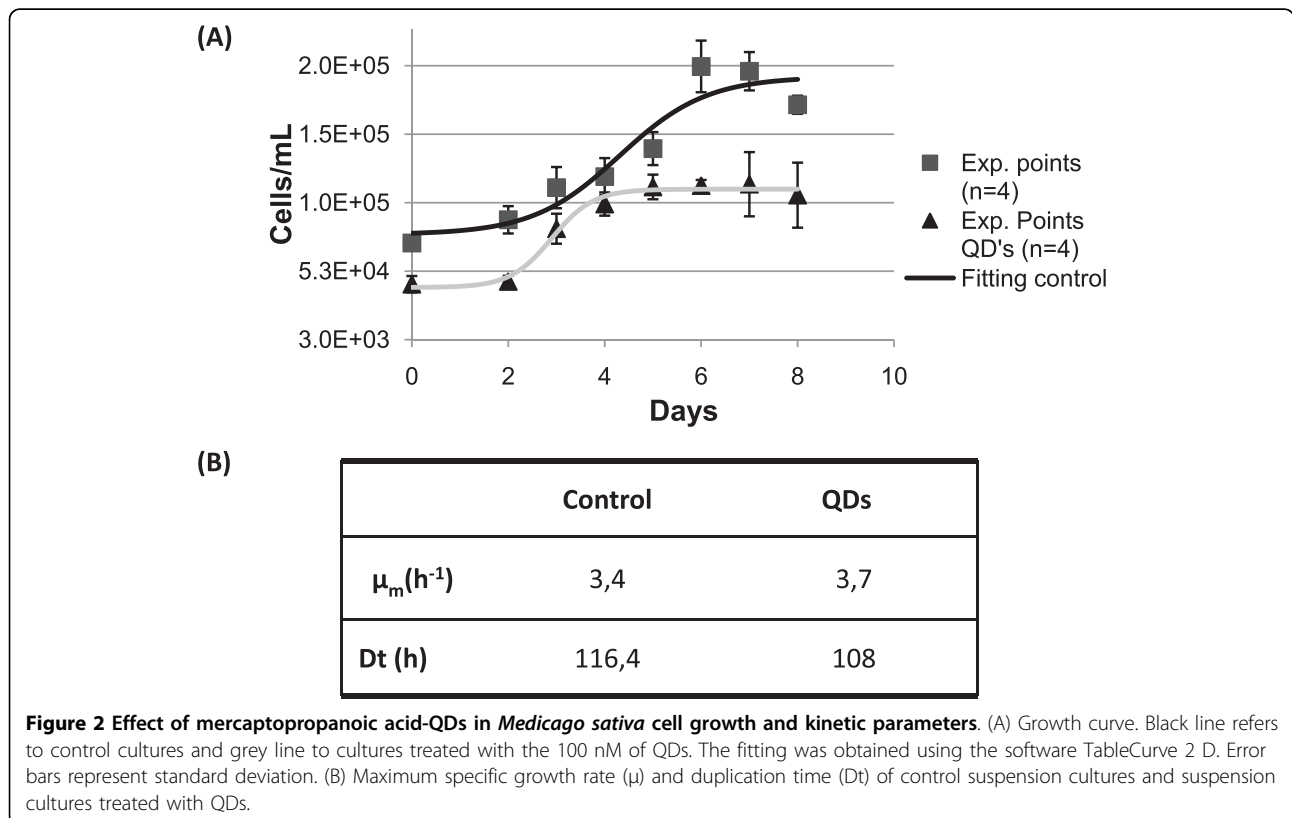


Figure 2 Effect of mercaptopropionic acid-QDs in *Medicago sativa* cell growth and kinetic parameters. (A) Growth curve. Black line refers to control cultures and grey line to cultures treated with the 100 nM of QDs. The fitting was obtained using the software TableCurve 2 D. Error bars represent standard deviation. (B) Maximum specific growth rate (μ) and duplication time (Dt) of control suspension cultures and suspension cultures treated with QDs.

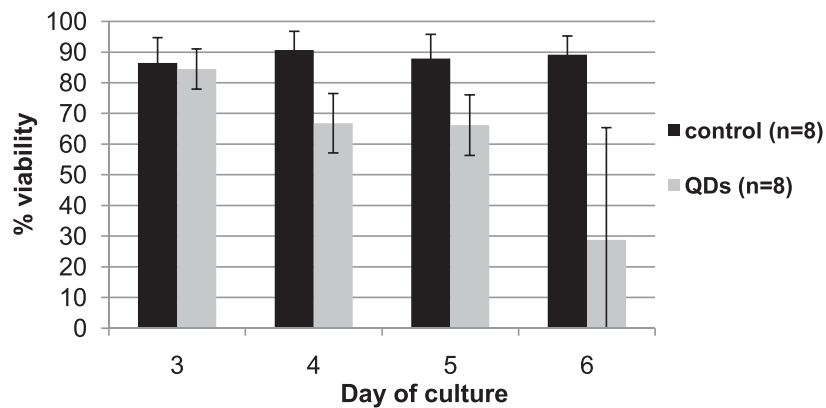


Figure 3 Effect of 100 nM of mercaptopropionic acid-QDs on cell viability determined with FDA method. Black line refers to control cultures and grey line to cultures treated with the QDs. Day 3 counts were performed before the QD addition. Error bars represent standard deviation.

After 72 hours in contact with mercaptopropionic acid-QDs, isolated cells, or cells in small aggregates, were not viable and most of them were plasmolysed. Less than 50% of the isolated cells were viable when compared with the control. However, most cells were found in large clusters. These clusters seemed to be viable, despite the significant decrease in fluorescence intensity when compared to the control (data not shown). This explains why subcultures previously subjected to mercaptopropionic acid-QDs continued to grow. Cell aggregation seemed to guarantee in this case a certain level of protection against toxicity probably

due to a certain impermeabilization of the cell wall in response to the imposed stress, as suggested previously.

Envisaging the application of this type of mercaptopropionic acid-QDs to plant organs our results showed that elevated concentrations of mercaptopropionic acid-QDs reduced significantly plant cell viability, mainly in cases where cells were isolated. They also showed that some cells in aggregates maintain a certain degree of viability.

Quantum dot uptake

M. sativa cells internalized mercaptopropionic acid-QDs as shown in Fig. 4a and 4b. Fluorescent spots due

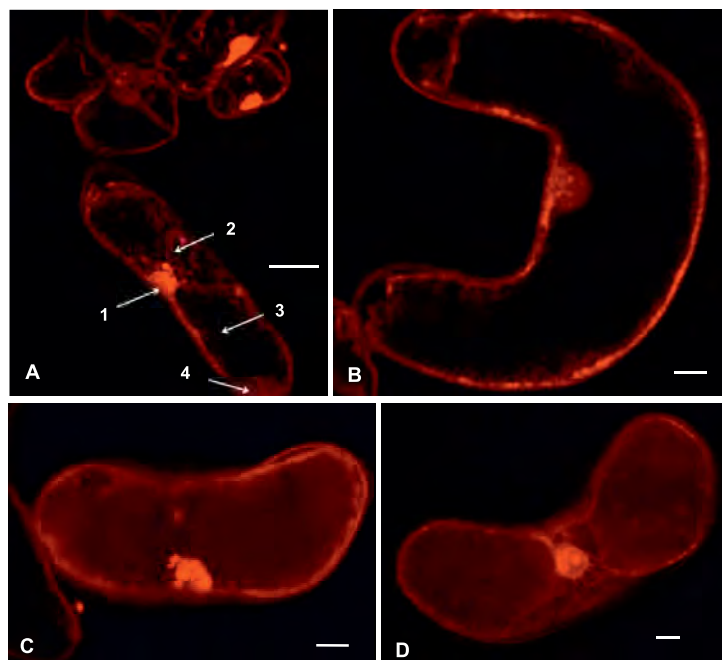


Figure 4 Confocal (A, B) and wide field (C, D) fluorescence images of *M. sativa* cells after 48 hours of incubation with 10 nM of mercaptopropionic acid-QDs showing QD internalization. Arrows point to 1- nucleus, 2- cytoplasmic strands, 3- vacuole and 4- hyaloplasm. Scale bar = 20 μ M.

to mercaptopropionic acid-QDs could be observed mainly in the nucleus and in the cytosol. Also cytoplasmic strands presented fluorescent particles, the vacuole, which occupies the majority of the cell volume, being the exception.

Images acquired using the inverted microscope (Fig. 4c and 4d) clearly showed the fluorescence of mercaptopropionic acid-QDs in several structures, such as the nucleus and nucleolus, the cytoplasm and cytoplasmic strands. In a recent study on the biogenic uptake of platinum (Pt), the roots of *Medicago sativa* were found to accumulate Pt *in vivo* in the form of nanoparticles on cell walls and organelles [24].

When the putative cytotoxicity of nanoparticles is determined, it is prudent to consider whether cells do in fact encounter individual nanoparticles, in contrast to aggregates of several nanoparticles; this becomes particularly relevant when studying internalization. Therefore it is necessary to have in mind that if the nanoparticles had not aggregated in the culture medium, probably more cells would internalize them.

ROS accumulation and oxidative stress

1) H_2O_2 detection

Cells treated with DAB (Fig. 5b), in the absence of any oxidative stress, did not present the typical brown precipitate. Cells heat treated for 20 min at 45°C with subsequent addition of DAB (Fig. 5c), showed a brownish colour as well as precipitates indicative of oxidative stress due to H_2O_2 presence. Cells treated with 10 mM of H_2O_2 , followed by the addition of DAB, showed the same brown precipitate (Fig. 5d) confirming that the cells were able to metabolize H_2O_2 .

The addition of 100 nM of mercaptopropionic acid-QDs to *M. sativa* cells did not seem to induce H_2O_2 production, as illustrated in Fig. 6. The resulting orange/brownish coloration around the cells was due to precipitated mercaptopropionic acid-QDs, which was confirmed by comparing the UV light picture (upper) with the UV image of cells and DAB (lower) where no orange coloured spots were detected.

The comparison of the cells reaction in the presence of mercaptopropionic acid-QDs with the reaction when H_2O_2 was added to the culture, led to the conclusion that the production of H_2O_2 induced by the addition of mercaptopropionic acid-QDs is far less than 10 mM, if any.

2) $O_2^- \cdot$ detection

After heating at 45°C for 20 minutes, cells exhibited dark blue formazan spots (Fig. 7b). These deposits indicated that $O_2^- \cdot$ was produced by the cells in response to heat stress, since no spots were seen in the controls (Fig. 7a). The presence of formazan deposits indicate that in these cells the rate of $O_2^- \cdot$ production had

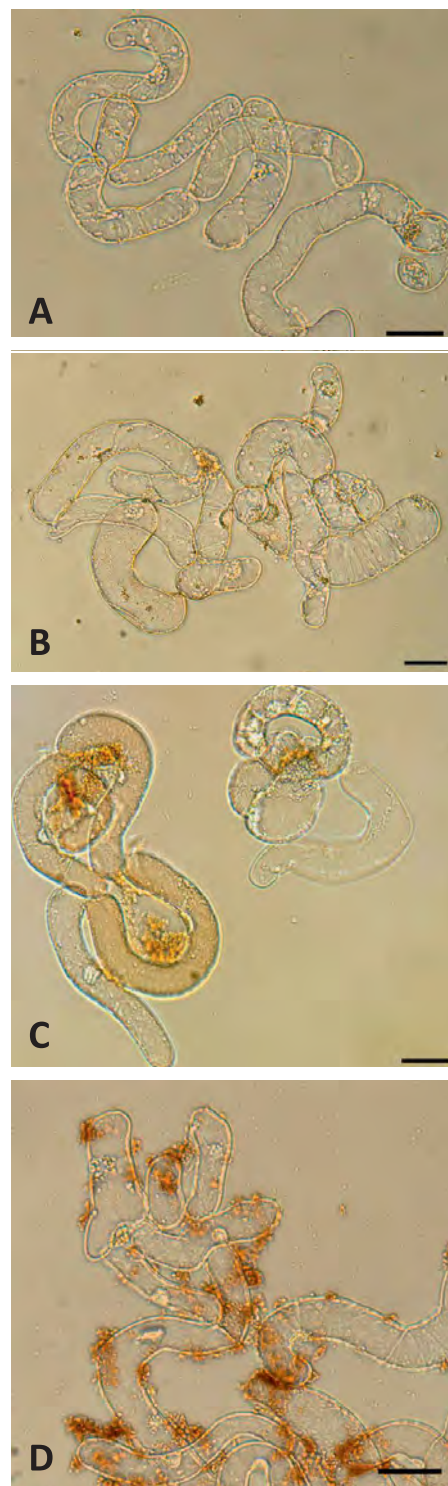


Figure 5 Cell suspension culture controls for the DAB assay. (A) Without treatment. (B) Treated with DAB (negative control). (C) Heat-treated (45°C for 20 minutes) to induce the production of H_2O_2 (positive control). (D) Treated with 10 mM H_2O_2 and DAB to visualize the peroxidase activity. All experiments were visualized 1 hour and half after the addition of DAB, in bright field. Scale bar = 50 μ M.

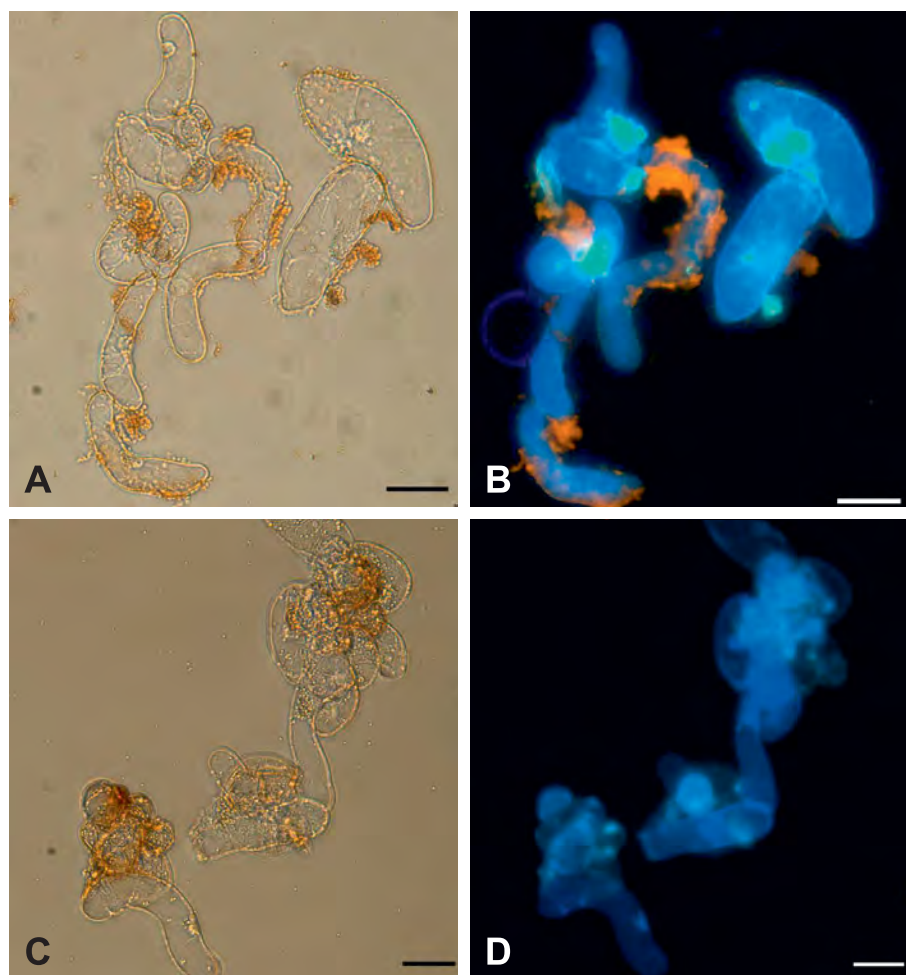


Figure 6 DAB assay for H_2O_2 detection. (A, B) Cell suspension culture treated with 100 nM of QDs plus DAB. (C,D) Cell suspension culture treated only with DAB. The orange/brownish precipitates around cells are QDs and not due to the DAB polymerization as revealed by UV light excitation. Scale bar = 50 μ M.

become significantly greater than the rate of detoxification [16].

Studies that applied the NBT technique were mainly focused on evaluating responses in plant tissues rather than in single cells. The few reports in cell suspension cultures that used this technique quantified the response spectrophotometrically, rather than study the precise location of the formazan deposits [26,19].

In *M. sativa* cell suspension cultures treated with mercaptopropionic acid-QDs, no blue formazan spots were detected, as shown in Fig. 7c, which could suggest that the interaction of 100 nM of mercaptopropionic acid-QDs did not induce the formation of $O_2^{\cdot -}$ after 4 hours of exposure. Also cultures exposed to mercaptopropionic acid-QDs for 48 and 72 hours (Fig. 7d and 7e respectively) did not show any noticeable production of $O_2^{\cdot -}$ since no blue formazan spots were detected.

A previous study [27] on the generation of free radicals (in an aqueous, cell-free system) by three types of mercaptopropionic acid-QDs revealed that while CdS QDs apparently had sufficient redox power to generate hydroxyl and superoxide radicals, CdSe QDs exclusively generate hydroxyl radicals.

Chloroplasts are a major site for ROS generation in plants due to the photosynthesis process. Peroxisomes and glyoxysomes are other major sites of ROS generation in plants during photorespiration and fatty acid oxidation, respectively [28]. However plant cell cultures used in this work are dark grown and therefore do not have differentiated chloroplasts. This also may explain why no $O_2^{\cdot -}$ was found in our system.

3) Cellular oxidative stress assay

When treated with H_2DCFDA , control cells showed a basal-level fluorescent signal (Fig. 8a) that accumulated uniformly in the cytoplasm. This has been also reported

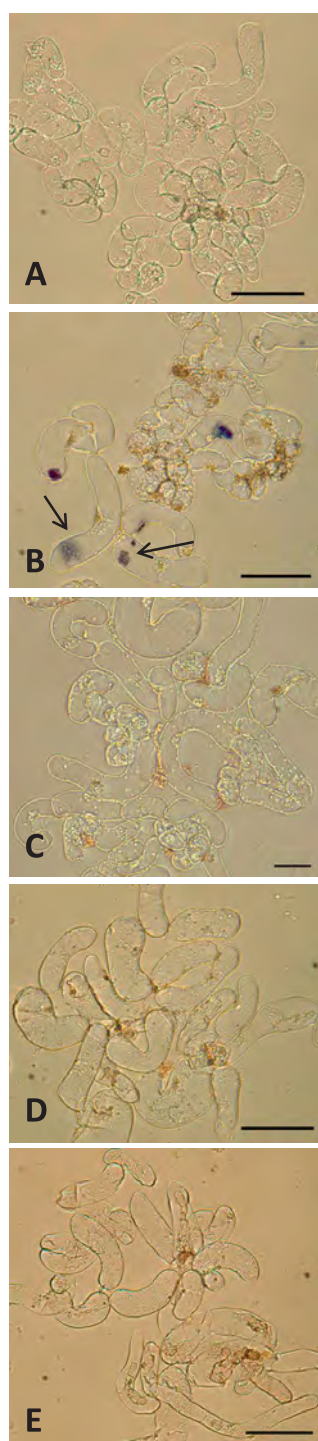


Figure 7 Detection of $O_2^{\cdot -}$ by the NBT assay in cell suspension cultures. (A) Treated with NBT. (B) Treated 20 minutes at 45°C and NBT exhibiting blue formazan spots due to $O_2^{\cdot -}$ production (indicated by arrows). (C) Treated with 100 nM QDs and stained with NBT showing no blue formazan spots. (D) Treated with 100 nM QDs for 48 hours and NBT and (E) treated with 100 nM QDs for 72 hours and NBT confirming that there is no $O_2^{\cdot -}$ production. All samples were visualized 4 hours after the NBT addition in bright field. Scale bar = 50 μM .

in tobacco cells by Ashtamker *et al.* [29]. In the heat treated ($45^\circ\text{C}/20$ min) cell suspension cultures, the DCF signal was significantly increased (Fig. 8b) showing a response in terms of ROS accumulation, also observed in the mercaptopropionic acid-QDs treated cell suspension cultures (Fig. 8c). These results confirmed the induction of an oxidative stress in cell suspension cultures treated with 100 nM of mercaptopropionic acid-QDs during 1.5 hours.

To evaluate the response of the cell suspension cultures when exposed to mercaptopropionic acid-QDs over a longer period of time, QDs addition was performed at day 3 of culture and the H_2DCFDA assay performed after 48 and 72 hours (Fig. 8d and 8e respectively). A progression of the intensity of the DCF signal could be seen in the cell cultures exposed to mercaptopropionic acid-QDs, when compared with the controls.

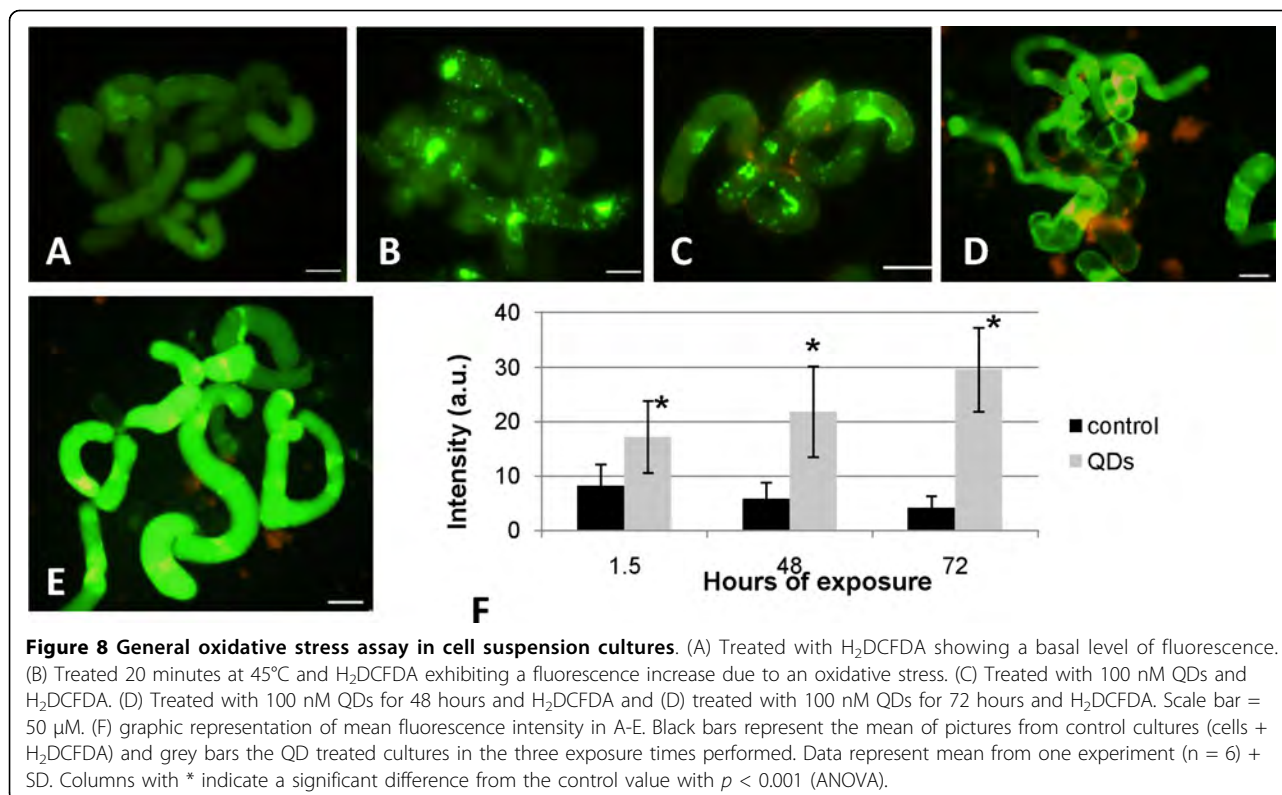
To further clarify the results in terms of the mean fluorescence intensity of DCF, a normalized graphic representation was obtained (Fig. 8f). Comparing the results of the three intensity values obtained over time, it can be concluded that while the control (cells plus H_2DCFDA) maintained an intensity below 8 a.u., cells treated with mercaptopropionic acid-QDs progressively increased the fluorescence intensity with the exposure time. mercaptopropionic acid-QD treated cultures increased ROS production in 52%, 73% and 85%, respectively 1.5, 48 and 72 hours after the mercaptopropionic acid-QD addition, showing that ROS production was intensified in a time dependent manner.

Conclusions about the specificity of H_2DCFDA are contradictory. DCFH oxidation to DCF can occur as a result of interaction with either H_2O_2 or $\cdot\text{OH}^-$ [30]. Myhrea *et al.* [31] suggest that H_2DCFDA is sensitive to the oxidation by ONOO^- (peroxynitrite, often included as ROS), H_2O_2 (in combination with cellular peroxidases), peroxidases alone, and $\cdot\text{OH}^-$, but not suitable to detect NO, HOCl, and $O_2^{\cdot -}$ radicals in biological systems. Due to the indiscriminate nature of DCFH, the increase of intracellular DCF fluorescence may not necessarily reflect the levels of ROS directly, but rather an overall oxidative stress index in cells [32,33].

4) Oxidative stress dose response

Since it is clear that the presence of mercaptopropionic acid-QDs in cell suspension cultures induces an oxidative stress, it is important to clarify if there is a relation between this cell response and the concentration of mercaptopropionic acid-QDs. Our results showed that fluorescence increased with the increasing concentrations of mercaptopropionic acid-QDs (Fig. 9a-i).

The mean fluorescence intensity of the cells subjected to the different QD concentrations was calculated, showing a linear increase (Fig. 9j). Regarding the range of concentrations used, it seems that to have a minor



impact in terms of oxidative stress, the concentration range of mercaptopropionic acid-QDs to be used should be between 1-5 nM, since cultures subjected to this concentration range presented a fluorescence intensity value that was not significantly different from the control. Concentrations above 5 nM led to the intensification of ROS production in more than 47%, measured in terms of fluorescence intensity, with a maximum of 85% at a concentration of 180 nM of mercaptopropionic acid-QDs.

Heterogeneity in cellular ROS production was also found to accompany the mercaptopropionic acid-QD concentration which is likely to reflect variability in the physiological conditions of the cells.

Conclusions

Here we report for the first time the response of *in vitro* cultured *Medicago sativa* plant cells when exposed to Quantum dots. Our results showed that concentrations above 1 nM of mercaptopropionic acid -CdSe/ZnS QDs induce a cyto-oxidative response in the plant cells.

Plant cells treated with 100 nM of mercaptopropionic acid-QDs showed a low cytotoxicity in short term exposure (24 hours) with a reduction of 6% in cell viability, which is probably related with the increase of 50% in ROS production. 72 Hours after the QD addition, less than 50% of the isolated cells were viable, when

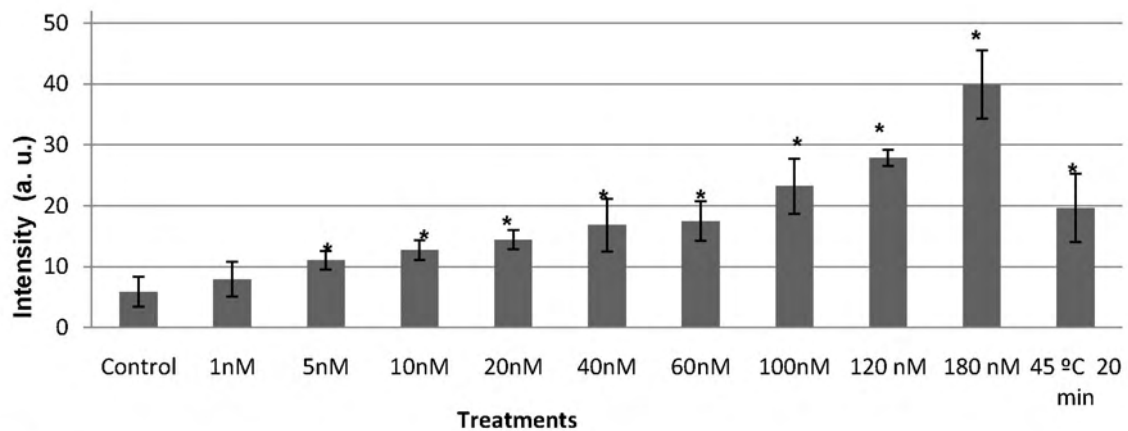
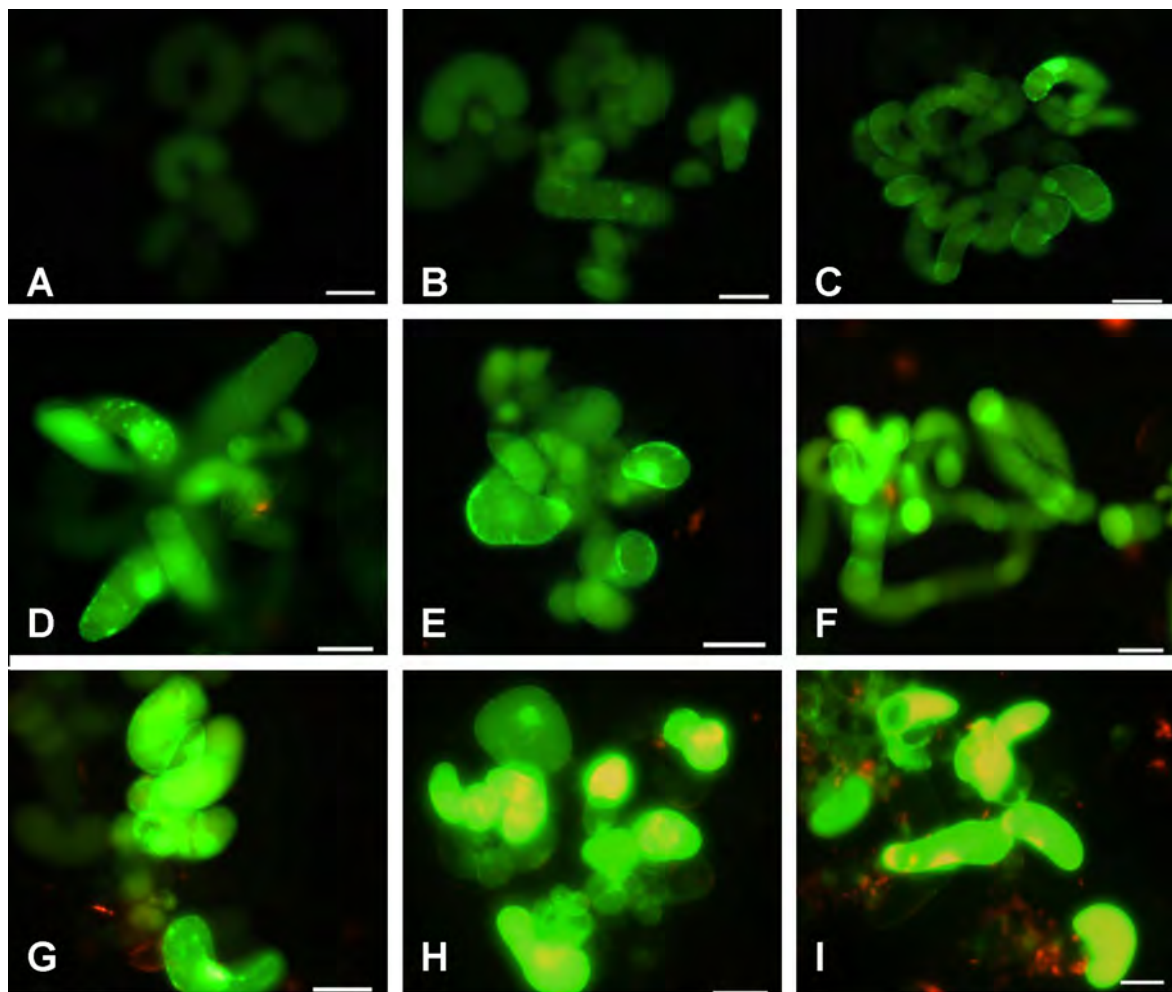
compared with the cells in the control, and ROS production was intensified in 85%.

Plant cells were found to increase the production of ROS in a dose dependent manner, and we shown that concentrations of 1-5 nM could be cyto-compatible for this type of QD. We also concluded that the superoxide anion is not the reactive species involved in the oxidative stress, since no superoxide anion production was detected upon 78 hours of exposure.

Mercaptopropionic acid -CdSe/ZnS QDs were taken up by the cells of *Medicago sativa* and found to accumulate in the nucleus and the cytoplasm, but not in the vacuoles. This uptake may explain the verified cyto-oxidative stress of QD treated cultures after only 1 hour of exposure.

Together these results confirm that the extent of QD cytotoxicity in plant cell cultures is dependent upon a number of factors including QD properties such as the coated material and surface chemistry, but also depends on the dose and on the environment where they are administered.

The intracellular formation of ROS is believed to be one of the causal factors of QD induced cytotoxicity [10]. Although mercaptopropionic acid coated CdSe/ZnS QDs are not completely innocuous to plant cells, a safe range of concentrations for biological application can be defined. The results presented in this work



J

Figure 9 Oxidative stress dose response assay. Cell suspension cultures treated with QDs and H₂DCFDA: (A) 1 nM QDs, (B) 5 nM QDs, (C) 10 nM QDs, (D) 20 nM QDs, (E) 40 nM QDs, (F) 60 nM QDs, (G) 100 nM QDs, (H) 120 nM QDs, (I) 180 nM QDs. Scale bar = 50 μm. (J) graphic representation of mean fluorescence intensity of pictures from cultures subjected to the different treatments. Data representing means from two independent experiments + SD (n = 6 in each experiment), except for the conditions 120 nM and 180 nM which represent one experiment (n = 7). Columns with * indicate a significant difference from the control value with $p < 0.001$ (ANOVA). Fluorescence intensity in cultures treated with QDs shows a linear behaviour represented by $Y = 0,1581x + 9,6342$ and $R^2 = 0,9735$. The H₂DCFDA assay was performed 48 hours after the QD addition.

contribute to the characterization of the parameters that regulate the toxicity of QDs in plant cell cultures, providing a basis for further work towards the improvement of nanoparticles functionalization and surface-coating strategies.

List of abbreviations

QDs: Quantum Dots; ROS: Reactive Oxygen Species; Mercaptopropionic acid-Mercaptopropionic acid; M&S: Murashige & Skoog; 2,4 D: Dichlorophenoxyacetic acid; FDA: Fluorescein diacetate; DAB: 3,3'-diaminobenzidine; NBT: Nitroblue tetrazolium; H₂DCFDA: 2',7'-dichlorodihydrofluorescein diacetate.

Competing interests

The authors declare that they have no competing interests.

Authors' contributions

ARS performed the majority of the experiments and wrote the first draft of the manuscript. ASM synthesized and characterized the quantum dots and wrote that part of the manuscript. LT contributed to the cell suspension culture establishment. RM contributed to the confocal and inverted microscopy and image processing. CM supervised the QD synthesis and contributed to the elaboration of the manuscript. MCVP contributed to the design of the project. PF participated in the design and coordination of the study, contributed to the interpretation of data and drafting of the manuscript. AO conceived the overall project and participated in the design of the work. All authors read, participated in the writing of the manuscript and approved the final manuscript.

Acknowledgements

This work was supported by the project "Development of ultra-sensitive detection methods and plant nano-vaccines for the fungi *Fusarium* spp. using nanotechnological devices" Iberian Capacitation Program in Nanotechnologies: Call 2006/2007". Ana Sofia Miguel acknowledge Fundação para a Ciência e Tecnologia for a PhD grant (SFRH/BD/40303/2007). We thank Benjamin Hardy Wunsch, MIT, Boston, USA for the TEM image.

Author details

¹Biomolecular Diagnostics Laboratory, Instituto de Tecnologia Química e Biológica, Universidade Nova de Lisboa, Apartado 127, 2781-901 Oeiras, Portugal. ²Plant Cell Biotechnology Laboratory, Instituto de Tecnologia Química e Biológica, Universidade Nova de Lisboa, Apartado 127, 2781-901 Oeiras, Portugal. ³Organic Synthesis Laboratory, Instituto de Tecnologia Química e Biológica, Universidade Nova de Lisboa, Apartado 127, 2781-901 Oeiras, Portugal. ⁴Universidade de Lisboa, Faculdade de Ciências, 1749-016 Lisboa, Portugal.

Received: 30 June 2010 Accepted: 7 October 2010

Published: 7 October 2010

References

- Lin DH, Xing BS: Phytotoxicity of nanoparticles: inhibition of seed germination and root elongation. *Environ Pollut* 2007, **150**:243-250.
- Zhu H, Han J, Xiao J, Jin Y: Uptake, translocation, and accumulation of manufactured iron oxide nanoparticles by pumpkin plants. *J Environ Monit* 2008, **10**:713-717.
- Joseph T, Morrison M: Nanotechnology in agriculture and food. 2007 [http://nanoforum.org].
- Auffan M, Rose J, Wiesner M, Bottero J: Chemical stability of metallic nanoparticles: A parameter controlling their potential cellular toxicity *in vitro*. *Environ Pollut* 2009, **157**:1127-1133.
- Fischer H, Chan W: Nanotoxicity: the growing need for *in vivo* study. *Curr Opin Biotechnol* 2007, **18**:565-571.
- Saez G, Moreau X, Jong L, Thiéry A, Dolain C, Bestel I, Giorgio C, Méo M, Barthélémy P: Development of new nano-tools: Towards an integrative approach to address the societal question of nanotechnology? *Nano Today* 2010, **5**:251-253.
- Wang J, Zhang X, Chen Y, Sommerfeld M, Hu Q: Toxicity assessment of manufactured nanomaterials using the unicellular green alga *Chlamydomonas reinhardtii*. *Chemosphere* 2008, **73**:1121-1128.
- Müller F, Houben A, Barker P, Xiao Y, Käs A, Melzer M: Quantum dots - a versatile tool in plant science? *J Nanobiotechnology* 2006, **4**:5.
- Fernández-Suárez M, Ting AY: Fluorescent probes for super-resolution imaging in living cells. *Nat Rev Mol Cell Bio* 2008, **9**:929-943.
- Jones C, Grainger D: *In vitro* assessments of nanomaterial toxicity. *Adv Drug Deliv Rev* 2009, **61**:438-456.
- Aldana J, Wang Y, Peng X: Photochemical instability of CdSe nanocrystals coated by hydrophilic thiols. *J Am Chem Soc* 2001, **120**:8844-8850.
- Xie R, Kolb U, Li J, Basché T, Mews A: Synthesis and Characterization of Highly Luminescent CdSe-Core CdS/Zn_{0.5}Cd_{0.5}S/ZnS Multishell Nanocrystals. *J Am Chem Soc* 2005, **127**:7480-7488.
- Widholm J: The use of fluorescein diacetate and phenosafranine for determining viability of cultured plant cells. *Stain Technol* 1972, **47**:189-194.
- Stepan- Sarkissian G, Grey D: Plant Cell and Tissue Culture. In *Methods in Molecular Biology*. Edited by: Pollard J, Walker J. New Jersey, The Humana Press; 1984:6:14-17.
- Thordal-Christensen H, Zhang Z, Wei Y, Collinge D: Subcellular localization of H₂O₂ in plants. H₂O₂ accumulation in papillae and hypersensitive response during the barley-powdery mildew interaction. *Plant J* 1997, **11**:1187-1194.
- Fryer J, Oxborough K, Mullineaux P, Baker N: Imaging of photo-oxidative stress responses in leaves. *J Exp Bot* 2002, **53**:1249-1254.
- Tarpey M, Fridovich I: Methods of Detection of Vascular Reactive Species Nitric Oxide, Superoxide, Hydrogen Peroxide, and Peroxynitrite. *Circulation Res* 2001, **89**:224-236.
- Armstrong J, Whiteman M: Measurement of reactive oxygen species in cells and mitochondria. *Methods Cell Biol* 2007, **80**:355-377.
- Romero-Puertas M, Rodriguez-Serrano M, Corpas F, Gomez M, del Rio L, Sandalio L: Cadmium-induced subcellular accumulation of O₂⁻ and H₂O₂ in pea leaves. *Plant, Cell and Environ* 2004, **27**:1122-1134.
- Ortega-Villasante C, Rellán-Alvarez R, del Campo F, Carpena-Ruiz R, Hernández L: Cellular damage induced by cadmium and mercury in *Medicago sativa*. *J Exp Bot* 2005, **56**:2239-2251.
- Sahu S, Casciano D: Nanotoxicity: from *in vivo* and *in vitro* models to health risks. Wiley, John Wiley & Sons, Ltd 2009.
- Mahendra S, Zhu H, Colvin V, Alvarez P: Quantum Dot Weathering Results in Microbial Toxicity. *Environ Sci Technol* 2008, **42**:9424-9430.
- Koeneman B, Zhang Y, Hristovski K, Westerhoff P, Chen Y, Crittenden J, Capco D: Experimental approach for an *in vitro* toxicity assay with non-aggregated quantum dots. *Toxicol Vitro* 2009, **23**:955-962.
- Bali R, Siegele R, Harris A: Biogenic Pt uptake and nanoparticle formation in *Medicago sativa* and *Brassica juncea*. *J Nanopart Res* 2010.
- Parak W, Pellegrino T, Plank C: Labelling of cells with quantum dots. *Nanotechnology* 2005, **16**:R9-R25.
- Chang E, Thekkekk N, Yu W, Colvin V, Drezek R: Evaluation of Quantum Dot Cytotoxicity Based on Intracellular Uptake. *Small* 2006, **2**:1412-1417.
- Żróbek-Sokolnik A, Asard H, Górska-Koplińska K, Górecki R: Cadmium and zinc-mediated oxidative burst in tobacco BY-2 cell suspension cultures. *Acta Physiol Plant* 2009, **31**:43-49.
- Ipe B, Lehnig M, Niemeyer C: On the Generation of Free Radical Species from Quantum Dots. *Small* 2005, **7**:706-709.
- Gechev T, Breusegem F, Stone J, Denev I, Laloi C: Reactive oxygen species as signals that modulate plant stress responses and programmed cell death. *BioEssays* 2006, **28**:1091-1101.
- Ashtamker C, Kiss V, Sagi M, Davydov O, Fluhr R: Diverse subcellular locations of cryptogei-induced reactive oxygen species production in tobacco bright yellow-2 cells. *Plant Physiol* 2007, **143**:1817-1826.
- Hoek T, Li C, Shao Z, Schumacker P, Becker L: Significant Levels of Oxidants are Generated by Isolated Cardiomyocytes During Ischemia Prior to Reperfusion. *J Molec Cell Cardiol* 1997, **29**:2571-2583.
- Myhrea O, Andersena J, Aarnesc H, Fonnuma F: Evaluation of the probes 2',7'-dichlorofluorescein diacetate, luminol, and lucigenin as indicators of reactive species formation. *Biochem Pharmacol* 2003, **65**:1575-1582.

33. Wang H, Joseph J: **Quantifying cellular oxidative stress by dichlorofluorescein assay using microplate reader.** *Free Radic Biol Med* 1999, **27**:612-616.

doi:10.1186/1477-3155-8-24

Cite this article as: Santos *et al.*: The impact of CdSe/ZnS Quantum Dots in cells of *Medicago sativa* in suspension culture. *Journal of Nanobiotechnology* 2010 **8**:24.

**Submit your next manuscript to BioMed Central
and take full advantage of:**

- Convenient online submission
- Thorough peer review
- No space constraints or color figure charges
- Immediate publication on acceptance
- Inclusion in PubMed, CAS, Scopus and Google Scholar
- Research which is freely available for redistribution

Submit your manuscript at
www.biomedcentral.com/submit



Synthesis and Laser Immobilization onto Solid Substrates of CdSe/ZnS Core–Shell Quantum Dots

E. György,^{*,†,‡} A. Pérez del Pino,[§] J. Roqueta,[†] B. Ballesteros,[†] A. S. Miguel,^{||} C. D. Maycock,^{||,‡} and A. G. Oliva^{||}

[†]Centre d'Investigació en Nanociència i Nanotecnologia, Institut Català de Nanotecnologia, Consejo Superior de Investigaciones Científicas, (CIN2, ICN-CSIC), Campus UAB, 08193 Bellaterra, Spain

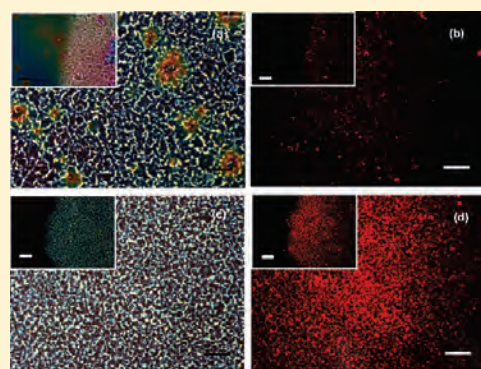
[‡]National Institute for Lasers, Plasma and Radiation Physics, P.O. Box MG 36, 76900 Bucharest V, Romania

[§]Instituto de Ciencia de Materiales de Barcelona, Consejo Superior de Investigaciones Científicas (ICMAB-CSIC), Campus UAB, 08193 Bellaterra, Spain

^{||}Instituto de Tecnologia Química e Biológica, Universidade Nova de Lisboa, 2781-901 Oeiras, Portugal

[‡]Departamento de Química e Bioquímica, Faculdade de Ciências, Universidade de Lisboa, 1749-016 Lisboa, Portugal

ABSTRACT: CdSe/ZnS core–shell quantum dots (QDs) have been immobilized by ultraviolet matrix-assisted pulsed laser evaporation (UV-MAPLE) onto SiO₂ glass substrates covered by silica thin films. The silica thin films were deposited by the sol–gel method. An UV KrF* ($\lambda = 248$ nm, $\tau_{\text{fwhm}} \cong 25$ ns) excimer laser source was used for the laser immobilization experiments. Toluene was chosen as solvent material for the preparation of the composite MAPLE targets. The surface morphology and growth mode of the deposited structures were investigated by optical and atomic force microscopy in acoustic (dynamic) configuration. The crystalline structure and chemical composition of the base material used for the preparation of the MAPLE targets as well as the laser transferred QDs were studied by transmission electron microscopy and energy dispersive X-ray spectroscopy. The functional properties of the immobilized QDs were studied by fluorescence microscopy. The immobilized materials form self-organized 2D arrays constituted by complex CdSe/ZnS core–shell QDs preserving the functional properties of the base material used for the preparation of the MAPLE targets.



1. INTRODUCTION

Semiconductor quantum dots (QD) are nanocrystals composed of hundreds to up to a few thousand atoms. These nanostructures can be prepared in a variety of compositions, and shapes as nearly spherical,¹ elongated nanorods,² or crystals with more complex shapes such as tetrapods.³ The small size of these systems leads to a quantum confinement effect, resulting in a strong modification of their band structure. In these conditions, effects such as an expansion of the band gap, the quantization of the energy levels to discrete values and the strong enhancement of the Coulomb interaction between the charge carriers take place. Such phenomena have a great effect in the e–h dynamical behavior, arising exciting mechanisms such as the direct generation of multiexcitons by single photons (carrier multiplication).⁴

As known, the physical properties of the QDs are size dependent.^{5,6} Thus, remarkable electronic and photonic characteristics can be tuned by simply controlling their shape and size, adding up significant functionality in applications as biological labeling, nonlinear optics, or photovoltaics technology.^{7,8} A step forward consists in overcoating such QDs with a shell of a second semiconductor, resulting in core–shell systems that exhibit novel properties as compared to simple dots.⁹ Overcoating the nanocrystals with higher band gap inorganic materials has been

found to improve the photoluminescence quantum yields by passivating surface nonradiative recombination sites.^{10,11} In addition, nanoparticles passivated with inorganic shells are more robust than those passivated with organic materials and withstand more severe processing conditions when incorporated into solid state structures. Besides, by the appropriate choice of the core and shell materials, it is possible to adjust the emission wavelength in a larger spectral range than with both materials alone.^{12,13} These features make them promising besides emitters for quantum information, also for biological labeling,^{14,15} design of devices such as thin film LEDs,^{16–18} or nanocrystal quantum dot lasers.^{19–21}

CdSe/ZnS core–shell QDs are usually deposited on solid substrates from colloidal solutions by conventional methods as drop casting or spin coating. These techniques are rather simple and cost-effective. However, they do not guarantee an accurate control over the amount of the immobilized material and its surface uniformity. In addition, conventional methods are not suitable for multilayer structures growth since they imply

Received: April 1, 2011

Revised: June 30, 2011

Published: July 01, 2011

repeated use of solvents. Laser technologies could represent an alternative solution for these drawbacks: the amount of evaporated and deposited material on the substrate surface can be controlled through the number and/or irradiance of the laser pulses, offering high reproducibility and versatility for multilayer synthesis. However, immobilization of nanoparticles with a narrow size distribution by conventional pulsed laser deposition technique can be a difficult task. Usually the deposited nanoparticles have a broad size distribution range and often form aggregates with dimensions in the micrometer range. An additional problem in the case of multicomponent materials represents the selective evaporation of elements making difficult to reproduce structures with identical chemical composition as the base materials used as targets submitted to laser irradiation.

Matrix-assisted pulsed laser evaporation (MAPLE) is a laser-based deposition technique developed more recently, mostly for organic and bio-organic materials processing.²² The material to be immobilized on a solid substrate surface is diluted in a laser-absorbing solvent. After the solution is frozen in liquid nitrogen it is submitted to laser radiation. The laser energy is mainly absorbed by the solvent which is vaporized and transports the material of interest toward the substrate placed in front of the target ensuring a gentle transfer mechanism. Besides organic species, some recent works have demonstrated the possibility to transfer TiO₂ and SnO₂²³ or carbon nanoparticles²⁴ by ultraviolet (UV)-MAPLE as well as CdSe QDs²⁵ by resonant infrared (RIR)-MAPLE techniques.

We report in this paper the creation of self-organized 2D arrays constituted by complex CdSe/ZnS core-shell QDs immobilized on solid substrates by UV-MAPLE technique. The networklike structures synthesis can be controlled by the incident laser fluence value. The formation of a photonic band gap due to the periodically changing refractive index can be used for future photonic applications implying guided light propagation or enhanced spontaneous emission.

2. EXPERIMENTAL SECTION

2.1. Synthesis of Core-Shell CdSe/ZnS QDs. The chemical reagents and solvents used for the CdSe/ZnS QDs synthesis were obtained from Sigma-Aldrich and Fluka. Air-sensitive materials were handled in a Braun MB150-GI glovebox under dry argon atmosphere. All solvents were spectrophotometric grade. Trioctylphosphine oxide (TOPO)/hexadecylamine (HDA) capped CdSe QDs were synthesized using standard procedures,²⁶ generating nanocrystals with the first absorption peak around 560–570 nm and diameters of 3.6–4.5 nm. The growth of the ZnS shell coating is based on SILAR method²⁷ which consists of injections of Zn and S precursors to the solution containing CdSe nanocrystals suspended in octadecene (ODE)/HDA. 0.1 M solutions of ZnO in ODE/oleic acid and S in ODE were used. For each monolayer shell growth, a calculated amount of these solutions were simultaneously injected via syringe into the dot suspension at 245 °C using standard gas-free conditions. A period of 10 min between each addition was left for the reaction to be complete. The CdSe cores were covered with 5 ZnS monolayers, which took about 1 h and 30 min. Then, the solution was kept for another 30 min at 260 °C and finally cooled down to room temperature. After extraction with methanol, centrifugation, and decantation, the particles were dispersed in chloroform and capped with a layer of TOPO/HDA.

2.2. Laser Immobilization of CdSe/ZnS QDs on SiO₂ Glass Substrates. The laser immobilization experiments were performed inside a stainless steel deposition chamber. A pulsed UV KrF* ($\lambda = 248$ nm, $\tau_{\text{fwhm}} \cong 25$ ns, $\nu = 10$ Hz) COMPexPro 205 Lambda Physik excimer laser source was used for the irradiations. Prior to each experiment, the irradiation chamber was evacuated down to a residual pressure of 10^{-3} Pa. This pressure value was maintained during the experiments.

For the preparation of the composite MAPLE targets 2.5 μg CdSe/ZnS core-shell QDs were added to 3 mL of toluene. The obtained solutions were introduced into a special double wall target holder and flash-frozen at -190 °C circulating liquid nitrogen inside the holder walls. The targets were kept frozen during the irradiation experiments. The complete MAPLE workstation was purchased from SURFACE.

To avoid significant morphological changes upon irradiation, the laser beam scanned the targets' surface at a constant velocity of 2 mm/s. The irradiated XY surface area was 1×1 cm². The angle between the laser beam and the target surface was chosen of 45°. The number of subsequent laser pulses applied for the deposition of the nanostructures was 5×10^3 . The laser pulses succeeded each other with a repetition rate of 10 Hz. The laser fluence value incident on the target's surface was fixed at 0.1 or 0.2 J/cm².

Silica films coated on SiO₂ glass substrates were placed parallel to the target at a separation distance of 5 cm. The silica films were deposited by sol gel technique based on the method described previously.^{28,29} The solution was composed by two types of precursors, tetraethyl orthosilicate (TEOS) and methyltriethoxysilane (MTES). The TEOS/MTES molar ratio was 1:1. The films were deposited by dip-coating onto 6.5 mm \times 50 mm SiO₂ glass substrates in a two step process with 1 min interval between them. Drying was performed at room temperature for 24 h followed by thermal treatment at 70 °C for 24 h. For the described experimental conditions a film porosity of 26% was estimated from nitrogen absorption isotherms, with a pore size ranging between 2 and 10 nm.²⁹ Prior to introduction inside the irradiation enclosure the substrates were carefully cleaned in ultrasonic bath in acetone. During the laser irradiations the substrates were kept at room temperature.

The CdSe/ZnS core shell QDs were investigated by transmission electron microscopy (TEM). A JEOL 2011 transmission electron microscope operated at an acceleration voltage of 200 kV was used for observing the CdSe/ZnS QDs. The samples were purified by acetone precipitation from their chloroform or hexane solutions. The laser immobilized QDs were prepared for TEM analysis by placing a droplet of milli-Q water on the deposited nanostructures with a subsequent mild stirring to suspend the QDs. The droplet was then transferred with a pipet onto a carbon-coated copper grid and left to evaporate. Energy dispersive X-ray spectroscopy (EDX) analyses were carried out using an Oxford Instruments EDX detector controlled by INCA software. Quantum yields (QY) measurements were performed with the aid of a SPEX-Fluorolog fluorometer spectrometer relative to Rhodamine 6G dye, at 530 nm excitation wavelength. Solutions of QDs in chloroform and dye in ethanol were optically matched at the excitation wavelength. Fluorescence spectra of solutions containing QDs and dye were taken under identical spectrometer conditions. To calculate QY the optical density at the peak was kept below 0.05, and the integrated intensities of the emission spectra were corrected for differences in index of refraction and concentration. The hydrodynamic

diameter (HD) of the synthesised CdSe/ZnS core–shell QDs was measured by dynamic light scattering analysis using a Nano series dynamic light scatterer from Malvern. The samples were measured in CHCl_3 with QD concentrations between 0.06 and $0.30 \mu\text{M}$ and filtered through a $0.2 \mu\text{m}$ filter before analysis. The surface morphology and growth mode of the deposited nanostructures were investigated by atomic force microscopy (AFM) by intermittent contact (dynamic) configuration with a 5100 AFM/SPM apparatus from Agilent Technologies. The AFM measurements were studied with MountainsMap software from Digital Surf. Fluorescence optical images were acquired using a Carl Zeiss Axio Observer Z1 inverted microscope equipped with a motorized XY stage. A 100-W Hg lamp was used as excitation light source. Microscope images were acquired with an Axio-CamHR digital CCD Color Camera and image capture and exposure times were controlled using Axio Vision Rel 4.6 software.

3. RESULTS AND DISCUSSIONS

The synthesized CdSe/ZnS core–shell QDs were analyzed by TEM (Figure 1). As can be observed in the higher resolution TEM image (Figure 1b), the QDs have a narrow size distribution, with dimensions between 4 and 6 nm. High-resolution TEM (HRTEM) investigations showed that the particles have two different crystalline structures. The measured interplanar distances correspond to the ZnS hexagonal wurtzite as well as ZnS cubic zinc-blende phases. No significant difference can be observed as concerns the crystalline structure between the QDs immobilized with different laser fluence values as well as the nonirradiated base material (Figure 2). The interplanar distances correspond to the bulk ZnS hexagonal wurtzite and ZnS cubic zinc-blende crystalline phases. These measured bulk interplanar distances can be explained by the high ~ 5 ZnS monolayers shell coverage, since it has been reported that a

coverage higher than ~ 2 monolayers ZnS shells grow with the bulk ZnS lattice parameter, with incoherence between the CdSe core and the ZnS shell.¹¹ As in our case, TEM micrographs correspond to the ZnS structure and the growth of the thick ZnS overlayer was described as epitaxial but incoherent.¹¹ The EDX data confirms that the laser deposited nanostructures are composed by CdSe and ZnS (Figure 3).

For the QY measurements the integrated intensity areas of the fluorescence emission spectra for both solutions, one containing QDs and the other dye, were corrected for differences in index of refraction and concentration. The optical absorbance of QDs containing solution at the excitation wavelength was about 0.05. The QY was calculated by the relative method³⁰ according to the equation

$$QY_{QD} = QY_{dye} (A_{dye}/A_{QD}) (E_{QD}/E_{dye}) (n_{QDsolvent})^2 / (n_{dyesolvent})^2$$

Where QY_{dye} stands for the QY of the solution containing the Rhodamine 6G dye, A the absorbance of the solutions, E the corrected intensity areas, and n the average refractive index of the solutions. A QY of 0.12 was estimated. The relatively low QY value could be associated with the high coverage of QDs, approximately 5 ZnS monolayers. It was reported that the QY begins to decrease as the surface coverage exceeds approximately a completed ZnS shelling.^{11,12,31} This behavior was attributed to the effect of strain created at the interface due to the 12% lattice mismatch between CdSe and ZnS leading to an incoherent epitaxial mechanism for the growth of the ZnS shell at high coverage, as suggested also by our HRTEM results. The relaxation of the crystallographic structure should be associated with formation of structural defects, dislocations, and grain boundaries and creation of sources for nonradiative recombination sites in the ZnS shell.¹¹

Figure 4 shows the tilted AFM image (a) and surface profile (b) across the line marked in the AFM image of silica films deposited by sol gel technique on SiO_2 glass substrate. The formation of dome-shaped structures of the films surface can be observed, with an average in-plane diameter of about $0.5\text{--}1 \mu\text{m}$ and height around 30 nm. The density of these structures is about $0.1 \mu\text{m}^{-2}$. A root-mean-square (rms) roughness of 1.5 nm was measured. We would like to note that the porous structure of the layers can not be observed due to the small size of the pores, smaller or similar to the AFM tip diameter of 10 nm. Then, the surface roughness is underestimated, including also the contribution of the AFM tip.

Figure 5 shows the tilted (a, b, d, e) AFM images as well as surface profiles (c, f) across the line marked in the AFM images of

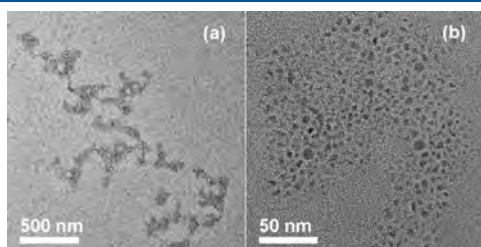


Figure 1. TEM images of CdSe/ZnS core shell QDs deposited on SiO_2 glass substrates covered by silica sol gel deposited film at 0.1 J/cm^2 laser fluence.

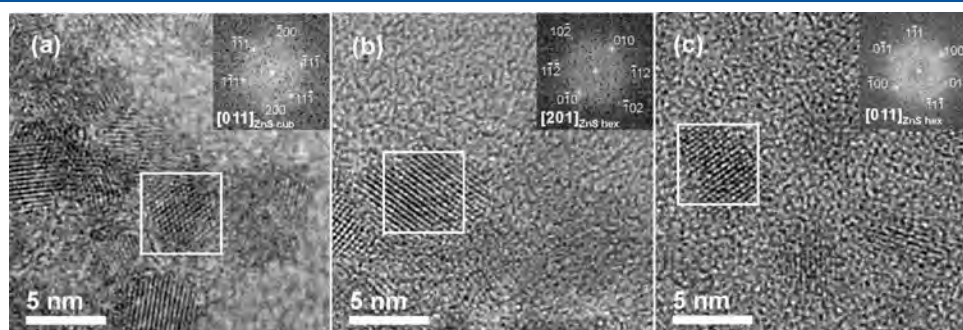


Figure 2. HRTEM images and fast Fourier transform patterns of (a) reference drop-cast sample and CdSe/ZnS core shell QDs deposited on SiO_2 glass substrates covered by silica sol gel deposited film at (b) 0.2 and (c) 0.1 J/cm^2 laser fluence.

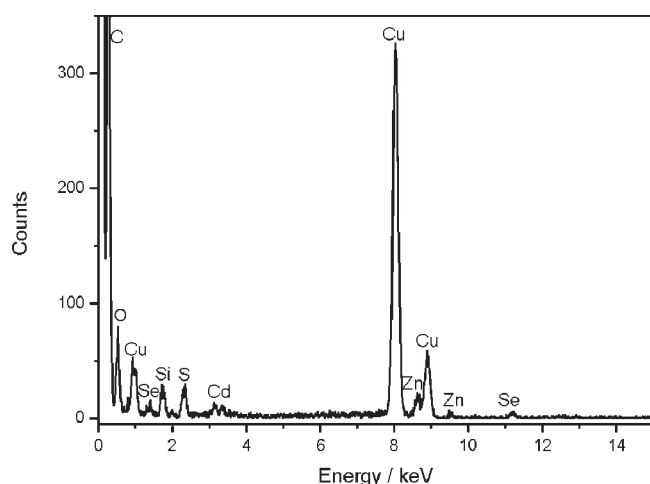


Figure 3. EDX spectrum of CdSe/ZnS core shell QDs deposited on SiO₂ glass substrates covered by silica sol gel deposited film at 0.1 J/cm² laser fluence.

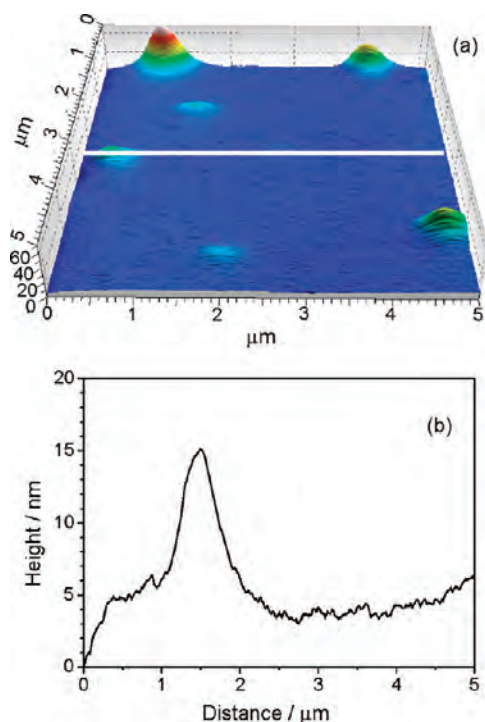


Figure 4. Tilted AFM micrograph and surface profile across the line marked in the AFM micrograph of sol gel deposited silica film on SiO₂ glass substrates.

CdSe/ZnS core–shell nanoparticles immobilized on SiO₂ glass substrates coated with silica films, at incident laser fluence values of 0.2 (a–c) and 0.1 J/cm² (d–f). The particulates present on the surface of films deposited at both laser fluence values have a quite homogeneous size distribution. As can be observed, the deposited material consists of tens of nanometer sized clusters. However, at 0.2 J/cm² laser fluence the deposition is not continuous over the substrate surface forming an interconnected line-structure (marked in Figure 5a). At higher magnification the individual particles can be clearly distinguished (Figure 5 b).

With the decrease of the laser fluence the deposited films surface is characterized by a more uniform morphology, constituted by tens of nanometer sized particulates (parts d and e of Figure 5).

The efficiency and homogeneity of the QDs attachment is superior on the silica buffer layer related to the nontreated glass slide surface (data not shown). This could be due to the porosity of the surface and the presence of dome-shaped structures providing a higher specific surface area and therefore a larger available area for QDs attachment as compared to the completely flat glass substrate. Moreover, the porous silica structure can be broken locally by the laser transferred particles. Note that at higher magnification the particles seem to be embedded in the silica matrix (parts b and e of Figure 5). In addition, it was reported that multivalent hydrophobic interactions provide a strong driving force for efficient immobilization of TOPO surfactant-coated QDs in silica nanopores.³² A further advantage of the silica film is that allows for the utilization of different support materials (glass, fiber optics, polymeric or plastic, etc.) keeping similar characteristics as regards surface topography for the QDs deposition.

The optical micrographs (parts a and b of Figure 6) of immobilized CdSe/ZnS core–shell nanoparticles evidence the formation of a long-range self-organized networklike morphology. The network is constituted by interconnected lines as observed also by AFM (see Figure 5a) composed by CdSe/ZnS QDs with transversal dimensions reaching about one micrometer and lengths of several micrometers. Figure 5b shows a detail of one of these lines constituted by tens of nm sized clusters. The density of the lines increases with the decrease of the laser fluence, resulting in a percolated structure.

Figure 7 shows the optical microscope (a) and the fluorescence (b) images corresponding to the same surface area of a positive reference (blank) sample prepared by the deposition onto SiO₂ glass substrate of a drop from the solution, 2.5 μg of CdSe/ZnS core shell QDs in 3 mL toluene, used for the frozen composite targets preparation in the MAPLE experiments. The observed orange fluorescence (Figure 7b) is characteristic for the CdSe/ZnS QDs using UV light for excitation.

The optical microscopy images and the fluorescence patterns corresponding to the same surface area of the deposited QDs on the SiO₂ glass substrates coated by silica films are presented in Figure 8. The insets belong to the edge of the depositions, the border between the substrate surface and the laser transferred QDs. The fluorescence image corresponding to the sample obtained with 0.1 J/cm² (Figure 8d) is more intense as compared to that of the QDs immobilized using higher, 0.2 J/cm² laser fluence (Figure 8b) and reproduces the characteristic organized, networklike surface morphology. On the other hand, the intensity of the fluorescence patterns of the laser immobilized QDs can not be compared to that of the reference drop-cast sample (Figure 7b). A direct comparison would be possible only if the quantity of the laser evaporated QDs would be equal to the quantity of the QDs deposited by drop-casting. The few randomly distributed large micrometer sized particulates visible also in parts a and b of Figure 6 are the most probably characteristic for the substrate surface morphology since they are present on the uncovered substrate areas as well (see inset of Figure 8a).

The QDs are transported to the substrate surface the most probably by the solvent vapor. The laser pulses incident onto the frozen target cause melting of the composite target followed by the vaporisation of the liquid solvent. We would like to note that we chose toluene as solvent for the frozen composite targets

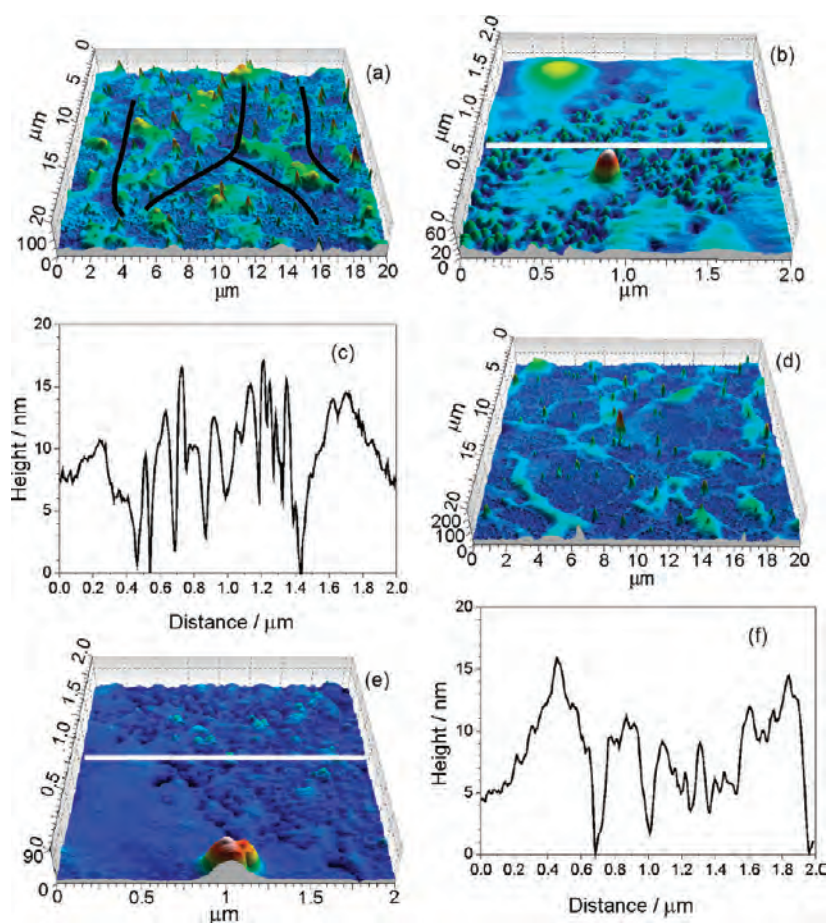


Figure 5. Tilted AFM micrographs (a, b, d, e) as well as surface profiles (c, f) across the lines marked in the AFM micrographs of CdSe/ZnS core shell QDs thin films obtained on SiO₂ glass substrates covered by silica sol gel deposited film at (a, b, c) 0.2 and (d, e, f) 0.1 J/cm² laser fluence.

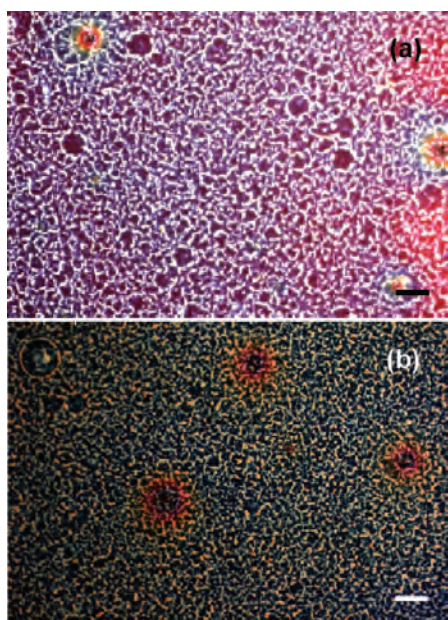


Figure 6. Optical microscopy images of CdSe/ZnS core shell nanostructures obtained on SiO₂ glass substrates covered by silica sol gel deposited film at 0.2 (a) and 0.1 J/cm² (b) laser fluence. Scale bars correspond to 20 μm.

preparations due to its highly absorption at the wavelength of the incident laser radiation. This is the typical situation in MAPLE experiments, where the solvents are highly absorbing at the incident laser wavelength in order to ensure a protection for the material to be irradiated and transferred to the substrate surface.

On the other hand, the laser radiation is also absorbed by the QDs. The threshold laser fluences necessary for ablation and plasma ignition upon KrF* excimer laser irradiation of CdSe and ZnS with a pulse width of 14 ns were estimated to be 0.1 and 1.3 J/cm² for CdSe and ZnS, respectively. These laser fluence values correspond to incident laser irradiances of 7.1 and 92.8 MW/cm², respectively.³³ Moreover, it was found that due to the low sublimation temperature of ZnS, the sublimation process is responsible for the onset of ablation, before the material reaches its melting temperature.³⁴ Theoretical calculations showed that a threshold laser irradiance value of 16.6 MW/cm² is sufficient to reach the sublimation temperature on the surface of ZnS:Mn thin films.³⁵ We would like to note that the 0.2 J/cm² laser fluence used in our experiments corresponds to an irradiance of 8 MW/cm², well below the calculated sublimation threshold value. However, the thermal diffusion length in ZnS for 25-ns laser pulses can be estimated at around 900 nm.³⁶ As a consequence, the ablation process in case of the only 5 monolayer thick ZnS shells is governed by the CdSe cores, the incident laser irradiance being at the limit of the estimated plasma ignition threshold.³³ Then, part of the irradiated QDs especially those situated in the

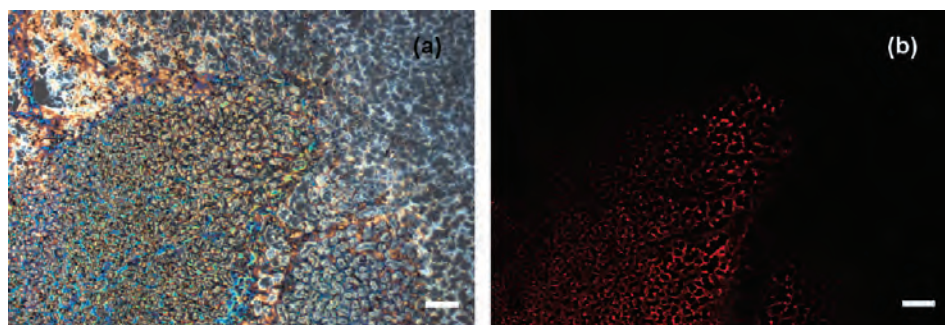


Figure 7. Optical microscopy (a) and fluorescence (b) images corresponding to the same surface area of positive reference (blank) sample prepared by the deposition onto SiO_2 glass substrate of a drop from the solution, $2.5 \mu\text{g}$ of CdSe/ZnS core shell QDs in 3 mL toluene, used as targets in the MAPLE experiments. Scale bars correspond to $20 \mu\text{m}$.

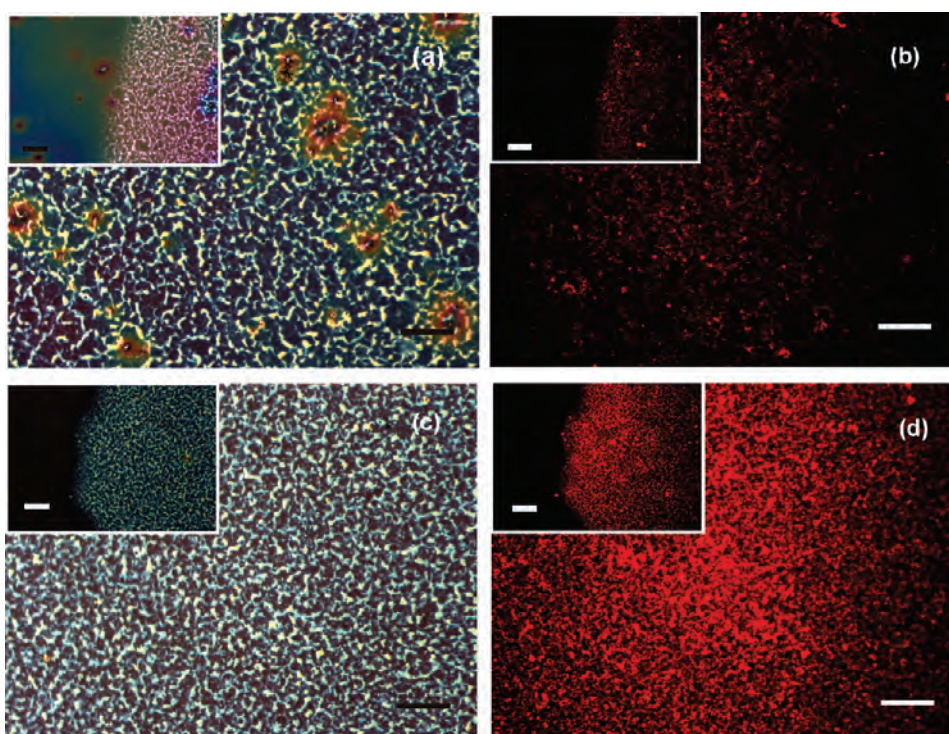


Figure 8. Optical microscopy (a, c) and fluorescence (b, d) images corresponding to the same surface area of CdSe/ZnS core shell nanostructures obtained on SiO_2 glass substrates covered by silica sol gel deposited film at 0.2 (a, b) and 0.1 J/cm^2 (c, d) laser fluence. The insets belong to the border between the substrate and CdSe/ZnS QDs thin films. Scale bars correspond to $20 \mu\text{m}$.

outmost surface layer of the frozen composite target could be damaged. However, the solvent vapor can carry QDs toward the substrate surface from deeper zones, where the temperature just surpasses the evaporation temperature of toluene.

Conversely, the laser fluence value of 0.1 J/cm^2 , with the corresponding 4 MW/cm^2 irradiance, remains below the plasma ignition threshold of CdSe. Indeed, as can be observed in the AFM and optical microscopy images, a higher amount of material were transferred and immobilized at 0.1 J/cm^2 laser fluence as compared to 0.2 J/cm^2 , and the fluorescence patterns are more intense. Besides, at 0.1 J/cm^2 laser fluence the fluorescence pattern reproduces the specific networklike surface morphology visible in Figure 8c. These results confirm that the CdSe/ZnS core-shell QDs were transferred at 0.1 J/cm^2 incident laser

fluence to the substrate surface without damage or selective evaporation.

CONCLUSION

The synthesized CdSe/ZnS core-shell QDs have a narrow size distribution, with dimensions between 4 and 6 nm. The obtained CdSe/ZnS QDs were immobilized by UV-MAPLE onto SiO_2 glass substrates covered by silica films. The formation of a specific self-organized network-like morphology was observed, built from micrometer-sized lines of CdSe/ZnS core-shell QDs. At high laser fluence value damage of QDs situated in the outmost surface layer of the frozen composite target can explain the reduced fluorescence of the processed and transferred material. At lower incident laser fluence the deposited QDs

structure the fluorescence pattern is more intense and reproduces the specific network-like surface morphology, proving that laser techniques are suitable for the immobilization of CdSe/ZnS QDs. The preserved functional properties make the immobilized QDs suitable for key applications as biosensors, lasers, or high performance electronic devices.

AUTHOR INFORMATION

Corresponding Author

*Phone: +34 93 581 37 25. Fax: +34 93 581 37 17. E-mail: egyorgy@cin2.es.

ACKNOWLEDGMENT

The authors acknowledge the financial support from the Spanish National Research Council under the Contract Nos. 200860I211 and 200960I015, the Spanish Ministry of Science and Innovation for the PTA2008-1108-I contract, the Portugal-Spanish Bilateral Agreement No. 2007PT0007, and the Romanian National University Research Council under the Contract IDEAS No. 652.

REFERENCES

- (1) Du, K.; Ernst, F.; Pelsozy, M. C.; Barthel, J.; Tillmann, K. *Acta Mater.* **2010**, *58*, 836.
- (2) Ayyub, P. J. *Cluster Sci.* **2009**, *20*, 429.
- (3) Shen, L.; Zhang, H.; Guo, S. *Mater. Chem. Phys.* **2009**, *114*, 580.
- (4) Klimov, V. I. *J. Phys. Chem. B* **2006**, *110*, 16827.
- (5) Sun, C. Q.; Chen, T. P.; Tay, B. K.; Li, S.; Huang, H.; Zhang, Y. B.; Pan, L. K.; Lan, S. P.; Sun, X. W. *J. Phys. D* **2001**, *34*, 3470.
- (6) Jasleniak, J.; Smith, L.; van der Embden, J.; Mulvaney, P. J. *Phys. Chem. C* **2009**, *113*, 19468.
- (7) Feng, M.; Cundiff, S. T.; Mirin, R. P.; Silverman, K. L. *IEEE J. Quantum Electron.* **2010**, *46*, 951.
- (8) Kamat, P. V. *J. Phys. Chem. C* **2008**, *112*, 18737.
- (9) Reiss, P.; Protière, M.; Li, L. *Small* **2009**, *5*, 154.
- (10) Ziegler, J.; Merkulov, A.; Grabolle, M.; Resch-Genger, U.; Nanni, T. *Langmuir* **2007**, *23*, 7751.
- (11) Dabbousi, B. O.; Rodriguez-Viejo, J.; Mikulec, F. V.; Heine, J. R.; Mattoussi, H.; Ober, R.; Jensen, K. F.; Bawendi, M. G. *J. Phys. Chem. B* **1997**, *101*, 9463.
- (12) Zhu, C. Q.; Wang, P.; Wang, X.; Li, Y. *Nanoscale Res. Lett.* **2008**, *3*, 213.
- (13) Smith, A. M.; Mohs, A. M.; Nie, S. *Nat. Nanotechnol.* **2009**, *4*, 56.
- (14) Alivisatos, A. P. *Nat. Biotechnol.* **2004**, *22*, 47.
- (15) Riegler, J.; Diténgou, F.; Palme, K.; Nann, T. *J. Nanobiotechnol.* **2008**, *6*, 7.
- (16) Nizamoglu, S.; Demir, H. V. *J. Appl. Phys.* **2009**, *105*, 083112.
- (17) Gopal, A.; Hoshino, K.; Kim, S.; Zhang, X. *Nanotechnology* **2009**, *20*, 235201.
- (18) Kazes, M.; Saraidarov, T.; Reisfeld, R.; Banin, U. *Adv. Mater.* **2009**, *21*, 1716.
- (19) Klimov, V. I.; Mihailovsky, A. A.; McBranch, D. W.; Bawendi, M. G. *Science* **2000**, *287*, 1011.
- (20) Mikhailovsky, A. A.; Malko, A. V.; Hollingsworth, J. A.; Bawendi, M. G.; Klimov, V. I. *Science* **2000**, *90*, 314.
- (21) Smirnova, T. N.; Sakhno, O. V.; Yezhov, P. V.; Kothtych, L. M.; Goldenberg, L. M.; Stumpe, J. *Nanotechnology* **2009**, *20*, 245707.
- (22) Wu, P. K.; Ringeisen, B. R.; Krizman, D. B.; Frondoza, C. G.; Brooks, M.; Bubb, D. M.; Auyeung, R. C. Y.; Piqué, A.; Spargo, B.; McGill, R. A.; Chrisey, D. B. *Rev. Sci. Instrum.* **2003**, *74*, 2546.
- (23) Caricato, A. P.; Luches, A.; Rella, R. *Sensors* **2009**, *9*, 2682.
- (24) Hunter, C. N.; Check, M. H.; Bultman, J. E.; Voevodin, A. A. *Surf. Coat. Technol.* **2008**, *203*, 300.
- (25) Pate, R.; Lantz, K. R.; Stiff-Roberts, A. D. *Thin Solid Films* **2009**, *517*, 6798.
- (26) Aldana, J.; Wang, Y. A.; Peng, X. *J. Am. Chem. Soc.* **2001**, *123*, 8844.
- (27) Xie, R.; Kolb, U.; Li, J.; Basche, T.; Mews, A. *J. Am. Chem. Soc.* **2005**, *127*, 7480.
- (28) McDonagh, C.; Bowe, P.; Mongey, K.; MacCraith, B. D. *J. Non-Cryst. Solids* **2002**, *306*, 138.
- (29) Yu, S.; Wong, T. K. S.; Hu, X.; Pita, K. J. *Electrochem. Soc.* **2003**, *150*, F116.
- (30) Williams, A. T. R.; Winfield, S. A.; Miller, J. N. *Analyst* **1983**, *108*, 1067.
- (31) Baranov, A.; Rakovich, Y.; Donegan, J.; Perova, T.; Moore, R.; Talapin, D.; Rogach, A.; Masumoto, Y.; Nabiev, I. *Phys. Rev. B* **2003**, *68*, 165306.
- (32) Gao, X.; Nie, S. *J. Phys. Chem. B* **2003**, *107*, 11575.
- (33) Gallardo, I.; Hoffmann, K.; Keto, J. W. *Appl. Phys. A Mater. Sci. Process* **2009**, *94*, 65.
- (34) Sands, D.; Key, P.; Hoyland, J. *Appl. Surf. Sci.* **1999**, *138–139*, 240.
- (35) Mastio, E. A.; Fogarassy, E.; Cranton, W. M.; Thomas, C. B. *Appl. Surf. Sci.* **2000**, *154*, 35.
- (36) Sands, D.; Wagner, F. X.; Key, P. H. *J. Appl. Phys.* **1999**, *85*, 3855.

Synthesis and characterization of CdSe/ZnS core-shell quantum dots immobilized on solid substrates through laser irradiation

E. György^{*1,2}, A. Pérez del Pino³, J. Roqueta¹, B. Ballesteros¹, A. S. Miguel⁴, C. Maycock⁴, and A. G. Oliva⁴

¹ Centre d'Investigacions en Nanociència i Nanotecnologia, Institut Català de Nanotecnologia, Consejo Superior de Investigaciones Científicas (CIN2, ICN-CSIC), Campus UAB, 08193 Bellaterra, Spain

² National Institute for Lasers, Plasma and Radiation Physics, P. O. Box MG 36, 76900 Bucharest V, Romania

³ Instituto de Ciencia de Materiales de Barcelona, Consejo Superior de Investigaciones Científicas (ICMAB, CSIC), Campus UAB, 08193 Bellaterra, Spain

⁴ Instituto de Tecnologia Química e Biológica, Universidade Nova de Lisboa (ITQB-UNL), 2781-901 Oeiras, Portugal

Received 19 December 2011, revised 4 June 2012, accepted 13 July 2012

Published online 10 August 2012

Keywords core-shell quantum dots, immobilization, laser processing, luminescence

* Corresponding author: e-mail egyorgy@cin2.es, Phone: +34-93-581-37-25, Fax: +34-93-581-37-17, Web: www.cin2.es

CdSe/ZnS core-shell quantum dots (QDs) have been immobilized onto solid substrates by matrix assisted pulsed laser evaporation (MAPLE). An UV KrF* ($\lambda = 248$ nm, $\tau_{FWHM} \cong 25$ ns) excimer laser source was used for irradiations of the composite MAPLE targets. The targets were prepared by the dispersion of the CdSe/ZnS QDs in a solvent with high absorption at the incident laser radiation. The dependence of the surface morphology,

crystalline structure, chemical composition, and functional properties of the laser transferred CdSe/ZnS QDs on the processing conditions as incident laser fluence value and ambient atmosphere inside the irradiation chamber was investigated. The possible physical mechanisms implied in the laser ablation process were identified.

© 2012 WILEY-VCH Verlag GmbH & Co. KGaA, Weinheim

1 Introduction CdSe/ZnS core-shell quantum dots (QDs) have received special interest from the scientific community due to their high photoluminescence (PL) quantum yield (QY) with narrow bandwidth, large band gap tunability across the visible spectrum and robustness for being processed [1]. Composite materials containing CdSe/ZnS nanocrystals are promising for a wide range of high-performance applications, as biosensors [2, 3], high efficiency quantum-LEDs [4–6], photovoltaic devices [7, 8], and lasers [9].

As compared to conventional processes used for the immobilization of inorganic nanoparticles, drop casting or spin coating from colloidal solutions, laser technologies offer several advantages: high reproducibility, practically any kind of substrate materials can be used without any pre-treatment procedure, good control over the immobilized material structure and composition, and thus the possibility of tailoring its functional properties. Additionally, the technique allows for multilayers growth and due to its

pulsed character offers a good control over the amount of evaporated and immobilized material through the number of laser pulses. Matrix assisted pulsed laser evaporation (MAPLE) is a laser-based deposition technique in which the material to be immobilized on a solid substrate surface is suspended in a solvent and frozen in liquid nitrogen [10]. The obtained target is subsequently irradiated using laser pulses. The MAPLE technique has already been tested for a large variety of materials, such as functional polymers [11–14], proteins [15–18], bacteria, and even living cells [10]. Some recent studies have demonstrated the use of this technique for the successful deposition of TiO₂ and SnO₂ colloidal nanoparticles [19] and carbon nanopearl films [20] by ultraviolet (UV)-MAPLE, or CdSe QDs [21] by resonant infrared (RIR)-MAPLE techniques.

In this work, UV-MAPLE technique was applied for the transfer and immobilization onto solid substrates of CdSe/ZnS core-shell QDs. These investigations represent a

continuation of our previous work on CdSe/ZnS QDs immobilization in vacuum conditions at low laser fluence values [22]. The main purpose of the present research was to elucidate the influence of the experimental conditions such as incident laser fluence value and ambient atmosphere inside the irradiation chamber on the structure, chemical composition, and fluorescence properties of CdSe/ZnS QDs. The possible physical phenomena taking place during UV-MAPLE process were also identified and discussed.

2 Experimental For the synthesis of CdSe/ZnS QDs standard procedures were used, as described in Refs. [23, 24]. The details of the synthesis process were presented in our previous work [22]. The laser irradiations were performed inside a stainless steel deposition chamber with the aid of a pulsed UV KrF* ($\lambda = 248$ nm, $\tau_{\text{FWHM}} \cong 25$ ns, $\nu = 10$ Hz) COMPexPro 205 Lambda Physik excimer laser source. Before each experiment the irradiation chamber was evacuated down to a residual pressure of 1.6×10^{-3} Pa. The laser immobilization experiments were performed in vacuum or in 0.3 Pa N₂ atmosphere. Toluene was used as solvent for the preparation of the composite MAPLE targets. The target preparation conditions and details of laser irradiation experiments were described in Ref. [22]. 10^4 laser pulses were applied for the deposition of each nanostructure. SiO₂ glass plates were used as substrates. The laser fluence value incident on the target's surface was fixed at 0.25 or 0.45 J cm⁻². The MAPLE workstation was purchased from Surface Systems & Technology GmbH & Co KG, (Hückelhoven, Germany).

The structure of the QDs before and after deposition was studied by transmission electron microscopy (TEM). The samples preparation procedure was described in Ref. [22]. TEM images were acquired on a Jeol JEM-2011 system operated at 200 kV. Energy dispersive X-ray spectroscopy (EDX) analyses were carried out using an Oxford Instruments EDX detector controlled by INCA software. The surface morphology and growth mode of the deposited nanostructures were investigated by atomic force micro-

scopy (AFM) by means of intermittent contact (dynamic) configuration with a 5100 SPM apparatus from Agilent Technologies. The AFM data were processed with the aid of MountainsMap software from Digital Surf. The fluorescence properties of the QDs were investigated with the aid of an inverted microscope model TE2000-S from Nikon equipped with a Nikon HMX-4 100 W Mercury lamp as a light source. Microscope images were acquired with an Evolution MP 5.1 megapixel digital CCD Color Camera (Media Cybernetics) and image capture as well as exposure times were controlled using Image Pro Plus 5.0 software (Media Cybernetics).

3 Results and discussion Figure 1 shows the TEM images of (a) the reference CdSe/ZnS core shell QDs drop-cast sample as well as nanostructures immobilized at (b) 0.45 J cm⁻² laser fluence in vacuum and at (c) 0.25 J cm⁻² laser fluence in 0.3 Pa N₂ atmosphere. The reference sample was deposited by drop-casting from the liquid MAPLE target solution, 2.5 μg CdSe/ZnS core-shell QDs in 3 ml of toluene, on SiO₂ glass substrate, identical to those used in the laser immobilization experiments. As can be observed, both the spherical shape and dimensions, around 5 nm in diameter, of the particles were preserved after the laser processing and transfer. However, in the case of the sample deposited at 0.45 J cm⁻² laser fluence besides the spherical particles, elongated whisker like nanostructures called in literature quantum rods [25], can be identified with high, about 2.5, aspect ratio (Fig. 1b). We mention that nanorods are not present in the reference sample suggesting that they were formed as an effect of laser irradiation possibly during the transit of the laser irradiated material from the target towards the substrate surface.

The HRTEM image of the reference sample (Fig. 2) contains particles with two different crystalline structures. The measured interplanar distances of (A) 0.33 nm can be assigned to the {100}, {110} and respectively {010} lattice plane reflection of the ZnS hexagonal wurtzite (JCPDS file no. 036-1450) as well as (B) 0.31 and 0.27 nm assigned to the {111} and respectively {200} lattice plane reflections of

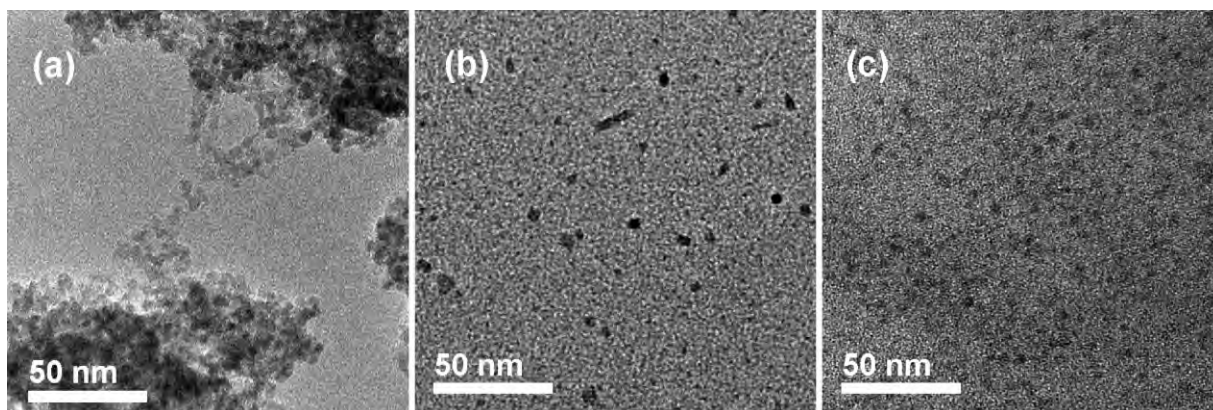


Figure 1 TEM images of (a) reference drop-cast sample prepared by the deposition onto SiO₂ glass substrate of a drop from the solution, 2.5 μg of CdSe/ZnS core shell QDs in 3 ml toluene, used as targets in the MAPLE experiments and CdSe/ZnS core shell QDs deposited on SiO₂ glass substrates at (b) 0.45 J cm⁻² laser fluence in vacuum as well as (c) 0.25 J cm⁻² laser fluence in 0.3 Pa N₂ atmosphere.

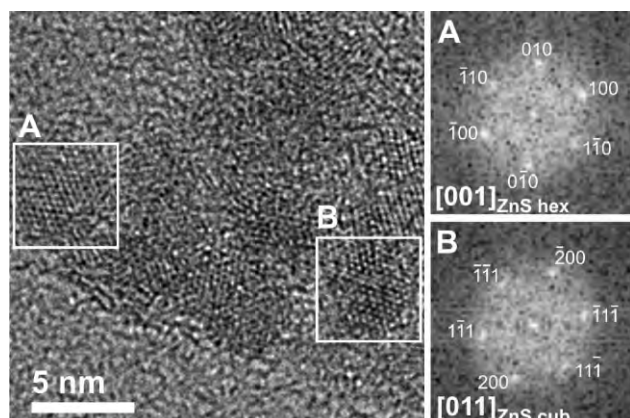


Figure 2 HRTEM image of reference drop-cast sample prepared by the deposition onto SiO_2 glass substrate of a drop from the solution, $2.5 \mu\text{g}$ of CdSe/ZnS core shell QDs in 3 ml toluene, used as targets in the MAPLE experiments. The insets correspond to FFT patterns of the selected areas.

the ZnS $F\bar{4}3m$ (zinc blende) cubic (JCPDS file no. 005-0566) phases. The insets correspond to the fast Fourier transformation (FFT) patterns of the selected areas. The FFT of the selected areas are viewed along the [001] and [011] zone axis of the ZnS hexagonal and cubic phases. It has been reported that the thickness of the ZnS shell determines the crystalline structure of the core-shell QDs [26]. At low-coverage ZnS growth is coherent and epitaxial on the CdSe nanocrystals used as nucleation centers and the lattice fringes are similar to the bulk CdSe. However, at coverage higher than ~ 2 monolayers ZnS shells grow with the bulk ZnS lattice parameter, with incoherence between the core and the shell. Indeed, as in our case with ~ 5 ZnS monolayers, TEM micrographs correspond to the ZnS shell and the growth of the thick overlayer was described as epitaxial but incoherent. Indeed, X-ray diffraction peaks for the core-shell structures has been reported to shift towards the position of the bulk values of the shell [1, 26, 27]. Two distinct mechanisms were proposed to explain this behavior [1]: (i) the growth could be

coherent at low coverage but as the thickness of the shell increases, the strain due to the lattice mismatch between CdSe and ZnS of 12% could induce the formation of dislocations relaxing the structure and thus the growth progresses incoherently or (ii) the growth begins in form of small islands of ZnS with a structure coherent with the CdSe core and as the thickness of the shell increases the islands coalesce to form a shell with a relaxed structure similar to that of bulk ZnS.

The HRTEM images of the laser transferred QDs prove that the crystalline structure of the laser transferred particles was unchanged as compared to that of the reference non-irradiated QDs deposited by drop-cast method from the liquid MAPLE target solution (Fig. 3). The measured interplanar distances correspond to the lattice plane reflections of the hexagonal and cubic zinc-blende ZnS phases (Fig. 3a and c). In case of the sample deposited at the highest laser fluence the measured interplanar distance of the quantum rods (Fig. 3b) of 0.25 nm can be assigned to the {102} lattice plane reflection of the hexagonal CdSe phase (JCPDS file no. 008-0459).

The EDX spectra of reference non-irradiated drop-cast sample and laser deposited sample at 0.25 J cm^{-2} incident fluence value are presented in Fig. 4. Both the spectrum of the reference (Fig. 4a) as well as laser deposited sample (Fig. 4b) are composed by the lines corresponding to the CdSe/ZnS core shell QDs.

The additional lines in the EDX spectra are specific to the substrate as well as the TEM specimen grid. The intensity of the lines is proportional to the amount of material present on the microscope grids. However, at high, 0.45 J cm^{-2} laser fluence, most probably due to the smaller amount of material immobilized on the substrate surface and transferred to the microscope grid, it was not possible to record EDX spectra.

Figure 5 shows the top view (a, d, and g) and tilted higher magnification (b, e, and h) AFM images as well as surface profiles (c, f, and i) of CdSe/ZnS core-shell nanostructures immobilized on SiO_2 glass substrates, at incident laser fluence values of 0.45 (a–c) and 0.25 J cm^{-2} (d–f) in vacuum

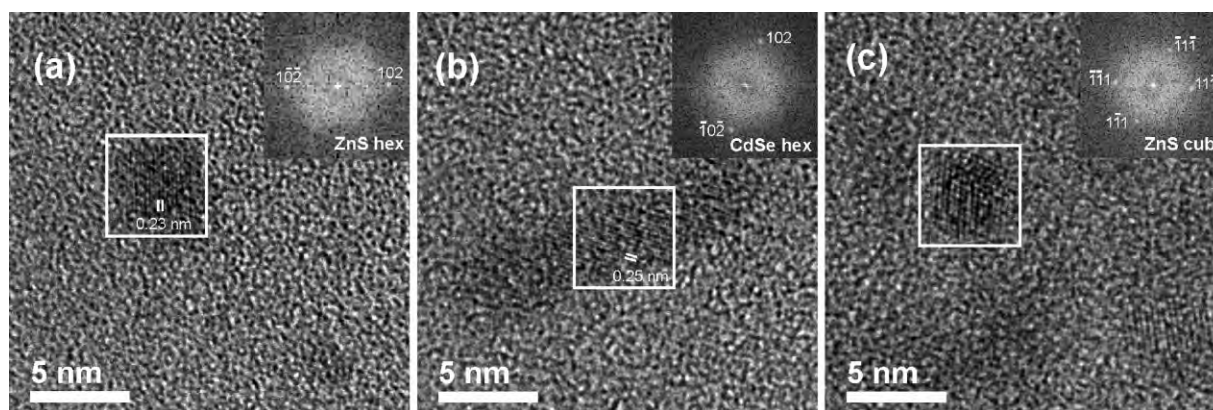


Figure 3 HRTEM images and FFT patterns of CdSe/ZnS core shell QDs deposited on SiO_2 glass substrates at (a and b) 0.45 J cm^{-2} laser fluence in vacuum as well as (c) 0.25 J cm^{-2} laser fluence in 0.3 Pa N_2 atmosphere.

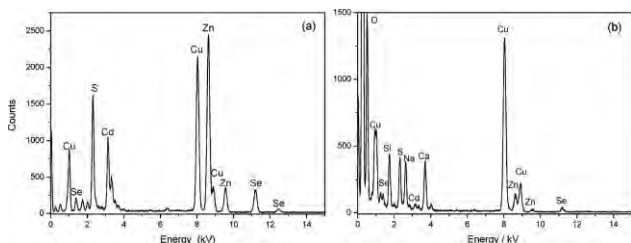


Figure 4 EDX spectra of (a) reference drop-cast sample prepared by the deposition onto SiO₂ glass substrate of a drop from the solution, 2.5 μg of CdSe/ZnS core shell QDs in 3 ml toluene, used as targets in the MAPLE experiments and (b) CdSe/ZnS core shell QDs deposited on SiO₂ glass substrates at 0.25 J cm⁻² laser fluence in 0.3 Pa N₂ atmosphere.

as well as at 0.25 J cm⁻² fluence and 0.3 Pa N₂ atmosphere (g–i). As can be observed, at high, 0.45 J cm⁻² laser fluence the deposited material consists of particulates forming separate islands without covering completely the substrate surface (Fig. 5a). The particulates have an average in plane diameter and height of around 100 nm (Fig. 5b and c). With the decrease of the incident laser fluence to

0.25 J cm⁻², the surface morphology of the immobilized material changes being characterized by continuous coverage over the substrate surface and the presence of circular features with diameters from about 1 to a few μm (Fig. 5d and e). Similar surface morphology can be observed also for the sample deposited at the same laser fluence but in 0.3 Pa N₂ atmosphere (Fig. 5g and h). The corresponding surface profiles are presented in Fig. 5c, f, and i, across the lines marked in the AFM images (Fig. 5b, e, and h). The profile of the deposition obtained at 0.45 J cm⁻² fluence reproduces the shape of the particulates present on the surface (Fig. 5c). At lower, 0.25 J cm⁻² laser fluence both in vacuum and N₂ atmosphere the profiles show the shape of the circular features, containing high amount of material over their whole area (Fig. 5e and f) or ring-shape, concentrating the material at their edges with heights of tens of nm (Fig. 5h and i).

Figure 6 shows the optical microscope (a) and the fluorescence (b) images corresponding to the same surface area of the reference drop-cast sample. An intense orange fluorescence can be observed in Fig. 6b, which is typical for the CdSe/ZnS QDs. The fluorescence signal follows the surface morphology. Its intensity is due to the large

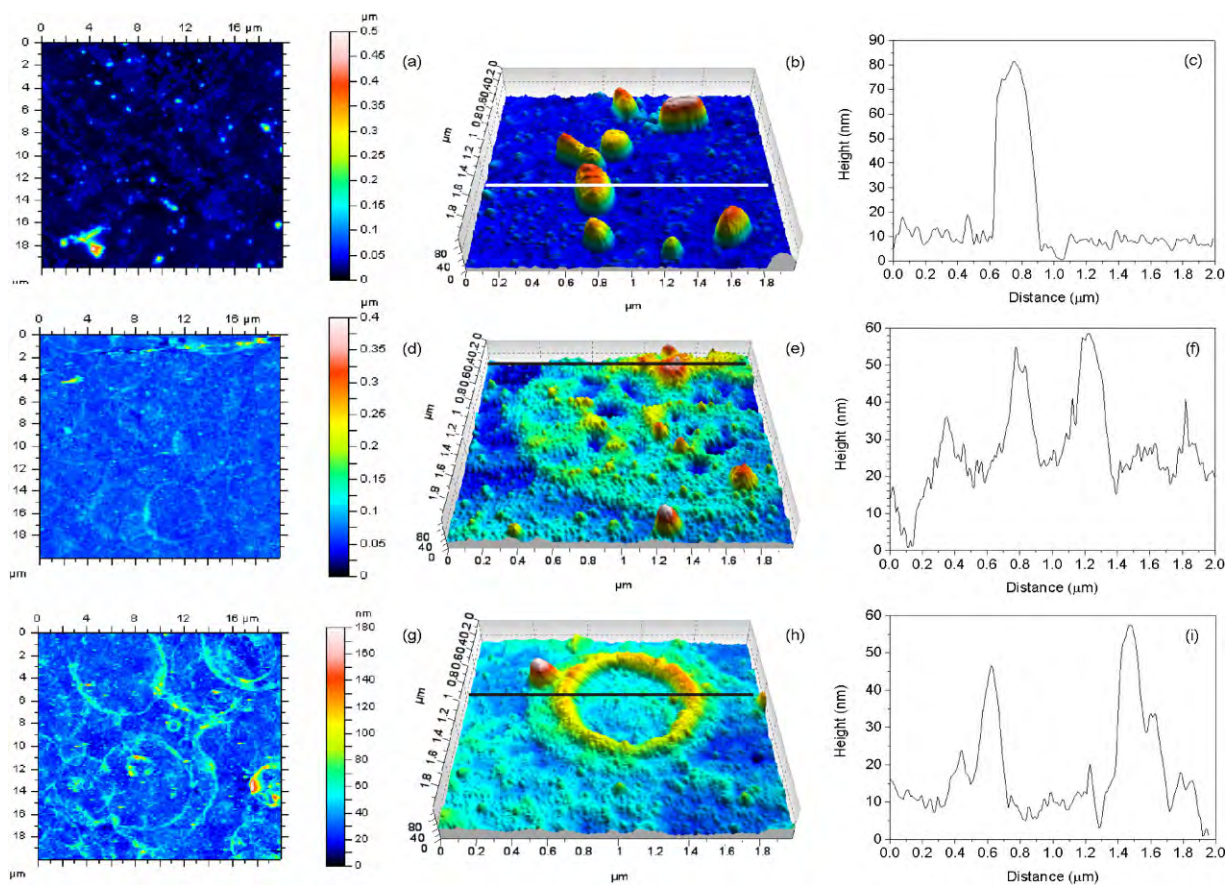


Figure 5 (online color at: www.pss-a.com) Top view and tilted AFM micrographs as well as surface profiles across the lines marked in the AFM micrographs for CdSe/ZnS core shell QDs deposited on SiO₂ glass substrates in vacuum at (a–c) 0.45 and (d–f) 0.25 J cm⁻² laser fluence, as well as at (g–i) 0.25 J cm⁻² laser fluence in 0.3 Pa N₂ atmosphere.

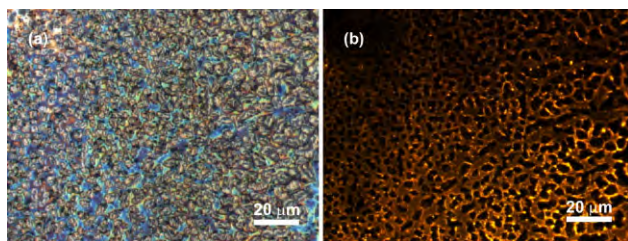


Figure 6 (online color at: www.pss-a.com) Optical microscopy (a) and fluorescence (b) images corresponding to the same surface area of reference drop-cast sample prepared by the deposition onto SiO_2 glass substrate of a drop from the solution, $2.5 \mu\text{g}$ of CdSe/ZnS core shell QDs in 3 ml toluene, used as targets in the MAPLE experiments.

amount of QDs transferred by drop-casting method. The fluorescence images of the laser immobilized CdSe/ZnS core-shell QDs are shown in Fig. 7. Representative intensity profiles of each image are also included. For the deposition obtained at high, 0.45 J cm^{-2} laser fluence in vacuum small number of intense orange fluorescent dots (with a maximum intensity of about 200 a.u.) was observed on reduced intensity (~ 25 a.u.) fluorescence background (Fig. 7a). The fluorescent dots correspond the most probably to the large particles and aggregates observed by AFM, composed by QDs. With the decrease of the laser fluence to 0.25 J cm^{-2} a

pale orange tonality fluorescent background (~ 50 a.u.) can be observed over the whole deposited area proving the formation of a more uniform and continuous surface layer composed by QDs. Fluorescent lines and spots can be also distinguished (Fig. 7b). For the sample obtained at the same, 0.25 J cm^{-2} , laser fluence and 0.3 Pa N_2 atmosphere the fluorescence pattern shows more intense fluorescent orange tonality background (~ 60 a.u.) and several bright orange dots (up to 210 a.u.), corresponding to CdSe/ZnS core-shell QDs aggregates (Fig. 7c). Circular fluorescent areas can be also distinguished, corresponding to the specific ring-shape surface features observed by AFM, concentrating significant amount of QDs at their edges. The intensity of the fluorescent background diminished towards the periphery of the sample to approximately 25 a.u. (Fig. 7d).

The observed surface morphology can be assigned to photothermal ablation mechanisms. Indeed, according to our numerical calculations assuming that the incident light energy is entirely converted into thermal one, even at the lowest, 0.25 J cm^{-2} incident laser fluence the surface temperature reaches the boiling point of toluene, 110°C , at atmospheric pressure [28]. Thus, explosive boiling can take place. Note also that under vacuum the boiling point is lower than at atmospheric pressure. Molecular dynamic simulation results suggested that explosive decomposition of the MAPLE target leads to the expulsion of liquid droplets with dimensions comparable to the optical penetration depth of

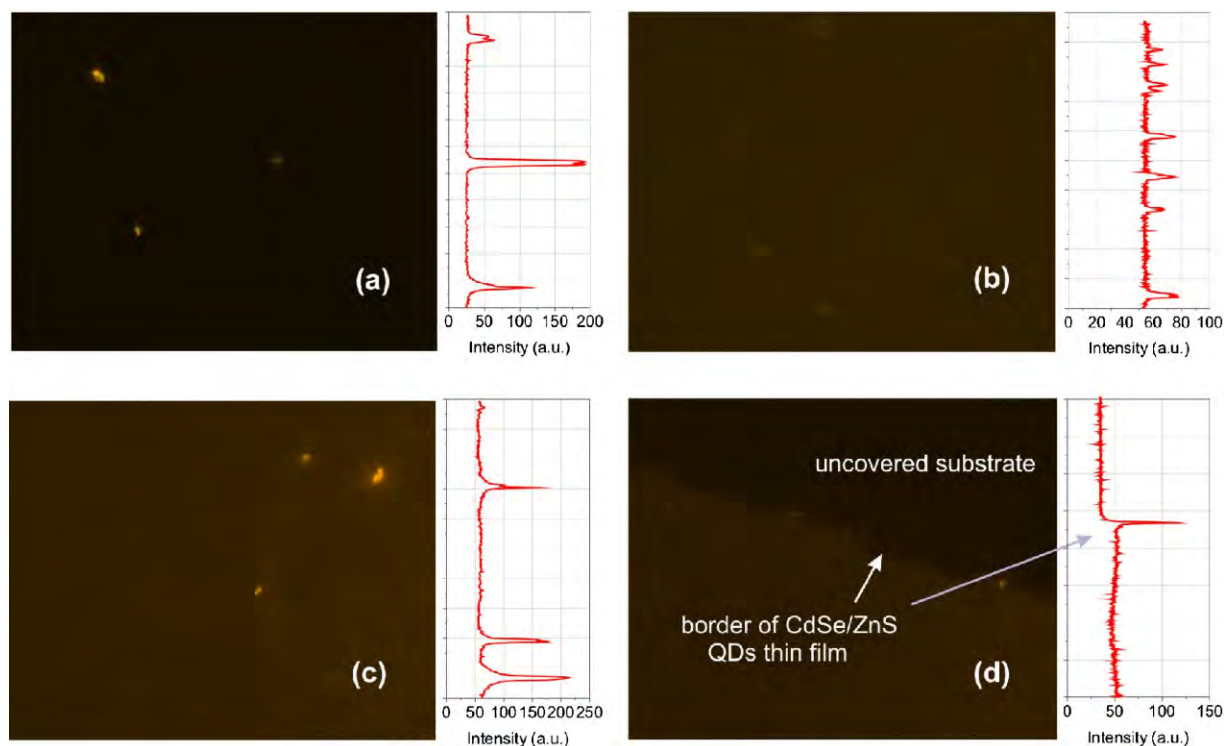


Figure 7 (online color at: www.pss-a.com) Fluorescence images and corresponding characteristic intensity profiles of CdSe/ZnS core shell QDs deposited on SiO_2 glass substrates in vacuum at (a) 0.45 and (b) 0.25 J cm^{-2} laser fluence, as well as at (c and d) 0.25 J cm^{-2} laser fluence in 0.3 Pa N_2 atmosphere.

the matrix, incorporating and transporting the material of interest towards the substrate surface [29]. The optical penetration depth in toluene matrix was estimated at 8.9 μm from the inverse of the linear optical absorption coefficient at 248 nm [30]. However, the laser radiation is also absorbed by the QDs. It was found that in the case of laser irradiation of ZnS sublimation is the controlling factor for the onset of ablation process, before reaching the melting temperature [31]. This behavior is attributed to the low sublimation temperature of ZnS. According to theoretical calculations the laser intensity threshold value to reach the sublimation temperature of ZnS:Mn thin films under KrF*, 248 nm wavelength excimer laser irradiation is around 16.6 MW cm^{-2} , in agreement with the threshold determined experimentally, around 15 MW cm^{-2} [32].

In our experiments, the higher, 0.45 J cm^{-2} laser fluence, corresponding to an intensity value of 18 MW cm^{-2} , surpasses this threshold value. On the other hand, ZnS sublimation can be followed by vaporization of the CdSe particles. The threshold laser fluence necessary to ablate CdSe was determined to be 1.3 J cm^{-2} for a KrF* 248 nm wavelength excimer laser with a pulse width of 14 ns, around 7 MW cm^{-2} [33], well below our laser intensity value. Sublimation of the ZnS shell with high QY as well as CdSe nanoparticles vaporization could explain the low particulates density observed by AFM on the substrate surface (Fig. 5a and b) and the low fluorescence emission of the laser processed and transferred material (Fig. 7a). We would like to note that CdSe nanoparticles are covered with ZnS shell specially to enhance its fluorescence QY [34]. Indeed, uncoated CdSe nanoparticles could be identified by HRTEM studies (Fig. 3b).

The 0.25 J cm^{-2} laser fluence, corresponding to an intensity value of 10 MW cm^{-2} , remains below the sublimation threshold of ZnS [31], but still exceeds the reported ablation threshold of CdSe. The thermal diffusion length in ZnS for 25 ns laser pulses was estimated at around 900 nm [35]. As a consequence, the ablation process in case of the only 5 monolayer thick ZnS shells is governed by the CdSe cores. Then, part of the laser irradiated QDs, especially those situated in the outmost surface layer of the frozen composite target could be damaged. The presence of an ambient gas inside the irradiation chamber produces plasma confinement and an increase of the density of the ejected species in the plasma [36]. As a consequence, the amount of material reaching the substrate surface is higher than under vacuum conditions, resulting in a more intense fluorescence background (Fig. 7c and d).

The micrometer sized circular surface features (Fig. 5d, e, g, and h) could be attributed to liquid droplets coming from the target. We recall that we used toluene as solvent material for the preparation of the MAPLE targets, with high absorption at the wavelength of the incident laser radiation. Molecular dynamics simulation of laser interactions with polymers in a toluene matrix explain the formation of “deflated balloon” structures as the result of droplet ejections during explosive boiling of the overheated

surface region of the MAPLE target [29]. The droplets consist of a mixture of liquid solvent, polymer, and vapor-phase solvent molecules. The solvent vapor inside the droplet pushes the polymer molecules to the surface of the droplet. Following the deposition of the droplet onto the room-temperature substrate, the solvent evaporates leaving behind the characteristic circular surface features. To a certain extent, similar surface features were observed in the case of carbon nanopearls films deposited by MAPLE using the same incident laser wavelength and highly absorbing solvents such as acetone, dimethyl formamide, ethyl acetate, and toluene [20]. Conversely, the effect was minimal in the case of solvents with low absorption at the incident laser radiation such as dimethyl sulfoxide and methanol.

4 Conclusion CdSe/ZnS QDs were immobilised on the surface of SiO_2 glass substrates by UV-MAPLE technique using a solvent with high absorption at the wavelength of the incident laser radiation. The influence of ablation process parameters such as incident laser fluence value and ambient gas pressure inside the irradiation chamber on the surface morphology, crystalline structure, chemical composition, and functional properties of the immobilised material was investigated. At low fluence values and in the presence of ambient gas the shape, dimensions, composition, and structure of the QDs were preserved after the laser processing and immobilisation. With the increase of the laser fluence the onset of sublimation processes and selective evaporation of the QDs could explain the loss of fluorescence properties of the processed and transferred material.

Acknowledgements The authors acknowledge with thanks the financial support from the Spanish National Research Council under the Contracts No. 200860I211 and 200960I015, the Spanish Ministry of Science and Innovation for the PTA2008-1108-I contract, and the Portugal-Spanish Bilateral Agreement No. 2007PT0007.

References

- [1] B. O. Dabbousi, J. Rodriguez-Viejo, F. V. Mikulec, J. R. Heine, H. Mattoussi, R. Ober, K. F. Jensen, and M. G. Bawendi, *J. Phys. Chem. B* **101**, 9463 (1997).
- [2] D. Bas and J. H. Boyaci, *Electroanalysis* **21**, 1829 (2009).
- [3] G. J. Kim, K. W. Kim, M. K. Oh, and Y. M. Sung, *Nanotechnology* **20**, 175503 (2009).
- [4] S. Nizamoglu and H. V. Demir, *J. Appl. Phys.* **105**, 083112 (2009).
- [5] A. Gopal, K. Hoshino, S. Kim, and X. Zhang, *Nanotechnology* **20**, 235201 (2009).
- [6] M. Kazes, T. Saraidarov, R. Reisfeld, and U. Banin, *Adv. Mater.* **21**, 1716 (2009).
- [7] E. Mutlugun, J. M. Soganci, and H. V. Demir, *Opt. Express* **16**, 3537 (2008).
- [8] T. López-Luque, A. Wolcott, L. Xu, S. Chen, Z. Wen, J. Li, E. De La Rosa, and J. Zhang, *J. Phys. Chem. C* **112**, 1282 (2008).

- [9] T. N. Smirnova, O. V. Sakhno, P. V. Yezhov, L. M. Kothtych, L. M. Goldenberg, and J. Stumpe, *Nanotechnology* **20**, 245707 (2009).
- [10] P. K. Wu, B. R. Ringeisen, D. B. Krizman, C. G. Frondoza, M. Brooks, D. M. Bubb, R. C. Y. Auyeung, A. Piqué, B. Spargo, R. A. McGill, and D. B. Chrisey, *Rev. Sci. Instrum.* **74**, 2546 (2003).
- [11] A. Piqué, R. C. Y. Auyeung, J. L. Stepnowski, D. W. Weir, C. B. Arnold, R. A. McGill, and D. B. Chrisey, *Surf. Coat. Technol.* **163/164**, 293 (2003).
- [12] J. M. Fitz-Gerald, G. Jennings, R. Johnson, and C. L. Fraser, *Appl. Phys. A Mater. Sci. Process.* **80**, 1109 (2005).
- [13] A. Gutierrez-Llorente, G. Horwitz, R. Perez-Casero, J. Perriere, J. L. Fave, A. Yassar, and C. Sant, *Organic Electron.* **5**, 29 (2004).
- [14] B. Toftmann, M. R. Papantonakis, R. C. Y. Auyeung, W. Kim, S. M. O'Malley, D. M. Bubb, J. S. Horwitz, J. Schou, P. M. Johnsen, and R. F. Haglund, *Thin Solid Films* **453/454**, 177 (2004).
- [15] B. R. Ringeisen, J. Callahan, P. K. Wu, A. Piqué, B. Spargo, R. A. McGill, M. Bucaro, H. Kim, D. M. Bubb, and D. B. Chrisey, *Langmuir* **17**, 3472 (2001).
- [16] A. Doraiswamy, R. J. Narayan, R. Cristescu, I. N. Mihailescu, and D. B. Chrisey, *Mater. Sci. Eng. C* **27**, 409 (2007).
- [17] M. Jelinek, R. Cristescu, T. Kocourek, V. Vorliček, J. Remsa, L. Stamatina, D. Mihailescu, I. Stamatina, I. N. Mihailescu, and D. B. Chrisey, *J. Phys. Conf. Series* **59**, 22 (2007).
- [18] E. György, A. Pérez del Pino, G. Sauthier, and A. Figueras, *J. Appl. Phys.* **106**, 114702 (2009).
- [19] A. P. Caricato, A. Luches, and R. Rella, *Sensors* **9**, 2682 (2009).
- [20] C. N. Hunter, M. H. Check, J. E. Bultman, and A. A. Voevodin, *Surf. Coat. Technol.* **203**, 300 (2008).
- [21] R. Pate, K. R. Lantz, and A. D. Stiff-Roberts, *Thin Solid Films* **517**, 6798 (2009).
- [22] E. György, A. Pérez del Pino, J. Roqueta, A. S. Miguel, C. Maycock, and A. G. Oliva, *J. Phys. Chem. C* **115**, 15210 (2011).
- [23] J. Aldana, Y. A. Wang, and X. Peng, *J. Am. Chem. Soc.* **123**, 8844 (2001).
- [24] R. Xie, U. Kolb, J. Li, T. Basche, and A. Mews, *J. Am. Chem. Soc.* **127**, 7480 (2005).
- [25] X. Peng, L. Manna, W. Yang, J. Wickham, E. Scher, A. Kadavanich, and A. P. Alivisatos, *Nature* **404**, 59 (2000).
- [26] A. B. Sharma, S. K. Sharma, M. Sharma, R. K. Pandey, and D. S. Reddy, *Spectrochim. Acta A* **72**, 285 (2009).
- [27] A. M. Smith, A. M. Mohs, and S. Nie, *Nature Nanotechnol.* **4**, 56 (2009).
- [28] Y. Tsuboi, K. Hatanaka, H. Fukumura, and H. Masahara, *J. Phys. Chem. A* **102**, 1661 (1998).
- [29] E. Leveugle, A. Sellinger, J. M. Fitz-Gerald, and L. V. Zhigilei, *Phys. Rev. Lett.* **98**, 216101 (2007).
- [30] H. H. Perkampus, *UV-Vis Atlas of Organic Compounds*, 2nd ed. (VCH, Weinheim, 1992).
- [31] D. Sands, P. Key, and J. Hoyland, *Appl. Surf. Sci.* **138/139**, 240 (1999).
- [32] E. A. Mastio, E. Fogarassy, W. M. Cranton, and C. B. Thomas, *Appl. Surf. Sci.* **154**, 35 (2000).
- [33] I. Gallardo, K. Hoffmann, and J. W. Keto, *Appl. Phys. A Mater. Sci. Process.* **94**, 65 (2009).
- [34] J. Ziegler, A. Merkulov, M. Grabolle, U. Resch-Genger, and T. Nann, *Langmuir* **23**, 7751 (2007).
- [35] D. Sands, F. X. Wagner, and P. H. Key, *J. Appl. Phys.* **85**, 3855 (1999).
- [36] D. Geohegan, in: *Pulsed Lased Deposition of Thin Films*, edited by D. B. Chrisey and G. K. Hubler (Wiley, New York, 1994), p. 115.

Metadata of the chapter that will be visualized online

Series Title	Methods in Molecular Biology	
Chapter Title	Synthesis and Functionalization of CdSe/ZnS QDs Using the Successive Ion Layer Adsorption Reaction and Mercaptopropionic Acid Phase Transfer Methods	
Chapter SubTitle		
Copyright Year	2012	
Copyright Holder	Springer Science + Business Media, LLC	
Corresponding Author	Family Name	Miguel
	Particle	
	Given Name	Ana Sofia
	Suffix	
	Division	Organic Synthesis Laboratory, Instituto de Tecnologia Química e Biológica
	Organization	Universidade Nova de Lisboa
	Address	Apartado 127, 2781-901, Oeiras, Portugal
	Division	Biomolecular Diagnostics Laboratory, Instituto de Tecnologia Química e Biológica
	Organization	Universidade Nova de Lisboa
	Address	Apartado 127, 2781-901, Oeiras, Portugal
	Email	sofmig@itqb.unl.pt
Author	Family Name	Maycock
	Particle	
	Given Name	Christopher
	Suffix	
	Division	Organic Synthesis Laboratory, Instituto de Tecnologia Química e Biológica
	Organization	Universidade Nova de Lisboa
	Address	Apartado 127, 2781-901, Oeiras, Portugal
	Division	Faculdade Ciências da Universidade de Lisboa
	Organization	Campo Grande
	Address	Edifício C5, 1149-016, Lisboa, Portugal
	Email	
Author	Family Name	Oliva
	Particle	
	Given Name	Abel
	Suffix	
	Division	Biomolecular Diagnostics Laboratory, Instituto de Tecnologia Química e Biológica
	Organization	Universidade Nova de Lisboa
	Address	Apartado 127, 2781-901, Oeiras, Portugal
	Email	

Abstract

Detailed protocols for the preparation of CdSe nanocrystals coated with a multishell structure of ZnS and their surface modification based on the successive ion layer adsorption and reaction method are described. The first phase of the synthesis produces a hydrophobic surface consisting of a TOPO/HDA ligand mixture. This is followed by a surface modification of the quantum dots (QDs) with 3-mercaptopropionic acid by the phase transfer method. The modified QDs become soluble in aqueous systems such as water or buffers for further biological applications.

Key words: (separated by '-') Quantum dots - 3-Mercaptopropionic acid - Water-soluble - Phase transfer method - Hydrodynamic diameter - ζ -Potential - Bio-conjugation

Synthesis and Functionalization of CdSe/ZnS QDs Using the Successive Ion Layer Adsorption Reaction and Mercaptopropionic Acid Phase Transfer Methods 2 3 4

Ana Sofia Miguel, Christopher Maycock, and Abel Oliva 5

Abstract 6

Detailed protocols for the preparation of CdSe nanocrystals coated with a multishell structure of ZnS and their surface modification based on the successive ion layer adsorption and reaction method are described. The first phase of the synthesis produces a hydrophobic surface consisting of a TOPO/HDA ligand mixture. This is followed by a surface modification of the quantum dots (QDs) with 3-mercaptopropionic acid by the phase transfer method. The modified QDs become soluble in aqueous systems such as water or buffers for further biological applications. 7 8 9 10 11 12

Key words: Quantum dots, 3-Mercaptopropionic acid, Water-soluble, Phase transfer method, Hydrodynamic diameter, ξ -Potential, Bio-conjugation 13 14

1. Introduction 15

Quantum dots (QDs) have emerged as a new class of fluorescent label with unique optical properties. The development of water-soluble and bio-conjugated QDs has made them very appealing for applications in bio-sensing and bio-imaging. QDs made of CdSe core and ZnS shells have been widely used for bio-conjugation (1). Several procedures for the synthesis of CdSe/ZnS QDs have been reported; including the method of successive ion layer adsorption and reaction (SILAR) (2–4). The core-shell CdSe/ZnS QDs synthesis reported here is based upon modified SILAR technique. The obtained cores are monodisperse and after coating of the CdSe (TOPO/HDA) with at least five monolayers of ZnS show a high fluorescence, are stable in organic solutions and are suitable for the posterior functionalization reactions with different ligands to 16 17 18 19 20 21 22 23 24 25 26 27 28

29 obtain hydrophilic and biocompatible QDs. However, CdSe/ZnS
30 core-shell QDs are synthesized in organic medium and have a sur-
31 face layer of lipophilic ligands which makes them insoluble in aque-
32 ous solution. We describe here the generation of water-soluble
33 CdSe/ZnS QDs by ligand exchange of TOPO/HDA with
34 3-mercaptopropionic acid (MPA). Ligand exchange by the phase
35 transfer method leads to a change of the surface polarity from
36 hydrophobic to hydrophilic and yields water-soluble nanoparticles.
37 The reported technique is advantageous due to its practical sim-
38 plicity and the potential for further derivatization through the
39 introduced carboxylic acid groups (5, 6).

40 2. Materials

41 All of the reagents used for the synthesis of CdSe/ZnS and
42 functionalization of MPA-coated QDs can be stored at room tem-
43 perature, unless indicated otherwise. All solutions should be freshly
44 prepared under an argon atmosphere. We recommend using Pt 100
45 probe and a digital thermometer for the temperature control. Place
46 the probe inside the reaction flask. For aqueous solutions, ultra-
47 pure water is recommended (18 M Ω at 25 °C, Millipore Milli-Q).
48 All common solvents should be p.a. ACS grade.

49 2.1. CdSe Core 50 Nanocrystal 51 Components

- 52 1. UV/Vis spectrophotometer Beckman DU-70 or similar
instrument.
- 53 2. Dynamic light scattering (DLS) instrument, Zetasizer Nano
54 ZS (Malvern Instruments).
- 55 3. Precision cells made of Quartz Supracil[®], Type Nr 101-QS,
56 10 mm, Hellma.
- 57 4. Centrifuge for use with 50 mL centrifuge tubes and capable of
58 5,000 $\times g$, e.g., Eppendorf 5804R.
- 59 5. Rotary evaporator, BUCHI rotavapor R-205 with vacuum
60 controller V-800 and heating bath B-490.
- 61 6. Ultrasound bath, Banson 1200.
- 62 7. Vortex mixer.
- 63 8. pH meter.
- 64 9. High vacuum pump.
- 65 10. Heating mantle.
- 66 11. Magnetic stirrer.
- 67 12. Digital thermometer with Pt 100 sensor.
13. Glass Pasteur pipettes (230 mm).
14. Disposable syringe (1, 2, and 5 mL)

	15. Polypropylene centrifuge tubes (50 mL).	68
	16. Syringe needles (19-gauge stainless steel, 10 in., with Luer hub and deflecting tip).	69 70
	17. 100 mL three-neck flask.	71
	18. 10 mL two-neck flask.	72
	19. Chloroform.	73
	20. Methanol (puriss. p.a., Reag. ACS).	74
	21. Cadmium oxide (99.99 %).	75
	22. Trioctylphosphine oxide (TOPO, technical grade).	76
	23. Oleic acid (Ph Helv).	77
	24. 1-Hexadecylamine (HDA, tech. 90 %).	78
	25. Selenium/trioctylphosphine (Se/TOP) solution: add 0.0632 g of selenium powder (99.5 %, powder, 100 mesh) into a 10 mL two-neck flask under an argon flow. Add 2.4 mL of trioctylphosphine (TOP, tech. 90 %) and sonicate the solution until a colorless optically clear solution is obtained.	79 80 81 82 83
2.2. CdSe/ZnS Core-Shell Nanocrystal Components	1. Centrifuge for use with 50 mL centrifuge tubes and capable of 8,000 × g, e.g., Eppendorf 5804R.	84 85
	2. Rotary evaporator, BUCHI rotavapor R-205 with vacuum controller V-800 and heating bath B-490.	86 87
	3. Ultrasound bath, Branson 1200.	88
	4. High vacuum pump.	89
	5. Heating mantle.	90
	6. Magnetic stirrer.	91
	7. Digital thermometer with Pt 100 sensor.	92
	8. Glass Pasteur pipettes (230 mm).	93
	9. Filter (PTFE membrane, 0.2 μm pore size, filter-Ø: 15 mm).	94
	10. Polypropylene centrifuge tubes (15 and 50 mL).	95
	11. Single-use syringes (1, 2, and 5 mL).	96
	12. Syringe needles (19-gauge stainless steel, 10 in., with Luer hub and deflecting tip).	97 98
	13. 100 mL three-neck flask.	99
	14. 10 mL two-neck flasks.	100
	15. 250 mL glass funnel.	101
	16. Chloroform.	102
	17. Methanol (puriss. p.a., Reag. ACS).	103
	18. Hexane.	104
	19. Acetone.	105
	20. TOPO (technical grade).	106

- 107 21. 1-Hexadecylamine (tech. 90 %).
- 108 22. Zinc oxide precursor solution. To prepare 0.1 M solution
- 109 transfer 0.041 g of ZnO to a 10 mL two-neck flask, under
- 110 argon flow and add 1.4 mL of oleic acid (Ph Helv). Heat the
- 111 mixture at 300 °C until the solution is completely clear. Add
- 112 3.6 mL of 1-octadecene (tech. 90 %) and keep the final solu-
- 113 tion at 80 °C until the growth shell procedure is complete.
- 114 23. Elemental sulfur solution: The sulfur precursor solution,
- 115 0.1 M, is prepared by dissolving sulfur in 1-octadecene (tech.
- 116 90 %) at 180 °C. In a 10 mL two-neck flask, under argon, con-
- 117 taining 0.016 g of elemental sulfur (99.98 %, powder), add
- 118 5 mL of 1-octadecene. Heat the solution until a clear solution
- 119 is obtained, indicating that all sulfur is completely dissolved in
- 120 the noncoordinating solvent. Maintain this solution at 80 °C
- 121 until the shell growth procedure is complete.

122 **2.3. MPA-Coated QDS**

123 **Components**

- 124 1. UV/Vis spectrophotometer, Beckman DU-70.
- 125 2. Centrifuge for use with 15 mL centrifuge tubes and capable of
- 126 7,500 × *g*, e.g., Eppendorf 5804R.
- 127 3. pH meter.
- 128 4. Glass Pasteur pipettes (230 mm).
- 129 5. Centrifugal filter devices (Vivapsin 6, MWCO 10 kDa PES
- 130 membrane).
- 131 6. Polypropylene centrifuge tubes (15 mL).
- 132 7. 10 mL volumetric flask.
- 133 8. Glass vials with polypropylene snap cap (5 and 10 mL).
- 134 9. Polypropylene micro tubes (2 mL).
- 135 10. 250 mL Duran Shott Bottle.
- 136 11. Chloroform.
- 137 12. Sodium hydroxide (p.a. ACS grade).
- 138 13. Stock solution of MPA: In a 10 mL graduated volumetric flask,
- 139 add 400 μL of MPA (99 %) (4.59 mmol) to 10 mL of MeOH
- 140 followed by the addition of 500 mg of KOH.
- 141 14. 10 mM NaOH in deionized water (pH 12).

142 **2.4. Optical**

143 **Characterization**

144 **Components**

- 145 1. UV/Vis spectrophotometer, Beckman DU-70.
- 146 2. Fluorescence spectrophotometer SPEX Fluorolog or
- 147 Fluoromax-4 (Horiba Jobin Yvon).
3. DLS instrument, Zetasizer Nano ZS (Malvern Instruments).
4. Precision cells made of Quartz Supracil®, Type Nr 101-QS,
- 10 mm.
5. Universal “Dip” cell (ZEN 1002, Malvern Instruments) (see
- Note 1).

6. Filters (PTFE membrane, 0.2 μm pore size, filter- \varnothing : 15 mm). 148
7. Rhodamine 6G in EtOH solution. Adjust concentration to achieve the optical density at the peak of approximately 0.1 or less. 149
150
151
8. 10 mM NaOH in deionized water (pH 12). 152
9. Single-use syringes (1 and 2 mL). 153
10. Disposable needles ($\varnothing 0.80 \times 50$ mm). 154

3. Methods

155

3.1. Synthesis of CdSe Core Nanocrystals

1. In a 100 mL three-neck flask, under an argon atmosphere, place 0.042 g of cadmium oxide (CdO) and 0.6 mL of oleic acid. Heat the mixture under stirring to 100 $^{\circ}\text{C}$ to obtain a yellow optically clear solution. 156
157
158
159
2. Then, remove the flask from the heat source and add 2 g of 1-hexadecylamine (HDA) and 2 g of TOPO. Heat the solution again, but this time to 280–300 $^{\circ}\text{C}$. When all is completely dissolved, the temperature is stabilized at 280 $^{\circ}\text{C}$ and the mixture should be optically clear. 160
161
162
163
164
3. While keeping the mixture at 280 $^{\circ}\text{C}$, in one single injection, add 2.4 mL of Se/TOP solution prepared previously (see Note 2). 165
166
167
4. After 2 min at 280 $^{\circ}\text{C}$ remove the heating mantle. When the temperature reaches 85 $^{\circ}\text{C}$ inject 20 mL of MeOH, to precipitate the nanoparticles. Leave the reaction mixture to cool to room temperature. 168
169
170
171
5. Transfer the nanoparticle suspension to five 50 mL polypropylene centrifuge tubes (10 mL in each tube). Add 20 mL of chloroform to each tube to force the precipitation of nanocrystals and shake the tubes by hand to mix the solutions. Leave the tubes to stand for 90 min at room temperature. 172
173
174
175
176
6. Centrifuge the tubes at $5,000 \times g$ at room temperature for a period of 10 min and discard the cloudy supernatant. 177
178
7. Wash the concentrated pellet at the bottom of the tubes at least three times with 20 mL of MeOH, centrifuging at $5,000 \times g$ for a period of 10 min each time. 179
180
181
8. Dry the final red-brownish pellet under vacuum and the nanocrystals can then be dispersed in chloroform or hexane for further processing. Otherwise, they can be stored as a powder in the dark at 4 $^{\circ}\text{C}$ for several months. 182
183
184
185
9. This procedure typically yields CdSe nanocrystals with the first absorption peak at 568 nm with a diameter of about 3.5 nm. 186
187

188 **3.2. Synthesis of CdSe/
189 ZnS Core-Shell
190 Nanocrystals, Based
191 on Successive Ion
192 Layer Adsorption
193 Reaction Method**
194
195
196
197
198
199
200
201

For shell growth, the SILAR method was found to be the best approach. This technique is based on alternating injections of precursor's solutions containing metal oxides such as ZnO and elemental sulfur into the solution containing the CdSe-core nanocrystals. Using this method, layers of ZnS can be grown successively around the core. The noncoordinating solvent, 1-octadecene is the most appropriate solvent for the growth of high-quality nanocrystals in general. It has a low melting point, high boiling point, low cost, low toxicity, low reactivity to precursors and excellent solvation power for many compounds at elevated temperatures (7, 8). 1-Hexadecylamine (HDA) is used as ligand for the core-shell nanocrystals because alkylamines have proven to be very good ligands for highly luminescent plain CdSe/ZnS core-shell nanocrystals (9).

- 202 1. Add 3 mL of 1-octadecene and 1 g of 1-hexadecylamine to a
203 100 mL three-neck flask. Heat the flask under vacuum at 70 °C
204 during 1 h to remove any traces of water and then cool to
205 room temperature.
- 206 2. Disperse ~30 mg of CdSe nanocrystals (from Subheading 3.1),
207 in a polypropylene tube in 15 mL of chloroform and filter
208 using a 0.2 µm PTFE membrane.
- 209 3. Place the chloroform suspension containing the CdSe nano-
210 crystals in the flask and remove the chloroform and other vola-
211 tiles by heating under vacuum at 70 °C for 30 min (see
212 Note 3).
- 213 4. Remove the vacuum and heat the system under an argon atmo-
214 sphere to 245 °C. Maintain the reaction at this temperature for
215 the duration of the shell growth procedure.
- 216 5. To calculate the amount of Zn- and S-precursor for the growth
217 of the first monolayer, assume that the surface of the CdSe-
218 cores consists equally of Se and Cd atoms. For a solution con-
219 taining CdSe nanocrystals with 3.5 nm (1.01×10^{-4} mmol),
220 0.47 mL of Zn and S precursor solutions should be added for
221 the first layer; 0.64 mL of each injection solution for the sec-
222 ond layer; 0.84 mL of each injection solution for the third
223 layer; 1.064 mL of each injection solution for the fourth layer,
224 and 1.32 mL of each injection solution for the fifth layer (see
225 Note 4).
- 226 6. After the final injection, incubate the reaction mixture for
227 30 min at 260 °C.
- 228 7. Cool the reaction to room temperature and add 30 mL of
229 hexane. Transfer the solution to a 250 mL glass extraction fun-
230 nel and remove the unreacted compounds and possible byprod-
231 ucts by successive MeOH extractions (20 mL, 6–8 washes)
232 (see Note 5).

8. Transfer the hexane/ODE phase containing the nanoparticles to a 50 mL centrifuge tube and wash with acetone. Centrifuge at $8,000\times g$ at room temperature for 10 min (see Note 6).
9. Suspend the final pellet in about 15 mL of hexane and precipitate the nanoparticles with the addition of the same volume of MeOH. Centrifuge at $8,000\times g$ at room temperature for 10 min.
10. Discard the colorless supernatant and dry the final red-brownish pellet under high vacuum for 1 h. The final QDs can be dispersed in chloroform or hexane for further processing. Otherwise, it can be stored as a powder in the dark at $4\text{ }^{\circ}\text{C}$ for several months.

3.3. Water-Soluble QDs: QDs Capped with 3-Mercaptopropionic Acid

The MPA-coated QDs are obtained by the phase transfer method (4, 10). When reacted with ZnS-capped CdSe QDs in chloroform, the mercapto-group binds to the Zn atom and the polar carboxylic acid group renders the QDs water-soluble. The free carboxyl group is also available for covalent coupling to various biomolecules (such as proteins, peptides, and nucleic acids) by cross-linking to reactive amine groups (6).

1. Add 10 mg of CdSe/ZnS (ODE/HDA) QDs to a 5 mL glass vial and disperse in about 1.5 mL of chloroform to give a high concentration solution (optical density, $\text{OD}=1.5$). Then, add 200 μL of a fresh stock solution containing MPA, close the vial with a snap cap and manually shake for 2 min (see Note 7).
2. Add 1.5 mL of NaOH solution 10 mM (pH 12) to the flocculate solution and manually shake it again. Two phases appear which correspond to the transfer of QDs from the organic to the aqueous phase.
3. For the complete phase separation, transfer the two-phase solution to a 15 mL polypropylene tube and centrifuge at $5,500\times g$ at room temperature for 5 min. Recover the aqueous phase (colored phase). Repeat steps 2 and 3 to ensure the total collection of water-soluble QDs.
4. Purify and concentrate the aqueous solution containing the MPA-capped CdSe/ZnS QDs using a Vivapsin 6 tube (cutoff 10 kDa) at $7,500\times g$, at room temperature for 15 min and wash (three times) with NaOH solution 10 mM (pH 12).
5. Disperse the concentrated sample in 1 mL of NaOH solution 10 mM (pH 12) affording an orange optically clear solution. The sample can be stored in the dark at $4\text{ }^{\circ}\text{C}$ (see Note 8).

273 **3.4. Characterization**
 274 **of CdSe/ZnS and**
 275 **Corresponding**
 276 **MPA-QDs**

277 *3.4.1. Optical*
 278 *Characterization*

Record UV–Vis absorption spectra using a spectrometer and photoluminescence (PL) spectra with a spectrofluorometer. Quantum yields (QY) can be measured relative to Rhodamine 6G in ethanol solution with excitation at 530 nm. Solutions of QDs in chloroform (CdSe/ZnS QDs) or water (MPA-QDs) and dye in ethanol are optically matched at the excitation wavelength ($\lambda=530$ nm). Fluorescence spectra of QDs and dye are measured under identical spectrometer conditions. The optical density at the peak should be maintained below 0.1, and the integrated intensities of the emission spectra, corrected for differences in index of refraction and concentration, should be used to calculate QY using the expression (see Note 9):

$$QY_{\text{QD}} = QY_{\text{Dye}} \times (\text{abs}_{\text{Dye}}/\text{abs}_{\text{QD}}) \times (\text{peak area}_{\text{QD}}/\text{peak area}_{\text{Dye}}) \times (\eta_{\text{QD solvent}})^2/(\eta_{\text{Dye solvent}})^2$$

where $QY_{\text{Dye}} = 0.95$ (the quantum yield of the solution containing Rhodamine 6G dye in EtOH), “abs” is absorbance of the solutions, “peak area” = corrected areas under the emission peaks, and η is average of refractive indexes of QDots and the dye solvents.

1. Using standard 10 mm path length Quartz cuvettes, record the UV–Vis absorbance spectra of the CdSe@ ZnS QDots in chloroform, MPA-QDots in water and Rhodamine 6G (dye) in ethanol. The optical density for both samples and dye at excitation wavelength should be below 0.1.
2. Record the emission spectra at 530 nm of the solutions prepared in step 1 in the 10 mm fluorescence cuvettes (Fig. 1).
3. Correct the fluorescence spectra obtained in step 2 for both samples and dye and calculate the integrated fluorescence intensity, that is, the area of the fluorescence spectra, using the appropriate spectrometer software.
4. Calculate the Quantum Yield using integrated intensities of the emission spectra, corrected for differences in index of refraction and concentration. Use the formula shown above (see Note 9).

306 *3.4.2. Concentration*
 307 *Determination*
 308 *of QD Solutions*

The determination of QD concentration in solution, water, or a given medium is not straightforward (see Note 10). Measurements of optical density can in principle be used to find molar concentrations if there are established extinction coefficients for these materials. However, the published extinction coefficients for quantum dots vary by more than an order of magnitude. These discrepancies may arise in part from the sensitivity of absorption coefficients to both quantum dot diameter and composition. According to some literature, the absorption spectrum method seems to be the most practical and convenient way to determine the particle concentrations. Thus, the optical density in water is measured and an

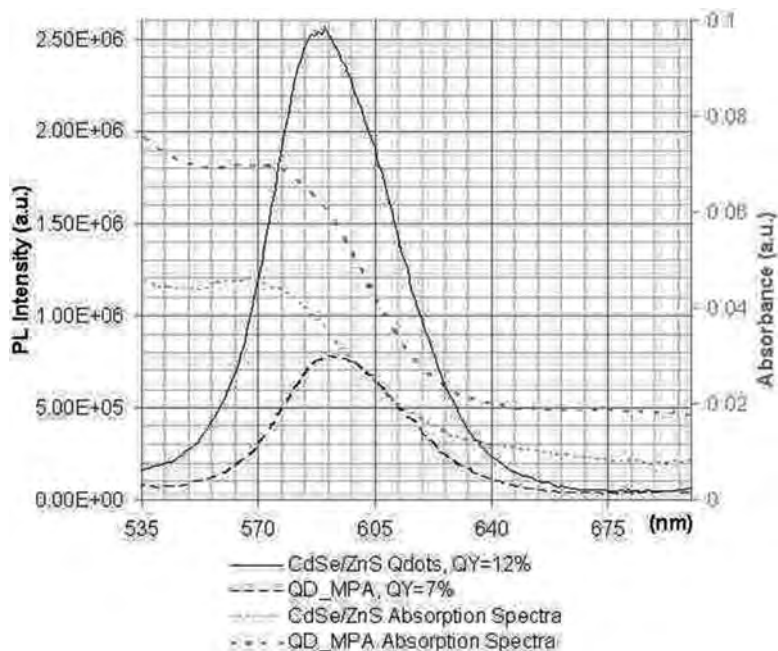


Fig. 1. Absorbance and fluorescence spectra. Absorbance spectrum of CdSe/ZnS core-shell (QD585) in CHCl_3 and MPA-coated QDs in water (gray lines). Fluorescence spectra with absorption normalized at the excitation of QD585 ($\lambda = 530 \text{ nm}$) in CHCl_3 (QY = 12 %) and in water after ligand exchange with MPA (QY = 7 %) (black lines).

absorption coefficient reported in the literature (see Note 11) for CdSe core QDs is applied (to calculate the concentration using the Lambert–Beer’s Law, $A = \epsilon bC$, where A is the optical density, b is the light path length, C is the core/shell QD concentration, and ϵ is the extinction coefficient) (see Note 12).

1. Resuspend ~10 mg of CdSe core QDs in 1.5 mL of chloroform.
2. Using 10 mm standard path length Quartz cuvettes, record the UV–Vis absorbance spectra of the solution prepared in step 1.
3. From the UV–Vis spectra obtained in the previous step, take the absorbance value of the highest absorption wavelength (absorption maximum) between 400 and 700 nm and determine NPs concentration (see Note 12).

3.4.3. Dynamic Light Scattering Measurements of Hydrophobic and Hydrophilic CdSe/ZnS QDs

Light scattering analysis is performed using a dynamic light scatterer. With this equipment, it is possible to analyze the hydrodynamic diameter (HD) and zeta potential (ζ) of synthetic lipophilic CdSe/ZnS QDs and their corresponding hydrophilic variant. HD is obtained from number-weighted size distribution analysis and reported as the mean of triplicate measurements. ζ -Potential is

337
338
339
340
341
342
343
344
345
346
347
348
349
350
351
352
353
354
355
356
357

measured only for hydrophilic QDs, because synthetic CdSe/ZnS QDs have no charge density on their surface. Values are reported as the average of triplicate runs consisting of 20 measurements at 25 °C.

1. Prepare 2 mL of each sample in the appropriate solvent and concentration: CdSe/ZnS QDs in chloroform and MPA-QDs in 10 mM NaOH (pH 12). For CdSe/ZnS and their corresponding hydrophilic QDs, sample concentrations between 0.06 and 0.3 μM should be prepared. The samples concentration should be adjusted to accommodate the scattering properties of your sample and/or the optical requirements of your specific instrument.
2. Take 1 mL of each sample solution using a 1 mL disposable syringe and filter the sample through a 0.2 μm PTFE membrane filter.
3. Transfer the filtered sample into the cuvette for analysis. The cuvette should be filled slowly to avoid the formation of air bubbles. For hydrodynamic diameter measurements, close the cuvette with supplied cap before analysis to avoid contamination and solvent evaporation. In zeta potential measurements, the cap is replaced by the universal “dip” cell which has to be

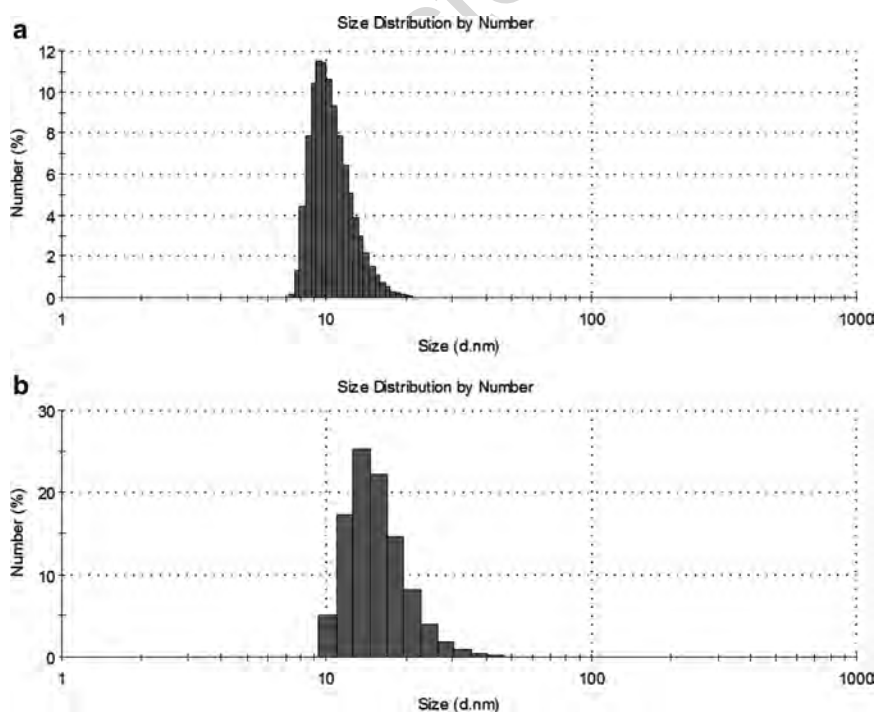


Fig. 2. Dynamic light scattering measurements. Representative dynamic light scattering histogram of (a) CdSe/ZnS QDs in CHCl_3 and (b) after ligand exchange with MPA, giving HD = 9.3 and 13.5 nm respectively.

- inserted inside the cuvette according to the manufacturer's instructions (see Note 13). 358 359
- Place the cuvette correctly in the sample holder (quartz windows should be facing the incident beam and detector). 360 361
 - Perform three measurements per sample at 25 °C (± 1 min) (during 1 min/20 runs for size and zeta potential measurements respectively) with an equilibration time of 2 min. 362 363 364
 - To analyze the obtained data, use the instrument's software to evaluate parameters such as autocorrelation data, size distribution, count rate, and zeta potential values (Fig. 2). 365 366 367

4. Notes 368

- 10 mm precision cells made of quartz should be used to ensure that the optimum signal is achieved in size and zeta potential measurements and due to their high resistance to aqueous and nonaqueous solutions. Therefore, an additional universal "dip" cell is required (according to instrument manufacturer's specifications) to measure zeta potential of the aqueous samples. 369 370 371 372 373 374 375
- After the addition of the Se/TOP solution, there is always a decrease in the temperature of the mixture inside the flask and could reach 255–265 °C. In this case, you should wait until the temperature stabilizes again to 280 °C to control the crystal growth time. 376 377 378 379 380
- As the system is under high vacuum, the temperature should not exceed 70 °C in order to avoid possible evaporation/loss of the mixture of solvent/ligand 1-octadecene/1-hexadecylamine from the reaction vessel. 381 382 383 384
- With fast stirring in place, there is no need for dropwise injections. A period of 10 min between each addition is sufficient for the reaction to be completed. The whole procedure for covering CdSe cores with five monolayers takes about 1 h 30 min. 385 386 387 388 389
- In the extraction procedure, the undesired products are soluble in MeOH. Therefore this phase should be discarded, keeping the hexane/ODE phase which contains the nanocrystals. 390 391 392
- This step is important for the elimination of excess ODE. This noncoordinating solvent can be retained by the nanoparticles during the MeOH washes. If it is not removed completely, it may appear on the walls of the tube in the form of a pale yellow powder. Washing with acetone helps to eliminate ODE, which will be discarded in the yellow cloudy supernatant. Repeat this wash four times for a complete removal of ODE. 393 394 395 396 397 398 399

- 400 7. With the addition of MPA stock solution, the chloroform
401 solution may flocculate and became turbid. The solution is not
402 optically clear at a pH = 5–7, possibly due to inter-particle hydro-
403 gen bonding between the carboxyl functions of the ligands.
- 404 8. With time, the functionalized MPA-QDs can form aggregates.
405 To remove them, centrifuge the sample in 2 mL polypropylene
406 tube at $2,000 \times g$ at room temperature for 2 min. Recover the
407 supernatant and store again in the dark at 4 °C for further use.
408 In this case, the new concentration has to be determined.
- 409 9. This formula is from ref. (11).
- 410 10. The published extinction coefficients for QDs can vary by more
411 than an order of magnitude. Some authors (12) measure the
412 optical density of the core-shell-structured QDs in water apply-
413 ing an absorption coefficient that is the average of three
414 reported in the literature (13–15). In this case, a large error on
415 the extinction coefficient could exist and the optical density
416 can at best give concentrations that are only accurate to 50 %.
- 417 11. Accurate determination of the extinction coefficient for QDs is
418 described in ref. (13). The results show that the extinction
419 coefficient of nanocrystals in the strong quantum confinement
420 size regime increases as their size increases approximately as a
421 square to a cubic function. Furthermore, the integrated ϵ of
422 the first absorption peak seemed to be independent of tem-
423 perature, nature of the surface capping groups, the refractive
424 index of the solvents, the photoluminescence, and the meth-
425 ods employed for the synthesis of the QDs.
- 426 12. For example, for CdSe core nanocrystals with the first exci-
427 tonic absorption peak at 568 nm, according to a sizing curve
428 from Peng and colleagues (13) the typical size is around 3.5 nm
429 and consequently the size-dependent extinction coefficient of
430 these nanocrystals is about 1.5×10^5 M/cm. If the solution
431 measured has $A = 1.5$ in a 1 cm path length,
- 432
$$c = A / \epsilon = 1.5 / 1.5 \times 10^5 = 1 \times 10^{-5} \text{ M} = 10 \mu\text{M}$$
- 433 13. For both measurements, inspect the cuvette to ensure that no
434 air bubbles are clinging to the optical window area or interfer-
435 ing with the metal electrodes of “dip” cell in zeta potential
436 analysis.

437 Acknowledgements

438 This work was supported by a grant to A.S.M. from the Fundação
439 para a Ciência e Tecnologia (SFRH/BD/40303/2007) and the
440 national funded project NTec/SQA/0131/2007 of FCT.

441 References

- 442 1. Liu W, Howarth M, Greytak AB, Zheng Y, 477
443 Nocera DG, Ting AY, Bawendi MG (2008) 478
444 Compact biocompatible quantum dots func- 479
445 tionalized for cellular imaging. *J Am Chem Soc* 480
446 130:1274–1284
- 447 2. Aldana J, Wang YA, Peng X (2001) 481
448 Photochemical instability of CdSe nanocrystals 482
449 coated by hydrophilic thiols. *J Am Chem Soc* 483
450 123:8844–8850
- 451 3. Li JJ, Wang A, Guo W, Keay JC, Mishima TD, 484
452 Johnson MB, Peng X (2003) Large-scale syn- 485
453 thesis of nearly monodisperse CdSe/CdS core/ 486
454 shell nanocrystals using air-stable reagents via 487
455 successive ion layer adsorption and reaction. *J* 488
456 *Am Chem Soc* 125: 489
457 12567–12575
- 458 4. Xie R, Kolb U, Li J, Bashé T, Mews A (2005) 490
459 Synthesis and characterization of highly lumi- 491
460 nescent CdSe-core CdS/Zn_{0.5}Cd_{0.5}S/ZnS 492
461 multishell nanocrystals. *J Am Chem Soc* 127: 493
462 7480–7488
- 463 5. Wang Q, Xu Y, Zhao X, Chang Y, Liu Y, 494
464 Jiang L, Sharma J, Seo D, Yan H (2007) A fac- 495
465 ile one-step in situ functionalization of quan- 496
466 tum dots with preserved photoluminescence 497
467 for bioconjugation. *J Am Chem Soc* 129: 498
468 6380–6381
- 469 6. Chan WCW, Nie S (1998) Quantum dot bio- 499
470 conjugates for ultrasensitive nonisotopic detec- 500
471 tion. *Science* 281:2016–2018
- 472 7. Yu WW, Peng X (2002) Formation of high- 501
473 quality and other II–VI semiconductor nano- 502
474 crystals in noncoordinating solvents: tunable 503
475 reactivity of monomers. *Angew Chem Int Ed* 504
476 41:2368–2371
8. Battaglia D, Peng X (2002) Formation of high 477
quality InP and InAs nanocrystals in a nonco- 478
ordinating solvent. *Nano Lett* 2:1027–1030 479
9. Peng X, Schlamp MC, Kadavanich AV, 480
Alivisatos AP (1997) Epitaxial growth of highly 481
luminescent CdSe/CdS core/shell nanocrystals 482
with photostability and electronic accessi- 483
bility. *J Am Chem Soc* 119:7019–7029 484
10. Gill R, Freeman R, Xu J, Willner I, Winograd S, 485
Shweky I, Banin U (2006) Probing biocatalytic 486
transformations with CdSe-ZnS QDs. *J Am* 487
Chem Soc 128:15376–15377 488
11. Williams ATR, Winfield SA, Miller JN (1983) 489
Relative fluorescence quantum yields using a 490
computer-controlled luminescence spectrome- 491
ter. *Analyst* 108:1067–1071 492
12. Yu WW, Chang E, Falkner JC, Zhang J, Al-Somali 493
AM, Sayes CM, Johns J, Drezek R, Colvin VL 494
(2007) Forming biocompatible nonaggregated 495
nanocrystals in water using amphiphilic poly- 496
mers. *J Am Chem Soc* 129:2871–2879 497
13. Yu WW, Qu L, Guo W, Peng X (2003) 498
Experimental determination of the extinction 499
coefficient of CdTe, CdSe and CdS nanocrystal- 500
s. *Chem Mater* 15:2854–2860 501
14. Leatherdale CA, Woo WK, Mikulec FV, 502
Bawendi MG (2002) On the absorption cross 503
section of CdSe nanocrystal quantum dots. 504
J Phys Chem B 106:7619–7622 505
15. Striolo A, Ward J, Prausnitz JM, Parak WJ, 506
Zanchet D, Gerion D, Milliron D, Alivisatos AP 507
(2002) Molecular weight, osmotic second virial 508
coefficient and extinction coefficient of colloidal 509
CdSe nanocrystals. *J Phys Chem B* 510
106:5500–5505 511

Metadata of the chapter that will be visualized online

Series Title	Methods in Molecular Biology	
Chapter Title	Evaluation of Cytotoxicity of 3-Mercaptopropionic Acid-Modified Quantum Dots on Medicago sativa Cells and Tissues	
Chapter SubTitle		
Copyright Year	2012	
Copyright Holder	Springer Science + Business Media, LLC	
Corresponding Author	Family Name	Santos
	Particle	
	Given Name	Ana Raquel
	Suffix	
	Division	Biomolecular Diagnostics Laboratory
	Organization	Instituto de Tecnologia Química e Biológica, Universidade Nova de Lisboa
	Address	Apartado 127, 2781-901, Oeiras, Portugal
	Division	Plant Cell Biotechnology Laboratory
	Organization	Instituto de Tecnologia Química e Biológica, Universidade Nova de Lisboa
	Address	Apartado 127, 2781-901, Oeiras, Portugal
	Email	anaraqssantos@gmail.com
Author	Family Name	Miguel
	Particle	
	Given Name	Ana Sofia
	Suffix	
	Division	Biomolecular Diagnostics Laboratory
	Organization	Instituto de Tecnologia Química e Biológica, Universidade Nova de Lisboa
	Address	Apartado 127, 2781-901, Oeiras, Portugal
	Division	Organic Synthesis Laboratory
	Organization	Instituto de Tecnologia Química e Biológica, Universidade Nova de Lisboa
	Address	Apartado 127, 2781-901, Oeiras, Portugal
	Email	
Author	Family Name	Fevereiro
	Particle	
	Given Name	Pedro
	Suffix	
	Division	Plant Cell Biotechnology Laboratory
	Organization	Instituto de Tecnologia Química e Biológica, Universidade Nova de Lisboa
	Address	Apartado 127, 2781-901, Oeiras, Portugal
	Division	
	Organization	Universidade de Lisboa
	Address	1749-016, Lisbon, Portugal
	Email	
Author	Family Name	Oliva

Particle	
Given Name	Abel
Suffix	
Division	Biomolecular Diagnostics Laboratory
Organization	Instituto de Tecnologia Química e Biológica, Universidade Nova de Lisboa
Address	Apartado 127, 2781-901, Oeiras, Portugal
Email	

Abstract Like most of the new technologies designed to interact with biological systems, the applications of - nanomaterials needs a proper assessment for their potential impacts. It is only through addressing the issues raised by toxicological studies that nanotechnology will be able to acquire its full potential. Here, we describe the detailed protocols to study the responses of plant cells to their exposure to nanoparticles, including viability, oxidative stress detection, and reactive oxygen species enzymatic detoxification, as well as particle uptake.

Key words: (separated by '-') Quantum dots - Cytotoxicity - ROS detection - Oxidative stress - Uptake - Antioxidant enzyme activity - Cell suspension cultures - Medicago sativa

Evaluation of Cytotoxicity of 3-Mercaptopropionic Acid-Modified Quantum Dots on *Medicago sativa* Cells and Tissues 2 3 4

Ana Raquel Santos, Ana Sofia Miguel, Pedro Fevereiro, and Abel Oliva 5

Abstract 6

Like most of the new technologies designed to interact with biological systems, the applications of nanomaterials needs a proper assessment for their potential impacts. It is only through addressing the issues raised by toxicological studies that nanotechnology will be able to acquire its full potential. Here, we describe the detailed protocols to study the responses of plant cells to their exposure to nanoparticles, including viability, oxidative stress detection, and reactive oxygen species enzymatic detoxification, as well as particle uptake. 7
8
9
10
11
12

Key words: Quantum dots, Cytotoxicity, ROS detection, Oxidative stress, Uptake, Antioxidant enzyme activity, Cell suspension cultures, *Medicago sativa* 13
14

1. Introduction 15

As a result of the rapid development of nanotechnology an emerging area of research is now focused on studying the short and medium term impacts of nanomaterials on the environment. This new discipline, named nano-ecotoxicology is now being developed to adequately evaluate the global impact of these new devices and their multiple applications (1). Cell-based in vitro studies play an essential role on meaningful toxicity testing. They allow the setting up of high-throughput systems for rapid and cost-effective screening of hazards, while targeting the biological responses under highly controlled conditions (2). Mechanisms of nanotoxicity should include the identification of the routes of uptake and intracellular accumulation of nanoparticles, the modes of its action, the damage to cellular structures, and the kinetics of toxi- and detoxification (3). The following protocols were developed to evaluate the plant 16
17
18
19
20
21
22
23
24
25
26
27
28
29

cell responses when in contact with quantum dots (QDs), including cell viability, the histochemistry of reactive oxygen species (ROS) production and accumulation, the activity of ROS detoxification enzymes, and cell/plant–particle uptake.

Fluorescein diacetate (FDA) is a widely used viability test due to quickness and because it can be visualized within individual cells with the help of a fluorescence microscope and therefore not only it is used as a general viability assay but also facilitates the determination of the number of live cells in a population (4). FDA is converted into a fluorescent product if cell membrane is intact and therefore viable cells present a bright green fluorescence when excited at 488 nm (5).

Using light microscopy we can monitor ROS production and accumulation with ROS-specific tracer dye 3-3' diaminobenzidine (DAB) for hydrogen peroxide (H_2O_2) and the nitroblue tetrazolium (NBT) for $O_2^{\cdot-}$. 2',7'-Dichlorodihydrofluorescein diacetate (H_2DCFDA) was applied to measure oxidative responses in cell suspension cultures. This probe is oxidized due to the presence of ROS, and the emitted fluorescence intensity is directly proportional to the level of dichlorofluorescein (DCF) formed intracellularly (6).

There is much evidence obtained from various plant systems showing that the concentration and activity of enzymes involved in scavenging ROS are altered by different stresses. The measurement of the activity of three major antioxidative enzymes is described: superoxide dismutases (SOD), catalase (CAT), and glutathione reductase (GR) from the ascorbate-glutathione cycle.

2. Materials

2.1. Initiation of *Medicago sativa* Cell Suspension Cultures

1. Eight week dark grown callus from roots or petioles of *Medicago sativa*.
2. Murashige & Skoog (M&S) liquid medium supplemented with 0.5 mg/L of Dichlorophenoxyacetic acid and 0.5 mg/L of kinetin. pH of medium should be adjusted to 5.8 with 1 M NaOH before autoclaving (121 °C, 20 min). Growth regulators are filter sterilized (0.2 µm) and added to the cooled autoclaved medium.
3. Orbital shaker at 120 rpm in the dark, at 24 °C.

2.2. Determination of Cell Viability

1. Stock solution of CdSe nanocrystals filter sterilized (0.2 µm). To illustrate the methods we will be using Mercaptopropionic acid (MPA)-QDs nanocrystals coated with a multishell structure of ZnS (see Note 1).
2. Eight days old *M. sativa* cell suspension culture.

3. Stock solution of FDA: dissolve 10 mg of FDA in 2 mL of acetone and keep at -20°C . 72
73
4. Fluorescence microscope with a filter set at 488 nm. 74
5. Murashige & Skoog (M&S) liquid medium supplemented with 0.5 mg/L of Dichlorophenoxyacetic acid and 0.5 mg/L of kinetin. pH of medium should be adjusted to 5.8 with 1 M NaOH before autoclaving (121°C , 20 min). Filter-sterilize the growth regulators (0.2 μm) and add to the cooled autoclaved medium. 75
76
77
78
79
80

2.3. QDs Uptake by Cells of *M. sativa* in Suspension Cultures

1. Stock solution of CdSe nanocrystals filter sterilized (0.2 μm). To illustrate the methods we will be using MPA-QDs nanocrystals coated with a multishell structure of ZnS (see Note 1). 81
82
83
2. Eight days old *M. sativa* cell suspension culture. 84
3. Fluorescence microscope with a filter set at 588 nm. 85
4. Murashige & Skoog (M&S) liquid medium supplemented with 0.5 mg/L of Dichlorophenoxyacetic acid and 0.5 mg/L of kinetin. pH of medium should be adjusted to 5.8 with 1 M NaOH before autoclaving (121°C , 20 min). Filter-sterilize the growth regulators (0.2 μm) and add to the cooled autoclaved medium. 86
87
88
89
90
91

2.4. In Vitro Uptake of QDs by Roots of *Medicago truncatula* Plantlets

1. Fourteen days old *Medicago truncatula* plantlets with roots of 1 cm length, grown in solid Murashige & Skoog (M&S) medium with 0.2 % (w/v) of gelrite. 92
93
94
2. Murashige & Skoog liquid medium supplemented with 200 mM of mannitol. 95
96
3. Four percent paraformaldehyde (PFA) solution in PBS: in a fume hood heat 20 mL of PBS to 60°C in a water bath. Weigh 1 g of (PFA) and add to the PBS while continuously stirring and maintain on heating plate at 60°C (do not allow water bath to go over 70°C , or formaldehyde will vaporize!). Add one or two drops of 5 M NaOH with a Pasteur pipette. The solution should become almost clear fairly rapidly, but will still have some fine particles that will not disappear. Remove from heat and complete the volume up to 25 mL with PBS. Cool the solution to room temperature and adjust the pH to 7.2 with a solution of 1 M HCl. Filter, aliquot into tubes, and freeze at -20°C . 97
98
99
100
101
102
103
104
105
106
107
4. Phytotron set to a 16 h photoperiod and a day/night temperature of 24/22 $^{\circ}\text{C}$. 108
109
5. Fluorescence microscope with a filter set at 588 nm. 110
6. PBS: 8 g of NaCl, 0.2 g of KCl, 1.44 g of Na_2HPO_4 , and 0.24 g of KH_2PO_4 . Adjust pH to 7.4 with HCl and add distilled water to 1 L. 111
112
113
7. Vibratome. 114

115 **2.5. ROS Detection**116 **2.5.1. Hydrogen Peroxide**
117 **Detection**

- 118
- 119
- 120
- 121
- 122
- 123
- 124
- 125
- 126
- 127
- 128
- 129
1. Stock solution of CdSe nanocrystals filter sterilized (0.2 μm). To illustrate the methods we will be using MPA-QDs nanocrystals coated with a multishell structure of ZnS (see Note 1).
 2. Three days old *M. sativa* cell suspension culture.
 3. 10 mg/mL DAB stock solution: 20 mg of DAB in 2 mL DMSO. Vortex the solution and centrifuge because the DAB does not dissolve completely and filter with a 0.2 μm pore. Store in dark at 4 °C (see Note 2).
 4. 0.5 M H_2O_2 solution: mix 102 μL of H_2O_2 and 2 mL of distilled water. Sterilize with a 0.2 μm filter and store in the dark at 4 °C. Prepare this solution fresh, just before running the assay.
 5. Optical microscope.
 6. Sterile 6-well plates.
 7. Orbital shaker.

130 **2.5.2. Superoxide Anion**
131 **($\text{O}_2^{\cdot-}$) Detection**

- 132
- 133
- 134
- 135
- 136
- 137
- 138
1. Stock solution of CdSe nanocrystals filter sterilized (0.2 μm). To illustrate the methods we will be using MPA-QDs nanocrystals coated with a multishell structure of ZnS (see Note 1).
 2. Three days old *M. sativa* cell suspension culture.
 3. 12 mM NBT stock solution: dissolve 20 mg of NBT in 2 mL of distilled water. Vortex and sterilize with a 0.2 μm filter. Store at 4 °C.
 4. Optical microscope.
 5. Orbital shaker.

139 **2.5.3. Oxidative Stress**
140 **Detection**

- 141
- 142
- 143
- 144
- 145
- 146
- 147
- 148
1. Stock solution of CdSe nanocrystals filter sterilized (0.2 μm). To illustrate the methods we will be using MPA-QDs nanocrystals coated with a multishell structure of ZnS (see Note 1).
 2. Three days old *M. sativa* cell suspension culture.
 3. 10 mM H_2DCFDA stock solution: dissolve 9.7 mg of H_2DCFDA in 2 mL of DMSO. Vortex and sterilize with a 0.2 μm filter. Store at -20 °C.
 4. Fluorescence microscope with a filter set at 488 nm.
 5. Orbital shaker.
 6. Heated water bath.

149 **2.5.4. Oxidative Stress**
150 **Dose Response Assay**

- 151
- 152
1. Stock solution of CdSe nanocrystals filter sterilized (0.2 μm). To illustrate the methods we will be using MPA-QDs nanocrystals coated with a multishell structure of ZnS (see Note 1).
 2. Three days old *M. sativa* cell suspension culture.

3. 10 mM H₂DCFDA stock solution: dissolve 9.7 mg of H₂DCFDA in 2 mL of DMSO. Vortex and sterilize with a 0.2 μm filter. Store at -20 °C. 153-155
 4. Fluorescence microscope with a filter set at 488 nm, with a color camera. 156-157
 5. Open source software ImageJ (<http://rsbweb.nih.gov/ij/>) for quantification of the image intensity. 158-159
- 2.6. Antioxidant Enzymatic Activity**
- 2.6.1. Enzyme Extraction**
1. Stock solution of CdSe nanocrystals filter sterilized (0.2 μm). To illustrate the methods we will be using MPA-QDs nanocrystals coated with a multishell structure of ZnS (see Note 1). 160-162
 2. Three days old *M. sativa* cell suspension culture. 163
 3. 100 mM Tris-HCl extraction buffer, pH 7.5: for 100 mL add 1.22 g of Tris, 3 mM DTT, 1 mM EDTA, 0.2 % triton X-100. Adjust to pH 7.5 with 1 M HCl and store at 4 °C, use within 2-3 weeks. 164-167
 4. Centrifuge capable of 12,000 × g. 168
- 2.6.2. Determination of SOD Activity**
1. Extracts from cell suspension cultures. 169
 2. 100 mM potassium phosphate buffer, pH 7.5. First make solution A by dissolving 13.61 g of KH₂PO₄ in 1 L of distilled water; and solution B by dissolving 14.2 g of Na₂HPO₄ in 1 L of distilled water. Add solution A to solution B until the required pH 7.5 is reached. Keep at 4 °C. The solution can be used for 2-3 weeks. 170-175
 3. 0.5 mM xantine stock solution: dissolve 47.6 mg of xantine in 25 mL of potassium phosphate buffer, pH 7.5. Add 1 M NaOH dropwise with constant stirring, until a clear solution is obtained. Store at 4 °C, use within 2-3 weeks. 176-179
 4. 0.1 mM EDTA stock solution: dissolve 23.27 mg of EDTA in 25 mL potassium phosphate buffer. Store at 4 °C, use within 2-3 weeks. 180-182
 5. Solution A (superoxide production): dissolve 6.1 mg of Cytochrome C in 12.5 mL of potassium phosphate buffer, add 0.5 mL of EDTA stock solution, and 0.5 mL of xantine stock solution. Prepare fresh before use. 183-186
 6. Solution X (xantine oxidase): Prepare a diluted solution containing 0.72 U of xantine oxidase in 800 μL of potassium phosphate buffer. Prepare fresh before sue and keep on ice. 187-189
 7. Spectrophotometer. 190
 8. Disposable polystyrene cuvettes with 10 mm optical light path. 191-192

- 193 **2.6.3. Determination**
194 **of CAT Activity**
195
196
197
1. Extracts from cell suspension cultures.
 2. 10 mM H₂O₂ stock solution: 170 μL of H₂O₂ (30 %) in 50 mL potassium phosphate buffer. Prepare fresh before use.
 3. UV/Vis spectrophotometer.
 4. Quartz cuvette 10 mm optical light path.
- 198 **2.6.4. Determination**
199 **of GR Activity**
200
201
202
203
204
205
206
207
208
209
210
211
212
213
214
1. Extracts from cell suspension cultures.
 2. 100 mM potassium phosphate buffer, pH 7.5 with 1 mM EDTA: dissolve 372 mg of EDTA in 100 mL of potassium phosphate buffer. Store at 4 °C, use within 2–3 weeks.
 3. 0.75 mM 5,5'-Dithiobis(2-nitrobenzoic acid) (DTNB) stock solution: dissolve 11.8 mg of DTNB in 10 mL potassium phosphate buffer. Prepare just before use, protect from direct light.
 4. 0.1 mM NADPH stock solution: dissolve 3 mg of NADPH in 2 mL of potassium phosphate buffer. Prepare fresh before use.
 5. 1 mM of Oxidized Glutathione (GSSG): dissolve 24.3 mg of GSSG in 2 mL of potassium phosphate buffer. Prepare fresh just before use.
 6. Spectrophotometer.
 7. Disposable polystyrene cuvettes with 10 mm optical light path.

215 3. Methods

216 All procedures should be carried out in a laminar flow chamber and
217 with sterilized material unless otherwise specified. Unless men-
218 tioned otherwise, all cell suspension cultures are grown and main-
219 tained on the orbital shaker at 120 rpm in the dark, at 24 °C.

220 **3.1. Initiation of** 221 ***Medicago sativa* Cell** 222 **Suspension Culture**

- 223
224
225
226
227
228
229
230
1. Place two friable portions of 8 week grown callus in 50 mL of liquid M&S medium. Grow cells for 8 days. After 8 days, add 100 mL of fresh M&S liquid medium.
 2. Grow cells for another 8 days.
 3. Remove the cells from the shaker and allow the suspension to settle for 3–4 min and pipette 20 mL of cells to another flask with 100 mL of M&S liquid medium (see Note 3).
 4. Grow cells until a density of 4×10^4 cells/mL is obtained. Change the medium every 8 or 9 days by transferring 20 mL of cell culture to 100 mL of fresh medium (in 250 mL Erlenmeyer flasks).

3.2. Determination of Cell Viability

1. Take 2 mL aliquots of 8-day-old cell suspension culture of *M. sativa* and subculture in a 50 mL Erlenmeyer flask containing 10 mL of fresh M&S liquid medium. 231-233
2. On the third day of culture determine the viability of cells. Prepare fresh diluted solution of FDA by adding 20 μ L of the FDA stock solution and 1 mL of M&S liquid medium, then on a microscope slide mix 20 μ L of suspension culture and 20 μ L of diluted FDA and cover with a cover slip. Incubate 5 at room temperature and perform the counts under the fluorescence microscope. FDA is converted into a fluorescent product if cell membrane is intact and therefore viable cells present a bright green fluorescence when excited at 488 nm. Count five random spots per slide and calculate the percentage of viability: 234-243

$$\text{viability \%} = (\text{number of viable cells} / \text{total number cells}) * 100$$
 244
3. After determining of the cellular viability add the MPA-QDs to the cell suspension cultures (use different concentrations ranging from 10 to 100 nM). 245-247
4. Grow cells for 5 days (until the eighth day of culture) and determine the cell culture viability as described above (see Note 4). 248-249

3.3. QDs Uptake by Cells of *M. sativa* in Suspension Cultures

MPA-QDs may accumulate intracellularly due to the hydrophilic character of MPA and the reduced size of the particles. The exact mechanisms of QDs attachment to the plant cells are not known. It has been shown that MPA-QDs can accumulate in different cellular compartments when contacted with *M. sativa* cells in suspension cultures (7). 250-255

1. Inoculate 2 mL aliquot of 8 days old *M. sativa* cell suspension culture in 50 mL Erlenmeyer flasks containing 10 mL of fresh M&S liquid medium. 256-258
2. Culture the cells for 3 days. 259
3. Add the MPA-QDs to the cell suspension cultures (final concentration ranging from 10 to 100 nM). 260-261
4. Grow the cells for 48 h. 262
5. Visualize samples using a confocal and fluorescent microscope (Fig. 1). 263-264
6. Acquire thin time-course confocal optical sections (~ 2 μ m thick) using <20 % laser intensity and operating in the mode 1,024 \times 1,024, 400 Hz ($\sim 1/2$ s per frame). A $\times 20$ Plan Apo dry objective (NA=0.75) (Leica) should be used. 265-268

3.4. In Vitro Uptake of QDs by Roots of *Medicago truncatula* Plantlets

1. Gently take out the 14-day-old plantlets from the agar using forceps (make sure that the roots are taken intact) and place it in 50 mL Falcon sterilized tubes with 200 μ L of M&S liquid medium with mannitol. Cover with parafilm and incubate in a 269-272

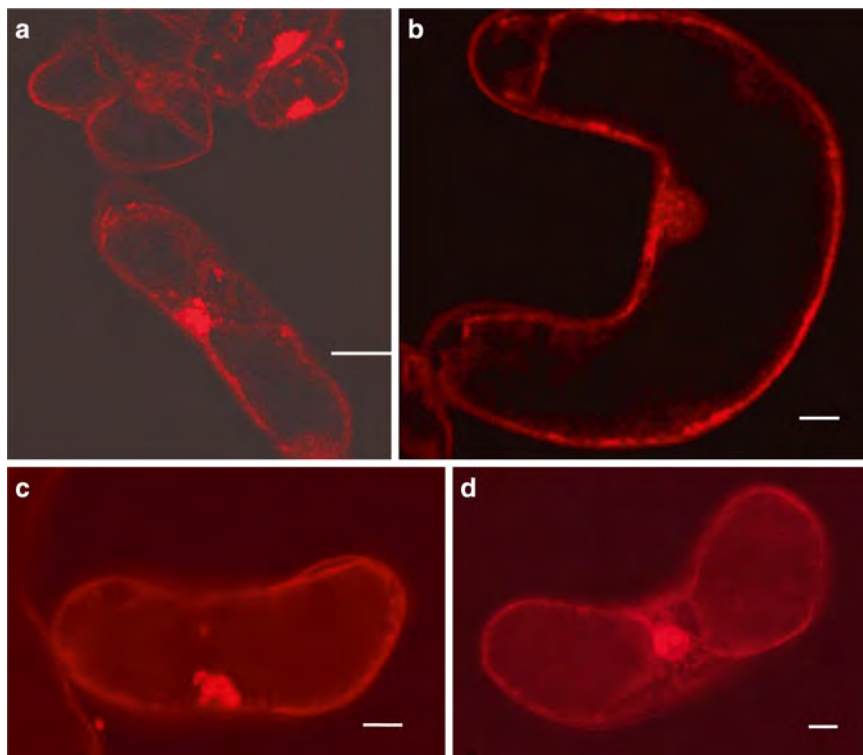


Fig. 1. Internalization of MPA-QDs in *Medicago sativa* cells. Confocal (a, b) and wide field (c, d) fluorescence images of *M. sativa* cells after 48 h of incubation with MPA-QDs. Scale bar = 20 μ M. Reproduced from ref. (7).

273

274

275

276

277

278

279

280

281

282

283

284

285

286

287

288

289

Phytotron under standard culture conditions mentioned above.

2. After 48 h remove the plantlets from the tubes and place them in a petri dish with a drop of fixation solution. Cut the root into three pieces no larger than 1 cm: root cap, zone of maturation, and zone of differentiation.
3. Transfer the pieces into 15 mL Falcon tubes with 4 % PFA solution (approximately ten times the volume of the samples) at 4 °C. Then place the samples under vacuum for approximately 10 min (to facilitate the fixative penetration into the samples).
4. Let the fixation process run overnight (about 18 h) at 4 °C with smooth agitation.
5. Wash the samples three times 10 min in PBS and store it in 0.1 % PFA in PBS at 4 °C (see Note 5).
6. Make longitudinal cuts using a vibratome and visualize them on a fluorescence microscope under UV light.

3.5. ROS Detection**3.5.1. Hydrogen Peroxide
Detection**

1. Take seven 2 mL aliquots from 3-day-old cell suspension cultures of *M. sativa* and transfer into sterile 6-well plate. Add MPA-QDs to the cell suspension cultures to 0, 1, 5, 10, 20, 50, 100 nM final concentration. 290-293
2. Grow the cells for 48 h. 294
3. Add 0.1 mg/mL of DAB to all cell suspension cultures (see Note 6). As control, heat 2 mL of suspension culture at 45 °C for 20 min (heated in a water bath) and add 0.1 mg/mL of DAB (see Note 7), as a second control add 40 µL of H₂O₂ stock solution into 2 mL of suspension culture plus 0.1 mg/mL of DAB (see Note 8). 295-300
4. Incubate cells on the orbital shaker for 90 min and check cell cultures using a fluorescence microscope (see Note 9). 301-302

**3.5.2. Superoxide Anion
(O₂^{-•}) Detection**

1. Take seven 2 mL aliquots from 3-day-old cell suspension cultures of *M. sativa* and transfer into sterile 6-well plate. Add MPA-QDs to cell suspension cultures to 0, 1, 5, 10, 20, 50 and 100 nM final concentrations 303-306
2. Grow the cells for 48 h. 307
3. Add 10 µL of NBT stock solution to all cell suspension cultures (final concentration of 60 nM). As control, heat 2 mL of suspension culture at 45 °C for 20 min (heated in a water bath) and add 10 µL of NBT stock solution (final concentration of 60 nM). 308-312
4. Incubate cells on the orbital shaker for 4 h and visualize cells using a microscope under bright field illumination (see Note 10). 313-314

**3.5.3. Oxidative Stress
Detection**

1. Take seven 2 mL aliquots from 3-day-old cell suspension cultures of *M. sativa* and transfer into sterile 6-well plate. Add MPA-QDs to cell suspension cultures to 0, 1, 5, 10, 20, 50 and 100 nM final concentrations. 315-318
2. Grow the cells for 48 h. 319
3. Add 1 µL of H₂DCFDA stock solution to all cell suspension cultures (to a final concentration of 5 µM). As control, heat 2 mL of suspension culture at 45 °C for 20 min (heated in a water bath), and add 1 µL of H₂DCFDA stock solution (to a final concentration of 5 µM). 320-324
4. Incubate cells on the orbital shaker for 1 h and visualize the samples using a fluorescence microscope (see Note 11). 325-326

**3.5.4. Oxidative Stress
Dose Response Assay**

1. Take 27 2 mL aliquots from 3-day-old cell suspension cultures of *M. sativa* and add to sterilized 6 well plates. Aliquots of MPA-QDs are added to each well to obtain the following final concentrations: 1, 5, 10, 20, 40, 60, 100, 120, and 180 nM (all in triplicates). All plates are placed on an orbital shaker at 110 rpm in the dark at 24 °C. 327-332

- 333
334
335
336
337
338
339
340
341
342
343
344
2. After 48 h of incubation, 1 μL of H_2DCFDA is added to all treatments, to obtain a final concentration of 5 μM .
 3. The fluorescence is quantified in terms of average pixel intensity, using the open source software ImageJ. Images are acquired 1 h after the H_2DCFDA addition, always with the same settings, and exposure time. For each treatment at least 15 pictures should be taken.
 4. Using the ImageJ program split the channels of the pictures in red, blue, and green. Using the green channel histogram (to exclude the QDs fluorescence), multiply the number of pixels with their respective intensity value (0–255) and divide it for the total number of pixels of the image.

3.6. Antioxidant Enzyme Activity

3.6.1. Enzyme Extraction

- 345
346
347
348
349
350
351
352
353
354
355
356
357
358
359
360
361
362
1. Transfer four 10 mL aliquots from 3-day-old cell suspension cultures of *M. sativa* to 50 mL Erlenmeyer flasks. Add MPA-QDs to a final concentration of 0 (control), 10, 50, or 100 nM.
 2. Grow the cells for 48 h.
 3. Harvest the cells by filtration, wash for a few seconds with distilled water and make aliquots of about 500 mg and proceed with the enzyme extraction.
 4. Prepare a positive control consisting of cell suspension culture heated at 50 °C for 20 min, and performing the same aliquoting procedure as described in previous step.
 5. Homogenize each aliquot in a mortar with a pestle in 2 mL of 100 mM Tris-HCl buffer (pH 7.5) and 2 % (w/v) insoluble polyvinylpyrrolidone (PVP-40). Carry this procedure at 4 °C.
 6. Pipette the homogenate into a microcentrifuge tube and centrifuge at 12,000 $\times g$ for 30 min at 4 °C.
 7. Store the supernatant in small aliquots at -80 °C, until use (CAT, GR, SOD, and protein analyses) (see Note 12).

3.6.2. Determination of SOD Activity

- 363
364
365
366
367
368
369
370
371
372
1. Determine the enzyme activity using disposable cuvettes. Add 50 μL of the extract (supernatant obtained in Subheading 3.6.1) to a reaction mixture composed of 0.5 mM xanthine, 0.05 mM ferricytochrome-C, 0.1 mM EDTA, and 0.01 U of xanthine-oxidase to the final volume of 1 mL (see Table 1) (see Note 13). Prepare the negative control by heating the extract containing the enzyme (SOD) at 90 °C for 10 min.
 2. Mix by inverting the cuvette several times and measure the increase in absorbance at 550 nm for 2 min (10 s interval).
 3. Calculate the enzymatic activity (see Note 14).

$$\% \text{ inhibition} = (\Delta\text{Abs control} - \Delta\text{Abs sample}) / \Delta\text{Abs control} * 100$$

$$\text{Units/mg protein} = (\% \text{ inhibition} / 50 \%) * (1 / v) / \text{mg of total protein}$$

Table 1
Reagents and proportions for SOD activity measurement

	Control sample (μL)	Sample (μL)	
Solution A ^a	500	500	t1.4
Phosphate buffer	487.5	437.5	t1.5
Solution X ^b	12.5	12.5	t1.6
Extract	–	50	t1.7

^a Solution A is defined in Subheading 2.6.2, item 5

^b Solution X is defined in Subheading 2.6.2, item 6

Table 2
Reagents and proportions for CAT activity measurement

	Blank (μL)	Sample (μL)	
Phosphate buffer	963	593	t2.4
Extract	37	37	t2.5
H ₂ O ₂ stock solution	–	370	t2.6

where 50 % = inhibition of cytochrome C reduction rate as per
 Unit definition; v is volume of extract in the cuvette
 ($v = 0.05$ mL, Table 1).

3.6.3. Determination of CAT Activity

1. In a quartz cuvette prepare 1 mL of solution containing the reagents in the order and proportions described in Table 2. Prepare a negative control by heating an extract with the enzyme (CAT) at 90 °C for 10 min.
2. Mix by inverting the cuvette several times and measure the decrease in absorbance at 240 nm for 2 min (10 s intervals) against the H₂O₂-free blank.
3. Calculate the CAT enzymatic activity (see Note 15):

Units per mg of protein = $(\Delta\text{Abs}/\Delta t) * (1 / \epsilon) * (1 / L) * (1 / v) / \text{mg of total protein}$

where ϵ is extinction coefficient of H₂O₂ (0.00394 μmol/mm); L is path length (10 mm); and v is volume of extract in the cuvette (0.037 mL, Table 2).

3.6.4. Determination of GR Activity

1. In a disposable cuvette prepare 1 mL of solution containing 1 mM EDTA in phosphate buffer, 0.75 mM DTNB, 0.1 mM NADPH, and 1 mM GSSG by pipetting the reagents in the

t3.1 **Table 3**
 t3.2 **Reagents and proportions for GR activity measurement**

t3.3		Sample volume (μL)
t3.4	Phosphate buffer + 1 mM EDTA stock solution	600
t3.5	0.75 mM DTNB stock solution	250
t3.6	0.1 mM NADPH stock solution	50
t3.7	Extract	50
t3.8	1 mM GSSG stock solution	50

394 order and proportions described in Table 3. Prepare a negative
 395 control by heating the extract with the enzyme (GR) at 90 °C
 396 for 10 min.

- 397 2. Mix by inverting the cuvette several times and measure the
 398 increase in absorbance at 412 nm (10 s interval during
 399 2 min).
- 400 3. Calculate the activity of the enzyme (see Note 16):

401 Units per mg of protein = $(\Delta\text{Abs} / \Delta T) * (1 / \epsilon) * (1 / L) * (1 / v) / \text{mg of total protein}$
 402

403 where ϵ is extinction coefficient of GSSG (0.62 mL $\mu\text{mol}/$
 404 mm); L is path length (10 mm); v is volume of extract in the
 405 cuvette (0.05 mL, Table 3).

406 4. Notes

- 407 1. *Making of CdSe* nanocrystals coated with a multishell structure
 408 of ZnS and their surface modification based on the successive
 409 ion layer adsorption and reaction (SILAR) method has been
 410 described elsewhere in this book. The first phase of the synthe-
 411 sis produces a hydrophobic surface consisting of a TOPO/
 412 HDA ligand mixture. This is followed by a surface modification
 413 of the Quantum Dots (QDs) with 3-mercaptopropionic acid
 414 (MPA) by the phase transfer method. The modified QDs
 415 become soluble in aqueous systems such as water or buffers for
 416 further biological applications.
- 417 2. DAB in solution can be kept at 4 °C for a maximum of 2 days;
 418 however, it is advisable to prepare a fresh solution for each set
 419 of experiments. DAB is difficult to dissolve in water unless the
 420 pH is reduced. An alternative procedure to dissolve DAB is to
 421 prepare a solution of water by adding HCl until pH 3.6 is

- reached and then add the DAB. Shake the solution until all the DAB is dissolved (8). 422
423
3. For subculture use a pipette with an orifice narrow enough to allow single cells and small aggregates to pass through. The suspension culture is allowed to rest in order to settle down the large clumps, and the inoculum is taken from the upper part of the culture. Regular practice of this procedure should allow obtaining a fine cell suspension culture. 424
425
426
427
428
429
 4. The presence of QDs can promote cell aggregation so be aware of this fact to have an accurate cell counting. The metabolism of FDA to fluorescein reflects the metabolic response of organisms when exposed to toxicants. Furthermore, the degree of fluorescence depends on the physical and metabolic state of the cell (5), therefore pay attention to the variations in the fluorescence. 430
431
432
433
434
435
436
 5. Samples stored this way are stable for weeks. 437
 6. The majority of studies investigate acute toxicity, generally 24 h, but longer incubation times are required to see the influence of nanoparticles (9). We also tested after 48 h of incubation with QDs, but extended periods can also be used. Note that the QDs should always be added at day 3 of culture (beginning of the exponential phase). 438
439
440
441
442
443
 7. The treatment of cell suspension cultures at 45 °C for 20 min is a positive control to ensure a cellular stress. 444
445
 8. The use of DAB technique requires the presence of endogenous peroxidase activity in order to ensure the polymerization, thus a simple test to check the required peroxidase activity is to expose cells to DAB and H₂O₂ (10). 446
447
448
449
 9. DAB reacts rapidly with H₂O₂ in the presence of peroxidase, forming a brown polymerized product (10). 450
451
 10. NBT is reduced by O₂^{•-} to form an insoluble blue formazan deposit (6). 452
453
 11. H₂DCFDA is a nonfluorescent product that is converted by ROS into DCF (2',7'-dichlorofluorescein), which can easily be visualized as a green fluorescence around 525 nm when excited at 488 nm (11). H₂DCFDA treated cells show a basal-level signal that accumulates in all cytoplasmic areas, including the nucleoplasm (12). DCF signal can suffer quenching and decrease the fluorescence within 5–10 min when continuously exposed to light. 454
455
456
457
458
459
460
461
 12. To normalize the results the total cellular protein concentration must be determined. The Bradford method is commonly followed by using a protein assay kit, and BSA as a standard (13). 462
463
464

- 465
466
467
468
469
470
471
472
473
474
475
476
477
13. The extract volume can be adjusted according to the activity of the enzymes, e.g., if for a determined enzyme the activity is too high you should use a smaller volume, but always maintaining the described proportions.
 14. The enzymatic activity of SOD is defined as the quantity necessary for the inhibition of 50 % of cytochrome-C reduction per minute under the assay conditions (14).
 15. The enzymatic activity of CAT is defined as the consumption of 1 μmol of H_2O_2 per minute per mL at room temperature, under the assay conditions (15).
 16. The enzymatic activity of GR is expressed in U/mL mg protein wherein unit activity is the amount of enzyme which reduces 1 mM of GSSG per minute at 24 °C under assay conditions (16).

478 Acknowledgments

479
480
481
482

This work was supported by the project “Development of ultra-sensitive detection methods and plant nano-vaccines for the fungi *Fusarium* spp. using nanotechnological devices” Iberian Capacitation Program in Nanotechnologies: Call 2006/2007.

483 References

- 484
485
486
487
488
489
490
491
492
493
494
495
496
497
498
499
500
501
502
503
504
505
506
507
508
509
1. Saeza G, Moreau X, Jonga L, Thiéry A et al (2010) Development of new nano-tools: towards an integrative approach to address the societal question of nanotechnology? *Nano Today* 5:251–253
 2. Auffan M, Rose J, Wiesner M, Bottero J (2009) Chemical stability of metallic nanoparticles: a parameter controlling their potential cellular toxicity in vitro. *Environ Pollut* 157:1127–1133
 3. Kristen U (1997) Use of higher plants as screens for toxicity assessment. *Toxicol In Vitro* 11:181–191
 4. Duncan D, Widholm J (1990) Measurements of viability suitable for plant tissue cultures. In: Pollard J, Walker M (eds) *Plant cell and tissue culture*, vol 6. The Humana Press, London, p 33
 5. Regel R, Ferris J, Ganf G, Brookes J (2002) Algal esterase activity as a biomeasure of environmental degradation in a freshwater creek. *Aquat Toxicol* 59:209–223
 6. Gerber I, Dubery A (2003) Fluorescence microplate assay for the detection of oxidative burst products in tobacco cell suspensions using 2',7'-dichlorofluorescein. *Methods Cell Sci* 25:115–122
 7. Santos A, Miguel A, Tomaz L, Malhó R, Maycock C, Patto M, Feveireiro P, Oliva A (2010) The impact of CdSe/ZnS quantum dots in cells of *Medicago sativa* in suspension culture. *J Nanobiotechnology* 8:24
 8. Driever S, Fryer M, Mullineaux P, Baker N (2009) Imaging of reactive oxygen species in vivo. In: Pfannschmidt T (ed) *Plant signal transduction*, vol 479. Humana Press, London, p 115
 9. Gormley A, Ghandehari H (2009) Evaluation of toxicity of nanostructures in biological systems. In: Sahu S, Casciano D (eds) *Nanotoxicity from in vivo and in vitro models to health risks*. Wiley, United Kingdom, p 137
 10. Thordal-Christensen H, Zhang Z, Wei Y, Collinge D (1997) Subcellular localization of H_2O_2 in plants. H_2O_2 accumulation in papillae and hypersensitive response during the barley-powdery mildew interaction. *Plant J* 11:1187–1194
 11. Ortega-Villasante C, Rellán-Alvarez R, del Campo F, Carpena-Ruiz R, Hernández L (2005) Cellular damage induced by cadmium and mercury in *Medicago sativa*. *J Exp Bot* 56:2239–2251

- 536 12. Ashtamker C, Kiss V, Sagi M, Davydov O, 548
537 Fluhr R (2007) Diverse subcellular locations of 549
538 cryptogein-induced reactive oxygen species 550
539 production in tobacco bright yellow-2 cells. 551
540 Plant Physiol 143:1817–1826
- 541 13. Ma Y (2009) In vitro models for nanotoxicity 552
542 testing. In: Sahu S, Casciano D (eds) 553
543 Nanotoxicity from in vivo and in vitro models 554
544 to health risks. Wiley, United Kingdom, p 365 555
- 545 14. McCord J, Fridovich I (1969) Superoxide dis- 556
546 mutase. An enzymic function for erythrocyte 557
547 (hemocuprein). J Biol Chem 244:6049–6055
15. Aebi E (1983) Catalase. In: Bergmeyer H (ed) 548
Methods of enzymatic analysis, vol III, 549
Oxidoreductases, transferases. Verlag Chemie, 550
Germany, pp 273–277 551
16. Shanker A, Djanaguiraman M, Sudhagar R, 552
Chandrashekar C, Pathmanabhan G (2004) 553
Differential antioxidative response of ascor- 554
bate glutathione pathway enzymes and 555
metabolites to chromium speciation stress 556
in green gram (*Vigna radiata* (L.) R. 557
Wilczek. cv CO 4) roots. Plant Sci 166: 558
1035–1043 559

Uncorrected Proof

Author Queries

Chapter No.: 36 0001528607

Query	Details Required	Author's Response
AU1	Please check the clarity of the following sentence: "Incubate 5 at room temperature and perform the counts under the fluorescence....."	

Uncorrected Proof

CdSe/ZnS Quantum Dots trigger DNA repair and antioxidant enzyme systems in *Medicago sativa* cells in suspension culture

Ana Raquel Santos^{1,2}, Ana Sofia Miguel^{1,3}, Anca Macovei⁴, Christopher Maycock^{3,5}, Alma Balestrazzi⁴, Abel Oliva¹ and Pedro Fevereiro^{2,5,§}

¹ Biomolecular Diagnostics Laboratory, Instituto de Tecnologia Química e Biológica, Universidade Nova de Lisboa, Apartado 127, 2781-901 Oeiras, Portugal

² Plant Cell Biotechnology Laboratory, Instituto de Tecnologia Química e Biológica, Universidade Nova de Lisboa, Apartado 127, 2781-901 Oeiras, Portugal

³ Organic Synthesis Laboratory, Instituto de Tecnologia Química e Biológica, Universidade Nova de Lisboa, Apartado 127, 2781-901 Oeiras, Portugal

⁴ Department of Biology and Biotechnology, via Ferrata 1, 27100 Pavia, Italy

⁵ Universidade de Lisboa, Faculdade de Ciências, 1749-016 Lisboa, Portugal

§Corresponding author

Email addresses:

A R S: anaraqssantos@gmail.com

A S M: sofmig@itqb.unl.pt

A M: anca.macovei@unipv.it

C M: maycock@itqb.unl.pt

A B: alma.balestrazzi@unipv.it

A O: oliva@itqb.unl.pt

P F: psalema@itqb.unl.pt

Abstract

Background

Nanoparticles appear to be promising devices for application in the agriculture and food industries but information regarding the response of plants to the contact with nanodevices is scarce. Toxic effects may be imposed depending on the type of nanoparticle as well as its concentration and time of exposure. A number of mechanisms were envisaged underlying the ability of nanoparticles to cause genotoxic DNA damage, besides the activation of ROS scavenging mechanisms. In a previous study we showed that plant cells increased the production of undifferentiated ROS in a dose dependent manner when exposed to mercaptopropanoic acid-CdSe/ZnS quantum dots (MPA-QDs) and that a maximum concentration of 5 nM should be cyto-compatible for this type of QDs.

Results

When *Medicago sativa* cells were exposed to 10, 50 and 100 of MPA-QDs a correspondent increase in the activity of Superoxide dismutase, Catalase and Glutathione reductase was registered. Different versions of the COMET assay were used to assess the genotoxicity of

Quantum dots. The number of DNA single and double strand breaks increased with increasing concentrations of MPA-QDs. At the highest concentrations tested purine bases were more oxidized than the pyrimidine ones. The transcription of the DNA repair enzymes Formamidopyrimidine DNA glycosylase, Tyrosyl-DNA phosphodiesterase I and DNA Topoisomerase I is up-regulated in the presence of increasing concentrations of MPA-QDs.

Conclusions

Concentrations as low as 10 nM of quantum-dots (MPA-QDs) although not lethal are cytotoxic and genotoxic to plant cells. This sets a limit for the concentrations to be used when experiments on plants using nanoparticles of this type are being considered. This work describes for the first time the genotoxic effect of Quantum dots in plant cells and demonstrates that both the DNA repair genes (*Tdp1 β* , *Top1 β* and *Fpg*) and the ROS scavenging mechanisms are activated during the MPA-QDs treatments in *M. sativa* cells.

Background

Nanoparticles offer many technological solutions since they are valuable as carriers, coaters, repellents, screens and conductors. Nanoparticles may also be useful as nanosensors, cell imaging devices and smart delivery systems and appear to be promising devices for application in the agriculture and food industries.

While the full potential of the different and new nanomaterials is still far from being explored, their impact on living systems shows that different types of toxic effects may be imposed, depending on the type of nanoparticle as well as its concentration and time of exposure among other factors. Properties that characterize nanomaterials such as nanoscale size, large surface area and high reactivity are also major points of concern, opening the development of a new area of research called nanotoxicology.

Nanotoxic effects have been detected at relatively high, in many cases unrealistic, particle concentrations and associated with cell death. But subtler effects that arise at lower concentrations without necessarily causing cell death also need to be considered. In particular a number of mechanisms were envisaged underlying the ability of nanoparticles to cause DNA damage [1].

Little information about the expression and activity of plant detoxifying enzymes and DNA repairing enzymes in response to contact with nanoparticles is found in the literature. Plants respond to toxicity producing ROS that trigger the activation of ROS scavenging mechanisms. These mechanisms include the superoxide dismutase (SOD) enzyme, the water-water cycle (WWC), the ascorbate-glutathione cycle (AGC), the glutathione peroxidase cycle (GPXC) and the catalase (CAT) enzyme [2].

In a previous study we showed that plant cells increased the production of undifferentiated ROS in a dose dependent manner when exposed to mercaptopropionic acid-CdSe/ZnS quantum dots (MPA-QDs) and that a maximum concentration of 5 nM should be cyto-compatible for this type of QDs [3]. The cells accumulated MPA-QDs in the cytoplasm and in the nucleus. We also showed that cell suspension cultures exposed to 100 nM of QDs during 48 hours did not show any noticeable production of superoxide radicals ($O_2^{\bullet-}$), and the production of H_2O_2 was far less than 10 nM, if any [3].

There is much evidence obtained from various plant systems showing that the amounts and activities of enzymes involved in scavenging ROS are altered by different stresses [4]. Several biotic and abiotic stress events such as pathogen attack, drought, chilling, heat shock, heavy metals, and ultraviolet (UV) radiation exposure, trigger ROS production and enhance their steady-state level in the cell [2]. Reactive oxygen species (ROS) can cause oxidative damage, to DNA, lipids, and proteins [5] and occur frequently in all cells.

Genotoxic effects have been reported when nanoparticles interact with living systems. Silver nanoparticles exhibited cytotoxicity by decreasing the mitotic index in a dose dependent manner in root tips of *Allium cepa* [6]. In particular two studies have demonstrated that 0.5 nM of CdSe/ZnS QDs cause DNA fragmentation and nicking in cell-free systems [7]. Another study demonstrated that Mercaptoacetic acid-CdSe QDs or Mercaptoacetic acid-QDs doped with cobalt had the potential to cause indirect *in vivo* genetic damage in mice [8], but so far there are no reports about the genotoxicity of MPA-QDs on plant cells.

Since 1996 the COMET assay has been used to quantify the genotoxic effects of different stress factors in plants [9]. This is an easy, inexpensive, and sensitive test for DNA damage and was first described in 1988 by Singh *et al.* [10]. This method has been used to assess the genotoxic impact of 2-10 mM of titanium oxide nanoparticles on *Allium cepa* roots [11].

Cytotoxic and genotoxic responses should be accompanied by variations in gene expression. These variations should corroborate the observable responses as a function of the variation in enzyme activities. The different ROS forms affect gene expression in specific and sometimes antagonistic ways [12]. Increases in oxidative stress induce cells to synthesize higher levels of antioxidants, antioxidant enzymes, repair enzymes, and other molecules that mitigate the effects of such stress [5].

Genes codifying DNA repair enzymes are also induced by stress factors. DNA topoisomerase I is essential for vital cellular processes, namely DNA replication, transcription, translation, recombination and repair [13]. *Nicotiana tabacum Top1* expression was found to be regulated by light, cold and also by ABA [14]. Macovei *et al* (2010) [15] showed that in *Medicago truncatula Top1* and also the gene encoding tyrosil-DNA phosphodiesterase (*Tdp*) are overexpressed when plants were subject to elevated copper concentrations or to osmotic stress induced by PEG 6000.

In this work we analyze the cyto- and genotoxic effects of MPA-QDs in *Medicago sativa* cells in suspension culture. We show that some of the ROS scavenging mechanisms are active at the cellular level, preventing the accumulation of some specific ROS when cells contact QDs. We also show that extensive DNA damage occurs when 100 mM of MPA-QDs are placed in contact with plant cells, and that the expression of the DNA repair genes *Top 1* and *Tdp* is activated by the stress imposed by this type of nanoparticle.

Results and Discussion

MPA-QDs trigger the activity of antioxidant enzymes

Cells of *Medicago sativa* in suspension culture take up MPA-QDs that accumulate in the cytoplasm and the nucleus (figure 1) as described in [3].

When *M. sativa* cells were exposed to 10, 50 and 100 of MPA-QDs an increase in SOD activity of 12%, 27% and 88% respectively, was observed when compared with the control (figure 2A). An increase of 50% to 70% of SOD activity was recorded when cells were submitted, as a positive control experiment, to 50°C (without QDs) for the period of 20 min.

The contact of MPA-QDs with plant cells triggers SOD activity and this may explain why, in our previous work [3], we could not detect $O_2^{\bullet-}$ accumulation when *M. sativa* cells were exposed to MPA-QDs.

Within a cell, SODs constitute the first line of defence against ROS, catalyzing the dismutation of $O_2^{\bullet-}$. Oxygen activation may occur in different compartments of the cell wherever an electron transport chain is present, including the cytosol, mitochondria, chloroplasts, peroxisomes and glyoxisomes [16]. In plant cells the increase in SOD activity appears to be an important protection mechanism to reduce the oxidative stress caused by the cytotoxic effects of the MPA-QDs.

An increase of 8%, 16% and 72 % of CAT activity was observed when *M. Sativa* cells were exposed to 10, 50 and 100 nM of MPA-QDs respectively (figure 2b). The significant increase in the activity of CAT suggests the role of this enzyme in constant detoxification of H_2O_2 when *M. sativa* cells are exposed to MPA-QDs. An increase in the activity of CAT was reported in plants exposed to toxic concentrations of heavy metals, namely Cd, Cu and Pb [17]. Catalase is active only at relatively high H_2O_2 concentrations. Lower H_2O_2 levels are eliminated by APX and other peroxidases with the aid of various reducing metabolites like ascorbate and glutathione [18]. Catalase and the ascorbate-glutathione cycle enzymes are both important in H_2O_2 scavenging. Although their properties and requirements are different, they effectively act in parallel [19] (Table 2).

Glutathione reductase (GR) activity increased by 5% and 23% when *M. sativa* cells were exposed to 50 and 100 nM of MPA-QDs (figure 2c), while the addition of 10 nM of MPA-QDs induced a GR activity not significantly different from the control.

Previous studies on the exposure of plants to cadmium (Cd) show that GR activity increases as part of the defence against Cd stress, an alteration which has been shown to be often dose dependent and variable over time [4,20].

As seen for other oxidative stresses in plants, mainly when the agent is a metal ion, plant cells respond to the presence of quantum dots by activating ROS scavenging mechanisms, to protect the cells from activated oxygen forms. This activation seems to be dose dependent and to effectively prevent the accumulation of H_2O_2 and $O_2^{\bullet-}$ when exposed to MPA-QDs at concentrations between 10 and 100 nM.

MPA-QDs induce DNA damage in exposed plant cells

We used four different versions of the Comet assay to estimate the range and type of genotoxicity imposed by MPA-QDs in *M. sativa* cells in a suspension culture: the neutral version useful to assess DNA double strand breaks (DSBs); the alkaline/neutral version (A/N) that detect mainly DNA single strand breaks (SSBs); the A/N version followed by an enzymatic treatment with Formamidopyrimidine DNA glycosylase (FPG) to evaluate the extent of purine base oxidation; and the A/N version followed by the enzymatic treatment with Endonuclease III (EndoIII) to evaluate the amount of oxidized pyrimidine bases. The two

enzymes remove the oxidized bases and generate a DNA strand break at the position of the excised base that can be detected via the comet assay [21].

The A/N Comet assay histogram distribution of cell suspension cultures added to 10, 50 and 100 nM of MPA-QDs, or heated at 50 °C for 20 minutes, is shown in figure 3a). The control shows that 77% of the comets fall in class 1 and 2, while only 4% fall in classes 3 and 4. This may be considered as a basal level of damage that may reflect the impact of protoplastization.

The histogram shows that an increment of MPA-QD concentration induces an increase in the frequency of comets in the higher classes, except for the 10 nM concentration that shows no significant difference from the control. When cells are exposed to 100 nM MPA-QDs 78% of the comets fall in class 2 and 13% and 8% of the comets fall in class 3 and 4, respectively. Heat treated cells present 25% of comet frequencies in classes 0, 1 and 2 and 10 % in class 3 and 4. Figure 3b show images of comets that represent the five classes used for visual scoring. These results demonstrate that stressed plant cells suffer DNA SSBs, as seen when comparing the heat treated cells with the control and that increasing concentrations of MPA-QDs increment the percentage of damage.

In figure 4 the results of the four variants of the Comet assay are plotted together. Strikingly the contact of 10 nM of MPA-QDs induced an increase in the number of DSBs when compared to the control, contrasting with the results obtained for the single strand break analysis. Also it can be seen that at the highest MPA-QD concentration tested purine bases are more oxidized than the pyrimidine ones.

The accumulation of SSBs and oxidatively induced base lesions can lead to DSBs considered to be the most lethal type of DNA oxidative damage. Compared with other types of DNA damage, DSBs are intrinsically more difficult to repair and as little as one DSB lesion in the DNA can kill the cell if the lesion inactivates a critical gene. SSBs and oxidatively induced DNA base lesions are definitely not harmless, and are known to block DNA transcription and replication processes, resulting in accelerated cytotoxicity and genomic instability [21]. It seems that even 10 nM of MPA-QDs may induce DNA double strand breaks in plant cells, being potentially deleterious and that the increment of nanoparticles induces an increase of genotoxicity.

MPA-QDs up-regulate DNA repair and antioxidant defence genes

Oxidative DNA damage is typically associated with the accumulation of 7,8-dihydro-8-oxoguanine (8-oxo-dG), an oxidized form of guanine. The 8-oxo-dG is highly mutagenic frequently inducing mispairs with the incoming dAMP during DNA replication and causing G:C to T:A transversions. The Base Excision Repair (BER) is responsible for recognizing and excising damaged bases by a multi-step process using different enzymes, such as DNA glycosylases, AP endonucleases or DNA ligases. Formamidopyrimidine DNA glycosylase (FPG) is a DNA glycosylase/ AP lyase enzyme involved in the repair of oxidized purines such as 8-oxo-dG and imidazole-ring opened purines (FapyA, FpyG) [22]. The presence of FPG was initially considered to be a unique feature of prokaryotes, but recently it has also been detected in plants [23,24,25].

The transcript accumulation of the FPG gene was evaluated in *M. sativa* cell suspension cultures treated with 10, 50 and 100 nM of MPA-QDs. Changes in the expression levels of the FPG gene were observed during the induced treatments (Fig 5). An up-regulation was observed when the higher QDs concentrations (50 and 100 nM) were used (0.7-fold and 2.0-

fold, respectively), which is in agreement with the Comet results: cells tend to respond to the genotoxic effect by increasing the expression of FPG to increase the enzyme activity.

Tyrosyl-DNA phosphodiesterase (Tdp1) is a key enzyme that hydrolyzes the phosphodiester bond between the tyrosine residue of DNA topoisomerase I (topo I) and the DNA 3'-phosphate, and thus it is involved in the repair of topoisomerase I – mediated DNA damage [26]. Macovei *et al.* (2010) reported on the presence of a *Tdp1* gene family (*Tdp1 α* and *Tdp1 β*) in *M. truncatula* and demonstrated its involvement in oxidative stress responses, while Lee *et al.* (2010) [27] isolated Tdp1-depleted *Arabidopsis* mutants that exhibited a dwarf phenotype and cell death events, suggesting the important role that this enzyme plays during plant development.

The accumulation of transcripts of the β isoforms of *Tdp1* and *Top1* transcripts was evaluated in *M. sativa* cell suspension cultures treated with 10, 50 and 100 nM of MPA-QDs. Results (Fig 5) show an increase in the transcript accumulation of both *Tdp1 β* and *Top1 β* mRNAs. In the case of *Tdp1 β* a 2.0-fold increase was observed at 10 nM and 50 nM, while the treatment with 100 nM QDs induced a 7.0-fold transcript accumulation. For the *Top1 β* gene, at the lower concentrations (10 nM and 50 nM) the results are not statistically different from the control, while at 100 nM a 4.0-fold increase was observed.

This is the first time that the expression of genes of DNA repair enzymes has been evaluated when nanoparticles are placed in contact with plant cells. The over accumulation of transcripts of *FPG*, *Tdp1 β* and *Top1 β* transcripts shows that the nanoparticles are exerting a genotoxic effect that the cells try to counteract by increasing the expression of these genes. This is corroborated by the data obtained with the Comet assays, that show that even 10 nM of MPA-QDs may induce a genotoxic response by plant cells. The fact that the expression of *APX* and *SOD* genes is also up-regulated by the nanoparticles (fig 5), mostly at the highest concentrations is in agreement with the results obtained for the antioxidant enzyme activities and our previous results [3]. The balance between ascorbate peroxidase and superoxide dismutase activity in cells is considered to be crucial for determining the steady-state level of reactive oxygen species [4]. These enzymatic antioxidant defences protect the cells by directly scavenging hydrogen peroxide and superoxide radicals, converting them into less reactive species [28].

Conclusions

Concentrations as low as 10 nM of quantum-dots (MPA-QDs) although not lethal are cytotoxic and genotoxic to plant cells. This sets a limit for the concentrations to be used when experiments on plants using nanoparticles of this type are being considered.

M. sativa cells responded to the oxidative stress caused by the addition of MPA-QDs by activating their antioxidant enzyme systems. In this study, three antioxidant enzymes: SOD, CAT and GR were activated within 48 hours of MPA-QDs exposure, preventing over-accumulation of oxygen reactive species, as described previous [3]. Higher concentrations of MPA-QDs induced the accumulation of ROS that are able to damage the plasma membrane, mitochondria and nucleus.

Cells may adapt to stress by up-regulating antioxidant and/or repair systems. This may protect them against damage to some extent but not completely, or sometimes even overprotect; the cells are then resistant to higher levels of oxidative stress imposed subsequently [29]. This work describes for the first time the genotoxic effect of Quantum dots in plant cells and demonstrated that both the DNA repair genes (*Tdp1 β* , *Top1 β* and *FPG*) and the ROS scavenging mechanisms are activated during the MPA-QD treatments in *M. sativa* cells.

Methods

Synthesis and characterization of QDs

Mercaptopropionic acid coated CdSe/ZnS QDs were synthesized, solubilised and characterized based in our previous report [3]. In brief, the Mercaptopropionic acid coated nanocrystals were synthesized by the phase transfer method and the obtained Mercaptopropionic acid coated CdSe/ZnS QDs were then concentrated using a Sartorius Vivaspin 6 tube (cutoff 10KDa) at 7.500g.

For the characterization of the synthesized CdSe/ZnS QD nanoparticles Transmission Electron Microscopy (TEM) was used. Low resolution images were obtained using a JEOL 200CX traditional TEM operating at an acceleration voltage of 200kV. Dynamic Light Scattering (DLS) analysis was performed using a Nano series dynamic light scatterer from Malvern. The nanoparticles had a hydrodynamic diameter of 13.5 nm and a zeta potential of -26.2 mV and an emission wavelength of 620 nm.

Cell suspension cultures treatments

M. sativa cell suspension cultures previously established [3] were used and maintained in an orbital shaker at 110 rpm (Innova 4900, New Brunswick Scientific, Germany) in the dark at 24°C. A MPA-QDs stock solution was added to cell suspension cultures at day 3 of culture (beginning of exponential phase) at different final concentrations (0, 10 nM, 50 nM and 100 nM). After 48 hours of incubation cells were harvested for RNA or enzyme extraction and frozen at -80°C or used directly for the Comet assays. Cell suspension cultures heat treated at 50 °C for 20 min were used as an abiotic stress control.

Antioxidant enzyme activity

1) Enzyme extraction

The following steps were carried out at 4 °C unless stated otherwise. The *in vitro* cultured *Medicago sativa* cells (about 500 mg of fresh weight) were homogenized in a mortar with 2 mL of 100 mM Tris-HCl buffer (pH 7.5) containing 1 mM ethylenediaminetetraacetic acid (EDTA), 3 mM DL-dithiothreitol, 0.2 % Triton X-100 and 2% (w/v) insoluble PVPP. The homogenate was centrifuged at 12000g for 30 min and the supernatant was stored in separate aliquots at -80 °C, until CAT, GR, SOD and protein quantification.

For the enzyme assays three types of controls were used: a stress control (heated cells), a control with no treatment and a negative control consisting of a boiled extract of the non-treated cells (inactivated enzyme).

2) Protein Quantification

Protein concentration was quantified spectrophotometrically at 595 nm according to the Bradford method [31] with BSA as a standard.

Protein quantification and all enzyme activities were measured using Ultrospec 4000 UV/Visible Spectrophotometer (Pharmacia Biotech).

3) Quantification of Superoxide Dismutase activity

Total SOD activity was quantified according to the modified method described by Rubio et al [32], measuring the increase in absorbance at 550 nm for 2 minutes (10 seconds interval) in a 1 mL solution containing 0.5 mM xanthine, 0.05 mM ferricytochrome-C, 0.1 mM EDTA and 0.01 U of xanthine-oxidase in 100 mM potassium phosphate buffer (pH 7.5). The enzymatic activity was estimated as the quantity of enzyme necessary for the inhibition of 50% of ferricytochrome-C reduction per minute under the assay conditions [33]:

% inhibition = $(\Delta\text{Abs control} - \Delta\text{Abs sample}) / \Delta\text{Abs control} * 100$

Units/mg protein = $(\% \text{ inhibition} / 50\%) * (1/v) / \text{mg of total protein}$

Where 50 % = inhibition of the rate of cytochrome C reduction; $v = 0.05 \text{ mL}$.

4) Quantification of Catalase activity

Total CAT activity was measured as described in [34]. Briefly, the decrease in absorbance was measured at 240 nm for 2 minutes (10 seconds intervals), in a 1 mL solution containing 10 mM of H_2O_2 in 50 mM phosphate buffer (pH 7.5). CAT enzymatic activity was defined as the consumption of 1 μmol of H_2O_2 per minute per ml at room temperature, under the assay conditions, according to the following equation:

$$(\Delta\text{Abs}/\Delta\text{T}) * (1/\epsilon) * (1/L) * (1/v) / \text{mg of total protein}$$

Where $\epsilon \text{ H}_2\text{O}_2 = 0.00394 \text{ } \mu\text{mol}^{-1}\text{mm}^{-1}$; $L = 10 \text{ mm}$; $v = 0.037 \text{ mL}$

5) Quantification of Glutathione reductase activity

GR activity was quantified based on the increase in absorbance at 412 nm (10 seconds interval during 2 minutes) when 5,5'-dithiobis (2-nitrobenzoic acid) (DTNB) was reduced by GSH [35]. The 1 mL reaction mixture contained 100 mM potassium phosphate buffer at pH 7.5, 1mM EDTA, 0.75 mM DTNB, 0.1 mM NADPH and 1 mM GSSG. The components of the reaction mixture were added in the stated order and the reaction was initiated by the addition of GSSG. The activity of the enzyme was expressed in U/mL*mg protein wherein unit activity is the amount of enzyme which reduces 1 mM of GSSG per minute at 24 °C under assay conditions:

$$(\Delta\text{Abs}/\Delta\text{T}) * (1/\epsilon) * (1/L) * (1/v) / \text{mg of total protein}$$

Where $\epsilon \text{ GSSG} = 0.62 \text{ mL } \mu\text{mol}^{-1}\text{mm}^{-1}$; $L = 10 \text{ mm}$; $v = 0.05 \text{ mL}$

Comet assay

1) Protoplast preparation

Cells from the suspension culture were pelleted by centrifugation at 1000 rpm for 10 min and incubated with a protoplastization solution consisting of 10 mM of MES buffer pH 5.8, 10 mM of CaCl_2 , 0.4 M of mannitol, 1% of Macerozyme and 1% of Cellulase (for about 1 g of cells 5 mL of enzymatic solution was added) at room temperature in the dark for 3-4 hours under gentle agitation. After the incubation the protoplasts were sieved through a 90 μm mesh without applying pressure.

200 μL of protoplasts were mixed with 200 μL of 0.75% LMP agarose (at 37 °C) and 80 μL aliquots were placed on a microscope slide previously coated with 0.75% agarose. A 22x22 mm glass cover slip was placed on each gel and the slides were allowed to set on ice for a few minutes, the coverslips were then removed. The slides were marked as “control” (protoplasts from cultures with no treatment), “heat treated” (protoplasts treated for 20 min at 50 °C), “10 nM, 50 nM or 100 nM” (protoplast from cultures treated with one of the three QDs concentrations), “buffer” (protoplasts from cultures treated with one of the three QDs concentrations plus enzyme buffer), “FPG” (protoplasts from cultures treated with one of the three QDs concentrations plus FPG enzyme) and “Endo III” (protoplasts from cultures treated with one of the three QDs concentrations plus Endo III enzyme).

2) Alkaline unwinding/ neutral electrophoresis

The modification of the comet assay described by Angelis *et al.* 1999 [36] employs various combinations of neutral and alkali pH solutions immediately prior to and during electrophoresis. Exposure of DNA to high alkali prior to electrophoresis under neutral conditions (N/A protocol) allows for the preferential detection of DNA SSBs.

Briefly, cells embedded in agarose were lysed in a Coplin jar for 1 hour in 2.5 M NaCl, 0.1 M EDTA, 10 mM Tris-HCl pH 10, 1% Triton X-100 at 4 °C. The slides marked with “buffer”, “FPG” and “EndoIII” were then washed 3 times for 5 minutes at 4 °C with enzyme buffer containing 40 mM HEPES, 0.1 M KCl, 0.5 mM EDTA, 0.2 mg/mL BSA, pH 8 adjusted with KOH. After the last wash the excess was drained with the tissue and the slides were placed on ice. Then 50 µL of enzyme buffer, FPG (10⁴ dilution) or Endo III (10⁴ dilution) were added to the respective gels and covered with a coverslip. The slides were then transferred to a moisten box and incubated at 37 °C for 30 min.

During this time the slides marked as “control”, “heat treated” and “10 nM, 50 nM or 100 nM” were kept in the lysis solution. At the end of the incubation period, the coverslips were removed and all the slides were placed in 0.3 M NaOH and 1 mM EDTA, pH approximately 13.0, at 4 °C for 20 minutes.

The samples were then neutralized by dipping in 0.4 M Tris-HCl, pH 7.5, 3 times for 5 minutes at 4 °C. The slides were transferred to the electrophoresis tank and placed in TBE (pH 8) for a few minutes and then electrophoresed for 10 min at 25V, 10 mA at 4 °C. After being electrophoresed they were fixed in ethanol 70% 2 times 5 min and left to dry overnight. 20 µL of 1 µg/mL DAPI was placed on each gel and covered with a coverslip, and scored after 5 min.

3) Neutral incubation/ neutral electrophoresis

DNA unwinding and electrophoresis at neutral pH (pH 7–8) facilitates the detection of double-strand breaks and crosslinks and the total DNA damage is much less pronounced than at alkaline conditions [36].

In brief, slides marked as “control”, “heat treated” and “10 nM, 50 nM or 100 nM” were lysed in the Coplin jar for 1 hour at 4 °C in 2.5 M NaCl, 0.1 M EDTA, 10 mM Tris-HCl pH 7.5. They were then equilibrated in TBE 2 times for 5 min and electrophoresed in TBE 10 min at 25 V, 10 mA. They were fixed, stained as above and scored.

4) Scoring for DNA damage

Visual image analyses of DNA damage were carried out in accordance with the protocol described [37]. Slides were examined at 200 X magnification on a Nikon Eclipse TE2000-S (Japan) inverted microscope equipped with a HMX-4 100 W Mercury lamp and UV excitation filter. One hundred randomly selected non overlapping nucleoids were analyzed by visual inspection giving each comet a value of 0-4 according to the degree of damage. Two to three slides were evaluated per treatment and each treatment was repeated at least twice.

Images were acquired with an Evolution MP 5.1 megapixel digital CCD Color Camera (Media Cybernetics) controlled by Image Pro Plus 5.0 software (Media Cybernetics).

For the lesion-specific enzymes we used the standard procedure that is to include a control slide (incubated with buffer alone) in parallel with the slide treated with the enzyme, and to subtract the mean Comet score of the control from the mean score of the slide treated with the enzyme. Net enzyme-sensitive sites were then the measure of the oxidized bases concerned.

Real Time Quantitative Polymerase Chain Reaction

1) RNA extraction

The RNA extraction protocol was based on the protocol developed by Chang *et al.* [38] with some modifications. Frozen cells were ground in the presence of liquid nitrogen in a mortar and the powder was transferred to a 2 mL microcentrifuge tube. The extraction buffer containing 2% CTAB, 2% PVP, 100 mM Tris-HCl pH 8, 25 mM EDTA, 2 M Na Cl, 0.5 g/L spermidine and 2 % β-mercaptoethanol (added just before use) was heated at 65°C for 10 min

in a water bath. 900 μ L of extraction buffer was added to each sample and quickly mixed and vortexed vigorously. Samples were incubated for 15 min at 65 °C, after that placed on ice for 5 min and 900 μ L of chloroform:isoamyl alcohol (CIA) (24:1) were added. Each sample was vigorously vortexed until a unique phase was observed and again placed on ice for 5 min. Then samples were centrifuged for 15 min at 20 000g. The CIA extraction was repeated 3 times. The final combined supernatant was placed into a new microcentrifuge tube and 65 μ L of 4M NaOAc (pH 5.2) and 1500 μ L of ethanol were added. Each sample was mixed by inversion and allowed to precipitate at -20 °C for one hour. The samples were then centrifuged for 30 min at 20 000g and the supernatant was carefully decanted. 250 μ L Of 70% ethanol at 4 °C was then added, centrifuged and the supernatant again discarded. An additional washing with absolute ethanol at 4 °C was carried out. The pellet was dried and re-suspended in 50 μ L of MilliQ water and 50 μ L of 12 M LiCl and left to precipitate overnight at -20 °C. It was then centrifuged 1 hour at 20 000g and the supernatant discarded. The residue was subsequently washed with 70% ethanol and stored in absolute ethanol. Total RNA was quantified in the Nanodrop1000 spectrophotometer (Thermo Fisher Scientific) and quality assessed by agarose gel electrophoresis. Only the samples with purity (A260/280 ratio) between 1.8- 2.0 were used for QRT-PCR.

2) cDNA synthesis and Real Time Quantitative Polymerase Chain Reaction (QRT-PCR)

The total RNA was reversely transcribed into cDNAs using the iScript cDNA Synthesis Kit (Bio-Rad), as indicated by the supplier.

The high degree of sequence identity and remarkably conserved genome structure and function between *Medicago truncatula* (barrel medic) and *M. sativa* (alfalfa) provides the opportunity to use the model legume *M. truncatula* as a surrogate [39,40,41] to design the oligonucleotide sequences of *Tdp1 β* , *Top1 β* , *FPG*, *SOD* and *APX* genes. Primers were designed using the Real-Time PCR Primer Design, GenScript software, (<https://www.genscript.com/ssl-bin/app/primer>) covering their highly conserved motifs. The used primer sequences are listed in Table 1. The *ELF1 α* gene was used as a reference gene for the QRT-PCR reactions [42].

QRT-PCR was carried out in a Rotor-Gene 6000 PCR apparatus (Corbett Robotics, Australia) by adding 10 μ l of SsoFast EvaGreen Supermix (Bio-Rad), 200 ng of cDNA, 0.5 pmol of each primer and water to a final volume of 20 μ L. After one initial incubation step at 95°C for 30 sec, amplification was performed for 40 cycles with the following profile: denaturation at 95°C for 5 sec, annealing at 60°C for 10 sec and extension at 72°C for 10 sec. Fluorescence data were collected during the extension (72°C) step and the specificity of PCR products was confirmed by performing a melting temperature analysis at temperatures ranging from 55°C to 95°C at intervals of 0.5°C. The PCR products were subsequently run on a 2.5% agarose gel to confirm the presence of a unique band with the expected size. The resulting PCR efficiency and Ct (Treshold Cycle) were used for transcript quantification. The Pfaff method [43] was used for the relative quantification of the transcript accumulation. For all the tested genes and treatments, three independent replicates were performed.

Statistical analysis

All results are presented as the mean \pm standard deviation (SD). The One Way ANOVA test of significance was used to compare the different conditions by Tukey Test (VassarStat Website for Statistical Computation, <http://faculty.vassar.edu/lowry/VassarStats.html>).

List of abbreviations

CAT – Catalase

DSBs – Double Strand Breaks

Endo III – Endonuclease III

FPG – Formamidopyrimidine DNA glycosylase

GR – Glutathione reductase

M&S – Murashige & Skoog

MPA – 3-Mercaptopropanoic acid

QDs – Quantum Dots

ROS – Reactive Oxygen Species

SOD – Superoxide dismutase

SSBs – Single Strand Breaks

Tdp – Tyrosyl-DNA phosphodiesterase

Top – Topoisomerase

Competing interests

The authors declare that they have no competing interests.

Authors' contributions

ARS, ASM and AM participated equally in the execution of the experiments and wrote the first draft of the manuscript. CM supervised the QD synthesis and contributed to the revision of the manuscript. AB, AO and PF participated in the design and coordination of the study, contributed to the interpretation of data and revision of the manuscript. All authors read, participated in the writing of and approved the final manuscript.

Acknowledgements

This work was supported by Fundação para a Ciência e a Tecnologia through the grant # NANO/NTec-SQA/0131/2007 “Development of ultra-sensitive detection methods and plant nano-vaccines for the fungi *Fusarium* spp. using nanotechnological devices” Iberian Capacitation Program in Nanotechnologies: Call 2006/2007” and the grant # PEst-OE/EQB/LA0004/2011.

Ana Sofia Miguel acknowledge Fundação para a Ciência e Tecnologia for the PhD grant (SFRH/BD/40303/2007).

We are thankful to Mattia Donà for his kind help and for introducing us to the Comet technique.

References

1. Karlsson H: **The comet assay in nanotoxicology research.** *Anal Bioanal Chem* 2010, **398**:651–666.
2. Apel K, Hirt H: **Reactive Oxygen Species: Metabolism, Oxidative Stress, and Signal Transduction.** *Annu Rev Plant Biol* 2004, **55**:373-99.

3. Santos A, Miguel A, Tomaz L, Malhó R, Maycock C, Patto C, Fevereiro P, Oliva A: **The impact of CdSe/ZnS Quantum Dots in cells of *Medicago sativa* in suspension culture.** *J Nanobiotechnology* 2010, **8**:24.
4. Smeets K, Cuypers A, Lambrechts A, Semane B, Hoet P, Laere A, Vangronsveld J: **Induction of oxidative stress and antioxidative mechanisms in *Phaseolus vulgaris* after Cd application.** *Plant Physiol Biochem* 2005, **43**: 437-444.
5. Valentine S, Wertz D, Lyons T, Liou L, Goto J, Gralla E: **The dark side of dioxygen biochemistry.** *Curr Opin Chem Biol* 1998, **2**:253–262.
6. Kumari M, Mukherjee A, Chandrasekaran N: **Genotoxicity of silver nanoparticles in *Allium cepa*.** *Sci Total Environ* 2009, **407**:5243-6.
7. Green M, Howman E: **Semiconductor quantum dots and free radical induced DNA nicking.** *Chem Commun* 2005;**1**:121-3.
8. Anas A, Akita H, Harashima H, Itoh T, Ishikawa M, Biju V: **Photosensitized breakage and damage of DNA by CdSe–ZnS quantum dots.** *J Phys Chem B* 2008, **112**:10005-11.
9. Koppen G, Verschaeve L: **The alkaline comet test on plant cells: A new genotoxicity test for DNA strand breaks in *Vicia faba* root cells.** *Mutation Res* 1996, **360**: 3193-200.
10. Singh N, McCoy M, Tice R, Schneider E: **A simple technique for quantitation of low levels of DNA damage in individual cells.** *Exp Cell Res* 1988, **175**: 184–191.
11. Ghosh M, Bandyopadhyay M, Mukherjee A: **Genotoxicity of titanium dioxide (TiO₂) nanoparticles at two trophic levels: plant and human lymphocytes.** *Chemosphere* 2010, **81**:1253-62.
12. Foyer C, Noctor G: **Redox regulation in photosynthetic organisms: signaling, acclimation, and practical implications.** *Antioxid Redox Signal* 2009, **11**:861-905.
13. Gouveris P, Skopelitis E, Tsavaris N: **Topoisomerase I and II Expression in Recurrent Colorectal Cancer Cells: A Dubious Matter.** DNA Replication-Current Advances, Herve Seligmann (Ed.), 2011. ISBN: 978-953-307-593-8, InTech
14. Mudgil Y, Singh B, Upadhyaya B, Sopory S, Reddy M: **Cloning and characterization of a cell cycle-regulated gene encoding Topoisomerase I from *Nicotiana tabacum* that is inducible by light, low temperature and abscisic acid.** *Mol Genet Genomics* 2002, **267**: 380-390.
15. Macovei A, Balestrazzi A, Confalonieri M, Carbonera D: **The tyrosyl-DNA phosphodiesterase gene family in *Medicago truncatula* Gaertn.: bioinformatic investigation and expression profiles in response to copper- and PEG-mediated stress.** *Planta* 2010, **232**:393–407.
16. Alsher R, Erturk N, Heath L: **Role of superoxide dismutases (SODs) in controlling oxidative stress in plants.** *J Exp Botany* 2002, **53**: 1331- 1341.
17. Prasad K, Saradhi P, Sharmila P: **Concerted action of antioxidant enzymes and curtailed growth under zinc toxicity in *Brassica juncea*.** *Environ Exp Botany*, 1999, **42**: 1-10.
18. Gechev T, Breusegem F, Stone J, Denev I, Laloi C: **Reactive oxygen species as signals that modulate plant stress responses and programmed cell death.** *BioEssays*, 2006, **28**:1091-1101.
19. Dat J, Vandenberghe S, Vranová E, Van Montagu M, Inzé D *et al*: **Dual action of the active oxygen species during plant stress responses.** *Cell Mol Life Sci* 2000, **57**:779-795.

20. Gomes-Junior, Moldes C, Delite F, Pompeu G, Gratão P, *et al*: **Antioxidant metabolism of coffee cell suspension cultures in response to cadmium.** *Chemosphere* 2006, **65**:1330-1337.
21. Petersen E, Nelson B: **Mechanisms and measurements of nanomaterial-induced oxidative damage to DNA.** *Anal Bioanal Chem* 2010, **398**:613-650.
22. Dizdaroglu M: **Base-excision repair of oxidative DNA damage by DNA glycosylases.** *Mutat Res* 2005, **591**: 45-59.
23. Murphy T, George A: **A comparison of two DNA base excision repair glycosylases from *Arabidopsis thaliana*.** *Biochem Biophys Res Commun* 2005, **329**: 869-872.
24. Scortecci K, Lima A, Carvalho F, Silva U, Agnez-Lima L, Batistuzzo de Medeiros S : **A characterization of a MutM/FPG ortholog in sugarcane - A monocot plant,** *Biochem Biophys Res Commun* 2007, **361**: 1054-1060.
25. Macovei A, Balestrazzi A, Confalonieri M, Faé M, Carbonera D: **New insights on the barrel medic *MtOGGI* and *MtFPG* functions in relation to oxidative stress response in planta and during seed imbibitions.** *Plant Physiol Bioch* 2011, doi:10.1016/j.plaphy.2011.05.007
26. Yang S, Burgin A, Huizenga B, Robertson C, Yao K, Nash H: **A eukaryotic enzyme that can disjoin dead-end covalent complexes between DNA and type I topoisomerases.** *Proc Natl Acad Sci USA* 1996, **93**: 11534-11539.
27. Lee S, Kim H, Hwang H, Jeong Y, Na S, Woo J, Kim S: **Identification of Tyrosyl-DNA phosphodiesterase as a novel DNA damage repair enzyme in *Arabidopsis*.** *Plant Physiol* 2010, **154**: 1460-1469.
28. Scandalios J: **Oxidative stress: molecular perception and transduction of signals triggering antioxidant gene defences.** *Bras J Med Biol Res* 2005, **38**: 995-1014.
29. Halliwell B: **Reactive Species and Antioxidants. Redox Biology Is a Fundamental Theme of Aerobic Life.** *Plant Physiol*, 2006, **141**: 312-322.
30. Azqueta A, Shaposhnikov S, Collins A: **Detection of Oxidised DNA Using DNA Repair Enzymes.** In *Issues in Toxicology No, 5 The Comet assay in toxicology*.1st edition. Edited by Dhawan A, Anderson D Royal Society of Chemistry; 2009:57-78.
31. Bradford, M. **A rapid and sensitive method for quantitation of microgram quantities of protein utilizing the principle of protein-dye-binding.** *Anal Biochem* 1976, **72**:248-54.
32. Rubio M, Gonzalez E, Minchin F, Webb K, Arrese-Igor C *et al*: **Effects of water stress on antioxidant enzymes of leaves and nodules of transgenic alfalfa overexpressing superoxide dismutases.** *Physiol Plantarum*, 2002, **115**: 531–540.
33. McCord J, Fridovich I: **Superoxide dismutase. An enzymic function for erythrocyte (hemocuprein).** *J Biol Chem*, 1969, **244**: 6049-6055.
34. Aebi, H. E: **Catalase.** In *Methods of enzymatic analysis*, Vol III. Oxidoreductases, transferases, eds. U.S. Bergmeyer, Germany, Verlag Chemie 1983, 273-277.

35. Shanker A, Djanaguiraman M, Sudhagar R, Chandrashekar C, Pathmanabhan G: **Differential antioxidative response of ascorbate glutathione pathway enzymes and metabolites to chromium speciation stress in green gram (*Vigna radiata* (L.) R.Wilczek. cv CO 4) roots.** *Plant Sci* 2004, **166**: 1035-1043.
36. Angelis K, Dusinská M, Collins A: **Single cell gel electrophoresis: Detection of DNA damage at different levels of sensitivity.** *Electrophoresis* 1999, **20**: 2133-2138.
37. Collins A: **The Comet Assay for DNA Damage and Repair.** *Mol Biotech* 2004, **26**:249-261.
38. Chang S, Puryear J, Cairney J: **A simple and efficient method for isolating RNA from pine trees.** *Plant Mol Biol Repor* 1993, **11**, 113-116.
39. Boldon F, Marie D, Brown S, Kodorosi A: **Genome size and base comparison in *Medicago sativa* and *M. truncatula* species.** *Genome* 1994, **37**: 264-270.
40. Choi H, Kim D, Uhm T, Limpens E, Lim H, Mun J, Kalo P, Penmetsa R, Seres A, Kulikova O, Roe B, Biosseling T, Kiss G, Cook D: **A sequence based genetic map of *Medicago truncatula* and comparison of marker colinearity with *M. sativa*.** *Genetics* 2004, **166**: 1463-1502.
41. Yang S, Gao M, Xu J, Despande S, Lin S, Roe BA, Zhu H: **Alfalfa benefits from *Medicago truncatula*: the RCT1 gene from *M. truncatula* confers broad-spectrum resistance to anthracnose in alfalfa.** *PNAS* 2008, **34**: 12164-12169.
42. Kadar K, Wandrey M, Czechowski T, Gaertner T, Scheible W, Stitt M, Torres-Jerez I, Xiao Y, Redman J, Wu H, Cheuny F, Town C, Udvardi M: **A community resource for high-throughput quantitative RT-PCR analysis of transcription factor gene expression in *Medicago truncatula*.** *Plant Methods* 2008,**4**:18.
43. Pfaff M: **A new mathematical model for relative quantitation in real-time RT-PCR.** *Nucleic Acids Res* 2001, **29**: 2002-2007.
44. Mittler R, Vanderauwera S, Gollery M, Van Breusegem F: **Reactive oxygen gene network of plants.** *Trends Plant Sci* 2004, **9**:490-498.

Figures

Figure 1 – Confocal fluorescence image of *M. sativa* cells after 48 hours of incubation with 10 nM of mercaptopropionic acid-QDs showing QD internalization. The fluorescent spots due to mercaptopropionic acid-QDs are seen in in the cytosol and in the nucleus. Scale bar = 25 μ M.

Figure 2 – Effect of MPA-QDs on the activities of SOD, CAT and GR.

Enzymatic activity of extracts of cell suspension cultures treated with 0, 10, 50 or 100 nM of MPA-QDS for 48 hours. Activity results for SOD are expressed in relative activity, A/A₀, where A is the measured enzyme activity for the cells in the presence of MPA-QDs and A₀ is the enzyme activity for the control. For CAT and GR activities results are expressed as U mg⁻¹ protein. Bars indicate the standard deviation of mean values. Values with different letters are significantly different at p \leq 0.01.

Figure 3 - Histogram of comet distribution.

a) Histogram of comet distribution for cell suspension cultures added with 0, 10, 50 and 100 nM of MPA-QDs and subjected to 50 °C during 20 min based on the comet score with the A/N version. b) images of comets that represent the 0-4 classes for visual scoring.

Figure 4 - DNA damage in *Medicago sativa* cells in suspension cultures

DNA damage in cell suspension cultures treated with 0, 10, 50 and 100 nM of MPA-QDs for 48 hours or at 50 °C for 20 minutes, in alkaline unwinding and neutral electrophoresis (A/N), in neutral incubation and neutral electrophoresis (N/N), and also by incubation with lesion-specific FPG or EndoIII enzymes. Results are expressed as mean values with standard deviation. One –way ANOVA $P < 0.0001$. Values with different letters are significantly different at $p \leq 0.01$ with Tukey test.

Figure 5 - Expression of *Tdp1* β , *Top1* β , *Fpg*, *SOD* and *APX* genes in *Medicago sativa* cells treated with MPA-QDs.

Expression of *Tdp1* β , *Top1* β , *Fpg*, *SOD* and *APX* genes on cell suspension cultures of *M. sativa* treated for 48 hours with 0, 10, 50 and 100 nM of MPA-QDs and at 50 °C for 20 minutes. For each treatment, data represent the mean values of three independent replications. One –way ANOVA $P < 0.0001$ for *Tdp1b*, *Fpg*, *APX* and *SOD* and $P < 0.01$ for *Top1b*. Tukey test $P < 0.01$ except for * $P < 0.05$.

Tables

Table 1-Primer sequences

Gene	Forward Primer (5'-3')	Reverse Primer (5'-3')	Efficiency*
<i>Tdp1</i> β	GGTTGGTTTGAGCCATCTTT	GCAGGCACATTGTGATTCT	1.79
<i>Top1</i> β	ATACACGTGGGCTATTGTCG	TCACTTGGATGAATGCGTT	1.77
<i>FPG</i>	TCCTTTCAATTCGGTATGGC	GTCCAAACCATCGTCTAGC	1.76
<i>APX</i>	AGCTCAGAGTTTCATCGCT	CGAAAGGACCACCAGTCTTT	1.80
<i>SOD</i>	CCTGAGGATGAGACTCGACA	GAACAACAACAGCCCTTCCT	1.72
<i>ELF1</i> α	GACAAGCGTGTGATCGAGAGATT	TTTCACGCTCAGCCTTAAGCT	1.90

* Efficiency of the primer pair in QRT-PCR

Table 2 -Detoxifying enzymes

Detoxifying enzymes studied in this work and their functions and location.

Enzyme	Function	Location	Reference
Superoxide Dismutase	Dismutation of $O_2^{\cdot-}$, leads to H_2O_2 formation	Cytosol, chloroplasts, mitochondria, peroxisomes	[44]
Catalase	Detoxifies H_2O_2 , no reductor required	Mitochondria, peroxisomes, glyoxysomes	[19]
Glutathione reductase	Reduces oxidized glutathione with NADPH as reductor	Cytosol, chloroplasts, mitochondria, peroxisomes	[44]

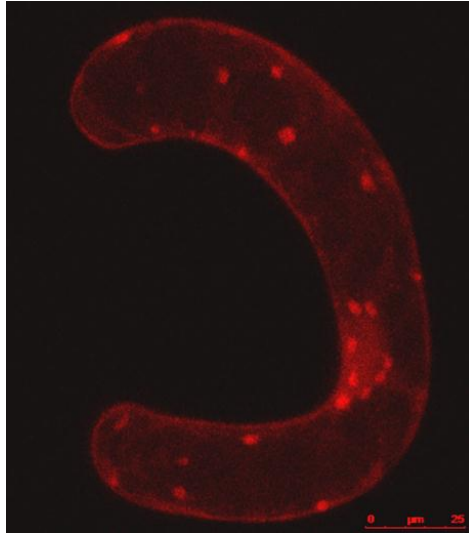


Fig.1

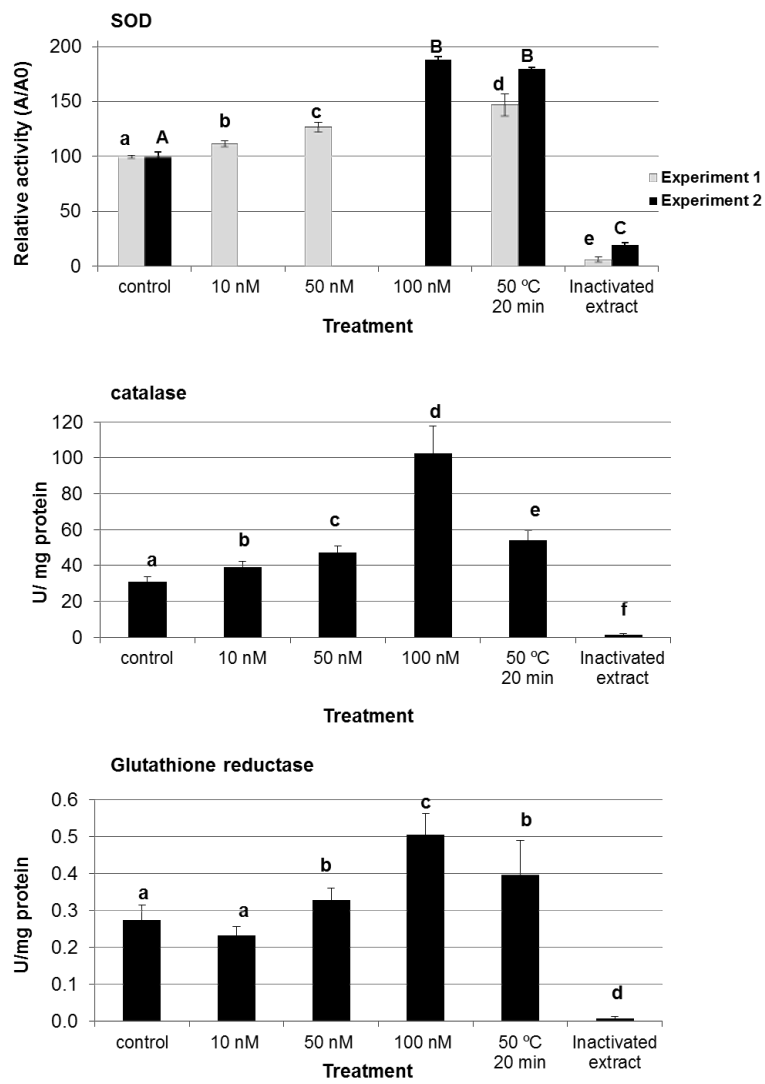


Fig. 2

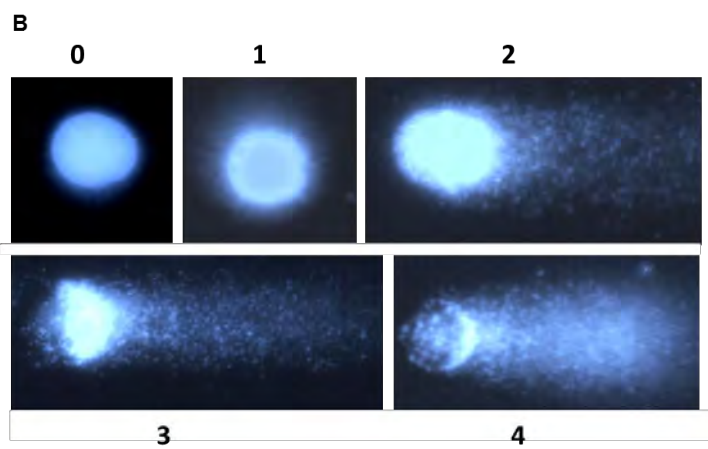
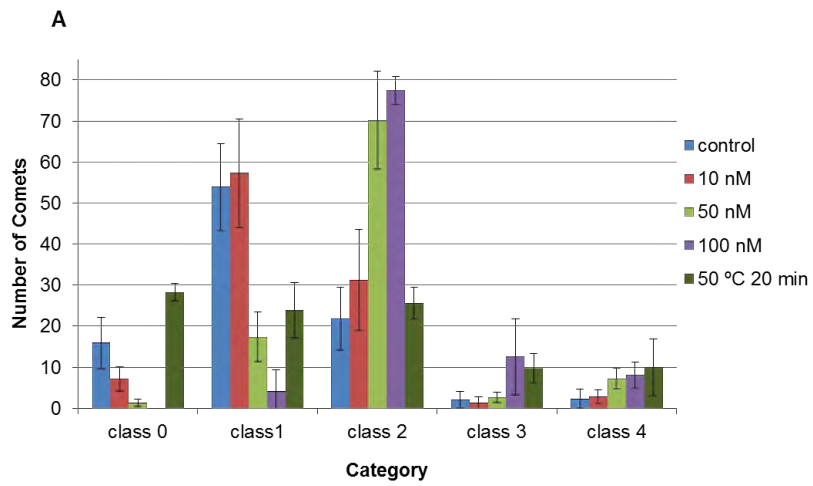


Fig. 3

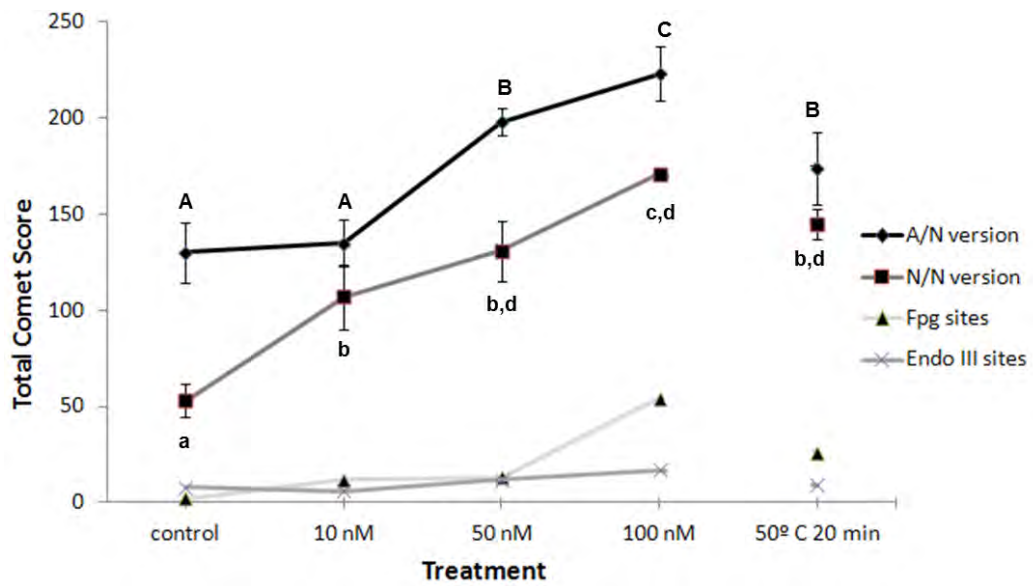


Fig. 4

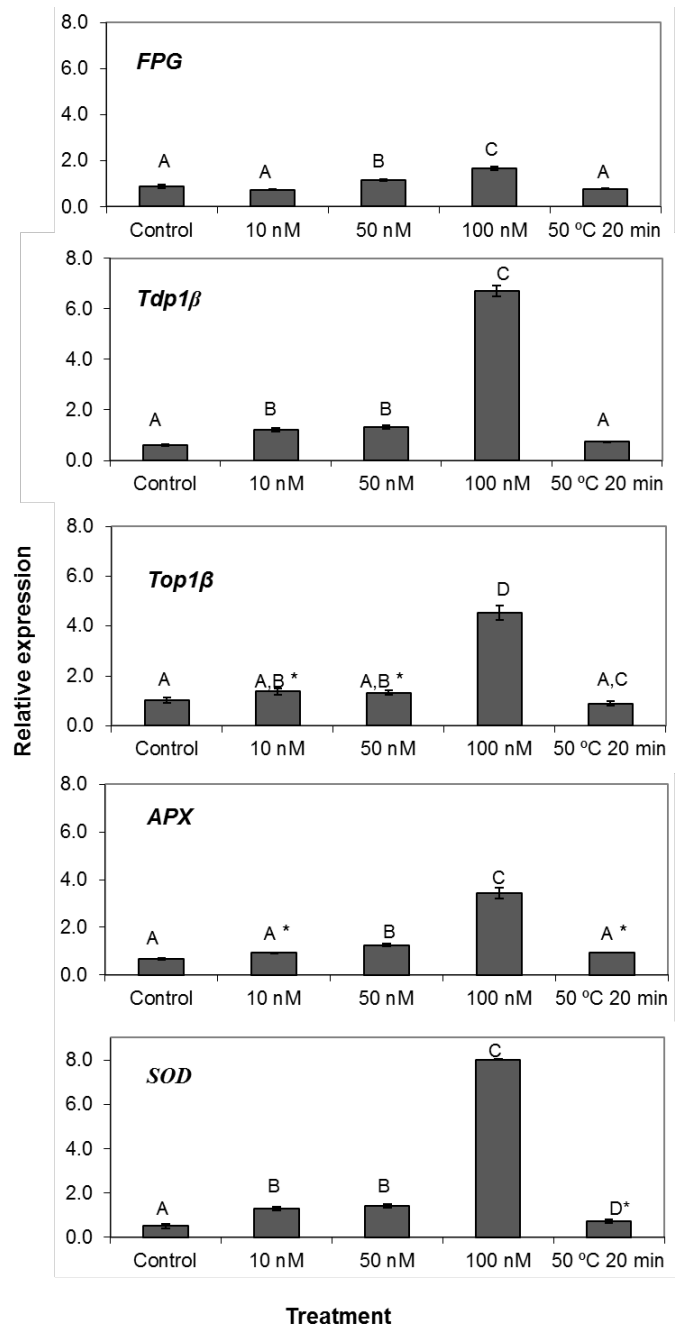


Fig. 5